

**Investigation of Chemical Constituents
in *Acacia saligna* (Labill.) H.L.Wendl.
Related to Antidiabetic Activity
by Anjar Purba Asmara**

Thesis submitted in fulfilment of the requirements for
the degree of

Doctor of Philosophy

under the supervision of A/Prof. Alison Ung (principal
supervisor) and Prof. Hui Chen (co-supervisor)

University of Technology Sydney
Faculty of Science

July 2023

Certificate of Original Authorship

I, Anjar Purba Asmara, declare that this thesis is submitted in fulfilment of the requirements for the award of Doctor of Philosophy, in the Faculty of Science at the University of Technology Sydney.

This thesis is wholly my own work unless otherwise referenced or acknowledged. In addition, I certify that all information sources and literature used are indicated in the thesis.

This document has not been submitted for qualifications at any other academic institution.

This research is supported by the Australian Government Research Training Program.

Signature:

Note: signature removed prior to publication

July 2023

Dedication

This thesis is dedicated to my beloved family for endless support and motivation.

Acknowledgement

All praise is due to Allah SWT for His blessings to the completion of my PhD study at UTS.

I would like to express my gratitude to my principal supervisor, Associate Professor Alison Ung, for her invaluable advice, guidance, encouragement, support, and motivation during my journey in this PhD study. I would also thank Professor Hui Chen as my co-supervisor for her advice and feedback on the research design and thesis writing.

I would gratefully acknowledge the full funding support from the Government of the Republic of Indonesia through *Program 5000 Doktor dan Beasiswa Indonesia Bangkit* organised by Ministry of Religious Affairs (MoRA) and Indonesia Endowment Funds for Education (LPDP) by Ministry of Finance.

I would also like to appreciate the assistance from Anchalee Prasansuklab, Ph.D. when setting up bioassay methods and during collecting data in Chulalongkorn University (CU), Bangkok, Thailand. I thank Dr. Tewin Tencomnao and his research group for the support during our collaborative research in CU, and Dr. Anchalee Chiabchalard for her administrative help within the data collection in CU.

All assistance from UTS lab and academic staff and my UTS laboratory mates, including Bishwajit Bokshi, Hugh Hiscock, Behjat Sheikholeslami, and Seyed Mostafa Hosseinpour Mashkani, is appreciated. All support from the Indonesian community in Sydney, especially within the difficult situation over the pandemic COVID 2020 – 2022, is also appreciated.

Last but not least, I would like to thank my wife, my sons, my mother, father, and sister in Indonesia for their unconditional support and motivation that make my life far from home less difficult.

List of Publications

- 1) Asmara, A.P.; Prasansuklab, A.; Tencomnao, T.; Ung, A.T. Identification of Phytochemicals in Bioactive Extracts of *Acacia saligna* Growing in Australia. *Molecules* **2023**, *28*(3), 1028. <https://doi.org/10.3390/molecules28031028>.
- 2) Asmara, A.P.; Prasansuklab, A.; Chiabchalard, A.; Chen, H.; Ung, A.T. Antihyperglycemic Properties of Extracts and Isolated Compounds from Australian *Acacia saligna* on 3T3-L1 Adipocytes. *Molecules* **2023**, *28*(10), 4054. <https://doi.org/10.3390/molecules28104054>.
- 3) Ung, A.T.; Asmara, A.P. Bioactive Phytochemicals of *Acacia saligna*. *Molecules* **2023**, *28*(11), 4396. <https://doi.org/10.3390/molecules28114396>.
- 4) Asmara, A.P.; Chen, H.; Ung, A.T. Preventing Adipogenesis and Preserving Mitochondria and GLUT-4 Functions by Extracts and Isolated Compounds of Australian *Acacia saligna*. *Molecules* **2023**, *28*(18), 6677. <https://doi.org/10.3390/molecules28186677>.

Table of Contents

Certificate of Original Authorship	ii
Dedication.....	iii
Acknowledgement	iv
List of Publications.....	v
Table of Contents	vi
List of Figures	x
List of Tables	xxii
List of Appendix	xxiv
Abbreviations.....	xxvii
Abstract	xxxii
CHAPTER 1: INTRODUCTION	1
1.1. General background.....	1
1.2. Diabetes mellitus	3
1.2.1. Classification of DM	3
1.2.2. Oxidative stress associated with DM.....	4
1.2.3. Postprandial hyperglycaemia	6
1.2.4. Potential targets to overcome insulin resistance	9
1.3. Pharmaceutical Treatments for Type 2 Diabetes Mellitus	15
1.4. Overview of <i>Acacia saligna</i>	19
1.4.1. Taxonomy.....	19
1.4.2. Reported chemical composition	21
1.4.3. Bioactivities of the plant	25
1.4.4. Other applications of <i>Acacia saligna</i>	30
1.5. Research aim.....	31
1.6. Research objectives	31
CHAPTER 2: RESULT AND DISCUSSION OF EXTRACTION AND BIOACTIVITIES OF EXTRACTS	33
2.1. Introduction of Chapter 2.....	33
2.2. Sequential extraction of flowers, leaves, and barks	34
2.3. Phenolic content and flavonoid content of the extracts	36
2.4. Phytochemicals screened by GCMS	38
2.5. Antioxidant activity of extracts against the DPPH	38
2.6. Antioxidant activity of extracts against the ABTS* ⁺	39
2.7. Inhibitory activity against α -glucosidase.....	41
2.8. Conclusion of Chapter 2.....	43

CHAPTER 3: RESULT OF CELL-BASED STUDIES OF EXTRACTS	44
3.1. Introduction of Chapter 3	44
3.2. Viability of 3T3-L1 preadipocytes treated with extracts	44
3.3. Cell differentiation.....	47
3.4. Viability of 3T3-L1 adipocytes treated with extracts	49
3.5. Oil Red-O assay of extracts.....	51
3.6. Measurement of cellular ROS level	53
3.7. Cellular glucose uptake assay of extracts.....	57
3.8. Conclusion of Chapter 3	58
CHAPTER 4: RESULT OF COMPOUND ISOLATION AND MOLECULAR ELUCIDATION	60
4.1. Introduction of Chapter 4	60
4.2. Structure identification of isolated compounds.....	60
4.2.1.1. Naringenin 42	60
4.2.1.2. Naringenin-7 <i>O</i> - α - <i>L</i> -arabinofuranoside 76	64
4.2.1.3. Isosalipurposide 1	74
4.2.1.4. Quercitrin 4 from flowers	78
4.2.1.5. <i>D</i> -(+)-pinitol 79a from flowers.....	82
4.2.2.1. (-)-Epicatechin 77 from leaves.....	86
4.2.2.2. 2,4-Di- <i>t</i> -butylphenol 78.....	90
4.2.2.3. Quercitrin 4 from leaves	94
4.2.2.4. Myricitrin 11	99
4.2.2.5. (-)-Pinitol 79b	103
4.2.2.6. 3-Hydroxy-5-(2-aminoethyl) dihydrofuran-2(3 <i>H</i>)-one 80	107
4.2.3.1. (-)-Epicatechin 77 from bark.....	115
4.2.3.2. <i>D</i> -(+)-Pinitol 79a from bark.....	120
4.2.3.3. Sucrose	124
4.3. Conclusion of Chapter 4	128
CHAPTER 5: RESULT OF BIOACTIVITIES OF ISOLATED COMPOUNDS.....	130
5.1. Introduction of Chapter 5.....	130
5.2. Antioxidant activities of isolated compounds.....	130
5.3. Inhibitory activity of isolated compounds against α -glucosidase	134
5.4. Cell viability of 3T3-L1 cell line treated with isolated compounds.....	137
5.5. Oil Red-O staining assay of adipocytes treated with isolated compounds ..	142
5.6. Cellular ROS reduction assay on adipocytes treated with isolated compounds	143

5.7. Measurement of mt-ROS and MMP on adipocytes treated with isolated compounds	145
5.8. Cellular glucose uptake of adipocytes treated with isolated compounds.....	149
5.9. Conclusion of Chapter 5.....	151
CHAPTER 6: RESULT OF IDENTIFICATION OF BIOLOGICAL PATHWAYS.....	152
6.1. Introduction of Chapter 6.....	152
6.2. AMPK pathway activation.....	153
6.3. Expression of mRNAs related to the mitochondrial biogenesis.....	155
6.4. Expression of mRNAs of inflammatory markers.....	158
6.5. Conclusion of Chapter 6.....	160
CHAPTER 7: CONCLUSION AND FUTURE DIRECTION.....	161
7.1. General conclusion.....	161
7.2. Future direction	163
CHAPTER 8: EXPERIMENTAL SECTION.....	164
8.1. Experiments of extraction	164
8.1.1. Materials	164
8.1.2. Extraction protocol	164
8.1.3. Spectrometric estimation of phenolic and flavonoid content.....	165
8.1.4. Screening of phytochemicals using gas chromatography-mass spectroscopy (GCMS) analysis.....	166
8.2. Experiments of DPPH and ABTS ^{•+} scavenging assays.....	167
8.3. Experiment of α -glucosidase inhibition assay	167
8.4. Cell-based studies.....	168
8.4.1. Protocol of cell subculture	168
8.4.2. Protocol of cell viability experiment on 3T3-L1 preadipocytes with MTT assay.....	169
8.4.3. Protocol of cell differentiation	169
8.4.4. Protocol of cell viability experiment on 3T3-L1 adipocytes	170
8.4.5. Experiment of ORO staining assay	170
8.4.6. Experiment of cellular ROS reduction assay using dichlorodihydrofluorescein diacetate (DCFH-DA).....	171
8.4.7. Experiment of cellular glucose uptake assay.....	171
8.5. Experiment of compound isolation and molecular structure elucidation	172
8.5.1. Materials for fractionation and isolation	172
8.5.2. Thin Layer Chromatography (TLC) experiment.....	172
8.5.2.1. Fractionation and TLC profile of FL-MeOH.....	172
8.5.2.2. Fractionation and TLC profile of LF-MeOH.....	175
8.5.2.3. Fractionation and TLC profile of BK-MeOH.....	177

8.5.3. Structure identification of isolated compounds	179
8.5.3.1. Spectral data analysis of compounds from FL-MeOH	179
8.5.3.2. Spectral data analysis of compounds from LF-MeOH	179
8.5.3.3. Spectral data analysis of compounds from BK-MeOH.....	180
8.6. Experiments of mt-ROS and MMP assays.....	181
8.6.1. Materials of mitochondrial assays	181
8.6.2. Mt-ROS level measurement using mitoSOX staining reagent	181
8.6.3. Mitochondrial membrane potential (MMP) measurement using JC-1 staining reagent	182
8.7. Experiment of immunoblot analysis	183
8.7.1. Materials for immunoblot study	183
8.7.2. Protocols for immunoblot study	183
8.8. Quantitative reverse transcription-polymerase chain reaction (RT-qPCR) ..	184
8.8.1. Materials for RT-qPCR.....	184
8.8.2. Protocol of the RT-qPCR experiment.....	184
8.9. Statistical analysis	185
REFERENCES	186

List of Figures

- Figure 1.** Percentage of global mortality factors for 41 million deaths in 2016 ². 1
- Figure 2.** Schematic representation of the link between inflammation mediators and adipocytes IR ¹⁷. GLUT-4: glucose transporter-4; ↑: increasing; ↓: decreasing. 2
- Figure 3.** Scheme of the T2DM progression due to insulin insufficiency promoted by inflammatory and oxidative state ²²⁻²⁴; ↑: increasing; ↓: decreasing. 3
- Figure 4.** An illustration of high glucose-induced ROS production in a cell. (1) Elevated blood sugar level causes comparably increased uptake of glucose into cells; (2) excess glucose induces glycation of protein to produce (3) Schiff base followed by rearrangement to form (4) Amadori compound as the intermediate of (5) advanced glycation end products (AGEs); (6) AGEs directly stimulate excess ROS production by NADPH oxidase due to neutralising endogenous antioxidants ⁴². Moreover, the glucose can also be oxidised in the cytoplasm resulting in elevated NADH and pyruvates; (7) pyruvates oxidised in the TCA cycle led to the increased NADH and FADH₂, (8) which are involved in the accumulated of electrons during ATP leading to overproduction of mt-ROS. The image was adapted from Kawahito et al. ⁴³ and created with BioRender.com. 5
- Figure 5.** An illustration of superoxide production in the mitochondrial ETC. Excess glucose and FFA-derived products lead to overproduced coenzymes (NADH and FADH₂) from the Krebs cycle. It causes accumulated electrons in coenzyme ubiquinone (CoQ) captured by O₂ to produce superoxide radicals (O₂[•]) or mt-ROS. The image was adapted from Rebolledo & Dato ⁴⁴ and created with BioRender.com. 6
- Figure 6.** Schematic diagram by which post-prandial hyperglycaemia plays its causal role in the onset of T2DM ⁵². 7
- Figure 7.** A representative flow of causes of T2DM-associated complications linked to polyol pathway. (1) In the presence of aldose reductase enzymes, excess glucose will be reduced to sorbitol that requires the oxidation of NADPH; (2) consequently, glutathione level will decrease due to the deficiency of its cofactor, NADPH, leading to elevated oxidative stress. (3) The increase of sorbitol resulted in increased intracellular osmolality and decreased the number of myoinositol, the upstream of adenosine-triphosphatase (ATPase) ⁶⁹. (4) The accumulated fructose from the reduction of sorbitol can be turnover to glyceraldehyde-3-phosphate as the precursor of all glycolytic intermediates that increase the glycation of proteins. (5) Finally, these processes exacerbate complications such as retinopathy, neuropathy, and renal

failure. The image was adapted from Taslimi et al.⁷⁰ and created with BioRender.com.

..... 8

Figure 8. A schematic flow chart of insulin-independent GLUT-4 activation induced by metformin inhibiting mitochondrial ATP synthase^{81, 95-97}. The increased ratios of ADP/ATP and AMP/ATP will activate AMPK by stimulating LKB1 to phosphorylate the AMPK- α and promoting the binding of AMP to AMPK- γ to maintain the phosphorylation. The activated AMPK can stimulate the phosphorylation of AS160 and ACC, eventually activating the translocation of GLUT-4. AMPK = adenosine 5'monophosphate-activated protein kinase; LKB1 = liver kinase B1; GLUT-4 = glucose transporter-4; ACC = acetyl-CoA carboxylase; AS160 = 160 kDa substrate of Akt Ser/Thr kinase; TBC1D4 = Tre-2/BUB2/cdc 1 domain family. 10

Figure 9. Schematic representation of possible mechanisms of the links between overproduced mt-ROS and insulin resistance, leading to disruption in GLUT-4 translocation^{79, 98}. mtROS = mitochondrial reactive oxygen species; ASK 1 = apoptosis signal-regulating kinase 1; JNK = c-jun NH₂-terminal kinases; MFN 1 and MFN2 = mitofusins 1 and 2; IRS-1 = insulin-receptor substrate 1. The image was created with BioRender.com. 11

Figure 10. An image represents a proposed mechanism of mitochondrial dysfunction as the primary cause of insulin resistance in an adipocyte model. The increased intracellular ROS triggered by obesity and metabolic challenges (e.g., excess nutrient intake) leads to mt-ROS overproduction, exacerbating the total ROS generation and decreasing mitochondrial membrane potential (MMP) and ATP production⁸¹. The impaired mitochondria reflected by the collapse of mt-DNA content and depletion of mitochondrial biogenesis alter adiponectin level, resulting in decreased OXPHOS due to reduced activation of AMPK and PGC-1 α as its regulator¹¹⁴. In addition, the compromised mitochondria function causes the accumulation of lipid metabolites due to the reduced β -oxidation and the increase of proinflammatory cytokines leading to the induction of PKC isoforms and Ser/Thr kinases^{28, 110}. Consequently, the inhibition of the insulin signalling cascade, including the disruption of GLUT-4 transduction, leads to the defect of the insulin-dependent glucose uptake pathway. Image was created with BioRender.com. 12

Figure 11. Schematic multiple steps mechanisms of insulin resistance induced by oxidative stress in 3T3-L1 adipocytes^{75, 78, 126}. \uparrow = increased; \downarrow = decreased..... 14

Figure 12. Schematic representation of some selected phytochemical roles as antidiabetic agents^{147, 159, 170, 171}. 18

Figure 13. A photograph of <i>A. saligna</i> subsp. <i>saligna</i> collected from Tasman St, Kurnell, NSW, on 7 October 2019 for this study.....	20
Figure 14. Phenolics and alkaloid derivatives identified in flowers ^{187, 188} , leaves ^{189, 190, 196, 215, 216} , and barks ²¹⁷ of <i>A. saligna</i>	24
Figure 15. Saponin derivatives elucidated in MeOH extract of <i>A. saligna</i> leaves ¹⁹⁶	25
Figure 16. Schematic diagrams of the outcomes of extraction of (a) flowers, (b) leaves, and (c) bark.	35
Figure 17. Estimation of (a) phenolic content and (b) flavonoid content of <i>A. saligna</i> extracts. GAE: gallic acid equivalent, QE: quercetin equivalent, FL-hex: hexane extract of flowers, FL-DCM: dichloromethane extract of flowers, FL-MeOH: methanol extract of flowers, FL-H ₂ O: aqueous extract of flowers, LF-hex: hexane extract of leaves, LF-DCM: dichloromethane extract of leaves, LF-MeOH: methanol extract of leaves, LF-H ₂ O: aqueous extract of leaves, BK-hex: hexane extract of bark, BK-DCM: dichloromethane extract of bark, BK-MeOH: methanol extract of bark, BK-H ₂ O: aqueous extract of bark. Data in mean ± SEM, **** <i>p</i> < 0.0001 (<i>n</i> = 3, One-way ANOVA, Tukey's post hoc).....	37
Figure 18. The dose-response curve of the active methanolic extract of flowers, leaves, and barks and vitamin C against radical DPPH. Data in mean ± SEM, <i>n</i> = 3.	39
Figure 19. The dose-response curve of the active methanolic extract of flowers, leaves, and barks and vitamin C against ABTS cation radicals, Data in mean ± SEM, <i>n</i> = 3.	40
Figure 20. Comparison of antioxidant activity in IC ₅₀ between methanolic flower, leaf, and bark extract of <i>A. saligna</i> and vitamin C in DPPH and ABTS ^{•+} scavenging assay. Data in mean ± SEM, **** <i>p</i> < 0.0001, vs vitamin C (<i>n</i> = 3, One-way ANOVA, Tukey's post hoc).....	40
Figure 21. The dose-response curve of the active methanolic extract of flowers (FL-MeOH), leaves (LF-MeOH), and barks (BK-MeOH), and acarbose against the yeast α-glucosidase enzyme. Data in mean ± SEM, <i>n</i> = 3.....	42
Figure 22. IC ₅₀ of active extracts and acarbose against the yeast α-glucosidase enzyme. Data in mean ± SEM, *** <i>p</i> = 0.0004; **** <i>p</i> < 0.0001, vs acarbose (<i>n</i> = 3, One-way ANOVA, Tukey's post hoc).	43
Figure 23. Viability of 3T3-L1 preadipocytes treated with FL extracts. FL-hex: hexane extract of flowers, FL-DCM: dichloromethane extract of flowers, FL-MeOH: methanol extract of flowers, FL-H ₂ O: aqueous extract of flowers. Data in mean ± SEM, * <i>p</i> = 0.04;	

** <i>p</i> = 0.004; *** <i>p</i> = 0.0001; **** <i>p</i> < 0.0001, vs vehicle control (<i>n</i> = 3, One-way ANOVA, Dunnett's post hoc).....	46
Figure 24. Viability of 3T3-L1 preadipocytes treated with LF extracts. LF-hex: hexane extract of leaves, LF-DCM: dichloromethane extract of leaves, LF-MeOH: methanol extract of leaves, LF-H ₂ O: aqueous leaves extract. Data in mean ± SEM, * <i>p</i> = 0.03; ** <i>p</i> = 0.006; *** <i>p</i> = 0.0004; **** <i>p</i> < 0.0001, vs vehicle control (<i>n</i> = 3, One-way ANOVA, Dunnett's post hoc).....	46
Figure 25. Viability of 3T3-L1 preadipocytes treated with BK extracts. BK-hex: hexane extract of bark, BK-DCM: dichloromethane extract of bark, BK-MeOH: methanol extract of bark, BK-H ₂ O: aqueous extract of bark. Data in mean ± SEM, * <i>p</i> = 0.03; ** <i>p</i> = 0.008; *** <i>p</i> = 0.0007; **** <i>p</i> < 0.0001, vs vehicle control (<i>n</i> = 3, One-way ANOVA, Dunnett's post hoc).....	47
Figure 26. Images of 3T3-L1 cells differentiation showing the cell appearance in the following stages: (1 & 2) preadipocytes growth at day -4 & -2 of differentiating induction; (3) confluent cell at the day of the induction with MDI or M2 and (4) second day defined as early phase; and (5) fourth day as the intermediate; (6) sixth and (7) eighth day of the induction called terminal phase. The cell photographs were captured with an inverse phase contrast microscope (Infinity 1, Nikon Eclipse TS100) at a magnification of 20×. M1 = DMEM, BCS, and PSG; M2 = DMEM, FBS, PSG, rosiglitazone 2 µM, insulin 5 µg/mL, IBMX 0.5 mM, and dexamethasone 1 µM; M3 = DMEM, FBS, PSG, and insulin 5 µg/mL; M4 = DMEM, FBS, PSG.....	48
Figure 27. Viability of 3T3-L1 adipocytes treated with FL extracts. FL-hex: hexane extract of flowers, FL-DCM: dichloromethane extract of flowers, FL-MeOH: methanol extract of flowers, FL-H ₂ O: aqueous extract of flowers. Data in mean ± SEM, * <i>p</i> = 0.02; ** <i>p</i> = 0.002, vs vehicle control (<i>n</i> = 3, One-way ANOVA, Tukey's post hoc).....	49
Figure 28. Viability of 3T3-L1 adipocytes treated with LF extracts. LF-hex: hexane extract of leaves, LF-DCM: dichloromethane extract of leaves, LF-MeOH: methanol extract of leaves, LF-H ₂ O: aqueous leaves extract. Data in mean ± SEM, * <i>p</i> = 0.02; ** <i>p</i> = 0.001; *** <i>p</i> = 0.0001, vs vehicle control (<i>n</i> = 3, One-way ANOVA, Tukey's post hoc).	50
Figure 29. Viability of 3T3-L1 adipocytes treated with BK extracts. BK-hex: hexane extract of bark, BK-DCM: dichloromethane extract of bark, BK-MeOH: methanol extract of bark, BK-H ₂ O: aqueous extract of bark. Data in mean ± SEM, * <i>p</i> = 0.02; ** <i>p</i> = 0.003, vs vehicle control (<i>n</i> = 3, One-way ANOVA, Tukey's post hoc).	51

Figure 30. The captured image of (a) unstained vs (b) stained 3T3-L1 adipocytes with ORO reagent. Images were photographed with an inverse phase-contrast microscope (Infinity 1, Nikon Eclipse TS100) at a magnification of 20×.52

Figure 31. Lipid content from ORO staining assay on the 3T3-L1 adipocytes treated with extracts during the progress of cell differentiation. FL-hex: hexane extract of flowers, FL-DCM: dichloromethane extract of flowers, FL-MeOH: methanol extract of flowers, FL-H₂O: aqueous extract of flowers, LF-hex: hexane extract of leaves, LF-DCM: dichloromethane extract of leaves, LF-MeOH: methanol extract of leaves, LF-H₂O: aqueous extract of leaves, BK-hex: hexane extract of bark, BK-DCM: dichloromethane extract of bark, BK-MeOH: methanol extract of bark, BK-H₂O: aqueous extract of bark, and NAC = *N*-acetyl cysteine. Data in mean ± SEM, **p* = 0.02; ***p* = 0.009, vs vehicle control (*n* = 3, One-way ANOVA, Tukey's post hoc)...53

Figure 32. Detected cellular ROS of 3T3-L1 adipocytes treated with (a) FL extracts, (b) LF extracts, and (c) BK extracts compared to NAC as the positive control. FL-hex: hexane extract of flowers, FL-DCM: dichloromethane extract of flowers, FL-MeOH: methanol extract of flowers, FL-H₂O: aqueous extract of flowers, LF-hex: hexane extract of leaves, LF-DCM: dichloromethane extract of leaves, LF-MeOH: methanol extract of leaves, LF-H₂O: aqueous extract of leaves, BK-hex: hexane extract of bark, BK-DCM: dichloromethane extract of bark, BK-MeOH: methanol extract of bark, BK-H₂O: aqueous extract of bark, and NAC = *N*-acetyl cysteine. Data in mean ± SEM, **p* = 0.03, vs vehicle control (*n* = 3, One-way ANOVA, Tukey's post hoc).55

Figure 33. Comparison of intracellular ROS level in 3T3-L1 adipocytes treated with methanolic extracts. Data in mean ± SEM, **p* = 0.01, ***p* = 0.008, vs vehicle control (*n* = 3, One-way ANOVA, Tukey's post hoc).55

Figure 34. Estimated 2-NBDG uptake by 3T3-L1 adipocytes treated with extracts of *A. saligna*. FL-hex: hexane extract of flowers, FL-DCM: dichloromethane extract of flowers, FL-MeOH: methanol extract of flowers, FL-H₂O: aqueous extract of flowers, LF-hex: hexane extract of leaves, LF-DCM: dichloromethane extract of leaves, LF-MeOH: methanol extract of leaves, LF-H₂O: aqueous extract of leaves, BK-hex: hexane extract of bark, BK-DCM: dichloromethane extract of bark, BK-MeOH: methanol extract of bark, BK-H₂O: aqueous extract of bark. Data in mean ± SEM, ***p* = 0.007 for FL-MeOH and ***p* = 0.006 for LF-MeOH, vs vehicle control (*n* = 3, One-way ANOVA, Dunnett's post hoc).58

Figure 35. The spectral image of ¹H NMR of naringenin **42** from methanolic extract of flowers61

Figure 36. The spectral image of ^{13}C NMR of naringenin 42 from methanolic extract of flowers	62
Figure 37. (a) The main skeleton of naringenin 42 ($\text{C}_{15}\text{H}_{12}\text{O}_5$; MW = 272.257), key connections of proton-to-proton ((b) \leftrightarrow COSY and (d) \leftrightarrow NOESY) and proton-to-carbon ((c) \leftrightarrow HMBC) of naringenin 42 isolated from the methanolic flowers extract.	64
Figure 38. Key connections of proton-to-proton (\leftrightarrow COSY; \leftrightarrow NOESY) and proton-to-carbon (\leftrightarrow HMBC) of naringenin-7- <i>O</i> - α -L-arabinofuranoside 76 ($\text{C}_{20}\text{H}_{20}\text{O}_9$; MW = 404.37) isolated from the methanolic flowers extract.	65
Figure 39. The spectral image of ^1H NMR of naringenin-7- <i>O</i> - α -L-arabinofuranoside 76 from methanolic extract of flowers.....	66
Figure 40. The spectral image of ^{13}C NMR of naringenin-7- <i>O</i> - α -L-arabinofuranoside 76 from methanolic extract of flowers.....	67
Figure 41. The spectral image of ^1H - ^1H COSY NMR of naringenin-7- <i>O</i> - α -L-arabinofuranoside 76 from methanolic extract of flowers	68
Figure 42. The spectral image of ^1H - ^{13}C HSQC NMR of naringenin-7- <i>O</i> - α -L-arabinofuranoside 76 from methanolic extract of flowers	69
Figure 43. The spectral image of ^1H - ^{13}C HMBC of naringenin-7- <i>O</i> - α -L-arabinofuranoside 76 from methanolic extract of flowers	70
Figure 44. The spectral image of ^1H - ^1H NOESY NMR of naringenin-7- <i>O</i> - α -L-arabinofuranoside 76 from methanolic extract of flowers	71
Figure 45. The spectral image of ^1H NMR of isosalipurposide 1 from methanolic extract of flowers.....	75
Figure 46. The spectral image of ^{13}C NMR of isosalipurposide 1 from methanolic extract of flowers.....	76
Figure 47. Molecular structure of isosalipurposide 1 ($\text{C}_{21}\text{H}_{22}\text{O}_{10}$; MW = 434.4) ¹⁸⁸ from the methanolic flower extract.	78
Figure 48. (a) The key connections of proton-to-proton (\leftrightarrow COSY) and (b) proton-to-carbon (\leftrightarrow HMBC) of isosalipurposide 1	78
Figure 49. The spectral image of ^1H NMR of quercitrin 4 from methanolic extract of flowers	79
Figure 50. The spectral image of ^{13}C NMR of quercitrin 4 from methanolic extract of flowers	80
Figure 51. Molecular structure of quercitrin 4 from the methanolic extract of flowers.	82

Figure 52. The spectral image of ^1H NMR of <i>D</i> -pinitol 79a from methanolic extract of flowers	83
Figure 53. The spectral image of ^{13}C NMR of <i>D</i> -pinitol 79a from methanolic extract of flowers	84
Figure 54. Molecular structure of 3- <i>O</i> -methyl- <i>D</i> -chiro-inositol (<i>D</i> -(+)-pinitol) ($\text{C}_7\text{H}_{14}\text{O}_6$) from the methanolic flower extract in (a) Haworth projection, (b) chair conformation, (c) COSY (\leftrightarrow) and HMBC (\leftrightarrow) relationship.....	86
Figure 55. (a) The main skeleton of catechin ($\text{C}_{15}\text{H}_{14}\text{O}_6$; MW = 290.97) and (b) key connections of proton-to-proton (\leftrightarrow COSY) and proton-to-carbon (\leftrightarrow HMBC) of the catechin derivative found in LF-MeOH-A1.....	86
Figure 56. The spectral image of ^1H NMR of (-)-epicatechin 77 from methanolic extract of leaves	87
Figure 57. The spectral image of ^{13}C NMR of (-)-epicatechin 77 from methanolic extract of leaves	88
Figure 58. (a) Key connections of proton-to-proton (\leftrightarrow NOESY) showing the spatial relationship of vicinal protons and (b) the molecular structure of (-)-epicatechin 77 with <i>cis</i> -2 <i>R</i> ,3 <i>R</i> stereochemical orientation.	90
Figure 59. The spectral image of ^1H NMR of 2,4-di- <i>t</i> -butylphenol 78 from methanolic extract of leaves	91
Figure 60. The spectral image of ^{13}C NMR of 2,4-di- <i>t</i> -butylphenol 78 from methanolic extract of leaves	92
Figure 61. (a) The molecular structure of phenol-2,4- <i>bis</i> (1,1-dimethylethyl) or 2,4-di- <i>t</i> -butylphenol 78 ($\text{C}_{14}\text{H}_{22}\text{O}$, MW = 206.32) from LF-MeOH-A3, (b) the structure with key connectivity according to COSY (\leftrightarrow), and (c) HMBC (\leftrightarrow) information.....	94
Figure 62. (a) Molecular structure of quercetin-3- <i>O</i> -rhamnoside from the methanolic extract of leaves (quercitrin 4 , $\text{C}_{21}\text{H}_{20}\text{O}_{11}$, MW = 448.1), and (b) key correlations within atoms based on HMBC.....	95
Figure 63. The spectral image of ^1H NMR of quercitrin 4 from methanolic extract of leaves	96
Figure 64. The spectral image of ^{13}C NMR of quercitrin 4 from methanolic extract of leaves	97
Figure 65. The spectral image of ^1H NMR of myricitrin 11 from methanolic extract of leaves	100
Figure 66. The spectral image of ^{13}C NMR of myricitrin 11 from methanolic extract of leaves	101

Figure 67. Molecular structure of myricetin-3- <i>O</i> -rhamnoside (myricitrin 11) from methanolic leaf extract showing 3-D conformation of the sugar ring.....	103
Figure 68. (a) Molecular structure of myricetin-3- <i>O</i> -rhamnoside (myricitrin 11 , C ₂₁ H ₂₀ O ₁₂ , MW = 464.37) and (b) key correlations within atoms based on selected HMBC.....	103
Figure 69. The spectral image of ¹ H NMR of (-)-pinitol 79b from methanolic extract of leaves	104
Figure 70. The spectral image of ¹³ C NMR of (-)-pinitol 79b from methanolic extract of leaves	105
Figure 71. Molecular structure of (-)-pinitol 79b (C ₇ H ₁₄ O ₆) from the methanolic extract of leaves in Haworth projection with HMBC information.	107
Figure 72. The spectral image of ¹ H NMR of compound 80 from methanolic extract of leaves	108
Figure 73. The spectral image of ¹³ C NMR of compound 80 from methanolic extract of leaves	109
Figure 74. The spectral image of ¹ H- ¹ H COSY NMR of compound 80 from methanolic extract of leaves	110
Figure 75. The spectral image of ¹ H- ¹³ C HSQC NMR of compound 80 from methanolic extract of leaves	111
Figure 76. The spectral image of ¹ H- ¹³ C HMBC NMR of compound 80 from methanolic extract of leaves	112
Figure 77. The spectral image of ¹ H- ¹ H NOESY NMR of compound 80 from methanolic extract of leaves	113
Figure 78. (a) The possible structure of the compound from LF-MeOH-D named as 3-hydroxy-5-(2-aminoethyl) dihydrofuran-2(3 <i>H</i>)-one 80 by ChemDraw (C ₆ H ₁₁ NO ₃ ; MW = 145.16), (b) COSY (↔) and NOESY (↔) information, (c) HMBC (↔) correlation, and (d) two possible enantiomers of the molecule (3 <i>R</i> ,5 <i>R</i> and 3 <i>S</i> ,5 <i>S</i>).....	114
Figure 79. (a) The main skeleton of catechin and (b) key connections of proton-to-proton (↔ COSY) and proton-to-carbon (↔ HMBC) of catechin derivative isolated from the methanolic bark extract.....	115
Figure 82. Key connections of (a) proton-to-proton (↔ NOESY) showing the spatial relationship of vicinal protons and (b) the molecular structure of (-)-epicatechin from BK-MeOH-A1 with <i>cis</i> -2 <i>R</i> ,3 <i>R</i> stereochemical orientation.....	116
Figure 80. The spectral image of ¹ H NMR of (-)-epicatechin 77 from methanolic extract of bark.....	117

Figure 81. The spectral image of ¹³ C NMR of (–)-epicatechin 77 from methanolic extract of bark.....	118
Figure 85. Molecular structure of 3-O-methyl- <i>D</i> -chiro-inositol (<i>D</i> -(+)-pinitol 79a) (C ₇ H ₁₄ O ₆) from the methanolic extract of bark in (a) Haworth projection and (b) chair conformation with HMBC information.....	120
Figure 83. The spectral image of ¹ H NMR of <i>D</i> -pinitol 79a from methanolic extract of bark	121
Figure 84. The spectral image of ¹³ C NMR of <i>D</i> -pinitol 79a from methanolic extract of bark	122
Figure 86. The spectral image of ¹ H NMR of sucrose isolated from methanolic extract of bark	125
Figure 87. The spectral image of ¹³ C NMR of sucrose isolated from methanolic extract of bark	126
Figure 88. Molecular structure of (a) sucrose isolated from the methanolic bark extract and (b) key connections of proton-to-proton (↔ COSY) and proton-to-carbon (↔ HMBC).....	128
Figure 89. An illustrative summary of isolated compounds from FL-, LF-, and BK-MeOH extracts of <i>A. saligna</i>	129
Figure 90. The dose-response curve of the isolated active compounds against radical DPPH. (a) isosalipurposide 1 , (b) quercitrin 4 , (c) <i>D</i> -(+)-pinitol 79a , (d) (–)-pinitol 79b , (e) (–)-epicatechin 77 , (e) myricitrin 11 . Data in mean ± SEM, <i>n</i> = 3.	131
Figure 91. The dose-response curve of the isolated active compounds against ABTS cation radicals. (a) naringenin 42 , (b) Compound 76 : naringenin-7- <i>O</i> - α - <i>L</i> -arabinofuranose 76 , (c) isosalipurposide 1 , (d) quercitrin 4 , (e) <i>D</i> -(+)-pinitol 79a , (f) (–)-pinitol 79b , (g) (–)-epicatechin 77 , (h) 2,4-di- <i>t</i> -butylphenol 78 , (i) myricitrin 11 . Data in mean ± SEM, <i>n</i> = 3.	133
Figure 92. Comparison of the IC ₅₀ of the compounds obtained by (a) DPPH and (b) ABTS ^{•+} scavenging assay. 1 : isosalipurposide; 4 : quercitrin; 11 : myricitrin; 42 : naringenin; 76 : naringenin-7- <i>O</i> - α - <i>L</i> -arabinofuranose 77 ; (–)-epicatechin; 78 : 2,4-di- <i>t</i> -butylphenol; 79a : <i>D</i> -(+)-pinitol, 79b : (–)-pinitol; Vit C: Vitamin C. Data in mean ± SEM, *** <i>p</i> = 0.0002; **** <i>p</i> < 0.0001, vs vitamin C (<i>n</i> = 3, One-way ANOVA, Tukey’s post hoc).	133
Figure 93. The dose-response curve of the isolated active compounds against α -glucosidase enzyme. (a) naringenin 42 , (b) compound 76 : naringenin-7- <i>O</i> - α - <i>L</i> -arabinofuranose, (c) isosalipurposide 1 , (d) quercitrin 4 , (e) <i>D</i> -(+)-pinitol 79a , (f) (–)-	

pinitol 79b , (g) (–)-epicatechin 77 , (h) myricitrin 11 , (i) 2,4-di- <i>t</i> -butylphenol 78 . Data in mean ± SEM, <i>n</i> = 3.	136
Figure 94. IC ₅₀ of isolated compounds compared to acarbose. 1 : isosalipurposide; 4 : quercitrin; 11 : myricitrin; 42 : naringenin; 76 : naringenin-7 <i>O</i> - α - <i>L</i> -arabinofuranose; 77 : (–)-epicatechin; 78 : 2,4-di- <i>t</i> -butylphenol; 79a : <i>D</i> -(+)-pinitol; 79b : (–)-pinitol. Data in mean ± SEM, * <i>p</i> = 0.03, **** <i>p</i> < 0.0001, vs acarbose (<i>n</i> = 3, One-way, ANOVA, Tukey's post hoc).....	136
Figure 95. Viability of (a) 3T3-L1 preadipocytes and (b) adipocytes treated with naringenin 42 for 24-, 48-, and 72-h. Data in mean ± SEM, * <i>p</i> = 0.013; ** <i>p</i> = 0.003, vs vehicle control (<i>n</i> = 3, One-way ANOVA, Dunnett's post hoc).....	138
Figure 96. Viability of (a) 3T3-L1 preadipocytes and (b) adipocytes treated with naringenin-7 <i>O</i> - α - <i>L</i> -arabinofuranoside 76 for 24-, 48-, and 72-h. Data in mean ± SEM, * <i>p</i> = 0.01; ** <i>p</i> = 0.004; *** <i>p</i> = 0.0008, vs vehicle control (<i>n</i> = 3, One-way ANOVA, Dunnett's post hoc).....	138
Figure 97. Viability of (a) 3T3-L1 preadipocytes and (b) adipocytes treated with isosalipurposide 1 for 24-, 48-, and 72-h. Data in mean ± SEM, * <i>p</i> = 0.04; *** <i>p</i> = 0.0008, vs vehicle control (<i>n</i> = 3, One-way ANOVA, Dunnett's post hoc).	139
Figure 98. Viability of (a) 3T3-L1 preadipocytes and (b) adipocytes treated with quercitrin 4 for 24-, 48-, and 72-h. Data in mean ± SEM, <i>n</i> = 3.	139
Figure 99. Viability of (a) 3T3-L1 preadipocytes and (b) adipocytes treated with <i>D</i> -(+)-pinitol 79a for 24-, 48-, and 72-h. Data in mean ± SEM, * <i>p</i> = 0.02, vs vehicle control (<i>n</i> = 3, One-way ANOVA, Dunnett's post hoc).	139
Figure 100. Viability of (a) 3T3-L1 preadipocytes and (b) adipocytes treated with (–)-pinitol 79b for 24-, 48-, and 72-h. Data in mean ± SEM, <i>n</i> = 3.	140
Figure 101. Viability of (a) 3T3-L1 preadipocytes and (b) adipocytes treated with (–)-epicatechin 77 for 24-, 48-, and 72-h. Data in mean ± SEM, * <i>p</i> = 0.03; ** <i>p</i> = 0.001, vs vehicle control (<i>n</i> = 3, One-way ANOVA, Dunnett's post hoc).....	140
Figure 102. Viability of (a) 3T3-L1 preadipocytes and (b) adipocytes treated with 2,4-di- <i>t</i> -butylphenol 78 for 24-, 48-, and 72-h. Data in mean ± SEM, * <i>p</i> = 0.01; ** <i>p</i> = 0.001; **** <i>p</i> < 0.0001, vs vehicle control (<i>n</i> = 3, One-way ANOVA, Dunnett's post hoc). ...	140
Figure 103. Viability of (a) 3T3-L1 preadipocytes and (b) adipocytes treated with myricitrin 11 for 24-, 48-, and 72-h. Data in mean ± SEM, * <i>p</i> = 0.05; ** <i>p</i> = 0.001; **** <i>p</i> < 0.0001, vs vehicle control (<i>n</i> = 3, One-way ANOVA, Dunnett's post hoc).....	141
Figure 104. Viability of (a) 3T3-L1 preadipocytes and (b) adipocytes treated with 3-hydroxy-5-(2-aminoethyl) dihydrofuran-2(3 <i>H</i>)-one) 80 for 24-, 48-, and 72-h. Data in	

mean \pm SEM, * p = 0.02; ** p = 0.002; *** p = 0.0002; **** p < 0.0001, vs vehicle control (n = 3, One-way ANOVA, Dunnett's post hoc). 141

Figure 105. Estimated lipid content from ORO staining assay on the 3T3-L1 adipocytes treated with isolated compounds during differentiation. NAC = *N*-acetyl cysteine. Data in mean \pm SEM, * p = 0.03; **** p = 0.00008, vs vehicle control (n = 3, One-way ANOVA, Tukey's post hoc). 142

Figure 106. Cellular ROS in 3T3-L1 adipocytes treated with isolated compounds and NAC compared to undifferentiated cells. Data in mean \pm SEM, * p = 0.05, ** p = 0.002, *** p = 0.0003, **** p = 0.00001, vs vehicle control (n = 3, One-way ANOVA, Tukey's post hoc). 144

Figure 107. Estimated mt-ROS level of 3T3-L1 adipocytes treated by (a) methanolic extracts, metformin, and (b) isolated compounds. Compound **2** = naringenin-7-*O*- α -*L*-arabinofuranoside, compound **80** = 3-hydroxy-5-(2-aminoethyl) dihydrofuran-2(3*H*)-one). Data in mean \pm SEM, * p = 0.02; ** p = 0.003; **** p = 0.00002, vs vehicle control (n = 3, One-way ANOVA, Tukey's post hoc). 146

Figure 108. Estimated ratio of J aggregates/JC-1 monomers percentage in 3T3-L1 adipocytes treated by (a) methanolic extracts and (b) isolated compounds. Data in mean \pm SEM, * p = 0.03, ** p = 0.001, *** p = 0.0002, **** p = 0.0002, ***** p = 0.000001, vs vehicle control (n = 3, one-way ANOVA, Tukey's post hoc tests). 147

Figure 109. Bar charts representing 2-NBDG uptake by 3T3-L1 adipocytes treated with isolated compounds. Data in mean \pm SEM, * p = 0.01, vs vehicle control (n = 3, One-way ANOVA, Dunnett's post hoc). 150

Figure 110. The ratio of p-AMPK- α to AMPK- α protein in 3T3-L1 adipocytes treated with (a) MeOH extracts and (b) isolated compounds. Data in mean \pm SEM, * p = 0.02; ** p = 0.003, *** p = 0.0002, vs vehicle control (n = 3, One-way ANOVA, Tukey's post hoc). FL-MeOH = methanolic extract of flower, LF-MeOH = methanolic extract of leaf, BK-MeOH = methanolic extract of bark, compound 42 = naringenin, 76 = naringenin-7-*O*- α -*L*-arabinofuranoside, 1 = isosalipurposide, 4 = quercitrin, 79a = *D*-(+)-pinitol, 79b = (-)-pinitol, 77 = (-)-epicatechin, and 11 = myricitrin. 154

Figure 111. The relative expression of (a) mRNA of adiponectin, (b) PGC-1 α , and (c) mtTFA of 3T3-L1 adipocytes treated with MeOH extracts. The gene expression was normalised by the housekeeping gene β -actin. Data in mean \pm SEM; * p = 0.02; ** p = 0.002, vs vehicle control (n = 3, One-way ANOVA, Tukey's post hoc). FL-MeOH = methanolic extract of flower, LF-MeOH = methanolic extract of leaf, BK-MeOH = methanolic extract of bark. 156

Figure 112. The relative expression of mRNA of (a) adiponectin, (b) PGC-1 α , and (c) mtTFA of 3T3-L1 adipocytes treated with isolated compounds. The gene expression was normalised by the housekeeping gene β -actin. Data were in mean \pm SEM; * p = 0.02; ** p = 0.002, vs vehicle control (n = 3, One-way ANOVA, Tukey's post hoc). 157

Figure 113. The relative expression of mRNA of (a) TNF- α and (b) IL-6 in 3T3-L1 adipocytes treated with MeOH extracts. The gene expression was normalised by the housekeeping gene β -actin. FL-MeOH = methanolic extract of flower, LF-MeOH = methanolic extract of leaf, BK-MeOH = methanolic extract of bark. Data were in mean \pm SEM; * p = 0.04, vs vehicle control (n = 3, One-way ANOVA, Tukey's post hoc). 158

Figure 114. The relative expression of mRNA of (a) TNF- α and (b) IL-6 in 3T3-L1 adipocytes treated with isolated compounds. The gene expression was normalised by the housekeeping β -actin. Data were in mean \pm SEM; * p = 0.04 and 0.02, vs vehicle control (n = 3, One-way ANOVA, Tukey's post hoc)..... 159

Figure 115. A summary of the effects of methanolic extracts of *A. saligna* and the isolated compounds on suppressing oxidative stress, promoting cellular glucose uptake *via* AMPK activation, and restoration of mitochondria of the adipocytes by increasing mRNA expression of key regulators and reducing mRNA expression of pro-inflammatory cytokines in the 3T3-L1 adipocytes (Blunt arrows (\perp): inhibiting, sharp arrows (\rightarrow): stimulating)..... 162

Figure 116. Illustration of the extraction procedures of the plant. 165

Figure 117. Representative illustration of the α -glucosidase inhibition assay. 168

Figure 118. Schematic workflow diagram of the cell differentiation. 170

Figure 119. Photographed images of TLC plates under a UV lamp at 254 nm for (a) FL-MeOH extract with a mobile phase of DCM/MeOH (75:25), (b) FL-MeOH-A fraction with EtOAc/MeOH/HCOOH/H₂O of 50:2:3:6, and (c) FL-MeOH-B fraction with EtOAc/MeOH/HCOOH/H₂O of 50:2:3:6..... 174

Figure 120. Photographed images of TLC plates under a UV lamp at 254 nm for (a) LF-MeOH extract with a mobile phase of DCM/MeOH (75:25), (b) LF-MeOH-A fraction with EtOAc/HCOOH/H₂O of 9:1:1, (c) LF-MeOH-B fraction with EtOAc/MeOH/HCOOH/H₂O of 50:2:3:6, and (d) LF-MeOH-C fraction with EtOAc/MeOH/HCOOH/H₂O of 50:2:3:6..... 177

Figure 121. Photographed image of TLC plate under a UV lamp at 254 nm for BK-MeOH extract with a mobile phase of EtOAc/HCOOH/H₂O (9:1:1). 178

Figure 122. A simplified oxidation reaction of the dihydroethidium group to form the red dyeing indicator of mt-ROS⁴³⁹. 181

Figure 123. Molecular structure of JC-1 labelling agent..... 182

List of Tables

Table 1. A list of common chemicals used in inducing 3T3-L1 cells in cell differentiation	13
Table 2. List of common pharmaceutical treatments of T2DM ¹³⁶⁻¹³⁸	15
Table 3. Some examples of secondary metabolites demonstrating α -glucosidase inhibitory and glucose uptake modulation	16
Table 4. Antifungal activities of MeOH extract of <i>A. saligna</i> leaves and its constituents ²²⁶	28
Table 5. Inhibitory activities of bark and leaf extracts of <i>A. saligna</i> against α -glucosidase ¹⁹⁷	28
Table 6. Quantified phenolic and flavonoid content of <i>A. saligna</i> extracts estimated using spectrophotometric analysis	36
Table 7. ¹ H NMR (400 MHz, CD ₃ OD), ¹³ C NMR (100 MHz, CD ₃ OD), and 2-D NMR data of compound from FL-MeOH-A1 compared to reported naringenin 42	63
Table 8. The 1- and 2-D NMR data of the isolate from FL-MeOH-A3 in CD ₃ OD	72
Table 9. ¹ H NMR (400 MHz, CD ₃ OD), ¹³ C NMR (100 MHz, CD ₃ OD), and 2D NMR data of compound from sub-fraction B1b of the methanolic flower extract compared to reported isosalipurposide 1	77
Table 10. ¹ H NMR (400 MHz, CD ₃ OD), ¹³ C NMR (100 MHz, CD ₃ OD), and 2D NMR data of compound from sub-fraction B2b of the methanolic extract of flowers compared to reported quercetin-3-O-rhamnoside (quercitrin 4)	81
Table 11. ¹ H NMR (400 MHz, D ₂ O), ¹³ C NMR (100 MHz, D ₂ O), and 2D NMR data of compound from FL-MeOH-B3b compared to reported 3-O-methyl-D-chiro-inositol (<i>D</i> -(+)-pinitol 79a)	85
Table 12. ¹ H NMR (400 MHz, D ₂ O), ¹³ C NMR (100 MHz, D ₂ O), and 2D NMR data of compound from LF-MeOH-A1 compared to reported (-)-epicatechin 77	89
Table 13. ¹ H NMR (400 MHz, CD ₃ OD), ¹³ C NMR (100 MHz, CD ₃ OD), and 2D NMR data of compound from LF-MeOH-A3 compared to reported 2,4-di- <i>t</i> -butylphenol 78	93
Table 14. ¹ H NMR (500 MHz, CD ₃ OD), ¹³ C NMR (125 MHz, CD ₃ OD), and 2D NMR data of compound from LF-MeOH-B2 compared to reported quercitrin 4	98
Table 15. ¹ H NMR (400 MHz, CD ₃ OD), ¹³ C NMR (100 MHz, CD ₃ OD), and 2D NMR data of compound from LF-MeOH-C2b compared to reported myricetin-3-O- α -L-rhamnopyranoside (myricitrin 11)	102

Table 16. ¹ H NMR (400 MHz, D ₂ O), ¹³ C NMR (100 MHz, D ₂ O), and 2D NMR data of compound from LF-MeOH-C3 compared to reported <i>D</i> -pinitol.....	106
Table 17. The 1- and 2-D NMR data of isolate from LF-MeOH-D in D ₂ O (400 MHz)	114
Table 18. ¹ H NMR (400 MHz, CD ₃ OD), ¹³ C NMR (100 MHz, CD ₃ OD), and 2D NMR data of compound from BK-MeOH-A1 compared to reported (–)-epicatechin 77 ...	119
Table 19. ¹ H NMR (400 MHz, CD ₃ OD), ¹³ C NMR (100 MHz, CD ₃ OD), and 2D NMR data of compound from BK-MeOH-B2 compared to reported 3- <i>O</i> -methyl- <i>D</i> -chiro-inositol (<i>D</i> -(+)-pinitol 79a)	123
Table 20. ¹ H NMR (400 MHz, D ₂ O), ¹³ C NMR (100 MHz, D ₂ O), and 2D NMR data of compounds from BK-MeOH-C2 compared to reported sucrose	127
Table 21. Summary of the possible pathways involved in the glucose uptake assay for the related phytochemicals based on the literature search	150
Table 22. Obtained fractions from the fractionation of FL-MeOH extract by the column chromatography.....	173
Table 23. Obtained sub-fractions from the fractionation of FL-MeOH-A extract by the column chromatography	173
Table 24. Obtained sub-fractions from the fractionation of FL-MeOH-B extract by the column chromatography	174
Table 25. Obtained fractions from the fractionation of LF-MeOH extract by the column chromatography.....	175
Table 26. Obtained sub-fractions from the fractionation of LF-MeOH-A extract by the column chromatography	176
Table 27. Obtained sub-fractions from the fractionation of LF-MeOH-B extract by the column chromatography	176
Table 28. Obtained sub-fractions from the fractionation of LF-MeOH-C extract by the column chromatography	176
Table 29. Obtained fraction from the fractionation of BK-MeOH extract by the column chromatography.....	178
Table 30. List of target primers used for the RT-qPCR experiments.....	184

List of Appendix

Table S1. Summary of reported bioactivities of various parts of <i>A. saligna</i> along with the possibly responsible phytochemicals	221
Figure S1. Spectral images of GCMS analysis of (A) FL-hex, (B) FL-DCM, (C) FL-MeOH, and (D) FL-H ₂ O extracts.....	224
Table S2. The list of identified compounds in hexane flower extract of <i>Acacia saligna</i> by GCMS	226
Figure S2. Spectral images of GCMS analysis of (A) LF-hex, (B) LF-DCM, (C) LF-MeOH, and (D) LF-H ₂ O extracts	231
Table S3. The list of identified compounds in <i>Acacia saligna</i> leaf extracts by GCMS	233
Figure S3. Spectral images of GCMS analysis of (A) BK-hex, (B) BK-DCM, (C) BK-MeOH, and (D) BK-H ₂ O extracts	238
Table S4. The list of identified compounds in <i>Acacia saligna</i> bark extracts by GCMS	240
Table S5. DPPH scavenging activity of the extracts of <i>A. saligna</i>	241
Table S6. Scavenging activity (%) and IC ₅₀ values of vitamin C from DPPH scavenging assay	242
Table S7. ABTS ^{•+} scavenging activity of the extracts of <i>A. saligna</i>	242
Table S8. ABTS ^{•+} scavenging activity (%) and IC ₅₀ values of vitamin C	243
Table S9. Percentage of α -glucosidase inhibition (%) of flower extracts	244
Table S10. Percentage of α -glucosidase inhibition (%) of methanolic flower extract	244
Table S11. Percentage of α -glucosidase inhibition (%) of leaf extracts	244
Table S12. Percentage of α -glucosidase inhibition (%) of the methanolic leaf extract	244
Table S13. Percentage of α -glucosidase inhibition (%) of bark extracts	244
Table S14. Percentage of α -glucosidase inhibition (%) of methanolic bark extract	245
Table S15. Percentage of α -glucosidase inhibition (%) of acarbose	245
Table S16. Viable 3T3-L1 preadipocytes treated with flower extracts for 24, 48, and 72 h	245
Table S17. Viable 3T3-L1 preadipocytes treated with leaf extracts for 24, 48, and 72 h	245
Table S18. Viable 3T3-L1 preadipocytes treated with bark extracts for 24, 48, and 72 h	246

Table S19. Viable 3T3-L1 adipocytes treated with flowers extracts for 24, 48, and 72 h	246
Table S20. Viable 3T3-L1 adipocytes treated with leaves extracts for 24, 48, and 72 h	247
Table S21. Viable 3T3-L1 adipocytes treated with barks extracts for 24, 48, and 72 h	247
Table S22. Estimated lipid content from adipogenesis assay with ORO staining agent on the 3T3-L1 adipocytes treated with extracts	247
Table S23. The estimated ROS level in adipocytes exposed to extracts for 48 h	248
Table S24. Observed data of glucose uptake simulation with the fluoroprobe 2-NBDG assay for all extracts on the 3T3-L1 adipocytes	248
Figure S4. Schematic representation of the outcomes of fractionation of FL-MeOH extract of <i>A. saligna</i>	249
Figure S5. Schematic representation of the outcomes of fractionation of LF-MeOH extract of <i>A. saligna</i>	250
Figure S6. Schematic representation of the outcomes of fractionation of BK-MeOH extract of <i>A. saligna</i>	251
Table S25. The DPPH scavenging properties of the isolated compounds	252
Table S26. The ABTS ^{•+} scavenging properties of the isolated compounds	252
Table S27. The quantified inhibitory activity of the isolated compounds against the α -glucosidase enzyme	253
Table S28. Viable 3T3-L1 preadipocytes and adipocytes treated with naringenin 42 for 24, 48, and 72 h	255
Table S29. Viable 3T3-L1 preadipocytes and adipocytes treated with naringenin-7O- α -L-arabinofuranoside 76 for 24, 48, and 72 h	255
Table S30. Viable 3T3-L1 preadipocytes and adipocytes treated with isosalipurposide 1 for 24, 48, and 72 h	255
Table S31. Viable 3T3-L1 preadipocytes and adipocytes treated with quercitrin 4 for 24, 48, and 72 h.....	255
Table S32. Viable 3T3-L1 preadipocytes and adipocytes treated with <i>D</i> -(+)-pinitol 79a for 24, 48, and 72 h	256
Table S33. Viable 3T3-L1 preadipocytes and adipocytes treated with (-)-pinitol 79b for 24, 48, and 72 h	256

Table S34. Viable 3T3-L1 preadipocytes and adipocytes treated with (–)-epicatechin 77 for 24, 48, and 72 h	256
Table S35. Viable 3T3-L1 preadipocytes and adipocytes treated with 2,4-di- <i>t</i> -butylphenol 78 for 24, 48, and 72 h	256
Table S36. Viable 3T3-L1 preadipocytes and adipocytes treated with myricitrin 11 for 24, 48, and 72 h	257
Table S37. Viable 3T3-L1 preadipocytes and adipocytes treated with 3-hydroxy-5-(2-aminoethyl) dihydrofuran-2(3 <i>H</i>)-one 80 for 24, 48, and 72 h	257
Table S38. Estimated lipid content from adipogenesis assay with ORO staining agent on the 3T3-L1 adipocytes treated with isolated compounds within the differentiation process (day-0 to day-8)	257
Table S39. The estimated ROS level of adipocytes exposed to isolated compounds for 48 h	257
Table S40. Estimated mt-ROS level (%) and J aggregates/JC-1 monomers percentage in 3T3-L1 adipocytes treated by methanolic extracts	258
Table S41. Estimated mt-ROS content and J aggregates/JC-1 monomers ratio in 3T3-L1 adipocytes treated by isolated compounds.	258
Table S42. Observed data of glucose uptake simulation with 2-NBDG fluorescence assay for isolated compounds on the 3T3-L1 adipocytes.....	259
Table S43. Quantitative data of ratio of expressed p-AMPK- α to AMPK- α (%) by adipocytes exposed to the tested MeOH extracts	259
Table S44. Quantitative data of ratio of expressed p-AMPK- α to AMPK- α (%) by adipocytes exposed to the tested isolated compounds	259
Table S45. Quantitative data of the expression of the target mRNA normalised by β -actin from the RT-qPCR of adipocytes treated with methanolic extracts	260
Table S46. Quantitative data of the expression of the target mRNA normalised by β -actin from the RT-qPCR of adipocytes treated with isolated compounds from methanolic extracts.....	261

Abbreviations

2-NBDG	2-Deoxy-2-[(7-nitro-2,1,3-benzoxadiazol-4-yl) amino]- <i>D</i> -glucose
ABTS	2,2'-Azino-bis-(3-ethylbenzothiazoline-6-sulphonic acid)
ACC	Acetyl-CoA carboxylase
AGEs	Advanced glycated end products
AMPK	Adenosine 5'-monophosphate-activated protein kinase
ANOVA	Analysis of variance
aP2	Adipocyte fatty acid binding protein 2
AS160	160 kDa substrate of Akt Ser/Thr kinase
ASK 1	Apoptosis signal-regulating kinase 1
ATP	Adenosine 5'-triphosphate
Bax	Bcl-2 associated X-protein
Bcl-2	B-cell leukemia/lymphoma 2 protein
BCS	Bovine calf serum
BHT	Butylated hydroxyl toluene
BK	Bark
BSA	Bovine serum albumin
BuOH	Butanol
C/EBP- α	CCAAT/enhancer-binding protein- α
cAMP	3',5'-Cyclic adenosine monophosphate
cDNA	Complementary deoxyribonucleic acid
cGMP	Guanosine 3',5'-cyclic monophosphate
COSY	Correlation spectroscopy
COX-2	Cyclooxygenase-2
CREB	cAMP response element-binding protein
DCFH-DA	Dichlorodihydrofluorescein diacetate
DCM	Dichloromethane
DEPT	Distortionless enhancement by polarisation transfer
DM	Diabetes melitus
DMEM	Dulbecco's modified eagle's medium
DMSO	Dimethylsulfoxide
DPPH	2,2-Diphenyl-1-picrylhydrazyl or 2,2-di(4-tert-octylphenyl)-1-picrylhydrazyl
DNA	Deoxyribonucleic acid

dNTP	Deoxyribose nucleotide triphosphate
DPP-4	Dipeptidyl peptidase 4
ECL	Enhanced chemiluminescence
EDTA	Ethylenediaminetetraacetic acid
ESI	Electrospray ionisation
ETC	Electron transport chain
EtOAc	Ethyl acetate
EtOH	Ethanol
FAS	Fatty acid synthetase
FBS	Fetal bovine serum
FC	Flavonoid content
FFA	Free fatty acid
FL	Flower
FTIR	Fourier transform infrared
GLUT-4	Glucose transporter 4
GSH	Glutathione
GSIS	Glucose-stimulated insulin secretion
Hex	Hexane
KRPH	Krebs-Ringer phosphate 4-(2-hydroxyethyl)-1-piperazineethanesulfonic acid
LDL	Low-density lipoprotein
LKB1	Liver kinase B1
GAE	Gallic acid equivalent
GCMS	Gas chromatography-mass spectroscopy
GDM	Gestational diabetes mellitus
GLP-1	Glucose-like peptide 1
HBSS	Hank's balanced salt solution
HMBC	Heteronuclear multiple bond correlation
HPLC	High performance liquid chromatography
HPLC-VWD	High performance liquid chromatography-variable wavelength detector
HRMS	High resolution mass spectroscopy
HRP	Horseradish peroxidase
HSQC	Heteronuclear single quantum coherence
IBMX	3-Isobutyl-1-methylxanthine
IgG	Immunoglobulin G

IGT	Impaired glucose tolerance
IRS-1	Insulin receptor substrate-1
IL-1 β	Interleukin-1 β
IL-6	Interleukin 6
IKK β	Inhibitor of nuclear factor kappa-B kinase subunit β
IR	Insulin resistance
IMT	<i>Myo</i> -inositol methyl transferase
JC-1	5,5,6,6'-Tetrachloro-1,1',3,3' tetraethylbenzimidazolylcarbocyanine iodide
JNK	c-Jun NH ₂ -terminal kinases
LF	Leaf
m/z	Mass per charge number of ions
MAPK	Mitogen-activated protein kinases
MDI	Medium of differentiation induction
MeOH	Methanol
MFN	Mitofusin
MGAM	Maltase-glucoamylase
MitoSOX	Hydroethidine triphenylphosphonium cation
MMP	Mitochondrial membrane potential
MnSOD	Manganese superoxide dismutase
mRNA	Messenger ribonucleic acid
MRSA	<i>Methicillin-resistant Staphylococcus aureus</i>
Mt-ROS	Mitochondrial reactive oxygen species
MTT	3-(4,5-Dimethylthiazol-2-yl)-2,5-diphenyltetrazolium bromide
mtTFA	Mitochondrial transcription factor A
NAC	<i>N</i> -acetyl cysteine
NADPH	Nicotinamide adenin dinucleotide phosphate
NF-kB	Nuclear factor kappa-light-chain-enhancer of activated B cells
NMR	Nuclear magnetic resonance
NO	Nitric oxide
NOESY	Nuclear Overhauser Effect Spectroscopy
NRF	Nuclear respiratory factor
ORO	Oil red-O
OXPHOS	Oxidative phosphorylation
p-AMPK- α	Phosphorylation of AMPK subunit α
PBS	Phosphate-buffered saline

PC	Phenolic content
PGC-1 α	Peroxisome proliferator-activated response- γ coactivator-1 α
PGE	Prostaglandin E2
PI3K-PKB/Akt	Phosphoinositide-3-kinase-protein kinase B/Akt
PKC	Protein kinase C
pNPG	4-Nitrophenyl α -D-glucopyranoside
PPAR- γ	Peroxisome proliferator- activated receptor γ
PSG	Penicillin streptomycin glutamine
PUFA	Polyunsaturated fatty acid
PDVF	Polyvinylidene fluoride
QE	Quercetin equivalent
QFOF	Quadrupole time-of-flight
RAGE	Receptor of advanced glycated end products
RNA	Ribonucleic acid
RNS	Reactive nitrogen species
RT-qPCR	Quantitative reverse transcription-polymerase chain reaction
ROS	Reactive oxygen species
RPM	Round per minute
SAR	Structure-activity relationships
SEM	Standard error of the mean
Ser/Thr	Serine/threonine
SGLT-2	Sodium-glucose co-transporter-2
SI	Sucrose-isomaltase
SIRT1	Silent information regulator 1
SOD	Superoxidase dismutase
SPLET	Sequential proton loss electron transfer
STAT3	Signal transducer and activator of transcription 3
T1DM	Type 1 diabetes mellitus
T2DM	Type 2 diabetes mellitus
TBARS	Thiobarbituric acid-reactive substances
TBC1D4	Tre-2/BUB2/cdc 1 domain family
TCA	Tricarboxylic acid
TCP15	Branched1-cycloidea-proliferating cell factor 15
TEMED	Tetramethylethylenediamine
TLC	Thin layer chromatography
TNF- α	Tumor necrosis factor α

TOCSY	Total correlation spectroscopy
TZD	Thiazolidinedione
UV	Ultraviolet
v/v	Volume per volume
w/w	Weight per weight
WAT	White adipose tissue
WHO	World Health Organisation

Abstract

Acacia saligna is native to Western Australia that can grow in extreme conditions such as drought, alkaline and saline soil, and frosty surroundings. This plant produces secondary metabolites, including diverse flavonoids, cinnamic acids, and benzoic acid derivatives, to support its defence system. Reports have revealed that extracts and phytochemicals of Middle Eastern and African species possess varied bioactivities, such as antioxidant, antibacterial, antifungal, antiinflammation, and antidiabetic properties. However, there has not yet been researched on Australian species. Therefore, this study aimed to investigate the active compounds as antidiabetic from Australian *A. saligna* by bioassay-guided fractionation using a combination of rapid *in vitro* assays and 3T3-L1 adipocyte-based assays.

This study discovered that the methanolic extract of flowers (FL-MeOH), methanolic extract of leaves (LF-MeOH), and methanolic extract of bark (BK-MeOH) have excellent properties as antioxidants, α -glucosidase inhibitors, inhibitors of cellular reactive oxygen species (ROS), and modulators of glucose uptake. Additionally, our mitochondrial study revealed that these extracts can restore adipocytes' mitochondria by reducing mitochondrial ROS (mt-ROS) and increasing mitochondrial membrane potential (MMP). Further fractionation of the methanolic extracts using column chromatography with normal silica gel afforded various phytochemicals. There are five compounds isolated from FL-MeOH, including naringenin **42**; naringenin-7-*O*- α -*L*-arabinofuranoside **76**; isosalipurposide **1**; quercitrin **4**; and *D*-(+)-pinitol **79a**. Six compounds were isolated from LF-MeOH: (-)-epicatechin **77**, quercitrin **4**; myricitrin **11**; 2,4-di-*t*-butylphenol **78**; (-)-pinitol **79b**; and (3*S**,5*S**)-3-hydroxy-5-(2-aminoethyl) dihydrofuran-2(3*H*)-one **80**. Isolated phytochemicals BK-MeOH were (-)-epicatechin **77**, *D*-(+)-pinitol **79a**, and sucrose. Except for compounds **1**, **4**, **42**, and **11**, this study suggested that the isolated compounds were found in the three parts of Australian *A. saligna* for the first time. Furthermore, the bioassay outcomes indicated that (-)-epicatechin **77** performed best in reducing cellular ROS and mt-ROS, aligning with its inhibitory activities against DPPH and ABTS^{•+} radicals. Marked increases in cellular glucose uptake and MMP values were observed from treatment with naringenin **42**, naringenin-7-*O*- α -*L*-arabinofuranoside **76**, *D*-(+)-pinitol **79a**, and (-)-epicatechin **77** reflecting the positive effect of their respective extracts in glucose uptake.

To gain more insight into possible mechanisms underlying the positive effects of *A. saligna* extracts on cells, further investigation was carried out using immunoblot and quantitative reverse transcription-polymerase chain reaction (RT-qPCR). Our

findings revealed that FL-MeOH exerted marked increases in glucose uptake and phosphorylated 5' adenosine monophosphate-activated protein kinase- α (p-AMPK- α) due to the presence of isosalipurposide **1**, quercitrin **4**, naringenin **42**, and naringenin-7-O- α -L-arabinofuranoside **76**. On the other hand, LF-MeOH showed corresponding effects due to quercitrin **4**, myricitrin **8**, and (-)-epicatechin **77**. FL-MeOH and its chemical constituents, naringenin **42** and *D*-(+)-pinitol **79a**, consistently increased MMP values, p-AMPK- α levels, and transcriptional levels of key regulators and reduced transcriptional levels of proinflammatory markers. Overall, the extracts and isolated chemical constituents of *A. saligna* demonstrated antidiabetic activities on 3T3-L1 adipocytes by reducing ROS and mt-ROS, stimulating glucose uptake through AMPK activation, and modulating transcriptional levels of adiponectin, PGC-1 α , and mtTFA while also reducing pro-inflammatory TNF- α and IL-6 mRNA levels to promote mitochondrial biogenesis.

CHAPTER 1: INTRODUCTION

1.1. General background

Diabetes mellitus (DM) is a chronic disease caused by defective insulin secretion or reduced cellular response to insulin to manage blood glucose levels ¹. Some chronic complications caused by this disorder ranked it the fourth noncommunicable disease (Figure 1) ^{1, 2}. Globally, the World Health Organization (WHO) estimated 422 million people living with DM in 2014, predominantly type 2 diabetes mellitus (T2DM) and projected to rise to 629 million by 2045 ^{3,4}. When lifestyle changes are not enough to manage blood glucose levels, antidiabetic medications must be prescribed to regulate blood sugar levels ^{2,4}. The approach is crucial in maintaining glucose homeostasis and preventing complications associated with hyperglycaemia.

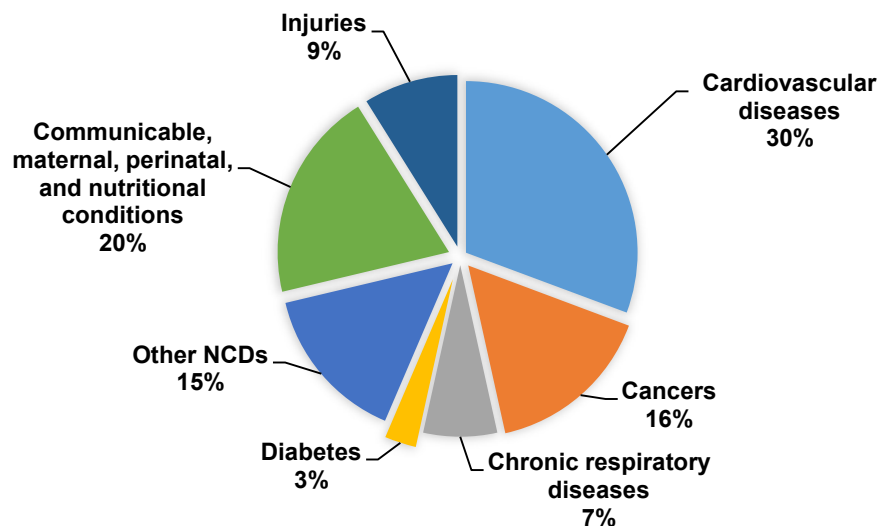


Figure 1. Percentage of global mortality factors for 41 million deaths in 2016 ².

T2DM is often linked to unhealthy lifestyles, such as physical inactivity, excessive intake of an energy-dense diet, smoking, and stress leading to the insensitivity of insulin in insulin-responsive cells followed by insufficient glucose-stimulated insulin secretion (GSIS) by pancreatic β -cells ^{1,5}. Fat accumulation occurs due to excessive calorie intake and lack of exercise, which initiates insulin resistance (IR) in the liver, skeletal muscle, and adipose tissue and triggers β -cells dysfunction in the pancreas ^{6,7}. In addition, IR relates to lipotoxicity, glucotoxicity, inflammation, and oxidative stress that impact the pancreatic β -cells ⁸.

Obesity closely correlates with T2DM since above 60–90% of T2DM patients are overweight or obese ^{6,7,9,10}. Insulin regulates the metabolism of non-esterified

fatty acids (FAs) by stimulating glucose uptake in adipose tissue to promote triglyceride storage and activating lipoprotein lipase in the vasculature ^{5, 11, 12}. Obese people with continuous physical inactivity have an increased number of macrophages infiltrating fat tissues, causing increased secretion of pro-inflammatory cytokines and prooxidant species damaging vital cellular components, which could eventually lead to insulin resistance (Figure 2) ¹³⁻¹⁶.

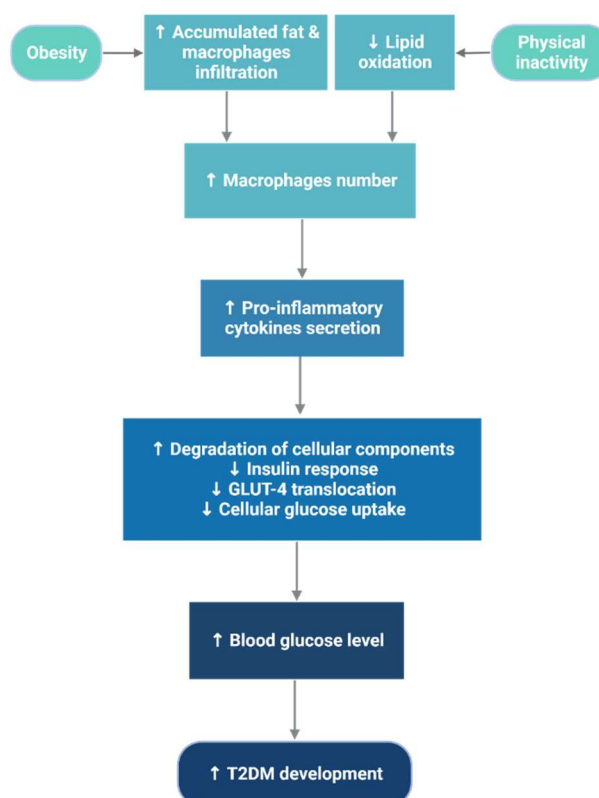


Figure 2. Schematic representation of the link between inflammation mediators and adipocytes IR ¹⁷. GLUT-4: glucose transporter-4; ↑: increasing; ↓: decreasing.

β -cell failure could also be associated with exposure to proinflammatory agents and oxidative stress induced by a high extracellular glucose level and free fatty acids (FFAs) (Figure 3). As a response to the high FFAs level, rapid macrophage infiltration under the obese condition in pancreatic cells could modulate reactive oxygen species (ROS) production ^{18, 19}. It could produce elevated cytokines and chemokines ²⁰, altering cellular function ²¹. Meanwhile, the oxidative environment could promote the antioxidant release to maintain the free radical proportion. On the other hand, the antioxidant can be exhausted if ROS is continuously overproduced, causing β -cell damage and death in the long term resulting in insulin insufficiency.

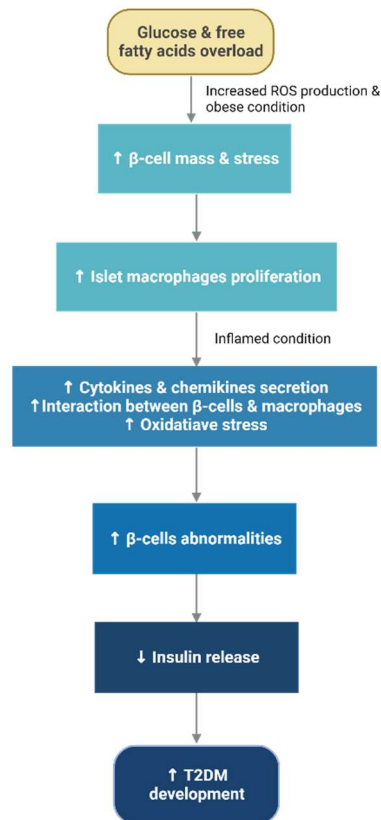


Figure 3. Scheme of the T2DM progression due to insulin insufficiency promoted by inflammatory and oxidative state ²²⁻²⁴; ↑: increasing; ↓: decreasing.

1.2. Diabetes mellitus

1.2.1. Classification of DM

DM is commonly classified into type 1 (T1DM), T2DM, gestational diabetes mellitus (GDM), and a special type of diabetes ³. T1DM is non-preventable, representing 10% of the global diabetes case, and is characterised by the absolute deficiency of insulin secretion due to the destruction of the pancreatic β -cells linked to the autoimmune action. Studies revealed that it could be caused by genetic, environmental, and/or immunologic factors ²⁵. Recently, at least two chromosomal regions from the human leukocyte antigen and the insulin gene have been associated with the pathogenesis of T1DM through apoptosis induced by lymphocytes. Moreover, viruses, diets, and gut microbiota, as environmental factors, have also been identified as the inducer of an autoimmune response that can lead to abnormal pancreatic tissue destruction and inflammation. Another factor is linked to the production of autoantibodies against glutamic acid decarboxylase 65-kilodalton isoform, tyrosyl phosphatase, insulin, and zinc transporter found in the β -cells ²⁶.

On the other hand, T2DM is associated with ineffective cellular response to insulin or insulin resistance (IR) and inadequate secretion of insulin due to β -cells dysfunction. The more severe the obesity is, the more severe IR develops ²⁷. As displayed in Figure 3, accumulated FFAs can lead to inflammation-induced insulin resistance. One theory from a muscle cell-based study suggests that obesity could lead to mitochondrial dysfunction, causing defective lipid oxidation. Consequently, lipid metabolites will increase, activating serine/threonine (Ser/Thr) kinases and protein kinase C (PKC) isoforms. This sequential event can inhibit the activation of insulin receptor substrate-1 (IRS-1) and glycogen synthase ²⁸. As a result, elevated blood sugar occurs due to the failure of glucose uptake by the liver, muscle, and adipose cells ²⁹.

1.2.2. Oxidative stress associated with DM

Obesity and high glucose intake can trigger the overproduction of oxidative species. Generally, oxidants can be defined as free radicals and reactive atoms or molecules, including ROS, reactive nitrogen species (RNS), and other organic species, such as alkyl sulfanyl radicals (RS^\bullet) ³⁰. Among them, ROS, such as hydroxyl radical ($^\bullet OH$), superoxide anion ($O_2^{\bullet -}$), and hydrogen peroxide (H_2O_2), is considered the predominant oxidant generated from the hyperglycaemia state. Oxidant species can generate spontaneous reactions by transferring an electron or a hydrogen atom from other molecules to compensate for their electron deficiency.

According to Brownlee ³¹, hyperglycaemia could induce the overproduced intracellular ROS via various mechanisms such as increased polyol pathway, increased formation of advanced glycated end products (AGEs), induction of PKC, and elevated hexosamine pathway flux. All these four pathogenic mechanisms have been hypothesised to occur when superoxides are overproduced by either glycation of protein or a mitochondrial electron transport chain (ETC) pathway (Figure 4). Cellular oxidation, such as NADPH oxidation, glucose autoxidation and low-density lipoprotein (LDL) peroxidation, is the major source of elevated cellular ROS levels due to accumulated fat in the 3T3L1–adipocyte cells ³²⁻³⁵. Furthermore, although the premature leaking of electrons in normal cells was estimated to be less than 1%, it is increased during hyperglycaemia ^{36, 37}. Given a markedly increased number of substrates entering the tricarboxylic acid (TCA) cycle, an over supplier of electron donors occurs in the mitochondrial ETC that could excessively transform molecular oxygens in between complex I and III into reactive species called mitochondrial ROS (mt-ROS) (Figure 5) ³⁸.

Abnormally high sugar level condition also contributes to the deficiency of endogenous antioxidant agents leading to oxidative stress. Superoxidase dismutase (SOD), the main enzymatic antioxidant, has been downregulated in the animal models fed by high fat and sugar diet ^{32, 39}. Previously, Arai et al. ⁴⁰ confirmed that glycosylation (glycation) and oxidation causing the reduction of the positive charge of Lysine residue located in the active site of the antioxidant could alter enzyme function and properties. Therefore, this process is most likely to play a significant role in the inactivation of the antioxidative components since glycated sites of protein are commonly observed due to prolonged exposure of glucose to protein generating covalent connection via either the Schiff base or the Amadori adduct ⁴¹.

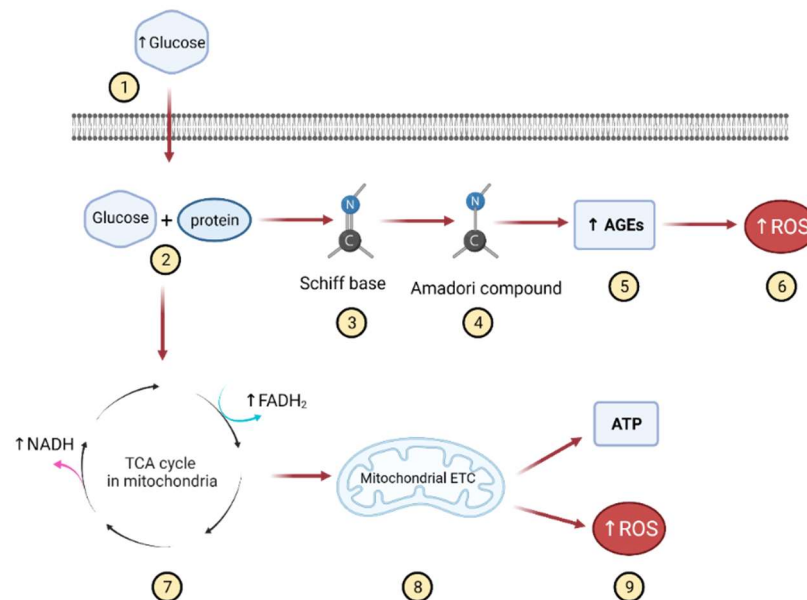


Figure 4. An illustration of high glucose-induced ROS production in a cell. (1) Elevated blood sugar level causes comparably increased uptake of glucose into cells; (2) excess glucose induces glycation of protein to produce (3) Schiff base followed by rearrangement to form (4) Amadori compound as the intermediate of (5) advanced glycation end products (AGEs); (6) AGEs directly stimulate excess ROS production by NADPH oxidase due to neutralising endogenous antioxidants ⁴². Moreover, the glucose can also be oxidised in the cytoplasm resulting in elevated NADH and pyruvates; (7) pyruvates oxidised in the TCA cycle led to the increased NADH and FADH₂, (8) which are involved in the accumulated of electrons during ATP leading to overproduction of mt-ROS. The image was adapted from Kawahito et al. ⁴³ and created with BioRender.com.

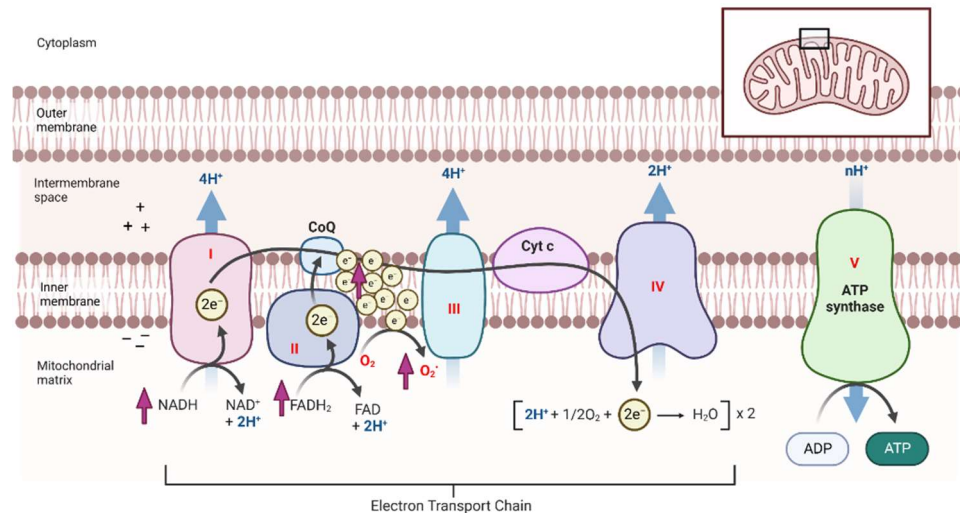


Figure 5. An illustration of superoxide production in the mitochondrial ETC. Excess glucose and FFA-derived products lead to overproduced coenzymes (NADH and FADH₂) from the Krebs cycle. It causes accumulated electrons in coenzyme ubiquinone (CoQ) captured by O₂ to produce superoxide radicals (O₂^{•-}) or mt-ROS. The image was adapted from Rebolledo & Dato ⁴⁴ and created with BioRender.com.

The role of cellular ROS in exacerbating T2DM and its complications has attracted some studies on targeting ROS as a therapeutic strategy for metabolic disease. Natural products have been reported to attenuate ROS production in obese mice and 3T3-L1 adipocytes. For instance, polyphenols, flavonoids ⁴⁵, and catechins from green tea ⁴⁶ effectively reduce the ROS level during hyperglycaemia, resulting in increased glucose uptake and improved IR. With their hydroxy groups and conjugated double bonds in aromatic rings, these compounds can interact directly with reactive species ⁴⁷ and/or induce cell signalling pathways to normalise ROS homeostasis ⁴⁸. *Acacia* extract treatment has also been reported to lower cellular ROS in other mammalian cells, as documented for *A. mearnsii* ⁴⁹, *A. shaffneri* and *A. farnesiana* ⁵⁰.

1.2.3. Postprandial hyperglycaemia

Following food ingestion in a healthy body, insulin secretion and the suppression of glucagon release are simultaneously generated in response to the increased blood glucose level. As a result, glucose uptake occurs in the liver, muscle, adipose tissue, kidney, and brain ⁵¹, which maintains postprandial glucose homeostasis ⁵². However, Mitrakou et al. ⁵³ reported that the rate of plasma glucose appearance was more pronounced in people who could not have proper insulin secretion in the first phase, which led to delayed insulin release in the next phase ⁵⁴, ⁵⁵.

Moreover, the lower rate of post-prandial glucose to return to the pre-prandial levels in individuals with normal insulin secretion was observed by Bock et al. ⁵⁶

manifesting decreased insulin action. Those people can be categorised as people with impaired glucose tolerance (IGT) or prediabetes, referred to as post-prandial hyperglycaemia⁵⁷.

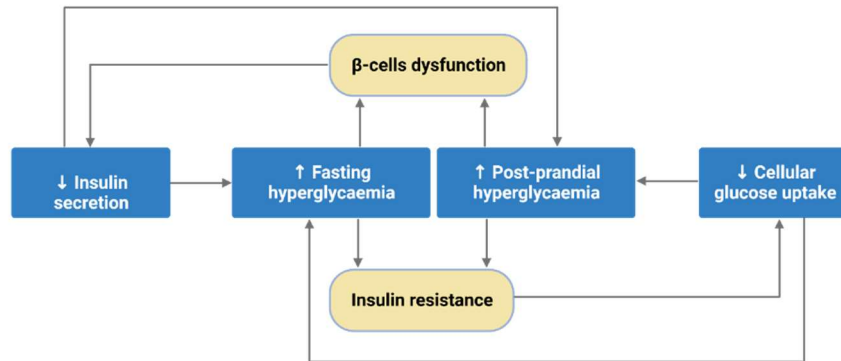


Figure 6. Schematic diagram by which post-prandial hyperglycaemia plays its causal role in the onset of T2DM⁵².

Post-prandial glucose, characterised by a rapidly elevated and significant plasma glucose level after a meal, has been considered one of the major risk factors leading to the progression of T2DM. One explanation was proposed by Yki-Järvinen⁵⁸ that long-term exposure of islets to glucose causes β -cells desensitisation due to glucose-induced phosphoinositide hydrolysis that activates PKC. In addition, long-term exposure of glucose to islet cells can also inhibit first-phase insulin secretory response linked to an increased prostaglandin E2 synthesis⁵⁹⁻⁶¹. These findings suggest that untreated IGT status could exacerbate T2DM development.

The delayed insulin secretory response could be linked to the decreased blood flow due to reduced arterioles and accelerated atherosclerosis in insulin-sensitive organs resulting in the early stage of IR due to insufficient insulin and glucose delivery into the cells⁶²⁻⁶⁴. As the insulin-mediated glucose uptake in muscle cells was estimated to be over 80%⁶⁵, the defect of glucose uptake into muscle cells could lead to more severe hyperglycaemia inducing ROS overproduction, sorbitol formation, and glyceraldehyde-derived AGEs as the predominant structure of toxic AGEs⁶⁶⁻⁶⁸.

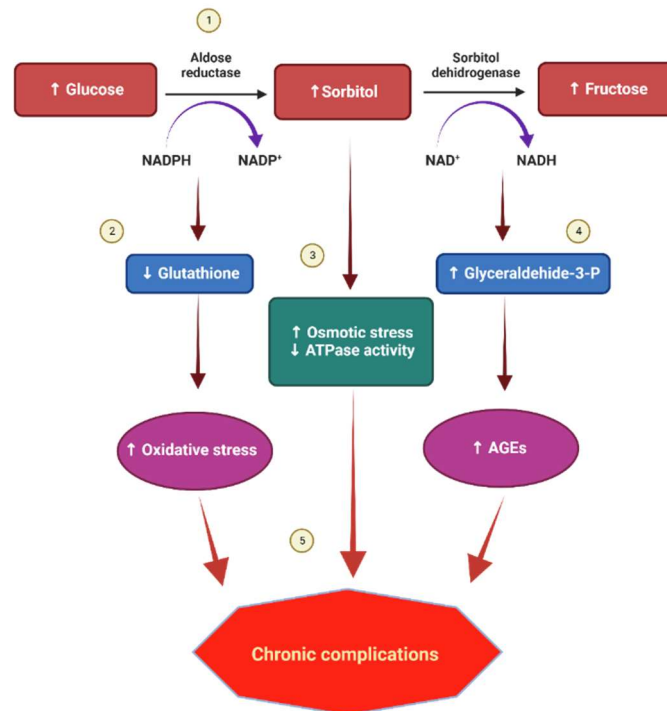


Figure 7. A representative flow of causes of T2DM-associated complications linked to polyol pathway. (1) In the presence of aldose reductase enzymes, excess glucose will be reduced to sorbitol that requires the oxidation of NADPH; (2) consequently, glutathione level will decrease due to the deficiency of its cofactor, NADPH, leading to elevated oxidative stress. (3) The increase of sorbitol resulted in increased intracellular osmolality and decreased the number of myoinositol, the upstream of adenosine-triphosphatase (ATPase) ⁶⁹. (4) The accumulated fructose from the reduction of sorbitol can be turnover to glyceraldehyde-3-phosphate as the precursor of all glycolytic intermediates that increase the glycation of proteins. (5) Finally, these processes exacerbate complications such as retinopathy, neuropathy, and renal failure. The image was adapted from Taslimi et al. ⁷⁰ and created with BioRender.com.

Excess extracellular glucose has also been reported to covalently attach to proteins or lipids *via* glycation reaction to form final polymers of AGEs. The AGEs interact with the broad components, including receptors of AGEs (RAGE), intracellular and circulating proteins (e.g. lipoprotein, albumin, haemoglobin, etc.), extracellular matrix, and nitric oxide (NO) that can alter their functions to injure blood vessels ⁴².

Therapy to reduce postprandial glucose update, such as the inhibitors of intestinal enzymes of saccharide hydrolysis, α -glucosidase, is one of the options in preventing and managing T2DM development. There are three clinical synthetic inhibitors: acarbose, miglitol, and voglibose, that have been applied since 1990. However, due to the long route of the synthetic process and its side effects, the search for alternative inhibitors, including research in natural products, is still underway ⁷¹. Extracts of some *Acacia* species have been displayed to serve as inhibitors against this enzyme. This is an additional advantage because the herbs can delay saccharide

degradation and maintain glucose homeostasis by restoring redox-regulated processes in the cells.

1.2.4. Potential targets to overcome insulin resistance

1.2.4.1. ROS as the cause of disrupted cellular glucose entry

Some studies have confirmed that two main pathways, i.e., phosphoinositide-3-kinase-protein kinase B/Akt (PI3K-PKB/Akt) and adenosine 5'-monophosphate-activated protein kinase (AMPK) pathway, involved in the glucose uptake by GLUT-4 translocation⁷²⁻⁷⁴. Oxidative stress has been demonstrated to activate stress-sensitive kinases such as IKK β and NF- κ B, impair tyrosine IRS-1 phosphorylation and disrupt the subcellular localisation of PI3K in 3T3-L1 adipocytes⁷⁵.

Interference of GLUT-4 translocation could result from defects in the insulin signalling pathway. Prolonged exposure to the cellular ROS in 3T3-L1 adipocytes also causes an impaired GLUT-4 translocation due to decreased GLUT-4 expression. On the other hand, treatment with *N*-acetyl cysteine (NAC)⁷⁶ restored the expression of GLUT-4 and glucose uptake. Moreover, one recent in vitro study⁷⁷ found that elevated mt-ROS were also sufficient to block GLUT-4 trafficking directly. Protein oxidation in the glucose transporter *via* direct interaction between mitochondria and endosomes has been postulated as the potential mechanism^{77, 78}.

The overproduced mt-ROS is also believed to disrupt insulin-dependent and insulin-independent glucose uptakes. Impaired tyrosine phosphorylation IRS-1 by the excess mt-ROS has been linked to the activation of apoptosis signal-regulating kinase 1 (ASK 1), leading to mitochondrial dysfunction^{79, 80}. Moreover, a cell-based study⁸¹ showed that increased mt-ROS production could inhibit the expression of essential enzymes for energy-generating pathways and mitochondrial membrane potential (MMP), significantly reducing ATP production. Nevertheless, treatment with metformin can inhibit the oxidation of NADH in complex I (Figure 5) by inducing peroxisome proliferator-activated response- γ coactivator-1 α (PGC-1 α) and manganese superoxide dismutase (MnSOD)^{82, 83} that results in the improvement of cellular glucose uptake^{84, 85}. Figure 9 illustrates that excessive mt-ROS production can result in reduced activation of mitofusins and mitochondrial enzymes.

Despite the safety level and effective treatment of metformin through AMPK-dependent and AMPK-independent pathways⁸⁶, side effects on gastrointestinal organs, such as nausea, diarrhoea, flatulence, abdominal pain, vomiting, and loss of appetite⁸⁷, and failure of metformin as a monotherapy of T2DM in the long term⁸⁸ encourage researchers to develop a better 2nd line option. An ethnomedicine using

herbal remedies can achieve multiple modes of action and safety. Several studies have revealed bioactive phytochemicals abilities in mt-ROS reduction ⁸⁹⁻⁹². Interestingly, phenolics and flavonoids are the most commonly reported to have modulation effects on the expression of mitofusins ⁹³ and mitochondrial enzymes, resulting in mitochondrial biogenesis ⁹⁴.

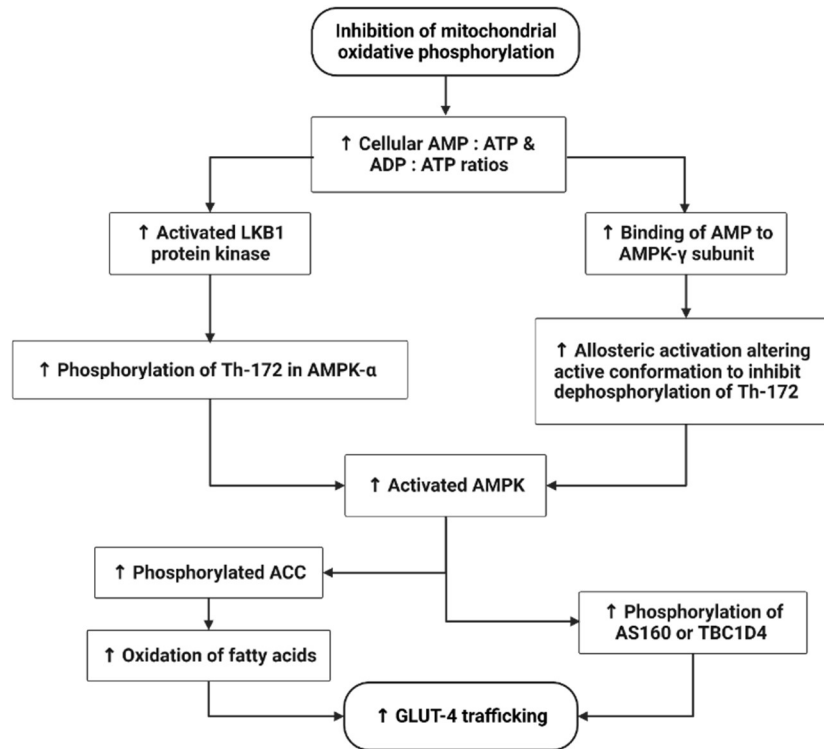


Figure 8. A schematic flow chart of insulin-independent GLUT-4 activation induced by metformin inhibiting mitochondrial ATP synthase ^{81, 95-97}. The increased ratios of ADP/ATP and AMP/ATP will activate AMPK by stimulating LKB1 to phosphorylate the AMPK- α and promoting the binding of AMP to AMPK- γ to maintain the phosphorylation. The activated AMPK can stimulate the phosphorylation of AS160 and ACC, eventually activating the translocation of GLUT-4. AMPK = adenosine 5' monophosphate-activated protein kinase; LKB1 = liver kinase B1; GLUT-4 = glucose transporter-4; ACC = acetyl-CoA carboxylase; AS160 = 160 kDa substrate of Akt Ser/Thr kinase; TBC1D4 = Tre-2/BUB2/cdc 1 domain family.

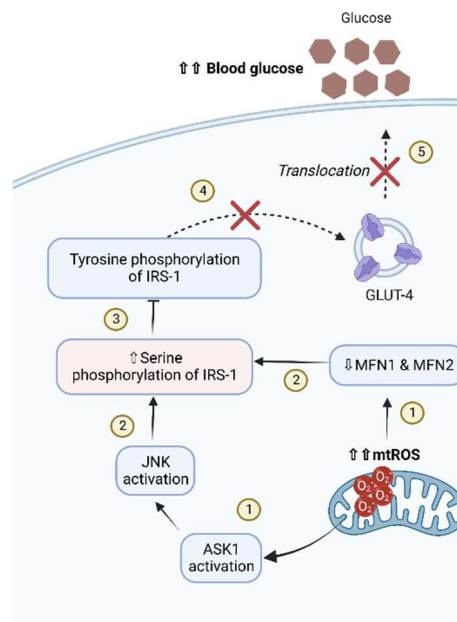


Figure 9. Schematic representation of possible mechanisms of the links between overproduced mt-ROS and insulin resistance, leading to disruption in GLUT-4 translocation ^{79, 98}. mtROS = mitochondrial reactive oxygen species; ASK 1 = apoptosis signal-regulating kinase 1; JNK = c-jun NH₂-terminal kinases; MFN 1 and MFN2 = mitofusins 1 and 2; IRS-1 = insulin-receptor substrate 1. The image was created with BioRender.com.

1.2.4.2. Targeting mitochondrial dysfunction

Studies revealed that a high level of glucose intake and obesity has directly stimulated impairments of mitochondria. Gao et al. ⁷⁶ confirmed that, under hyperglycaemia and fatty acids, some changes in adipocytes mitochondria occurred, such as overproduced mt-ROS, reduced mitochondrial membrane potential, and mitochondrial content. In addition, mitochondrial oxidative capacity in obese adults was significantly reduced compared to non-obese patients ⁹⁹. Alterations in mitochondrial oxidative phosphorylation (OXPHOS) can be considered one of the underlying factors of mitochondrial abnormalities. Studies on cell lines ⁷⁶, mice model ¹⁰⁰, and T2DM patients ¹⁰¹⁻¹⁰³ found that nuclear respiratory factors (NRFs) and peroxisome proliferator-activated receptor- γ coactivators-1 (PGCs-1) were lower than healthy controls. NRFs contribute to the expression of mitochondrial transcription factor A (mtTFA), a key regulator of the transcription of mitochondrial genes and mitochondrial DNA replication ¹⁰⁴. PGC-1 α is the primary regulator of mitochondrial replication and OXPHOS ¹⁰¹ and the co-activator of other genes in energy homeostasis ¹⁰⁵.

As depicted in Figure 10, mitochondria dysfunction can be linked to inflammation and metabolic disorders, including IR. Over-secretion of TNF- α , an inflammatory marker, can be considered a cause of mitochondrial malfunction ¹⁰⁶. Houstis et al. ¹⁰⁷ reported TNF- α -induced mt-ROS production on 3T3-L1 adipocytes.

The defective mitochondria can lead to a reduced β -oxidation rate in diabetic mice ¹⁰⁸. ATP synthases and levels of OXPHOS and palmitic acid oxidation were significantly lower in diabetic and obese animal models¹⁰⁸. According to Mello et al. ¹⁰⁹, excessive fatty acid level induces the infiltration of macrophages into the adipose tissue leading to increased pro-inflammatory cytokines. Furthermore, the inflammatory cytokines trigger the development of IR (see Figure 10). Hence, inflammation has a central position in T2DM, marking it as the potential target for treating hyperglycaemia.

Mitochondrial dysfunction impairs insulin sensitivity. Wang et al. ¹¹⁰ demonstrated the downregulated mitochondrial transcription factor A (mtTFA), a key regulator of transcription of mitochondrial genes and mitochondrial DNA replication, causing markedly decreased expression of phosphorylated Akt and GLUT-4 in 3T3-L1 adipocytes. Moreover, reduced PGC-1 α alters mtTFA in the adipocytes. Targeting AMPK phosphorylation can generate multiple impacts on IR and mitochondrial defects. AMPK has been confirmed as the key regulator of PGCs activation and expression ¹¹¹. In C2C12 myocytes, the activation of PGC-1 α requires adiponectin-induced AMPK activation ¹¹². Additionally, knocking out adiponectin inhibited the AMPK-PGC-1 α pathway in obese mice ¹¹³.

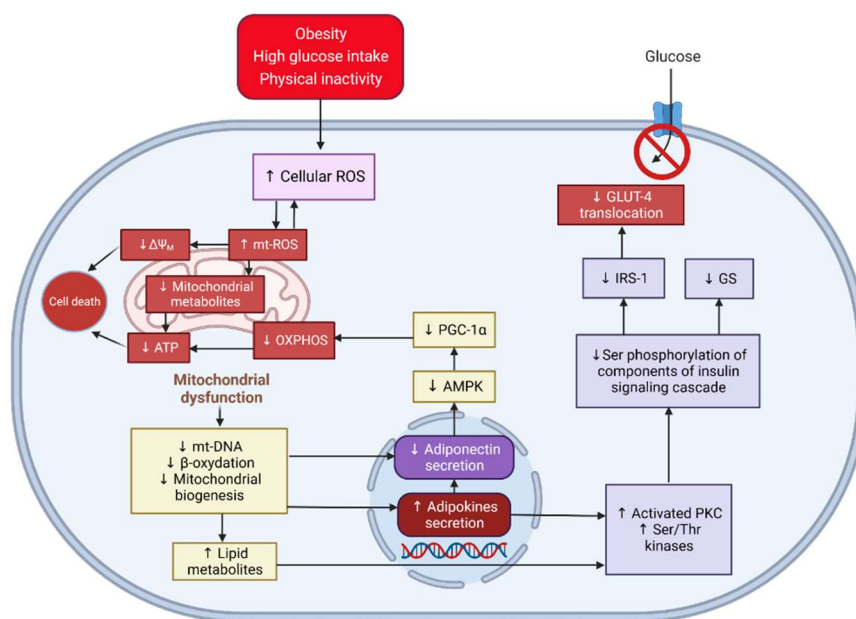


Figure 10. An image represents a proposed mechanism of mitochondrial dysfunction as the primary cause of insulin resistance in an adipocyte model. The increased intracellular ROS triggered by obesity and metabolic challenges (e.g., excess nutrient intake) leads to mt-ROS overproduction, exacerbating the total ROS generation and decreasing mitochondrial membrane potential (MMP) and ATP production ⁸¹. The impaired mitochondria reflected by the collapse of mt-DNA content and depletion of mitochondrial biogenesis alter adiponectin level, resulting in decreased OXPHOS due to reduced activation of AMPK and PGC-1 α as its regulator ¹¹⁴. In addition, the compromised mitochondria function causes the accumulation of lipid metabolites due to the reduced β -oxidation and the increase of proinflammatory cytokines

leading to the induction of PKC isoforms and Ser/Thr kinases ^{28, 110}. Consequently, the inhibition of the insulin signalling cascade, including the disruption of GLUT-4 transduction, leads to the defect of the insulin-dependent glucose uptake pathway. Image was created with BioRender.com.

Treatment with herbal products is beneficial for the activation of AMPK. Hawley et al. ¹¹⁵ summarised that some phytochemicals are the activator, i.e., berberine, quercetin, resveratrol, genistein, capsaicin, and epigallocatechin gallate. Among six different AMPK inducers, quercetin, a flavanol found in *Acacia*, is involved in multiple mechanisms, such as increasing ADP: ATP ratio, increasing phosphorylation of Thr-172, inhibiting basal O₂ uptake, inhibiting ATP synthase and NAD-dependent histone deacetylase SIRT1 ¹¹⁶. Moreover, oral consumption of this flavonoid also enhanced the adiponectin, resulting in a 12.3% increased level of AMPK compared to control patients ¹¹⁷. These studies again emphasised the considerably advantageous natural product-based treatment in T2DM.

1.2.4.3. Study using 3T3-L1 adipocytes

The 3T3-L1 cell line is a fibroblast-like cell from Swiss mouse embryonic fibroblast. It is used to study adipose differentiation and lipid accumulation during adipogenesis and related disorders ^{118, 119}. During the process, the synthesis of triglycerides is increased, leading to an acquisition of mature adipocytes. Hence, it is a practicable model for white adipose tissue (WAT), primary storage for reserving triacylglycerol under a positive energy balance ¹²⁰. Excess WAT has been linked to obesity and severe metabolic disorders, including T2DM, hypertension and cancer. Moreover, given the accumulated fats as the risk factor for the overproduction of ROS, IR, mitochondrial malfunction, and secretion of pro-inflammatory adipokines, the 3T3-L1 adipocytes could be considered an appropriate platform to understanding the possible mechanisms of development and management of the abnormalities.

Table 1. A list of common chemicals used in inducing 3T3-L1 cells in cell differentiation

No	Reagent	Reported concentration	Effect
1	Insulin	1 µg/mL	Stimulating triglyceride synthesis following the cellular absorption of excessive glucose ¹²¹
2	Dexamethasone	0.25 µM	Inhibiting the synthesis of prostaglandin E ₁ ¹²²
3	3-Isobutyl-1-methylxanthine	0.5 mM	Inhibiting cyclic nucleotide phosphodiesterase, increasing intracellular cAMP and cGMP ¹²³
4	Rosiglitazone	2 µM	Activating the PPAR-γ pathway results in increased glucose uptake ¹¹⁸

The conversion of the fibroblast-like cells into adipocytes was induced by prodifferentiative reagents affecting lipogenic or lipolytic processes. According to Zebisch et al. ¹¹⁸, some prodifferentiative agents were demonstrated to efficiently induce the conversion of preadipose cells to adipocytes, including insulin,

dexamethasone, 3-isobutyl-1-methylxanthine, and rosiglitazone (see Table 1). Once confluence, treatment with the reagents should be carried out for 48 h exposures to activate the cellular differentiation. The cells would start accumulating fat, observed as lipid droplets or intramyocellular triglycerides. The number and size are then increasing over the period. The differentiation time to acquire mature adipocytes is reported to be between 8 and 14 days ¹¹⁸. As the main accumulated lipid in the adipocytes is triglycerides ¹²⁴, the lipid droplets have commonly been selectively stained by oil red-O (ORO)-staining assay to quantify the intramyocellular lipid deposition ¹²⁵.

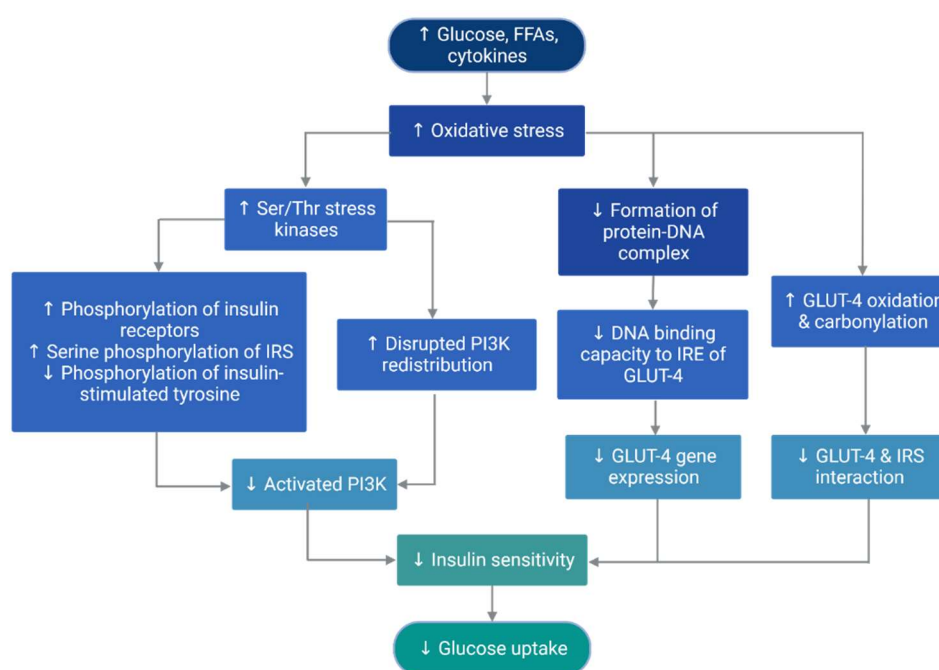


Figure 11. Schematic multiple steps mechanisms of insulin resistance induced by oxidative stress in 3T3-L1 adipocytes ^{75, 78, 126}. ↑ = increased; ↓ = decreased

The adipose 3T3-L1 can be used as a model of obesity to study cellular ROS production and IR (see Figure 11). The accumulated lipid in the cells can cause inflammatory and oxidative stress. Consequently, the proinflammatory mediators can inhibit the PI3K/PKB pathway. Moreover, the ROS can oxidise the protein binding sites for insulin-responsive elements (IRE) in GLUT-4 ⁷⁸, carbonylation of amino acids (Arg 246, Arg 265, and Lys 264) located in the glucose transport channel of GLUT-4 ¹²⁷, and/or complex formation with the DNA ¹²⁸. Eventually, these events can promote IR, characterised by the decline of cellular glucose uptake.

1.3. Pharmaceutical Treatments for Type 2 Diabetes Mellitus

Some medications have been applied to treat T2DM as individual or combination therapy. Their effects and disadvantages are summarised in Table 2. However, the disease is still progressive due to other metabolic disorders^{129, 130}. In some cases, treatment with metformin, the first-line drug, is inadequate due to its hydrophilic property causing minimal diffusion through cell membranes¹³¹. Hypertension and cardiovascular diseases are commonly associated with T2DM¹³², while therapy with sulfonylurea and exogenous insulin, for instance, have a greater risk of hypoglycaemia and weight gain¹³³. Sodium-glucose co-transporter-2 (SGLT-2) inhibitors and glucose-like peptide 1 (GLP-1) receptor agonists, the latest classes of antidiabetic medication, seem to have a lower risk of those side effects but are expensive^{134, 135}.

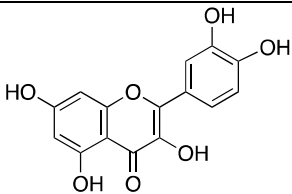
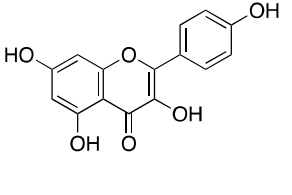
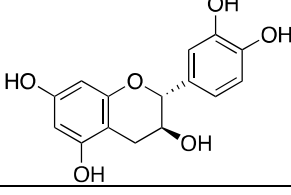
Table 2. List of common pharmaceutical treatments of T2DM¹³⁶⁻¹³⁸

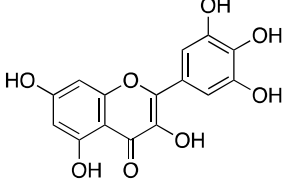
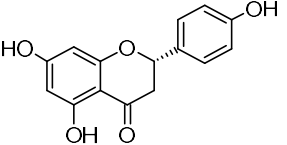
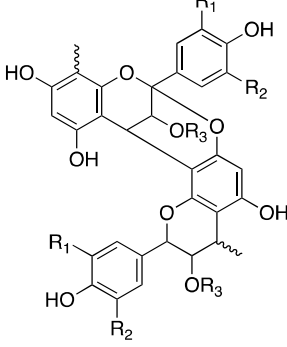
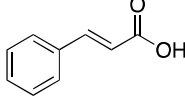
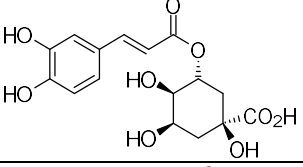
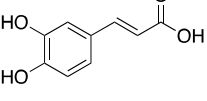
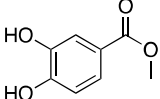
No	Class and examples	Year of introduction	Physiological actions	Disadvantages
1	Insulin injection	1920–1930	Act on insulin receptor	Hypoglycaemia, weight gain, mitogenic effect
2	Sulfonylureas <ul style="list-style-type: none"> ▪ Gliclazide ▪ Glipizide ▪ Glyburide 	1956	Increase insulin release	Hypoglycaemia, weight gain, renal or liver damage
3	Biguanides <ul style="list-style-type: none"> ▪ Metformin 	1957	Increase insulin sensitivity and decrease hepatic glucose production	Gastrointestinal side effects: diarrhoea and flatulence, multiple contraindications: renal or liver damage, hypoxia, acidosis
4	α-Glucosidase inhibitors <ul style="list-style-type: none"> ▪ Acarbose ▪ Miglitol ▪ Voglibose 	1995	Reduce intestinal carbohydrate hydrolysis rate	Gastrointestinal side effects related to potent inhibition of α-amylase enzyme
5	Meglitinides <ul style="list-style-type: none"> ▪ Nateglinide ▪ Repaglinide 	1997	Increase insulin release	Hypoglycaemia, weight gain, liver damage
6	Thiazolidinediones (TZDs) <ul style="list-style-type: none"> ▪ Pioglitazone ▪ Rosiglitazone 	1997	Improve insulin sensitivity	Weight gain, heart disorder, liver toxicity
7	Glucose-like peptide 1 (GLP-1) receptor agonists <ul style="list-style-type: none"> ▪ Exenatide ▪ Liraglutide ▪ Lixisenatide 	2005	Stimulate the GLP-1 receptors, Increase insulin release	Gastrointestinal side effects, renal impairment
8	Dipeptidyl peptidase 4 (DPP-4) inhibitors <ul style="list-style-type: none"> ▪ Sitagliptin ▪ Vildagliptin ▪ Saxagliptin ▪ Linagliptin ▪ Alogliptin 	2006	Inhibit DPP-4 enzyme, increase endogenous GLP-1 level	Liver impairment, pancreatitis risk

No	Class and examples	Year of introduction	Physiological actions	Disadvantages
9	Sodium/glucose cotransporter 2 (SGLT-2) inhibitors <ul style="list-style-type: none"> ▪ Canagliflozin ▪ Dapagliflozin ▪ Empagliflozin 	2012	Inhibit glucose reabsorption in the kidney	Polyuria, risk of urinary infections

Some studies have revealed that inhibiting the α -glucosidase enzyme and stimulating glucose uptake can be achieved using dietary flavonoids ¹³⁹⁻¹⁴². Flavonoid derivatives, such as polyphenolic compounds found in flowers, leaves, fruit, and bark, have been reported to exhibit those activities ¹⁴³. By binding the enzyme through non-covalent and reversible interactions performed by the hydroxyl group ¹⁴⁴, the phytochemicals exert strong inhibitory activity on the enzyme resulting in glucose homeostasis ¹⁴⁵. Interestingly, the natural products show lower interaction with α -amylase that could overcome the side effects of maldigestion ¹⁴⁶. In addition, the hydroxyl-contained compounds have been confirmed to stimulate GLUT-4 translocation via both IRS-1/PI3K and AMPK activations and inhibit lipid deposition resulting in an antiobesity activity (Figure 14) ^{145, 147, 148}. For example, myricitrin has been reported to increase the phosphorylation of IRS1 and Akt ^{149, 150} due to the strong intermolecular interaction with PI3K ¹⁵⁰. This compound has also been confirmed to phosphorylate AMPK by suppressing mRNA and protein expression of TNF- α and IL-6 ¹⁵¹.

Table 3. Some examples of secondary metabolites demonstrating α -glucosidase inhibitory and glucose uptake modulation

No	Compound and source	Structure	Target activity	Effects	Reference
1	Quercetin Source: • Apple • Red onion • Broccoli		α -glucosidase enzyme	↓ Postprandial hyperglycaemia	He et al. ¹⁵² , Zygmunt et al. ¹⁵³
			GLUT-4 via AMPK pathway	↑ Glucose uptake ↓ Fat accumulation in 3T3-L1 cells	Dhanya et al. ¹⁴⁷ , Yang et al. ¹⁵⁴
2	Kaempferol Source: • Tea • Grape • Onion		α -glucosidase enzyme	Altering the secondary structure of the enzyme	Peng et al. ¹⁵⁵
			GLUT-4 via AMPK pathway	↑ Glucose uptake ↑ β -cells survival	Zhang et al. ¹⁵⁶
3	(–)-Catechin Source: • Tea • Grape		α -glucosidase enzyme	Inhibiting maltose breakdown	Matsui et al. ¹⁵⁷
			GLUT-4 via IRS-1/PI3K pathway	↑ Glucose uptake	Daisy et al. ¹⁵⁸

No	Compound and source	Structure	Target activity	Effects	Reference
	• Leguminous plants				
4	Myricetin Source: • Grape • Berries • Onion		α-glucosidase enzyme	Showing strong binding capacity to the enzyme	He et al. ¹⁵⁹
			GLUT-4 via IRS-1/PI3K pathway	↑ GLUT-4 signalling pathway	Kandasamy et al. ¹⁶⁰
5	Naringenin Source: • Grape • Orange • Tomatoes		α-glucosidase enzyme	↓ Postprandial hyperglycaemia	Proença et al. ¹⁶¹
			GLUT-4 via IRS-1/PI3K pathway	↑ Glucose uptake	Zymunt et al. ¹⁵³
6	Condensed tannins Source: • Leguminous plants • Acacia plants • Berries • Grape		α-glucosidase enzyme	↓ Postprandial hyperglycaemia	Chai et al. ¹⁶²
			GLUT-4 via IRS-1/PI3K and AMPK pathways	↑ Glucose uptake	Pinent et al. ¹⁴⁸
7	Cinnamic acid Source: • Sweet potatoes • Celery • Garlic		α-glucosidase enzyme	↓ Postprandial hyperglycaemia	Ernawati et al. ¹⁶³
			GLUT-4 via IRS-1/PI3K pathway	↑ Glucose uptake	Prabhakar et al. ¹⁶⁴
8	Chlorogenic acid Source: • Coffee		α-glucosidase enzyme	↓ Postprandial hyperglycaemia	Zheng et al. ¹⁶⁵
			GLUT-4 via AMPK pathway	↑ Glucose uptake and antiobesity	Ong et al. ¹⁶⁶
9	Caffeic acid Source: • Coffee		α-glucosidase enzyme	Inhibiting the enzyme	Oboh et al. ¹⁶⁷
			GLUT-4 via IRS-1/PI3K pathway	↑ Glucose uptake	Huang et al. ¹⁶⁸
10	Methyl 3,4-dihydroxybenzoate Source: • Nutmeg		α-glucosidase enzyme	Inhibiting of the enzyme	Megawati et al. ¹⁶⁹

↑ = increased; ↓ = decreased

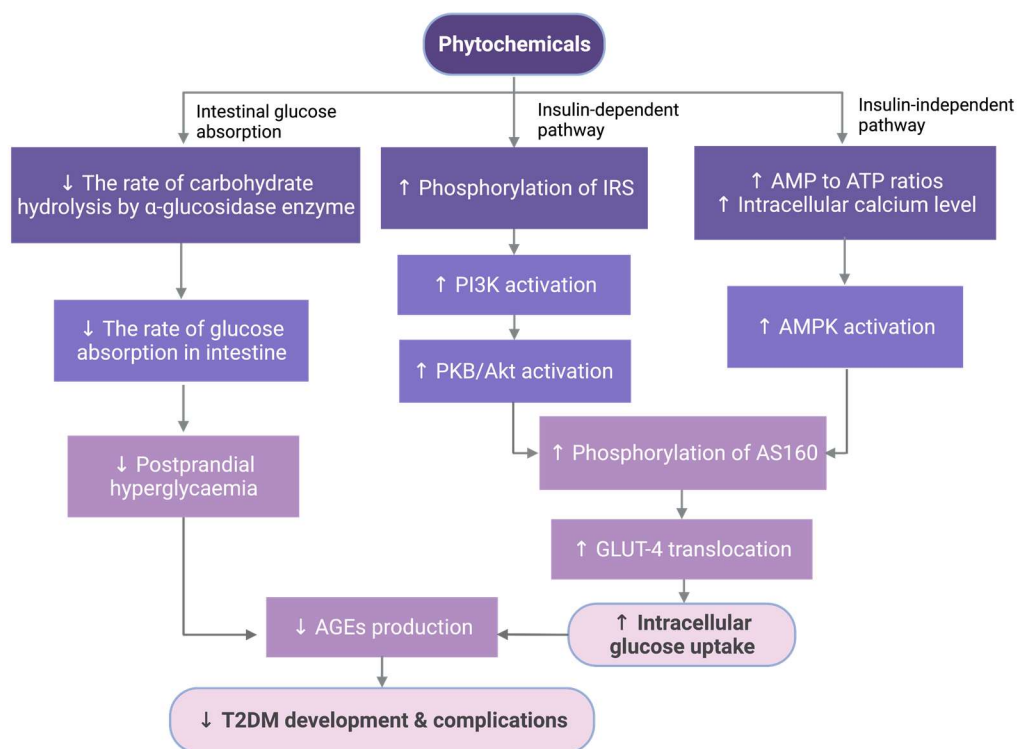


Figure 12. Schematic representation of some selected phytochemical roles as antidiabetic agents ^{147, 159, 170, 171}.

Indigenous Australia's knowledge of the medicinal properties of *Acacia* species ^{172, 173} has been scientifically confirmed to provide important bioactive constituents that show antidiabetic activities and prevent related complications and side effects. Flavonoid and phenolic derivatives such as kaempferol, caffeic acid, *p*-coumaric acid, (+)-catechin, (-)-epicatechin, and chlorogenic acid have been reported to contribute to the properties ¹⁷⁴⁻¹⁷⁷. However, the information regarding which compound is the primary antidiabetic agent remains unclear.

There are 1,380 species of *Acacia* worldwide, and two-thirds are native to Australia. Indigenous Australians have used the leaves, bark, and flowers as medicinal agents for centuries ¹⁷⁸. Decoction and infusion are the most common preparation of the ethnomedicinal plant applied by those people ^{173, 179, 180}. The Australian continent consisting of some arid, semiarid and dry subtropical regions, allows *Acacia* to grow and produce unique secondary metabolites ¹⁸¹. The compounds have various benefits for human health, such as anti-digestive disorder (tannins, saponins, flavonoids); antiplasmodial (tryptamine, tannins, organic acids, saponins); antioxidant (polyphenols); anticancer (triterpenoids, saponins); nutraceutical, diuretic therapy, and natriuretic therapy (polysaccharide, glucosides, gum) ^{182, 183}. Moreover, some Australian polyphenol-containing species such as *Acacia kempeana*, *A.*

ligulata, *A. tetragonophylla*, *A. mearnsii*, and *A. pycnantha* exhibit potential properties as antihyperglycemic agents ^{172, 173, 184-186}.

A. saligna, an Australian species, is constituted by various phytochemicals despite being considered a weed. Its flowers contain isosalipurposide **1** and chalcononaringenin 4-glucoside **2** ¹⁸⁶, quercetin **3**, kaempferol **22**, naringenin **42** ^{187, 188}, and some polyphenols ¹⁸⁹. The leaves contain quercetin **3**, catechin **14**, kaempferol **22**, and myricetin **11** derivatives ^{190, 191}. Other phenolic series in the phyllode, namely gallic acid **25**, syringic acid **28**, vanillin **29**, protocatechic acid **30**, *p*-hydroxybenzoic acid **31**, *p*-coumaric acid **37**, salicylic acid **32**, and chlorogenic acid **40**, have been identified by Gumgumjee and Hajar ¹⁹¹. In the barks, some compound groups were identified as the derivatives of benzoic acid **24**, cinnamic acid **34**, phenolics, and condensed tannins ¹⁹²⁻¹⁹⁵. Some structures can be seen in Table 3.

The chemical components of *A. saligna* have been reported to have potential bioactivities. Ghribia et al. ¹⁸⁸ and Al-Huqail et al. ¹⁸⁷ demonstrated the flavonoids from the flowers with antioxidant, anti-acetylcholinesterase, and antibacterial activities. Its volatile phytochemicals possessing allelopathic activity indicate their possibility as a green herbicide ¹⁹² (see Table S1, pages 221–223). The phyllode extracts containing polyphenols have demonstrated antibacterial, anticandidal, and antifungal activities, while the pure compounds have exhibited antioxidant effects and cytotoxicity against liver cancer cells linked to the acetylation ^{190, 191, 196}. Buttner et al. ¹⁹⁷ reported the potential inhibition of the α -glucosidase enzyme by the leaf and bark extracts. However, the information on the cell-based study of antidiabetic activity of *A. saligna* is lacking.

1.4. Overview of *Acacia saligna*

1.4.1. Taxonomy

Acacia saligna (Labill.) H. L. Wendl. (1820) is the current scientific name for the species characterised by 2–10 m tall as a shrub or small tree, grey to red-brown bark, linear to lanceolate; 8–25 × 0.4–2 cm; green to glaucous leaves, and bright yellow flowers with 5–10 mm diameter ¹⁹⁸. It is native to Western Australia and was previously named *Acacia cyanophylla* Lindl, *A. bracteata* Maiden & Blakeley, *A. lindleyi* Meissner, *Mimosa saligna* Labill., and *Racosperma salignum* (Labill.) Pedley ¹⁹⁹. More recent studies have revealed that this highly polymorphic species has four subspecies (subsp.), i.e., "subsp. *saligna*" referred to the cyanophylla variant, "subsp. *pruinescens*" referred to the Tweed River variant, "subsp. *lindleyi*" referred to the typical variant, and "subsp. *stolonifera*" referred to the forest variant ²⁰⁰. On the other hand, people recognise the plant with familiar names such as Port Jackson wattle,

Coojong, blue-leaved wattle, and Western Australia golden wattle. The following information shows the detailed taxonomic tree of the species taken from Maslin ¹⁹⁸.

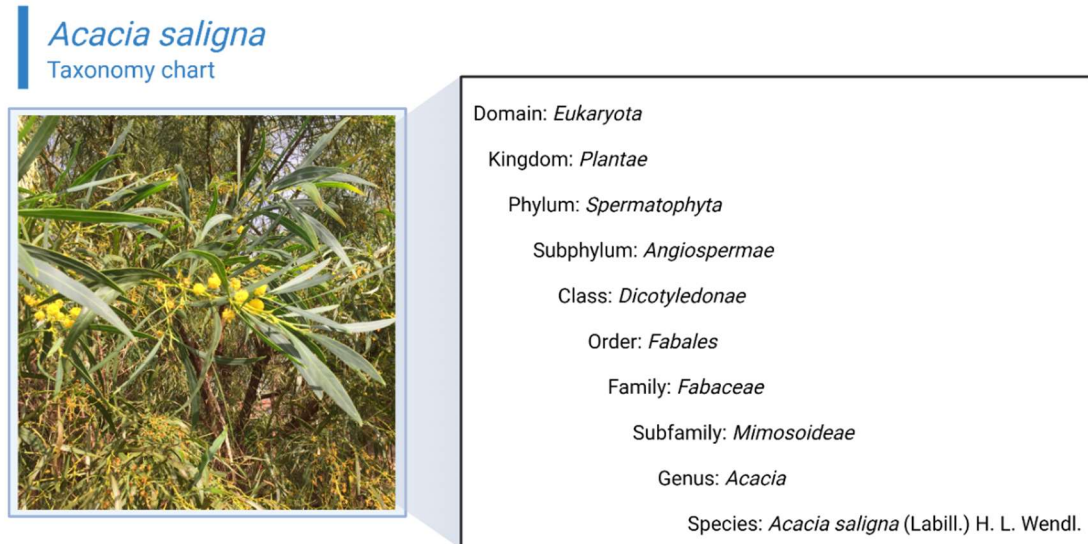


Figure 13. A photograph of *A. saligna* subsp. *saligna* collected from Tasman St, Kurnell, NSW, on 7 October 2019 for this study.

A. saligna is commonly found on poor sandy soils and coastal dune systems within South-west Western Australia. The tree is highly tolerant against drought, saline and alkaline surroundings, and frosty locations ²⁰¹. Due to the ability to stabilise a coastal dune system, this species was cultivated in the Southern and Eastern States of Australia, such as South Australia, Queensland, New South Wales, Victoria, and Tasmania ²⁰², and some countries abroad. It has been naturalised in semi-arid areas of the Middle East and Africa including Iran, Iraq, Jordan, Syria, Saudi Arabia, Egypt, Lybia, Tunisia, Morocco, Algeria, Tunisia, Ethiopia, Namibia, Kenya, Tanzania, and South Africa ²⁰³. The species was also introduced to European countries, for example Greece, Turkiye, Cyprus, Spain, Portugal, France, and to America countries of United States of America, Mexico, Uruguay, and Chile ²⁰⁴. The flowering season is usually between August and October, while mature legumes appear from November to January ¹⁹⁸.

Studies were found to report the intraspecific variation of *A. saligna* and its distribution in Australia and some naturalisation countries. Millar et al. ²⁰⁵ and George et al. ²⁰⁶ have revealed the distribution of all four subspecies in Western Australia based on their genetic structure characteristics assigned by using a polymerase chain reaction (PCR) method called Bayesian analysis. The studies found that subsp. *lindleyi* has the largest population followed by subsp. *saligna*, subsp. *stolonifera*, and

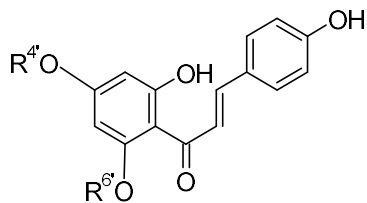
subsp. *pruinescens* in its native land. Using the same approach, however, Millar et al.²⁰⁷ identified only three intraspecific variation in Tigray (Ethiopia), including subsp. *lindleyi*, subsp. *saligna*, and subsp. *stolonifera*. Moreover, more comprehensive report²⁰⁸ also showed the distribution of these three with varied number of population in the wider locations, including eastern Australia, Israel, Italy, New Zealand, Portugal, South Africa, Spain and the USA. Interestingly, a unique subspecies different from those found in Western Australia assigned as a South African subspecies²⁰⁹ was found in that regions.

1.4.2. Reported chemical composition

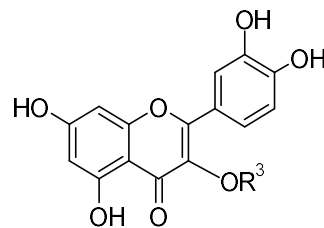
1.4.2.1. Flowers

Studies have revealed that flavonoid derivatives were the most common phytochemicals reported from the flowers of *Acacia saligna*, along with beneficial effects as an antioxidant^{187, 188, 196}. Isosalipurposide **1**^{210, 211}, chalcononaringenin 4-glucoside **2**¹⁸⁶, and quercetin **3**¹⁸⁸ (Figure 14) have been isolated from the ethyl acetate (EtOAc) extract of the yellow-rounded flowers of *A. saligna* growing in Tunisia. Moreover, an HPLC-based study conducted by Al-Huqail et al.¹⁸⁷ on *A. saligna* from Egypt documented the presence of quercetin **3**, kaempferol **22**, benzoic acid **24**, syringic acid **28**, *p*-hydroxybenzoic acid **31**, salicylic acid **32**, caffeic acid **35**, *o*-coumaric acid **36**, *p*-coumaric acid **37**, ferulic acid **38**, naringenin **42**, ellagic acid **44**, catechol **45**, and caffeine **46** in the water-soluble extract of flowers. To the best of our knowledge, there is no documented information about phytochemicals isolated from the flowers of this species growing in Australia.

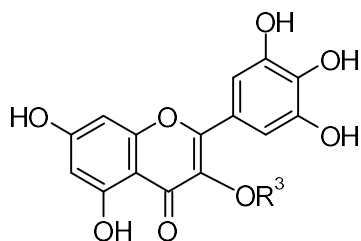
As plants require secondary metabolites for survival and defence, biosynthesising the compounds depends on environmental factors, including rainfall, soil, salt, temperature, and geographical variations²¹². Environmental stress can stimulate the accumulation of bioactive compounds to cope with severe conditions. For instance, uncommon saccharides grouped in polyol derivatives are produced by plants living in a water shortage and high salinity area. These factors have induced the transcription of all genes of catalysts of pinitol biosynthesis, *myo*-inositol methyl transferase (IMT) group²¹³. Anthocyanins, common groups found in *Acacia* species, are synthesised by the plant at a higher level when light and drought stresses occur²¹⁴. This has been linked to the inactivation of teosinte branched1-cycloidea-proliferating cell factor 15 (TCP15), an inhibitor of anthocyanin biosynthesis, by the high light intensity. In this regard, the Australian species growing in different environments facing different challenges may produce different phytochemicals from those identified in the Middle East and Africa.



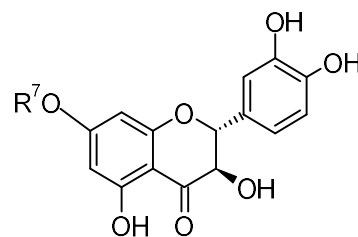
R⁴ = H, R⁶ = β -D-glucoside, Isosalipurposide **1**
 R⁴ = β -D-glucoside, R⁶ = H, Chalconaringen 4'-glucoside **2**



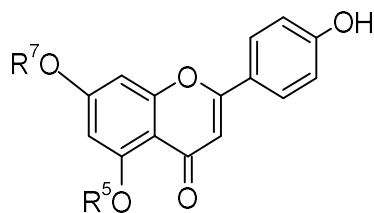
R³ = H, Quercetin **3**
 R³ = α -L-rhamnoside, Quercitrin **4**
 R³ = α -L-arabopyranoside, Quercetin-3-O-arabinoside **5**
 R³ = rhamnosyl-glucosyl, Rutin **6**
 R³ = β -D-glucopyranoside, Miquelianin **7**
 R³ = β -D-glucofuranoside, Isoquercetin **8**
 R³ = β -D-galactopyranoside, Hyperoside **9**



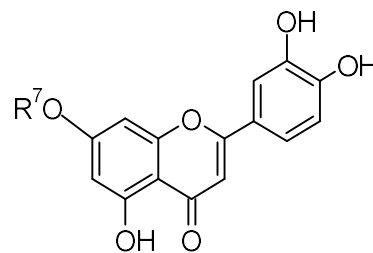
R³ = H, Myricetin **10**
 R³ = α -L-rhamnopyranoside, Myricitrin **11**
 R³ = α -L-arabinopyranoside, Myricetin-3-O-arabinoside **12**
 R³ = β -D-glucopyranoside, Myricetin-3-O-glucoside **13**



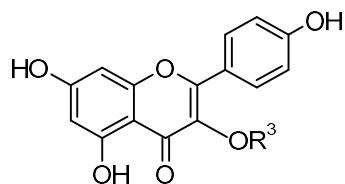
R⁷ = H, (+)-Catechin **14**
 R⁷ = galloyl, 7-O-Galloyl-catechin **15**



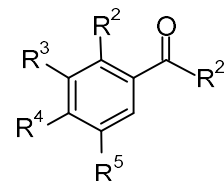
R⁵ = R⁷ = H, Apigenin **16**
 R⁵ = H, R⁷ = β -D-glucopyranoside, Apigenin **17**
 R⁵ = β -D-glucopyranoside, R⁷ = H, Salipurpin **18**



R⁷ = H, Luteolin **19**
 R⁷ = β -D-glucopyranoside, Luteolin-7-O-glucoside **20**
 R⁷ = β -D-arabinopyranoside, Luteolin-7-O- β -arabinoside **21**



R³ = H, Kaempferol **22**
 R³ = β -D-glucopyranoside, Astragalin **23**



R² = R³ = R⁴ = R⁵ = H, R² = OH, Benzoic acid **24**
 R² = H, R³ = R⁴ = R⁵ = R² = OH, Gallic acid **25**

$R^2 = H, R^3 = R^4 = R^5 = OH, R^2' = OMe,$
Methyl gallate **26**

$R^2 = H, R^3 = R^4 = R^5 = OH, R^2' = OPr,$
Propyl gallate **27**

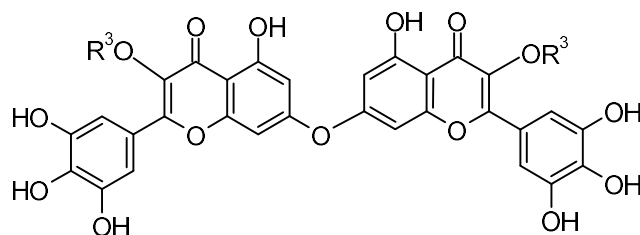
$R^2 = H, R^4 = R^5 = OH, R^3 = R^5 = OMe,$
Syringic acid **28**

$R^2 = R^3 = R^5 = H, R^4 = OH, R^5 = OMe,$
Vanillin **29**

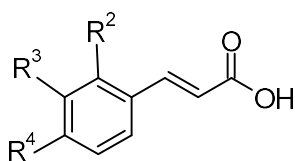
$R^2 = R^3 = H, R^4 = R^5 = R^2' = OH,$
Protocatechuic acid **30**

$R^2 = R^3 = R^5 = H, R^4 = R^2' = OH,$ *p*-Hydroxy
benzoic **31**

$R^3 = R^4 = R^5 = H, R^2 = R^2' = OH,$ Salicylic
acid **32**



$R^3 = \alpha$ -L-rhamnopyranoside, Myricetin-3-O-rhamnoside (C^7 -O- C^7) myricetin-3-O-rhamnoside **33**



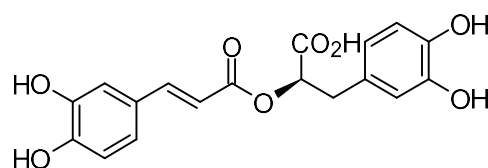
$R^2 = R^3 = R^4 = H,$ Cinnamic acid **34**

$R^2 = H, R^3 = R^4 = OH,$ Caffeic acid **35**

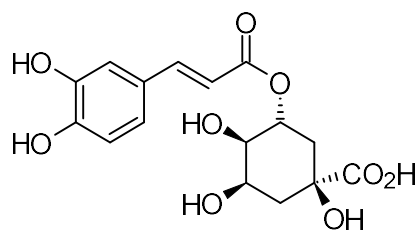
$R^2 = OH, R^3 = R^4 = H,$ *o*-Coumaric acid **36**

$R^2 = R^3 = H, R^4 = OH,$ *p*-Coumaric acid **37**

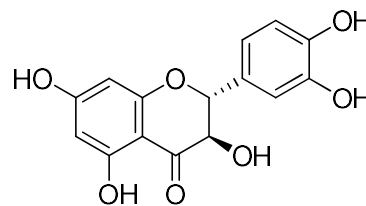
$R^2 = H, R^3 = OMe, R^4 = OH,$ Ferulic acid **38**



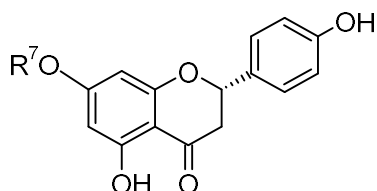
Rosmarinic acid **39**



Chlorogenic acid **40**

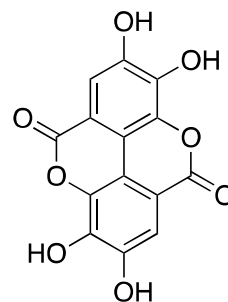


Taxifolin **41**

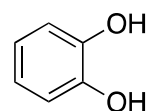


$R^7 = H,$ Naringenin **42**

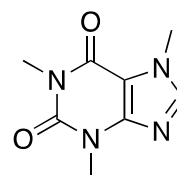
$R^7 = \alpha$ -L-rhamnosyl-(1→2)- β -D-glucopyranoside, Naringin **43**



Ellagic acid **44**



Catechol **45**

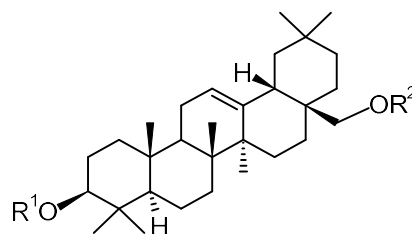


Caffeine **46**

Figure 14. Phenolics and alkaloid derivatives identified in flowers ^{187, 188}, leaves ^{189, 190, 196, 215, 216}, and barks ²¹⁷ of *A. saligna*.

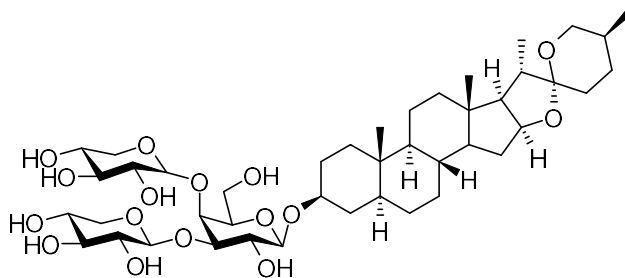
1.4.2.2. Leaves

Some flavonoid derivatives such as astragalins **23** ¹⁸⁹; quercetin derivatives **3–5**; myricetin derivatives **10–13**, catechin derivatives **14, 15** ^{190, 196, 216}; rutin **6**; taxifolin **41**; naringenin **42** ²¹⁸; and luteolin derivatives **19–21** ²¹⁵ have been identified in its polar extract of leaves. In addition, using HPLC, benzoic acid derivatives (gallic acid **25**, syringic acid **28**, vanillin **29**, protocatechuic acid **30**, and *p*-hydroxybenzoic **31**), cinnamic acid derivatives (cinnamic acid **34**, caffeic acid **35**, *p*-coumaric acid **37**, ferulic acid **38**, and chlorogenic acid **40**), phenolic esters (methyl gallate **26** and propyl gallate **27**), and a coumarin derivative (ellagic acid **44**) observed by Guneidy et al. ²¹⁸ from ethanol (EtOH) extract, Elansary et al. ²¹⁶ from methanol (MeOH) extract, and Gumgumjee et al. ¹⁹¹ from EtOH extract showed that its leaves could be considered the source of bioactive phenolic compounds. Other groups of compounds were also identified in the leaves. For instance, the methanolic extract of the leaves gave three derivatives of saponin (**73–75**, Figure 15) ¹⁹⁶. All the reported phytochemicals in the leaves were obtained from *A. saligna* collected from Middle East regions, while no phytochemicals have been reported in the leaves found in the plant growing in Australia.



$R^1 = R^2 = H$, Erythrodiol **73**

$R^1 = p\text{-coumaric}$, $R^2 = H$, $3\beta\text{-O-}trans\text{-}p\text{-coumaryl}$ erythrodiol **74**



(25S)-5 β -spirostan-3 β -yl-3-O- β -D-xylopyranosyl(1 \rightarrow 3)-O- β -D-xylopyranosyl(1 \rightarrow 4)- β -D-galactopyranoside **75**

Figure 15. Saponin derivatives elucidated in MeOH extract of *A. saligna* leaves ¹⁹⁶.

Accumulated flavonols have been found co-localising with ROS in the plant cells. This phenomenon responds to abiotic-induced ROS production in plants' cytoplasm, nucleus, and cell wall ²¹⁴. Abiotic factors can influence the chemical composition of the plant extracts. For example, the leaves harvested from the Albahah region of South-west Saudi Arabia ²¹⁹ had lower gallic acid and *p*-coumaric acid content of 0.0054% and 0.0008%, respectively, than those in the leaves collected from Orman Botanical Garden Giza, Egypt ²¹⁵ with the percentage of 19.2% and 6.4%, respectively. A literature search found that the Al-Bahah region is a dry area with an annual mean rainfall of 142.6 mm/year ²²⁰ and medium to high soil salinity ²²¹ while the Giza area is an arid area estimated at 1.2 mm/year of annual rainfall ²²² with high soil salinity ²²³. Moreover, studies on drought and saline stress showed a significantly elevated level of gallic acid and *p*-coumaric acid in Lentil seeds varieties Tina ²²⁴ and wheat *Aegilops cylindrica* ²²⁵ compared to their controls. These findings imply the influences of abiotic stresses in phenolic biosynthesis.

1.4.2.3. Bark

Although no paper has reported the isolation of any single chemical from the bark of *A. saligna*, a recent study from Salem and colleagues ²²⁶ by screening the EtOH extract of barks *via* HPLC-VWD detected the presence of quercetin **3**, rutin **6**, kaempferol **22**, benzoic acid **24**, gallic acid **25**, vanillin **29**, caffeic acid **35**, *o*-coumaric acid **36**, *p*-coumaric acid **37**, ferulic acid **38**, rosmarinic acid **39**, chlorogenic acid **40**, and caffeine **46**. The barks of *Acacias* have also been documented as a source of gums and tannin derivatives ²²⁷. Indigenous Australians have applied *Acacia* barks to cure cough, rheumatic fever, and dysentery ¹⁸⁰.

1.4.3. Bioactivities of the plant

Like other species of *Acacia*, *A. saligna* also has been potential to manage the risk factors of certain disorders, including microorganisms and prooxidants. Leaves were frequently documented for this purpose, followed by flowers, as they

have been recognised as a flavonoid-rich source ^{190, 196, 228}. Several methods were employed to determine the responsible compounds. For instance, proximate analysis, including phenolic and flavonoid content quantification, was the primary method used by most authors (60%), followed by single compound isolation and identification (23%), HPLC analysis (14%), and GCMS analysis (3%). Table S1 (Appendix A, pages 221–223) shows flavonoid derivatives were the predominant active compounds linked to the properties, followed by phenolic acids such as benzoic and cinnamic acid derivatives.

1.4.3.1. Antioxidant

Some reports have confirmed the antioxidant activity of *A. saligna* through *in vitro* assays such as DPPH and ABTS. Its flowers extracted by water demonstrated a weaker IC₅₀ value against DPPH than the positive control, butylated hydroxyl toluene (BHT) ¹⁸⁷. Phenolic and flavonoid derivatives screened using HPLC were associated with the activity. Another HPLC-based screening identified quercitrin **4**, rutin **6**, miquelianin **7**, isoquercetin **8**, hyperoside **9**, gallic acid **25**, and *p*-coumaric acid **37** as the significant contributors to the antioxidant activity of MeOH leaf extract ²¹⁶. In addition, a chromatographic study ²²⁶ on EtOH bark extract showed a high content of benzoic acid **24**, catechol **45**, naringenin **42**, quinol, and rutin **6**. This ethanolic extract possessed remarkable antioxidant activity against DPPH and β -carotene-linoleic acid (a bleach).

Interestingly, biflavonoid glycoside of myricetin-3-*O*-rhamnoside (C⁷-O-C⁷) myricetin-3-*O*-rhamnoside **33** along with myricitrin **11** isolated from a MeOH extract of the leaves neutralised ABTS cation radicals ¹⁹⁶. Isosalipurposide **1**, quercetin **3**, and naringenin **42** isolated from flowers by EtOAc were responsible for the antioxidant activity of the extract in DPPH and ABTS ¹⁸⁸. Other phytochemical groups were also recognised to contribute to the antioxidant property of *A. saligna*. Polyunsaturated fatty acids (PUFAs) were detected in the MeOH seeds extract that displayed free radical scavenging activity in DPPH and ABTS ²²⁹.

1.4.3.2. Antimicrobial

A. saligna possesses antibacterial activities. The water extract of flowers inhibited the growth of *Agrobacterium tumefaciens* (minimum inhibitory concentration or MIC = 200 μ g/mL), *Enterobacter cloacae* (MIC = 300 μ g/mL), *Erwinia amylovora* (MIC = 300 μ g/mL), and *Pectobacterium carotovorum* subsp. *carotovorum* (MIC = 100 μ g/mL) ¹⁸⁷. Another work on its leaves ¹⁹⁰ documented the antibacterial activities of the EtOAc fraction against gram-positive bacteria, including *Staphylococcus aureus*

(MIC = 0.41 $\mu\text{g/mL}$), *Streptococcus pyogenes* (MIC = 0.46 $\mu\text{g/mL}$), *Bacillus cereus* (MIC = 0.41 $\mu\text{g/mL}$) and *B. subtilis* (MIC = 0.14 $\mu\text{g/mL}$), and the yeast *Candida albicans* (MIC = 3.7 $\mu\text{g/mL}$).

This study also found thirteen flavonoid derivatives (**3** – **5**, **10** – **17**, and **19**) and two phenolic acids (**25** and **26**) from the active fraction. However, the activity of the single compound was not reported. Moreover, the EtOH extract of the leaves contains predominantly phenolic acids, including gallic acid **25**, syringic acid **28**, vanillin **29**, protocatic acid **30**, *p*-hydroxybenzoic acid **31**, salicylic acid **32**, *p*-coumaric acid **37**, and chlorogenic acid **40** which was also found to be active against not only gram-positive bacteria such as *Micrococcus* (diameter of inhibition zone or DIZ = 27.66 mm) and *Methicillin-resistant Staphylococcus aureus* (MRSA) (DIZ = 27.66 mm), but also gram-negative bacteria, *Escherichia coli* (DIZ = 25.66 mm), *Klebsiella pneumonia* (DIZ = 29.33 mm), and *Pseudomonas aeruginosa* (DIZ = 25.66 mm)¹⁹¹. The MeOH extract of the leaves was also an inhibitor of *Listeria monocytogenes* (MIC = 0.47 mg/mL), *E. coli* (MIC = 0.31 mg/mL), *S. aureus* (MIC = 0.30 mg/mL), *B. cereus* (MIC = 0.35 mg/mL), *Micrococcus flavus* (MIC = 0.41 mg/mL), and *P. aeruginosa* (MIC = 0.37 mg/mL)²¹⁶.

1.4.3.3. Antifungal

This plant has been reported to inhibit numerous species of pathogenic fungi. For instance, 3% of the aqueous extract of the flowers significantly prevented *Melia azedarach* wood from discolouration caused by *Fusarium culmorum* (38.51% of inhibition), *Rhizoctonia solani* (41.48%), and *Penicillium chrysogenum* (65.92%)¹⁸⁷. Moreover, a preventive activity against the growth of *Aspergillus niger* (DIZ = 20 mm), *A. fumigatus* (DIZ = 25.67 mm), *A. flavus* (DIZ = 21.33 mm), and *Candida albicans* (DIZ = 23.33 mm) has also been found¹⁹¹ in the EtOH extract of the leaves. The activity of some pathogenic fungi such as *A. ochraceus*, *A. niger*, *A. flavus*, *C. albicans*, *P. ochrochloron*, and *P. funiculosum* was also suppressed by methanolic leaves extract containing quercetin **3**, rutin **6**, miquelianin **7**, hyperoside **9**, and *p*-coumaric acid **37** as the possible contributors²¹⁶ (Table 4).

The EtOH extract of the barks displayed fungicidal properties indicated by the inhibition of the growth of six types of *Fusarium oxysporum* isolated from different plant hosts, *Pisum sativum* L. (*F. oxysporum* 1 with MIC = 125 mg/L), *Cucurbita pepo* L. (*F. oxysporum* 2 with MIC = 125 mg/L), *Oryza sativa* L. (*F. oxysporum* 3 with MIC = 64 mg/L), *Capsicum annum* L. (*F. oxysporum* 4 with MIC = 64 mg/L), *Physalis*

peruviana L. (*F. oxysporum* 5 with MIC = 64 mg/L), and *Vicia faba* L. (*F. oxysporum* 6 with MIC = 64 mg/L) ²²⁶.

Table 4. Antifungal activities of MeOH extract of *A. saligna* leaves and its constituents ²²⁶

Sample	MIC, MFC (mg/mL) against					
	<i>A. ochraceus</i>	<i>A. niger</i>	<i>A. flavus</i>	<i>C. albicans</i>	<i>P. ochrochloron</i>	<i>P. funiculosum</i>
<i>A. saligna</i> extract	0.30, 0.91	0.38, 0.95	0.48, 1.02	0.58, 1.42	0.43, 1.01	0.44, 1.31
Quercetin 3	0.31, 0.63	0.20, 0.75	0.21, 0.75	0.06, 0.33	0.24, 0.70	0.29, 0.63
Miquelianin 7	0.26, 0.52	0.17, 0.61	0.18, 0.62	0.06, 0.27	0.21, 0.60	0.26, 0.54
Rutin 6	0.21, 0.45	0.18, 0.55	0.28, 0.62	0.25, 0.51	0.30, 0.71	0.23, 0.43
Hyperoside 9	0.10, 0.46	0.13, 0.50	0.15, 0.52	0.21, 1.03	0.25, 1.03	0.31, 1.19
<i>p</i> -Coumaric acid 36	0.22, 0.43	0.23, 0.45	0.21, 0.41	0.32, 0.60	0.22, 0.59	0.20, 0.40

1.4.3.4. Inhibition of α -glucosidase

Only a few studies investigated the antidiabetic property of *A. saligna*. Buttner *et al.* ¹⁹⁷ reported the inhibitory effects of aqueous and ethanolic leaf and bark extracts on α -amylase and α -glucosidase (Table 5). The extracts have a high flavonoid and phenolic content. Moreover, MeOH extracts of flowers, leaves, seeds, and branches can also be inhibitors of the α -glucosidase ²³⁰. In diabetic rats, the aqueous-alcoholic leaf extract decreased blood sugar levels from 255 to 117 mg/dL, indicating a change from diabetic to pre-diabetic status ²¹⁵. Although quercetin **3**, myricetin **10**, and luteolin **19** and their glycone forms, i.e., quercitrin **4**, quercetin-3-*O*- β -arabinopyranoside **5**, miquelianin **7**, myricetrin **11**, myricetin-3-*O*- β -arabinopyranoside **12**, myricetin-3-*O*- β -glucopyranoside **13**, luteolin-7-*O*- β -glucopyranoside **20**, and luteolin-7-*O*- β -arabinopyranoside **21** were also isolated from the extract, none presented the antihyperglycemic effects alone.

Table 5. Inhibitory activities of bark and leaf extracts of *A. saligna* against α -glucosidase ¹⁹⁷

Sample	IC ₅₀ (μ g/mL) against	
	α -Amylase	α -Glucosidase
Aqueous bark extract	34.78	3.41
EtOH bark extract	10.45	2.35
Aqueous leaf extract	45.10	5.35
EtOH leaf extract	17.67	3.64

1.4.3.5. Anti-inflammation

Acacia plants, including *A. saligna*, have anti-inflammatory activities due to the rich content of bioactive constituents. A butanol (BuOH) extract of the shoots

showed potent inhibition of inflammatory markers, PGE₂, COX-2, and IL-1 β in a rat model of ulcerative colitis induced by acetic acid ²³¹. Some bioactive compounds, including quercetin **3**, rutin **6**, catechin **14**, kaempferol **22**, gallic acid **25**, methyl gallate **26**, syringic acid **28**, cinnamic acid **34**, caffeic acid **35**, coumaric acid **37**, ferulic acid **38**, chlorogenic acid **40**, taxifolin **41**, naringenin **42**, and ellagic acid **44** were linked to the anti-inflammatory effects.

1.4.3.6. Antiparasitic

A. saligna, rich in phenolic and flavonoid compounds, has been believed to control the activity of parasites such as ticks. A study ²¹⁸ documented that the EtOH extract of the leaves contains a high level of condensed and hydrolysable tannin as well as derivatives of benzoic acid, cinnamic acid, flavonoids, phenolic esters, and coumarin, which might be responsible for antiparasitic activity. Furthermore, the acaricidal bioassay against *Rhipicephalus annulatus* Say indicated that the extract inhibited the catalytic activity of glutathione S-transferases of the hematophageal ectoparasites ²¹⁸. Consequently, the risk of drug resistance by the ticks against acaricide can be minimised.

1.4.3.7. Allelopathic

The allelopathy characteristics of *A. saligna* contribute to its invasive nature ²³². Methanolic extracts of the flowers and leaves can inhibit the germination of *Hordeum murinum* ²³³. Bioactive compounds contributing to such action include terpenes, tannins, flavonoids, and phenolics allelochemicals. Furthermore, various essential oils have been extracted from the flowers, leaves, and pods, which can restrict seed germination and the growth of lettuce (*Lactuca sativa* L.) ¹⁹². The major allelochemical component analysed by GC-MS was dodecanoic acid.

1.4.3.8. Cytotoxicity

Some *in vitro* studies revealed the cytotoxic activity of the plant and phytochemicals on cancer cell lines. Gedara and Galala ¹⁹⁶ reported that a spirostane saponin, erythrodiol, and flavonoid series in the MeOH extract of the leaves inhibited the development of liver cancer line HEPG2 cells. This study showed that the anticancer activity of myricitrin **11** was stronger than quercitrin **4** and myricetin-3-O-rhamnoside (C⁷-O-C⁷) myricetin-3-O-rhamnoside **33**. The finding supported the structure-activity relationships (SAR) observation that less OH in ring B and the bulky group at C-7 decreased the cytotoxicity ²³⁴. MeOH leaf extract containing quercitrin **4**, rutin **6**, miquelianin **7**, isoquercetin **8**, hyperoside **9**, and *p*-coumaric acid **37** also

induced apoptosis in several cancer cell lines, such as HT-29, HeLa, MCF-7, HEK-293, and Jurkat ²¹⁶. Chang et al. ²³⁵ and Touil et al. ²³⁶ highlighted the important features of the structure of flavonoids in cytotoxic activities. These are (i) the C2=C3 double bond, (ii) the appropriate number and position of OH, 3-OH, and (iii) 3',4'-*ortho*-hydroxylation of ring B.

1.4.3.9. Other bioactivities

A publication from Ghribia and co-workers ¹⁸⁸ suggested the anti-acetylcholinesterase effects of three different extracts of flowers, i.e., dichloromethane, EtOAc, and butanol extract, due to its unique phytoconstituent, isosalipurposide. Isosalipurposide has been reported as a cholinesterase enzyme inhibitor through intermolecular interactions between enzyme active sites and the major functional groups. For instance, π - π interaction and hydrogen bindings have been formed due to the lipophilic aromatic rings A and B and the carbonyl group, respectively ²³⁷. Moreover, hydroxyls at C7 of ring A and C4' of ring B also contributed to the inhibitory properties ²³⁸.

Apart from the bioactivities mentioned above, which are beneficial for human health, *A. saligna* has also been recognised to exert a beneficial impact on ruminants. For example, aqueous extracts of flowers, leaves, and stems have prevented acidosis and microbial fermentation of ruminant feeds ²³⁹. Furthermore, the foliage of this species applied for forage demonstrated an antinematode effect by significantly reducing faecal egg count in a study with Barbarine lambs ²⁴⁰, attributed to tannins. A study on rabbits fed by *A. saligna* phyllode showed that the *Acacia* supplementation has increased reproductive parameters, such as total sperm output, sperm motility, and total functional sperm fraction ²⁴¹. In addition, due to the decreased level of thiobarbituric acid-reactive substances (TBARS) and the increased activity of glutathione S-transferase, the improved reproduction performance was also in line with the protecting action of phytochemicals of the leaves to the sperms from toxic by-products of peroxidation of unsaturated fatty acids ²⁴¹.

1.4.4. Other applications of *Acacia saligna*

1.4.4.1. Fodder

Livestock farmers in arid and semiarid areas have struggled with feedstock deficit during the autumn and summer, whereas *A. saligna* grows well in all seasons in such dry environments. Following this situation, the species has been utilised as either a sole or combined source of fodder ²⁴². *A. saligna* has a good nutrition content

to meet the demand for elementary substances for ruminants ²⁴³. On the other hand, McDonald et al. ¹⁹⁹ reported that the nutritional value of *Acacias* seems to be lower than expected when they grow in drought lands. Applying *A. saligna* as supplementary fodder is preferable ^{244, 245} since the high tannin content has been associated with unfavourable impacts on the animal, such as weight loss, when applied as the sole fodder ^{246, 247}. In contrast, when *Acacia* foliage was supplied to the goats, tannins were linked to the protective effect against protein degradation by catalytic enzymes in the rumen ²⁴⁸. As a result, the level of post-ruminal amino acids was higher, improving the growth of the life stock.

1.4.4.2. Food source

Seeds of *A. saligna* have been a food source for humans documented in recent years. The plant produces edible seeds (with >30% content rich in protein and soluble carbohydrate ^{249, 250}) consumed by indigenous Australians ^{251, 252} and Tigrayan people in Ethiopia ²⁵³. Moreover, study ²⁵⁴ also showed a high level of lipids (10% of dried weight), carotenoids, tocopherols, and sterols in the seeds. The methods for processing the seeds for food consumption were soaking, boiling, and roasting to eliminate toxic substances ²⁴⁹. For example, a toxic amino acid called djenkolic acid has been identified in *Acacia* seeds, including *A. saligna*, with 1.9% bioactive chemicals interfering with gut nutrient digestion to protect against predators ²⁵⁵. Roasting the seeds is the best way to reduce such content to a negligible concentration and increase phenolic compounds ^{249, 250, 256}. Furthermore, the seeds have also been considered a source of ω 6 fatty acids. A report from Youzbachi et al. ²²⁹ uncovered the high level of principal fatty acids, including linoleic (61–65%), oleic (20–23%) and palmitic acids (9–10%) in the seeds.

1.5. Research aim

This work investigated the biological activities and mechanism of actions of extracts and isolated compounds from Australian *A. saligna* (Labill.) H.L.Wendl. subs. *saligna* (flowers, leaves, and bark) against common causes of T2DM.

1.6. Research objectives

The objectives of this study were:

- 1.6.1. To determine the active extracts from the flowers, leaves, and barks of *A. saligna* (Labill.) H.L.Wendl. using the free radicals scavenging assay, α -glucosidase inhibition assay, and 3T3-L1 adipocytes, an *in vitro* model of white adipose tissue.

- 1.6.2. To isolate and elucidate the structure of bioactive compounds from the identified biologically active crude extracts through spectroscopic methods.
- 1.6.3. To determine the possible pathway involved in the cellular glucose uptake in the 3T3-L1 adipocytes treated by the active extracts and isolated compounds.
- 1.6.4. To determine the effects of *A. saligna* extracts and compounds on the mitochondrial function in 3T3-L1 adipocytes.

CHAPTER 2: RESULT AND DISCUSSION OF EXTRACTION AND BIOACTIVITIES OF EXTRACTS

2.1. Introduction of Chapter 2

This chapter aims to discuss the outcomes of plant extraction, including the yield, phenolic and flavonoid content and identified phytochemicals in the extracts using a GCMS analysis. Enormous aspects, including sample preparation, the polarity of solvents, the ratio of sample and solvent, the type of extraction, temperature, the chemical nature of the desired compounds, and the interfering substances, strongly influence the acquired bioactive phytochemicals^{257, 258}. Among them, selecting the proper solvent for extraction is most likely the main factor in the effectiveness of desired bioactive compound isolation with solvent extraction²⁵⁹. For instance, hexane and acetone are common solvents to extract aliphatic groups, fatty acid, terpene, and steroid derivatives, while ethanol and methanol are effective for extracting phenolic, flavonoid, and polyol derivatives²⁶⁰. A single type of solvent is usually used for solvent extraction of plants using various traditional methods such as maceration, percolation, reflux, or soxhlation, followed by solvent fractionation. However, this approach may result in extracts with complex extracted compounds that require more plant materials, time, and solvents for purification. Hence, sequential extraction or liquid-liquid partitioning can be alternative to selectively separate polarity-based compounds at the first stage of the process. As a result, the obtained extract can be less complex as compounds have been pooled into the same polarity with solvents. This approach generally starts with a less polar solvent, such as hexane, to remove lipophilic groups, followed by higher polarity to extract phenolics, flavonoids, and polar non-phenolic compounds.

A bioassay-guided separation can be applied to achieve the efficiency and effectivity of the isolation of possibly active compounds. *In vitro* assays are believed to be faster, inexpensive, and less complicated than the *in vivo* screening of active compounds²⁶¹. The antioxidant assay is an appropriate method to meet the specificity, simplicity, and efficiency of the purification²⁶². Moreover, as mentioned in the previous chapter, oxidative stress has been commonly linked to T2DM. Being obese and consuming a diet high in fat and glucose can induce the development of T2DM due to the overproduction of ROS. ROS can cause spontaneous reactions *via* transferring an electron or a hydrogen atom from other molecules to compensate for the electron deficiency²⁶³. Indeed, previous studies have shown that compounds with antioxidant activity can improve glycaemic control in animal models of T2DM¹⁰⁷. Furthermore, antioxidant and α -glucosidase inhibition assays-based fractionation

may help select the most promising extracts for further developing antidiabetic compounds from *A. saligna*. As part of this research project, we aimed to use these methods to screen the antioxidant potential of *A. saligna* extracts using vitamin C as the positive control ²⁶⁴⁻²⁶⁷.

As the main source of energy for human activities, recommended 40–70% of energy intake, dietary carbohydrates such as cereal grains, bread, and potatoes, comprise starch (60%), sucrose (20–30%), and maltose (10%) ²⁶⁸. Enzymes must hydrolyse such complex carbohydrates into monosaccharides before their absorption into the blood. One endogenous enzyme involved in carbohydrate breakdown is α -glucosidase, classified into maltase-glucoamylase (MGAM) and sucrose-isomaltase (SI) ²⁶⁹. Both enzymes consist of N-terminal (Nt-MGAM and Nt-SI) and C-terminal (Ct-MGAM and Ct-SI) catalytic sites ²⁷⁰.

One primary target for managing T2DM is α -glucosidase, as the enzyme inhibition has been associated with a 36% decrease in T2DM progression and a 34% and 49% risk reduction in hypertension and cardiovascular events, respectively ²⁷¹. Such enzymes consist of N-terminal and C-terminal catalytic sites ²⁷⁰ that cleave polysaccharides following glycosylation and hydrolysis. However, flavonoids have been evidenced to neutralise the active sites *via* hydrogen bindings by suggested groups, namely hydroxyls at C-3, -5, -7, and -8, -4', and 5' and carbonyl oxygen at C-4 ^{161, 272}. Moreover, double bonds of C2=C3 and C α =C β for chalcone have been recognised to stabilise the link between rings A and B and form a near-planar structure that supports the compounds to quickly enter the enzyme's hydrophobic pockets ^{161, 273}. As *A. saligna* is the source of such phytochemicals, and thus we also aimed to explore if any bioactive extract from *A. saligna* can exert an inhibition against a yeast α -glucosidase activity.

2.2. Sequential extraction of flowers, leaves, and barks

Twelve extracts were obtained from the sequential extraction of flowers, leaves, and bark of *A. saligna* with varied yields. Dried flowers were sequentially extracted through a four-step extraction followed by *in vacuo* solvent evaporation to give the following extracts: hexane extract of flowers (FL-hex) (1.71 g), dichloromethane extract of flowers (FL-DCM) (1.79 g), methanol extract of flowers (FL-MeOH) (26.17 g) and aqueous extract of flowers (FL-H₂O) (36.31 g). The FL-hex and FL-DCM are sticky yellow gums, while FL-MeOH and FL-H₂O are yellow powder. The dried leaves were sequentially extracted to give hexane extract of leaves (LF-hex) (3.08 g), dichloromethane extract of leaves (LF-DCM) (4.98 g), methanol extract

of leaves (LF-MeOH) (25.37 g) and aqueous extract of leaves (LF-H₂O) (13.32 g) after evaporation. The extracts appeared like flower extracts. The dried bark was also sequentially extracted to give hexane extract of bark (BK-hex) (0.68 g), dichloromethane extract of bark (BK-DCM) (2.12 g), methanol extract of bark (BK-MeOH) (18.26 g) and aqueous extract of bark (BK-H₂O) (4.34 g). Even though both BK-hex and BK-DCM are brown solids, different from the less polar-soluble extracts from the previous parts, the appearance of BK-MeOH and BK-H₂O is the same, brown powder. All extracts were stored in a -20°C freezer before further use.

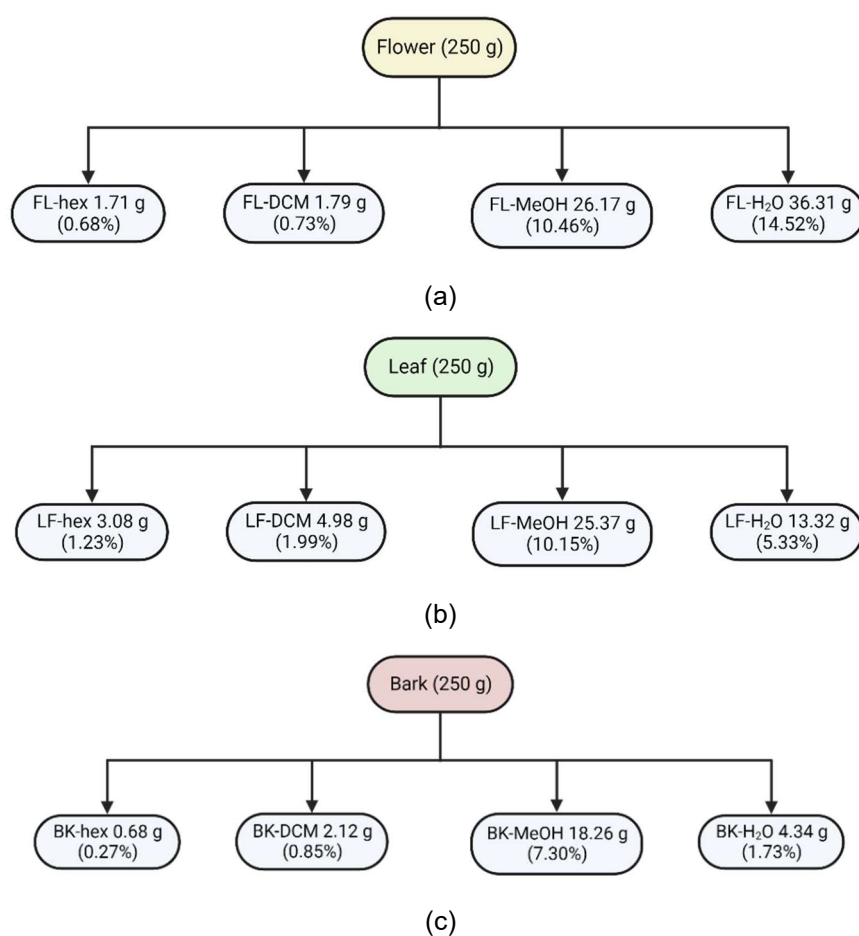


Figure 16. Schematic diagrams of the outcomes of extraction of (a) flowers, (b) leaves, and (c) bark.

Figure 17 shows that more polar solvents gave higher yields than those with less polarity. The same finding was confirmed by Missio et al.²⁷⁴ by extracting *A. mearnsii* using *n*-hexane, ethyl acetate (EtOAc), pentanol, propanol, and MeOH. The research reported that flavonoids, tannins, and saccharides were the major components of the polar extracts. Our phenolic and flavonoid content evaluation quantified compound groups in the MeOH extracts with higher estimations than those

in the hexane, dichloromethane, and water extracts. Furthermore, the GCMS analysis also indicated more extracted polar ingredients (e.g., hydroxy and amine groups) in the MeOH and aqueous extracts. Some of them are derivatives of the primary metabolites. According to Enev et al. ²⁷⁵, solvents with a higher polarity have been thought to disrupt intermolecular interactions within the matrix compounds to create a strong hydrogen bonding to the desired phytochemicals. This process allows the solvent to withdraw the target compounds from the plant tissues.

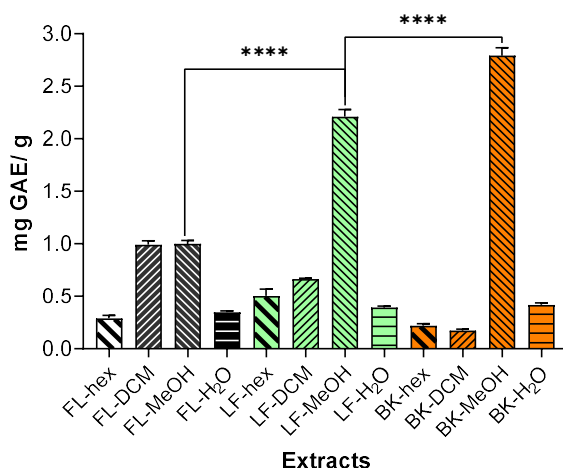
2.3. Phenolic content and flavonoid content of the extracts

The phenolic and flavonoid contents were estimated using a spectrophotometric method expressed in gallic acid equivalent (GAE) and quercetin equivalent (QE), respectively. Table 6 and Figure 17 show that all methanolic extracts have a higher estimated phenolic and flavonoid content in each part extract. This finding may support the report ²³³ that MeOH extract of Egyptian *A. saligna* flowers and leaves possessed a greater allelopathic property than non-alcoholic extract. When compared within the methanolic group, the estimated phenolic and flavonoid content can be expressed in a trend of increasing values order as FL-MeOH < LF-MeOH < BK-MeOH.

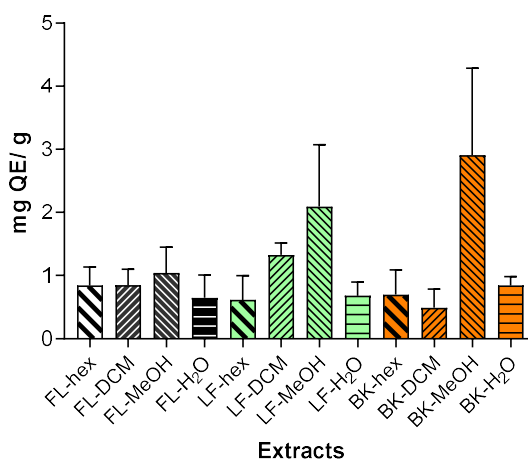
Table 6. Quantified phenolic and flavonoid content of *A. saligna* extracts estimated using spectrophotometric analysis

No	Extract	Phenolic content (mg GAE/g extract)	Flavonoid content (mg QE/g extract)
1	FL-hex	0.291 ± 0.03	0.845 ± 0.29
2	FL-DCM	0.99 ± 0.04	0.850 ± 0.25
3	FL-MeOH	0.998 ± 0.03	1.04 ± 0.41
4	FL-H ₂ O	0.349 ± 0.01	0.647 ± 0.36
5	LF-hex	0.503 ± 0.06	0.615 ± 0.38
6	LF-DCM	0.663 ± 0.01	1.325 ± 0.19
7	LF-MeOH	2.211 ± 0.07	2.093 ± 0.98
8	LF-H ₂ O	0.395 ± 0.01	0.679 ± 0.22
9	BK-hex	0.220 ± 0.01	0.699 ± 0.39
10	BK-DCM	0.173 ± 0.02	0.489 ± 0.30
11	BK-MeOH	2.79 ± 0.08	2.908 ± 1.38
12	BK-H ₂ O	0.420 ± 0.02	0.844 ± 0.14

FL-hex: hexane extract of flowers, FL-DCM: dichloromethane extract of flowers, FL-MeOH: methanol extract of flowers, FL-H₂O: aqueous extract of flowers, LF-hex: hexane extract of leaves, LF-DCM: dichloromethane extract of leaves, LF-MeOH: methanol extract of leaves, LF-H₂O: aqueous extract of leaves, BK-hex: hexane extract of bark, BK-DCM: dichloromethane extract of bark, BK-MeOH: methanol extract of bark, BK-H₂O: aqueous extract of bark, GAE: gallic acid equivalent, QE: quercetin equivalent



(a)



(b)

Figure 17. Estimation of (a) phenolic content and (b) flavonoid content of *A. saligna* extracts. GAE: gallic acid equivalent, QE: quercetin equivalent, FL-hex: hexane extract of flowers, FL-DCM: dichloromethane extract of flowers, FL-MeOH: methanol extract of flowers, FL-H₂O: aqueous extract of flowers, LF-hex: hexane extract of leaves, LF-DCM: dichloromethane extract of leaves, LF-MeOH: methanol extract of leaves, LF-H₂O: aqueous extract of leaves, BK-hex: hexane extract of bark, BK-DCM: dichloromethane extract of bark, BK-MeOH: methanol extract of bark, BK-H₂O: aqueous extract of bark. Data in mean ± SEM, *****p* < 0.0001 (*n* = 3, One-way ANOVA, Tukey's post hoc).

The phenolic content of our methanolic leaves and barks extract has higher values than those reported for ethanolic extract of leaves and barks extracts of *A. saligna* in South Africa of 0.95 and 1.2 mg gallic acid equivalent (GAE)/mL, respectively¹⁹⁷. Previous studies by Gedara & Galala¹⁹⁶ and El-Toumy et al.¹⁹⁰ confirmed that *A. saligna* leaves extract from 70% aqueous methanol extraction afforded various isolated compounds of polyphenols such as two different phenolic acids, flavan-3-ol, and flavonoid derivatives. Even though there is little documentation of the flowers' quantitative phenolic and flavonoid content from other studies, *A.*

saligna flower is believed to be rich in phenolic acid, chalcone, and flavanol derivatives.

2.4. Phytochemicals screened by GCMS

Following the detected compounds in the *A. saligna* extracts using the GCMS, a selective analysis was carried out through screening phytochemicals reports to ensure the presence of the volatile compounds in the plant. In brief, various phytochemical groups have been found in the samples. For instance, volatile molecules, including the derivatives of alkane, alkene, aldehyde, ether, and fatty acid, were predominantly observed in the FL-hex and LF-hex extract. Furthermore, terpenoid derivatives were found in the DCM extracts of flowers and leaves. On the other hand, more polar groups were detected in the methanolic and water extracts of all three parts of the plant. They were members of the carboxylic acid, sugar, polyol, amino acid, peptide, and heteroatom ring group.

Hexane has been reported as an effective solvent to extract long-chain carbon compounds, such as hydrocarbons, oxygenated long-chain hydrocarbon, terpenoid, and fatty acids^{276, 277}. Many long-chain carbon compounds were also identified from the FL-, LF-, and BK-hexane extracts. For instance, saturated and unsaturated hydrocarbons were present in the extracts, along with carboxylic acid derivatives, in trace levels between 0.01% and 0.46%. Two terpene derivatives, α - and β -amyrin, were detected in our DCM extract of the flowers at a very low level of 0.43 and 0.68%, respectively. Moreover, broader levels of steroids were also found in the DCM extracts of the plant, from 0.83% to 4.96%. Allelochemicals such as chondrillasterol were detected in both FL- and LF-DCM extracts, estimated for 0.83% and 4.96%, respectively. A polyol derivative, 4-C-methyl-*myo*-inositol or lamitol, was found at higher levels in the MeOH extracts. It was quantified for 6.42%, 42.74%, and 2.94% in FL-, LF-, and BK-MeOH extract, respectively. This compound was also found in LF-H₂O, with a high percentage of 18.99%. Further information on the phytochemicals analysed by the GCMS is presented in Figure S1–S3 (pages 221–223) and Tables S2–S4 (pages 226–241).

2.5. Antioxidant activity of extracts against the DPPH

Figure 18 and Table S5 (Appendix A, pages 241–242) show the dose-response DPPH scavenging activity of flowers, leaves, and bark extracts obtained in this study. All non-methanolic extracts demonstrated lower activity of free radical neutralisation, whereas the methanolic samples possessed a better scavenging property. This trend agrees with the previously reported finding that polar organic

solvent extract seemed to have better antioxidant activity due to its high polyphenols content ²⁶⁷. Our study also showed that phenolic and flavonoid content was higher in the methanolic extracts. The BK-MeOH extract has the highest antioxidant activity with IC₅₀ of 94.24 ± 19.89 µg/mL, followed by LF-MeOH (IC₅₀ = 190.1 ± 59.15 µg/mL) and FL-MeOH (IC₅₀ = 331.5 ± 17.21 µg/mL). Compared to vitamin C (49.97 ± 10.76 µg/mL), the decreasing order of DPPH scavenging potency among the methanolic extracts is MeOH-bark > MeOH-leaf > MeOH-flower.

Using a similar DPPH method, the crude ethyl acetate extract from flowers of *A. saligna* collected in Tunisia was shown to have an IC₅₀ of 67 µg/mL ²⁷⁸, while the water flower extract from Egyptian species showed poor activity with an IC₅₀ of 461.7 µg/mL ²²⁸. Elansary et al. ²⁷⁹ showed that their crude methanolic extract of leaves collected in Saudi Arabia has a potent antioxidant activity with an IC₅₀ of 17 µg/mL. The crude methanolic extract from barks collected in Egypt was reported ²⁸⁰ to have an IC₅₀ of 10.1 µg/mL. The variation in activities may mainly be attributed to each extract's different chemical compositions affected by the growing conditions ²⁸¹ and methods of extraction and assay.

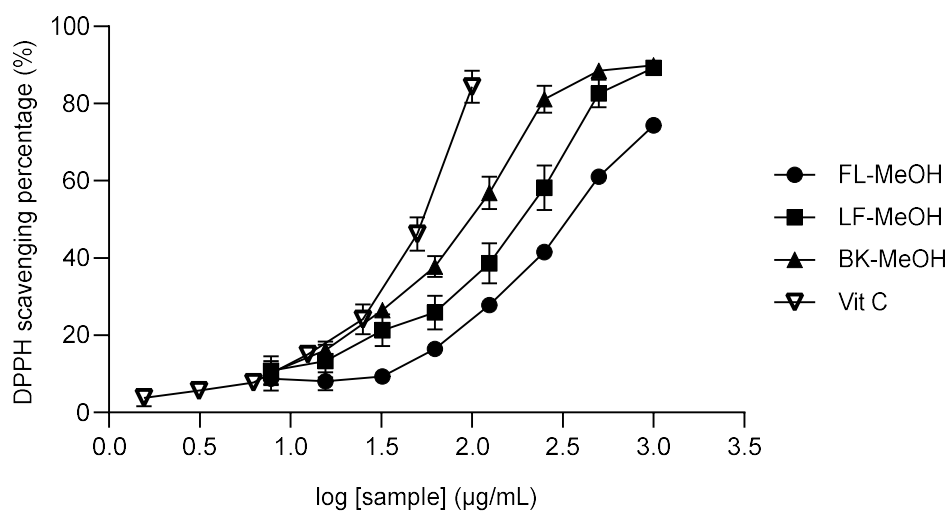


Figure 18. The dose-response curve of the active methanolic extract of flowers, leaves, and barks and vitamin C against radical DPPH. Data in mean ± SEM, n= 3.

2.6. Antioxidant activity of extracts against the ABTS^{•+}

Table S7 (pages 242–243) shows the dose-response ABTS^{•+} scavenging activity of all extracts, and Figure 19 displays the dose-response curves of ABTS^{•+} scavenging capacity for all alcoholic extracts. Similar to the DPPH scavenging assay, the trend of antioxidant activity in this ABTS^{•+} radical decolourisation assay indicates

that all methanolic extracts exert higher potential than their counterparts. It is not surprising because methanol has been considered a highly effective solvent for extracting phenolic compounds with antioxidant properties. According to Figure 20, the decreasing trend of antioxidant order of the alcoholic extracts can be expressed as MeOH-bark > MeOH-leaf > MeOH-flower. Interestingly, the activity of the methanolic extract of the bark was slightly higher than the ascorbic acid, whereas its IC₅₀ value appears higher compared to the methanolic extract of bark of *A. seyal*, i.e. 27 µg/mL²⁸². This outcome suggests that the methanolic extracts could neutralise both free radicals. As Litwinienko & Ingold²⁸² and Foti et al.²⁸³ proposed, active extracts dissolved in alcoholic solvent could follow sequential proton loss electron transfer (SPLET) as the solvent may partially ionise the compounds.

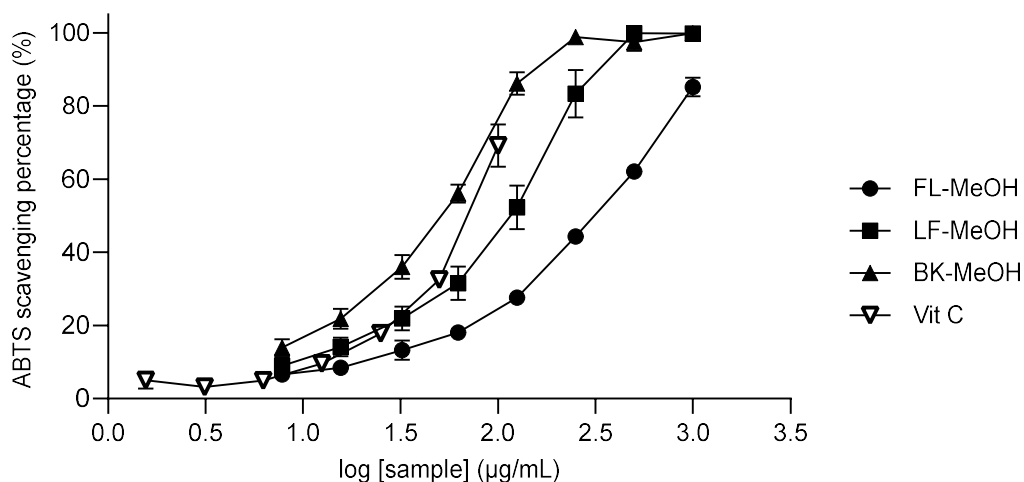


Figure 19. The dose-response curve of the active methanolic extract of flowers, leaves, and barks and vitamin C against ABTS cation radicals, Data in mean ± SEM, $n = 3$.

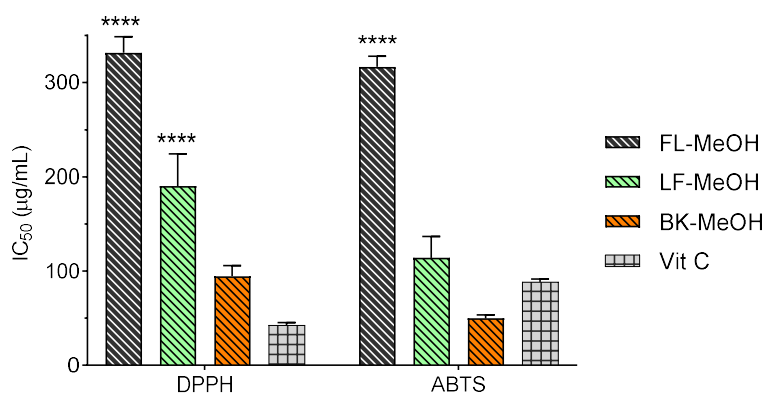


Figure 20. Comparison of antioxidant activity in IC₅₀ between methanolic flower, leaf, and bark extract of *A. saligna* and vitamin C in DPPH and ABTS^{••} scavenging assay. Data in mean ± SEM, **** $p < 0.0001$, vs vitamin C ($n = 3$, One-way ANOVA, Tukey's post hoc).

2.7. Inhibitory activity against α -glucosidase

This assay screened the potentially active α -glucosidase inhibitor found in *A. saligna*. In a recent report, Buttner et al.¹⁹⁷ presented the excellent inhibitory properties of EtOH extract of South African *A. saligna* leaves and bark, indicating the presence of active inhibitors in the species. They have correlated the activities with the high content of phenolic compounds¹⁹⁷. Moreover, the study suggested further investigation to isolate and identify the responsible compounds with the activity since there has been a gap in information regarding active compounds from this species.

Tables S9–S15 (pages 243–244) present the observed dose-response inhibition of the plant extracts and the positive control acarbose against the yeast α -glucosidase enzyme. Both hexane extracts from leaves and bark possessed similar IC_{50} values ($IC_{50} = 285.5 \pm 100.9$ and 289.9 ± 29.17 $\mu\text{g/mL}$, respectively) with the positive control, acarbose ($IC_{50} = 254 \pm 22.18$ $\mu\text{g/mL}$). The GCMS analysis could not detect potentially active phytochemicals from these two extracts. In addition, BK-H₂O extract exerted a potent inhibition by IC_{50} of 23.27 ± 3.88 or a nine-fold change more active than the positive control. However, its ¹H NMR spectrum revealed that the aqueous bark extract predominantly contained sucrose. Sucrose is a natural substrate of α -glucosidase to be hydrolysed into glucose and fructose²⁸³. This may interfere with the absorbance reading of the test substrate, 4-nitrophenyl α -D-glucopyranoside, leading to a false-lowered chromophore absorbance. Therefore, further separation was not conducted on the extract.

Many groups working on crude extracts have highlighted the proportional relationship between the quantified total phenolic and flavonoid contents and the inhibitory activity. These compounds can inactivate the enzyme due to the formation of non-covalent bindings such as hydrogen bonding, salt bridge interactions, cation- π interactions, or electrostatic forces²⁸⁴. However, Wu and Xu²⁸⁵ pointed out that these compound groups are not the only ones responsible for the activities. Other classes, such as terpenes, alkaloids, or even saccharide derivatives, can also contribute to the activities of plant crude extracts.

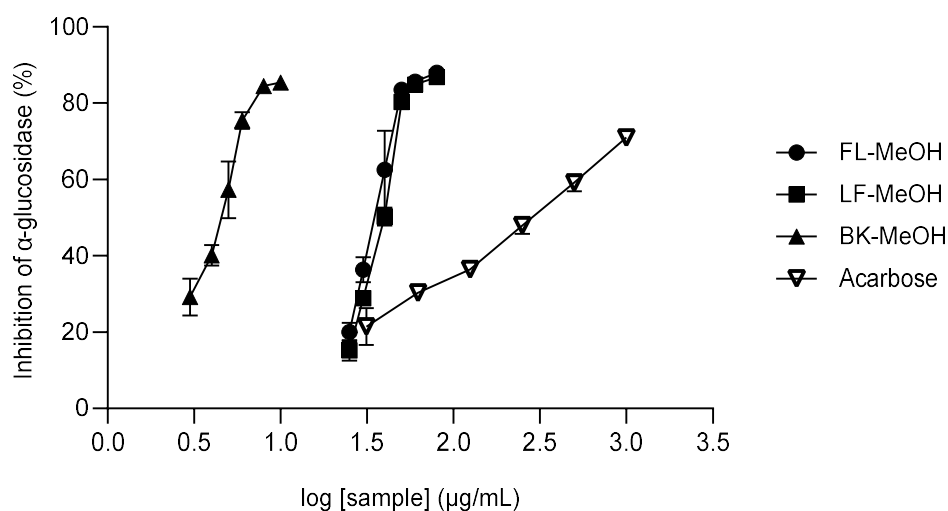


Figure 21. The dose-response curve of the active methanolic extract of flowers (FL-MeOH), leaves (LF-MeOH), and barks (BK-MeOH), and acarbose against the yeast α -glucosidase enzyme. Data in mean \pm SEM, $n = 3$.

All methanolic extracts demonstrated better activities than the other extracts of each plant part. The GCMS analysis showed the presence of a reported inhibitor of the enzyme, *trans*-cinnamic acid^{286, 287}, in all the alcoholic extracts. Upon analysis, it is evident that the BK-MeOH extract exhibits greater inhibitory activity against the yeast α -glucosidase enzyme. Its IC_{50} value of 4.37 ± 0.24 μ g/mL surpasses the other two alcoholic extracts by over eight-fold. According to the phenolic and flavonoid content quantification, BK-MeOH has the highest estimated values of phenolic and flavonoid content. This finding aligned with those reported for the ethanolic barks extract of South African *A. saligna* with the highest inhibition and phenolic content by Buttner et al.¹⁹⁷. These results are consistent with those of Subhan¹⁷³ and Gulati¹⁷² reported that alcoholic extracts from Australian *Acacias* were active against the enzyme.

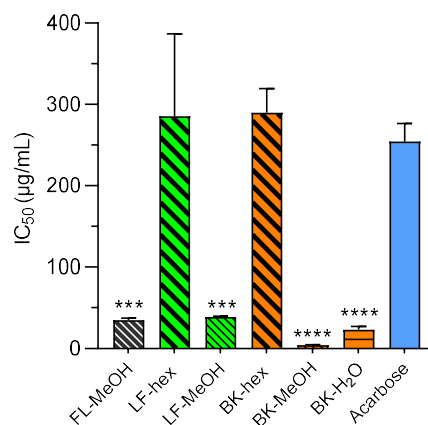


Figure 22. IC₅₀ of active extracts and acarbose against the yeast α -glucosidase enzyme. Data in mean \pm SEM, *** p = 0.0004; **** p < 0.0001, vs acarbose (n = 3, One-way ANOVA, Tukey's post hoc).

2.8. Conclusion of Chapter 2

This study showed that more extract yield was obtained from a higher polarity solvent, such as methanol, in the sequential extraction of flowers, leaves, and bark of *A. saligna*. The methanolic extracts had higher estimated phenolic and flavonoid contents than other extracts. Further screening of compounds using GCMS analysis grouped detected compounds into two groups: long-chain hydrocarbon and terpene derivatives, found in hexane and DCM extracts and electronegative group-rich compounds detected in MeOH and aqueous extracts. The *in vitro* assays of antioxidant and α -glucosidase inhibition demonstrated the positive effects of all MeOH extracts in scavenging DPPH and ABTS^{•+} radicals and inhibiting the α -glucosidase enzyme. Thus, the methanolic extracts have been selected for further separation to isolate the active compounds.

CHAPTER 3: RESULT OF CELL-BASED STUDIES OF EXTRACTS

3.1. Introduction of Chapter 3

Chapter 3 presents an *in vitro* study using 3T3-L1 adipocytes treated with crude extracts. The intracellular ROS production was detected by dichlorodihydrofluorescein diacetate (DCFH-DA), a ROS-sensitive reagent. It has widely been applied to detect oxidative stress in cellular models due to its simplicity, high sensitivity of changes in cellular redox state, and low cost ²⁸⁸. Cellular ROS will rapidly oxidise H₂DCF to a fluorescent product of dichlorofluorescein (DCF) that can be observed using a fluorescent spectrophotometer. The measured fluorescent intensity is directly proportional to the number of ROS formed ²⁸⁹.

The 2-deoxy-2-[(7-nitro-2,1,3-benzoxadiazol-4-yl) amino]-D-glucose (2-NBDG) was then used to evaluate the real-time glucose uptake into the cytosol of 3T3-L1 adipocytes as it has a remarkable similarity of the cellular transport properties to those of glucose ^{290, 291}. This fluorescent tracer, reported as a suitable substrate for glucose transporters (GLUTs) ²⁹², enters cells and is trapped in the inner space of the cells after phosphorylation by hexokinase ²⁹³. Therefore, the fluorescent emission intensity of the detected tracer in the intracellular space can reflect the concentration of transported 2-NBDG.

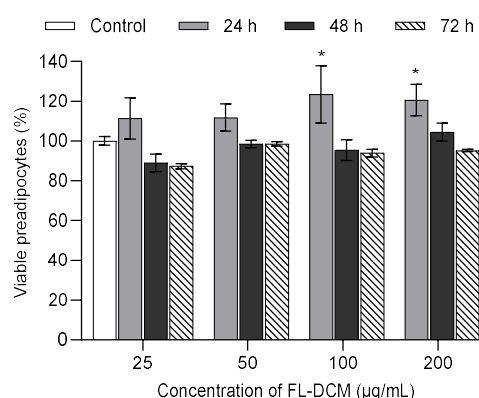
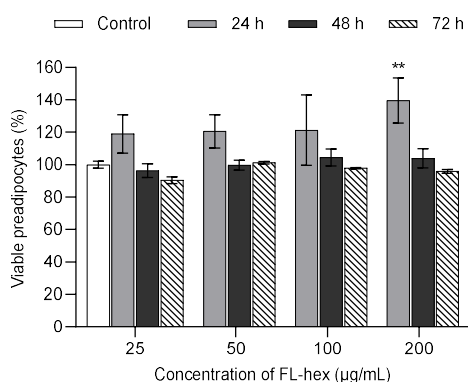
The adipocytes-based study on the extracts aims to screen the suitable active extracts from the flowers, leaves, and bark of *A. saligna* as the inhibitor of cellular ROS production and modulator of cellular glucose uptake. The information from this section is also important to justify the potential extract for the next fractionation step for compound isolation.

3.2. Viability of 3T3-L1 preadipocytes treated with extracts

Our literature search found that active extract and compounds as antioxidants ²⁹⁴ and anti-obesity ²⁹⁵ tend to exert an inhibitory property on the dividing growth of pre-confluent 3T3-L1 preadipocytes. To examine the impact of extracts on the proliferation of the pre-adipose cells, an MTT (3-(4,5-dimethylthiazolyl-2)-2,5-diphenyltetrazolium bromide) was conducted on the fibroblast-like cells exposed to all extracts in three different incubation times. The assay is based on the reduction of the MTT tetrazolium (yellow) to (*E,Z*)-5-(4,5-dimethylthiazol-2-yl)1,3-diphenylformazan (purple) by cellular oxidoreductase enzymes such as NAD(P)H-dependent. This conversion is only generated by viable cells with an active metabolism, while dead cells lose this ability. Therefore, the appeared purple colour can represent cell viability.

Figure 23 and the detailed data in Table S16 (Appendix A, page 245) showed no toxic effect from flower extracts after the treatment and incubation for 24, 48, and 72 h. Cell viability was above 70% at the highest tested concentration. Figure 24 and Table S17 (Appendix A, page 245) show that all non-methanolic did not inhibit cell growth within the tested concentration range for leaf extracts. However, the LF-MeOH extract exhibited anti-proliferative activity as the number of viable cells was below 70 % at 50 (for 72 h incubation only), 100 (except 24 h) and 200 $\mu\text{g}/\text{mL}$. The same results were documented for BK-MeOH, which had a toxic effect starting at a concentration of 50 $\mu\text{g}/\text{mL}$ (except for 24 h of incubation).

Interestingly, fewer viable cells were observed for the treatment with 200 $\mu\text{g}/\text{mL}$ of the water extract of the bark. However, all bark hexane and DCM extracts were non-toxic for the preadipocytes. The same trend was found in similar research by Lin et al.²⁹⁶, highlighting the toxicity of the EtOAc extract against the preadipocytes compared to the non-toxic effect of less polar-soluble hexane extract. They revealed higher content of phenolic compounds and flavonoids in the EtOAc-soluble extract. Among methanolic extracts, FL-MeOH treatment for up to 200 $\mu\text{g}/\text{mL}$ at all exposure times showed a harmless effect of the growth of fibroblast-like 3T3-L1 cells, whereas LF-MeOH and BK-MeOH treatment displayed toxicity in a time- and dose-dependent manner.



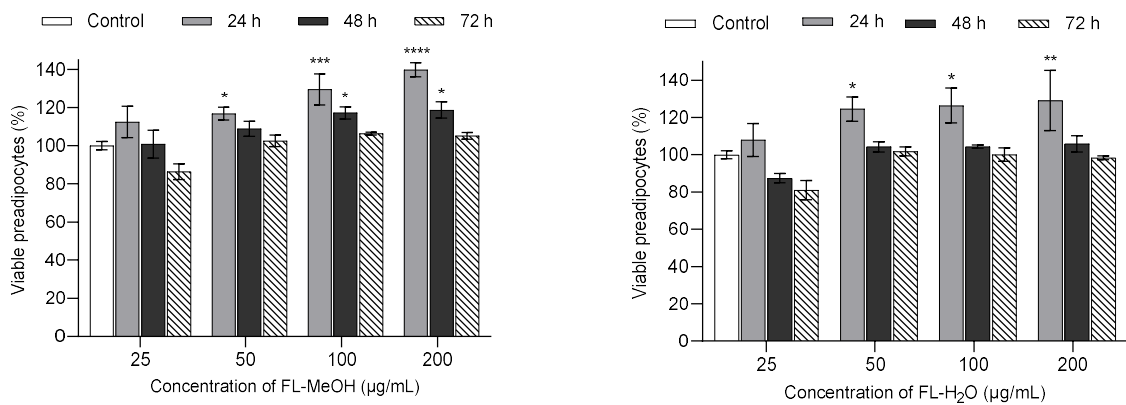


Figure 23. Viability of 3T3-L1 preadipocytes treated with FL extracts. FL-hex: hexane extract of flowers, FL-DCM: dichloromethane extract of flowers, FL-MeOH: methanol extract of flowers, FL-H₂O: aqueous extract of flowers. Data in mean \pm SEM, * p = 0.04; ** p = 0.004; *** p = 0.0001; **** p < 0.0001, vs vehicle control (n = 3, One-way ANOVA, Dunnett's post hoc).

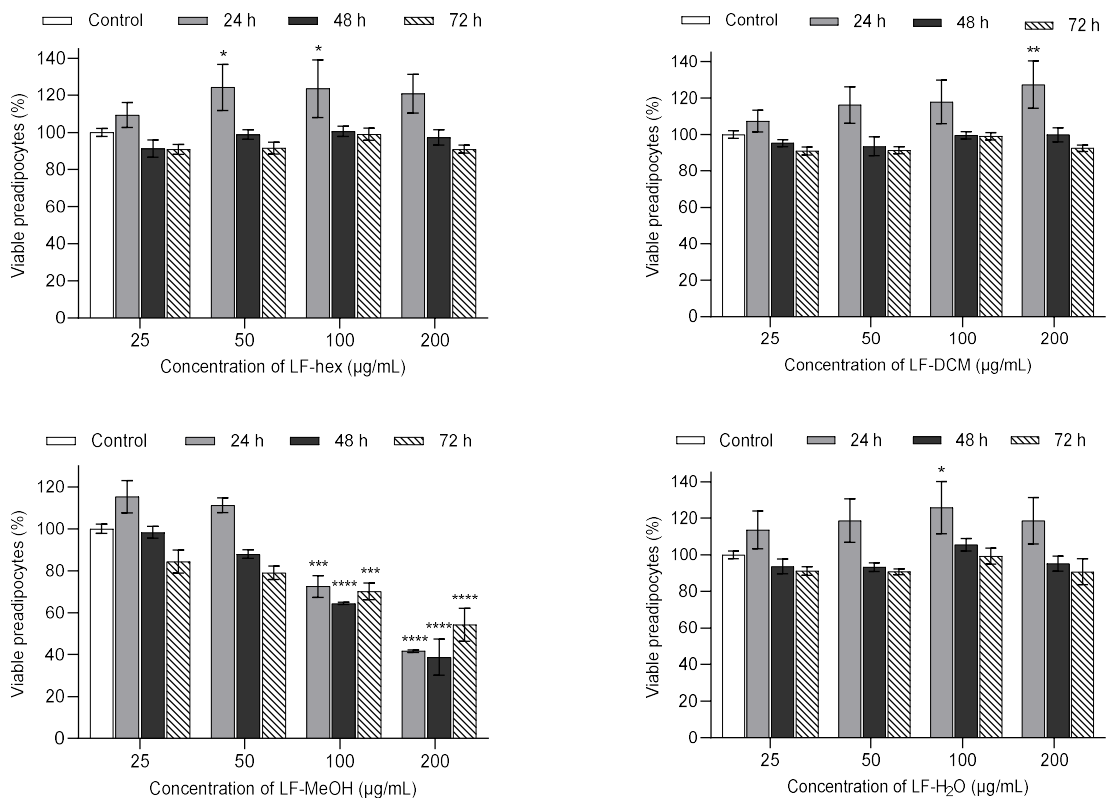


Figure 24. Viability of 3T3-L1 preadipocytes treated with LF extracts. LF-hex: hexane extract of leaves, LF-DCM: dichloromethane extract of leaves, LF-MeOH: methanol extract of leaves, LF-H₂O: aqueous leaves extract. Data in mean \pm SEM, * p = 0.03; ** p = 0.006; *** p = 0.0004; **** p < 0.0001, vs vehicle control (n = 3, One-way ANOVA, Dunnett's post hoc).

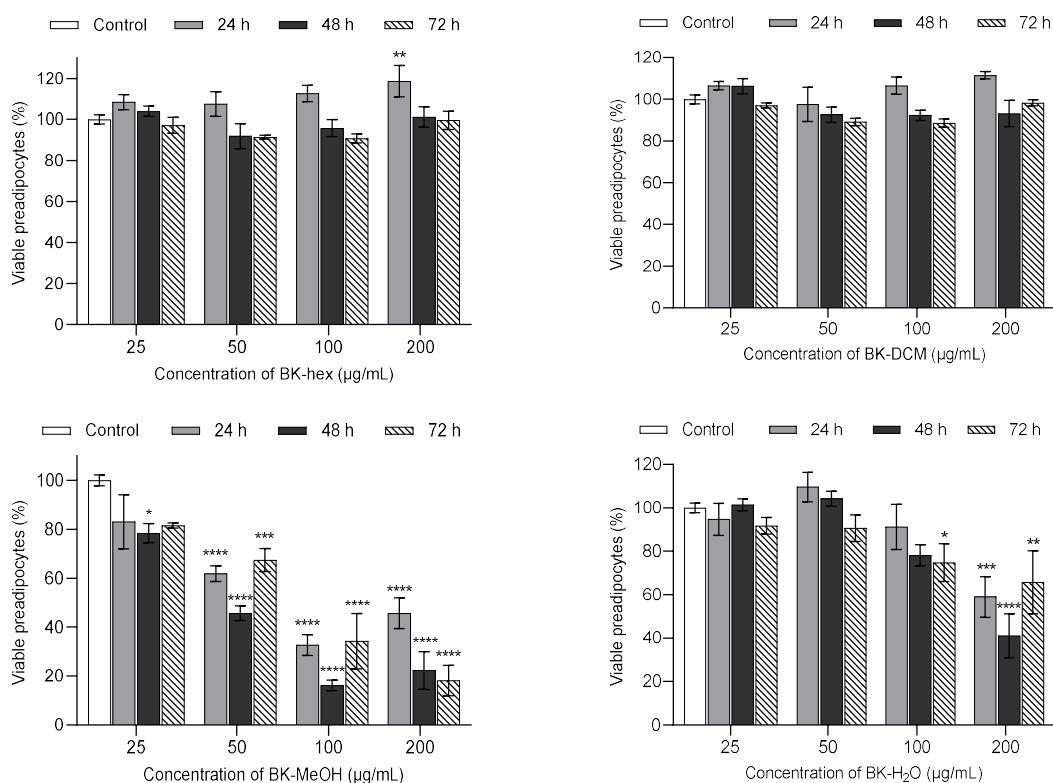


Figure 25. Viability of 3T3-L1 preadipocytes treated with BK extracts. BK-hex: hexane extract of bark, BK-DCM: dichloromethane extract of bark, BK-MeOH: methanol extract of bark, BK-H₂O: aqueous extract of bark. Data in mean \pm SEM, * p = 0.03; ** p = 0.008; *** p = 0.0007; **** p < 0.0001, vs vehicle control (n = 3, One-way ANOVA, Dunnett's post hoc).

3.3. Cell differentiation

The progression of the differentiation experiment of this study is illustrated in Figure 27. The pre-adipose 3T3-L1 cells were grown in 96-well plates to achieve a confluent or growth-arrested state, followed by differentiation induction with a medium of differentiation induction (MDI) (set as day 0). It is important to note that fibroblast conversion into adipocytes occurs only after the cells have reached confluency¹²⁴. Instead of adipose conversion, treatment with MDI in the dividing stage will affect the proliferation of pre-confluent cells through signal transducer and activator of transcription 3 (STAT3) induction activator. On the second day, the first phase of differentiation, clonal expansion¹²⁰, was observed by the appearance of a small number and size of cytoplasmic lipid droplets. Madsen et al.²⁹⁷ suggested the vital role of lipoxygenases in activating peroxisome proliferator-activated receptors (PPAR γ) in this stage. Antiadipogenic activity by many natural products was observed from the treatment in this early stage by decreasing the expression of CCAAT/enhancer-binding protein- α (C/EBP- α), PPAR γ ²⁹⁸, and fatty acid synthetase (FAS)²⁹⁹. As the intermediate stage, this phase continued for the following 48 h (day-

2 to day-4). After day 4, the rate activity of FAS enzymes was reported to be declined to achieve a plateau on day 6³⁰⁰.

On day 6, the third phase, defined as the maturation or terminal stage, appeared characterised by some spherical lipid droplets. In this late phase, adipocyte fatty acid binding protein 2 (aP2) is the primary marker³⁰¹. Tzeng and Liu also documented downregulating aP2 and FAS expression as a practical approach to suppress adipogenesis in cells²⁹⁹. This study demonstrated the inhibitory effects on the modulation of both proteins by the treatment with 6-gingerol (5, 10, and 15 µg/mL) at day 8. The complete maturation phase was achieved on day-8 as the rounded lipid droplets covered most spaces. The mature adipocytes are marked by their altered morphological appearance, such as bigger size, rounded, and filled with abundant lipid droplets³⁰², whereas MDI-untreated cells retain their native fibroblast form. Synthesis of triglycerides in the differentiated cells was reported 19.5-fold higher than those observed in undifferentiated cells³⁰⁰. According to Zebisch et al.¹¹⁸, the mature adipocytes remain unchanged for at least four days. Any bioassay between day-8 and day-12 can generate a reliable outcome.

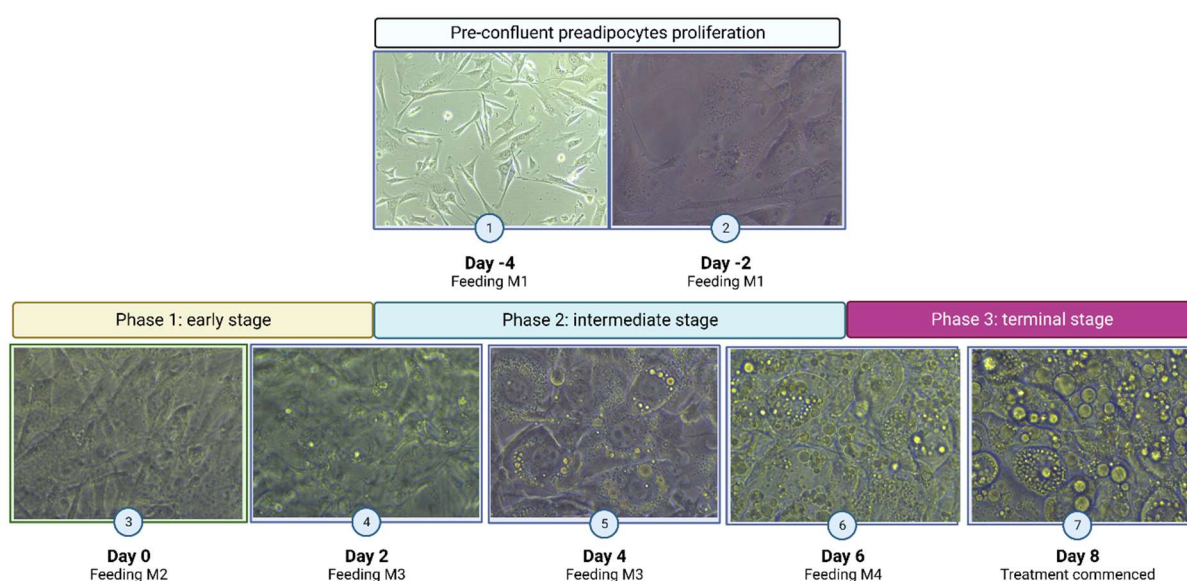


Figure 26. Images of 3T3-L1 cells differentiation showing the cell appearance in the following stages: (1 & 2) preadipocytes growth at day -4 & -2 of differentiating induction; (3) confluent cell at the day of the induction with MDI or M2 and (4) second day defined as early phase; and (5) fourth day as the intermediate; (6) sixth and (7) eighth day of the induction called terminal phase. The cell photographs were captured with an inverse phase contrast microscope (Infinity 1, Nikon Eclipse TS100) at a magnification of 20×. M1 = DMEM, BCS, and PSG; M2 = DMEM, FBS, PSG, rosiglitazone 2 µM, insulin 5 µg/mL, IBMX 0.5 mM, and dexamethasone 1 µM; M3 = DMEM, FBS, PSG, and insulin 5 µg/mL; M4 = DMEM, FBS, PSG.

3.4. Viability of 3T3-L1 adipocytes treated with extracts

Figure 27 shows the results of the MTT assay on 3T3-L1 adipocytes treated with four different flower extracts in a range of concentrations (25–200 µg/mL) for 24, 48, and 72 h. All flower extracts did not show significantly toxic effects at that range as none of the differentiated cell viability was under 80%. In the previous experiments with preadipocytes, all flower extracts were non-toxic in the same concentration range. In addition, the FL-MeOH extracts showed synergistic effects on cell growth in the MTT assay of preadipocytes. Here, the methanolic flower extracts exhibited similar effects to those demonstrated by hexane, DCM, and water extract of flowers, where the viable cell percentages were between 90 and 119%.

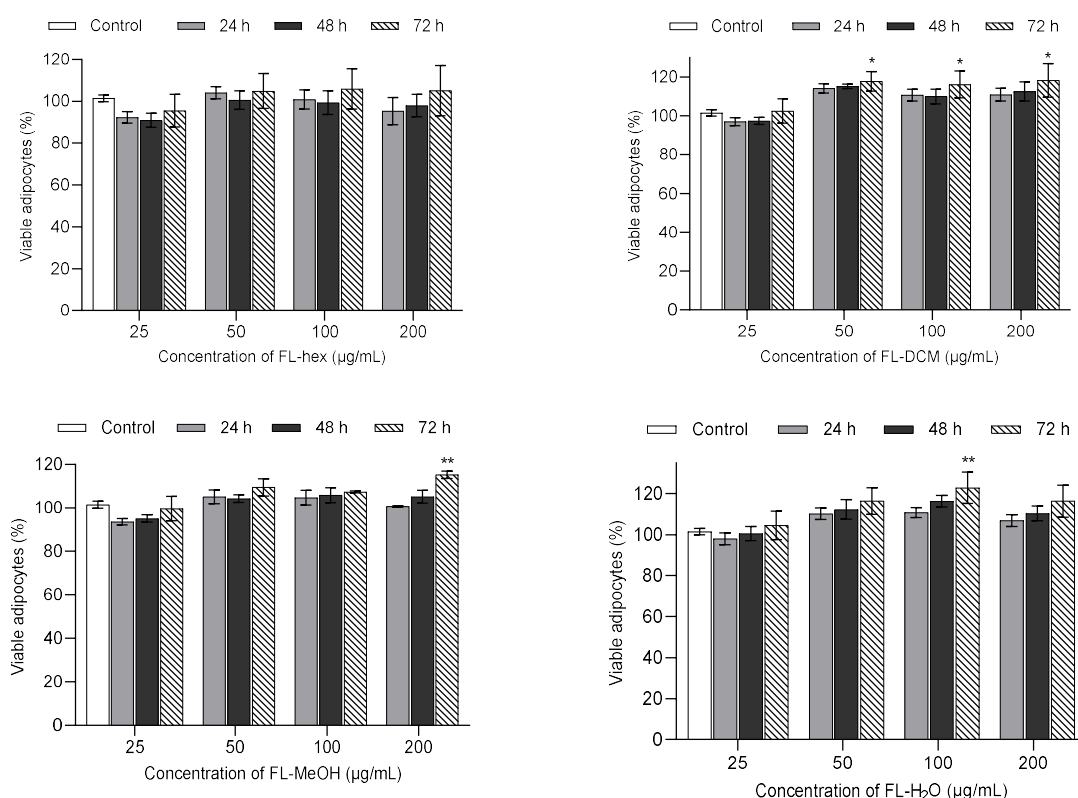


Figure 27. Viability of 3T3-L1 adipocytes treated with FL extracts. FL-hex: hexane extract of flowers, FL-DCM: dichloromethane extract of flowers, FL-MeOH: methanol extract of flowers, FL-H₂O: aqueous extract of flowers. Data in mean ± SEM, **p* = 0.02; ***p* = 0.002, vs vehicle control (*n* = 3, One-way ANOVA, Tukey's post hoc).

As shown in Figure 28, the cell viabilities of the adipocytes were from 93 to 125% when incubated with hexane, DCM, MeOH, and water extracts of the leaves. This means no cytotoxic effect with an incubation time of 24 to 72 h. This aligns with the previous trend in preadipocytes except for LF-MeOH extract. The methanolic extract starting from 100 µg/mL in the preadipocytes showed inhibitory effects in cell

growth. In contrast, the effect was not observed in the same assay on the adipose state, even in the higher 200 µg/mL concentration.

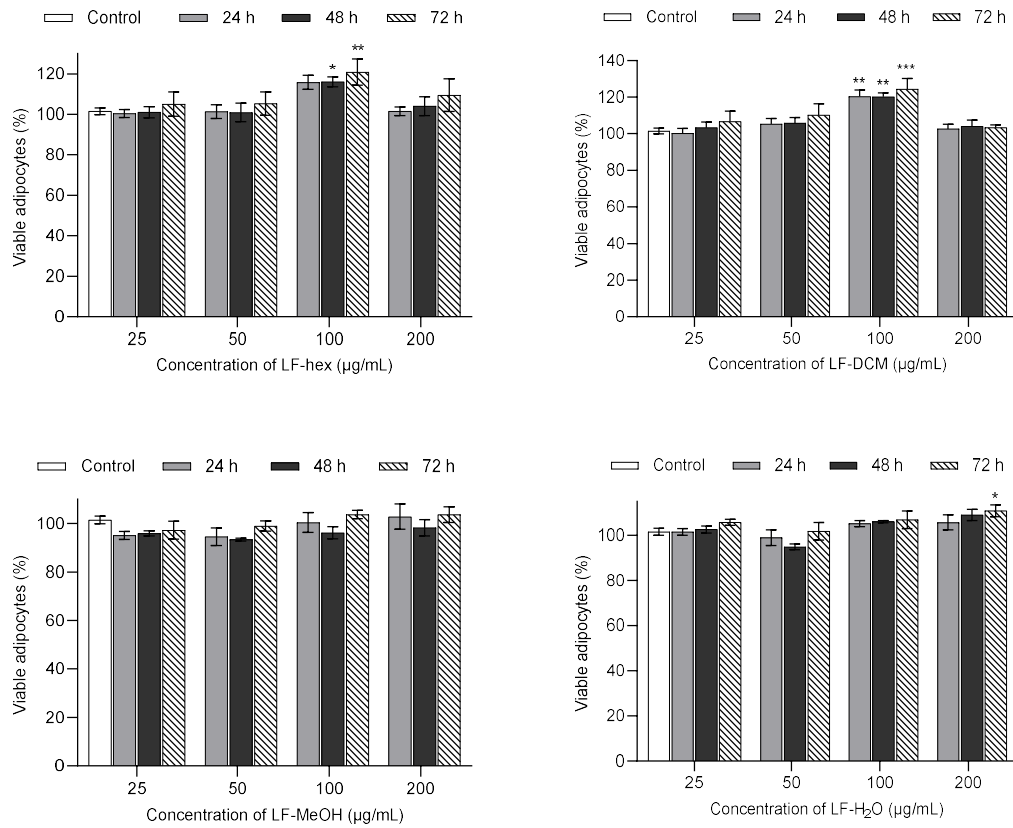
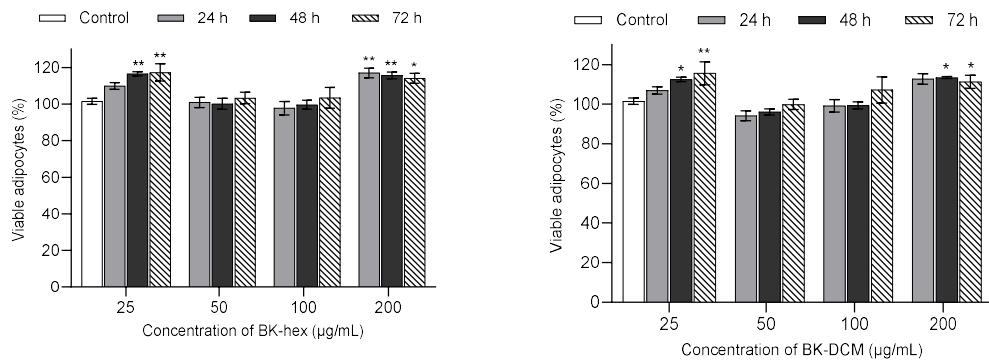


Figure 28. Viability of 3T3-L1 adipocytes treated with LF extracts. LF-hex: hexane extract of leaves, LF-DCM: dichloromethane extract of leaves, LF-MeOH: methanol extract of leaves, LF-H₂O: aqueous leaves extract. Data in mean ± SEM, **p* = 0.02; ***p* = 0.001; ****p* = 0.0001, vs vehicle control (*n* = 3, One-way ANOVA, Tukey's post hoc).



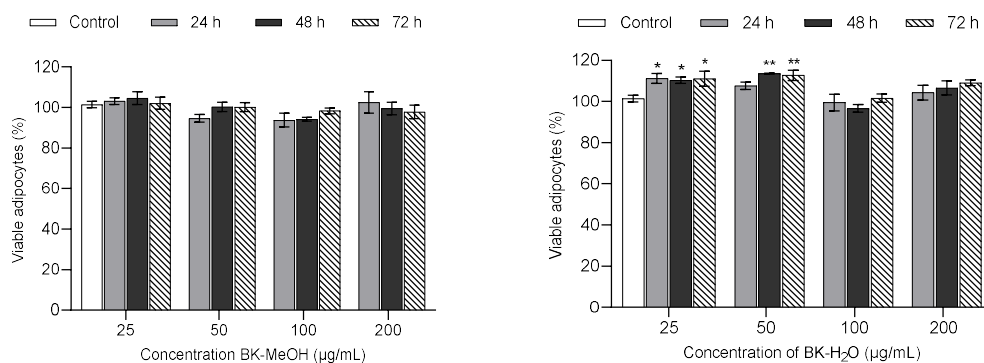


Figure 29. Viability of 3T3-L1 adipocytes treated with BK extracts. BK-hex: hexane extract of bark, BK-DCM: dichloromethane extract of bark, BK-MeOH: methanol extract of bark, BK-H₂O: aqueous extract of bark. Data in mean \pm SEM, * p = 0.02; ** p = 0.003, vs vehicle control (n = 3, One-way ANOVA, Tukey's post hoc).

Similar to the above observations, in the range between 25 and 200 $\mu\text{g/mL}$, all bark extracts demonstrated non-toxic effects within all three incubation times. The cell viability was estimated between 93 and 116%. Though the bark methanolic barks extract inhibited the preadipocyte growth at 25 $\mu\text{g/mL}$ in the previous test, it demonstrated no significant difference in cell viability at all incubation times compared to the vehicle control (see Figure 29). According to this work, all twelve extracts in the highest test concentration of 200 $\mu\text{g/mL}$ could be safe for further assay in the mature 3T3-L1 adipocytes.

3.5. Oil Red-O assay of extracts

Adipogenesis is a process behind transforming fibroblast-like cells into mature adipocytes³⁰³, characterised by developing lipid droplets. The excessively accumulated fat in mature adipocytes can cause dysfunction of metabolic processes due to oxidative stress and decrease cellular glucose uptake leading to insulin resistance. Primary regulators of cell differentiation, including C/EBPs and PPARs^{304, 305}, have been well-studied as promising targets for developing antiobesity and antiadipogenic drugs. The study of antiadipogenic effects can also be employed to link insulin resistance development and oxidative stress³⁰⁶. Therefore, an ORO-staining assay has been carried out to evaluate the effect of *A. saligna* to the adipogenesis of cells.

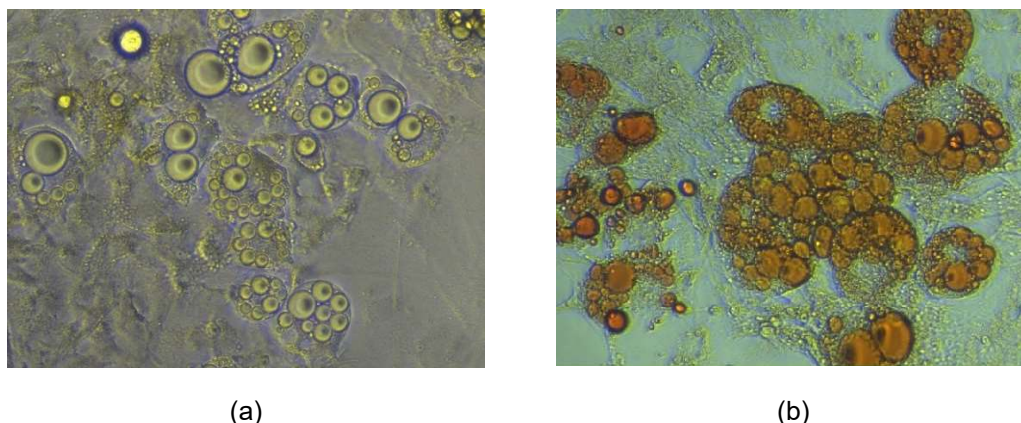


Figure 30. The captured image of (a) unstained vs (b) stained 3T3-L1 adipocytes with ORO reagent. Images were photographed with an inverse phase-contrast microscope (Infinity 1, Nikon Eclipse TS100) at a magnification of 20 \times .

There are fluctuated percentages of quantified lipid droplets between the extract-treated adipocytes and the vehicle control. According to data from Figure 31, significant anti-adipogenic activity was observed from the LF-MeOH-treated adipocytes at 50 $\mu\text{g}/\text{mL}$. It was estimated to be 28.68% of reduced lipid droplets compared to the vehicle control. A similar effect was observed in the positive control treatment with NAC at 10 mM for 29.55%. A slight decrease of lipid droplets was observed from treatment with hexane leaf extract (LF-hex) 50 $\mu\text{g}/\text{mL}$, BK-MeOH 50 $\mu\text{g}/\text{mL}$, LF-MeOH 12.5 $\mu\text{g}/\text{mL}$, FL-H₂O 12.5 $\mu\text{g}/\text{mL}$, and *N*-acetyl cysteine (NAC) 5 mM for 10.18, 11.9, 15.35, 16.81, and 22.14, %, respectively. On the other hand, a significantly increased lipid droplets percentage was shown from the treatment with BK-MeOH 12.5 $\mu\text{g}/\text{mL}$, dichloromethane leaf extract (LF-DCM) 50 $\mu\text{g}/\text{mL}$, dichloromethane bark extract (BK-DCM) 12.5 $\mu\text{g}/\text{mL}$ for 30.4, 40.9, and 45.9%, respectively.

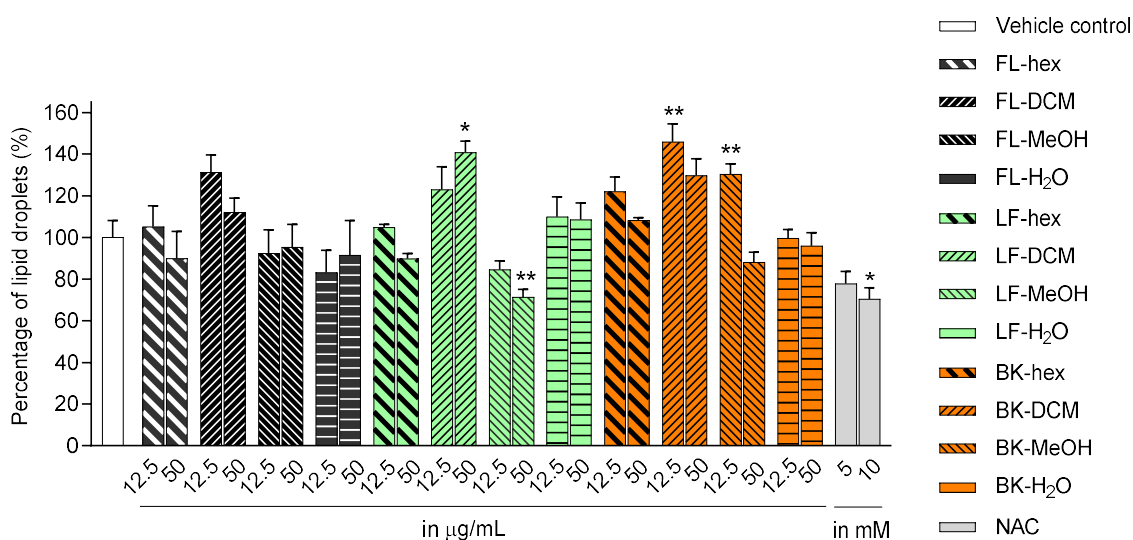


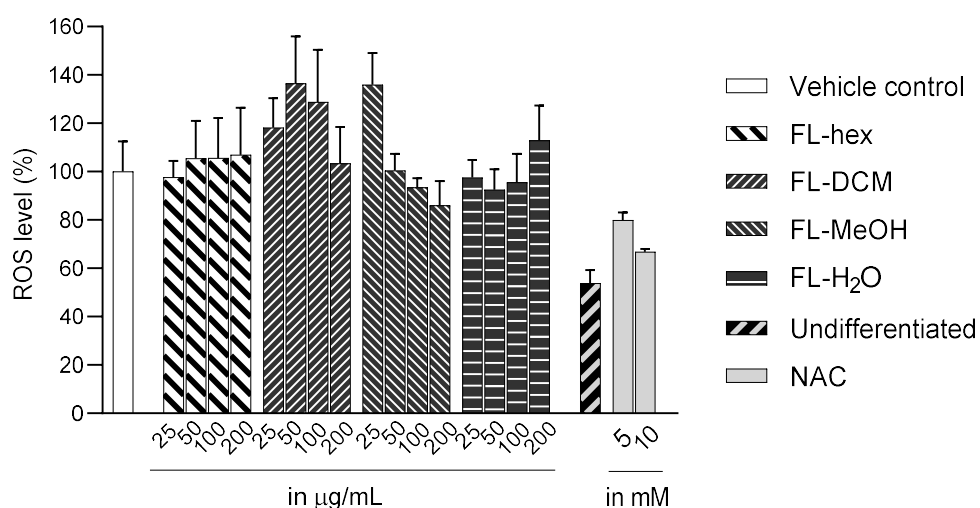
Figure 31. Lipid content from ORO staining assay on the 3T3-L1 adipocytes treated with extracts during the progress of cell differentiation. FL-hex: hexane extract of flowers, FL-DCM: dichloromethane extract of flowers, FL-MeOH: methanol extract of flowers, FL-H₂O: aqueous extract of flowers, LF-hex: hexane extract of leaves, LF-DCM: dichloromethane extract of leaves, LF-MeOH: methanol extract of leaves, LF-H₂O: aqueous extract of leaves, BK-hex: hexane extract of bark, BK-DCM: dichloromethane extract of bark, BK-MeOH: methanol extract of bark, BK-H₂O: aqueous extract of bark, and NAC = *N*-acetyl cysteine. Data in mean \pm SEM, * p = 0.02; ** p = 0.009, vs vehicle control (n = 3, One-way ANOVA, Tukey's post hoc).

3.6. Measurement of cellular ROS level

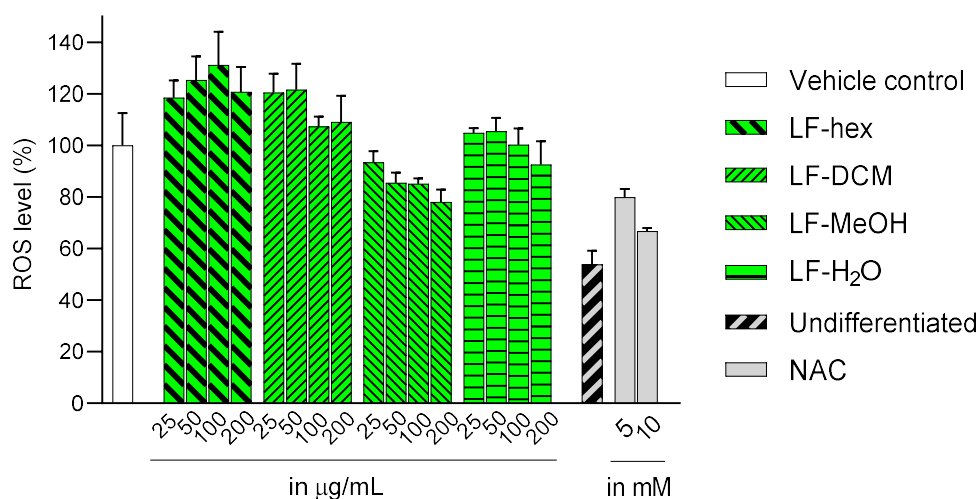
All extracts have been evaluated for their effect on intracellular ROS production in the white adipocytes to select the promisingly active fractions among twelve samples. The accumulation of lipids in the 3T3-L1 cells model can lead to ROS overproduction due to NADPH oxidation, glucose autoxidation and low-density lipoprotein (LDL) peroxidation. In the previous antioxidant assays, all alcoholic extracts demonstrated inhibitory properties against free radicals. Similarly, the plant's methanolic extracts also positively affected the reduction of cellular ROS production. Our study with DCFH-DA-staining assay found that the cellular ROS level in 3T3-L1 adipocytes was about 50% higher than those observed in non-differentiated 3T3-L1 cells. Among twelve *A. saligna* extracts, all methanolic extracts demonstrated a noticeable dose-dependent ROS reduction.

Methanolic extracts of leaf and bark reduced cellular ROS accumulation in 3T3-L1 adipocytes within the tested concentration, while FL-MeOH exerted reduction only between 100 and 200 μ g/mL. As shown in Figure 32, the decreasing pattern of ROS in the adipocytes appeared for all MeOH extracts. At the lowest dose, LF- and BK-MeOH decreased ROS by 6.56 and 10.89%, respectively, whereas no reduction was observed for FL-MeOH treatment. Furthermore, treatment with 200 μ g/mL of BK-

MeOH extract showed a significant decrease in the cellular ROS level, estimated for 37.43% of the adipocytes control, almost twice and thrice of those observed from LF- and FL-MeOH treatment, respectively. Taken together, the order of reduction of ROS accumulation can be expressed as BK-MeOH > LF-MeOH > FL-MeOH. The extracts' ability to reduce ROS accumulation in 3T3-L1 adipocytes reflects and follows the trend of their *in vitro* antioxidant activities found in our earlier finding³⁰⁷. Elansary et al. reported the connection between the significant reduction of ROS accumulation and the strong antioxidation of their methanolic leaf extract (17 µg/mL) of *A. saligna* in various cancer cell lines²¹⁶.



(a)



(b)

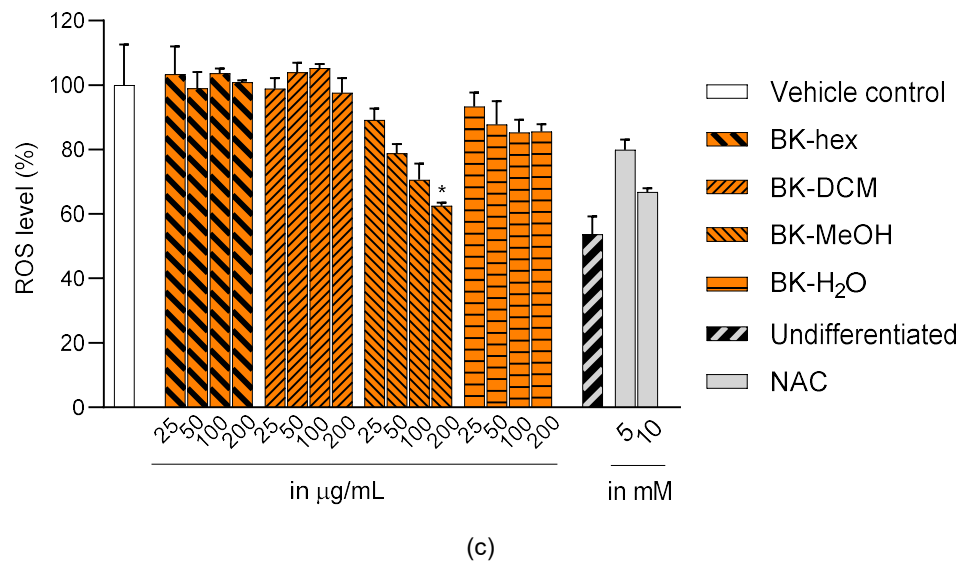


Figure 32. Detected cellular ROS of 3T3-L1 adipocytes treated with (a) FL extracts, (b) LF extracts, and (c) BK extracts compared to NAC as the positive control. FL-hex: hexane extract of flowers, FL-DCM: dichloromethane extract of flowers, FL-MeOH: methanol extract of flowers, FL-H₂O: aqueous extract of flowers, LF-hex: hexane extract of leaves, LF-DCM: dichloromethane extract of leaves, LF-MeOH: methanol extract of leaves, LF-H₂O: aqueous extract of leaves, BK-hex: hexane extract of bark, BK-DCM: dichloromethane extract of bark, BK-MeOH: methanol extract of bark, BK-H₂O: aqueous extract of bark, and NAC = *N*-acetyl cysteine. Data in mean \pm SEM, * p = 0.03, vs vehicle control (n = 3, One-way ANOVA, Tukey's post hoc).

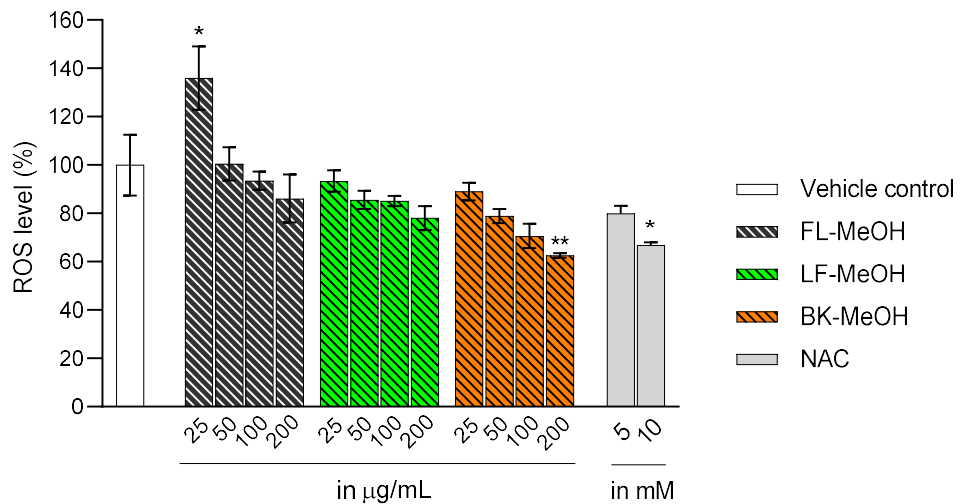


Figure 33. Comparison of intracellular ROS level in 3T3-L1 adipocytes treated with methanolic extracts. Data in mean \pm SEM, * p = 0.01, ** p = 0.008, vs vehicle control (n = 3, One-way ANOVA, Tukey's post hoc).

Polyphenol and flavonoid-rich herbal extracts have been demonstrated to ameliorate the overproduction of intracellular ROS from various models. A study by Marimoutou and co-workers³⁰⁸ compared the bioactive contents and antioxidant

capacity of leaves of three Indian Ocean medicinal plants for obesity and diabetes, namely *Antirhea borbonica*, *Doratoxylon apetalum*, and *Gouania mauritiana*. Among the three, *D. apetalum* possessed the highest values of phenolic and flavonoid contents (7% gallic acid equivalent and 2.8% catechin equivalent, respectively), antioxidant capacity against DPPH (61.1% compared to 75% inhibition by vitamin C), and ROS reduction in 3T3-L1 adipocytes (20%). This work suggested that cellular ROS's reductive effect aligned with the bioactive contents and DPPH scavenging capacity.

Studies on cellular ROS inhibition by *Acacia* species have also confirmed this property to be correlated with phenolic compounds. Methanolic barks extract of *A. mearnsii* reduced ROS level in mouse macrophage RAW 264.7 cell line ⁴⁹. This work showed that high content of polyphenol and flavonoid content (843.9 mg GAE/g and 30.3 mg QE/g, respectively) as well as ABTS scavenging activity (7.1 mmol Trolox/g equivalent) aligned with the inhibition of intracellular ROS level (roughly 25% compared to blank control). Moreover, two species of *A. shaffneri* and *A. farnesiana* have been reported to exert a similar trend in a study with pig kidney LLC-PK1 cells ⁵⁰. Methanolic pods extract of *A. farnesiana* with higher phenolic content than that quantified for *A. shaffneri* (213 and 76 mg GAE/g, respectively) showed a two-fold change higher on the ROS reduction percentage at 200 ppm treatment. The role of phenolic compounds is well known to involve direct scavenging against ROS and indirect impact through cell signalling pathways. Hydroxyl groups and conjugated C=C bonds are beneficial in stabilising the interaction between the phytochemicals and the free radicals ³⁰⁹. Furthermore, the phytochemicals have also been reported to inhibit three major MAP kinases, namely ERK, p38, and JNK, resulting in reduced NADPH oxidase-dependent formation of ROS and other superoxide anions ³¹⁰. The activity has been linked to the OH at C5 and C7 of ring A and C4 of ring B for flavonoids and the increased number of OH in other phenolics.

Our study also showed a similar finding. As presented in Chapter 2, the MeOH extracts with higher PC and FC content had higher ROS reduction percentages than those estimated for non-alcoholic extracts at concentrations ranging between 50 and 200 µg/mL. Interestingly, the decreasing order of PC and FC content among the three MeOH extracts agreed with the reductive ability of ROS, where BK-MeOH and FL-MeOH were quantified to have the highest and lowest values, respectively. This is the first report of the reductive activity of *A. saligna* extracts on the production of 3T3-L1 adipocytes ROS.

3.7. Cellular glucose uptake assay of extracts

This experiment aimed to assess the effects of all *A. saligna* extracts ranging between 12.5 and 50 µg/mL on the glucose uptake simulation in the adipose 3T3-L1 model. The 2-(*N*-(7-nitrobenz-2-oxa-1,3-diazol-4-yl)-amino)-2-deoxyglucose (2-NBDG) uptake assay was then performed to evaluate their activity. All extracts showed dose-dependent glucose uptake modulation at tested concentrations of 12.5 and 50 µg/mL. However, the increased uptake by hexane extracts of flowers and leaves, dichloromethane extracts of flowers and bark, and aqueous extracts of flowers and leaves were not observed. At 12.5 µg/mL, FL-MeOH, LF-DCM, LF-MeOH, BK-MeOH, and BK-H₂O showed an increase in glucose uptake in the 13.5-41.5% range compared to vehicle control. Marked increases in glucose uptake by 98 and 85% were observed when treated with 50 µg/mL LF-MeOH and FL-MeOH, respectively. At 50 µg/mL FL-, LF-, and BK-MeOH performed better than metformin at 10 µM. Overall improvement in the uptake of 2-NBDG at 50 µg/mL can be expressed as LF-MeOH > FL-MeOH > BK-MeOH > BK-hex > BK-H₂O > LF-DCM, as shown in Figure 34 and Table S24 (page 248). The methanolic extracts, once again, exerted more quantitative activity than their extract counterparts.

Some reports have detected phenolic and flavonoid derivatives in extracts related to the modulation of cellular glucose uptake in 3T3-L1 adipocytes. According to Luan and colleagues³¹¹, phenolic compounds from an aqueous extract of *Potentilla anserina* L. at 50 µg/mL, including derivatives of chlorogenic acids, caffeic acids, and myricetin glycones, were involved in the increased expression of phosphorylated Akt resulting in an enhanced level of glucose uptake (4 and 1.5 fold higher compared to untreated control, respectively). In another report, quercetin saccharides and benzoic acid derivatives in MeOH extract of *Ipomoea batatas* leaves were detected as the vital contributors in the enhanced Akt activation and glucose uptake³¹². This documentation suggested that phenolic and flavonoid-rich extracts demonstrated modulating effects on the 2-NBDG assay for cellular glucose uptake evaluation. Thus, the higher content of both compound groups in our methanolic extracts will likely play an essential role in glucose uptake. The involvement of these compounds in the multiple cellular pathways such as activation of Akt, induction of p-AMPK, inhibition of inflammatory markers (TNF-α, IL-6, and IL-1β)³¹³ and induction of adiponectin secretion³¹⁴ can be the possible mechanisms related to the effects.

Apart from the excellent outcomes of the methanolic extracts, other fractions, namely LF-DCM, BK-hex, and BK-H₂O extract, also demonstrated a positive impact.

Around 20% increase in glucose uptake was observed in the treatment by LF-DCM extract. Previously, our GCMS analysis showed some terpene groups in the extract, including chondrillasterol; (3 β ,5 α)-stigmasta-7,25-dien-3-ol; (3 β ,5 α ,22*E*)-ergosta-8(14),15,22-trien-3-ol; cholesta-5,17(20)-diene-3 β ,16-diol, 22,26-epoxy-; and (3 β ,5 α ,24*S*)-stigmast-7-en-3-ol. Many compounds with triterpenoid core structures have been reported to have a stimulatory effect on glucose uptake in the adipocytes by activating Akt³¹⁵ and inhibiting pro-inflammatory markers such as TNF- α , IL-6, and IL-1 β ³¹⁶. A treatment with hexane bark extract at 12.5 and 50 μ g/mL gave 9.4 and 40% of improved glucose uptake, respectively. From the GCMS experiment, phthalic acid of 2-methoxyethyl tetradecyl ester was found in the extract as the major volatile component. Interestingly, this compound has also been detected in the DCM extract of leaves. The last active extract, BK-H₂O, has a 21.8 and 32.2% of increasing effect at 12.5 and 50 μ g/mL, respectively. Two compounds were detected as 1-(1-propenylthio)-propane and 3-*O*-methyl-*D*-glucose. However, no documentation has been found for their activity in the related glucose uptake assays.

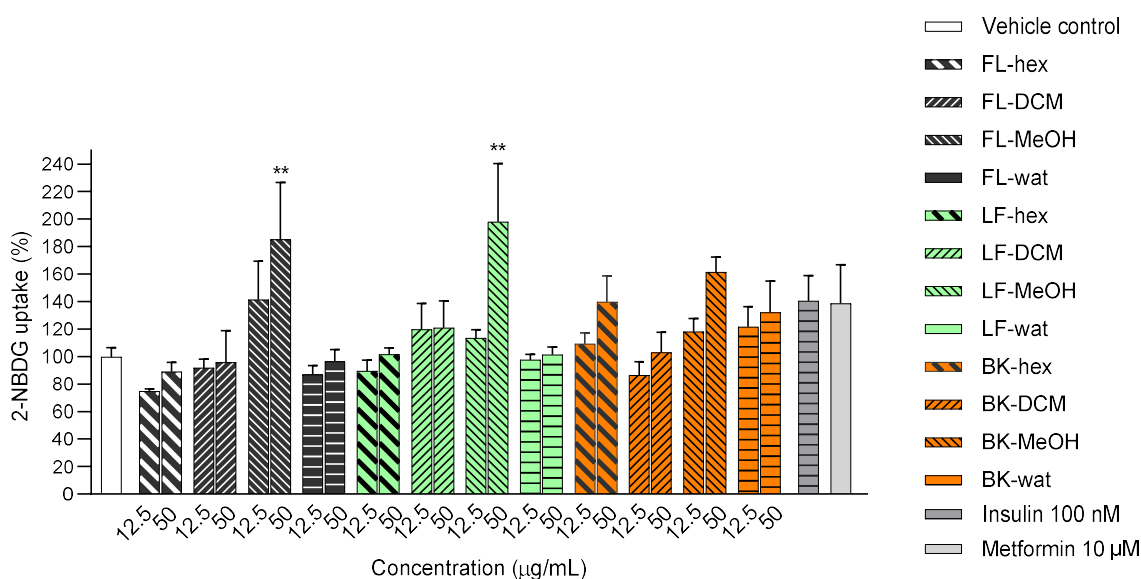


Figure 34. Estimated 2-NBDG uptake by 3T3-L1 adipocytes treated with extracts of *A. saligna*. FL-hex: hexane extract of flowers, FL-DCM: dichloromethane extract of flowers, FL-MeOH: methanol extract of flowers, FL-H₂O: aqueous extract of flowers, LF-hex: hexane extract of leaves, LF-DCM: dichloromethane extract of leaves, LF-MeOH: methanol extract of leaves, LF-H₂O: aqueous extract of leaves, BK-hex: hexane extract of bark, BK-DCM: dichloromethane extract of bark, BK-MeOH: methanol extract of bark, BK-H₂O: aqueous extract of bark. Data in mean \pm SEM, ***p* = 0.007 for FL-MeOH and ***p* = 0.006 for LF-MeOH, vs vehicle control (*n* = 3, One-way ANOVA, Dunnett's post hoc).

3.8. Conclusion of Chapter 3

Using *A. saligna*'s flower, leaf, and bark extracts on the 3T3-L1 cell-based tests has shown promising properties for T2DM remedies. Out of twelve extracts,

three methanolic extracts, namely FL-, LF-, and BK-MeOH extracts, demonstrated a consistent bioactivity outcome with those recorded from the previous *in vitro* assays of free radicals scavenging and inhibition of the yeast α -glucosidase enzyme. All three were active as inhibitors of cellular ROS production and stimulators of cellular glucose uptake on the differentiated 3T3-L1 cells in the safe concentration for the adipocytes below 200 $\mu\text{g}/\text{mL}$. In the study of lipid droplets level with ORO assay, the inhibitory activity of adipogenesis of 3T3-L1 cells was observed from the treatment with LF- and BK-MeOH extracts during the entire stages of differentiation. Furthermore, these data can justify the selected alcoholic extracts for further isolation of bioactive compounds.

CHAPTER 4: RESULT OF COMPOUND ISOLATION AND MOLECULAR ELUCIDATION

4.1. Introduction of Chapter 4

Our earlier works showed remarkable properties of all three alcoholic extracts over the non-alcoholic groups on neutralising free radicals and inhibiting α -glucosidase activity. The consistent trend of bioactivity of the methanolic extracts was found in the cell-mediated study, including intracellular ROS reduction and glucose uptake stimulation suggesting the need for fractionation and separation of the active extracts. Therefore, a study of compound isolation and identification described in this chapter was performed to reveal the molecular structure of phytochemical constituents in the FL-, LF-, and BK-MeOH extracts. The separation of compounds was carried out by column chromatography. The structure elucidation of isolated compounds was assigned by spectroscopic approach, including FTIR, NMR, and HRMS analysis. The information obtained from this chapter is essential to provide primary data on individual compounds isolated from Australian *A. saligna* for the first time. The data can assist those who work on drug design and discovery and natural product chemistry to attempt to lead compound-based drug development, optimised compound isolation, and structure-activity relationship (SAR) study.

4.2. Structure identification of isolated compounds

4.2.1. Four flavonoids and one cyclitol from the FL-MeOH fraction

4.2.1.1. Naringenin 42

A yellow powder subfraction A1 (10.5 mg, 9.63%, $R_f = 0.8$, EtOAc/MeOH/HCOOH/H₂O of 50:2:3:6 as the TLC eluent) was obtained from a column chromatography-based purification of FL-MeOH-A of methanolic extract of flower eluted by 100% of EtOAc with silica gel 60 as the stationary phase. As shown in Table 7, a geminal couple of protons resonating within upfield regions at δ 2.615 and 3.027 ($^2J_{H3a-H3b} = 17$ Hz, Figure 37b) ppm has cross-peaks correlations with the anomeric proton at δ 5.256 ppm ($^3J_{H2-H3a} = 12.92$ Hz and $^3J_{H2-H3b} = 3$ Hz). According to heteronuclear multiple bonds correlation (HMBC) information, a carbonyl was observed next to the geminal protons. This system is most likely to represent the ring C of a dihydroflavone (Figure 37a). The following information supports the statement:

1. An aromatic ring A with meta couple ($J = 2.16$ Hz, Figure 37b) by H6 (5.805 ppm) and H8 (5.818 ppm) links to it confirmed by HMBC cross-peaks relationships for H2 to C9, H3b to C10, and H6 to C4.

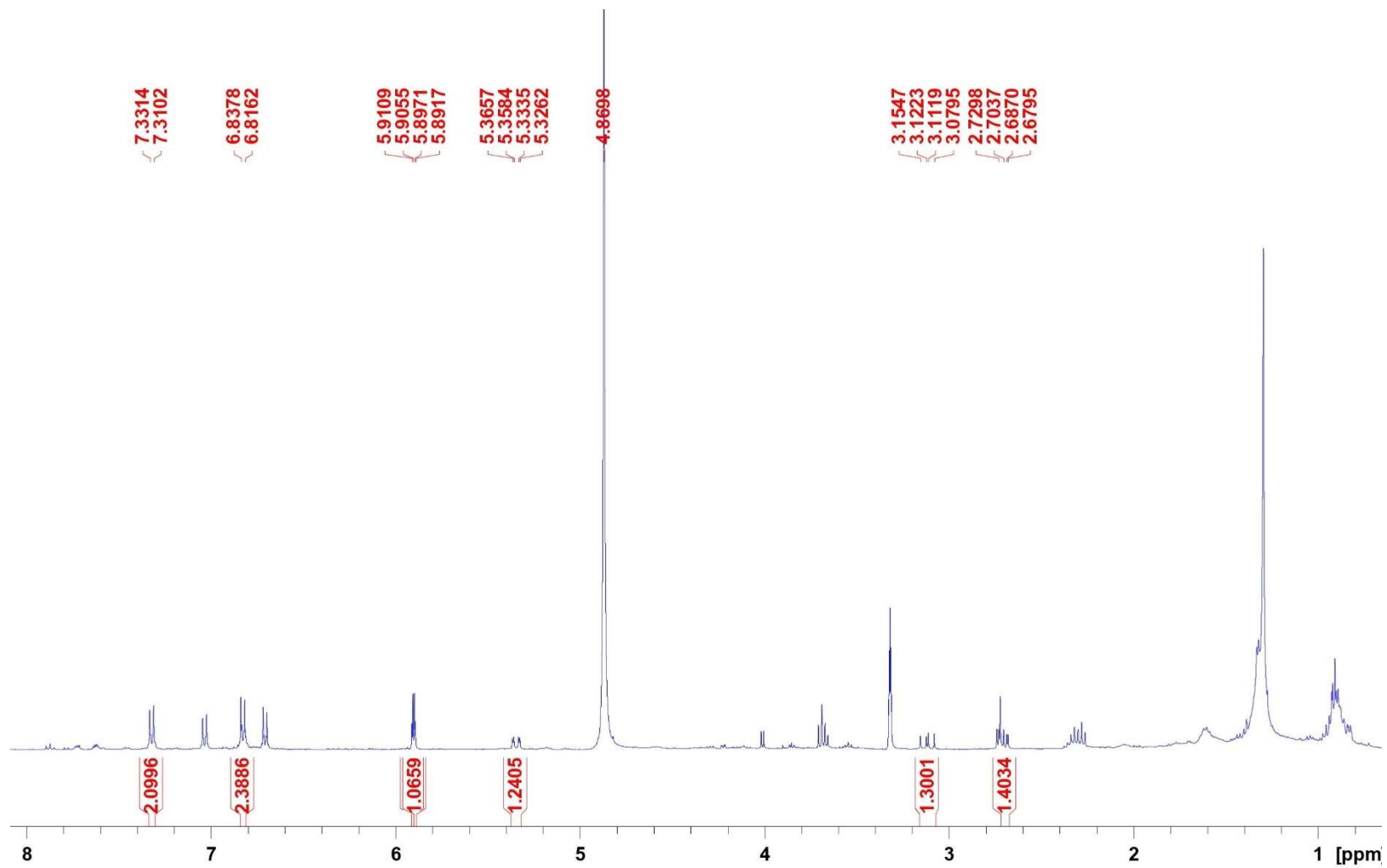


Figure 35. The spectral image of ¹H NMR of naringenin 42 from methanolic extract of flowers

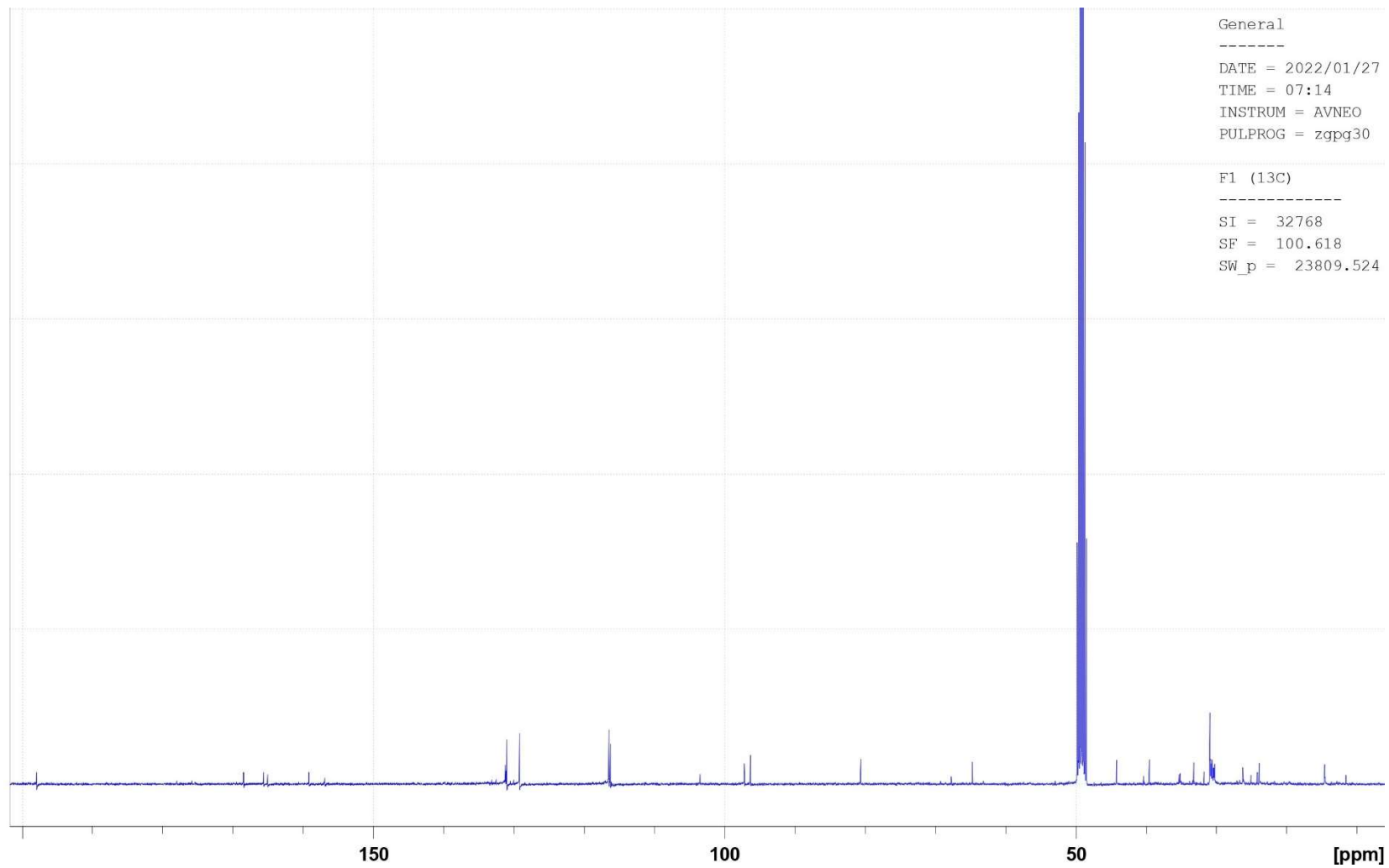


Figure 36. The spectral image of ^{13}C NMR of naringenin **42** from methanolic extract of flowers

Table 7. ¹H NMR (400 MHz, CD₃OD), ¹³C NMR (100 MHz, CD₃OD), and 2-D NMR data of compound from FL-MeOH-A1 compared to reported naringenin 42

No	FL-MeOH-A1					Naringenin ³¹⁷	
	δ ¹ H in ppm (m, J Hz, integration)	δ ¹³ C (ppm)	COSY	HMBC	NOESY	δ ¹ H in ppm (m, J Hz, integration)	δ ¹³ C (ppm)
2	5.26 (dd; 12.92, 2.9; 1H)	80.63	H3a, H3b	C4, C9, C1'	H3a (strong), H3b (weak), H2' (weak)	5.34 (dd; 13, 3; 1H)	80.5
3a	3.03 (dd; 17.12, 12.92; 1H)	44.20	H2, H3b	C2, C4, C1'	H2 (strong), H3b (strong), H2' (weak)	3.1 (dd; 17, 13; 1H)	44
3b	2.62 (dd; 17.04, 3.06; 1H)		H2, H3a	C1', C2, C4, C10	H2 (weak), H3a (strong)	2.7 (dd; 17, 3; 1H)	
4	-	197.93	-	-	-	-	197.8
5	-	165.62	-	-	-	-	165.5
6	5.81 (d; 2.16; 1H)	97.19	H8	C4, C5, C8, C10	-	5.88 (d; 2; 1H)	97.1
7	-	168.50	-	-	-	-	168.4
8	5.82 (d; 2.16; 1H)	96.31	H6	C6, C9, C10	-	5.9 (d; 2; 1H)	96.2
9	-	165.04	-	-	-	-	164.9
10	-	103.5	-	-	-	-	103.4
1'	-	131.22	-	-	-	-	131.1
2'	7.23 (dd; 6.76, 1.78, 1H)	129.18	H3	C2, C3', C6', C4'	H2 (weak), H3a (weak), H3' (strong)	7.31 (m; 1H)	129
3'	6.74 (dd; 6.64, 2.02, 1H)	116.47	H1	C1', C5', C4'	H2' (strong)	6.82 (m; 1H)	116.4
4'	-	159.18	-	-	-	-	159
5'	6.74 (dd; 6.64, 2.02; 1H)	116.47	H1	C1', C3', C4'	H6' (strong)	6.82 (m; 1H)	116.4
6'	7.23 (dd; 6.76, 1.78; 1H)	129.18	H3	C2, C2', C5', C4'	H5' (strong)	7.31 (m; 1H)	129

2. The linkage of the ring C to *p*-substituted aromatic ring B with two tall downfield peaks at δ 6.737 (H2' and H6') and 7.231 ppm (H3' and H5') was found by the HMBC cross-peaks for H2 to C1' as well as H2' to C2 (Figure 36c) and a weaker cross-peaks correlation from the nuclear overhauser effect spectroscopy (NOESY) spectrum attributing the farther through-space relationship between H2 and H2' (Figure 36d).

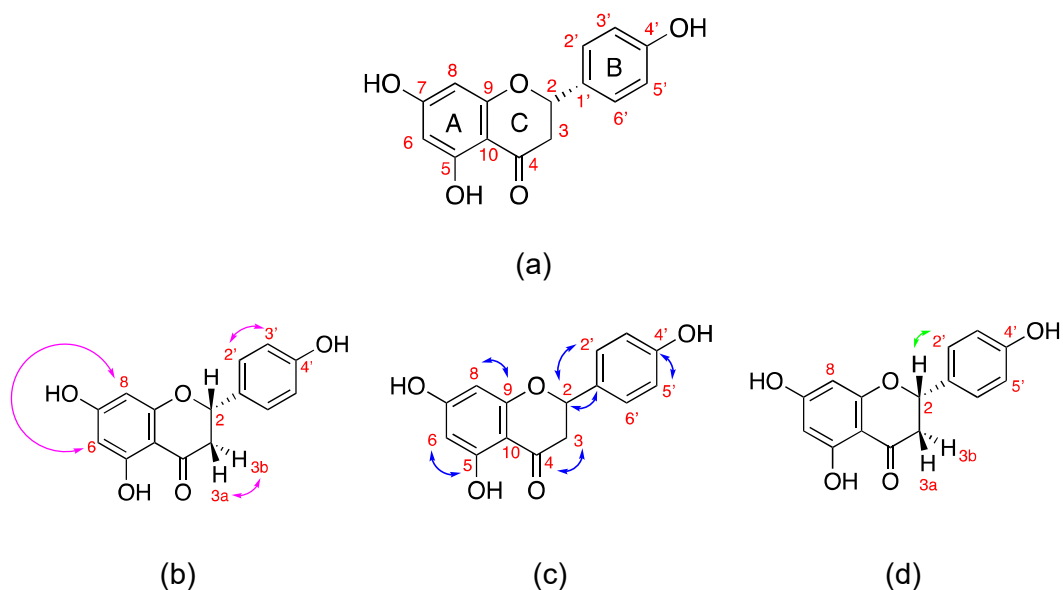


Figure 37. (a) The main skeleton of naringenin **42** (C₁₅H₁₂O₅; MW = 272.257), key connections of proton-to-proton ((b) \leftrightarrow COSY and (d) \leftrightarrow NOESY) and proton-to-carbon ((c) \leftrightarrow HMBC) of naringenin **42** isolated from the methanolic flowers extract.

Its NMR data agreed with those reported by Du et al.³¹⁷ for 5,7-dihydroxy-2-(4-hydroxyphenyl)chroman-4-one, known as naringenin **42**. Naringenin **42** has previously been detected in the crude water extract of *A. saligna* flowers by HPLC with weak DPPH scavenging activity¹⁸⁷. Nevertheless, the singly isolated compound has not been found in the literature. As the flavanone has an epimeric centre at C2, ring B can give two optically active configurations, (2*S*)- or (2*R*)-flavanone³¹⁸. Our study showed that the specific optical value of the isolate was $[\alpha]^{23} = -16.68^\circ$ (c 0.1, EtOH). This finding confirms a report that the laevorotatory (–)- or (2*S*)-flavanone is the most common one isolated from plants³¹⁸.

4.2.1.2. Naringenin-7*O*- α -L-arabinofuranoside **76**

A unique flavanone glycone was isolated from FL-MeOH-A3 of the methanolic flower extract (15.5 mg, 14.22%, R_f = 0.33 with TLC mobile phase of EtOAc/MeOH/AcOH/H₂O = 50:2:3:6). The δ of C-13 of the core skeleton of flavanone

moiety was identified as naringenin which is identical to those reported by Olsen et al.³¹⁹. The following data confirmed the typical proton peaks of flavanone:

1. An ABX-system comprising the geminal proton of H3a (2.606 ppm, td, $J = 17.64$, 2.95 Hz, 1H) and H3b (2.946 ppm, m, 1H) coupled to proton H2 (5.255 ppm, td, $J = 12.96$, 2.8 Hz, 1H) in ring C assigned by correlation spectroscopy (COSY) relationship (Figure 37).
2. The *p*-substituted aromatic ring B is represented by two stronger downfield signals of δ 7.223 ppm (dd, $J = 8.56$, 3.16 Hz, H2' and H6') and δ 6.735 ppm (dd, $J = 8.64$, 1.96 Hz, H3' and H5').
3. The catechol ring A identified by tiny upfield signals for aromatic at δ 6.406 ppm (d, $J = 2.2$ Hz, H8) *o*-coupled to δ 6.059 ppm (d, $J = 2.24$ Hz, H6).

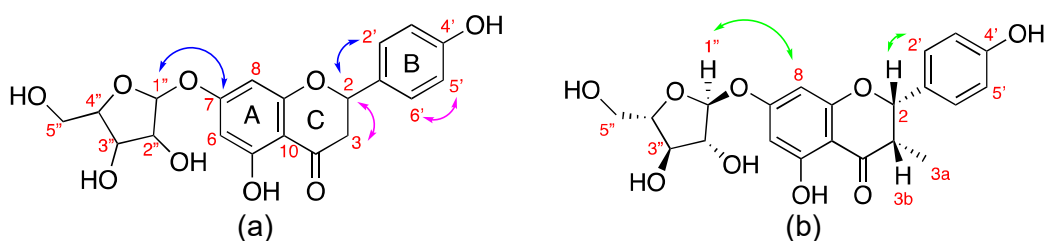


Figure 38. Key connections of proton-to-proton (\leftrightarrow COSY; \leftrightarrow NOESY) and proton-to-carbon (\leftrightarrow HMBC) of naringenin-7-*O*- α -*L*-arabinofuranoside **76** (C₂₀H₂₀O₉; MW = 404.37) isolated from the methanolic flowers extract.

Furthermore, the δ of C-13 of the sugar moiety is identical to those reported for arabinofuranoside by Zhang et al.³²⁰. The detailed descriptions of proton signals are as follows:

1. The anomeric proton of δ 4.78 ppm (d, $J = 7.48$ Hz, H1'') represented an α conformation with smaller J constants due to the equatorial-axial relationship of H1'' to H2'',
2. triplet couple of H3'' (3.45 ppm, $J = 8.4$ Hz) and H4'' (3.51 ppm, $J = 8.08$ Hz) with higher J constants representing equatorial-equatorial relationship as an indication of *L* orientation of the sugar,
3. geminal protons of 3.97 ppm (m, H5''a) and 3.78 ppm (m, H5''b) as the typical signals for a furanose ring. To confirm this, a total correlation spectroscopy (TOCSY) experiment showed that the sugar is a 5-membered ring.

FL-MeOH-A4b cc2 on 2021

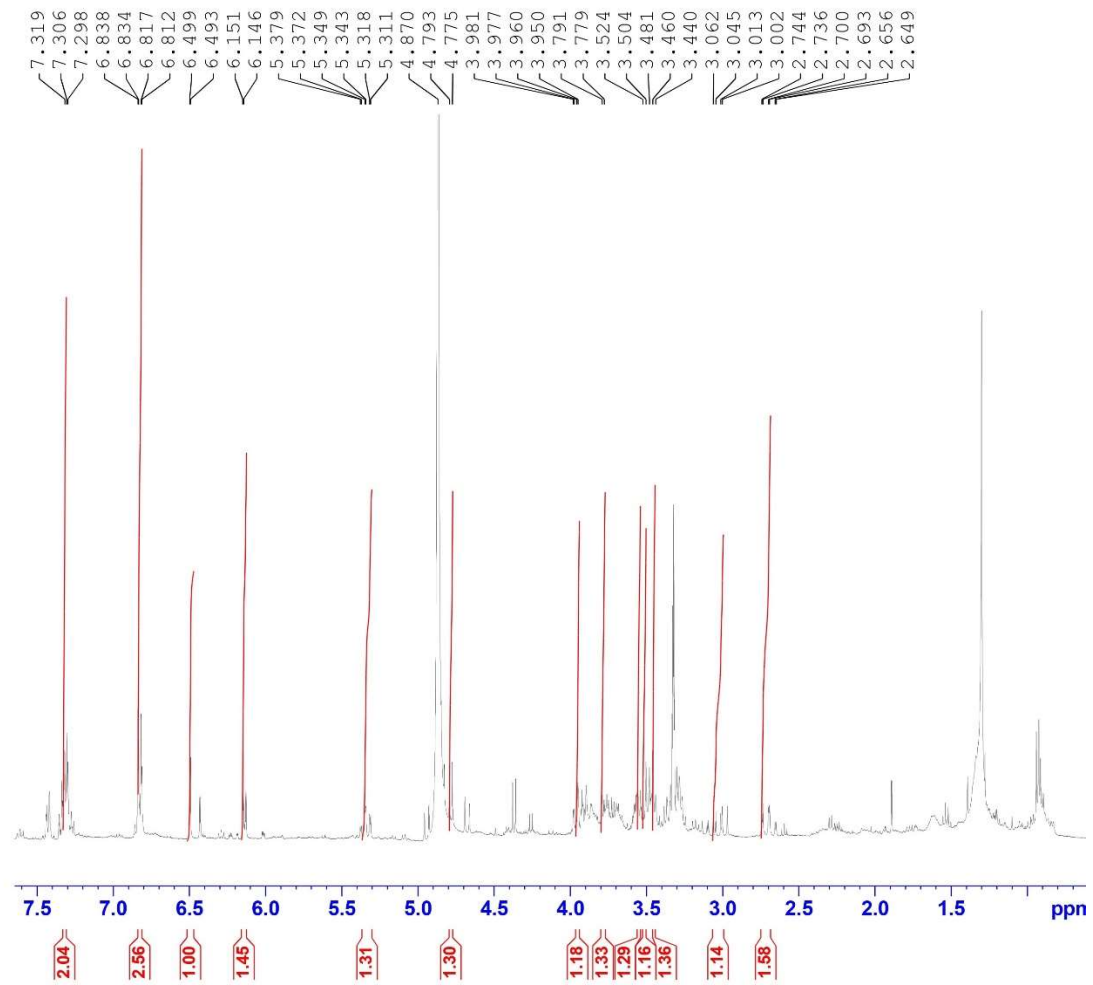


Figure 39. The spectral image of ^1H NMR of naringenin-7- O - α -L-arabinofuranoside **76** from methanolic extract of flowers

FL-MeOH-A4b cc2 on 2021

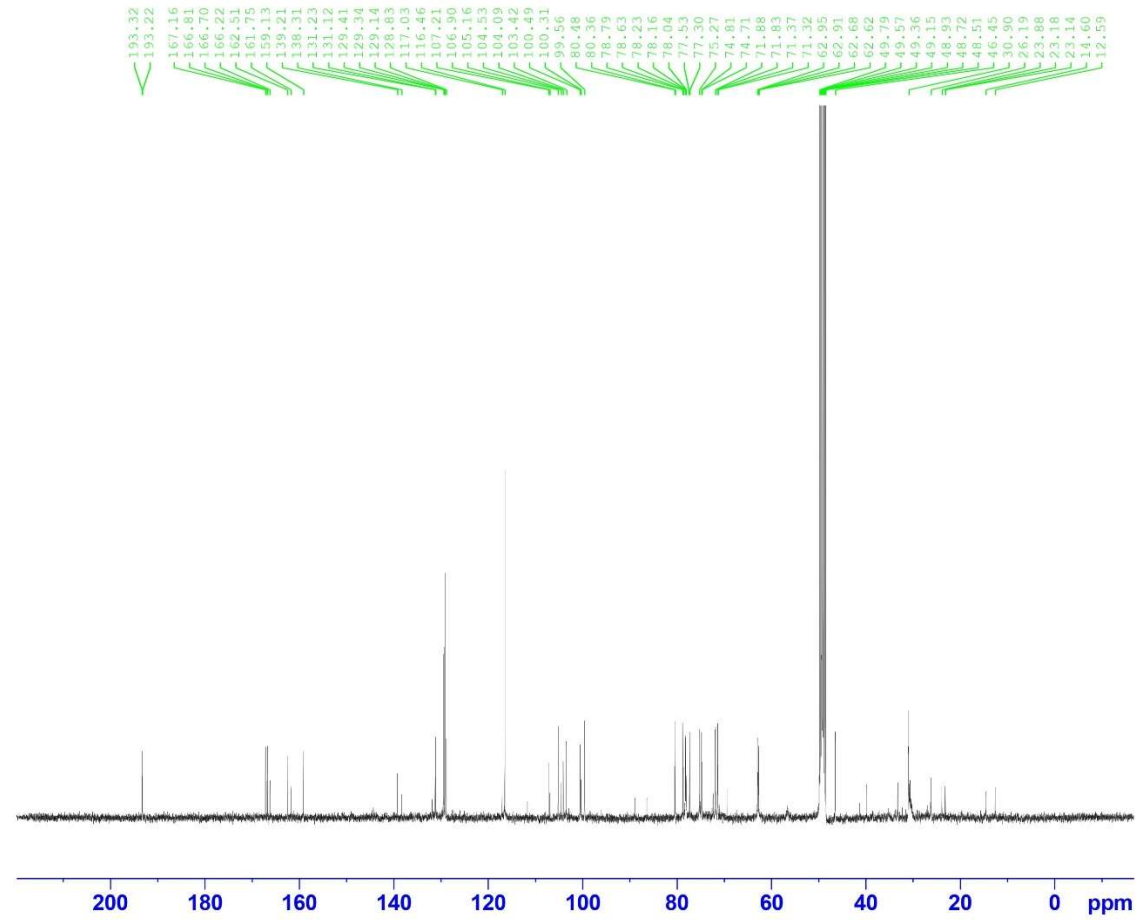


Figure 40. The spectral image of ^{13}C NMR of naringenin-7-*O*- α -*L*-arabinofuranoside **76** from methanolic extract of flowers

FL-MeOH-A4b cc2 on 2021

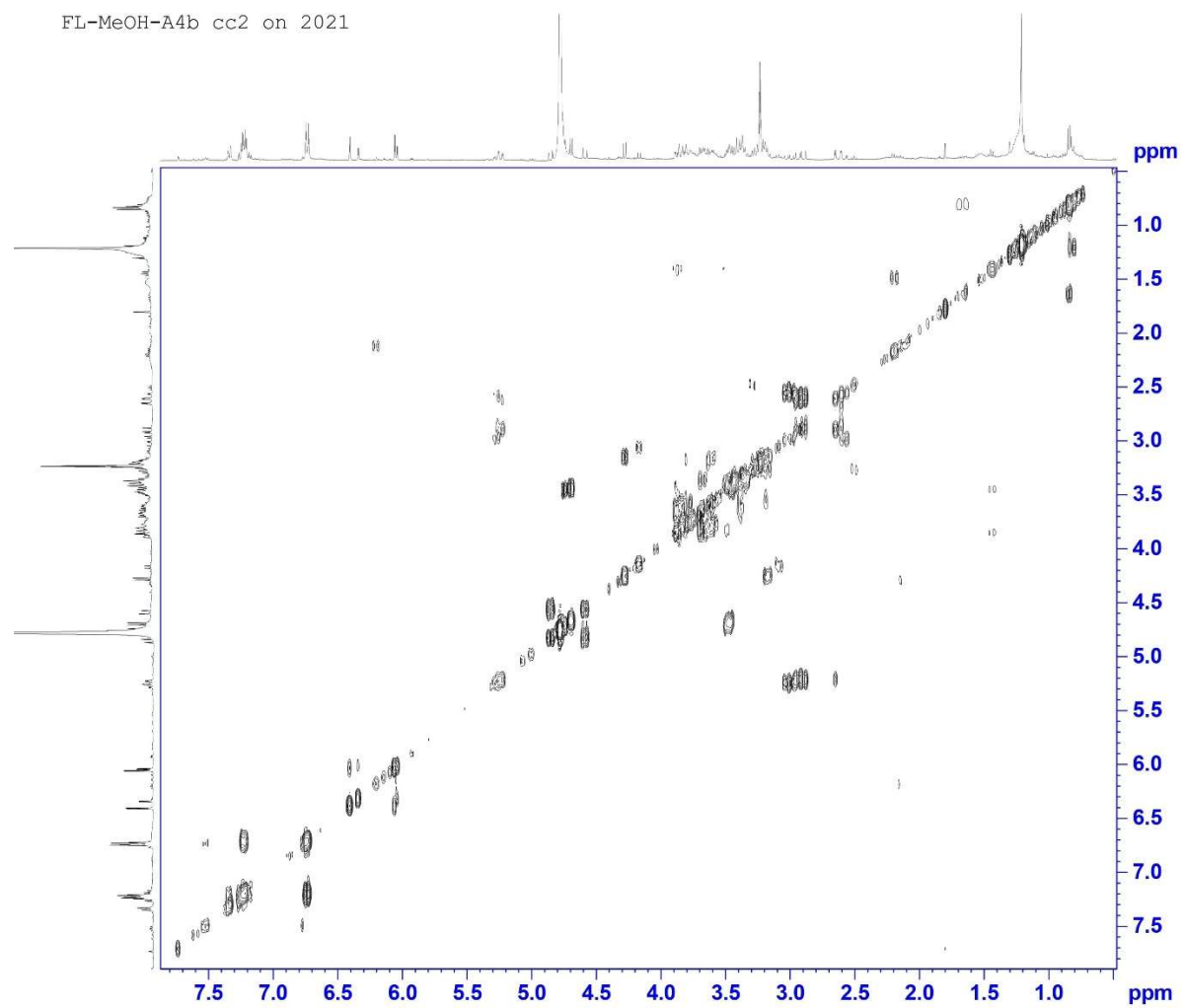


Figure 41. The spectral image of ¹H-¹H COSY NMR of naringenin-7-*O*- α -L-arabinofuranoside **76** from methanolic extract of flowers

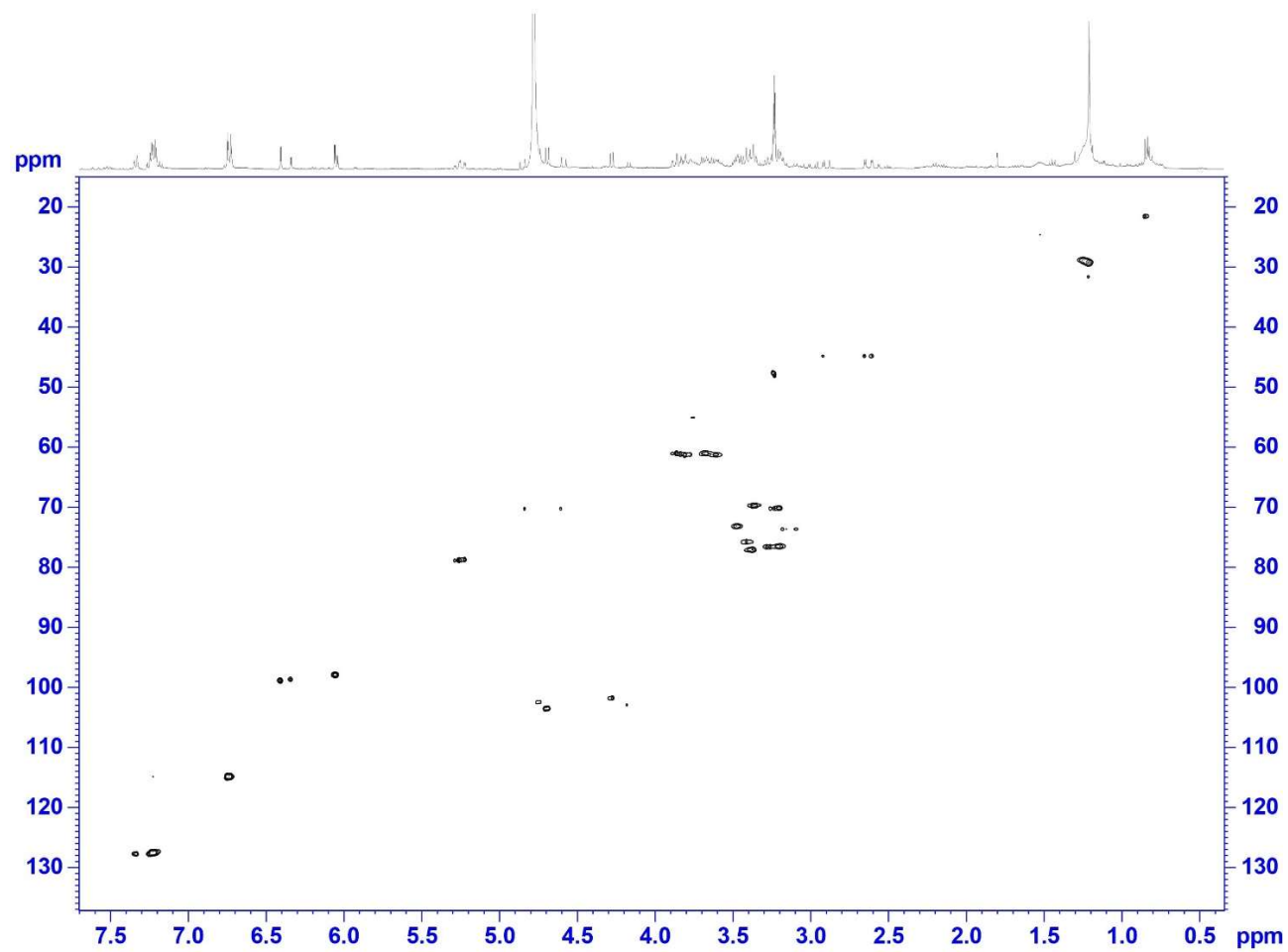


Figure 42. The spectral image of ^1H - ^{13}C HSQC NMR of naringenin-7- O - α -L-arabinofuranoside **76** from methanolic extract of flowers

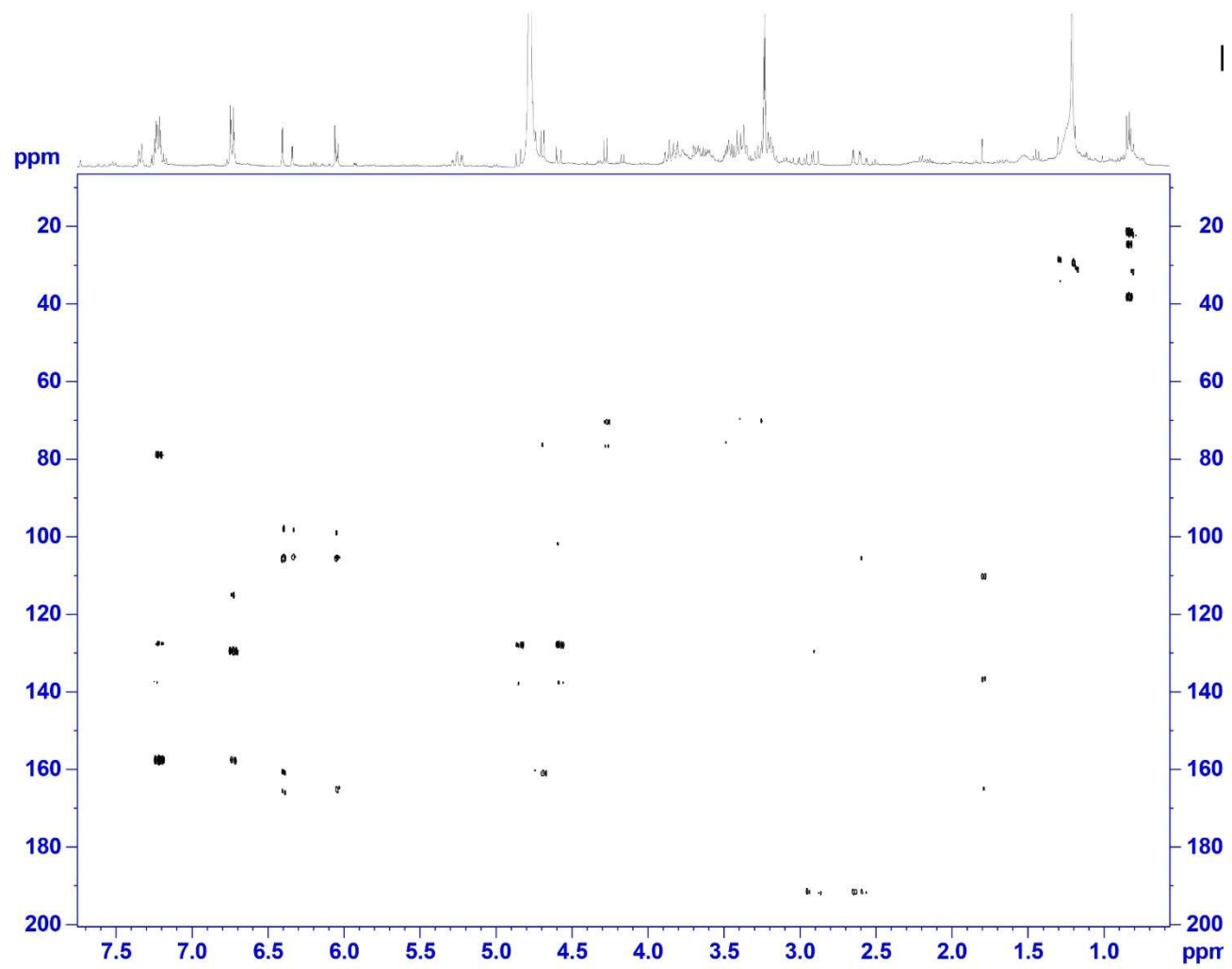


Figure 43. The spectral image of ^1H - ^{13}C HMBC of naringenin-7-*O*- α -*L*-arabinofuranoside **76** from methanolic extract of flowers

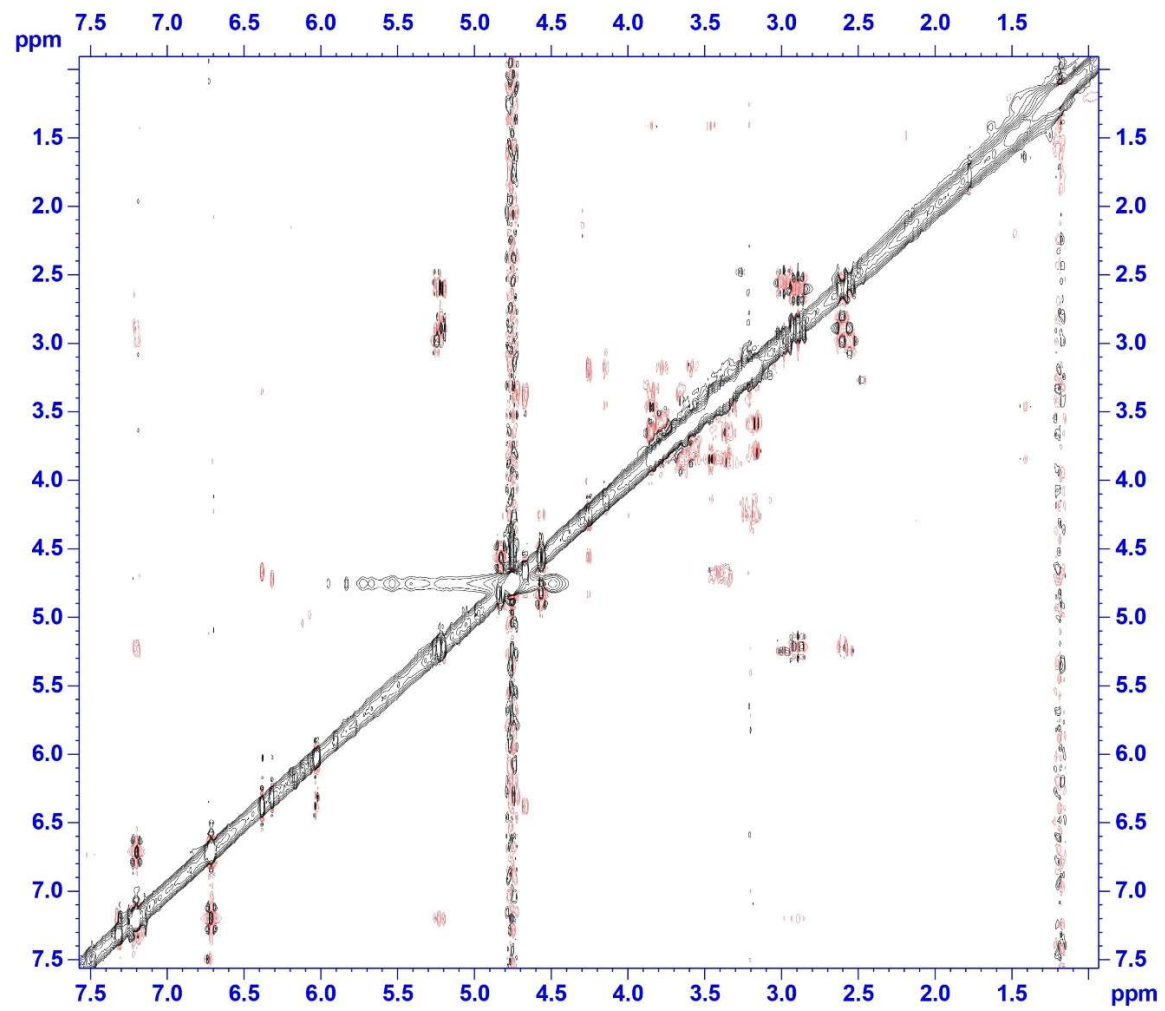


Figure 44. The spectral image of ^1H - ^1H NOESY NMR of naringenin-7- O - α - L -arabinofuranoside **76** from methanolic extract of flowers

Table 8. The 1- and 2-D NMR data of the isolate from FL-MeOH-A3 in CD₃OD

No	¹ H (δ ppm, m, J in Hz, integration)	δ ¹³ C (ppm)	COSY	TOCSY	NOESY	HMBC
2	5.35 (td; 12.96, 2.8; 1H)	80.48	H3a H3b	H3a, H3b	H3b (stronger), H3a (weaker)	C4, C2', C6'
3a	2.70 (td; 17.64, 2.95; 1H)	46.45	H2, H3b	H2, H3b	H2	C4, C10
3b	3.04 (m; 1H)		H2, H3a	H2, H3a	H2	C4, C2, C1'
4	-	193.22	-	-	-	-
5	-	166.70	-	-	-	-
6	6.15 (d; 2.24; 1H)	99.56	H6	H8	H8	C4, C5, C8 C10
7	-	167.16	-	-	-	-
8	6.50 (d; 2.2; 1H)	100.49	H8	H6	H6	C4, C7, C6, C9, C10
9	-	162.51	-	-	-	-
10	-	107.21	-	-	-	-
1'	-	131.12	-	-	-	-
2'	7.31 (dd; 8.56, 3.16; 1H)	129.14	H3', H6'	H3', H6'	H3' (stronger), H2 (weaker)	C2, C1', C3', C4'
3'	6.83 (dd; 8.64, 1.96; 1H)	116.46	H2', H5'	H2', H5'	H2'	C2', C4'
4'	-	159.13	-	-	-	-
5'	6.83 (dd; 8.64, 1.96; 1H)	116.46	H3', H6'	H3', H6'	H6'	C6', C4'
6'	7.31 (dd; 8.56, 3.16; 1H)	129.14	H2', H5'	H2', H5'	H5'	C2, C1', C5', C4'
1''	4.78 (d; 7.48; 1H)	105.16	H2''	H2'', H3'', H4''	H8 (stronger), H2'', H3'', H4''	C7, C2''
2''	3.57 (m; 1H)	74.81	H1''	H1'', H3'', H4'', H5''a, H5''b	H1'', H5''a	-
3''	3.45 (t; 8.4; 1H)	78.79	-	H1'', H2'', H4'', H5''a, H5''b	H1'', H5''a, H5''b	C2''
4''	3.51 (t; 8.08; 1H)	77.3	H5''b	H1'', H2'', H3'', H5''a, H5''b	H1'', H5''a, H5''b	C2''

No	¹ H (δ ppm, m, J in Hz, integration)	δ ¹³ C (ppm)	COSY	TOCSY	NOESY	HMBC
5" a	3.97 (m; 1H)	62.68	H5" b	H2", H3", H4", H5b"	H2", H3", H4", H5" b	-
5" b	3.78 (m; 1H)		H4", H5" a	H2", H3", H4", H5a"	H3", H4", H5" a	-

By a 2D NMR experiment of HMBC, the sugar moiety was confirmed to attach to 7O of the aromatic ring A (Figure 38). Moreover, NOESY data also showed a strong cross-peaks relationship between H1'' of the sugar and H8 of aromatic ring A, representing a closer space configuration. The IR spectra gave prominent numbers at 3300.70 (-OH stretching); 2920.64 (sp³ CH stretching); 1605.11 (C=O carbonyl stretching); 1515.07 (C=C aromatic stretching); and 1021.40 cm⁻¹ (C–O bending). The [M + H]⁺ of subfraction A3 was 405.1189. Therefore, this finding confirms the molecular formula of C₂₀H₂₀O₉ (calculated m/z [M + H]⁺ = 405.1186) for naringenin-7-O- α -L-arabinofuranoside **76** with a melting point of 229–230 °C and [α]²³ = -44.54° (c 0.1, MeOH).

4.2.1.3. Isosalipurposide 1

A chalcone glycoside derivative (yellow powder of B1b, 9.13 mg, 4.43%) was isolated from FL-MeOH of the methanolic flower extract. The *p*-coumaroyl group was confirmed by the downfield shift of the proton olefin skeleton ($\delta_{H\alpha}$ 8.01 ppm, $\delta_{H\beta}$ 7.69 ppm) with *E* geometric orientation (*J* ~16 Hz), a carbonyl (δ_C 194.44 ppm), and the two doublets ($\delta_{H_{2,6}}$ 7.61 ppm 8.61 Hz, $\delta_{H_{3,5}}$ 6.85 ppm 8.75 Hz) in the *para*-disubstituted aromatic ring. The second phenyl (ring A) was elucidated as a trioxygenated aromatic with *meta*-coupling of protons (~2.2 Hz) at two upfield chemical shifts due to the inductive effects of adjacent hydroxyls.

The glycone moiety was assigned as a cyclohexane-like chair ring of glucose due to a β -anomeric proton at 5.09 ppm with $J_{H1''-H2''} = 7.4$ Hz and the vicinal axial-axial couplings (7.5–8.75 Hz) of the H2''–H3'', H3''–H4'', and H4''–H5'' indicating the OH groups in the equatorial position¹⁸⁸. Furthermore, the protons on C6'' ($\delta_{H_{6a}}$ 3.62 ppm, $\delta_{H_{6b}}$ 3.99 ppm) were identified by the geminal coupling (~12 Hz) and their similar vicinal coupling (5.32 and 5.28 Hz) to H5'' indicating the *gauche* relationship between both and H5''. This glucopyranoside was linked to oxygen in C6', confirmed by its similar ¹³C chemical shift with that reported isosalipurposide (Table 9). Due to the close similarity of δ ¹³C, therefore, the compound could be considered as isosalipurposide (Figure 47), a member of isoliquiritigenin as a common group in *Leguminosae* plants³¹⁸, which was previously isolated by Imperato¹⁸⁶, Ghouila et al.²¹¹, and Ghribia et al.¹⁸⁸.

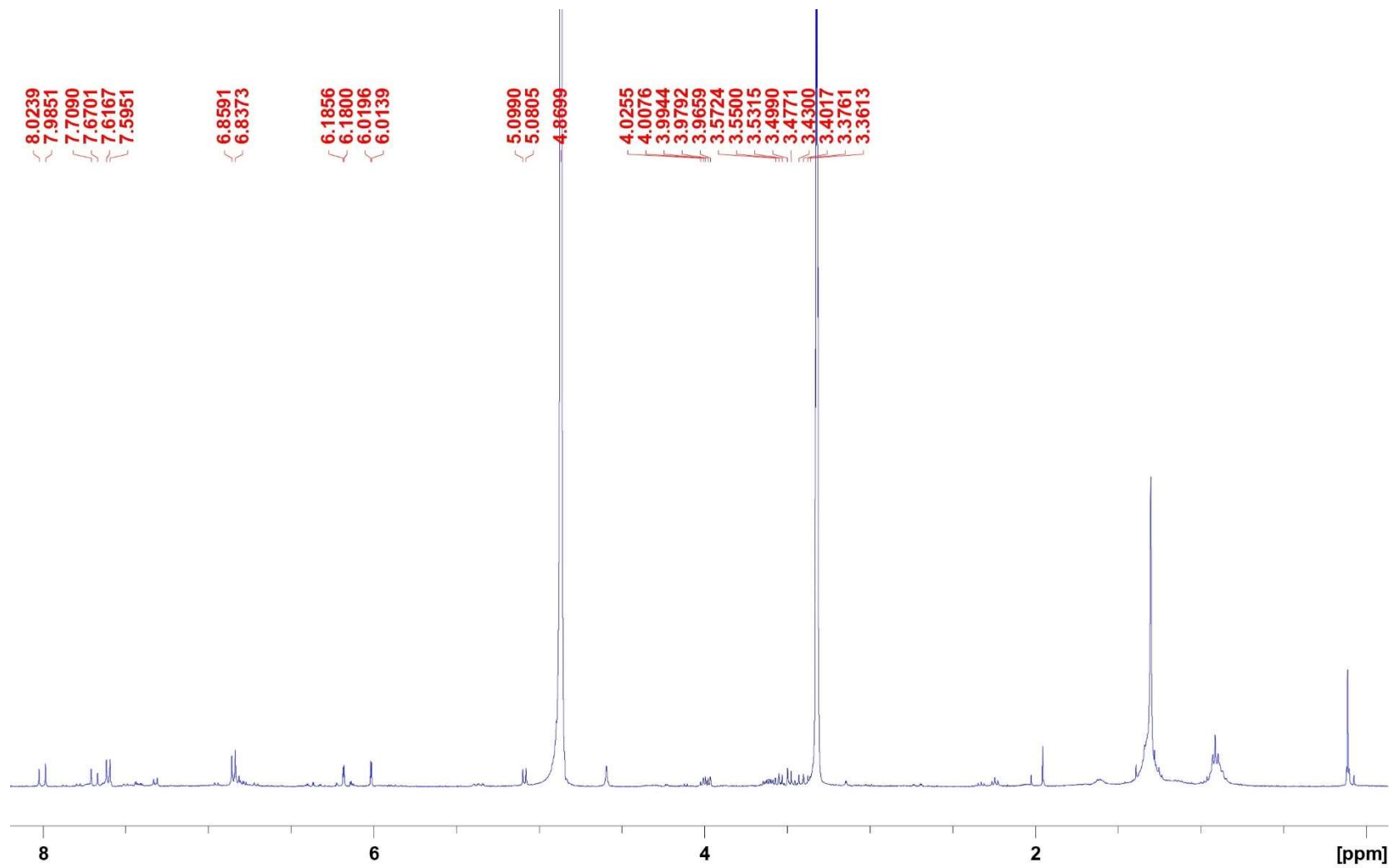


Figure 45. The spectral image of ^1H NMR of isosalipurside **1** from methanolic extract of flowers

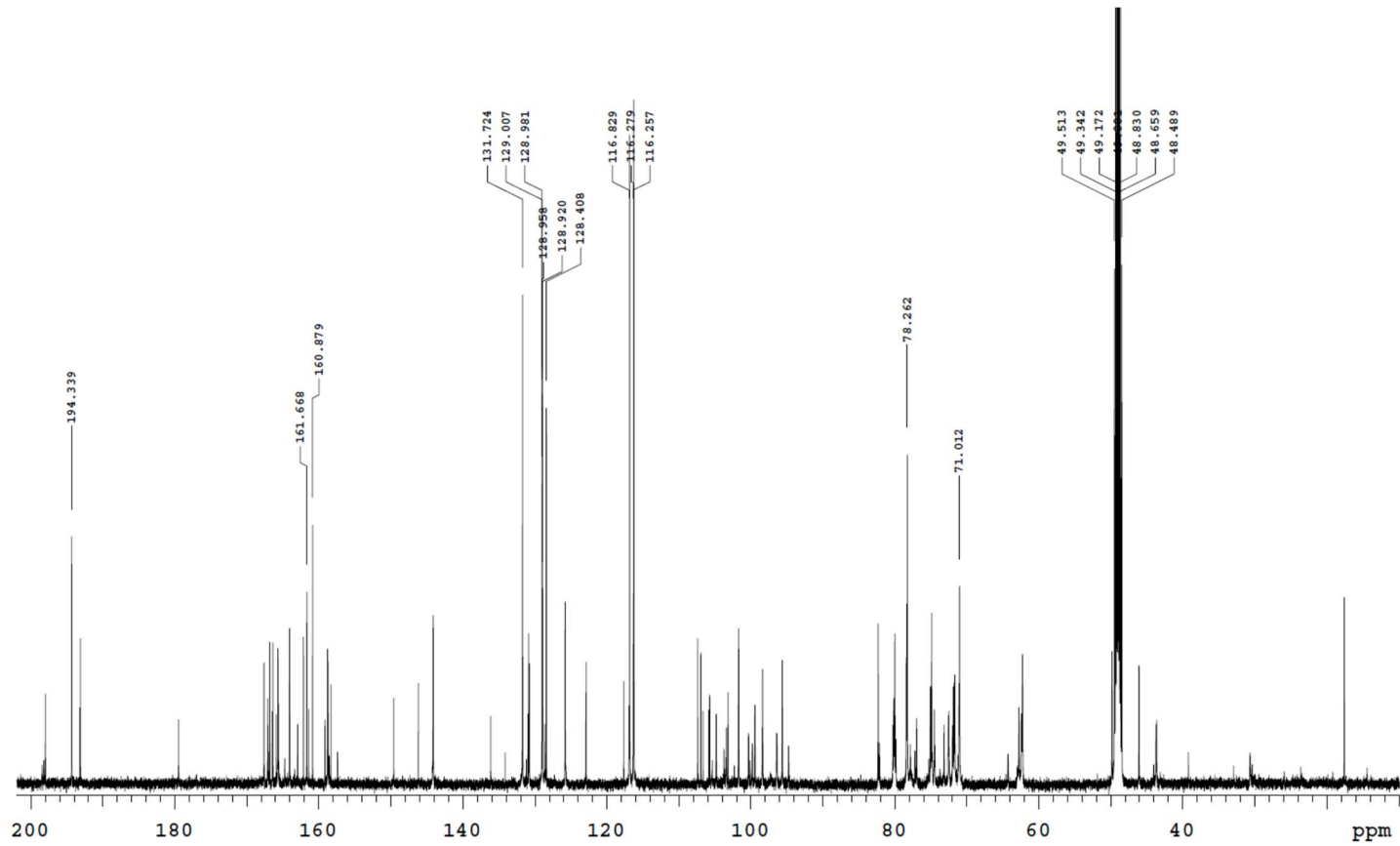


Figure 46. The spectral image of ^{13}C NMR of isosalipurposide **1** from methanolic extract of flowers

Table 9. ¹H NMR (400 MHz, CD₃OD), ¹³C NMR (100 MHz, CD₃OD), and 2D NMR data of compound from sub-fraction B1b of the methanolic flower extract compared to reported isosalipurposide **1**

No	FL-MeOH-B1b				Isosalipurposide ³²¹	
	δ ¹ H in ppm (m, J in Hz, integration)	δ ¹³ C (ppm)	COSY	HMBC	δ ¹ H in ppm (m, J Hz, integration)	δ ¹³ C (ppm)
1	-	128.47	-	-	-	128.3
2, 6	7.61 (d; 8.64; 2H)	131.74	H3, H5	C β , C3, C4	7.62 (d; 8.0; 1H), 7.62 (d; 8.0; 1H)	131.8, 132.2
3, 5	6.85 (d; 8.72; 2H)	116.85	H2, H6	C2, C6, C1, C4	6.87 (d; 8.0; 1H), 6.87 (d; 8.0; 1H)	116.9, 116.9
4	-	161.01	-	-	-	161.8
α	8.01 (d; 15.52; 1H)	125.88	H β	C1, C=O	8.02 (d; 15.0; 1H)	144.2
β	7.69 (d; 51.56; 1H)	144.12	H α	C α , C2, C1, C=O	7.68 (d; 15.0; 1H)	125.8
C=O	-	194.44	-	-	-	194.8
1'	-	107.46	-	-	-	107.8
2'	-	165.77	-	-	-	165.9
3'	6.18 (d; 2.24; 1H)	95.63	H5'	C1', C2', C4', C5', C=O	6.26 (s; 1H)	95.9
4'	-	161.75	-	-	-	161.1
5'	6.02 (d; 2.28; 1H)	98.35	H3'	C1', C2', C3', C6'	6.03 (s; 1H)	98.5
6'	-	167.70	-	-	-	161.4
1''	5.09 (d; 7.4; 1H)	101.82	H2''	C2'', C3''	5.15 (d; 7.8; 1H)	101.9
2''	3.44 (t; 8.75; 1H)	74.97	H1'', H3	C4'', C3''	3.39–3.46 (m; 1H)	75.3
3''	3.37 (t; 8.25; 1H)	78.45	H4'', H2''	C6'', C2''	3.60 (dd; 10.5, 7.5; 1H)	76.3
4''	3.47 (d; 7.5; 1H)	71.10	H3''	C1'', C2''	3.47–3.50 (m; 1H)	72.1
5''	3.39 (m; 1H)	78.41	H6''a, H6''b	C4'', C2'', C1'', C3'', C6''	3.54–3.57 (m; 1H)	76.7
6''a	3.62 (dd; 12, 5.32; 1H)	62.34	H6''b, H5''	C5''	3.76 (dd; 12.6, 1.5; 1H)	62.3
6''b	3.99 (dd; 11.36, 5.28; 1H)		H6''a, H5''	C5'', C2''	3.94 (dd; 12.6, 1.5; 1H)	62.3

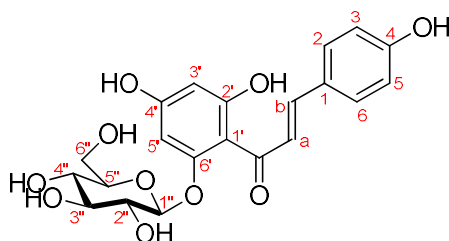


Figure 47. Molecular structure of isosalipurposide **1** (C₂₁H₂₂O₁₀; MW = 434.4)¹⁸⁸ from the methanolic flower extract.

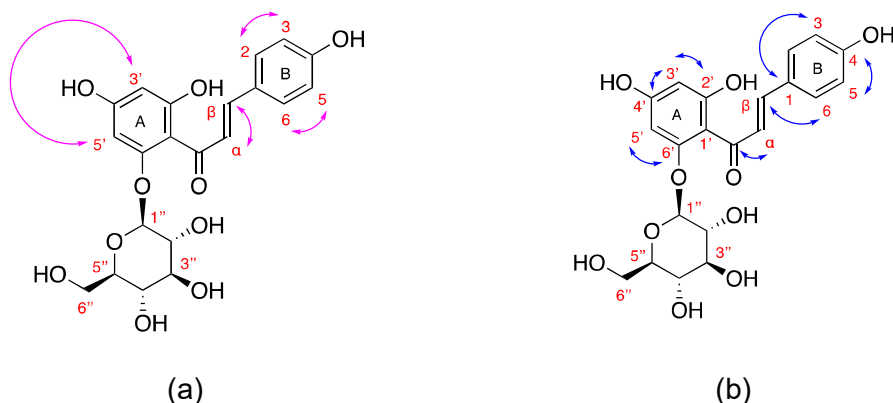


Figure 48. (a) The key connections of proton-to-proton (\leftrightarrow COSY) and (b) proton-to-carbon (\leftrightarrow HMBC) of isosalipurposide **1**.

4.2.1.4. Quercitrin **4** from flowers

Another structurally different flavonoid glycoside was obtained from the yellow powder of sub-fraction B2 of methanolic extract of flower (24.77 mg, 12.02%). Two different aromatic systems, trihydroxyl (ring A) and dihydroxyl (ring B), were assigned. Ring A has two shielded protons: H6 (6.21 ppm) *meta*-correlated to H8 (6.38 ppm) while, due to both electron-withdrawal (ring C) and -donation (-OH), ring B comprises benzene-generic protons, H6' (7.32 ppm) *meta*- and *ortho*-coupling to H2' (7.35 ppm) and H5' (6.92 ppm), respectively.

The glycone part has been assigned as α -rhamnoside with α -anomer (δ 1'' 5.36 ppm, 1.48 Hz), axial-equatorial couplings of H2''–H3'' (~3 Hz), axial-axial of H3''–H4'' (~9 Hz), and a proton methyl coupled to H5'' (6 Hz). The sugar unit has unique coupling constants of anomeric proton and methyl doublet of ~6 and ~1.3 Hz, respectively³²². The close similarity of the ¹³C NMR of C3 suggests that the monosaccharide is attached. In addition, the core skeleton has been confirmed as quercetin by comparison of δ ¹³C with those reported in Table 10. In other words, the isolated molecule could be quercetin-3-O-rhamnoside, trivially called quercitrin (Figure 51).

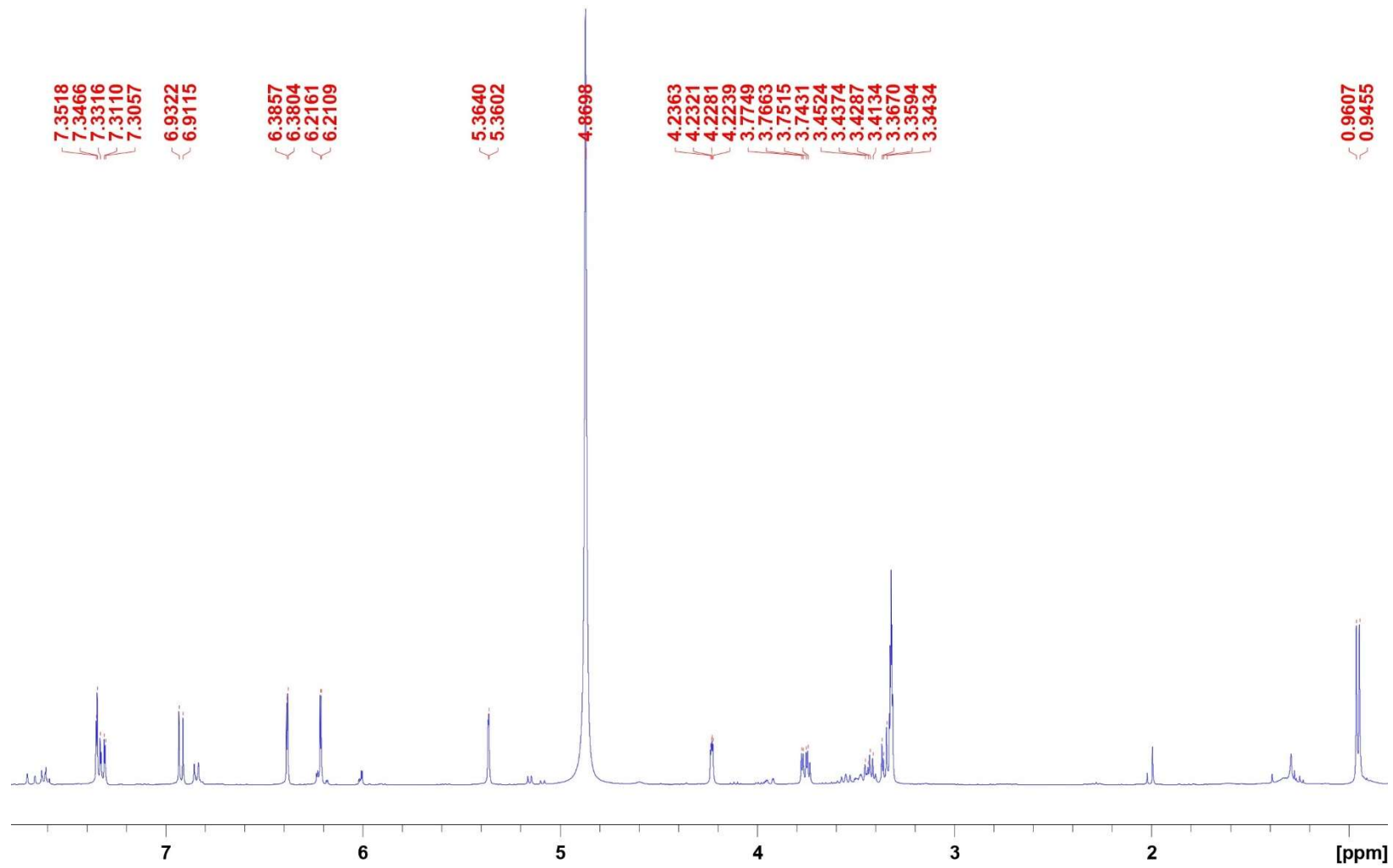


Figure 49. The spectral image of ¹H NMR of quercitrin **4** from methanolic extract of flowers

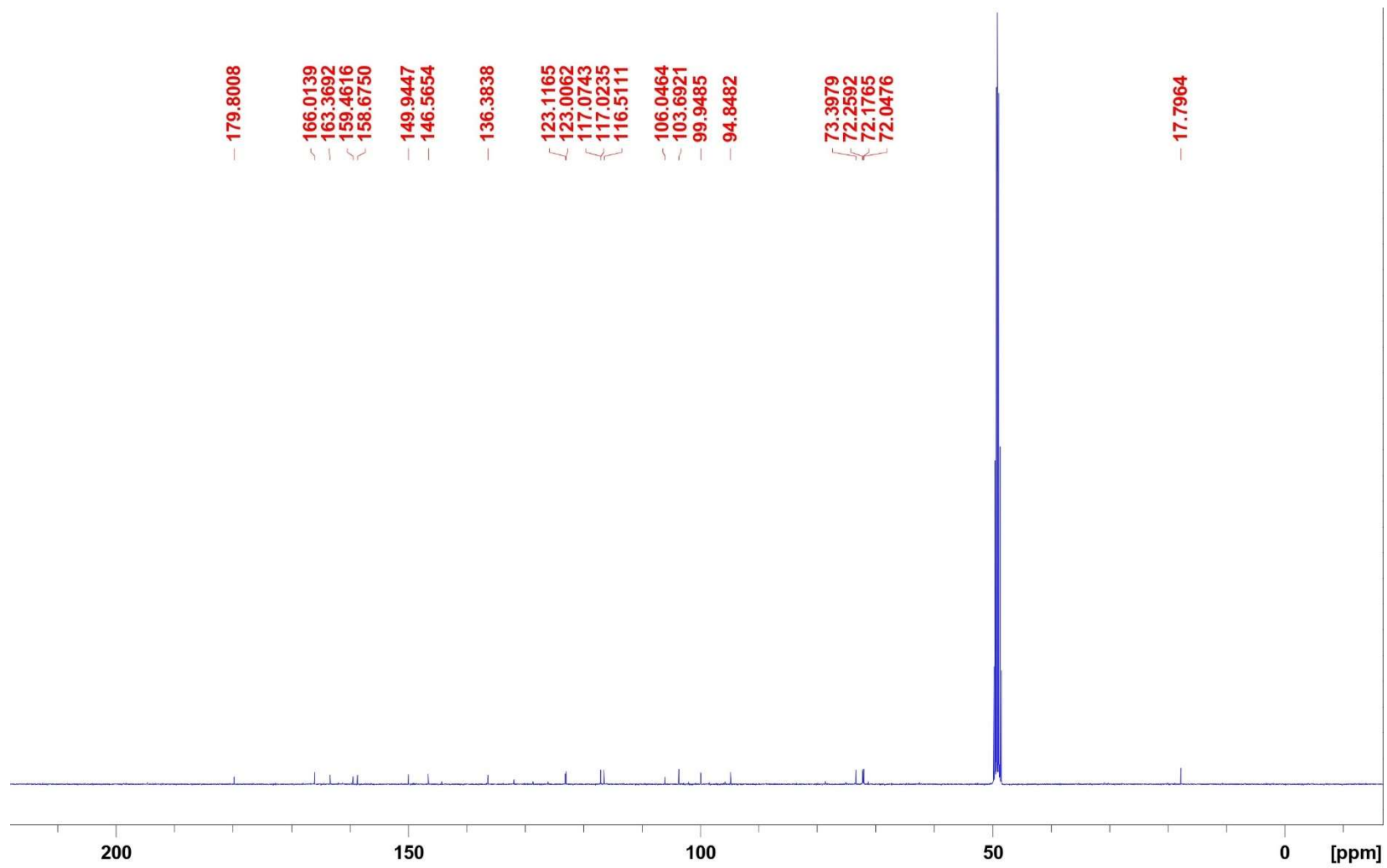


Figure 50. The spectral image of ^{13}C NMR of quercitrin 4 from methanolic extract of flowers

Table 10. ¹H NMR (400 MHz, CD₃OD), ¹³C NMR (100 MHz, CD₃OD), and 2D NMR data of compound from sub-fraction B2b of the methanolic extract of flowers compared to reported quercetin-3-O-rhamnoside (quercitrin **4**)

No	FL-MeOH-B2b				Quercitrin ³²³	
	δ ¹ H in ppm (m, J in Hz, integration)	δ ¹³ C (ppm)	COSY	HMBC	δ ¹ H ppm (m, J Hz, integration)	δ ¹³ C (ppm)
2	-	146.57	-	-	-	149.9
3	-	136.38	-	-	-	136.2
4	-	179.80	-	-	-	179.6
5	-	158.68	-	-	-	163.2
6	6.21 (d; 2.12; 1H)	99.95	H8	C4, C8, C10, C9	6.13 (d; 2.5; 1H)	100.2
7	-	166.01	-	-	-	167.2
8	6.38 (d; 2.08; 1H)	94.85	H6	C4, C5, C6, C7, C10	6.29 (d; 2.5; 1H)	95.3
9	-	163.37	-	-	-	158.6
10	-	106.05	-	-	-	105.6
1'	-	123.12	-	-	-	123.1
2'	7.35 (s; 1H)	117.07	-	C2, C6', C3', C4'	7.28 (s; 1H)	116.9
3'	-	149.95	-	-	-	146.4
4'	-	159.46	-	-	-	159.2
5'	6.92 (d; 8.28; 1H)	116.51	H6'	C2, C3, C2', C1', C3', C4', C6'	6.86 (d; 7.9; 1H)	116.4
6'	7.32 (dd; 8.28, 2.14; 1H)	123.01	H5'	C2, C2', C3', C4'	7.25 (d; 7.9; 1H)	122.8
1''	5.36 (d; 1.48; 1H)	103.69	H2''	C4''	5.29 (d; 1.2; 1H)	103.5
2''	4.23 (dd; 3.28, 1.68; 1H)	72.05	H1'', H3''	-	4.17 (m; 1H)	71.9
3''	3.76 (dd; 9.36, 3.44; 1H)	72.26	H4''	-	3.70 (d; 6.7; 1H)	72.2
4''	3.36 (t; 1H)	73.40	H3''	C5''	3.32 (d; 9.6; 1H)	73.4
5''	3.42 (d; 6.12; 1H)	72.18	H6''	-	3.35 (m; 1H)	72
6''	0.95 (d; 6.08; 3H)	17.80	H5''	-	0.86 (d; 6.1; 3H)	17.7

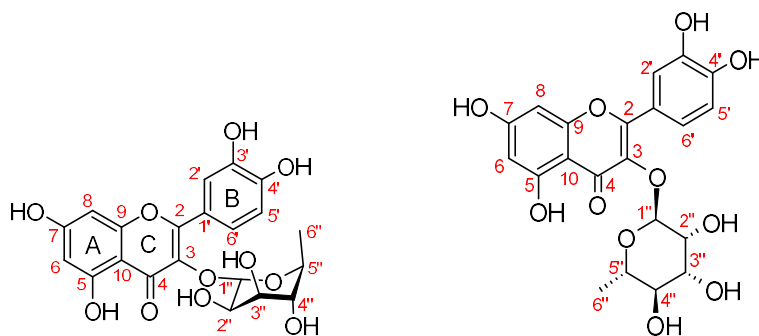


Figure 51. Molecular structure of quercitrin **4** from the methanolic extract of flowers.

This finding is not surprising as the isoliquiritigenin group is the precursor of flavonol derivatives in Leguminosae³¹⁸, like *A. saligna*, which may lead to the existence in the sample. Both compounds with quercetin were previously identified in crude ethanolic extract of *Coryloposis coreana* Uyeki flowers reported by Seo et al.³²⁴ and associated with its DPPH scavenging activity ($IC_{50} = 56.1 \mu\text{g/mL}$). Moreover, quercitrin has been well known as the active inhibitor of α -glucosidase from leguminous plants^{322, 325, 326}. Thus, these facts may justify the corresponding bioactive constituents in FL-MeOH extract to be further investigated, and the biological results of this investigation will be discussed in biological results and discussion in Chapter 5.

4.2.1.5. *D*(+)-pinitol **79a** from flowers

Table 11 shows 1D- and 2D-NMR data of the subfraction FL-MeOH-B3b from the methanolic flower extract (15 mg, 7.28%) by which the protons were found between 3 and 4 ppm. The connectivity among them can be summarised as follows:

1. Protons 1 and 6 couple have large vicinal coupling constants of 6.08 Hz representing geometrically different orientations (equatorial-equatorial).
2. Protons H1 to H2 and H6 to H5 shared the same coupling constants ($J = 2.08$ Hz), suggesting an equatorial-axial relationship.
3. Three equatorial-equatorial coupling systems ($J \sim 9$ Hz) are observed for H2 to H3, H3 to H4, and H4 to H5.
4. According to C-13 and C-DEPT data, H7 has been confirmed as a methoxy ($-\text{OCH}_3$).

The obtained data were identical to those reported for *D*-pinitol **79a** by Raya-Gonzalez et al.³²⁷. This inositol ether was first isolated in the sugar pine (*Pinus lambertiana*) by Anderson et al.³²⁸ and first documented in the genus *Acacia* in *A. nilotica*³²⁹. The compound has been actively confirmed as an antidiabetic^{330, 331}, antioxidant³³², and α -glucosidase inhibitor by its synthesised derivatives³³³. However,

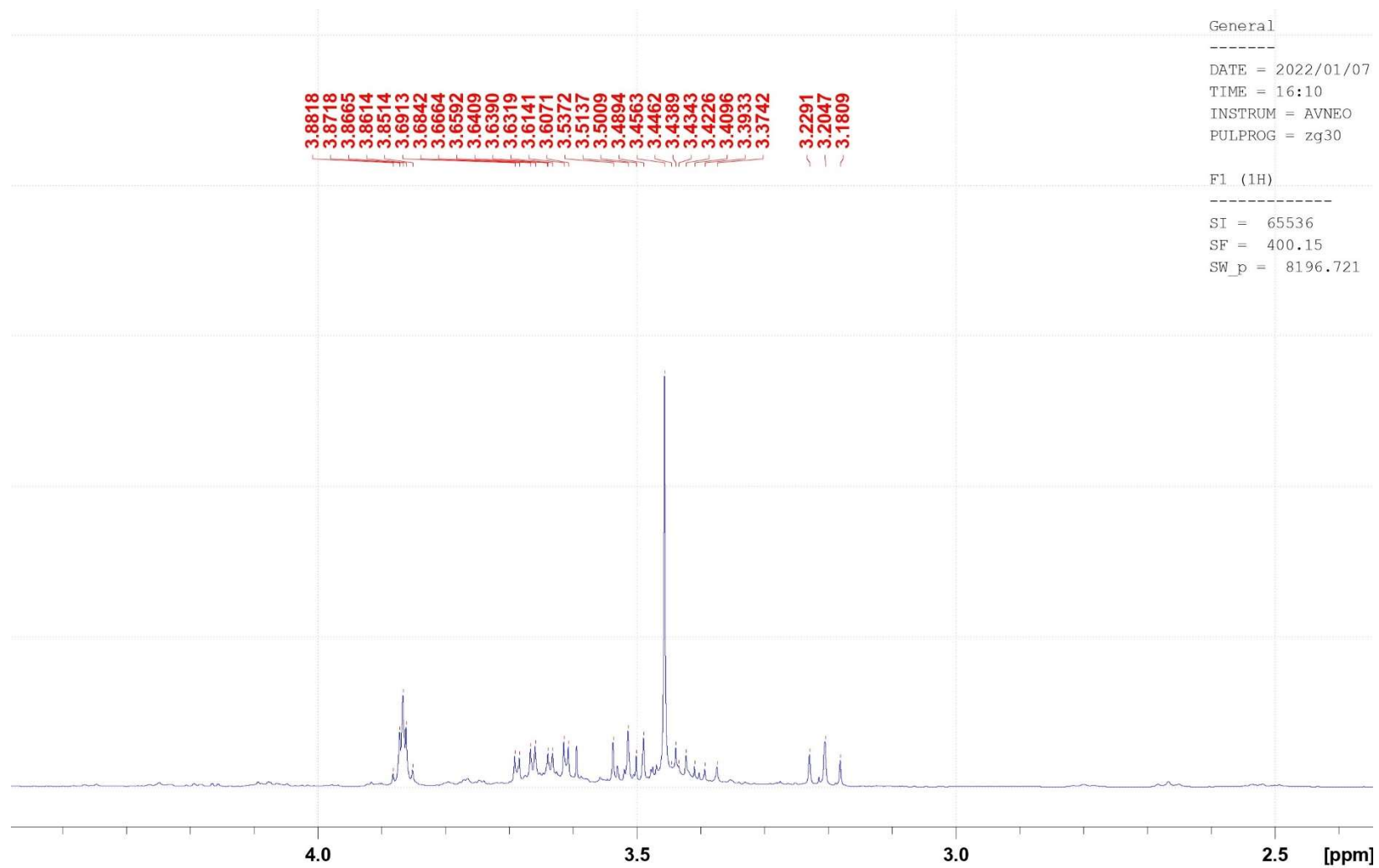


Figure 52. The spectral image of ^1H NMR of *D*-pinitol **79a** from methanolic extract of flowers

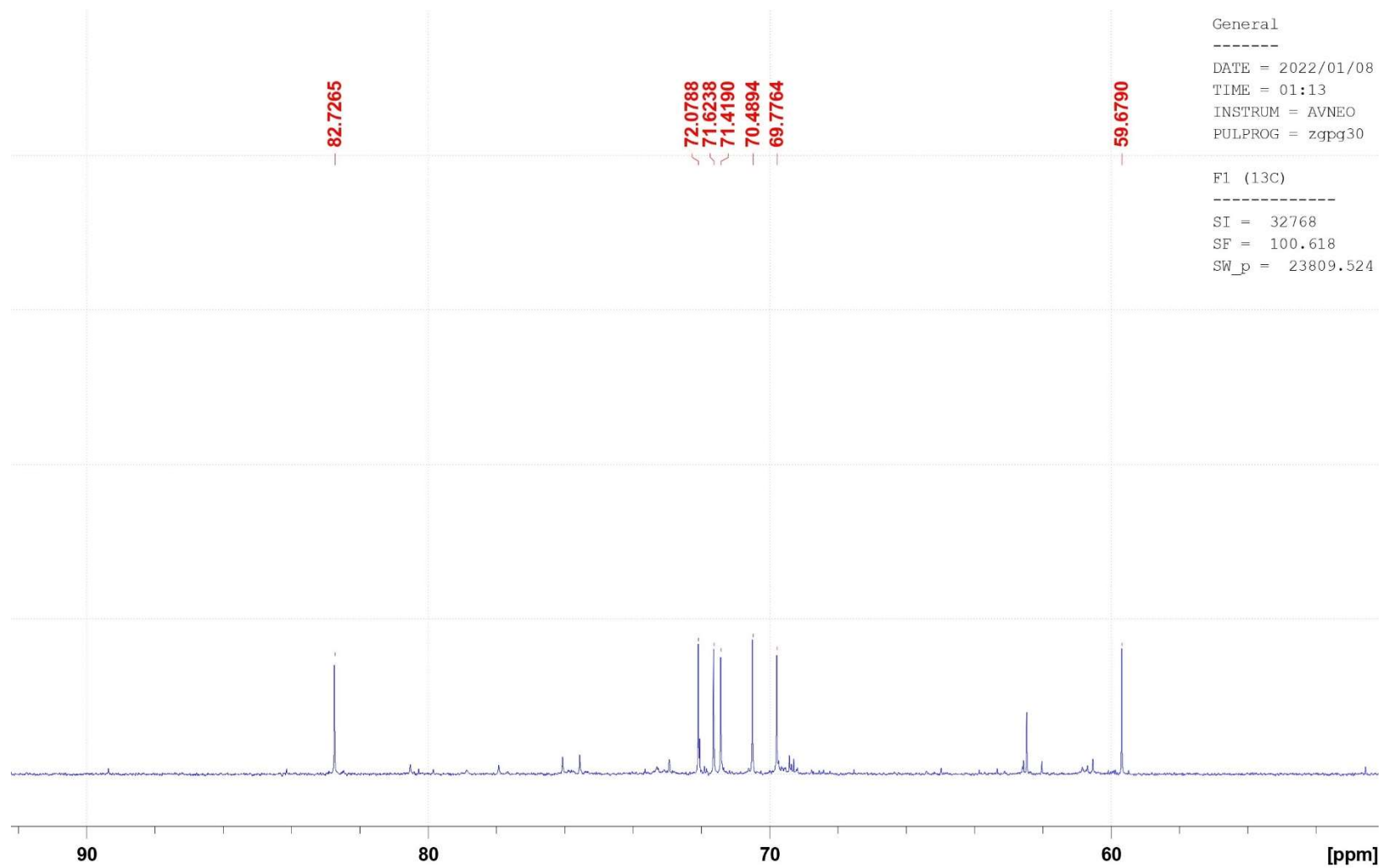


Figure 53. The spectral image of ^{13}C NMR of *D*-pinitol **79a** from methanolic extract of flowers

Table 11. ¹H NMR (400 MHz, D₂O), ¹³C NMR (100 MHz, D₂O), and 2D NMR data of compound from FL-MeOH-B3b compared to reported 3-O-methyl-*D*-chiro-inositol (*D*-(+)-pinitol **79a**)

No	FL-MeOH-B3b				Pinitol ³²⁷	
	δ H in ppm (m, J in Hz, integration)	COSY	δ C (ppm)	HMBC	δ ¹ H in ppm (m, J Hz, integration)	δ ¹³ C (ppm)
1	3.87 (m; 6.08, 2.08; 2H)	H2	71.62	C6, C2, C3	3.85 (m; 2H)	71.89
6		H5	71.42	C1, C4, C5		71.67
2	3.68 (dd; 9.96, 2.86; 1H)	H1, H3	69.78	C1, C3	3.66 (dd; 9.90, 2.60; 1H)	70.02
3	3.21 (t; 9.64, 1H)	H2, H4	82.73	C2, C4, C7	3.19 (t; 9.72; 1H)	82.96
4	3.51 (t; 9.56, 1H)	H3, H5	72.08	C3, C5	3.50 (t; 9.76; 1H)	72.32
5	3.62 (dd; 9.96, 2.86; 1H)	H4, H6	70.49	C4, C7	3.61 (dd; 9.98, 2.60; 1H)	70.73
7	3.46 (s; 3H)	-	59.68	C3	3.45 (s; 3H)	59.88

there seems to be no related documentation in any paper about isolating *D*-(+)-pinitol **79a** in any part of *A. saligna*.

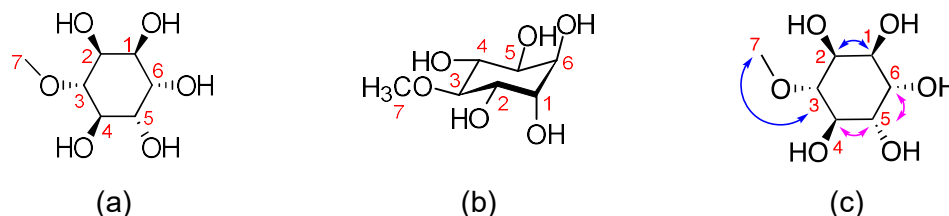


Figure 54. Molecular structure of 3-*O*-methyl-*D*-chiro-inositol (*D*-(+)-pinitol) (C₇H₁₄O₆) from the methanolic flower extract in (a) Haworth projection, (b) chair conformation, (c) COSY (↔) and HMBC (↔) relationship.

4.2.2. Three flavonoids, one substituted phenol, one cyclitol, and one lactone derivative from the LF-MeOH fraction

4.2.2.1. (-)-Epicatechin **77** from leaves

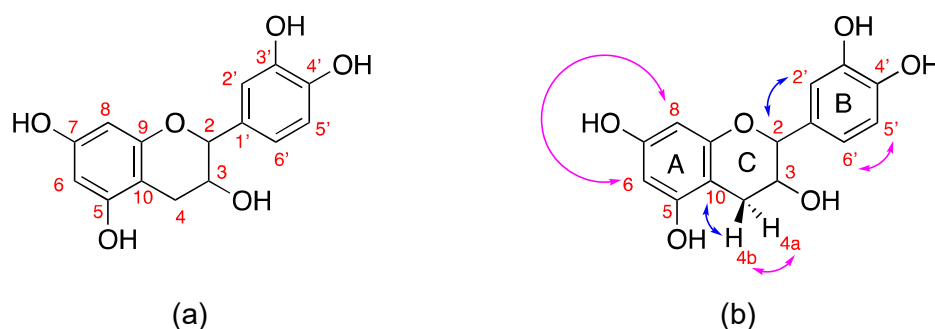


Figure 55. (a) The main skeleton of catechin (C₁₅H₁₄O₆; MW = 290.97) and (b) key connections of proton-to-proton (↔ COSY) and proton-to-carbon (↔ HMBC) of the catechin derivative found in LF-MeOH-A1.

The 1D- and 2D-NMR data (Table 12) shows that the compound in the subfraction LF-MeOH-A1 of the methanolic leaf extract (9 mg, 11.25%) could be an aglycone flavan-3-ol derivative. A geminal couple ($^2J = 16$ Hz) of protons 4 (δ_a 2.87 and δ_b 2.52 ppm) was also assigned, representing the typical proton resonance of catechin. In detail, the following information confirms the complete structure of the compound:

1. Proton 6 (5.83 ppm) and 8 (5.75 ppm) are meta couple ($J = 2.28$ Hz) representing ring A.
2. Meta couple of H6' (6.62 ppm) to H2' (6.74 ppm) with $J = 1.8$ Hz and ortho couple of H6' to H5' (6.66 ppm) with $J = 8$ Hz represent ring B.

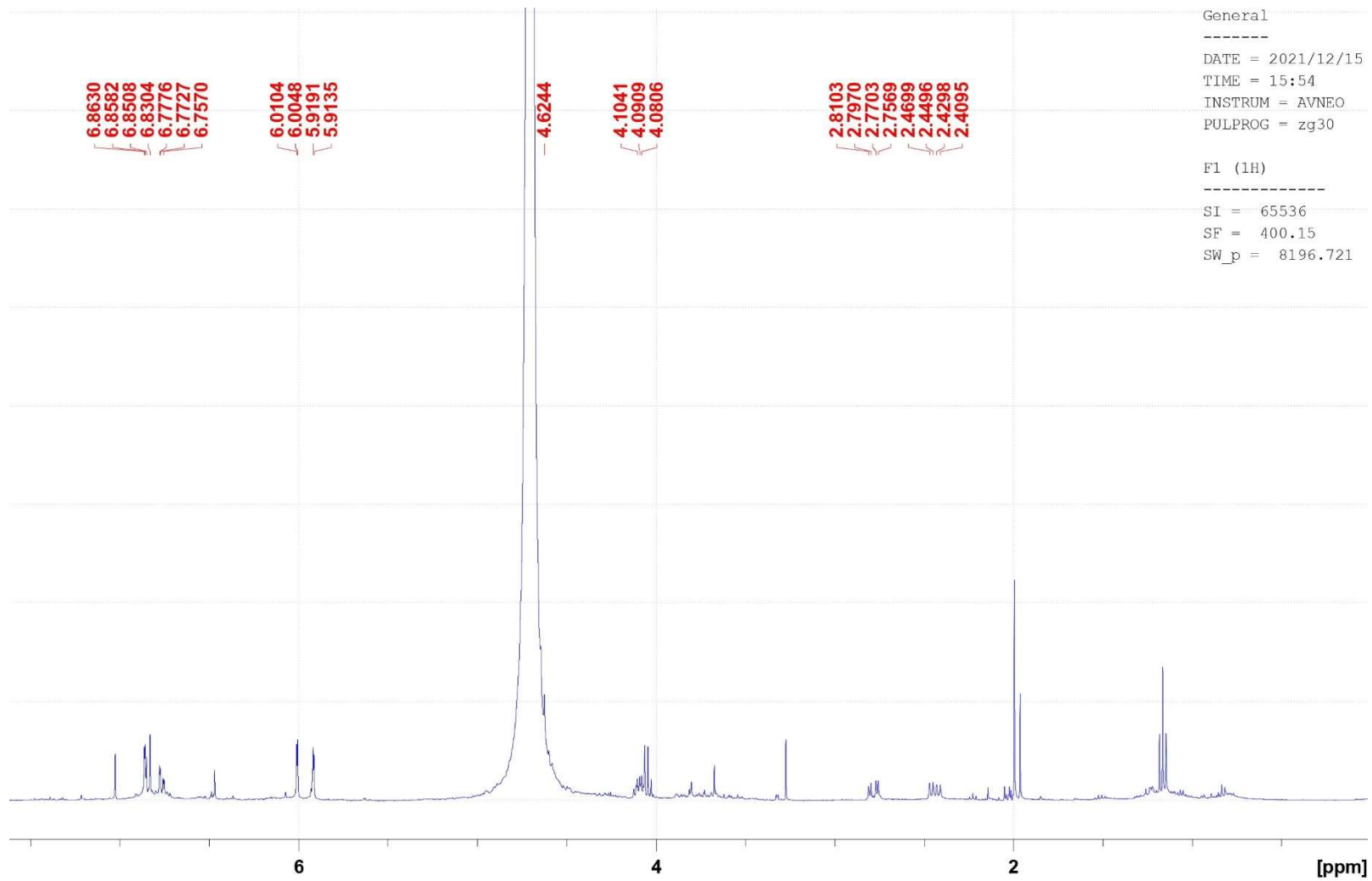


Figure 56. The spectral image of ^1H NMR of (-)-epicatechin **77** from methanolic extract of leaves

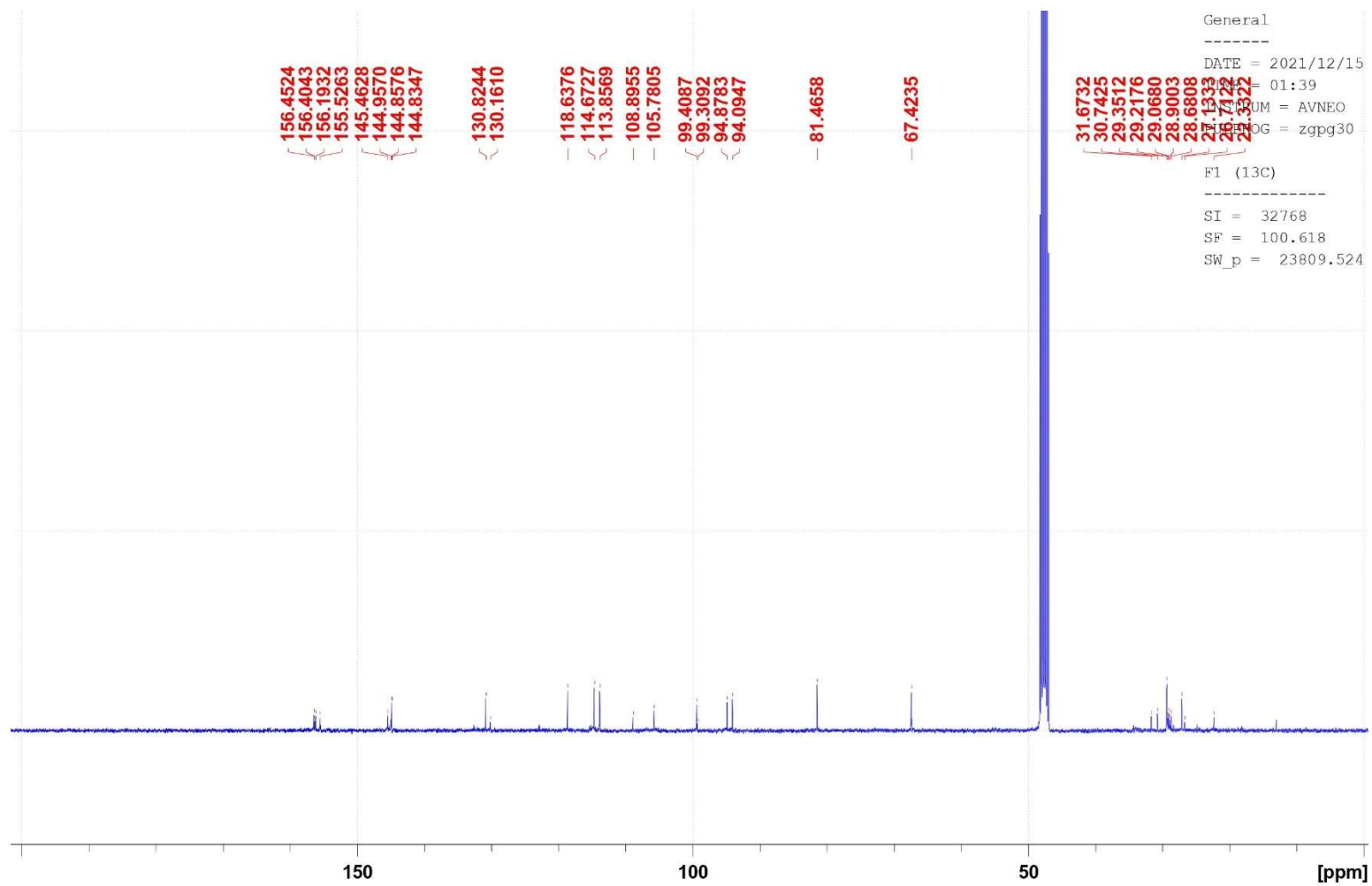


Figure 57. The spectral image of ^{13}C NMR of (-)-epicatechin **77** from methanolic extract of leaves

Table 12. ¹H NMR (400 MHz, D₂O), ¹³C NMR (100 MHz, D₂O), and 2D NMR data of compound from LF-MeOH-A1 compared to reported (–)-epicatechin 77.

No	LF-MeOH-A1					(–)-Epicatechin	
	δ ¹ H in ppm (m, J Hz, integration)	δ ¹³ C (ppm)	COSY	HMBC	NOESY	δ ¹ H in ppm (m, J in Hz, integration)	δ ¹³ C (ppm)
2	4.46 (d; 7.52; 1H)	82.99	H3	C3, C4, C2', C6', C1', C5	H4b	4.82 (br s; 1H)	79.88
3	3.87 (m; 1H)	68.95	H2, H4a, H4b		H4a (weaker), H4b (stronger)	4.19 (m; 1H)	67.49
4a	2.75 (dd; 16.16, 5.4; 1H)	28.69	H3, H4b	C2, C3, C5, C10	H4b	2.73 (dd; 16.8, 2.9; 1H)	29.26
4b	2.40 (dd; 16.12, 8.16; 1H)		H3, H4a	C3, C5, C10	H4a	2.87 (dd; 16.8, 4.5; 1H)	
5	-	157.72	-	-	-	-	158
6	5.83 (d; 2.28; 1H)	96.42	H8	C5, C10	-	5.94 (d; 2.3; 1H)	96.38
7	-	157.98	-	-	-	-	157.67
8	5.75 (d; 2.28; 1H)	95.64	H6	C6, C10	-	5.97 (d; 2.3; 1H)	95.88
9	-	157.06	-	-	-	-	157.37
10	-	100.95	-	-	-	-	100.06
1'	-	132.35	-	-	-	-	132.28
2'	6.74 (d; 1.84; 1H)	115.41	H5', H6'	C2, C6', C3'	H2, H3	6.98 (d; 1.9; 1H)	115.32
3'	-	146.36	-	-	-	-	145.78
4'	-	146.39	-	-	-	-	145.95
5'	6.66 (d; 8.12; 1H)	116.22	H6'	C2', C1', C4'	-	6.76 (d; 8.4; 1H)	115.88
6'	6.62 (dd; 1.88, 8.16; 1H)	120.18	H2', H5'	C2, C2', C4'	H2, H3	6.81 (dd; 8.4, 1.9; 1H)	119.39

- HMBC of H4 confirmed the connectivity between ring C to A and ring C to B to C10, and H2' to C2 (Figure 42b).
- The stronger cross-peaks correlation in the NOESY spectrum was observed for proton H2 and H3, H2 and H4b, and H3 and H4b, demonstrating the same spatial orientation among them.

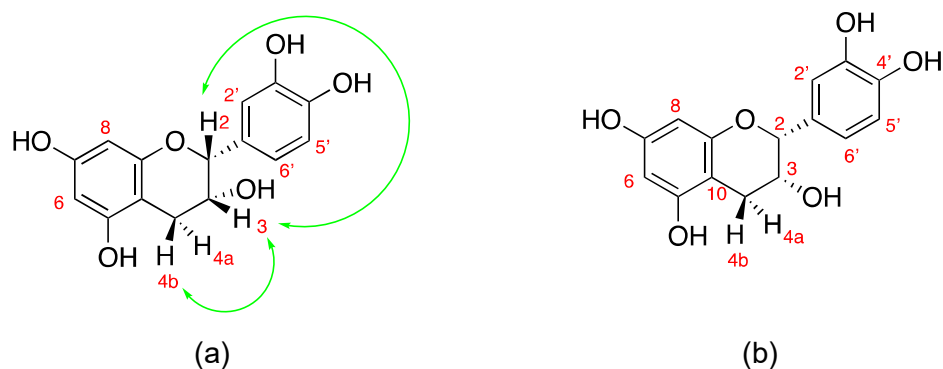


Figure 58. (a) Key connections of proton-to-proton (\leftrightarrow NOESY) showing the spatial relationship of vicinal protons and (b) the molecular structure of (-)-epicatechin **77** with *cis*-2*R*,3*R* stereochemical orientation.

Catechin derivatives are believed to be a ubiquitous component of vascular plants such as the *Acacia* genus. The isolation of catechin (the catechin isomer with *trans* configuration) and 7-galloylcatechin from *A. saligna* leaves was previously reported by E-Toumy et al.²¹⁵. However, this study did not show the specific rotation of the chiral protons. In our work, the *cis* isomer of catechin isolated from the leaves was identified as (-)-epicatechin **77**, demonstrated by its specific rotation value of $[\alpha]^{23} = -69.06^\circ$ (c 0.1, MeOH).

4.2.2.2. 2,4-Di-*t*-butylphenol **78**

A substituted monophenol derivative has been identified in the subfraction A3 of methanolic leaf extract (10 mg, 12.5%). According to the spectral information, the possible compound found in the subfraction A3 of methanolic leaves extract could be 2,4-di-*t*-butylphenol **78**. In addition, its δ proton and carbon data were also reported by those reported for 2,4-di-*t*-butylphenol **78** by Belghit et al.³³⁴ and Dharni et al.³³⁵ (Table 13). The data could be interpreted as follows:

- Tall peaks at 1.29 and 1.40 ppm were assigned as two *tert*-butyl groups.
- Two peaks of proton at 7.01 (H5) and 7.24 (H3) ppm have small *J* values (2.4 Hz), showing their *meta*-relationship. Moreover, H5 also has large *J* values of 8.32 Hz, suggesting an *ortho*-relationship to H6 (6.64 ppm).

LF-MeOH-A3 cc2 on 22 Dec 21

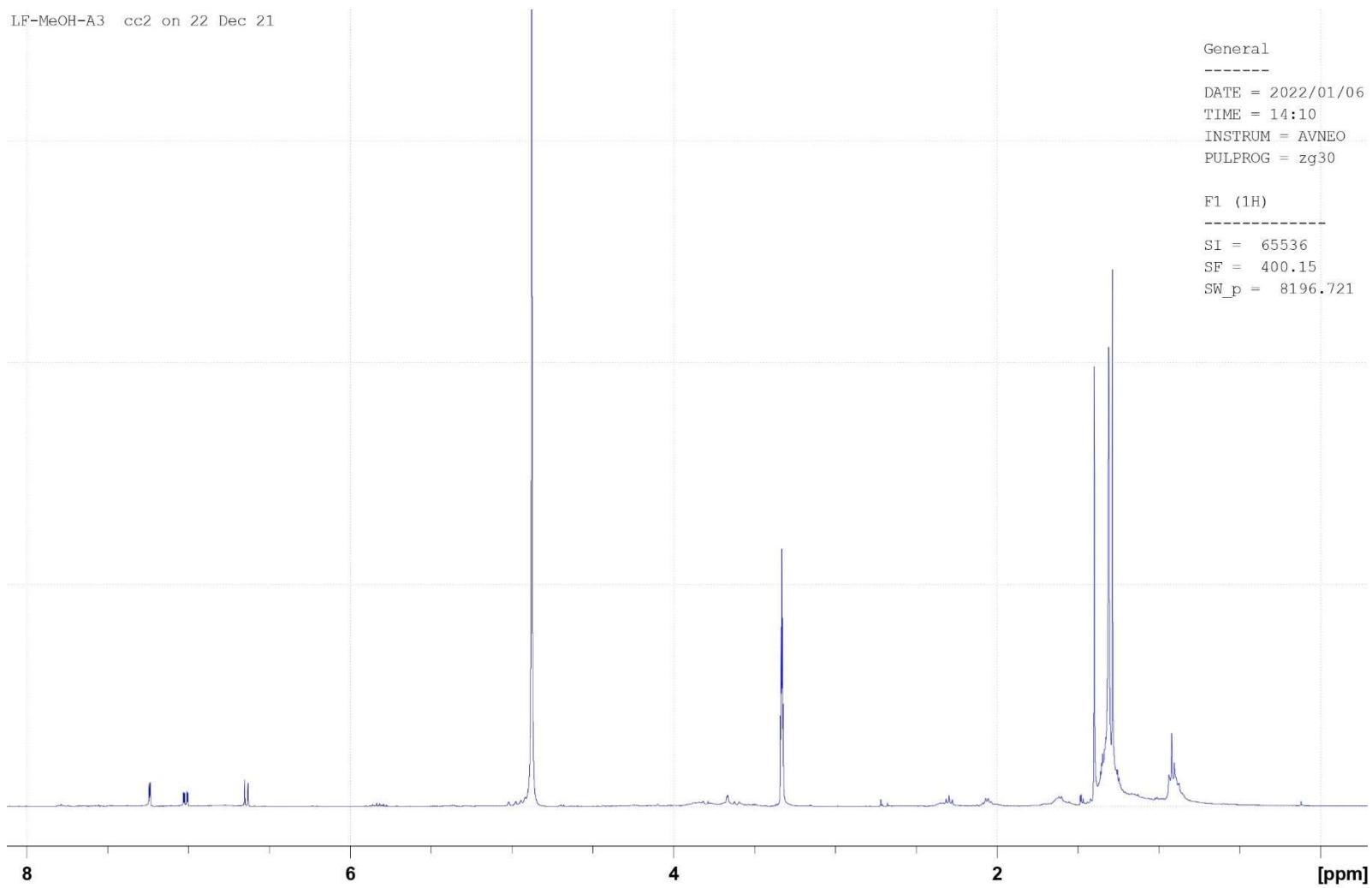


Figure 59. The spectral image of ^1H NMR of 2,4-di-*t*-butylphenol **78** from methanolic extract of leaves

LF-MeOH-A3 cc2 on 22 Dec 21

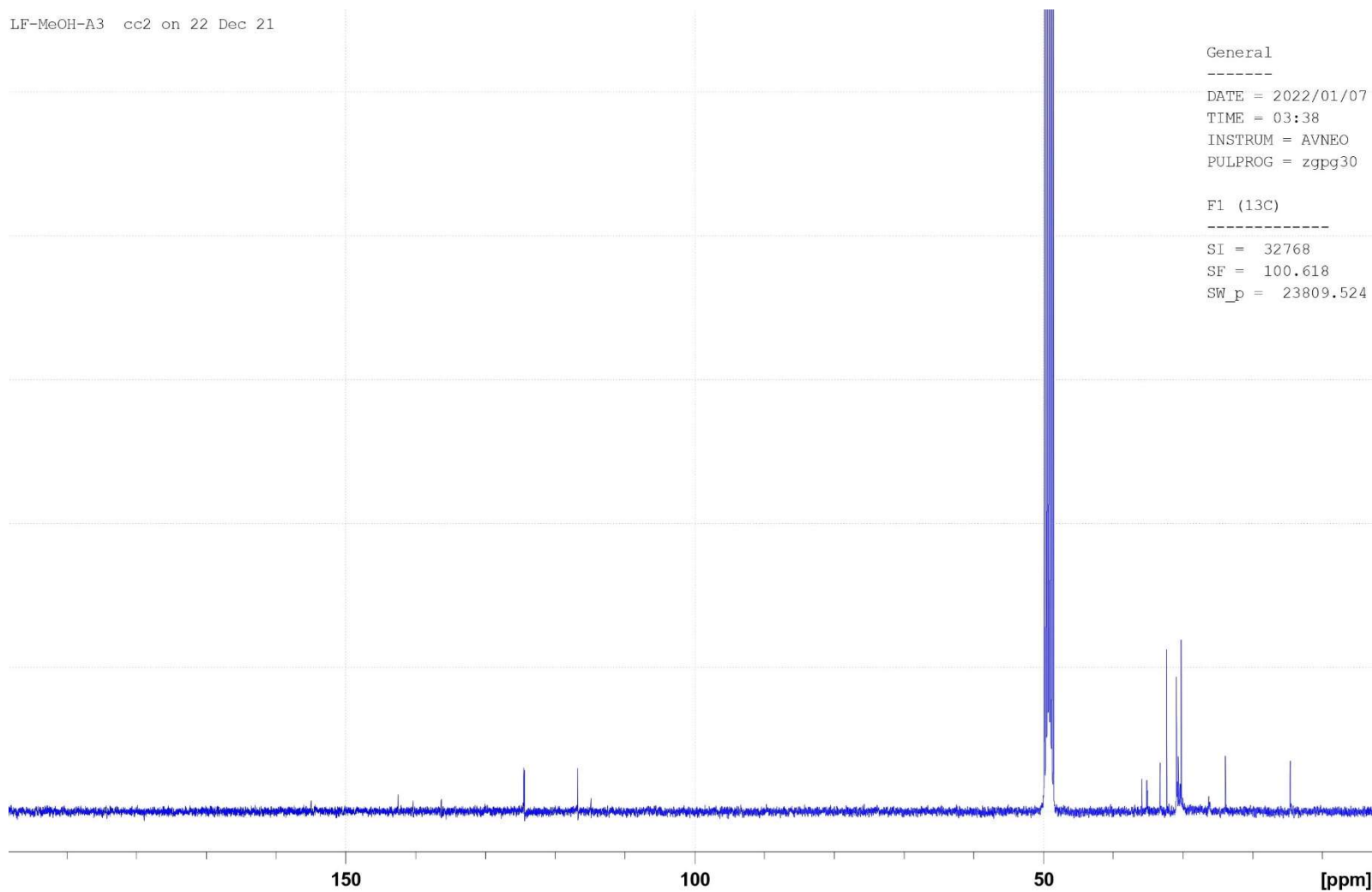


Figure 60. The spectral image of ^{13}C NMR of 2,4-di-*t*-butylphenol **78** from methanolic extract of leaves

Table 13. ¹H NMR (400 MHz, CD₃OD), ¹³C NMR (100 MHz, CD₃OD), and 2D NMR data of compound from LF-MeOH-A3 compared to reported 2,4-di-*t*-butylphenol **78**

No	LF-MeOH-A3				2,4-Di- <i>t</i> -butylphenol ^{334, 335}	
	δ H in ppm (m, J Hz, integration)	COSY	δ C (ppm)	HMBC	δ ¹ H in ppm (m, J Hz, integration)	δ ¹³ C (ppm)
1	-	-	154.93	-	-	153.38
2	-	-	136.27	-	-	134.77
3	7.24 (d; 2.44; 1H)	H5	124.45	C1, C5	7.24 (d; 2.4; 1H)	122.91
4	-	-	142.45	-	-	140.96
5	7.01 (dd; 8.32, 2.48; 1H)	H3, H6	124.37	C1, C3	7.02 (dd; 8.2, 2.4; 1H)	122.82
6	6.64 (d; 8.32; 1H)	H5	116.73	C1, C4	6.64 (d; 8.2; 1H)	115.19
7	-	-	35.85	-	-	34.31
8	-	-	35.12	-	-	33.58
9	1.40 (s, 9H)	-	30.22	C2, C3, C7	1.40 (s, 9H)	28.67
10	1.29 (s, 9H)	-	32.29	C4, C5, C8	1.29 (s, 9H)	30.76

- The shielded peak of H6 appears due to the shielding effect of the adjacent electron-donating group of hydroxyl.

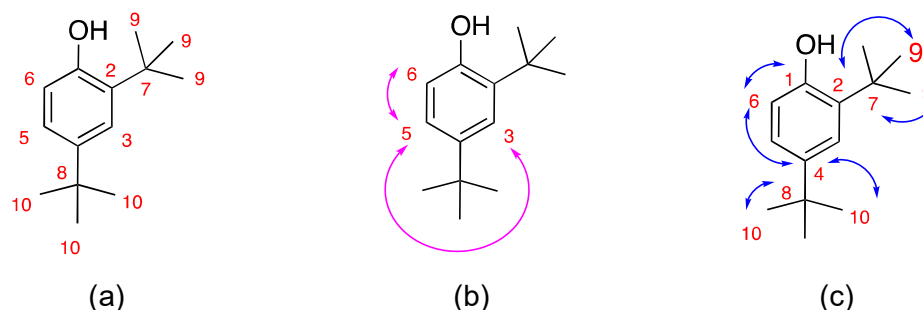


Figure 61. (a) The molecular structure of phenol-2,4-bis(1,1-dimethylethyl) or 2,4-di-*t*-butylphenol **78** (C₁₄H₂₂O, MW = 206.32) from LF-MeOH-A3, (b) the structure with key connectivity according to COSY (↔), and (c) HMBC (↔) information.

This compound has been isolated from different groups of organisms, including plants, e.g. sweet potatoes³²¹ and pine trees³³⁶, and animals, e.g. marine sponge *Zygomycale* sp³³⁷, such as the Chinese-red-headed centipede (*Scolopendra subspinipes*)³³⁸, bacteria, and fungi³³⁶. It has also been identified as an antioxidant³³⁹, anticancer, antiviral³⁴⁰, antibacterial, and antifungal³³⁵. Moreover, as 2,4-di-*t*-butylphenol **78** demonstrated allelopathic activities against weeds and lettuces^{341, 342}, this compound could also be linked to the herbicide properties of *A. saligna*, allowing this plant to grow uninterruptedly. Indeed, some previous works have demonstrated the strongly allelopathic^{192, 233, 343} and antifungal activities²¹⁶ of *A. saligna* leaves. Nevertheless, none of those reports identified 2,4-di-*t*-butylphenol **78** and tested its potential.

4.2.2.3. Quercitrin 4 from leaves

The sample of fraction LF-MeOH-B (60 mg) was eluted with an incremental gradient mobile phase (100:0, 95:5, and 9:1 of EtOAc/MeOH) through a packed column of silica gel 60 (4 g). Under a short-wave UV light inspection of its TLC plate, a major subfraction was obtained as LF-MeOH-B2 (28.6 mg, 47.67%). Table 14 shows 1D- and 2D-NMR data of an isolated compound in the sub-fraction B2. The chemical shifts of protons represent both oxygenated aromatics of ring A and B flavonol and a pyranose system. The data could be interpreted as follows:

- Upfield peaks at 6.21 and 6.37 ppm indicate a shielding effect of adjacent electron-donating groups attached to ring A (Figure 62). The small *J* values (2 Hz) show their *meta*-relationship. The peak at 6.21 ppm (H6) appears due to the *ortho*-substituent effects of two neighbouring hydroxyls, while the least shielded

of 6.37 ppm (H8) could probably be due to the *o*-substituent effects between ether and hydroxyl.

2. Three peaks in the downfield region reflecting an electron-withdrawing environment were assigned as protons of ring B. The electron withdrawal could occur due to an alkoxy group of ring C linked to C1' (123.11 ppm), leading to up shielded nucleus of *ortho* protons of H2' (7.35 ppm) and H6' (7.31 ppm). Moreover, the meta relationship of both protons was confirmed by their small *J* value of ~2 Hz. Apart from the electron-withdrawing effect, the next upfield proton at 6.92 ppm (H5') shows an electron-donating effect of the OH group (attached at C4') on the ortho position. This proton *o*-couples to H6' deduced by the *J* value of 8.5 Hz.
3. A duplet anomeric peak at 5.36 ppm (*J* = 1.5 Hz) could indicate a α conformation of the sugar substituent. Both small and large *J* values (3 and 9.5 Hz) represent axial-equatorial and axial-axial couplings of H2'–H3' and H3'–H4', respectively. Moreover, a triplet peak of 3.36 ppm (*J* = 9.5 Hz) demonstrates axial-axial relationships of C4' towards C3' and C5'. Finally, the C5' coupling to methyl protons suggests that the sugar could be a α -rhamnopyranoside assigned as *L*-form.
4. The connectivity between flavonol's sugar and core structure was established using HMBC. The HMBC cross-peaks of H1'' and C3 suggest that the sugar moiety was attached to the oxygen of C3. Furthermore, according to Table 14, the obtained data were identical to those reported for quercitrin **4**, a trivial name for quercetin-3-*O*-rhamnoside, by Kim et al.³²³.

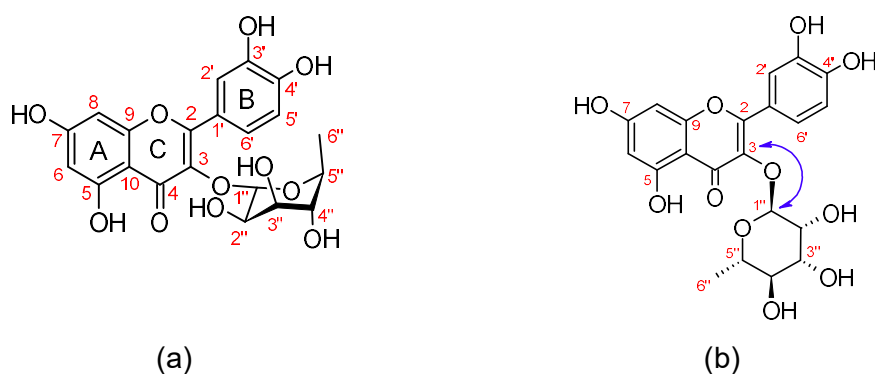


Figure 62. (a) Molecular structure of quercetin-3-*O*-rhamnoside from the methanolic extract of leaves (quercitrin **4**, C₂₁H₂₀O₁₁, MW = 448.1), and (b) key correlations within atoms based on HMBC.

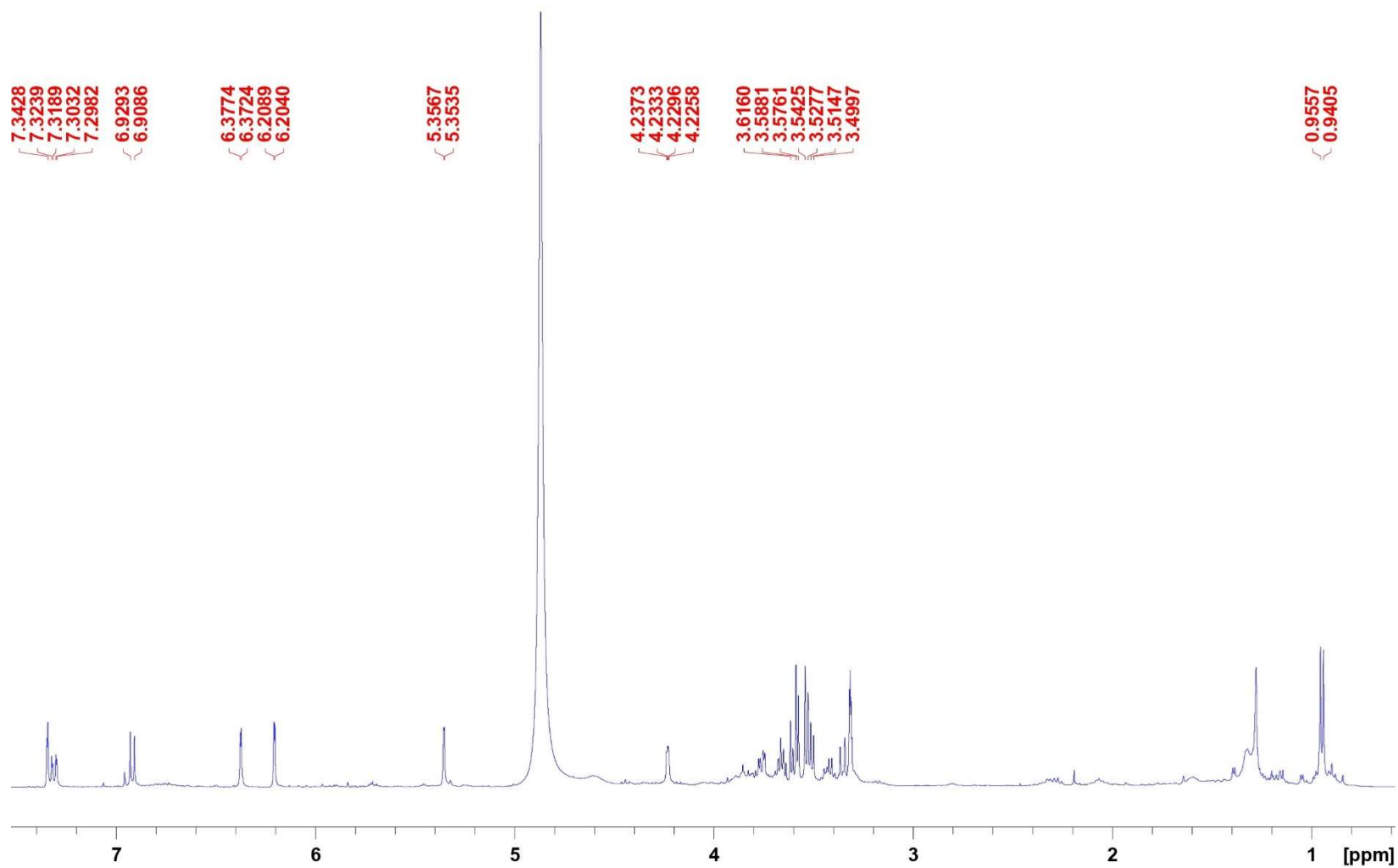


Figure 63. The spectral image of ¹H NMR of quercitrin **4** from methanolic extract of leaves

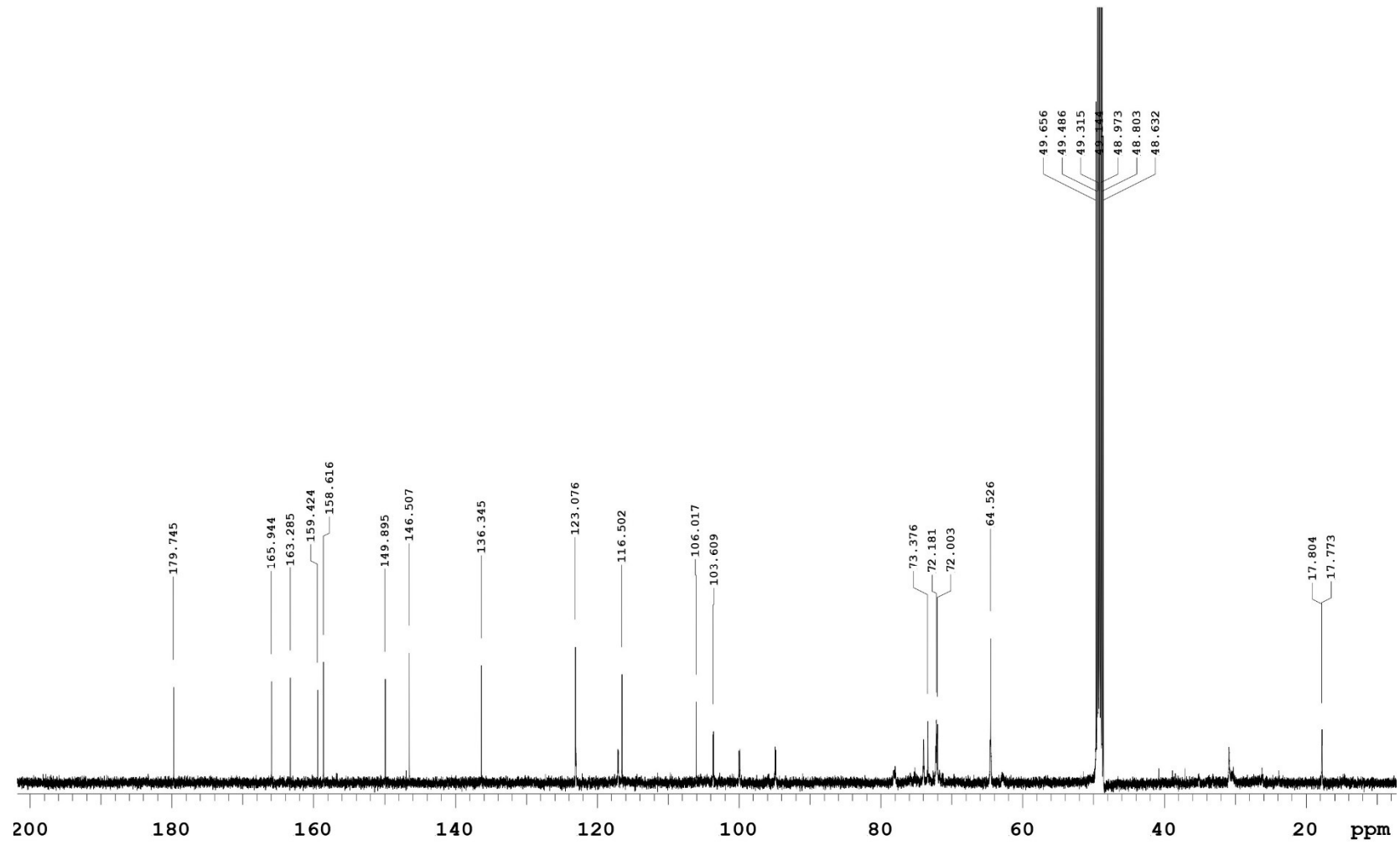


Figure 64. The spectral image of ¹³C NMR of quercitrin 4 from methanolic extract of leaves

Table 14. ¹H NMR (500 MHz, CD₃OD), ¹³C NMR (125 MHz, CD₃OD), and 2D NMR data of compound from LF-MeOH-B2 compared to reported quercitrin 4.

No	LF-MeOH-B2				Quercitrin ³²³	
	δ ¹ H in ppm (m, J in Hz, integration)	δ C (ppm)	COSY	HMBC	δ ¹ H ppm (m, J Hz, integration)	δ ¹³ C (ppm)
2	-	146.52	-	-	-	149.9
3	-	136.37	-	-	-	136.2
4	-	179.76	-	-	-	179.6
5	-	158.63	-	-	-	163.2
6	6.21 (d; 2; 1H)	99.94	H8	C5, C7, C10	6.13 (d; 2.5; 1H)	100.2
7	-	165.96	-	-	-	167.2
8	6.37 (d; 2; 1H)	94.85	H6	C7, C9, C10	6.29 (d; 2.5; 1H)	95.3
9	-	163.32	-	-	-	158.6
10	-	106.03	-	-	-	105.6
1'	-	123.11	-	-	-	123.1
2'	7.35 (d; 2.5; 1H)	116.50	H6'	C2, C1', C3', C4'	7.28 (s; 1H)	116.9
3'	-	149.90	-	-	-	146.4
4'	-	159.43	-	-	-	159.2
5'	6.92 (d; 8.5; 1H)	117.08	H6'	C2, C1', C3'	6.86 (d; 7.9; 1H)	116.4
6'	7.31 (dd; 8.5, 2; 1H)	123.02	H2', H5'	C3', C4'	7.25 (d; 7.9; 1H)	122.8
1''	5.36 (d; 1.5; 1H)	103.66	H2''	C3	5.29 (d; 1.2; 1H)	103.5
2''	4.24 (dd; 3, 2; 1H)	72.06	H1'', H3''	C3''	4.17 (m; 1H)	71.9
3''	3.77 (dd; 9.5, 3; 1H)	72.29	H2'', H4''	C4''	3.70 (d; 6.7; 1H)	72.2
4''	3.36 (t; 9.5; 1H)	73.40	H3''	C5''	3.32 (d; 9.6; 1H)	73.4
5''	3.42 (d; 6; 1H)	72.18	H5''		3.35 (m; 1H)	72
6''	0.95 (d; 6; 3H)	17.78	H6''	C5'', C4''	0.86 (d; 6.1; 3H)	17.7

According to these spectral data, the subfraction LF-MeOH-B2 could be considered quercitrin, a similar flavonol isolated from the methanolic extract of flowers. This compound was previously separated from ethanolic ¹⁸⁹, aqueous alcoholic ²¹⁵, and methanolic extract ¹⁹⁶ of the leaves. Furthermore, some reports demonstrated that several bioactivities, including ²¹⁵, antibacterial ¹⁹⁰, antioxidant and anticancer ¹⁹⁶ of the leaves, have been linked to this phytochemical.

4.2.2.4. Myricitrin 11

The sub-subfraction LF-MeOH-C2b (50 mg, 10.20%) was obtained through a further purification of LF-MeOH-C fraction (490 mg), which was the major fraction yielded from the fractionation of methanolic leaves extract (Figure S5, page 250). The yellow powder was collected by EtOAc/MeOH (90:10) elution out of the incremental gradient mobile phase (100:0, 95:5, 90:10, and 85:15 of EtOAc/MeOH) through a packed column of silica gel 60.

Table 15 shows 1D- and 2D-NMR data of the flavonol derivative isolated from the sub-subfraction C2b. The δ protons represent both oxygenated aromatics (two doublets at the upfield region and a singlet near the generic region of benzene) and a pyranose system (3 to 4 ppm and an anomeric peak of 5.33 ppm). The data could be interpreted as follows:

1. Upfield peaks at 6.21 and 6.37 ppm indicate a shielding effect of adjacent electron-donating groups attached to ring A (Figure 68). The small J values (1.8 and 2.3 Hz) show their *meta*-relationship. The peak at 6.21 ppm (H6) appears due to the *ortho*-substituent effects of two neighbouring hydroxyls, while the least shielded of 6.37 ppm (H8) could probably be due to the *o*-substituent effects between ether and hydroxyl.
2. A taller peak at 6.96 ppm represents two symmetric protons (H2' and H6') lying between electron-withdrawing (ring C) and -donating groups (hydroxyls) in ring B. The aromatic could be a parallel trihydroxyl substituents at C3', 4', and 5' of the ring, which were confirmed by typical δ s of C-13: a taller peak at 146.95 ppm representing C3' and 5' and a more upfield peak at 137.99 ppm for C4' due to the *o*-substituent effects of the adjacent groups.
3. An anomeric singlet peak at 5.33 ppm could indicate an α conformation of the glycone moiety. Both small and large J values (3.48 and 9.4 Hz) represent axial-equatorial and axial-axial couplings of H2'–H3' and H3'–H4', respectively. Moreover, a triplet peak of 3.37 ppm with larger J values (~9.5 Hz) demonstrates axial-axial relationships of C4' towards C3' and C5'. Finally, the C5' coupling to

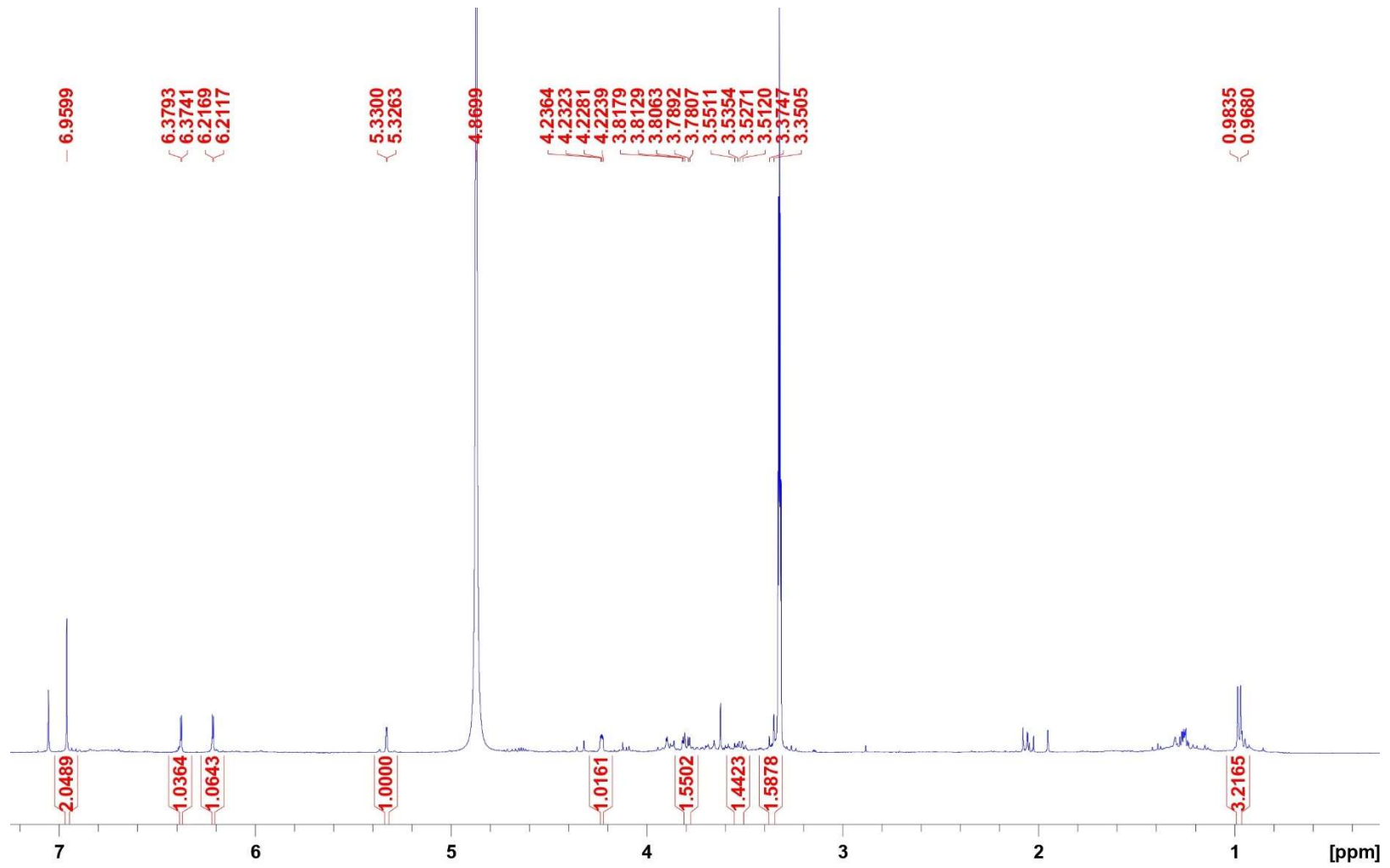


Figure 65. The spectral image of ¹H NMR of myricitrin 11 from methanolic extract of leaves

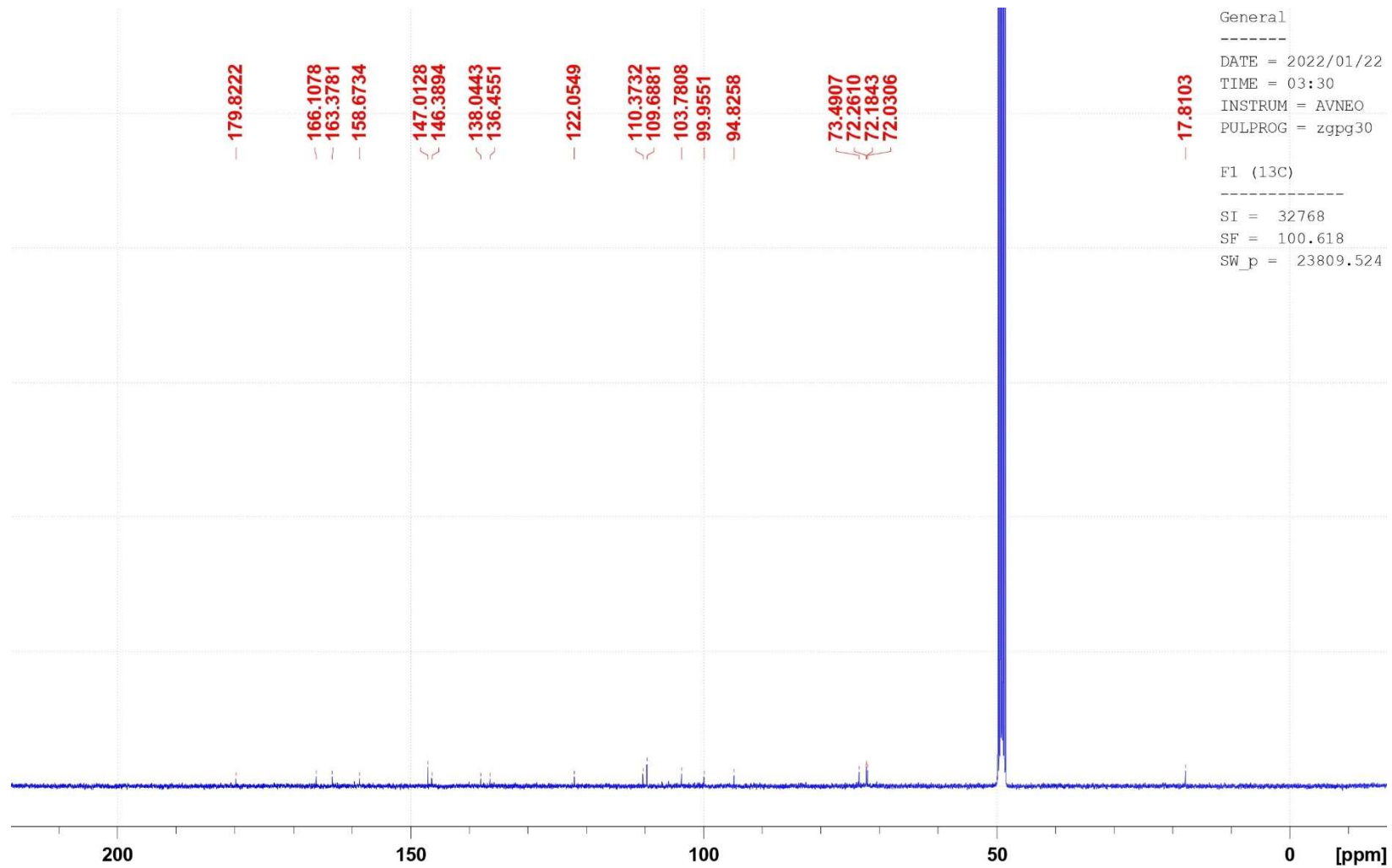


Figure 66. The spectral image of ^{13}C NMR of myricitrin **11** from methanolic extract of leaves

Table 15. ¹H NMR (400 MHz, CD₃OD), ¹³C NMR (100 MHz, CD₃OD), and 2D NMR data of compound from LF-MeOH-C2b compared to reported myricetin-3-O- α -L-rhamnopyranoside (myricitrin **11**)

No	LF-MeOH-C2b				Myricitrin ³⁴⁴	
	δ ¹ H in ppm (m, J in Hz, integration)	δ C (ppm)	COSY	HMBC	δ ¹ H ppm (m, J Hz, integration)	δ ¹³ C (ppm)
2	-	159.59	-	-	-	159.2
3	-	136.46	-	-	-	136.1
4	-	179.83	-	-	-	179.5
5	-	163.38	-	-	-	163.1
6	6.21 (d; 2; 1H)	99.96	H8	C5, C8, C10	6.19 (d; 1.8; 1H)	99.7
7	-	166.12	-	-	-	164.0
8	6.37 (d; 2; 1H)	94.83	H6	C6, C7, C9, C10	6.35 (d; 2.3; 1H)	94.6
9	-	158.61	-	-	-	158.4
10	-	106.00	-	-	-	105.6
1'	-	122.06	-	-	-	121.7
2'	6.96 (s; 2H)	109.69	-	C2, C1', C3', C4'	6.94 (s; 2H)	109.6
3'	-	147.02	-	-	-	146.7
4'	-	137.99	-	-	-	137.7
5'	-	147.02	-	-	-	146.7
6'	6.96 (s; 2H)	109.69	-	C2, C1', C3', C4'	6.94 (s; 2H)	109.6
1''	5.33 (s; 1H)	103.79	H2''	C3, C2''	5.30 (d; 1.8; 1H)	103.5
2''	4.24 (s; 1H)	72.04	H1'', H3''	-	4.21 (dd; 3.2, 1.8; 1H)	71.7
3''	3.8 (dd; 9.4, 3.48; 1H)	72.27	H2'', H4''	-	3.76–3.78 (dd; 9.4, 3.4; 1H)	72.0
4''	3.37 (t; 9.52; 1H)	73.50	H3'', H5''	-	3.31–3.34 (m; 1H)	73.2
5''	3.53 (dd; 9.66, 6.1; 1H)	72.19	H4'', H6''	-	3.48–3.54 (m; 1H)	71.9
6''	0.97 (d; 6.16; 3H)	17.82	H5''	C5''	0.94–0.96 (m; 3H)	17.5

methyl protons suggests that the sugar could be a α -rhamnopyranoside assigned as *L*-form.

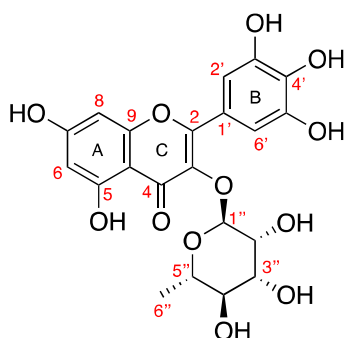


Figure 67. Molecular structure of myricetin-3-O-rhamnoside (myricitrin **11**) from methanolic leaf extract showing 3-D conformation of the sugar ring.

The connectivity of the main fragments of the molecule was established using an HMBC experiment. An HMBC-based correlation of H2 confirmed the link between ring B and C' and C2 (Figure 68). Moreover, the HMBC of H1'' and C3 suggests that the sugar part was attached to the carbon of ring C. Furthermore, the obtained data were identical to those reported for myricitrin, a trivial name for myricetin-3-O-rhamnoside, by Hwang & Chung³⁴⁴ (Table 15).

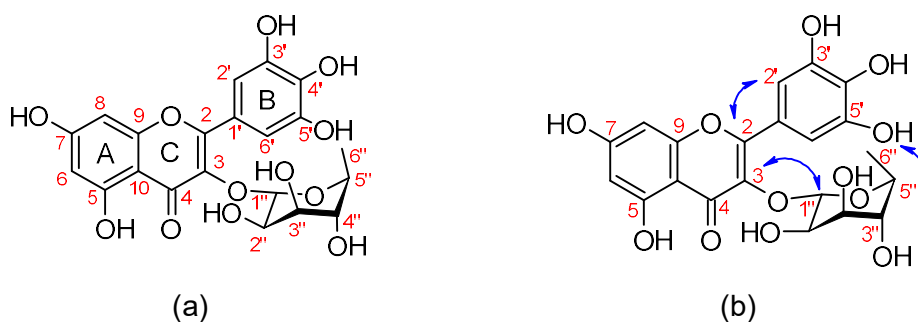


Figure 68. (a) Molecular structure of myricetin-3-O-rhamnoside (myricitrin **11**, C₂₁H₂₀O₁₂, MW = 464.37) and (b) key correlations within atoms based on selected HMBC.

4.2.2.5. (-)-Pinitol **79b**

The LF-MeOH-C3 was isolated from the methanolic leaf extract as a white solid (80 mg, 16.33%). Complete NMR and HRMS analysis initially revealed that this compound is identical to *D*-(+)-pinitol **79a**. The obtained data were identical to those reported for *D*-(+)-pinitol by Raya-Gonzalez et al.³²⁷ (Table 16). However, its optical rotation $[\alpha]^{23} = -79.44^\circ$ (c 0.1, H₂O) indicates that LF-MeOH-C3 is the enantiomer (-)-pinitol **79b** ($[\alpha]^{20} = -61.5^\circ$ (c 0.19, H₂O))³⁴⁵. It is known that both enantiomers of pinitol occur in various plants. However, this is the first time both enantiomers isolated

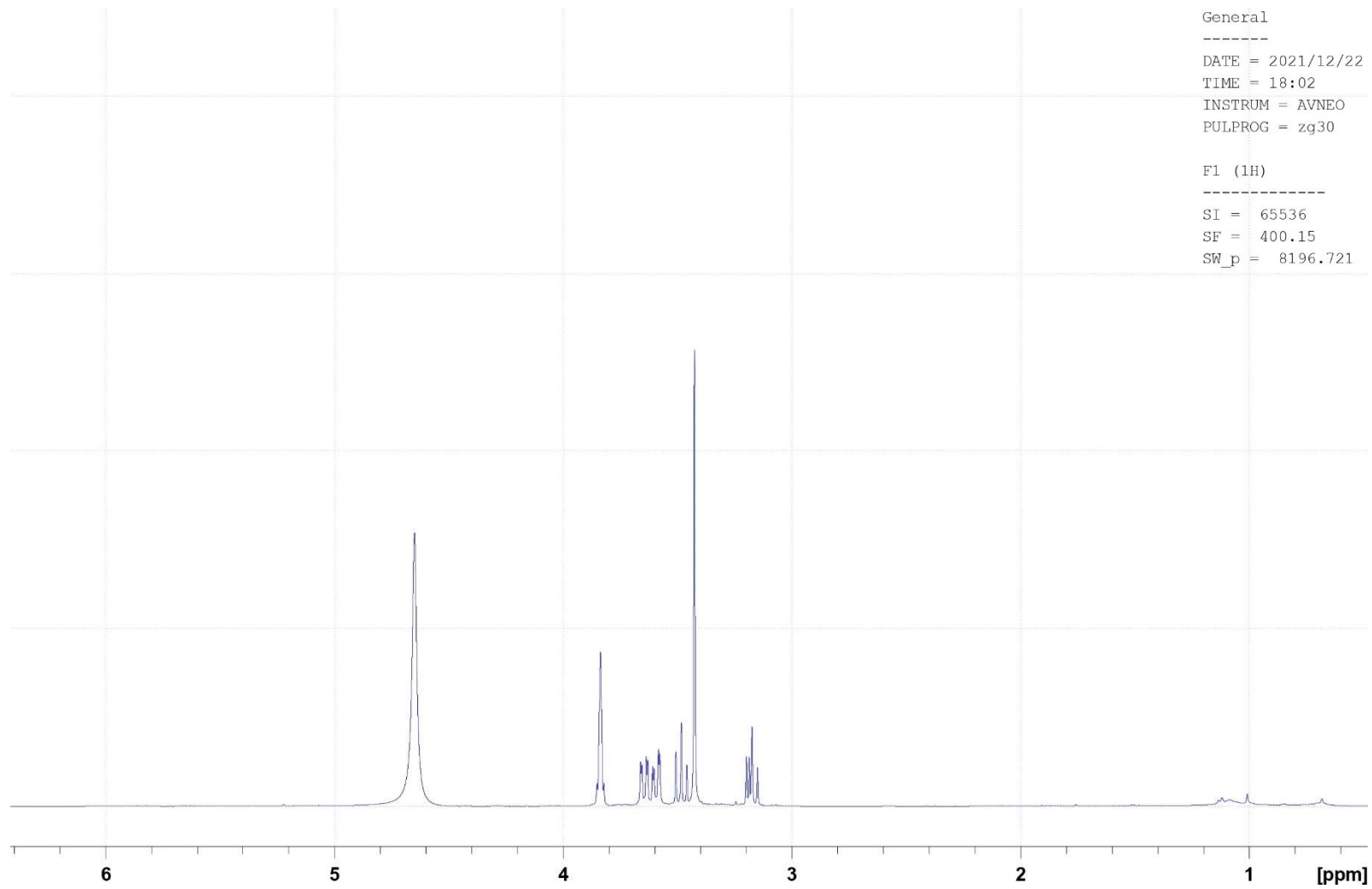


Figure 69. The spectral image of ^1H NMR of (-)-pinitol **79b** from methanolic extract of leaves

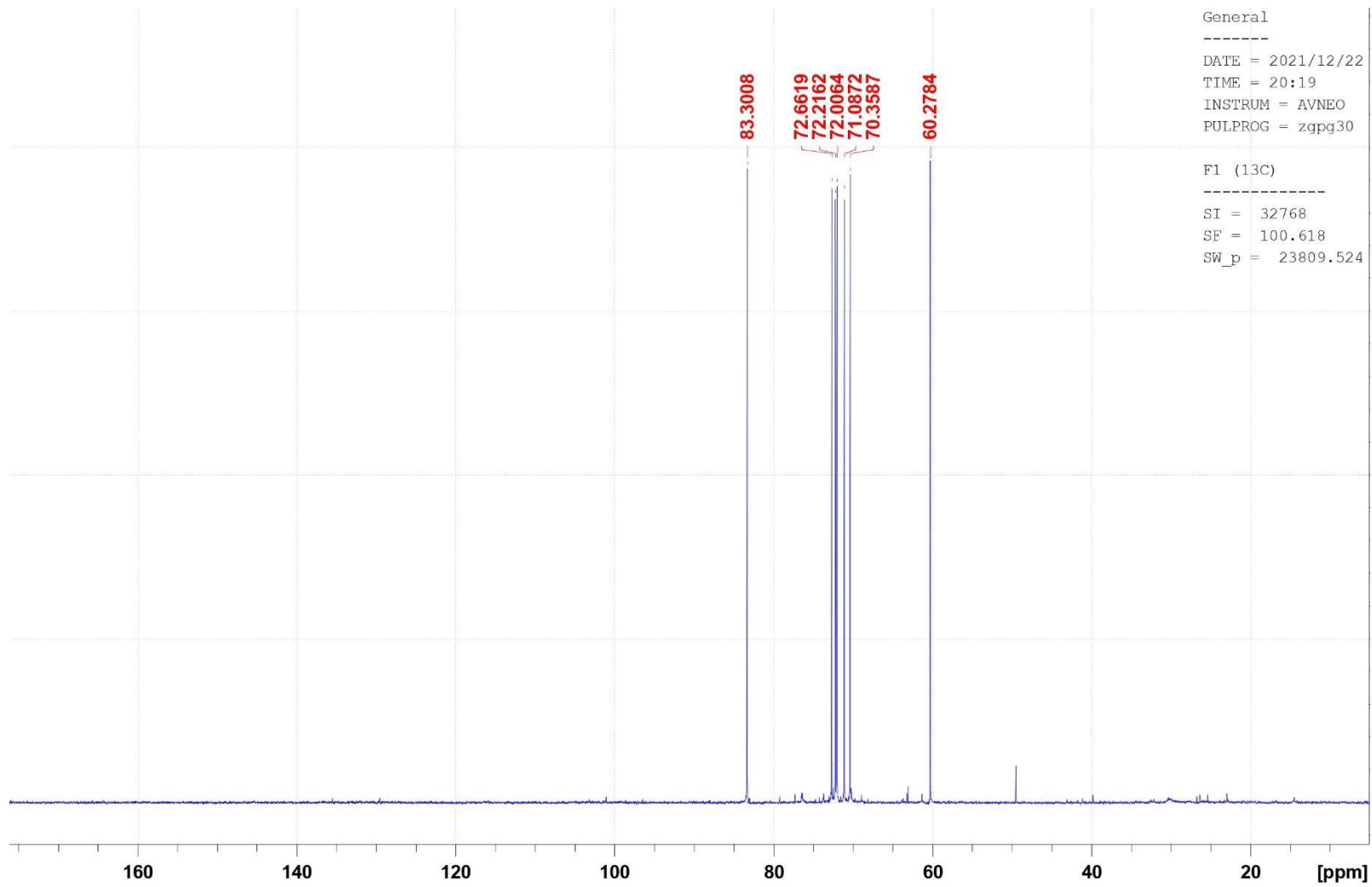


Figure 70. The spectral image of ^{13}C NMR of (-)-pinitol **79b** from methanolic extract of leaves

Table 16. ¹H NMR (400 MHz, D₂O), ¹³C NMR (100 MHz, D₂O), and 2D NMR data of compound from LF-MeOH-C3 compared to reported *D*-pinitol

No	LF-MeOH-C3				<i>D</i> -pinitol ³²⁷	
	δ ¹ H in ppm (m, <i>J</i> in Hz, integration)	δ C (ppm)	COSY	HMBC	δ ¹ H in ppm (m, <i>J</i> in Hz, integration)	δ ¹³ C (ppm)
1	3.99 (dd; 12, 6; 1H)	72.22	H2, H6	C2, C3	3.985 (m; 2H)	72.32
6	3.99 (dd; 12, 6; 1H)	72.01	H5, H1	C2		70.02
2	3.80 (dd; 9.92, 2.44; 1H)	70.36	H1, H3	C3	3.66 (dd; 9.90, 2.6; 1H)	71.67
3	3.32 (t; 9.66; 1H)	83.30	H2, H4	C1, C2, C7	3.19 (dd; 9.9, 9.53; 1H)	82.96
4	3.63 (t; 9.6; 1H)	72.66	H5, H3	C2, C3	3.50 (dd; 9.53, 9.98; 1H)	70.73
5	3.74 (dd; 9.88, 2.56; 1H)	71.09	H6, H4	C3, C6	3.61 (dd; 9.98, 2.6; 1H)	71.89
7	3.58 (s; 3H)	60.28	-	C3	3.45 (s; 3H)	59.88

from Australian *A saligna*. Furthermore, (-)-pinitol **79b** was exclusively isolated from the leaves of this plant.

D-pinitol is a typical secondary metabolite of plants living in water-deficit environments. This compound is a simple cyclic sugar derivative called cyclitol which is numbered counter-clockwise, indicating the *D*-configuration³⁴⁶. The *O*-methyl group has been observed to lead to dextrorotation (optically active structure)³⁴⁷. Both enantiomers of pinitol commonly occur in the same plant.

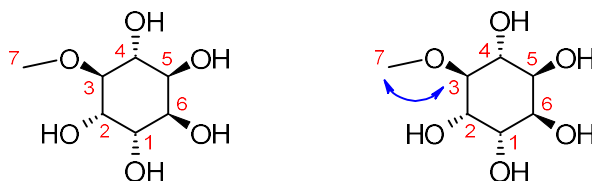


Figure 71. Molecular structure of (-)-pinitol **79b** (C₇H₁₄O₆) from the methanolic extract of leaves in Haworth projection with HMBC information.

4.2.2.6. 3-Hydroxy-5-(2-aminoethyl) dihydrofuran-2(3*H*)-one **80**

A polar colourless isolated compound was obtained from the methanolic extract of leaves (50 mg, 6%) with five proton peaks within 1.84 and 4.17 ppm. This isolate has six carbons, including three –CH₂s resonating in upfield (26.50 and 32.74 ppm) and mildly downfield region (38.53 ppm), two –CHs resonating in farther downfield of the singly-oxygenated saturated region (53.90 and 61.80 ppm), and a carbonyl (δ 175.27 ppm). The detailed interpreted information is as follows:

1. A geminal pair of protons (δ H4a and H4b of 2.16 and 1.91 ppm) was observed to couple to a doublet-doublet proton H3 bore in a chiral centre resonating in the region of singly-oxygenated carbon (δ C3 53.90 ppm).
2. A multiplete peak representing 2 protons (H7) bore in an electronegative group-substituted C-7 was coupled to an upfield peak corresponding to H6 as –CH₂. The group was assigned as a primary amine according to the δ C7 characteristics excluded from the singly-oxygenated region and the HRMS data.
3. Even though proton H5 was not observed to couple to any proton, data of TOCSY and NOESY showed that this proton with a multiplete downfield spectrum could be a part of the system. The cross-peaks correlation of TOCSY demonstrated three patterns for (1) H5 to H3 and H4, as well as (2) H5 to H6 and H7, and (3) H3 to H4a and H5. Therefore, a five-membered ring could be possible as the core of this compound, where H6 and H7 seem to be the chain-like substituent attached to the chiral centre of C5.

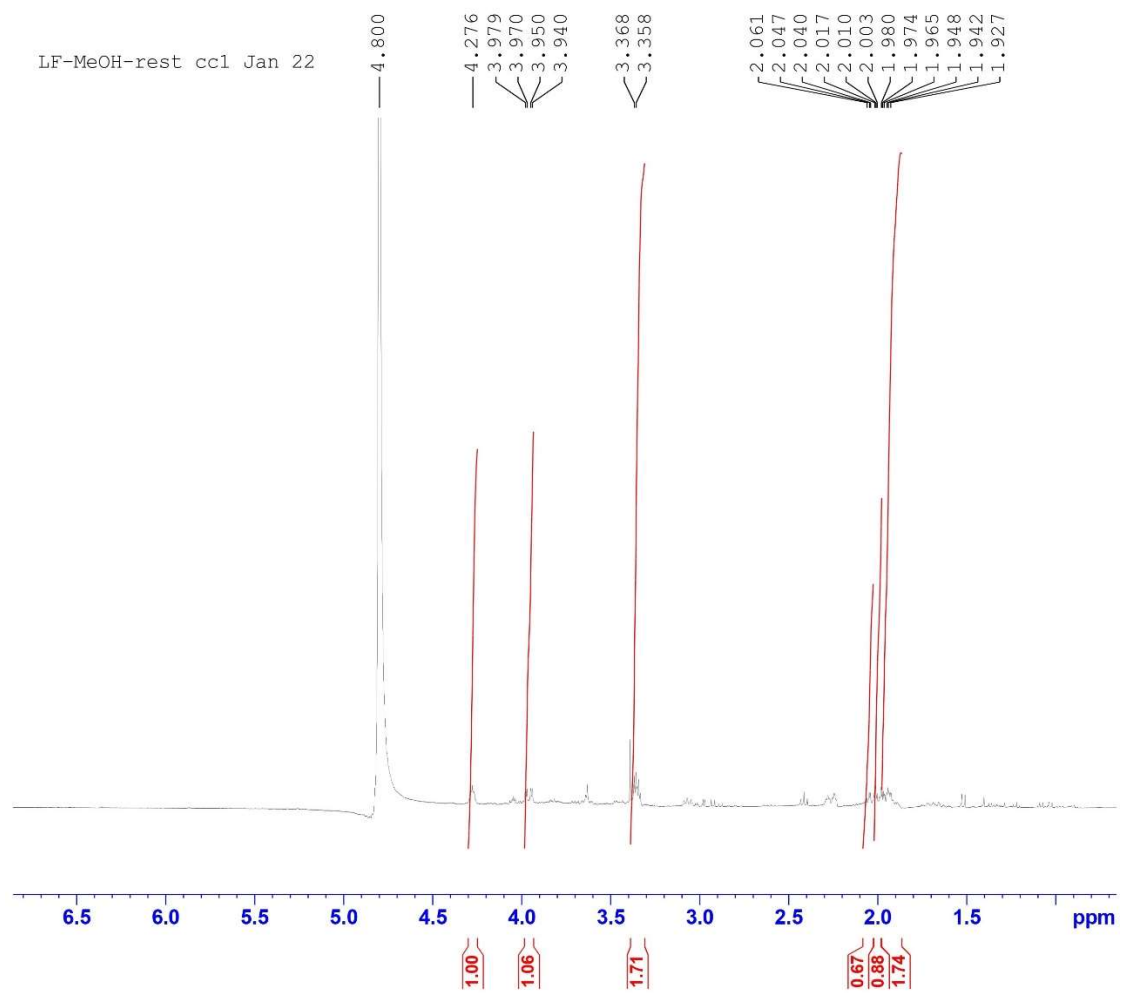


Figure 72. The spectral image of ^1H NMR of compound **80** from methanolic extract of leaves

LF-MeOH-rest ccl Jan 22

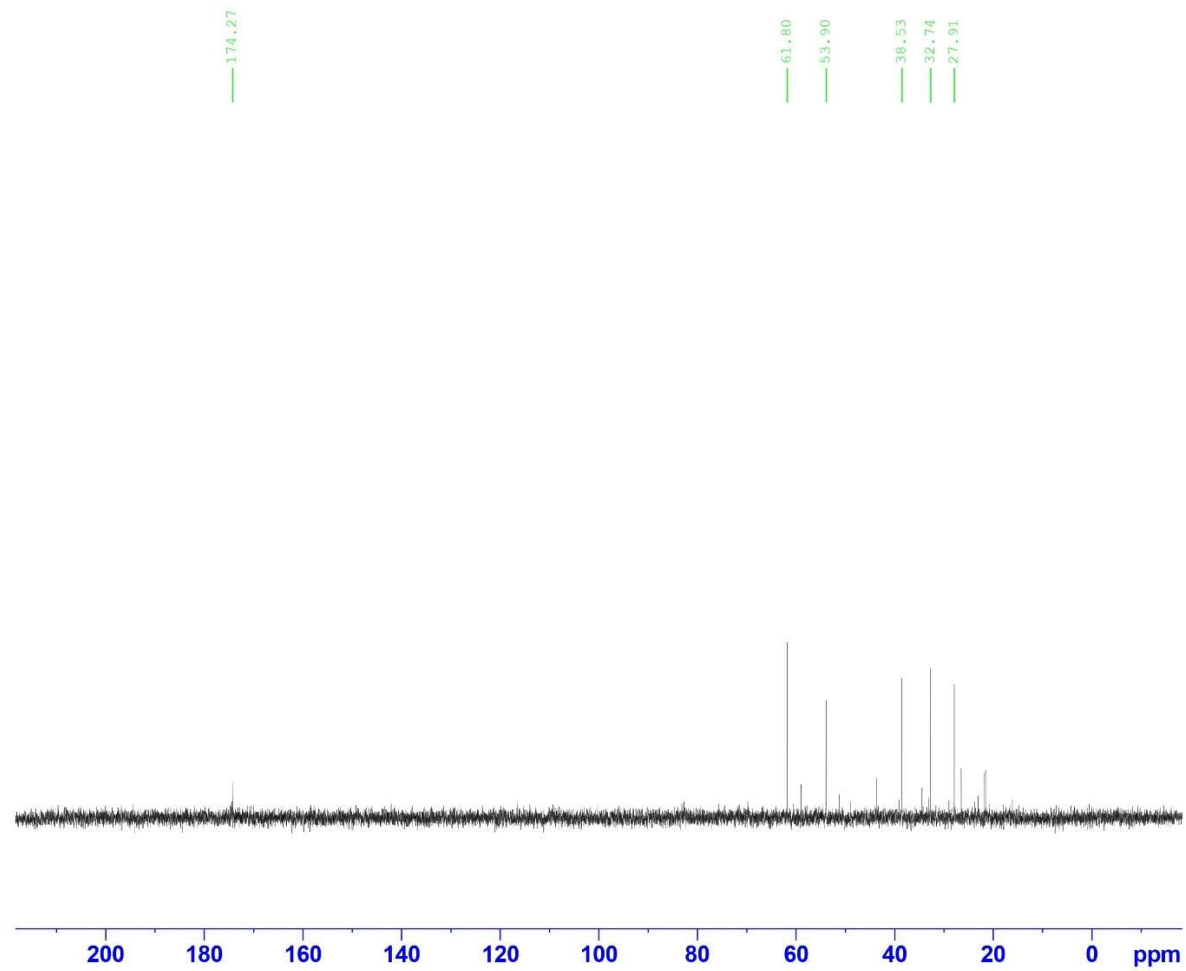


Figure 73. The spectral image of ^{13}C NMR of compound **80** from methanolic extract of leaves

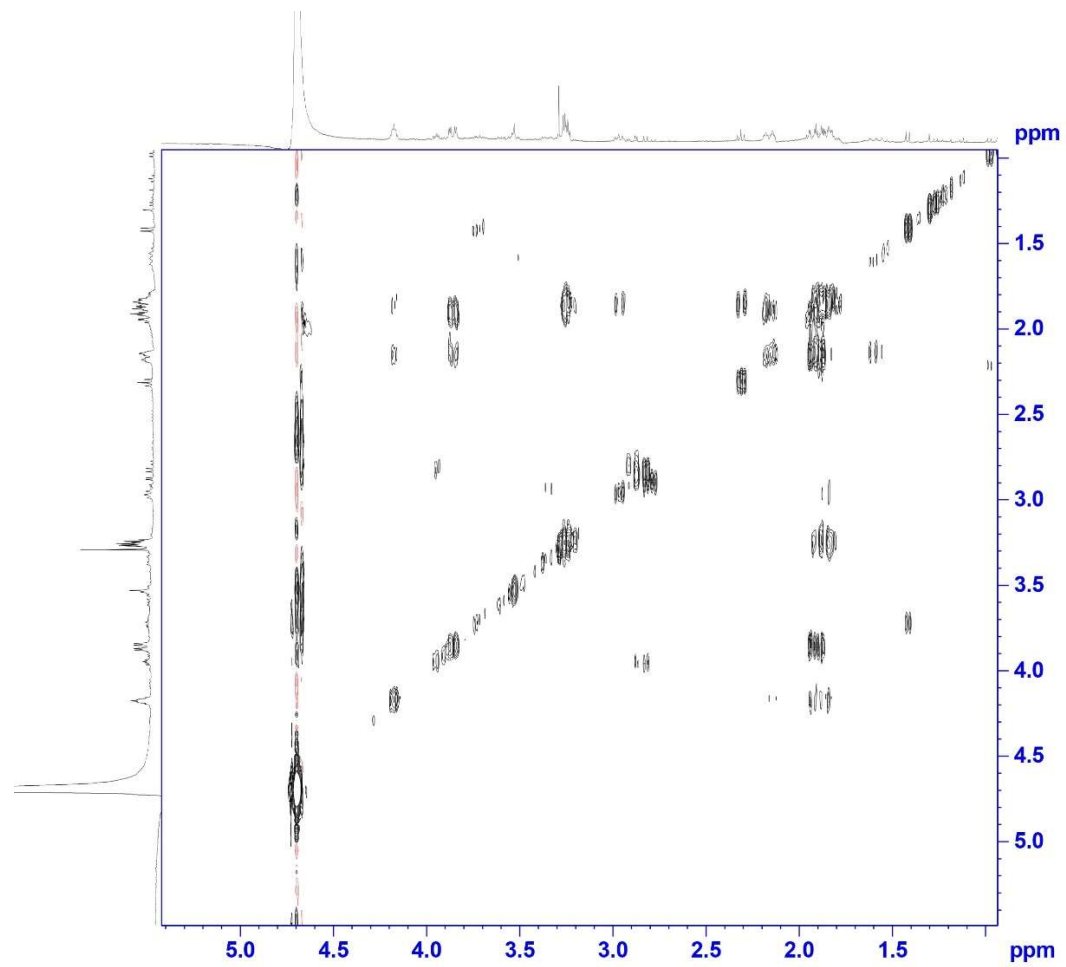


Figure 74. The spectral image of ^1H - ^1H COSY NMR of compound **80** from methanolic extract of leaves

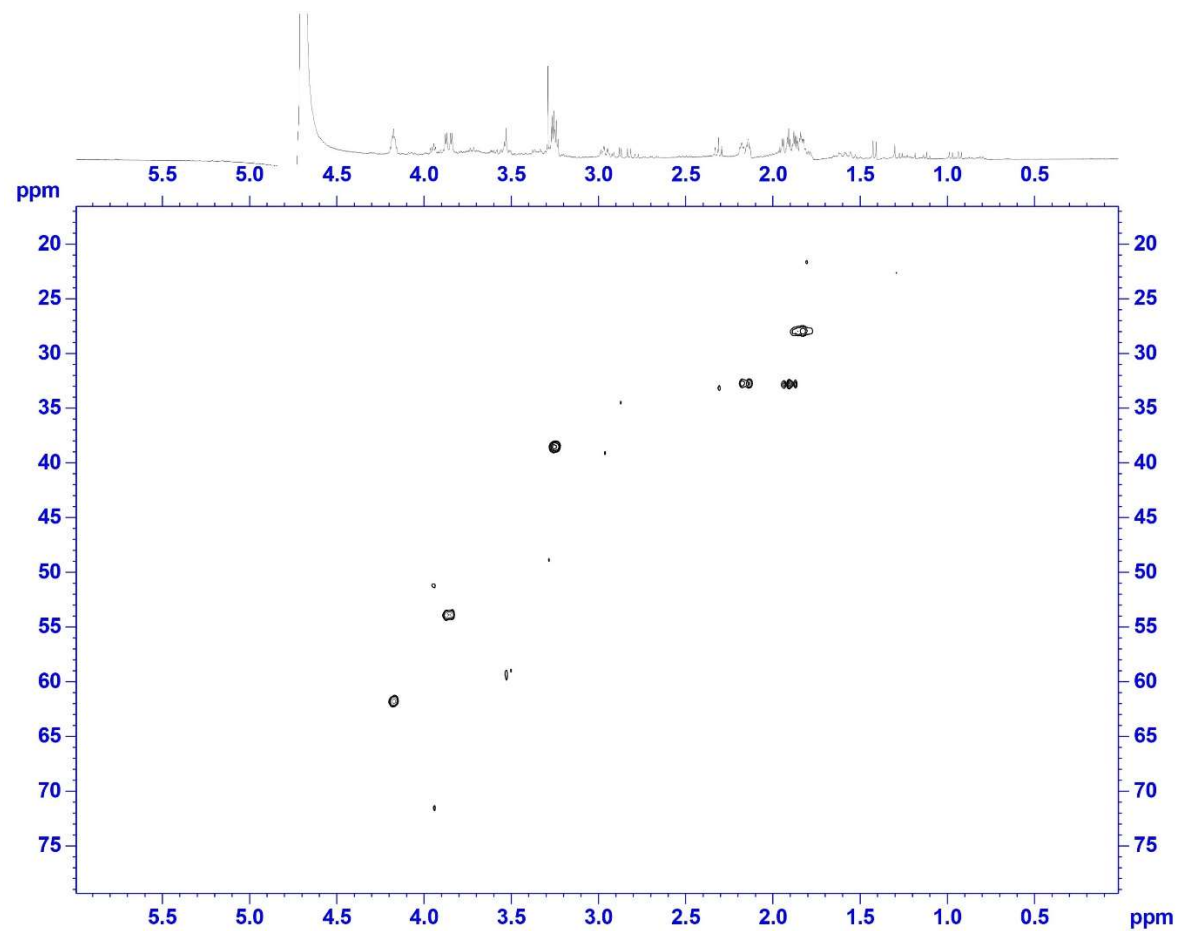


Figure 75. The spectral image of ^1H - ^{13}C HSQC NMR of compound **80** from methanolic extract of leaves

LF-MeOH-rest ccl Jan 22

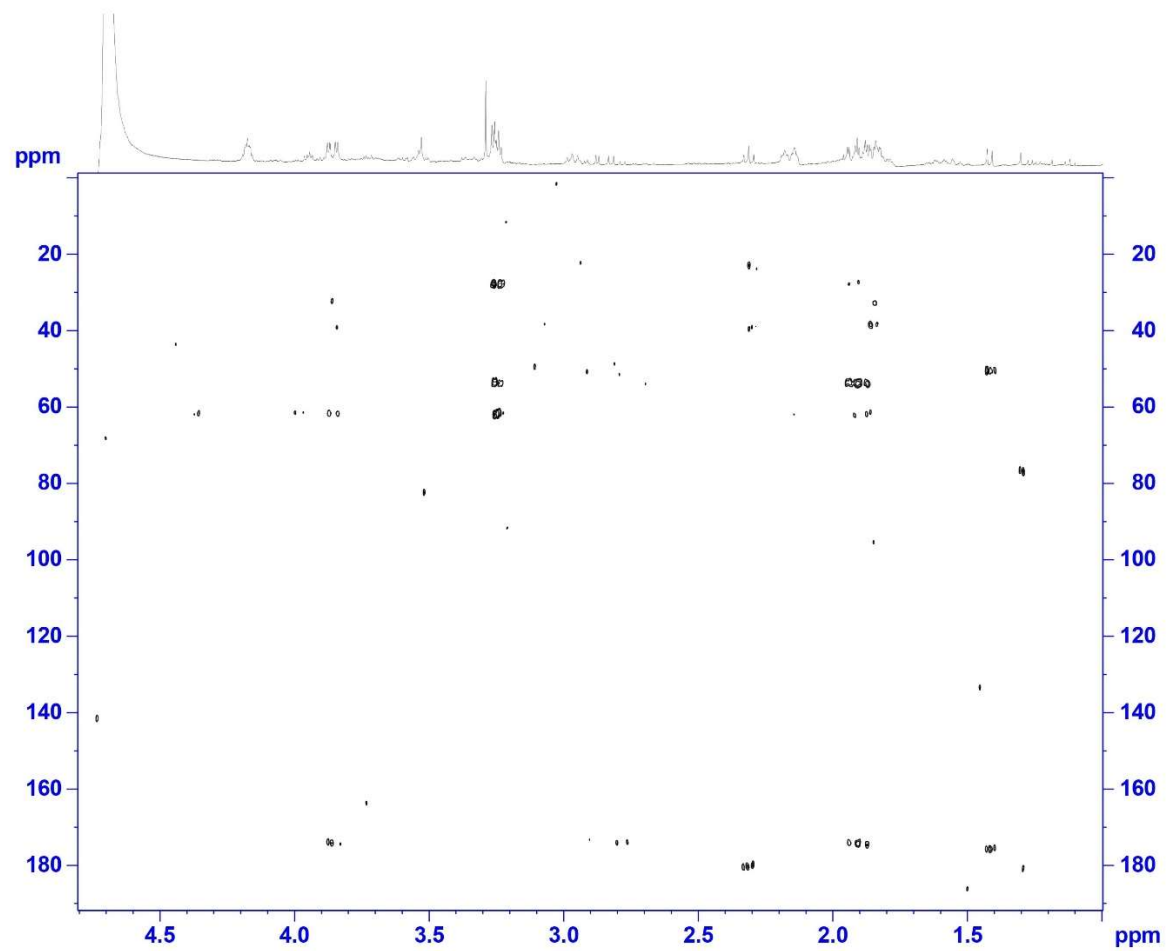


Figure 76. The spectral image of ^1H - ^{13}C HMBC NMR of compound **80** from methanolic extract of leaves

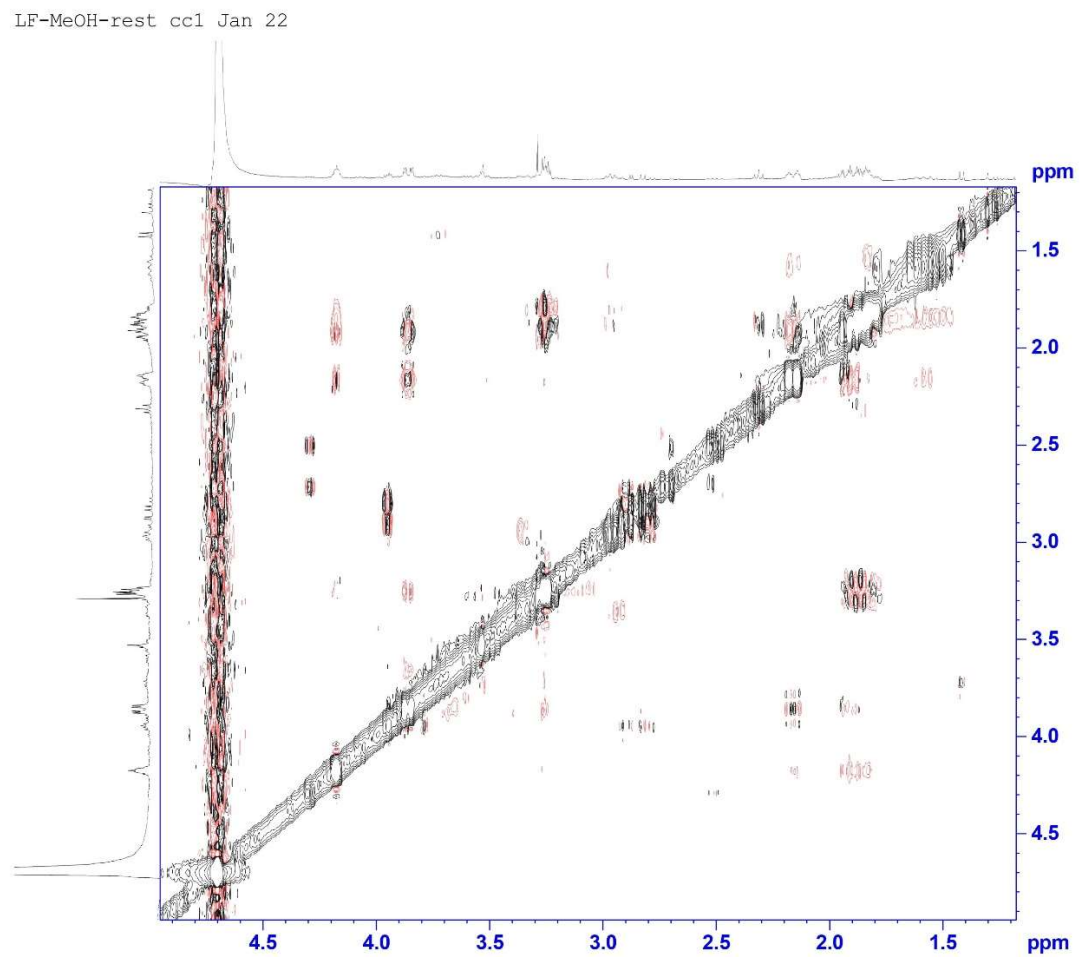


Figure 77. The spectral image of ^1H - ^1H NOESY NMR of compound **80** from methanolic extract of leaves

4. NOESY information gave that H5 seems to share the same space with H4b and H6, suggesting two possible isomers of the lactone, 3*R*,5*R* and 3*S*,5*S* (Figure 78d).

Table 17. The 1- and 2-D NMR data of isolate from LF-MeOH-D in D₂O (400 MHz)

No	¹ H (δ ppm, m, J Hz, integration)	¹³ C (δ ppm)	COSY	TOCSY	HMBC	NOESY
2	-	175.27	-	-	-	-
3	3.86 (dd; 11.8, 3.68; 1H)	53.90	H4b	H5, H4a, H4b	C2, C4, C5	H4a (strong), H4b
4a	2.16 (m; 1H)	32.74	H4b	H3, H4b, H5	-	H3 (strong), H4b (strong)
4b	1.91 (m; 1H)		H3, H4a	H3, H4a, H5	C2, C3, C5	H5 (strong), H3, H4a
5	4.17 (m; 1H)	61.80	-	H3, H4a, H4b, H6, H7	-	H4b (strong), H6
6	1.84 (m; 2H)	26.50	H7	H5, H7	C4, C5, C7	H5
7	3.26 (m; 2H)	38.53	H6	H5, H6	C5, C6	H6 (strong)

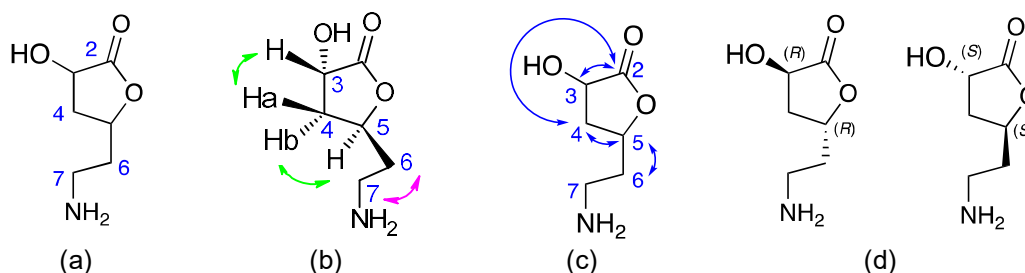


Figure 78. (a) The possible structure of the compound from LF-MeOH-D named as 3-hydroxy-5-(2-aminoethyl) dihydrofuran-2(3*H*)-one **80** by ChemDraw (C₆H₁₁NO₃; MW = 145.16), (b) COSY (↔) and NOESY (↔) information, (c) HMBC (↔) correlation, and (d) two possible enantiomers of the molecule (3*R*,5*R* and 3*S*,5*S*).

An aminoethyl substituent attached to the lactone ring at C5 via C6. The chemical shift of C-3 indicates that an OH is appropriately attached to C3. NOESY NMR analysis (Figure 78b) showed strong crossed peaks between H3-H4a and H5-H4b, indicating that H5 is trans to H3. The positive ESI-MS [M + H]⁺ of the isolate was 146.0818, corresponding to C₆H₁₁NO₃ (calculated m/z [M + H]⁺ = 146.0817). It has an optical rotation [α]²³ = -3.6° (c 0.1, H₂O). Its melting point was observed to be in the range of 347-350 °C. The IR spectra showed bands at 3212.08 (OH stretch); 2929.09 (CH sp³); 1707.74 (C=O stretch); and 1053.09 cm⁻¹ (C-O). Our spectral data analysis, therefore, concludes LF-MeOH-D to be (3*S*,5*S*)-3-hydroxy-5-(2-aminoethyl)-

dihydrofuran-2(3*H*)-one **80** or the (3*R*,5*R*)-enantiomer (Figure 49d). It is for the first time being isolated as a natural product from the leaves of *A. saligna*. Nothing in the literature indicates that (3*S*,5*S*)-3-hydroxy-5-(2-aminoethyl)-dihydrofuran-2(3*H*)-one **80** is a known natural product. The absolute configuration of (3*S*,5*S*)-3-hydroxy-5-(2-aminoethyl)-dihydrofuran-2(3*H*)-one **80** at C3 and C5 can be further confirmed by an X-ray crystallographic study or NMR analysis of Mosher diastereomeric esters of compound **80**.

4.2.3. One flavonoid, cyclitol, and disaccharide from the BK-MeOH fraction

4.2.3.1. (-)-Epicatechin **77** from bark

Table 18 shows 1D- and 2D-NMR data of the subfraction BK-MeOH-A1 (9 mg, 11.25%) from the methanolic bark extract. The data indicated that the compound consists of the flavan-3-ol skeleton with two patterns of aromatic rings representing rings A and B. A geminal couple ($^2J = 16$ Hz) of protons 4 (2.52 and 2.87 ppm) due to a chiral environment of the neighbouring carbon (C3) represents the typical proton resonance of a catechin derivative. Moreover, the connectivity among protons can be summarised as follows:

1. Proton 6 and 8 are meta couple in ring A with $J = 2.2$ Hz.
2. Proton 6' is meta couple to H2' ($J = 1.8$ Hz) and ortho couple to H5' ($J = 8$ Hz) in ring B.
3. HMBC of H4 has confirmed the connectivity between ring C to A and ring C to B to C10 and H2' to C2.

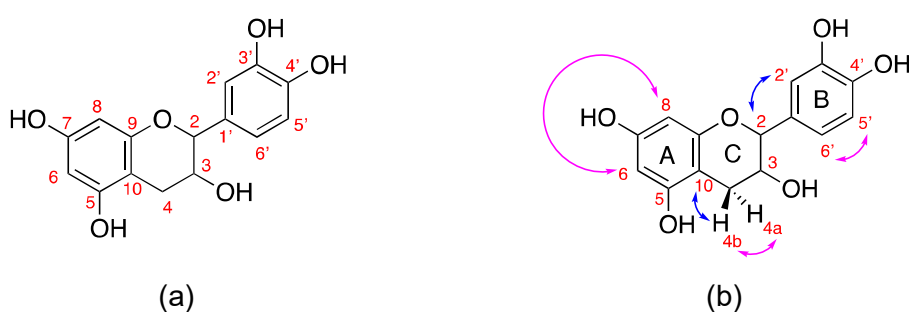


Figure 79. (a) The main skeleton of catechin and (b) key connections of proton-to-proton (\leftrightarrow COSY) and proton-to-carbon (\leftrightarrow HMBC) of catechin derivative isolated from the methanolic bark extract.

This finding shows that flavonoids can also be found in the bark beside the flowers and leaves. Acacia barks have been known as the source of condensed tannin, where catechin is one of the major units of group³⁴⁸. According to the NOESY spectrum, the type of stereochemical orientation of the isolate can be revealed. The

geminal proton of H4a and H4b showed a very strong cross-peaks correlation indicating the closer spatial distance. Moreover, proton H3 shared a stronger cross-peaks correlation with proton H4b than those with proton H4a meaning that H3 and H4b are in the same face (Figure 82a). Notably, the strong peaks correlation was also observed for proton H2 and H3 demonstrating the same spatial orientation among the twos. This relationship has also been confirmed by weak cross-peaks correlation between proton H2 and H4b, indicating they are positioned on the same face. Furthermore, its specific optical value of $[\alpha]^{23} = -28.72^\circ$ (c 0.1, MeOH) indicated that the possible compound could be (-)-epicatechin with 2*R*,3*R* orientation (Figure 51b).

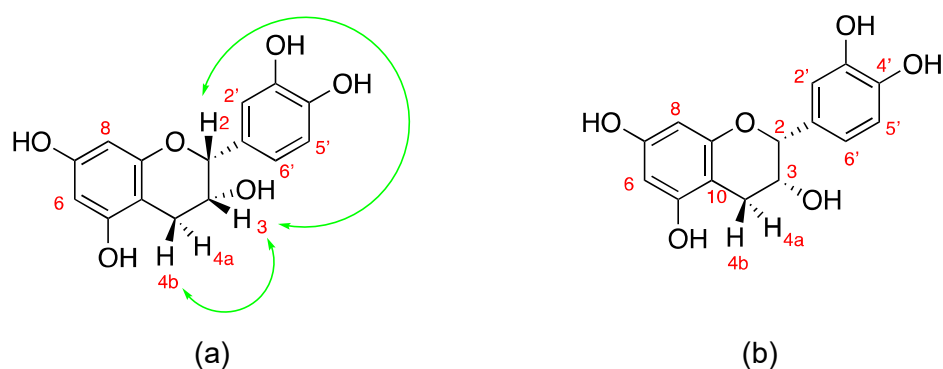


Figure 80. Key connections of (a) proton-to-proton (\leftrightarrow NOESY) showing the spatial relationship of vicinal protons and (b) the molecular structure of (-)-epicatechin from BK-MeOH-A1 with *cis*-2*R*,3*R* stereochemical orientation.

The isolation of (-)-epicatechin **77** from the barks was interesting since only flavonol derivatives were detected in the EtOH extract of *A. saligna* by Salem et al.²²⁶. (-)-Epicatechin **77** is a member of flavan-3-ol commonly found as one of the monomers of condensed tannins or proanthocyanidins of *Acacia* barks. For example, catechin was isolated as a unit from *A. mearnsii* barks in 1960 by Roux and Maihs³⁵⁰ and as a few of catechin-fisetinidol and catechin-robinetinidol by Drewes et al.³⁵¹.

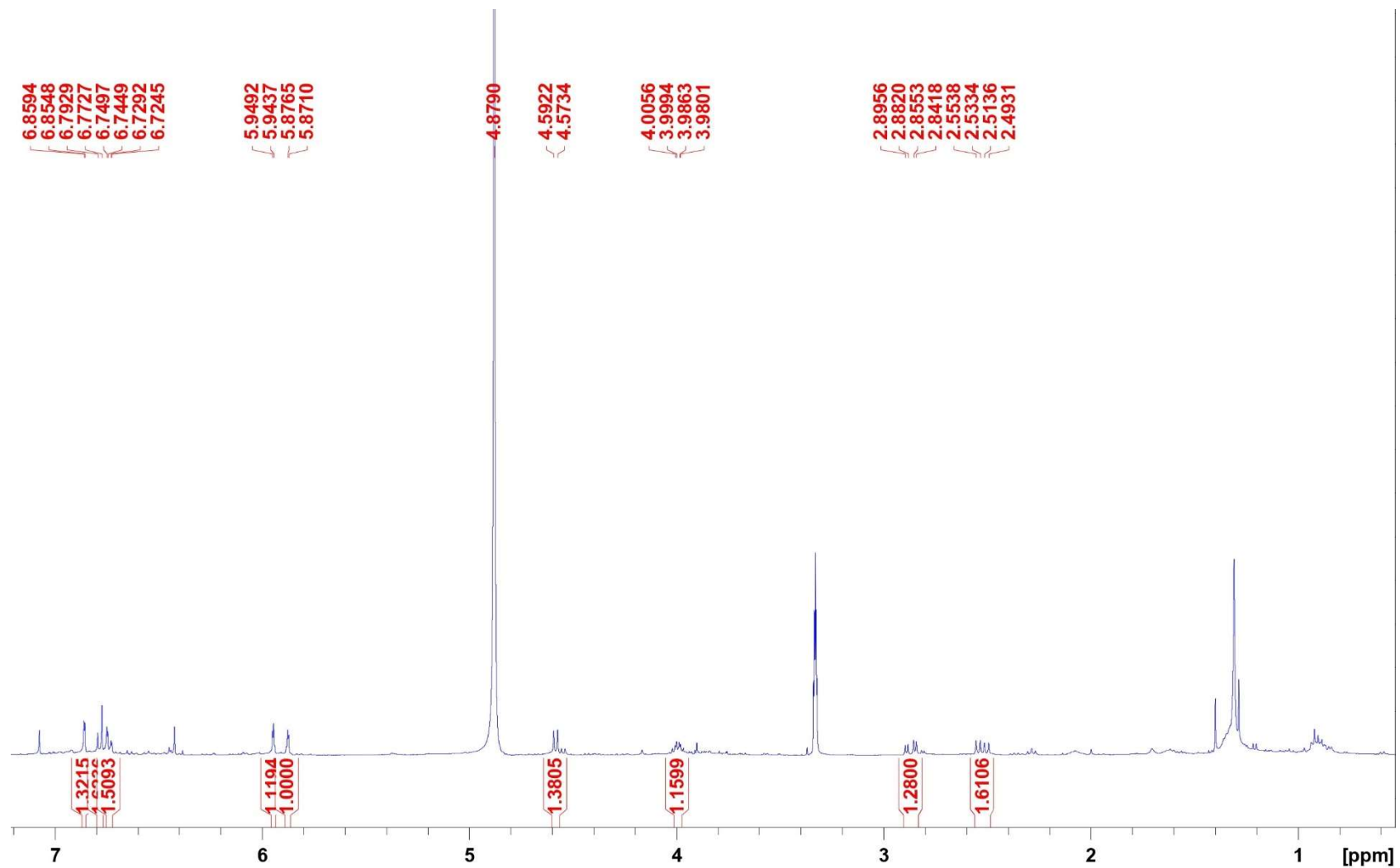


Figure 81. The spectral image of ^1H NMR of (-)-epicatechin **77** from methanolic extract of bark

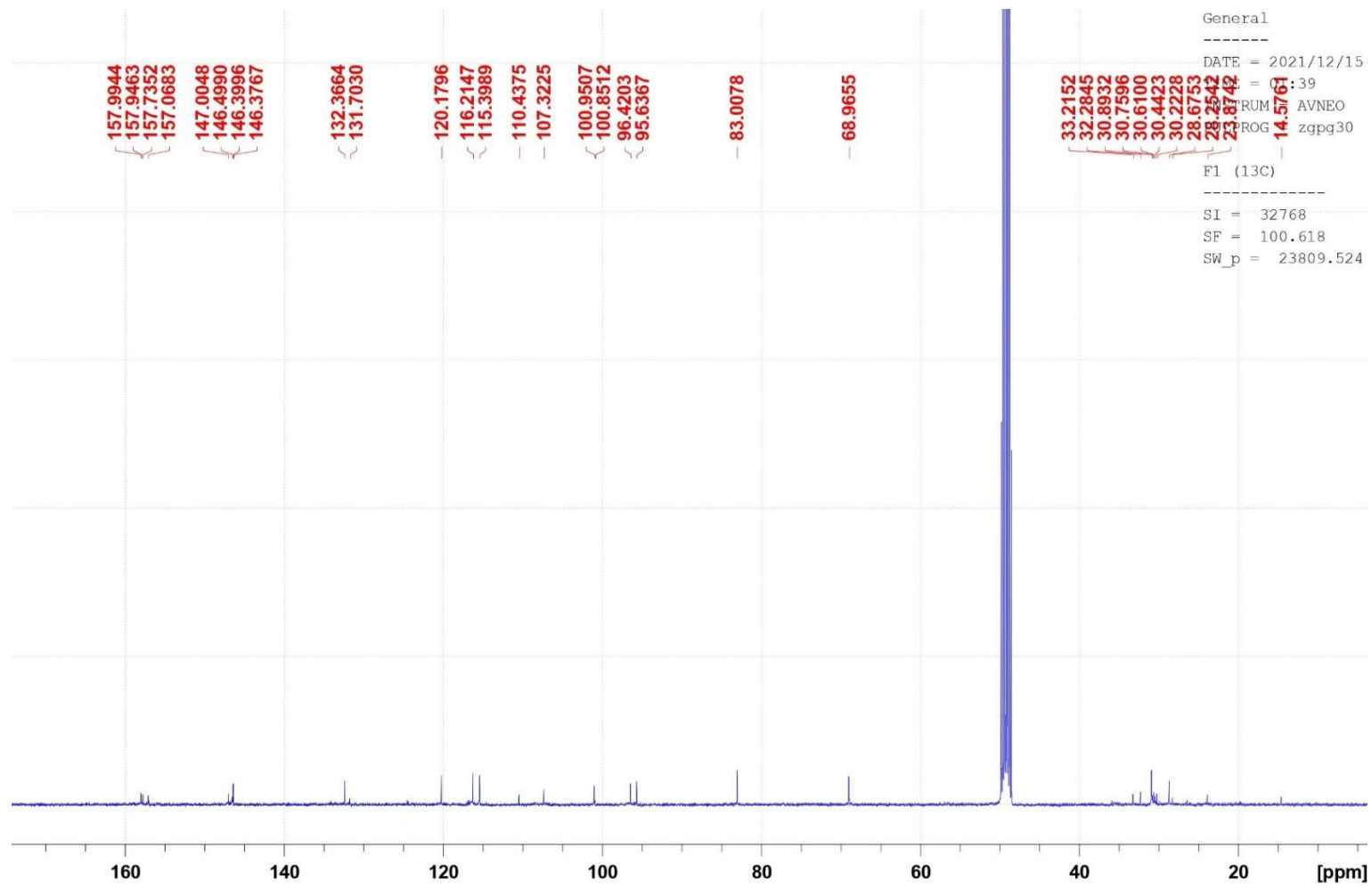


Figure 82. The spectral image of ^{13}C NMR of (-)-epicatechin **77** from methanolic extract of bark

Table 18. ¹H NMR (400 MHz, CD₃OD), ¹³C NMR (100 MHz, CD₃OD), and 2D NMR data of compound from BK-MeOH-A1 compared to reported (–)-epicatechin **77**.

No	BK-MeOH-A1				(–)-Epicatechin ³⁴⁹	
	δ ¹ H in ppm (m, J in Hz, integration)	δ ¹³ C (ppm)	COSY	HMBC	δ ¹ H in ppm (m, J in Hz, integration)	δ ¹³ C (ppm)
2	4.58 (d; 7.52; 1H)	81.47	H3	C3, C4, C2', C6', C1', C9	4.82 (br s; 1H)	79.88
3	3.99 (m; 1H)	67.42	H2, H4a, H4b	-	4.19 (m; 1H)	67.49
4a	2.52 (dd; 16.08, 8.2; 1H)	27.13	H3, H4b	C2, C3, C5, C9, C10	2.73 (dd; 16.8, 2.9; 1H)	29.26
4b	2.87 (dd; 16.12, 5.4; 1H)		H3, H4a		2.87 (dd; 16.8, 4.5; 1H)	
5	-	156.40	-	-	-	158
6	5.95 (d; 2.2; 1H)	94.88	H8	C5, C7, C10	5.94 (d; 2.3; 1H)	96.38
7	-	156.45	-	-	-	157.67
8	5.87 (d; 2.2; 1H)	94.09	H6	C6, C10, C7, C9	5.97 (d; 2.3; 1H)	95.88
9	-	155.53	-	-	-	157.37
10	-	99.41	-	-	-	100.06
1'	-	130.82	-	-	-	132.28
2'	6.86 (d; 1.6; 1H)	113.86	H6'	C2, C6', C1', C3'	6.98 (d; 1.9; 1H)	115.32
3'	-	144.83	-	-	-	145.78
4'	-	144.86	-	-	-	145.95
5'	6.78 (d; 8.08; 1H)	114.67	H6'	C2, C2', C1', C4'	6.76 (d; 8.4; 1H)	115.88
6'	6.74 (dd; 8.16, 1.88; 1H)	118.64	H2', H5'	C2, C2', C4'	6.81 (dd; 8.4, 1.9; 1H)	119.39

4.2.3.2. *D*-(+)-Pinitol **79a** from bark

Table 19 shows 1D- and 2D-NMR data of the subfraction BK-MeOH-B2 (10 mg, 12.5%) that allows us to establish the connectivity of the elements. All protons are likely to form a cyclohexane-like ring system with singly oxygenated groups, as the peaks are between 3 and 4 ppm. Protons 1 and 6 share the same peak indicating a symmetrical molecule due to their unique chemical environment. The connectivity among protons can be summarised as follows:

1. Protons 1 and 6 couple each other with large vicinal coupling constants of 9 Hz representing geometrically different orientations (equatorial-equatorial).
2. Two coupling constants of the same values ($J \sim 2$ Hz) that suggest sharing the same orientation: H1 to H2 and H6 to H5, represent the equatorial-axial relationship.
3. Three equatorial-equatorial coupling systems ($J \sim 9$ Hz) are observed for H2 to H3, H3 to H4, and H4 to H5.
4. According to HMBC data, H7 (methyl) links to C3, indicating that the carbon bonds an ether system instead of hydroxyl. The upfield shifting of H3 has also confirmed this due to an inductive effect of the attached ether (-OCH₃).

The obtained data were identical to those reported for *D*-pinitol **79a** by Kayed et al.³⁵² (Table 19). *D*-pinitol **79a** is a typical secondary metabolite of plants living in water-deficit and saline environments. This compound is a simple cyclic sugar derivative called cyclitol which is numbered counter-clockwise, indicating the *D*-configuration³⁵³. The *O*-methyl group has been observed to lead to dextrorotation (optically active structure)³⁴⁷.

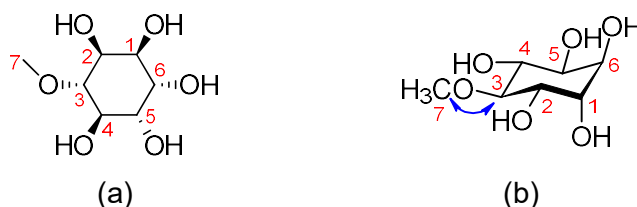


Figure 83. Molecular structure of 3-O-methyl-*D*-chiro-inositol (*D*-(+)-pinitol **79a**) (C₇H₁₄O₆) from the methanolic extract of bark in (a) Haworth projection and (b) chair conformation with HMBC information.

5.

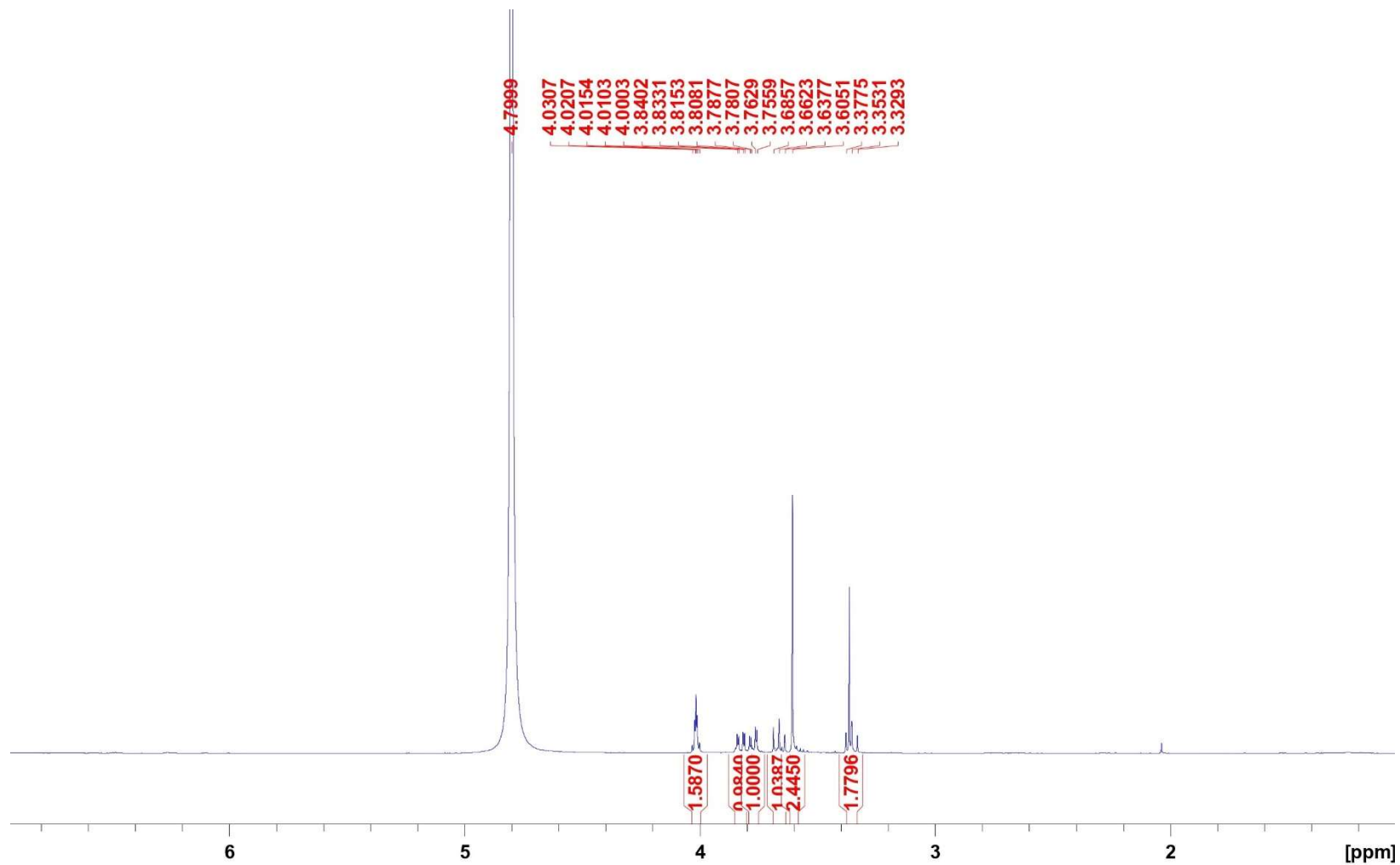


Figure 84. The spectral image of ^1H NMR of *D*-pinitol **79a** from methanolic extract of bark

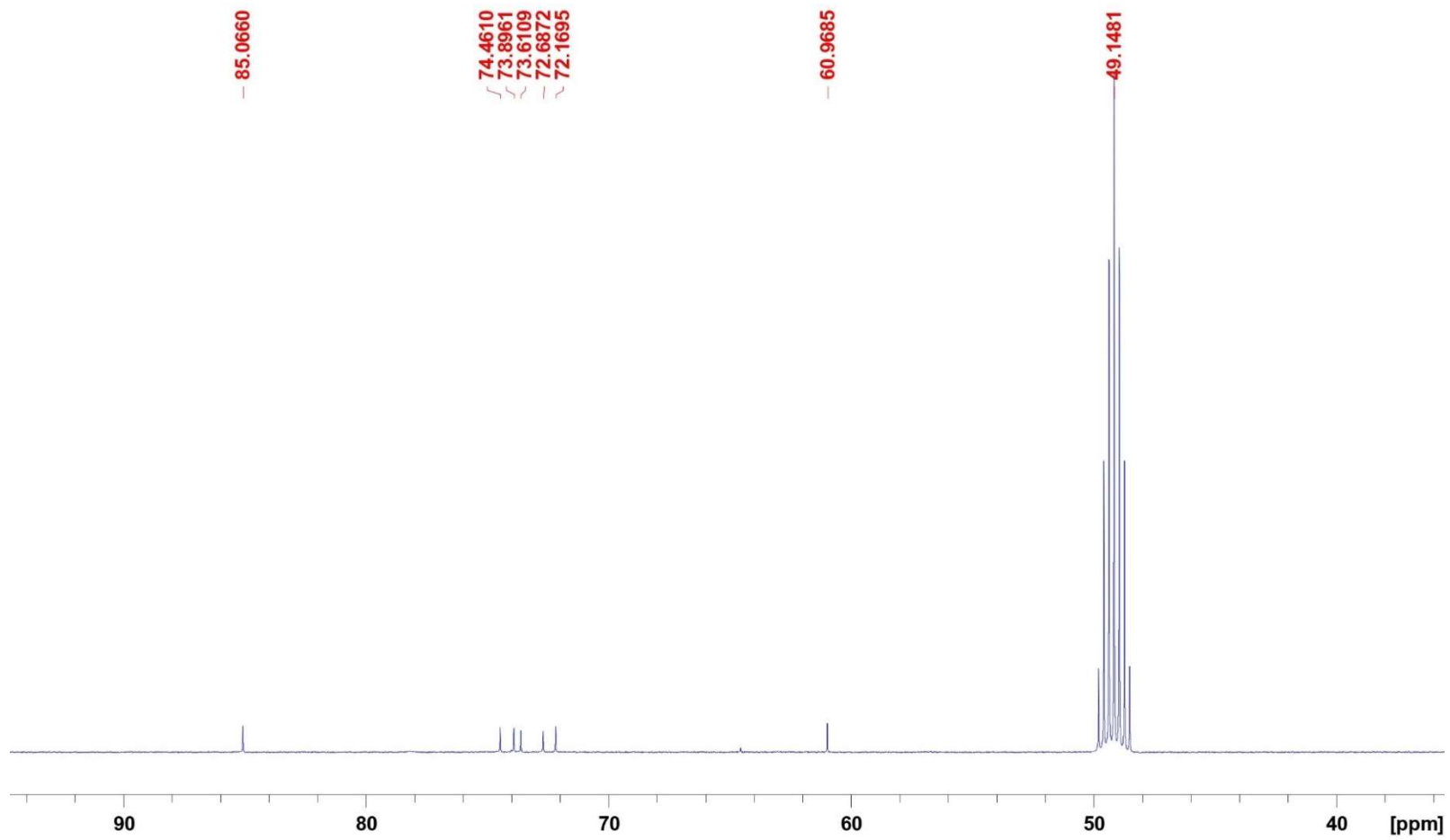


Figure 85. The spectral image of ^{13}C NMR of *D*-pinitol **79a** from methanolic extract of bark

Table 19. ¹H NMR (400 MHz, CD₃OD), ¹³C NMR (100 MHz, CD₃OD), and 2D NMR data of compound from BK-MeOH-B2 compared to reported 3-O-methyl-*D*-chiro-inositol (*D*-(+)-pinitol **79a**)

No	BK-MeOH-B2				<i>D</i> -pinitol ³⁵²	
	δ ¹ H in ppm (m, <i>J</i> in Hz, integration)	δ C (ppm)	COSY	HMBC	δ ¹ H in ppm (m, <i>J</i> in Hz, integration)	δ ¹³ C (ppm)
1	3.90 (dd; 9.2, 2.24; 1H)	73.89	H2, H6	-	3.91 (dd; 9.6, 2.6; 2H)	72.06
6	3.90 (dd; 9.2, 2.24; 1H)	73.61	H5, H1	-		71.14
2	3.76 (dd; 9.56, 2.32; 1H)	72.17	H1, H3	-	3.76 (dd; 9.68, 2.28; 1H)	70.61
3	3.27 (t; 9.42; 1H)	85.06	H2, H4	C7	3.27 (t; 9.44; 1H)	83.5
4	3.59 (t; 9.52; 1H)	74.46	H5, H3	-	3.61 (dd; 9.5; 1H)	72.89
5	3.71 (dd; 9.72, 2.14; 1H)	72.69	H6, H4	C3	3.72 (dd; 9.6, 2.6; 1H)	72.34
7	3.63 (s; 3H)	60.97	-	-	3.63 (s; 3H)	59.56

4.2.3.3. Sucrose

Table 20 shows 1D- and 2D-NMR data of the subfraction BK-MeOH-C2 (25 mg, 8.33%), which allows us to establish the connectivity of the elements. The data indicated that the compound consists of twelve carbons with a single quaternary carbon and a carbon with an anomeric proton (δ H1= 5.337 ppm). The heteronuclear experiment of HMBC showed that the proton seems linked to the quaternary carbon indicating a bridge between the two systems. The systems would be two different polyhydroxy rings. The following points describe the possible ring systems:

1. The anomeric proton resonates further downfield with a small J value (3.84 Hz) representing an equatorial proton coupled to H2. Furthermore, an axial-axial coupling system was observed for H3 and H4 and a multiplet signal for H5 next to the geminal protons of H6, indicating that this system is most likely an α -*D*-glucose.
2. In the second ring, the quaternary carbon resonates further downfield (δ HC2' = 104.238 ppm), indicating a doubly-oxygenated carbon species. The HMBC cross-peaks relationship confirmed that it could be directly linked to a methylene carbon (-CH₂- of H1') and a CH of H3'. The H3' couples to H4' as an axial-axial pair system (J = 8 Hz).
3. The H4' and H5' coupling was observed by a COSY cross-peaks correlation. This ring system is most likely a five-membered carbon ring as the C5' was observed to link to another methylene of H6' as shown by the HMBC data (Figure 88b). According to the NMR information, this ring would be a *D*-fructofuranose.

As mentioned above, both rings connect via a glycosidic linkage connecting C1 and C2'. This means that this compound could be a disaccharide of α -*D*-glucose and *D*-fructofuranose. In other words, this is most likely to be sucrose. In addition, their chemical shifts of ¹H and ¹³C are similar to reported data for sucrose by Hernández-García and co-workers³⁵⁴ (Table 20). The isolation of sucrose from Acacia bark was previously reported in *A. albida*³⁵⁵ and *A. mearnsii*³⁵⁶, while our work is the first report of the isolation of the disaccharide from this species.

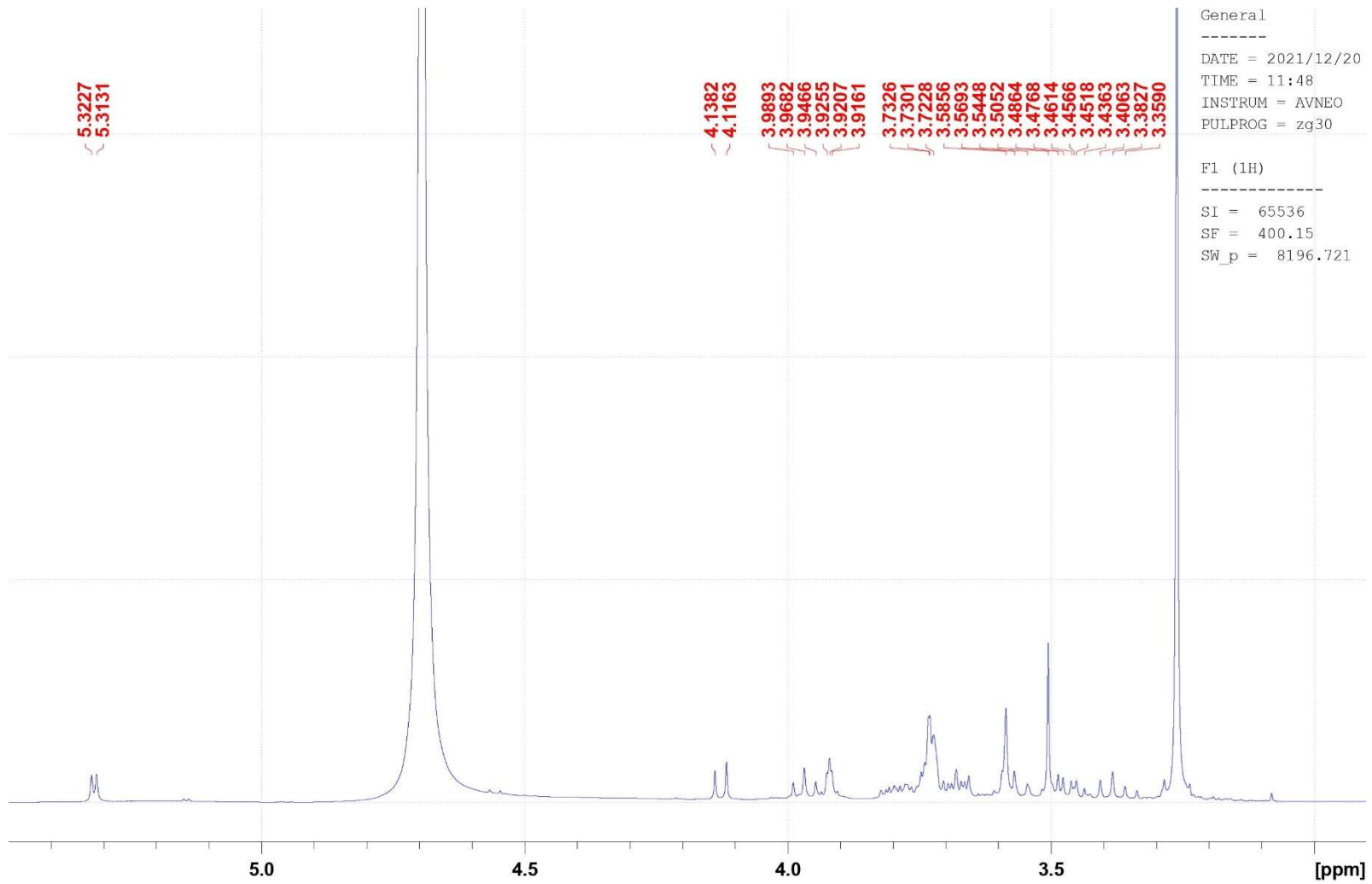


Figure 86. The spectral image of ^1H NMR of sucrose isolated from methanolic extract of bark

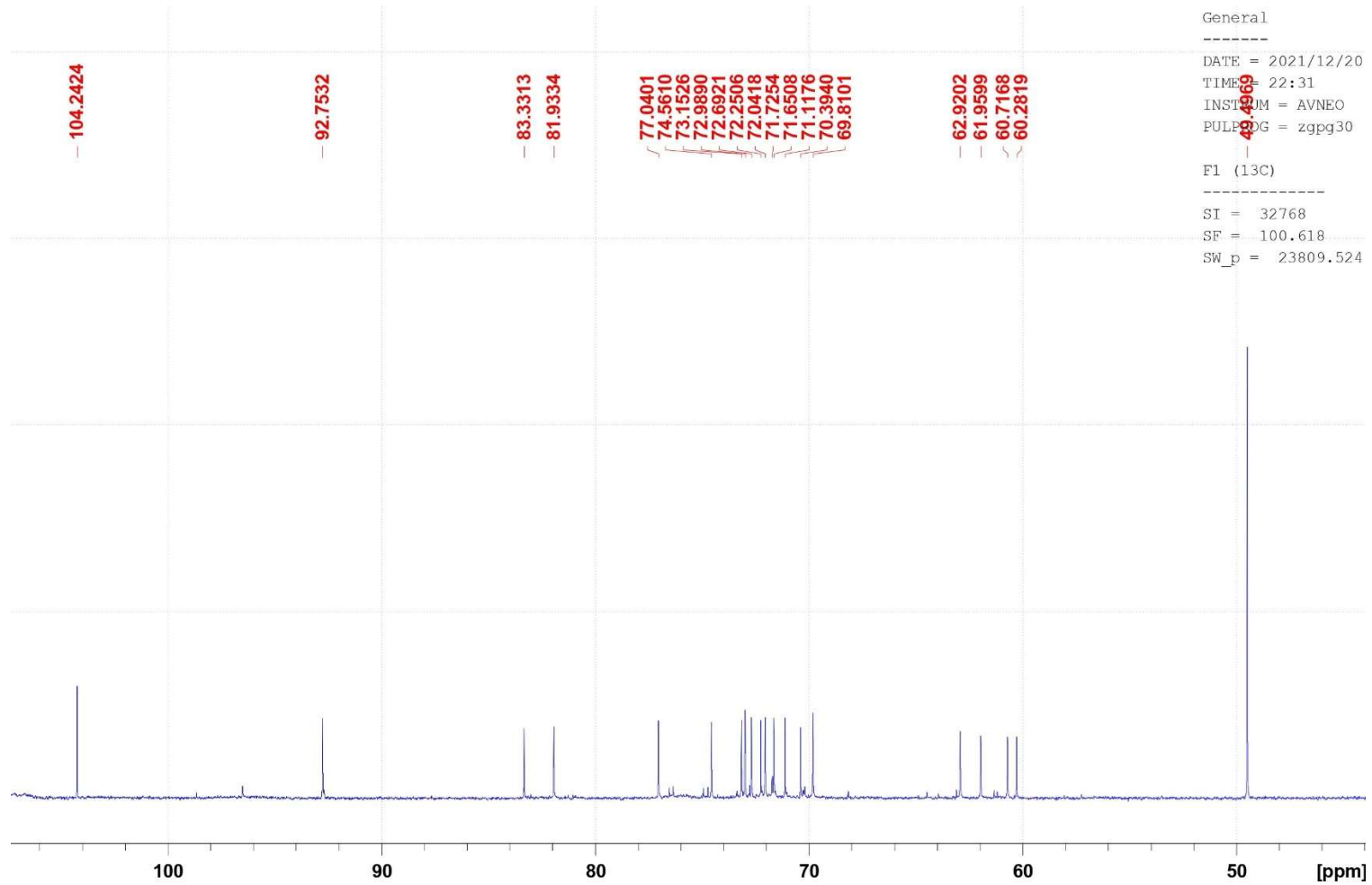


Figure 87. The spectral image of ^{13}C NMR of sucrose isolated from methanolic extract of bark

Table 20. ¹H NMR (400 MHz, D₂O), ¹³C NMR (100 MHz, D₂O), and 2D NMR data of compounds from BK-MeOH-C2 compared to reported sucrose

No	BK-MeOH-C2				Sucrose ³⁵⁴	
	δ ¹ H in ppm (m, J in Hz, integration)	δ ¹³ C (ppm)	COSY	HMBC	δ ¹ H in ppm (m, J Hz, integration)	δ ¹³ C (ppm)
1	5.44 (d; 3.84; 1H)	92.74	H2	C3, C2'	5.38 (d; 3.88; 1H)	94.66
2	3.58 (dd; 10, 3.84; 1H)	71.63	H1, H3	C3	3.52 (dd; 10, 3.84; 1H)	73.55
3	3.78 (t; 9.4; 1H)	73.12	H2, H4	C4	3.72 (t; 9.56; 1H)	75.05
4	3.49 (t; 9.46; 1H)	69.78	H4, H5	C3, C5, C6	3.43 (t; 9.42; 1H)	71.70
5	3.89 (m; 1H)	72.96	H4	-	3.83 (m; 1H)	74.88
6	3.85 (d; 2; 2H)	62.92	-	C4, C5	3.78 (d; 2.96; 2H)	62.59
1'	3.70 (s; 2H)	61.91	-	C2', C3'	3.63 (s; 2H)	63.82
2'	-	104.24	-	-	-	106.17
3'	4.24 (d; 8.76; 1H)	76.98	H4'	C1', C4', C5', C6'	4.18 (d; 8.76; 1H)	78.88
4'	4.00 (t; 8.54; 1H)	74.55	H4', H5'	C3', C5', C6'	4.01 (t; 1H; 8.56)	76.47
5'	3.93 (m; 1H)	81.92	H4'	C2', C4'	3.86 (m; 1H)	83.85
6'	3.84 (s; 2H)	60.68	-	C5'	3.79 (s; 2H)	64.84

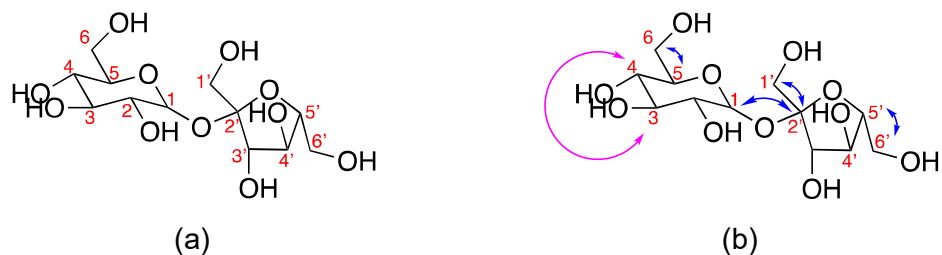


Figure 88. Molecular structure of (a) sucrose isolated from the methanolic bark extract and (b) key connections of proton-to-proton (\leftrightarrow COSY) and proton-to-carbon (\leftrightarrow HMBC).

4.3. Conclusion of Chapter 4

Natural products from methanolic extracts of *A. saligna* were successfully isolated using a column chromatography technique yielding eleven compounds grouped into four categories. They are (i) known compounds isolated from *A. saligna*, including isosalipurposide **1** (from FL-MeOH), myricitrin **11** (LF-MeOH), and (-)-epicatechin **77** (LF- and BK-MeOH); (ii) known compounds to exist in *A. saligna* but being isolated in this work: naringenin **42** (FL-MeOH) and quercitrin **4** (FL- and LF-MeOH), (iii) known phytochemicals found elsewhere but isolated from this plant for the first time: *D*-(+)-pinitol **79a** (FL- and BK-MeOH), sucrose (BK-MeOH), (-)-pinitol **79b**, and 2,4-di-*t*-butylphenol **78** (LF-MeOH), and (iv) two novel natural products assigned as naringenin-7-*O*- α -*L*-arabinofuranoside **76** (FL-MeOH) and (3*S**,5*S**)-3-hydroxy-5-(2-aminoethyl) dihydrofuran-2(3*H*)-one **80** (LF-MeOH).

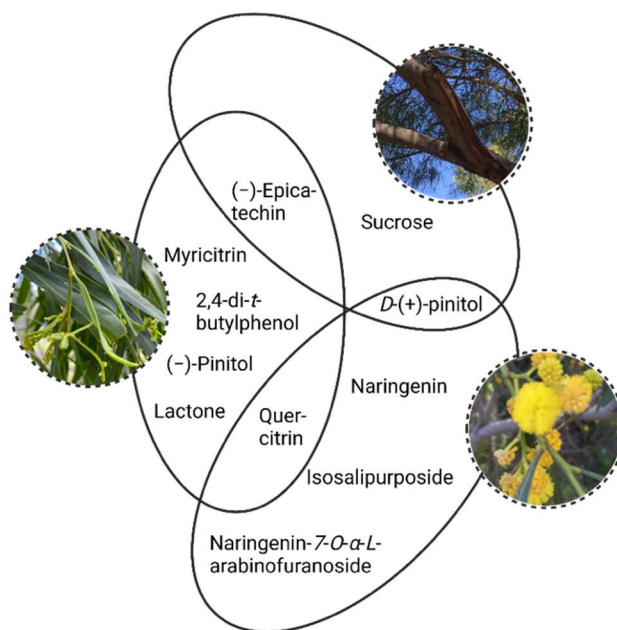


Figure 89. An illustrative summary of isolated compounds from FL-, LF-, and BK-MeOH extracts of *A. saligna*.

CHAPTER 5: RESULT OF BIOACTIVITIES OF ISOLATED COMPOUNDS

5.1. Introduction of Chapter 5

Mitochondrion³⁵⁷ is an essential cellular component for converting substrates into energy. The mitochondria respiratory chain gains excess electrons converted to extra mt-ROS, causing mitochondrial dysfunction³⁵⁸. Indeed, mitochondrial dysfunction leads to cellular insulin dysregulation³⁵⁹⁻³⁶¹, preventing glucose entry into cells³⁶², impaired insulin production^{296, 363-365}, resulting in obesity and other microvascular diseases³⁶⁶⁻³⁶⁹. Moreover, some studies on 3T3-L1 adipocytes^{76, 89, 106, 110} showed a marked ROS accumulation and a loss of mitochondrial membrane potential (MMP). Therefore, reducing excess mt-ROS and restoring MMP to maintain mitochondria function is a promising approach to managing T2DM, obesity and related metabolic disorders.

The main objective of Chapter 5 was to investigate the bioactivities of the isolated compounds from methanolic extracts of *A. saligna*. Nine identified compounds were collectively isolated from FL-, LF-, and BK-MeOH extracts subjected to the *in vitro* assays. The bioactivity data can inform us about the effectiveness of natural products from Australian *A. saligna* as an antioxidant, antihyperglycemic, and mitochondrial protectant.

5.2. Antioxidant activities of isolated compounds

The antioxidant activity of active isolated phytochemicals followed a dose-dependent manner, depicted in Figures 90 and 91. Of 10 isolated compounds, only three (–)-epicatechin **77**, quercitrin **4**, and myricitrin **11** showed consistently potent antioxidant activities against DPPH and ABTS free radicals (Figure 92). Previously, (–)-epicatechin **77**^{370, 371}, quercitrin **4**³⁷², and myricitrin **11**^{373, 374} demonstrated an excellent inhibition against both free radicals. These compounds have been confirmed to be involved in the electron and proton transfer in some standard antioxidant assays, including the two methods due to two substituted C3' and C4' of the ring B by hydroxyl groups³⁷⁵ forming a stable *ortho*-hydroxyl phenoxyl radical to increase the rate of proton transfer to the DPPH³⁷⁶. On the other hand, the IC₅₀ of naringenin **42**, naringenin-7*O*- α -L-arabinofuranoside **76**, 2,4-di-*t*-butylphenol **78**, and 3-hydroxy-5-(2-aminoethyl) dihydrofuran-2(3*H*)-one **80** did not reach 50% at the highest tested concentration (10 mM) in the DPPH assay (Table S25, Appendix C, page 252).

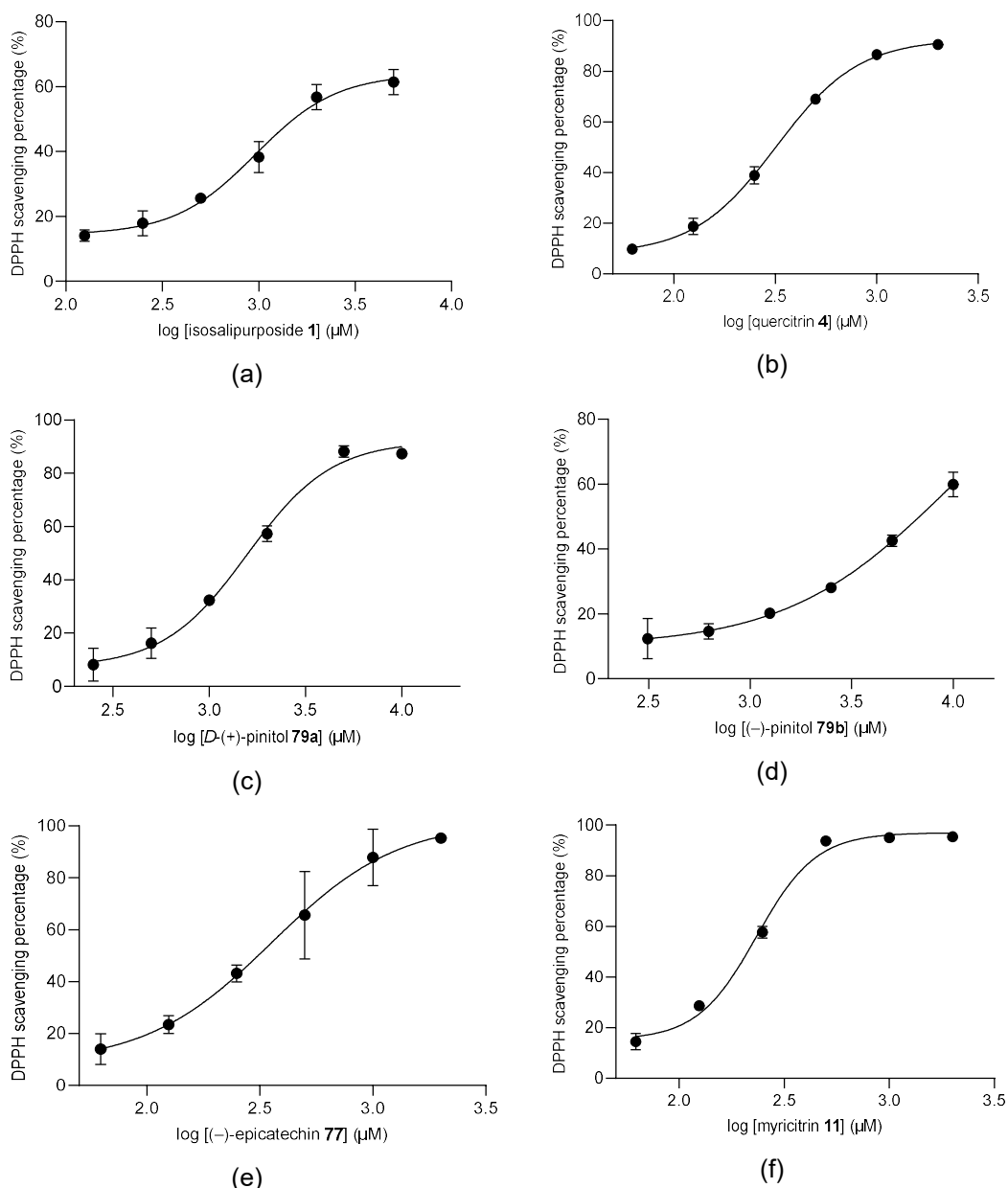
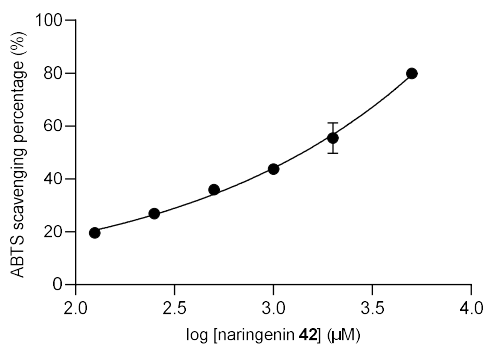


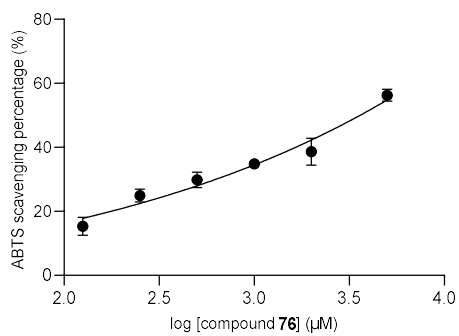
Figure 90. The dose-response curve of the isolated active compounds against radical DPPH. (a) isosalipurposide **1**, (b) quercitrin **4**, (c) *D*-(+)-pinitol **79a**, (d) (-)-pinitol **79b**, (e) (-)-epicatechin **77**, (f) myricitrin **11**. Data in mean \pm SEM, $n = 3$.

Furthermore, naringenin **42**, naringenin-7*O*- α -*L*-arabinofuranoside **76**, and 2,4-di-*t*-butylphenol **78** demonstrated a weaker neutralising activity against ABTS^{•+} cation radicals due to the relatively higher IC₅₀ values (Figure 92) than those of the three flavonoid derivatives. The activity of compound **80** was neglectable as its scavenging percentage remains under 50% even up to 10,000 μ M. Given that no extended π - π conjugation in ring C reduced the possibility of resonance of the phenolic radical intermediates after proton-abstracting³⁷⁷, it is not surprising that naringenin and its glycone form possessed lower scavenging activity in the DPPH

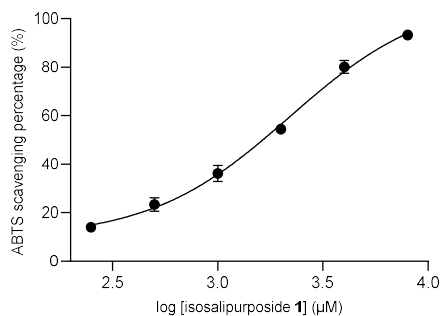
assay than their precursor, isosalipurposide. According to Ouyang et al.³⁷⁸, H-abstracting is the preferable starting step in the neutralisation of DPPH• radicals by accepting a proton to form a DPPH-H molecule.



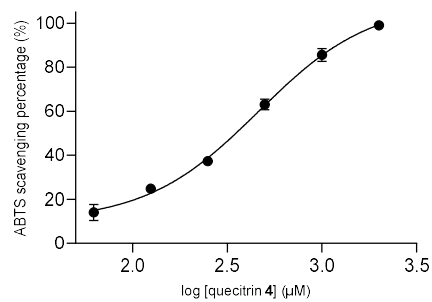
(a)



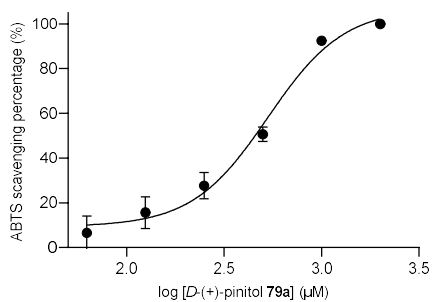
(b)



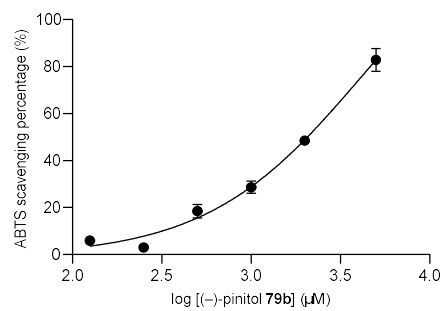
(c)



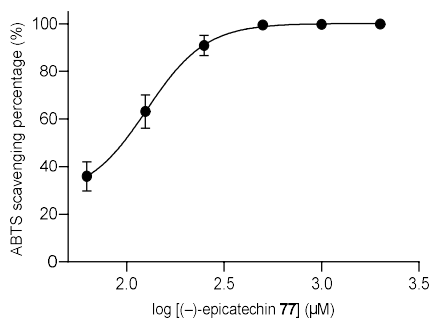
(d)



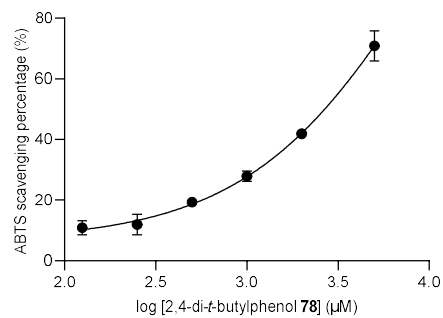
(e)



(f)



(g)



(h)

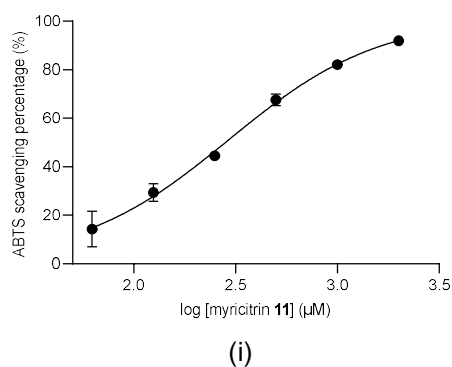


Figure 91. The dose-response curve of the isolated active compounds against ABTS cation radicals. (a) naringenin **42**, (b) Compound **76**: naringenin-7-*O*- α -L-arabinofuranose **76**, (c) isosalipurposide **1**, (d) quercitrin **4**, (e) *D*-(+)-pinitol **79a**, (f) (-)-pinitol **79b**, (g) (-)-epicatechin **77**, (h) 2,4-di-*t*-butylphenol **78**, (i) myricitrin **11**. Data in mean \pm SEM, $n = 3$.

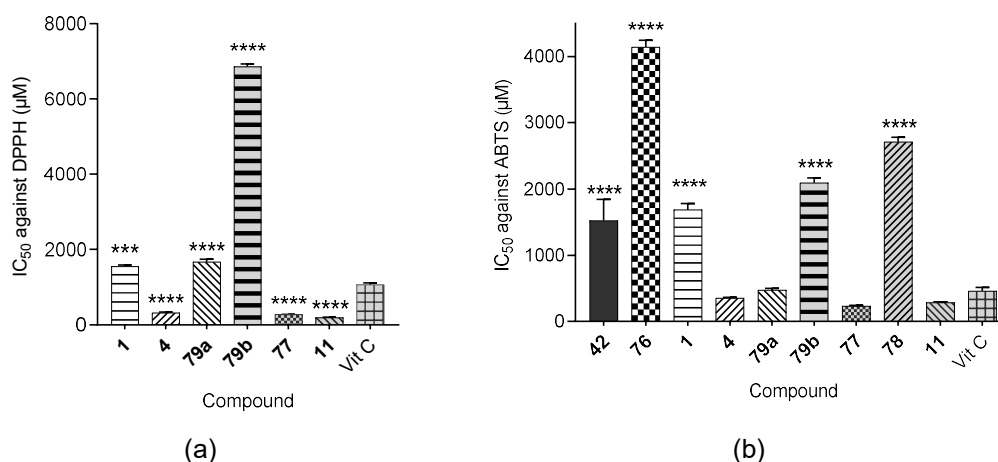


Figure 92. Comparison of the IC₅₀ of the compounds obtained by (a) DPPH and (b) ABTS^{•+} scavenging assay. **1**: isosalipurposide; **4**: quercitrin; **11**: myricitrin; **42**: naringenin; **76**: naringenin-7-*O*- α -L-arabinofuranose **77**; (-)-epicatechin; **78**: 2,4-di-*t*-butylphenol; **79a**: *D*-(+)-pinitol, **79b**: (-)-pinitol; Vit C: Vitamin C. Data in mean \pm SEM, *** $p = 0.0002$; **** $p < 0.0001$, vs vitamin C ($n = 3$, One-way ANOVA, Tukey's post hoc).

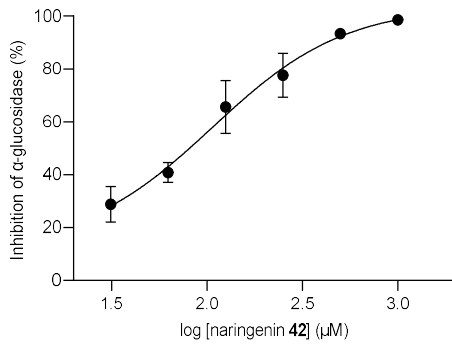
The presence of quercitrin **4** (4.13% w/w) and perhaps naringenin **42** (1.75% w/w) and isosalipurposide **1** (1.52% w/w) in FL-MeOH supports the activity exerted by this extract. The presence of the three active antioxidants, namely (-)-epicatechin **77** (0.9% w/w), quercitrin **4** (2.86% w/w), and myricitrin **11** (5% w/w), logically supports the activity of LF-MeOH observed in both DPPH and ABTS assays. Quercitrin **4** and myricitrin **11** were also found in the leaf extract of Egyptian *A. saligna*¹⁹⁶. The potent antioxidant activity of the leaf extract reported by Elansary et al.²⁷⁹ was extensively exerted by many other flavonoids and polyphenols in the extract, as indicated in their HPLC analysis.

BK-MeOH extract is the most active in DPPH and ABTS assays (Table S5 and S7, pages 241–243). However, only 2.53% w/w of active (–)-epicatechin **77** is present in this extract, in which *D*-(+)-pinitol **79a** (17.83% w/w) is the main component. In this case, the presence of (–)-epicatechin **77** may partly explain the high activity exerted by BK-MeOH in both assays. The inconsistent activities of *D*-(+)-pinitol **79a** found between DPPH and ABTS assays would inadequately support the activity exerted by BK-MeOH. In comparison, the antioxidant activity of Egyptian crude ethanolic bark extract was reported with $IC_{50} = 10.1 \mu\text{g/mL}$ ²⁸⁰. The potent activity of their bark extract was attributed to the presence of flavonoid antioxidant compounds (naringenin, kaempferol, and rutin) and phenolic group (gallic acid, vanillin acid, caffeic acid, ferulic acid, and chlorogenic acid).

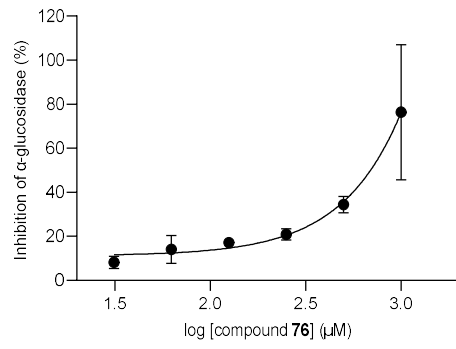
5.3. Inhibitory activity of isolated compounds against α -glucosidase

The inhibitory activity against yeast α -glucosidase enzymes was applied to screen the activity of the phytochemicals. They demonstrated dose-dependent inhibition on the cleavage of saccharide analogue by the enzyme (Figure 93). (–)-Epicatechin **77** ($IC_{50} = 63.58 \pm 11.83 \mu\text{M}$), *D*-(+)-pinitol **79a** ($IC_{50} = 74.69 \pm 0.226 \mu\text{M}$), naringenin **42** ($IC_{50} = 89.71 \pm 10.22 \mu\text{M}$), isosalipurposide **1** ($IC_{50} = 116.5 \pm 26.40 \mu\text{M}$), (–)-pinitol **79b** ($IC_{50} = 164.2 \pm 8.362 \mu\text{M}$), and quercitrin **4** ($IC_{50} = 177.3 \pm 11.34 \mu\text{M}$) inhibited the enzyme better than naringenin-7*O*- α -*L*-arabinofuranose **76**, 2,4-di-*t*-butylphenol **78**, myricitrin **11**, and the positive control, acarbose. Compound **80** showed no inhibition against the enzyme across the range of test concentrations. Notably, *D*-(+)-pinitol **79a** is a potent inhibitor and 2-fold more active than its enantiomer (–)-pinitol **79b**. It is important to note that acarbose exerts more inhibitory activity against mammalian α -glucosidase enzyme than the yeast enzyme. Pacillia et al.³⁷⁹ reported that naringenin **42** displayed an effective inhibition against the yeast enzyme ($IC_{50} = 6.51 \mu\text{M}$). However, it was poor when tested on the rat intestinal glucosidase ($IC_{50} = 384 \mu\text{M}$). They also reported that the positive control acarbose inhibited the rat α -glucosidase more effectively than the yeast enzyme. Therefore, further investigation is required to confirm the inhibitory activity of our extracts and active compounds against the mammalian α -glucosidase enzyme.

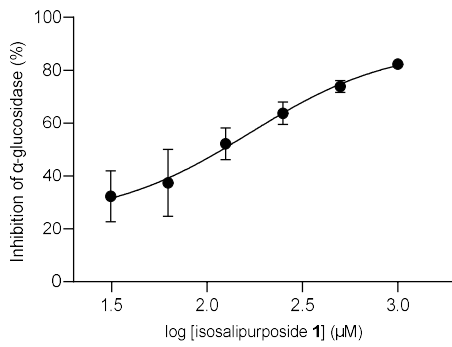
Naringenin **42** exhibited much better inhibition, calculated a 10-fold higher value of IC_{50} than its glycone derivative, the naringenin-7*O*- α -*L*-arabinofuranose **76**. This observation agrees with the report from Jung et al.³⁸⁰ that glycolised flavanone was linked to a lower inhibitory activity against the enzyme. The flavonol derivative of myricitrin **11** showed relatively lower activity in this study than quercitrin **4**.



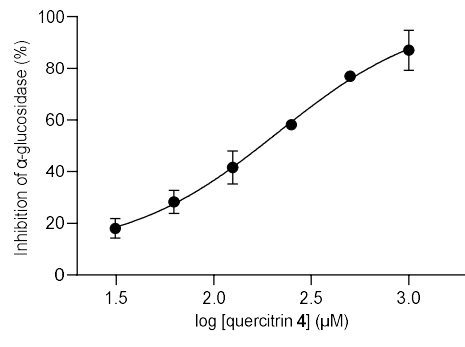
(a)



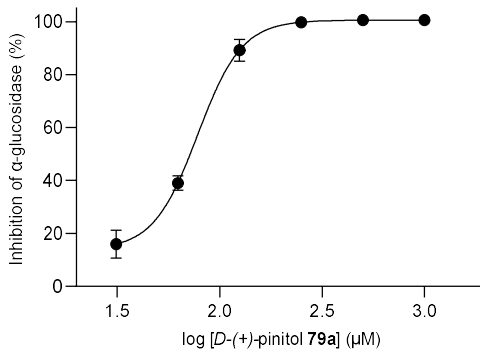
(b)



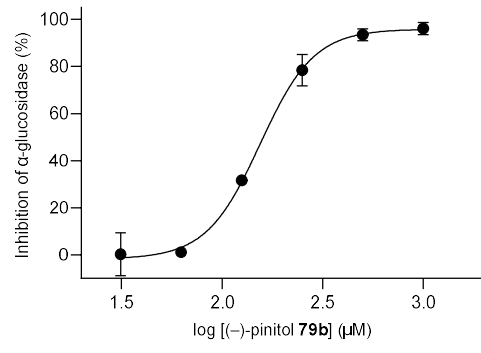
(c)



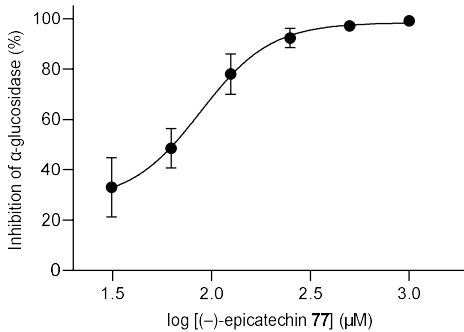
(d)



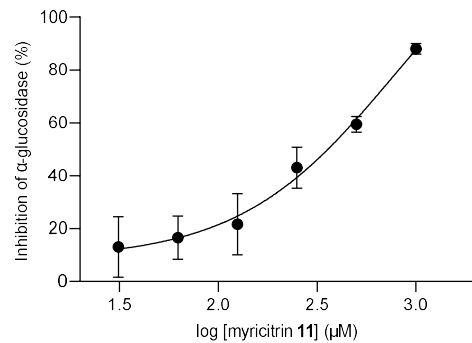
(e)



(f)



(g)



(h)

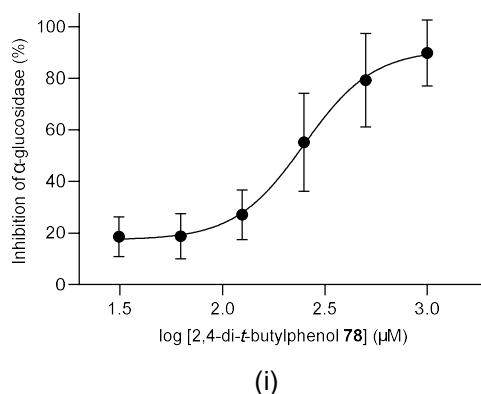


Figure 93. The dose-response curve of the isolated active compounds against α -glucosidase enzyme. (a) naringenin **42**, (b) compound **76**: naringenin-7O- α -L-arabinofuranose, (c) isosalipurposide **1**, (d) quercitrin **4**, (e) D-(+)-pinitol **79a**, (f) (-)-pinitol **79b**, (g) (-)-epicatechin **77**, (h) myricitrin **11**, (i) 2,4-di-*t*-butylphenol **78**. Data in mean \pm SEM, $n = 3$.

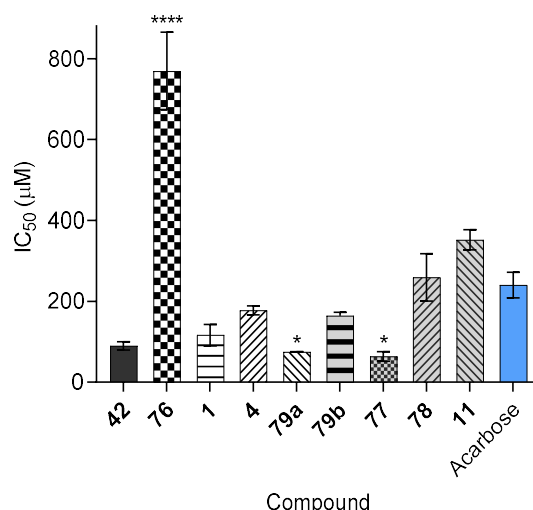


Figure 94. IC₅₀ of isolated compounds compared to acarbose. **1**: isosalipurposide; **4**: quercitrin; **11**: myricitrin; **42**: naringenin; **76**: naringenin-7O- α -L-arabinofuranose; **77**: (-)-epicatechin; **78**: 2,4-di-*t*-butylphenol; **79a**: D-(+)-pinitol; **79b**: (-)-pinitol. Data in mean \pm SEM, * $p = 0.03$, **** $p < 0.0001$, vs acarbose ($n = 3$, One-way, ANOVA, Tukey's post hoc).

The inhibitory activity of (-)-epicatechin **77** against α -glucosidase was reported to have IC₅₀ values of 0.95 μ M to 12.3 mM³⁸¹⁻³⁸³. For naringenin **42**, variable IC₅₀ values were also observed in the 6.51 to 75 μ M^{379,384}. Furthermore, the literature indicates that the reported IC₅₀ values of these compounds and other flavonoids are dispersed and variable³⁸⁵.

The structure-activity relationships (SAR) investigation by Proença et al.³⁸⁵ suggested that flavonoids with two phenolic groups at the A or B ring and a hydroxy group at C3 possessed the highest α -glucosidase inhibitory activity. He et al.³⁸⁶ and Şöhretoğlu et al.³⁸⁷ further reiterated that the number of phenolic groups on ring B is

vital for the activity. Their docking study indicated that the B ring of the flavonoids located deep inside the active side of the enzyme and the presence of the phenolics significantly improved interactions via hydrogen bonding. On the other hand, bulky flavonoid glycosides showed poor inhibition due to their inability to access the binding pocket, which explains the poor activity of naringenin-7-O- α -L-arabinofuranose **76**, quercitrin **4**, myricitrin **11**, and compound **80**. *D*-(+)-pinitol **79a** is a cyclic polyol known to have highly beneficial effects on inflammation and related diseases, such as T2D³⁸⁸. To the best of our knowledge, it is for the first time that both enantiomers of pinitol were shown to be inhibitors against the yeast α -glucosidase enzyme.

It is noteworthy that *D*-(+)-pinitol **79a** (17.83% w/w) is the principal component in BK-MeOH and would be the main contributor to the α -glucosidase inhibitory activity observed in the BK-MeOH ($IC_{50} = 4.37 \pm 0.24 \mu\text{g/mL}$) in combination from (-)-epicatechin **77** (2.53% w/w). *D*-(+)-pinitol **79a** has previously been documented as the weak α -glucosidase inhibitor³⁸⁹. (-)-Pinitol **79b** (8% w/w), (-)-epicatechin **77** (0.9%), and quercitrin **4** (2.86%) contribute to inhibitory activity exerted by LF-MeOH ($IC_{50} = 38.69 \pm 1.01 \mu\text{g/mL}$). In FL-MeOH, *D*-(+)-pinitol **79a** (2.5%) and three mid-range active compounds, namely naringenin **42** (1.75%, w/w), isosalipurposide **1** (1.52%), and quercitrin **4** (4.13%), are the main contributors to the activity found in FL-MeOH ($IC_{50} = 34.93 \pm 2.67 \mu\text{g/mL}$).

5.4. Cell viability of 3T3-L1 cell line treated with isolated compounds

According to Figures 95–104, all ten isolated compounds demonstrated varied toxic effects towards the growth of 3T3-L1 preadipocytes up to 125 μM . Naringenin derivatives from the flowers showed a non-toxic effect as more than 75% of viable cells³⁹⁰ incubated with the isolated compounds for 24-, 48-, and 72-h were observed. Previously, naringenin **42** has been reported by Nishina et al.³⁹¹ to demonstrate no significant toxicity for the same cells up to 100 μM , whereas no documentation has been found for naringenin-7-O- α -L-arabinofuranoside **76**. The isolated (-)-epicatechin **77** could be applied to the pre-confluent cell experiments within the range of more than 80% viable cells in all treatments, 24-, 48-, or 72-h. Our finding aligns with the report from Ardevol et al.³⁹² confirming the non-toxic effect on 3T3-L1 cells by epicatechin at 300 μM .

Some isolated compounds, however, exhibited a slightly different outcome. An alkylphenol (2,4-di-*t*-butylphenol **78**) is slightly toxic (< 75% viable cells) for the pre-adipocytes exposed to 125 μM for over 72-h. This compound was reported as an antiviral, antifungal, antioxidant, and antimicrobial component in some plants, such as

sweet potatoes³⁹³. Nevertheless, no study has been reported on this compound in the 3T3-L1 cells. Interestingly, the viable cells exposed to the chalcone isosalipurposide **1** for 48 h have been somewhat lower than the safe point, 70%. However, both 24- and 72-h incubation gave different observations with a much higher percentage of cell viability of 86.14 and 81.83%, respectively. Myricitrin **11**, in contrast, could be excluded for safe treatment between 62.5 and 125 μM due to significantly decreased cell viability in all incubation times. Therefore, the safe working concentration for myricitrin **11** is likely below 31.25 μM for the treatment of the preadipocytes.

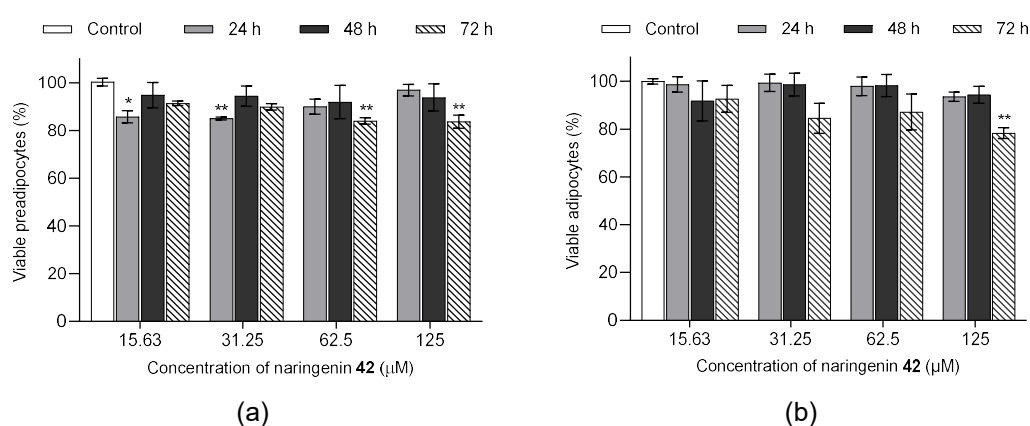


Figure 95. Viability of (a) 3T3-L1 preadipocytes and (b) adipocytes treated with naringenin **42** for 24-, 48-, and 72-h. Data in mean \pm SEM, * $p = 0.013$; ** $p = 0.003$, vs vehicle control ($n = 3$, One-way ANOVA, Dunnett's post hoc).

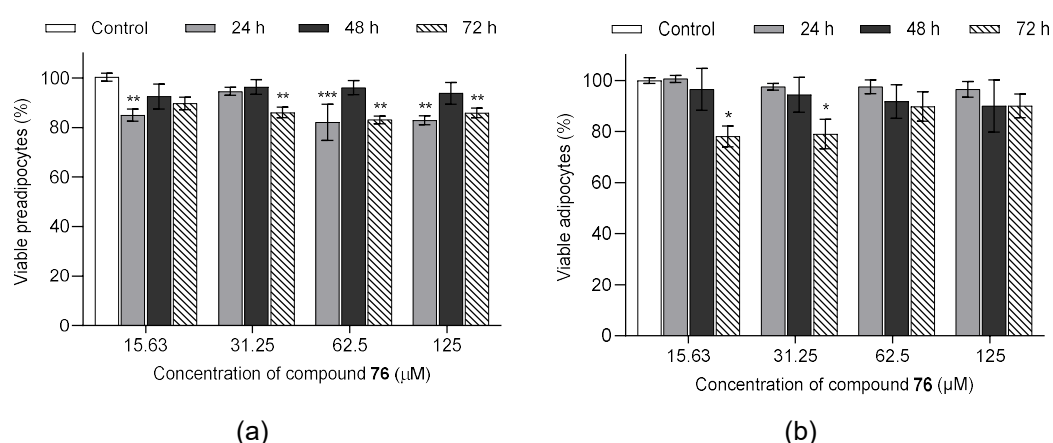


Figure 96. Viability of (a) 3T3-L1 preadipocytes and (b) adipocytes treated with naringenin-7O- α -L-arabinofuranoside **76** for 24-, 48-, and 72-h. Data in mean \pm SEM, * $p = 0.01$; ** $p = 0.004$; *** $p = 0.0008$, vs vehicle control ($n = 3$, One-way ANOVA, Dunnett's post hoc).

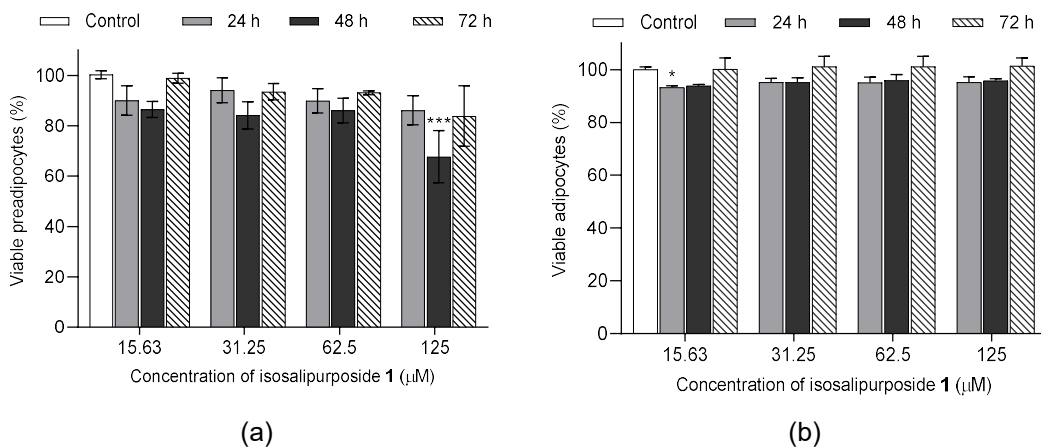


Figure 97. Viability of (a) 3T3-L1 preadipocytes and (b) adipocytes treated with isosalipurposide 1 for 24-, 48-, and 72-h. Data in mean \pm SEM, * $p = 0.04$; *** $p = 0.0008$, vs vehicle control ($n = 3$, One-way ANOVA, Dunnett's post hoc).

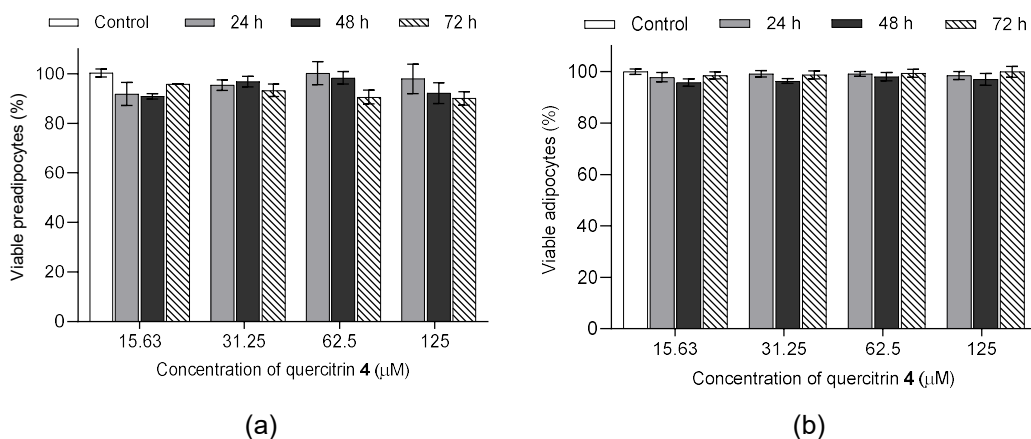


Figure 98. Viability of (a) 3T3-L1 preadipocytes and (b) adipocytes treated with quercitrin 4 for 24-, 48-, and 72-h. Data in mean \pm SEM, $n = 3$.

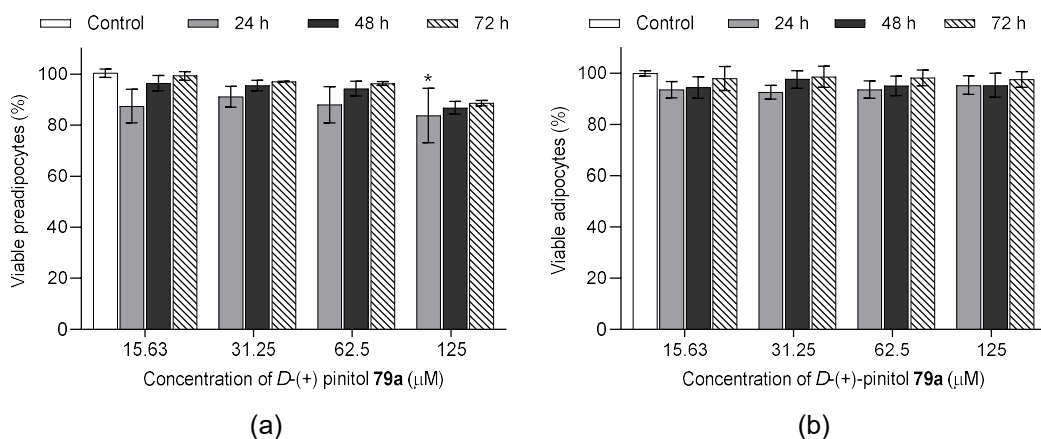


Figure 99. Viability of (a) 3T3-L1 preadipocytes and (b) adipocytes treated with D-(+)-pinitol 79a for 24-, 48-, and 72-h. Data in mean \pm SEM, * $p = 0.02$, vs vehicle control ($n = 3$, One-way ANOVA, Dunnett's post hoc).

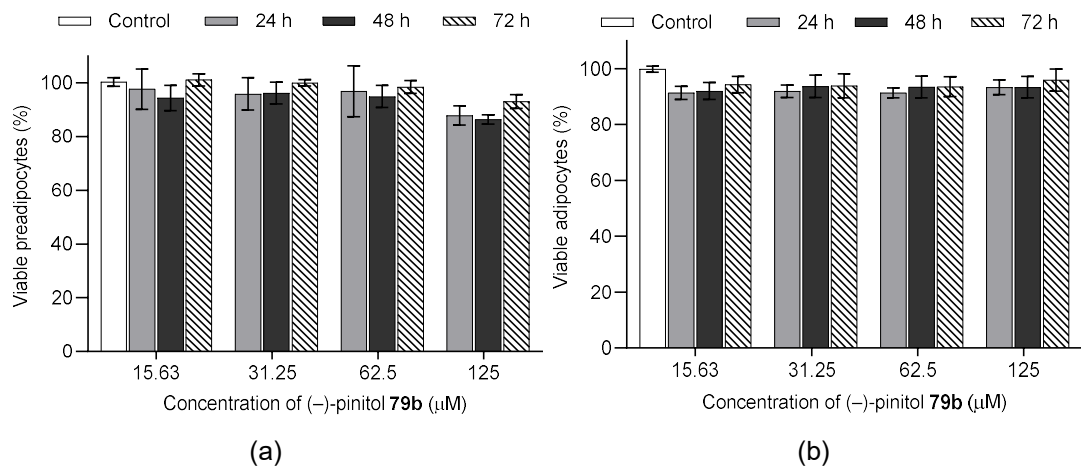


Figure 100. Viability of (a) 3T3-L1 preadipocytes and (b) adipocytes treated with (-)-pinitol **79b** for 24-, 48-, and 72-h. Data in mean \pm SEM, $n = 3$.

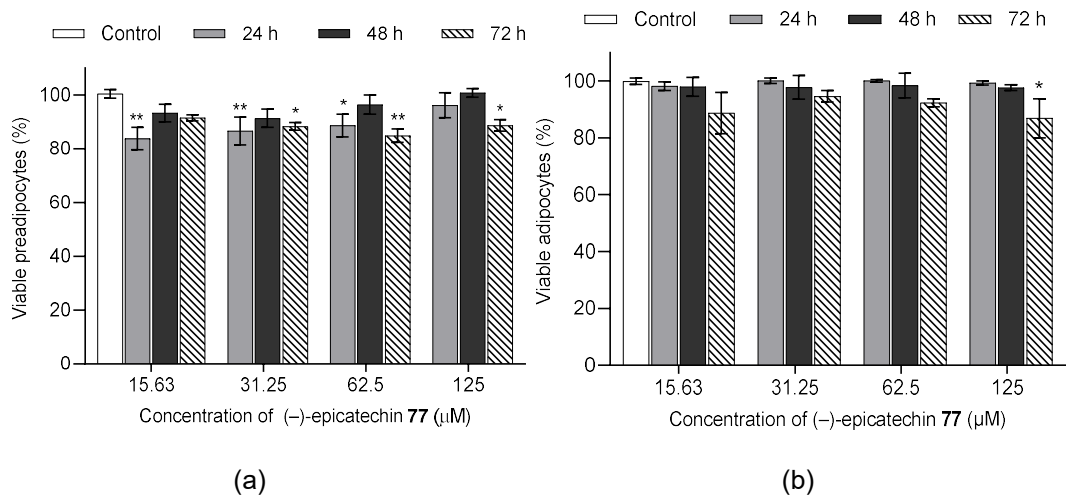


Figure 101. Viability of (a) 3T3-L1 preadipocytes and (b) adipocytes treated with (-)-epicatechin **77** for 24-, 48-, and 72-h. Data in mean \pm SEM, * $p = 0.03$; ** $p = 0.001$, vs vehicle control ($n = 3$, One-way ANOVA, Dunnett's post hoc).

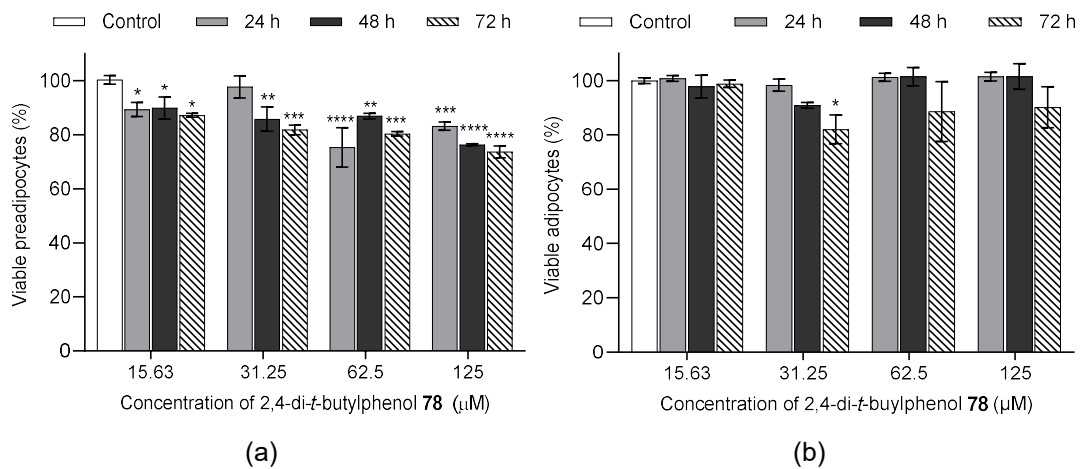


Figure 102. Viability of (a) 3T3-L1 preadipocytes and (b) adipocytes treated with 2,4-di-*t*-butylphenol **78** for 24-, 48-, and 72-h. Data in mean \pm SEM, * $p = 0.01$; ** $p = 0.001$; **** $p < 0.0001$, vs vehicle control ($n = 3$, One-way ANOVA, Dunnett's post hoc).

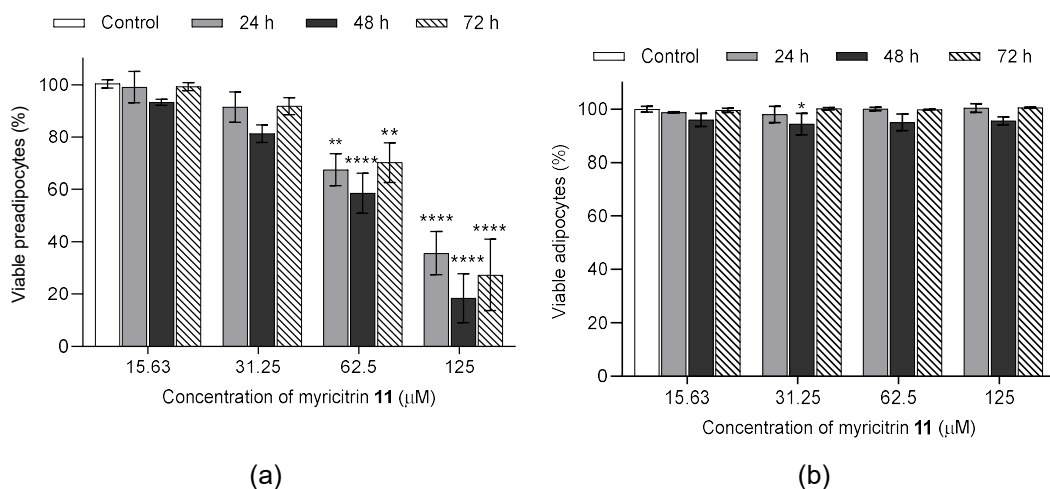


Figure 103. Viability of (a) 3T3-L1 preadipocytes and (b) adipocytes treated with myricitrin **11** for 24-, 48-, and 72-h. Data in mean \pm SEM, * p = 0.05; ** p = 0.001; **** p < 0.0001, vs vehicle control (n = 3, One-way ANOVA, Dunnett's post hoc).

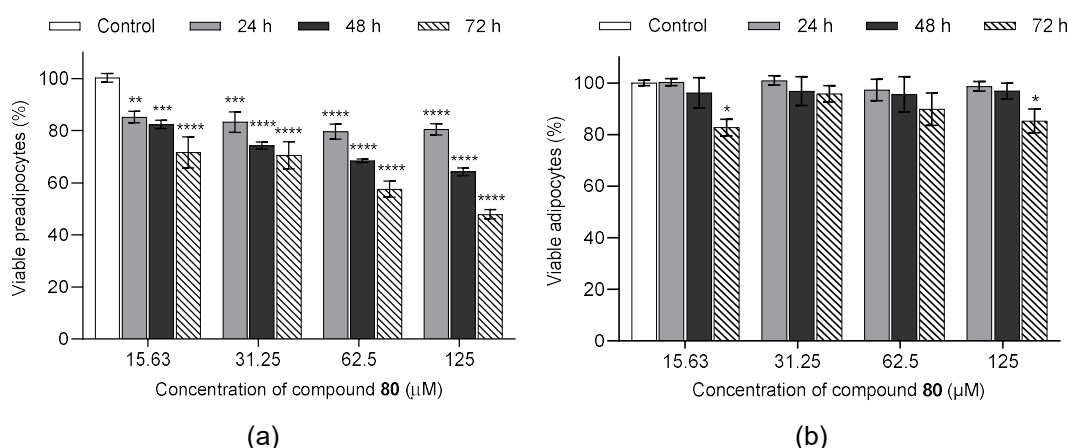


Figure 104. Viability of (a) 3T3-L1 preadipocytes and (b) adipocytes treated with 3-hydroxy-5-(2-aminoethyl) dihydrofuran-2(3H)-one **80** for 24-, 48-, and 72-h. Data in mean \pm SEM, * p = 0.02; ** p = 0.002; *** p = 0.0002; **** p < 0.0001, vs vehicle control (n = 3, One-way ANOVA, Dunnett's post hoc).

A cell viability test of 3T3-L1 adipocytes treated with isolated compounds was also carried out to evaluate the toxicity effects of the phytochemicals between 15.63 and 125 µM during 24, 48, and 72 h of incubation. According to Tables S28–S37 (pages 254–256) and Figures 95–104 above, all compounds could be considered safe for the adipose cells within the concentration range. This finding aligns with the previous MTT assay of the compounds in 3T3-L1 pre-adipocytes except for isosalipurposide **1** at 125 µM for 48-h, myricitrin **11** at 62.5 and 125 µM for all incubation times, and compound **80** at 62.5 and 125 µM for 72-h. The same trend was also observed for LF-MeOH and BK-MeOH extracts; although these were toxic at 100

µg/mL for pre-adipocytes, the harmful effect on adipocytes did not appear up to the highest concentration, 200 µg/mL. From here, it can be said that the compounds can be applied for other assays against the mature adipocytes in the indicated concentration.

5.5. Oil Red-O staining assay of adipocytes treated with isolated compounds

The ORO-staining assay was then applied to determine the impact of isolated compounds of methanolic extracts on lipid content in 3T3-L1 adipocytes. Most isolated compounds possessed anti-adipogenic activity during the differentiation process of 3T3-L1 cells, as depicted in Figure 105. The tested compounds exhibited higher lipid droplet percentage reductions at 10 µM than the vehicle control. At 10 µM, a slight reduction was observed for 2,4-di-*t*-butylphenol **78** (9.86%), *D*-(+)-pinitol **79a** (10.88%), quercitrin **4** (11.88%), naringenin **42** (14.41%), and (-)-pinitol **79b** (16.92%). Furthermore, the lactone derivative and (-)-epicatechin **77** showed moderate reductions of lipid droplets estimated at 19.13 and 21.15%, respectively. Myricitrin **11** significantly reduced lipid accumulation by 25.28%, seven times higher than that at 0.5 µM suggesting the change through a dose-dependent manner. This activity reflects the potent inhibition in lipid production by its corresponding LF-MeOH extracts. In contrast, naringenin-7-*O*- α -*L*-arabinofuranoside **76** did not alter the LDs content at 0.5 and 10 µM, while isosalipurposide did not affect the reduction of lipid droplets at 10 µM.

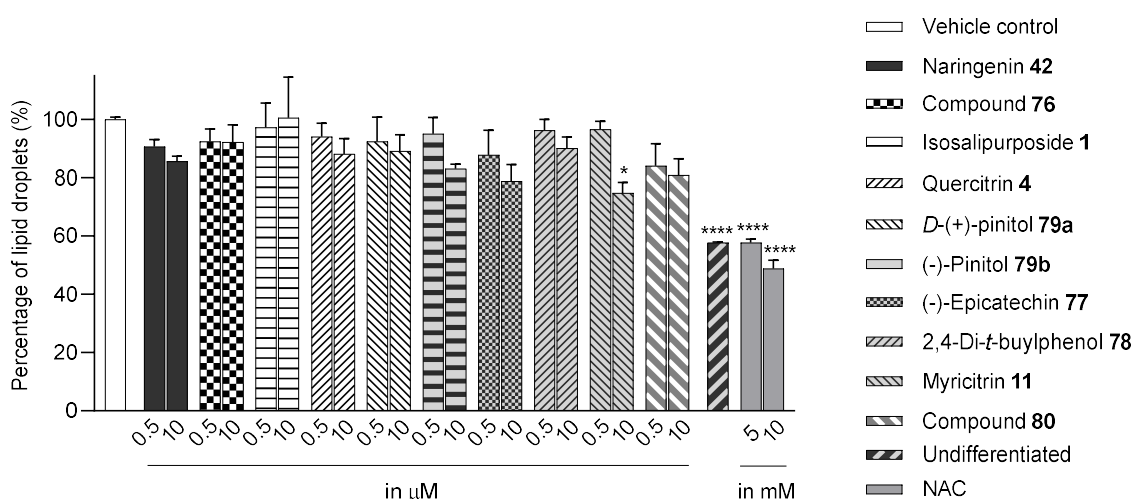


Figure 105. Estimated lipid content from ORO staining assay on the 3T3-L1 adipocytes treated with isolated compounds during differentiation. NAC = *N*-acetyl cysteine. Data in mean \pm SEM, * p = 0.03; **** p = 0.00008, vs vehicle control (n = 3, One-way ANOVA, Tukey's post hoc).

5.6. Cellular ROS reduction assay on adipocytes treated with isolated compounds

Isolated compounds, such as (–)-epicatechin **77**, quercitrin **4**, and myricitrin **11**, showed potent antioxidant activities against DPPH and ABTS free radicals³⁰⁷. This suggests that the strong antioxidant activities of these compounds may also affect ROS accumulation and help explain the observed reduction in ROS accumulation by the extracts. The ability of isolated compounds to reduce cellular ROS was evaluated using the same protocol. Figure 106 and Table S39 (pages 257–258) present the result of the DCFH-DA assay on the cells treated with 0.5 and 10 µM of isolated compounds. In general, treatment at 0.5 µM did not show a significant reducing effect compared to vehicle control of adipocytes. There was around one-tenth ROS reduction in the treatment with two enantiomers of pinitol, whereas relatively steady ROS levels were observed from treatment with other isolated compounds. A noticeable decreasing effect was found in the treatment with 10 µM of the two active compounds isolated from BK-MeOH extract, (–)-epicatechin **77** and *D*-(+)-pinitol **79a**, indicating the most active ones with a reduction percentage of 28.55 and 30.76%, respectively. *D*-(+)-pinitol **79a** demonstrated more activity than its enantiomer, (–)-pinitol **79b**, consistent with the previous finding on DPPH and ABTS scavenging.

Flavanol derivatives, including (–)-epicatechin **77**, have been reported to possess better scavenging activities on neutralising ROS than many monomeric flavones and flavonols³⁰⁹. The DPPH and ABTS assays outcome showed that (–)-epicatechin **77** exerted more inhibition percentage than flavone derivatives, including naringenin **42** and naringenin-7-*O*- α -*L*-arabinofuranoside **76** and flavanol derivatives, such as quercitrin **4** and myricitrin **11**. Furthermore, activation of the cell signalling system has also been reported to play a key role in the protective effect of bioactive compounds against overproduced ROS. For instance, activation of Akt and AMPK pathways has been correlated to the decreasing effects of glycoside flavonoids on ROS production in 3T3-L1 adipocytes³⁹⁴.

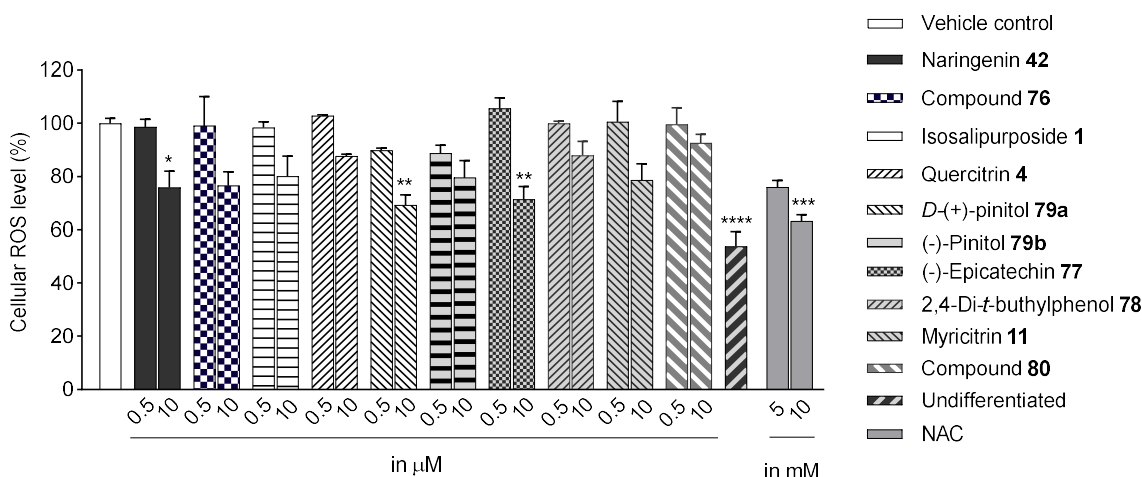


Figure 106. Cellular ROS in 3T3-L1 adipocytes treated with isolated compounds and NAC compared to undifferentiated cells. Data in mean \pm SEM, * p = 0.05, ** p = 0.002, *** p = 0.0003, **** p = 0.00001, vs vehicle control (n = 3, One-way ANOVA, Tukey's post hoc).

Furthermore, naringenin-7-*O*- α -*L*-arabinofuranoside **76** and 3-hydroxy-5-(2-aminoethyl) dihydrofuran-2(3*H*)-one **80** had an inhibitory effect at 10 μ M estimated for 23.36 and 7.33% reduction, respectively. However, this finding does not reflect the weak antioxidant activities observed in DPPH and ABTS assays, as reported in our previous study³⁰⁷. This anomaly is that naringenin-7-*O*- α -*L*-arabinofuranoside **76** and 3-hydroxy-5-(2-aminoethyl) dihydrofuran-2(3*H*)-one **80** might chemically interact with DPPH or ABTS differently than cellular ROS. They could possess cellular ROS reductive activity by directly scavenging the ROS and were indirectly involved in cellular signalling pathways. For instance, flavanone, the core skeleton of naringenin-7-*O*- α -*L*-arabinofuranoside **76**, scavenged hydroxyl and peroxide radicals attributed to the hydroxyl group at C4' of ring B³⁹⁵. Moreover, naringenin groups demonstrated modulation of endogenous glutathione³⁹⁶ and activation of the nuclear factor erythroid 2-related factor 2 (Nrf2) pathway³⁹⁷. Lactone derivatives have been reported to suppress a cellular redox regulator called nuclear factor- κ B (NF- κ B)³⁹⁸. Further investigation is needed to evaluate the possible mechanisms causing the antioxidant of both compounds in the adipocytes.

Naringenin-7-*O*- α -*L*-arabinofuranoside **76** showed slightly less percentage of ROS reduction at both tested concentrations (0.94 and 23.36% at 0.5 and 10 μ M) than those for naringenin (1.3 and 24.18 %). The glycosylated 7-OH of ring A can decrease anti-ROS activity³⁹⁹. The chalcone derivative, isosalipurposide, exerted lower activity (19.87% at 10 μ M) than naringenin and its glycoside derivative, naringenin-7-*O*- α -*L*-arabinofuranoside **76**. Saturated C2,3 and opened ring C of

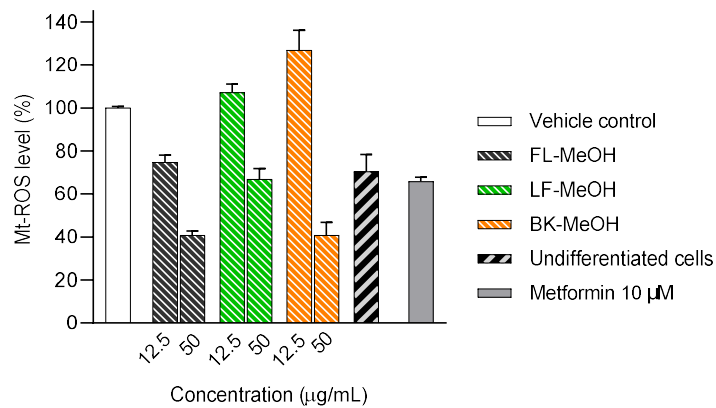
chalcone have been described as the factor of its decreased inhibition by Limasset et al.³⁹⁹ compared to flavanone.

5.7. Measurement of mt-ROS and MMP on adipocytes treated with isolated compounds

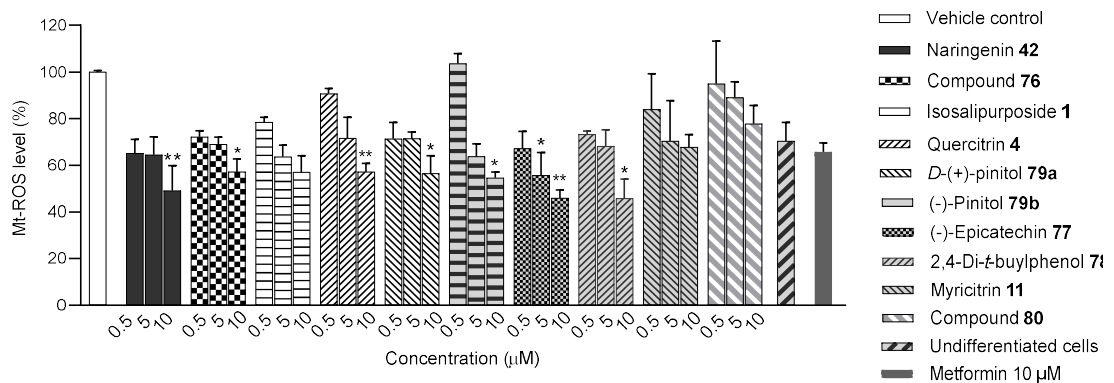
Given that accumulated mt-ROS on adipocytes can trigger carbonylation in mitochondrial proteins and affect the antioxidant enzymes such as superoxide dismutase of MnSOD and SOD2, reducing mt-ROS can restore mitochondrial health. An increasing MMP can manifest the restored mitochondria. The increased MMP has been reported to improve endogenous mitochondrial antioxidants to convert superoxide into harmless H₂O⁴⁰⁰.

Monitoring changes in MMP can be conducted using a membrane-permeant 5,5,6,6'-tetrachloro-1,1",3,3" tetraethylbenzimidazolcarbocyanine iodide (JC-1) dye assay. In the MMP study, the cationic lipophilic JC-1 dye accumulates in polarised mitochondria to form aggregates (J-aggregate) that fluoresce red. Upon depolarisation for the cytoplasm, JC-1 leaves the inner mitochondrial membrane, which disaggregates into monomers (JC-1 monomer) that fluoresce green. The degree of depolarisation is determined by the ratio of red: green fluorescence or J-aggregates/JC-1 monomers. A healthy mitochondrion possesses more negative charges in its mitochondrial matrix due to proton transfer from the matrix to intermembrane space. Therefore, healthy mitochondria admit red fluorescence compared to mitochondria with lower membrane potential, which fluoresce green. In other words, it has a higher ratio⁴⁰¹. Our study showed that the mt-ROS and J-aggregates/JC-1 monomers ratio of undifferentiated 3T3-L1 cells were 29.55% lower and 0.91-fold higher than those measured for the adipocytes, respectively. In addition, treatment with a mitochondria-targeted drug, metformin, demonstrated mt-ROS reduction of 34.26% and a 2-fold higher ratio of J-aggregates/JC-1 monomers than vehicle control. Thus, these parameters can reflect the normalisation of the mitochondria function.

As presented in Table S40 (page 258), the exposure to FL-, LF-, and BK-MeOH extracts at the higher concentration (50 µg/mL) seems to positively impact the health of adipocytes' mitochondria, indicated by the decreased mt-ROS level and increased value of the J-aggregates/JC-1 monomers ratios compared to untreated adipocytes group. All methanolic extracts demonstrated a reducing effect on mt-ROS levels at 50 µg/mL (Figure 107a). The methanolic flower extract reduced the level of mt-ROS by 31%, while LF- and BK-MeOH reduced it by 52% and 58%, respectively.

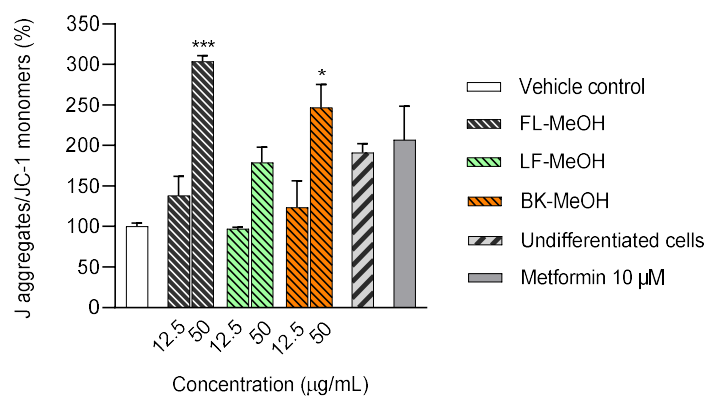


(a)

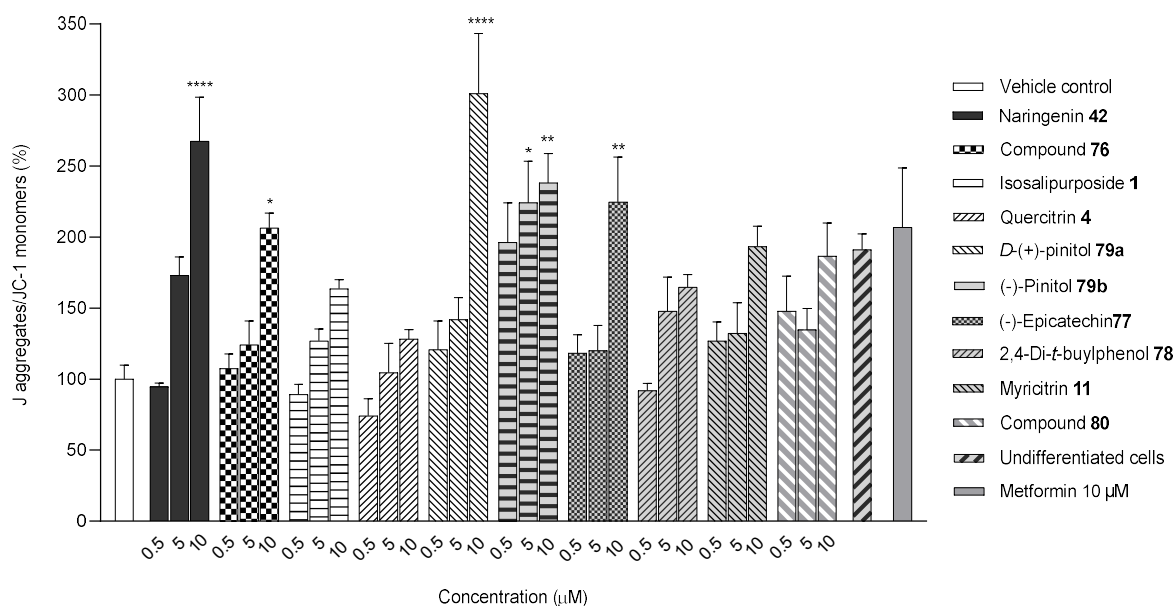


(b)

Figure 107. Estimated mt-ROS level of 3T3-L1 adipocytes treated by (a) methanolic extracts, metformin, and (b) isolated compounds. Compound **2** = naringenin-7-*O*- α -*L*-arabinofuranoside, compound **80** = 3-hydroxy-5-(2-aminoethyl) dihydrofuran-2(3*H*)-one). Data in mean \pm SEM, * p = 0.02; ** p = 0.003; **** p = 0.00002, vs vehicle control (n = 3, One-way ANOVA, Tukey's post hoc).



(a)



(b)

Figure 108. Estimated ratio of J aggregates/JC-1 monomers percentage in 3T3-L1 adipocytes treated by (a) methanolic extracts and (b) isolated compounds. Data in mean \pm SEM, * p = 0.03, ** p = 0.001, *** p = 0.0002, **** p = 0.00001, vs vehicle control (n = 3, one-way ANOVA, Tukey's post hoc tests).

The trend of decreasing mt-ROS level was also displayed in the incubation of adipocytes with all isolated compounds (see Table S41, page 258). The flavanone derivatives (naringenin **42** and naringenin-7-*O*- α -*L*-arabinofuranoside **76**), isosalipurposide, flavonol derivatives (quercitrin **4** and myricitrin **11**), pinitols, and (–)-epicatechin **77** showed better impacts on the reduction (ranged 28.37 to 54.18% of reduction) than those exerted by 3-hydroxy-5-(2-aminoethyl) dihydrofuran-2(3*H*)-one **80** at both tested concentrations of 0.5 and 10 μ M (10.88 and 22.22%, respectively). The reductive effect of lactone derivative was insignificant, reflecting similar findings with previous assays that this compound has poor antioxidant activity³⁰⁷. (–)-Epicatechin **77** demonstrated significant impacts at 5 and 10 μ M, indicating that this flavanol possesses strong antioxidant properties. This finding aligns with the marked inhibitory activities against DPPH and ABTS^{••} radicals, suggesting that a scavenger of both free radicals can inhibit cellular ROS production.

In the MMP study presented in Figure 108 and Table S40 and S41 (page 258), treatment with methanolic extracts and all isolated compounds at the higher concentration seems to maintain the health of adipocytes' mitochondria, indicated by more than 100% value of the J-aggregates/JC-1 monomers ratios. The FL-MeOH treatment exerted a fold-change of 3 of the ratios, while BK- and LF-MeOH showed 2.47- and 1.79-fold increases in the ratios, respectively. In addition to the marked

activity of FL-MeOH, its bioactive constituents, namely naringenin **42**, naringenin-7-*O*- α -*L*-arabinofuranoside **76**, and *D*-(+)-pinitol **79a**, demonstrated significant protective effects at 10 μ M on MMP status. Indeed, naringenin is well-studied to prevent mitochondrial dysfunction by improving the expression of Bcl-2 and down-regulating Bax and Caspase-3 of neuro 2A cells ⁴⁰².

Three isolated phytochemicals of LF-MeOH, namely (–)-epicatechin **77**, *D*-(+)-pinitol **79a**, and (–)-pinitol **79b**, demonstrated significant protective effects on mitochondria of the adipocytes at 10 μ M with J-aggregates/JC-1 monomers ratios between 18 to 94% higher than metformin. *D*-(+)-pinitol **79a**, showing excellent activity in mitochondrial protection, was also found as the active constituent of BK-MeOH along with (–)-epicatechin **77**. It is 1.5-fold more effective than metformin at the same test concentration of 10 μ M. Pinitol has been shown to protect mitochondria by increasing intracellular glutathione (GSH) and endogenous antioxidant of glutathione reductase in P12 cells ⁴⁰³. Notably, *D*-(+)-pinitol **79a** has been used as a natural health supplement to provide therapeutic benefits in treating T2D. It is also a natural antidiabetic and insulin regulator with anti-inflammatory ⁴⁰⁴ and hepatoprotective ³³² activities.

Apart from their role in the protein signalling pathway, flavonoids have been believed to modulate the level of endogenous antioxidant enzymes, such as SOD, catalase, glutathione peroxidase, and glutathione-S-transferase ⁴⁰⁵. Notably, naringenin **42** and (–)-epicatechin **77** demonstrated outstanding reduction of mt-ROS and protection of mitochondria. In studies on human vascular endothelial cells, (–)-epicatechin **77** has been confirmed to alter the mt-ROS production under a designed stress induction ⁴⁰⁶ through activating AMPK- α and SIRT1 (sirtuin 1) signalling pathway ⁴⁰⁷.

Here we showed that the mitochondrial health of adipocytes was enhanced by incubation with methanolic extracts of *A. saligna* and its isolated phytochemicals at the tested concentration. This was confirmed by the comparable data of reduction of mt-ROS concentration and increase of J-aggregates/JC-1 monomers ratio with those observed from the treatment with metformin and normal fibroblast-like 3T3-L1 cells. The normal MMP status allows protons produced by the mitochondrial respiratory chains to transfer proportionally from the mitochondrial matrix to the intermembrane. The recovered mitochondrial respiration is an indication of healthy mitochondria. Additionally, preventing excessive mt-ROS production helps safeguard

endogenous antioxidant enzymes from oxidation and maintain mitochondrial redox balance.

5.8. Cellular glucose uptake of adipocytes treated with isolated compounds

As the promising extract with outstanding activity in the modulation of glucose uptake, compounds isolated from the flowers, leaves, and bark extracts were subjected to the assay. We further evaluated the isolated compounds' ability to improve glucose uptake in 3T3-L1 adipocytes. The outcome would help to determine which compounds were responsible for stimulating the glucose uptake observed in the active extracts. The outcome is reported in Figure 109 and Table S42 (page 259). A slightly positive enhancement in the uptake stimulation was observed in the treatment at 0.5 μ M by naringenin-7-*O*- α -*L*-arabinofuranoside **76** (7.6% increase), isosalipurposide **1** (10.7%), *D*-(+)-pinitol **79a** (8.5%), (-)-epicatechin **77** (8.3%), and myricitrin **11** (22.7%) compared to vehicle control. At 10 μ M, an increase in 2-NBDG uptake was observed across all compounds (except lactone derivative). Interestingly, (-)-epicatechin **77** performed the best, about 50% better than metformin (10 μ M, 38% increase) and insulin (100 nM, 40.6%). Other compounds, such as naringenin-7-*O*- α -*L*-arabinofuranoside **76** (56.4% increase), isosalipurposide **1** (61%), quercitrin **4** (51%), *D*-(+)-pinitol **79a** (43.9%), 2,4-di-*t*-butylphenol **78** (31.2%) and myricitrin **11** (52.3%), showed marked improvement in glucose uptake. Therefore, their effects on glucose uptake support improving their respective extracts' glucose uptake.

A previous study by Gao et al. (2010) showed that the impaired mitochondria of white adipose tissue could reduce glucose uptake due to insulin resistance ⁷⁶. So far, we demonstrated that the most active extract, LF-MeOH at 50 μ g/mL, showed a 2-fold increase in glucose uptake of vehicle control, possessed mt-ROS reduction and J-aggregates/JC-1 monomers ratio 52.57% and 1.8-fold change, respectively. At 10 μ M, (-)-epicatechin **77** with 87.9% increased glucose uptake was observed to reduce 54.06% mt-ROS and 2.3-fold ratio change. This finding indicates that treatment with *A. saligna* methanolic extracts and compounds protect mitochondria in adipocytes and consequently enhances cellular glucose.

The well-known flavonoid derivatives such as (-)-epicatechin **77**, quercitrin **4**, and myricitrin **11**, as well as the inositol, *D*-(+)-pinitol **79a**, demonstrated modulating effect on this assay. Some publications, summarised in Table 21, have reported the insulin-dependent pathway as the major mechanism involved in their action. In addition, a molecular docking model has shown that quercitrin **4** has a great affinity to PI3K and Akt protein as a confirmation of the role of this compound in the activation

of GLUT 4 via PI3K/Akt pathway ⁴⁰⁸. Moreover, (-)-epicatechin **77** and myricitrin **11** have been confirmed to improve glucose uptake through the insulin-independent route by activating AMPK activity.

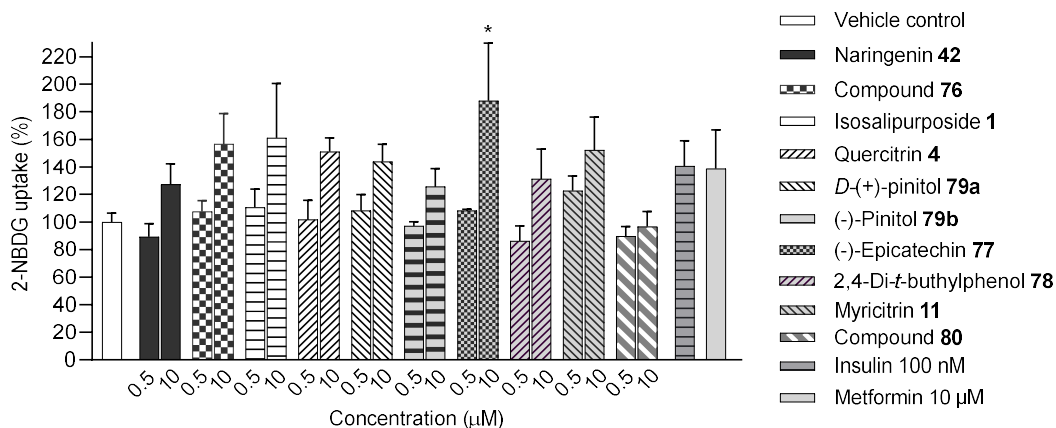


Figure 109. Bar charts representing 2-NBDG uptake by 3T3-L1 adipocytes treated with isolated compounds. Data in mean \pm SEM, * p = 0.01, vs vehicle control (n = 3, One-way ANOVA, Dunnett's post hoc).

Table 21. Summary of the possible pathways involved in the glucose uptake assay for the related phytochemicals based on the literature search

No	Compound	Reported pathway of glucose uptake (GU) modulation	
		IRS-PI3K/Akt	AMPK
1	Naringenin 42	Improving GU on HTR-8/SVneo and human umbilical vein endothelial cell (HUVEC) cells ⁴⁰⁹	Improving GU on L6 rat myotubes ¹⁵³
2	Naringenin-7-O- α -L-arabinofuranoside 76	n.d.	n.d.
3	Isosalipurposide 1	n.d.	n.d.
4	Quercitrin 4	Improving GU on human Simpson-Golabi-Behmel syndrome (SGBS) cells ⁴⁰⁸	n.d.
5	<i>D</i> -(+)-pinitol 79a	Improving GU on HepG2 cells ⁴¹⁰ ; 3T3-L1 adipocytes ^{411, 412}	n.d.
6	(-)-Pinitol 79b	n.d.	n.d.
7	(-)-Epicatechin 77	Improving GU on renal NRK-52E cells ^{413, 414} ; human HepG2 cells ⁴¹⁵ ; 3T3-L1 adipocytes ⁴¹⁶	Improving GU on renal NRK-52E cells ⁴¹³ ; human HepG2 cells ⁴¹⁵
8	2,4-Di- <i>t</i> -butylphenol 78	n.d.	n.d.
9	Myricitrin 11	Improving GU on 3T3-L1 adipocytes ¹⁴⁹ ; L6 myoblast cells ¹⁵⁰	Improving GU on 3T3-L1 adipocytes ¹⁴⁹
10	3-Hydroxy-5-(2-aminoethyl) dihydrofuran-2(3 <i>H</i>)-one 80	n.d.	n.d.

n.d = no documentation found

5.9. Conclusion of Chapter 5

This study confirmed that isolated compounds from the MeOH extracts of *A. saligna*, flavonoid and polyol groups could surpass oxidative stresses. It was reflected by the decreased cellular ROS and mt-ROS levels of 3T3-L1 adipocytes. As a result, the biogenesis of the mitochondria was maintained based on the increased values of MMP. These also aligned with previous observations that the active compounds were scavengers of DPPH and ABTS^{•+} free radicals. Moreover, treatment with the phytochemicals demonstrated improved glucose uptake in the adipocytes. This finding can be correlated to the protective impacts of the compounds against oxidative stress in the cells.

CHAPTER 6: RESULT OF IDENTIFICATION OF BIOLOGICAL PATHWAYS

6.1. Introduction of Chapter 6

An overproduction of hyperglycemia-induced cellular ROS correlates with altered GLUT-4 trafficking in 3T3-L1 adipocytes ⁴¹⁷. This study suggested that ROS can directly oxidise thiol (SH) groups (cysteine residues) in the nuclear protein binding site of the DNA, leading to decreased GLUT-4 expression. Moreover, a recent in vitro study ⁷⁷ found that elevated mt-ROS can oxidise proteins in the translocation machinery of GLUT-4, such as GLUT-4 storage vehicle and *trans*-Golgi network. This event leads to the degradation of the structure and function of GLUT. Furthermore, another in vitro study ⁴¹⁸ showed that increased mt-ROS could cause the lower expression of essential enzymes for energy-generating pathways and the reduction in MMP, significantly reducing ATP production. Consequently, the GLUT-4 translocation cannot occur due to the ATP shortage required for adenosine monophosphate-activated protein kinase (AMPK) activation.

The AMPK pathway regulates GLUT-4 translocation to the cellular membrane to facilitate glucose uptake in glucose deposition tissue, i.e., skeletal muscle and adipose tissue ⁷²⁻⁷⁴. Some of our isolated compounds from MeOH extracts, such as myricitrin **11**, naringenin **42**, and epicatechin **77**, are known to be involved in the pathways. Activation of AMPK is also linked to the biogenesis of mitochondria. Phosphorylation of AMPK subunit α (p-AMPK- α) has been shown to upregulate PGC- α , resulting in increased expression of mitochondrial transcription factor A (mtTFA). As the activation of AMPK can be induced by metformin, the first-line anti-diabetic drug, *via* inhibition of mt-ROS production ⁸⁴, the effect of MeOH extracts and the constituents on this pathway may need to be evaluated because they also have an antioxidant property demonstrated by our study.

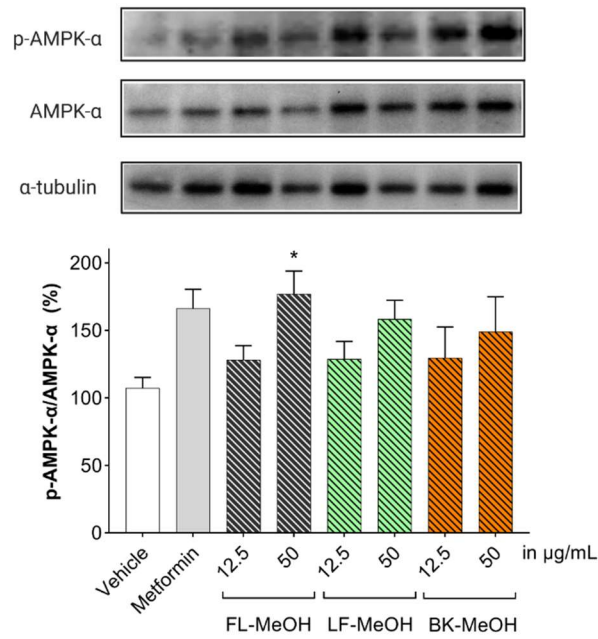
Natural products with antioxidant properties are suggested to act as antidiabetics through multiple mechanisms, such as reducing ROS, normalising mitochondrial biogenesis and function, and activating AMPK signalling. This chapter aimed to examine the effects of the *A. saligna* extracts and their isolated compounds on the p-AMPK- α quantified by immunoblot analysis to reflect the consequence of ROS scavenging activities on cellular glucose entry. A quantitative reverse transcription-polymerase chain reaction (RT-qPCR) was conducted to monitor vital genes involved in mitochondrial biogenesis, such as adiponectin, PGC-1 α , and mtTFA, as the key regulators. Previous studies reported that increased mRNA expression of these genes in adipocytes can trigger mitochondrial biogenesis ^{76, 106},

⁴¹⁹. Moreover, besides ROS production, the excessive triglyceride deposits in adipocytes can promote the pro-inflammatory response leading to impaired glucose homeostasis ⁴²⁰. The levels of cytokines increase proportionally to adiposity and insulin resistance ⁴²¹. Thus, the TNF- α and IL-6 mRNA levels as members of cytokines were also measured to assess the effect of samples on the transcription of the inflammatory markers.

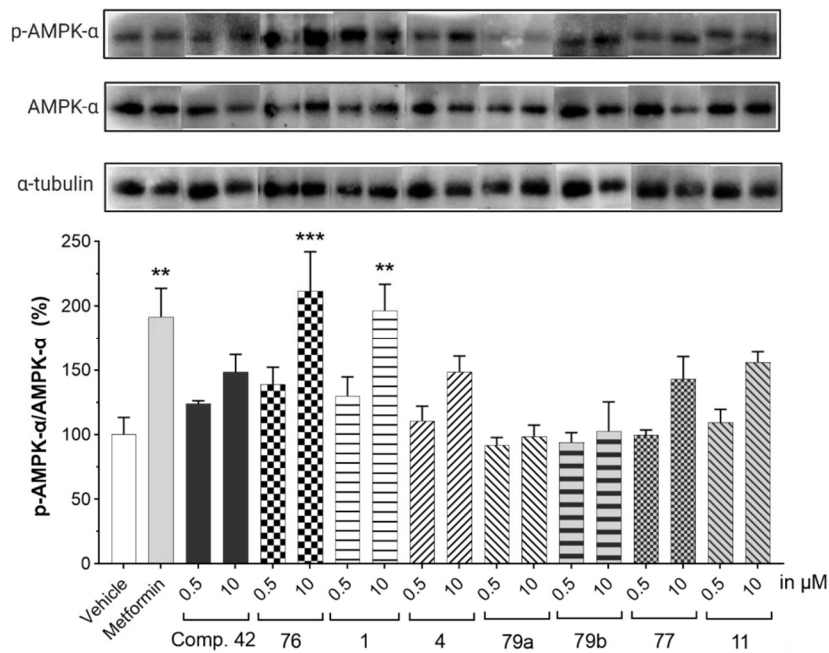
6.2. AMPK pathway activation

The decrease of AMPK- α has been reported as the primary cause of mitochondrial dysfunction due to the impaired activation of OXPHOS in the mitochondria ⁷⁶. The lower activation of AMPK is also thought as the consequence of the malfunction of mitochondria initiated by obesity-induced ROS overproduction. Hence, treatment with our alcoholic extracts and the isolated compounds seems promising to inhibit the mt-ROS production and suppress the insulin resistance in adipocytes by improving the insulin-independent glucose uptake pathway.

Our previous assays displayed the MeOH extracts of the *A. saligna* as the most active ones. Therefore, we further explored how the extracts and their isolated compounds, except for lactone **80**, increased glucose uptake in 3T3-L1 adipocytes. An evaluation of a signalling pathway involved in the glucose uptake in the differentiated 3T3-L1 cells treated with all methanolic extracts was carried out using the western blot analysis. The study focused on activating AMPK- α as this pathway has been reported to be linked to mitochondrial function. Impairment of AMPK- α occurs when the mitochondria function has been compromised. Supplementary Tables S43 and S44 (Appendix C, page 258) and Figure 110 show that phosphorylation of AMPK- α (p-AMPK- α) improved with the increased concentration of extracts or compounds. These results indicate that activation of AMPK- α and expression of p-AMPK- α occurred with increased dosing of the extracts. Treatment with FL-MeOH 50 μ g/mL showed the most potent expression of p-AMPK- α among the three extracts. One observes the correlation between the improvement of glucose uptake (Figure 35) and increases in AMPK phosphorylation (when treated with 50 μ g/mL of extracts). FL-, LF-, and BK-MeOH demonstrated increased glucose uptake and increased phosphorylation by 85.3 and 77%, 98 and 58.5%, and 61.6 and 49.1%, respectively. These results indicated that the extracts increased glucose uptake by activating AMPK- α signalling pathway.



(a)



(b)

Figure 110. The ratio of p-AMPK- α to AMPK- α protein in 3T3-L1 adipocytes treated with (a) MeOH extracts and (b) isolated compounds. Data in mean \pm SEM, * p = 0.02; ** p = 0.003, *** p = 0.0002, vs vehicle control (n = 3, One-way ANOVA, Tukey's post hoc). FL-MeOH = methanolic extract of flower, LF-MeOH = methanolic extract of leaf, BK-MeOH = methanolic extract of bark, compound 42 = naringenin, 76 = naringenin-7- O - α -L-arabinofuranoside, 1 = isosalipurposide, 4 = quercitrin, 79a = D -(+)-pinitol, 79b = (-)-pinitol, 77 = (-)-epicatechin, and 11 = myricitrin.

The possible link between glucose uptake and the AMPK signalling pathway of isolated compounds was also evaluated. After being treated with 10 μ M of the

compounds, we observed enhanced AMPK- α phosphorylation compared to the vehicle control across all compounds (except **79a**). A marked increase in the expression of phosphorylated AMPK- α was observed for naringenin **42** (48.4%), naringenin-7-O- α -L-arabinofuranoside **76** (111.8%), isosalipurposide **1** (96.6%), quercitrin **4** (48.6%), (-)-epicatechin **77** (43.2%), and myricitrin **11** (56%). The highest expression of p-AMPK- α was observed on the test of naringenin-7-O- α -L-arabinofuranoside **76** at 10 μ M. These mentioned compounds improved glucose uptake in 3T3-L1 adipocytes (Figure 109). Therefore, our study suggests that these compounds stimulate glucose uptake via AMPK (phosphorylation demonstrated by the methanolic extracts). D-(+)-pinitol **79a** was shown to improve glucose uptake; however, its ability to activate AMPK- α was not observed at 10 μ M.

As aforementioned, excessive levels of mt-ROS can decrease MMP in adipocytes, disrupting cellular uptake of glucose and AMPK- α . The decrease in p-AMPK- α has been suggested as the primary cause of mitochondrial dysfunction due to the impaired activation of oxidative phosphorylation in the mitochondria⁴²². Reduced activation of AMPK signalling is also thought of as the consequence of mitochondria dysfunction initiated by obesity-induced ROS overproduction.

A. saligna methanolic extracts and the isolated compounds are promising inhibitors of cellular ROS and mt-ROS production. Furthermore, the extracts and the compounds markedly increased glucose uptake and p-AMPK- α in 3T3-L1 adipocytes. Activation of the AMPK pathway has also been linked to reduced cellular ROS and mt-ROS production in 3T3-L1 adipocytes⁷⁸. In addition, this pathway can protect the downstream target GLUT-4 from structural degradation and dysfunction due to excessive ROS levels^{417, 419, 422}. These findings suggest that glucose transporters can be activated by the AMPK pathway to facilitate glucose entry into the fat cells.

6.3. Expression of mRNAs related to the mitochondrial biogenesis

Treatment with all methanolic extracts of *A. saligna* increased the expression of target mRNAs, including adiponectin, PGC-1 α , and mtTFA. A slightly increased expression of adiponectin (approximately 7% increase compared to the vehicle control group) was found from the treatment with all three MeOH extracts at 12.5 μ g/mL, whereas a significant increase, 28.92% higher than the control, was only observed by treatment with FL-MeOH extract at 50 μ g/mL. Meanwhile, at 12.5 μ g/mL, treatment with BK-MeOH demonstrated significantly increased expression of PGC-1 α and mtTFA estimated for 9.9% and 10.7%, respectively. Moreover, the expression of PGC-1 α was significantly upregulated when treating FL-, LF-, and BK-MeOH at 50

µg/mL by 11.4, 13.4, and 10.7% increased, respectively. On the other hand, only adipocytes treated with FL- and BK-MeOH extracts at 50 µg/mL showed a significant increase of mtTFA expression by 11.5 and 12.6%, respectively. Figure 111 and Table S45 (page 260) show that FL-MeOH extract consistently impacted the target gene expression. This information is consistent with the highest MMP change 2-fold from FL-MeOH treatment at 50 µg/mL. Overall, these findings iterate the positive effect of the methanolic extracts on the adipocytes' mitochondrial biogenesis, as previously monitored by the reduction of mt-ROS and improvement of MMP status, as observed through the decrease of mt-ROS and enhancement of MMP status. This was achieved by stimulating the transcriptional expression of adiponectin, PGC-1α, and mtTFA.

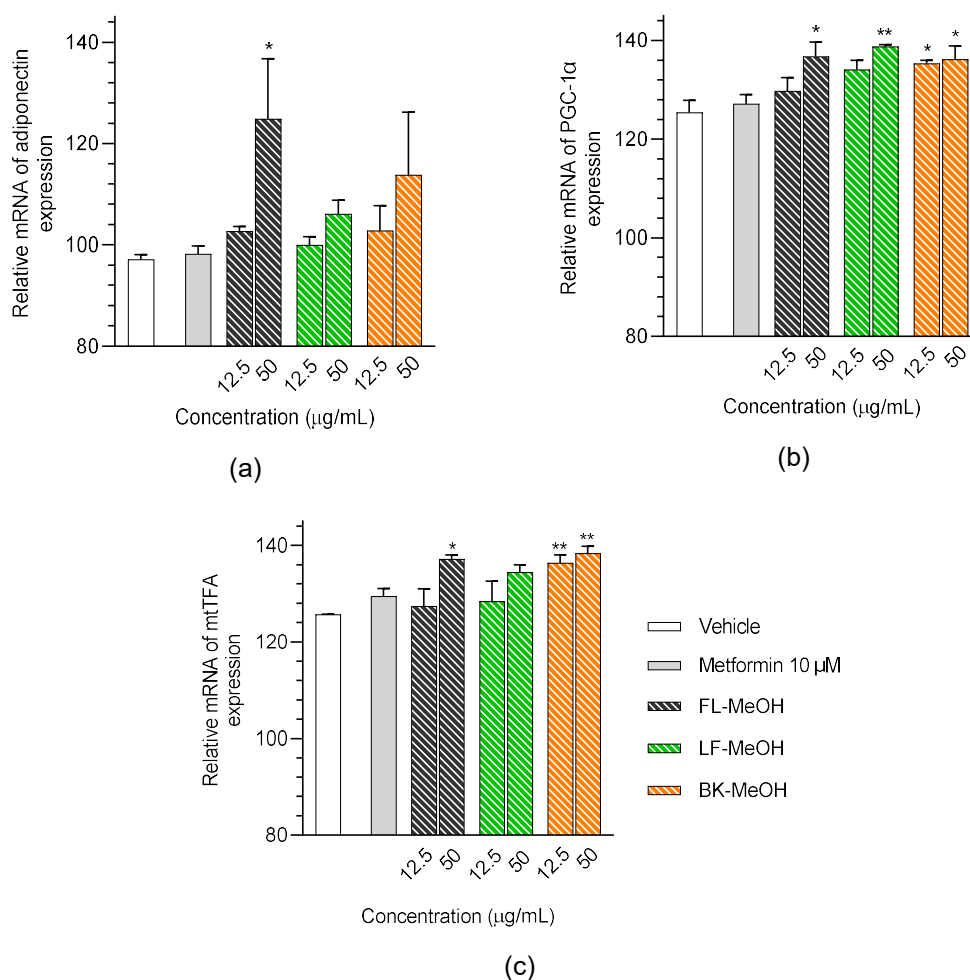


Figure 111. The relative expression of (a) mRNA of adiponectin, (b) PGC-1α, and (c) mtTFA of 3T3-L1 adipocytes treated with MeOH extracts. The gene expression was normalised by the housekeeping gene β-actin. Data in mean ± SEM; **p* = 0.02; ***p* = 0.002, vs vehicle control (*n* = 3, One-way ANOVA, Tukey's post hoc). FL-MeOH = methanolic extract of flower, LF-MeOH = methanolic extract of leaf, BK-MeOH = methanolic extract of bark.

Furthermore, to evaluate the effect of isolated compounds, the change in the gene level was then quantified using the same qPCR protocol. All compounds at 0.5 μM showed a slight increase in the transcriptional level of the adiponectin, PGC-1 α , and mtTFA mRNA (see Figure 112 and Table S46 page 261). In addition, treatment with 10 μM showed a slight change in the increased expression of mtTFA, ranging from 3% to 6%. However, significant elevation of adiponectin by 14.42% and PGC-1 α by 12.1% was observed over incubation at 10 μM with naringenin **42** and *D*-(+)-pinitol **79a**, respectively.

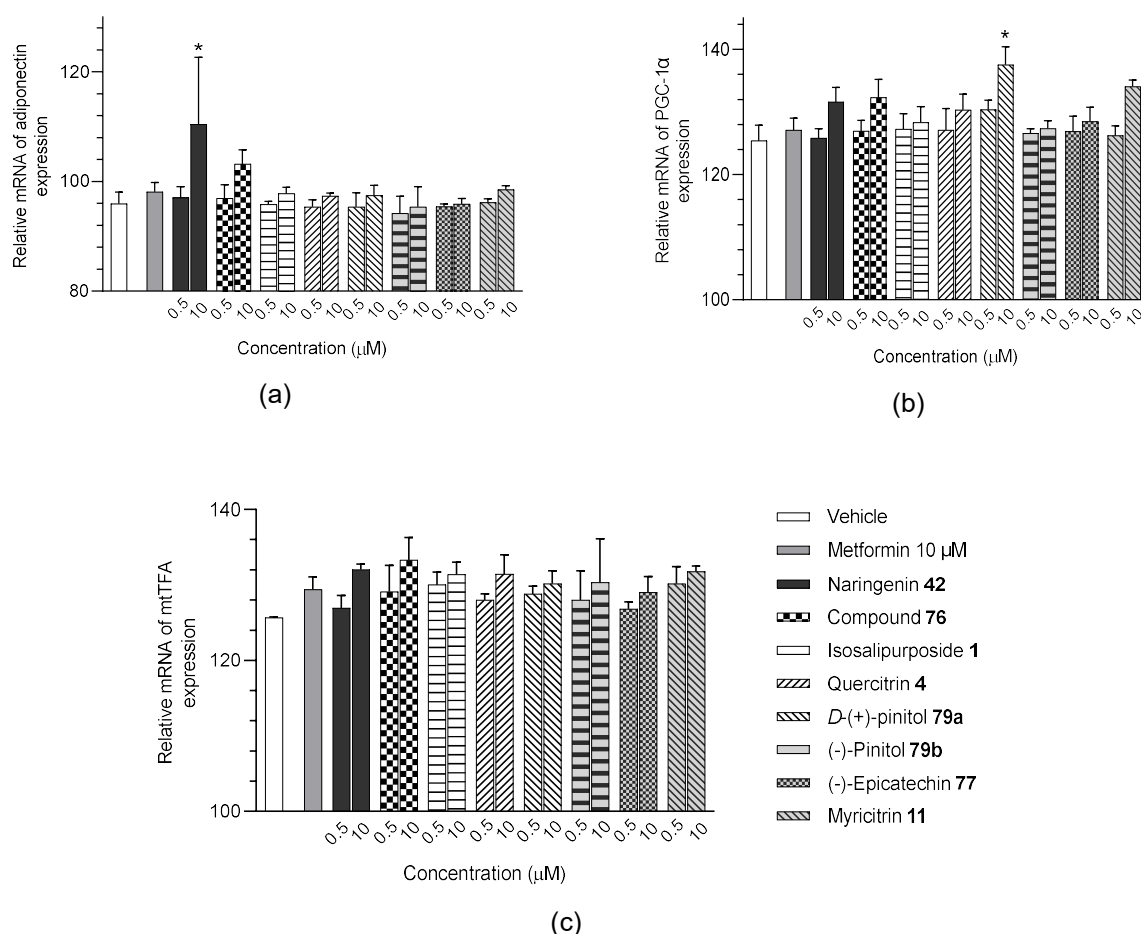


Figure 112. The relative expression of mRNA of (a) adiponectin, (b) PGC-1 α , and (c) mtTFA of 3T3-L1 adipocytes treated with isolated compounds. The gene expression was normalised by the housekeeping gene β -actin. Data were in mean \pm SEM; * p = 0.02; ** p = 0.002, vs vehicle control (n = 3, One-way ANOVA, Tukey's post hoc).

A consistent trend was also found between these data and those observed from their remarkable MMP change. In the MMP assay, exposure to naringenin **42** and *D*-(+)-pinitol **79a** increased MMP by 1.67- and 2-fold in the adipocytes. Interestingly, naringenin **42** and *D*-(+)-pinitol **79a** were found in FL-MeOH extract with percentages (w/w) of 1.75% and 2.5%, respectively. These two active compounds

can then be considered to reflect the noticeable impact of FL-MeOH extract on the change of the gene level. Naringenin **42** has previously been reported to modulate mRNA expression of adiponectin and PGC-1 α in human white adipocyte cultures linked to increased energy expenditure and insulin sensitivity⁴²³. In obese mice, *D*-(+)-pinitol **79a** induced PGC-1 α mRNA expression by up-regulating cAMP response element-binding protein (CREB)⁴²⁴.

6.4. Expression of mRNAs of inflammatory markers

The transcriptional levels of two common cytokines in adipocytes, TNF- α and IL-6, were altered in the *A. saligna* MeOH extract-treated adipocytes compared to the vehicle control group. Marked reducing effect on the expression of TNF- α and IL-6 can be seen from the FL-MeOH-treated adipocytes at 50 μ g/mL estimated for 15.9% and 10.5% decrease, respectively. At the same concentration, treatment with LF-MeOH extract demonstrated a somewhat lower impact than the methanolic extract of flowers with 11.6% and 10.4% decrease of TNF- α and IL-6, respectively, while treatment with BK-MeOH showed the lowest effect due to 12% reduction in TNF- α expression and the similar level of IL-6 with the vehicle control. In other words, this study suggests that treatment with FL-MeOH exhibited pronounced inhibition of the pro-inflammatory gene expression in the adipocytes.

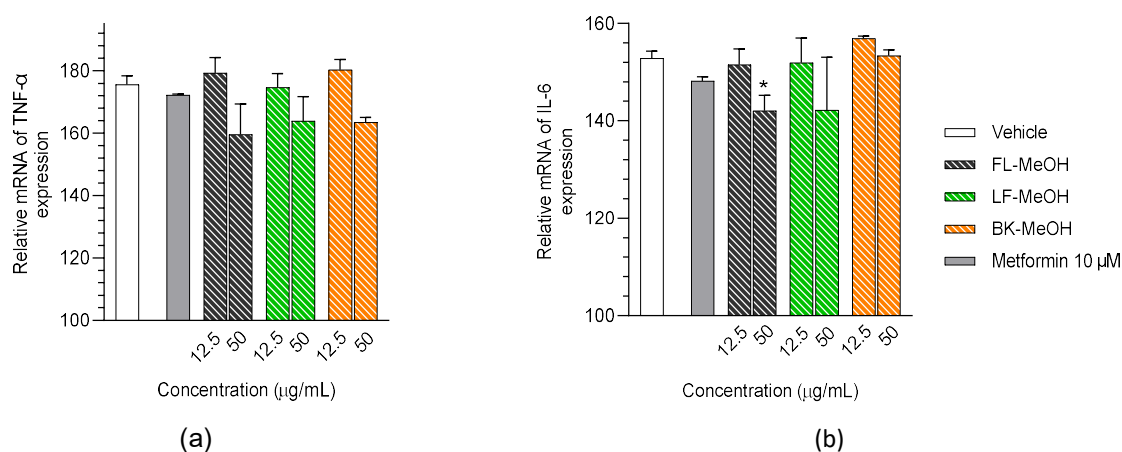


Figure 113. The relative expression of mRNA of (a) TNF- α and (b) IL-6 in 3T3-L1 adipocytes treated with MeOH extracts. The gene expression was normalised by the housekeeping gene β -actin. FL-MeOH = methanolic extract of flower, LF-MeOH = methanolic extract of leaf, BK-MeOH = methanolic extract of bark. Data were in mean \pm SEM; * p = 0.04, vs vehicle control (n = 3, One-way ANOVA, Tukey's post hoc).

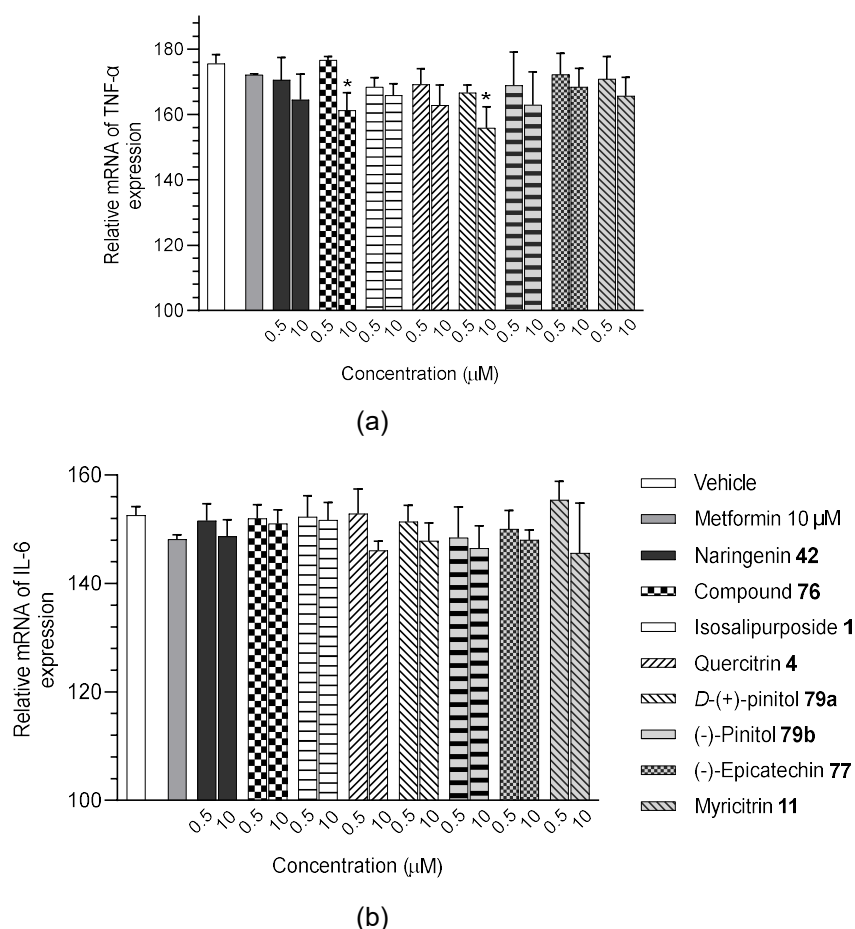


Figure 114. The relative expression of mRNA of (a) TNF- α and (b) IL-6 in 3T3-L1 adipocytes treated with isolated compounds. The gene expression was normalised by the housekeeping β -actin. Data were in mean \pm SEM; * p = 0.04 and 0.02, vs vehicle control (n = 3, One-way ANOVA, Tukey's post hoc).

The isolated compounds reduced the mRNA expression of two pro-inflammatory adipokines. Treatment with naringenin-7-*O*- α -*L*-arabinofuranoside **76** and *D*-(+)-pinitol **79a** at 10 μ M demonstrated a significant decrease in TNF- α expression by 14.2% and 19.6%, respectively. In addition, the noticeably decreased expression in TNF- α was also found by naringenin **42** and quercitrin **4** treatment at the same dose by 11% and 12.7%. For IL-6 mRNA expression, naringenin **42**, quercitrin **4**, *D*-(+)-pinitol **79a**, and naringenin-7-*O*- α -*L*-arabinofuranoside **76** exerted a non-significant inhibitory effect. All these phytochemicals isolated from FL-MeOH extract indicate the active constituents linked to the inhibitory activity of the methanolic extract of flowers against the two cytokines. Given that TNF- α and IL-6 can impair the adiponectin pathway and mitochondrial biogenesis^{425, 426}, our finding also suggests that *A. saligna* extracts and the phytoconstituents can protect the mitochondria in the adipocytes from the harmful effects of the pro-inflammatory cytokines.

6.5. Conclusion of Chapter 6

Our methanolic extracts and isolated compounds were involved in activating the AMPK- α of the 3T3-L1 adipocytes in a dose-dependent manner. This finding showed a consistent correlation between the improvement of glucose uptake and increases in phosphorylation of AMPK- α in 3T3-L1 adipocytes when treated with extracts and their corresponding isolated compounds. The markedly increased glucose uptake by (-)-epicatechin **77**, quercitrin **4**, and myricitrin **11** reflected the best glucose uptake of their corresponding LF-MeOH. FL-MeOH showed the highest expression of p-AMPK- α among the three extracts. These results were supported by the marked increase in p-AMPK- α when treated with isolated compounds such as naringenin **42**, naringenin-7-O- α -L-arabinofuranoside **76**, isosalipurposide **1**, and quercitrin **4**. Among them, (-)-epicatechin **77** performed well for all tested activities and significantly increased phosphorylated AMPK- α levels, suggesting that its effects could be partly mediated through activating the AMPK signalling pathway.

The methanolic extracts and phytochemicals have promoted mRNA levels of key regulators of mitochondrial biogenesis, including adiponectin, PGC-1 α , and mtTFA. Among the three methanolic extracts, FL-MeOH treatment showed a consistently marked increase in mRNA levels. The chemical constituents, naringenin **42** and *D*-(+)-pinitol **79a**, have been noticed as the active compounds related to the impact of FL-MeOH extract by the significant increase of the mRNA expression. Moreover, the methanolic flower extract also markedly reduced the transcriptional expression of pro-inflammatory TNF- α and IL-6. The activity of naringenin **42**, quercitrin **4**, *D*-(+)-pinitol **79a**, and naringenin-7-O- α -L-arabinofuranoside **76** was confirmed as the active constituents behind the impact of FL-MeOH against the cytokines. These findings align with the above outcome: FL-MeOH exerted the highest promoting impact on the restoration of MMP and phosphorylation of AMPK- α . This suggests that *A. saligna* extracts and the isolated compounds can promote adipocytes' mitochondria health by inducing adiponectin, PGC-1 α , and mtTFA expression and reducing the expression of inflammatory TNF- α and IL-6, resulting in increased AMPK phosphorylation and cellular glucose uptake.

CHAPTER 7: CONCLUSION AND FUTURE DIRECTION

7.1. General conclusion

Successive solvent extraction with *n*-hexane, dichloromethane (DCM), methanol (MeOH), and water solvent gave twelve different types of extracts of *A. saligna* with varied phytochemical contents. Using bioassays of antioxidants with DPPH and ABTS^{•+} radicals scavenging and α -glucosidase inhibition followed by 3T3-L1 adipocytes *in vitro* assays to measure essential parameters, including cellular and mitochondrial ROS, MMP, lipid droplets, and cellular glucose uptake, we confirmed that methanolic *A. saligna*'s flower, leaf, and bark extracts possessed the most promising properties for T2DM remedy. Our study found a consistent bioactivity of FL-, LF-, and BK-MeOH extracts between *in vitro* assays of free radicals scavenging, inhibition of the yeast α -glucosidase enzyme, and the cell-based assays. Furthermore, these data can be used to justify the bioactive extracts for further isolation of bioactive compounds.

Eleven compounds were obtained from FL-, LF-, and BK-MeOH extracts through isolation using column chromatography techniques. Spectroscopic methods using FTIR, 1D and 2D NMR, and HRMS suggested the presence of various classes of compounds, including chalcone, flavanone, flavan-3-ol, flavonol, alkyl phenol, cyclitols, and lactone derivatives. Five compounds were isolated from FL-MeOH, including naringenin **42**, naringenin-7-*O*- α -L-arabinofuranoside **76**, isosalipurposide **1**, quercitrin **4**, and *D*-(+)-pinitol **79a**. Flavonoid derivatives including (-)-epicatechin **77**, quercitrin **4**, and myricitrin **11** were the most isolated compounds found in the LF-MeOH, followed by 2,4-di-*t*-butylphenol **78**, (-)-pinitol **79b**, and (3*S**,5*S**)-3-hydroxy-5-(2-aminoethyl) dihydrofuran-2(3*H*)-one **80**. Isolated phytochemicals BK-MeOH were (-)-epicatechin **77**, *D*-(+)-pinitol **79a**, and sucrose. Except for compounds **1**, **4**, **42**, and **11**, this study suggests that the isolated compounds were found in three parts of Australian *A. saligna* for the first time.

The flavonoid and cyclitol derivatives isolated from MeOH extracts of *A. saligna* helped to reduce oxidative stress in adipocytes. These extracts were able to lower the levels of cellular ROS and mt-ROS. Among the derivatives, (-)-epicatechin **77** was found to be the most effective in reducing both types of ROS. This is consistent with its ability to inhibit DPPH and ABTS^{•+} radicals. The active compounds that increased MMP values were effective in repairing mitochondria in adipocytes. Significant increases in MMP were found in the adipocytes incubated with naringenin **42**, naringenin-7-*O*- α -L-arabinofuranoside **76**, *D*-(+)-pinitol **79a**, (-)-pinitol **79b**, and

(-)-epicatechin **77**. Moreover, the treatment with (-)-epicatechin **77** showed significant modulation of cellular glucose uptake. Based on the findings, the active compounds that produced positive results in the bioassays are consistent with those found in the methanolic extracts.

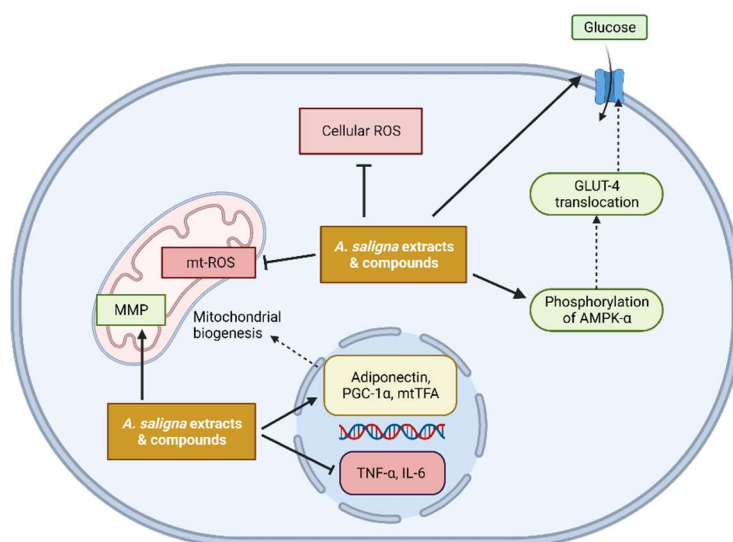


Figure 115. A summary of the effects of methanolic extracts of *A. saligna* and the isolated compounds on suppressing oxidative stress, promoting cellular glucose uptake via AMPK activation, and restoration of mitochondria of the adipocytes by increasing mRNA expression of key regulators and reducing mRNA expression of pro-inflammatory cytokines in the 3T3-L1 adipocytes (Blunt arrows (\perp): inhibiting, sharp arrows (\rightarrow): stimulating).

Our study also showed a consistent correlation between the improvement in glucose uptake and an increase in the p-AMPK- α in 3T3-L1 adipocytes when treated with extracts and their corresponding isolated compounds. The marked increases in glucose uptake and p-AMPK- α were observed from the FL-MeOH and LF-MeOH treatments. Naringenin **42**, naringenin-7-O- α -L-arabinofuranoside **76**, isosalipurposide **1**, and quercitrin **4** supported the activities of FL-MeOH while (-)-epicatechin **77**, quercitrin **4**, and myricitrin **8** were corresponding for LF-MeOH. This study, therefore, suggests that the cellular glucose uptake could be partly mediated via the activation of the AMPK signalling pathway.

The consistent trend between increasing effects on MMP values, p-AMPK- α , and increased transcriptional levels of key regulators of mitochondrial biogenesis, namely, adiponectin, PGC-1 α , and mtTFA, was also found in this study. The consistent data has been shown by FL-MeOH supported by its chemical constituents, naringenin **42** and *D*-(+)-pinitol **79a**. Moreover, our study also attributes the noticeably reducing effects of FL-MeOH against TNF- α and IL-6 to these two phytochemicals

along with quercitrin **4** and naringenin-7-*O*- α -L-arabinofuranoside **76**. Overall, *A. saligna* extracts and the isolated chemical constituents demonstrated antidiabetic activities on 3T3-L1 adipocytes by reducing ROS and mt-ROS, modulating transcriptional levels of adiponectin, PGC-1 α , and mtTFA and reducing pro-inflammatory TNF- α and IL-6 mRNA levels to promote mitochondrial biogenesis.

7.2. Future direction

This study demonstrated the potential of Australian *A. saligna* extracts and the chemical constituents for treating T2DM based on the studies using 3T3-L1 adipose cells. This is the first study of the *Acacia* species conducted in the 3T3-L1 adipocytes to reveal the active phytochemicals and the mode of action to stimulate cellular glucose uptake and restore mitochondria. This work can help those who work on natural product research, and the related field obtain effective successive polar solvent extraction on plants. Moreover, the information from bioassays can highlight the multiple actions of phytochemicals constituting the active extracts in scavenging free radicals, inhibiting α -glucosidase enzyme, stimulating vital components in adipocytes, such as AMPK phosphorylation; GLUT-4 transduction; PGC-1 α activation, and also inhibiting of pro-inflammatory markers. However, this study only focuses on white adipose tissue (WAT) as the study model. T2DM is a complex disorder that involves multiple metabolic tissues and organs, such as muscles, kidneys, liver, pancreas, and brain. In addition, this study only employed a single type of normal-phase silica gel to afford the isolated compounds. Therefore, further studies to provide guidelines for developing comprehensive data on the potential of this species as listed in the following points:

1. A study on animal models of T2DM is needed to confirm the findings in 3T3-L1 adipocytes. This study will also observe the effects of *A. saligna* extracts and compounds on glucose metabolism in muscles.
2. Further study in other cell lines, such as skeletal C2C12 cells, β -cells, renal tissues, and liver tissues, can be carried out to extend the effects of the plant on other tissues involved in the onset of T2DM. Moreover, further animal studies can be conducted to study the effects on several vital organs such as the pancreas, skeletal tissues, liver, kidney, and brain.
3. Separation using reverse-phase silica gels and reverse-phase HPLC can be carried out to discover more polar compounds, such as tannin derivatives, that were not isolated from this current study.

CHAPTER 8: EXPERIMENTAL SECTION

8.1. Experiments of extraction

8.1.1. Materials

Unless otherwise expressed, all chemicals were purchased from Sigma-Aldrich (St. Louis, MO, USA). The solvent for extraction includes *n*-hexane, dichloromethane, and methanol. The solvents for GCMS were acetonitrile and methanol of HPLC grade. Chemicals for phenolic and flavonoid content experiments were Folin-Ciocalteu reagent, sodium carbonate, ethanol (Point of Care Diagnostics, Australia), aluminium chloride, ammonium acetate, gallic acid, and quercetin. The antioxidant assay used DPPH (2,2-di(4-tert-octylphenyl)-1-picrylhydrazyl), ABTS (2,2'-azino-bis-(3-ethylbenzothiazoline-6-sulphonic acid)), and ascorbic acid (Merck, Germany). Chemicals for α -glucosidase inhibition were α -glucosidase enzyme from *Saccharomyces cerevisiae* (lyophilized powder, 23 units/mg), 4-nitrophenyl α -D-glucopyranoside (*p*NPG, $\geq 99\%$), acarbose (99%), and dimethylsulfoxide (DMSO), KH_2PO_4 and K_2HPO_4 (Ajax Chemicals, Australia), Na_2CO_3 (Chem-Supply, Australia). Ultrapure water was purified using an Aurium pro-VF ultrapure water system (Gottingen, Germany).

3T3-L1 murine cell lines were supplied by American Type Tissue Culture/ATCC (Manassas, USA). The following reagents were purchased from Sigma-Aldrich (USA): Dulbecco's Modified Eagle's Medium High Glucose (DMEM), bovine calf serum (BCS), penicillin, streptomycin glutamine (PSG), fetal bovine serum (FBS), rosiglitazone, dexamethasone, 3-isobutyl-1-methylxanthine (IBMX), insulin, phosphate-buffered saline (PBS), trypsin-EDTA solution 0.25%, bovine serum albumin (BSA), and dimethylsulfoxide (DMSO). Chemicals for cell-based studies were Oil Red-O (ORO), formaldehyde solution 10%, isopropanol, dichlorodihydrofluorescein diacetate (DCFH-DA), (3-(4,5 dimethylthiazol-2-yl)-2, 5 diphenyltetrazolium bromide) (MTT), metformin, N-acetylcysteine (NAC), and Hank's balanced salt solution (HBSS). A Krebs-Ringer phosphate HEPES (KRPB) buffer was prepared from NaCl 118 mM, KCl 5 mM, KH_2PO_4 1.2 mM, CaCl_2 1.3 mM, MgSO_4 1.2 mM, and HEPES 30 mM in a certain volume of milli-Q water. The 2-NBDG (2-deoxy-2-[(7-nitro-2,1,3-benzoxadiazol-4-yl) amino]-D-glucose) was purchased from Thermo-Fisher Scientific (USA).

8.1.2. Extraction protocol

The samples, including leaves, flowers, and stem barks, were collected from 12 Tasman Street, Kurnell, Sutherland Shire, NSW (34°00'48.2" S 151°12'27.7" E) on

7 October 2019. The plant was identified by Andrew Orme, a technical identification officer from the National Herbarium of NSW, as *Acacia saligna* (Labill.) H.L.Wendl. The wattle was further identified as subspecies *saligna* by Bruce Maslin from the Western Australia Herbarium. All samples were washed with flowing water to remove undesired matter, air-dried for a week, and finely powdered. The extraction applied a four-step sequential extraction with gradually increasing polarity of the solvents: *n*-hexane (hex), dichloromethane (DCM), methanol (MeOH) and water (H₂O) in a shaker over 48 hours at 30°C as shown in Figure 116.

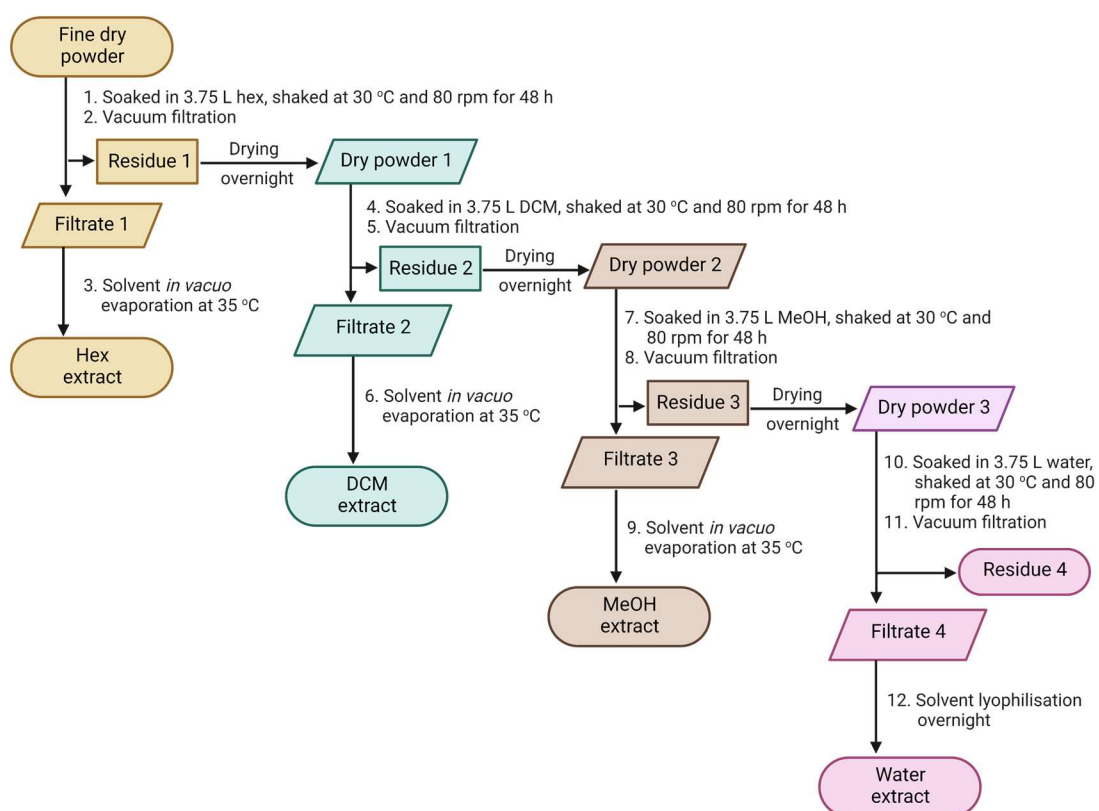


Figure 116. Illustration of the extraction procedures of the plant.

8.1.3. Spectrometric estimation of phenolic and flavonoid content

Phenolic and flavonoid content was estimated using a spectrophotometric method in microtiter plates.

8.1.3.1. Estimation of phenolic content (PC)

Phenolic content (PC) quantification was generated using a modified Folin-Ciocalteu method adapted from Zhang et al.⁴²⁷. Briefly, samples (1 mg/mL, 20 μ L) and the serial standard gallic acid solution (3.125–100 μ g/mL, 20 μ L) were individually mixed with Folin-Ciocalteu reagent (100 μ L) in a 96-well microplate. After 5 min, Na₂CO₃ solution (7.5%, 80 μ L) was added, followed by 2 h in the dark at room

temperature. The absorbance was measured with a Perkin Elmer (EnSpire 2300 Multilabel Reader) microplate reader at λ 750 nm after an auto mix for 1 min. The PC of the extracts were determined using the following formula:

$$PC = C \times \frac{V}{m}$$

PC is the phenolic content in the extract (mg gallic acid equivalent (GAE)/g extract), *C* is the estimated concentration of gallic acid of the samples established from the curve of calibration (mg/mL), *V* is the volume of extract (mL), and *m* is the mass of the extracts (g).

8.1.3.2. Estimation of flavonoid content (FC)

Using the method adapted from Nurcholis et al.⁴²⁸, each sample (1 mg/mL, 50 μ L) or standard quercetin ethanolic solution (3.125–100 μ g/mL, 50 μ L) and $AlCl_3$ ethanolic solution (10%, 10 μ L) were mixed in each well followed by adding EtOH (96%, 130 μ L) and then let to stand for 3–5 min. Ammonium acetate solution (1M, 10 μ L) was added into the mixture prior to a 40 min-incubation in the dark at room temperature. The optical density was measured at λ 415 nm, and the TFC was expressed in mg quercetin equivalent (QE)/g determined by:

$$FC = C \times \frac{V}{m}$$

FC is the flavonoid content in the extract (mg QE/g extract), *C* is the estimated concentration of quercetin of the samples established from the curve of calibration (mg/mL), *V* is the volume of extract (mL), and *m* is the mass of the extracts (g).

8.1.4. Screening of phytochemicals using gas chromatography-mass spectroscopy (GCMS) analysis

An analytical screening of volatile and lower molecular weight phytochemicals using a GCMS was performed to assist in analysing the potential bioactive of crude extracts. All extracts were dissolved in the analytical grade solvents (acetonitrile and methanol) and then made up to 1 ppm. The sample and the blank solvent were subjected to an Agilent 6890GC coupled with Agilent 5973n MS (EI) equipped with a capillary column (length of 30 m, diameter of 0.25 mm, and film thickness of 0.10 μ m) with a total run time of 30 min. The initial and working temperatures of the column were 50 and 340°C. Helium was used as the carrier gas at a 1 mL/min flow rate. Identification of the possible molecules was based on the library data of the instrument.

8.2. Experiments of DPPH and ABTS^{•+} scavenging assays

The DPPH-free radical scavenging study based on a 96-well plate reading approach was performed following Jiang, Li, Ma, Jiang, He, Qiu, Li and Wang⁴²⁹ and Chen, Bishop, Tanambell, Buchanan, Smith and Quek⁴³⁰ with slight modifications of the protocol. Briefly, a 180 μL of DPPH 0.2 mM ethanolic solution was pipetted into each well (Corning, USA), followed by 20 μL of ethanolic solution of extracts, isolated compounds, or ascorbic acid in a different concentration and, for the blank solution, 20 μL of ethanol. The blank extract and the blank positive solution were prepared by adding 180 μL of ethanol into 20 μL of samples and ascorbic acid solution. The plate was then incubated in a dark condition for 30 min at 30°C. The absorbance was observed using a microplate reader (Tecan Infinite M1000 PRO, Austria) at 517 nm.

The percentage of DPPH scavenging activity was determined by:

$$\text{DPPH scavenging activity (\%)} = \left[1 - \left(\frac{A_1 - A_2}{A_0} \right) \right] \times 100\%$$

A_0 is the absorbance of the blank solution (DPPH 0.2 mM + EtOH), A_1 is the absorbance of the sample (sample + DPPH 0.2 mM), and A_2 is the absorbance of the blank sample (sample in EtOH). The value was then converted into IC_{50} ($\mu\text{g}/\text{mL}$) from a graph correlating sample concentration ($\mu\text{g}/\text{mL}$) and DPPH scavenging activity (%). The results were expressed as mean \pm standard error mean (SEM) of three separate experiments ($n = 3$).

The ABTS^{•+} solution was prepared by generating a reaction between ABTS 7 mM and potassium persulfate 2.45 mM (1:1 of v/v) at room temperature for 16-18 h⁴³¹. The ABTS^{•+} solution was diluted to achieve an acceptable measurement at 734 nm⁴³². The same experimental procedure used in the DPPH radical scavenging assay was applied to measure the percentage of ABTS^{•+} radical scavenging. The absorbance was observed using a microplate reader (Tecan Infinite M1000 PRO, Austria) at 734 nm.

8.3. Experiment of α -glucosidase inhibition assay

The enzyme deactivation assay followed the modified microplates method adapted from Ning, Zhai, Huang, Peng, Hu, Xiao, Wen, Lin, Zhao and Bian⁴³³ with minor modifications. As illustrated in Figure 117, a volume of 20 μL of the plant extract or isolated compounds in different concentrations, acarbose solution (31.25–1000 $\mu\text{g}/\text{mL}$), or solvent control was mixed with α -glucosidase (40 μL , 0.075 U/mL in potassium phosphate buffer solution (PBS, 100 mM) with pH 6.8) in 96-well polystyrene plates (Corning Incorporated, NY, USA) and then incubated for 15 min at

37°C. Afterwards, *p*NPG solution in PBS (40 µL, 1 mM) was added to the mixture, followed by further incubation for 30 min at 37°C. In order to terminate the reaction, Na₂CO₃ (100 µL, 200 mM) was added to the wells. The spectrophotometric observation was then conducted to determine the absorbance of *p*-nitrophenol released from the reaction under 405 nm wavelength in a microplate reader (Tecan Infinite M1000 PRO, Austria). The percentage of inhibition was calculated from the following formula:

$$\text{Percentage of inhibition (\%)} = \frac{A_c - A_s}{A_c} \times 100\%$$

Where A_c is the absorbance of the solvent control and enzymatic reaction system and A_s is the absorbance of the sample with the enzymatic reaction system, the inhibitory activity was expressed in the value of half minimal inhibitory concentration (IC₅₀).

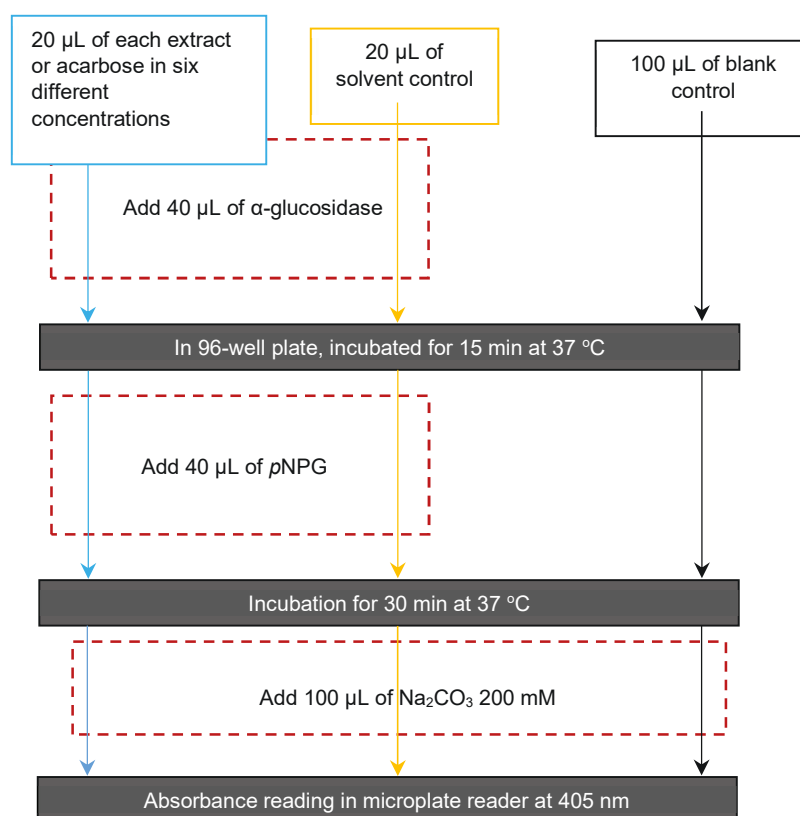


Figure 117. Representative illustration of the α -glucosidase inhibition assay.

8.4. Cell-based studies

8.4.1. Protocol of cell subculture

The parent cells were taken from passaged 2 (P2) cell stock stored on June 21st, 2019. The cells were cultivated in a 25 cm² of tissue culture flask (Corning, USA) with a density of 0.3 x 10⁵ cells/mL in a complete growth medium of DMEM (90%, v/v)

supplemented with BCS (9%, v/v) and PSG (1%, v/v). The cells were incubated in a humid environment of 37° C with 5% CO₂. Once 70–80 % confluent had been obtained, the medium was aspirated from the cells and washed with 5 mL of sterile PBS solution. The cells were detached from the flask by incubation for 3–5 minutes with 3 mL of trypsin-EDTA. Into the detached cells, a fresh medium of 3 mL was added to terminate the trypsinisation, followed by spinning down with a centrifuge at 150 rpm for 5 min at 25 °C. After resuspending with another complete medium and counting cell numbers, the other cell line works can be performed for cryopreservation, cell passage, or cell differentiation.

8.4.2. Protocol of cell viability experiment on 3T3-L1 preadipocytes with MTT assay

The preadipocytes were seeded in three different 96-well plates (3x10³ cells/mL per well) containing 100 µL of growth medium and then incubated for 24-h (37 °C/ 5% CO₂). The old medium was replaced by an identical volume of each fresh extract-containing medium in a range of concentration (25, 50, 100, and 200 µg/mL) or isolated compound-containing medium (15.63, 31.25, 62.5, and 125 µM) followed by incubation for a further 24- (plate A), 48- (plate B), and 72-h (plate C). After incubation and discarding solution, the cells were washed with PBS and then exposed to 100 µL of fresh medium containing 10 µL of MTT (5 mg/mL in PBS). After incubation for another 4 hours, the supernatant was replaced by 100 µL of DMSO and adequately mixed. The absorbance was measured using a microplate reader (Tecan Infinite M1000 PRO, Austria) at 570 nm. The percentage of cell viability is expressed in the:

$$\text{Cell viability (\%)} = \frac{\text{absorbance of sample}}{\text{absorbance of control}} \times 100\%$$

8.4.3. Protocol of cell differentiation

The 3T3-L1 preadipocytes (70–80% confluent from a culture flask) were grown in a 96-well microtiter plate (3x10³ cells/well in 100 µL final volume of basal medium 1 (M1 = 90% DMEM, 9% BCS, and 1% PSG)) and incubated for 48 h in a humid condition (37° C & 5% CO₂) for adherence of the cells. After 48 h, the old M1 was replaced with new M1, and the cells were incubated for another 48-h (day -2 to 0) to get 100% confluent. The M1 was replaced by an identical volume of M2 (9% FBS, 1% PSG, and 90% DMEM containing rosiglitazone 2 µM, dexamethasone 2.2 mM, IBMX 500 mM, and insulin 4 mg/mL) followed by incubation for 48 h (day 0 to 2). After incubation and M2 removal at day 2 of differentiation, new M3 (90% DMEM, 9%

FBS, 1% PSG and insulin) were added, followed by incubation to day 6 with medium replacement every 48-h. On day 6, M3 was replaced by M4 (90% DMEM, 9% FBS, and 1% PSG), followed by another 48-h incubation.

Cell growth		100% confluent	Lipid droplets formation and development			Excessive lipid droplets
48 h	48 h (day - 2 to 0)	48 h (day 0 to 2)	48 h (day 2 to 4)	48 h (day 4 to 6)	48 h (day 6 to 8)	Between day 8 & 12
Feed M1	Feed M1	Feed M2	Feed M3	Feed M3	Feed M4	Treatment with extracts/compounds
Preadipocyte			→			mature adipocyte

Figure 118. Schematic workflow diagram of the cell differentiation.

8.4.4. Protocol of cell viability experiment on 3T3-L1 adipocytes

The differentiated 3T3-L1 cells grown in three 96-well microtiter plates (Corning, USA) were exposed to 100 µL of fresh test solution containing flower, leaf, and bark extracts in a range of concentrations (25–200 µg/mL) or isolated compounds (15.63–125 µM) and incubated for a further 24 (plate A), 48 (plate B), and 72 h (plate C). After incubation, the solution was replaced with 100 µL of fresh medium containing 10 % MTT solution (5 mg/mL in PBS). The treated cells were then incubated for additional 4 hours. Once finished the last incubation, the MTT solution was replaced by 100 µL of DMSO to homogenous. The absorbance was measured at wavelength 570 via a multiwell plate reader (Tecan Infinite M1000 PRO, Austria). Each concentration was performed twice times whereby each experiment was done in triplicate. The percentage of cell viability is expressed in the:

$$\text{Cell viability (\%)} = \frac{\text{absorbance of sample}}{\text{absorbance of control}} \times 100\%$$

8.4.5. Experiment of ORO staining assay

This assay protocol was adapted from Kraus et al. ⁴³⁴. On the day of induction of differentiation (day 0), the confluent preadipocytes are exposed to the differentiation medium of induction in the presence of extracts (12.5 and 50 µg/mL) or isolated compounds (0.5 and 10 µM) followed by 48 hours incubation. The cells were fed with fresh basal media containing insulin in the presence of the extracts every other 2 days until day 8 of the induction. On the day of staining (day 8), the treated

cells and control are washed with PBS and then fixed with 10% of formalin solution (dissolved in PBS, 100 μ L/well) for 30 min at room temperature. The cells were washed with 60% of isopropanol and then stained with 60% of Oil Red O (0.7 g of ORO/200 mL of isopropanol, 100 μ L/well) for 1 h at room temperature. After liquid removal, the stained cells are washed with water and eluted with 100% isopropanol. The plate was incubated for 10 min at room temperature with a shaker. The absorbance was measured at 510 nm through a microplate reader. The lipid level was expressed by:

$$\text{Fold change of adipogenesis} = \frac{\text{Absorbance of treated adipocytes}}{\text{Absorbance of control}} \times 100\%$$

8.4.6. Experiment of cellular ROS reduction assay using dichlorodihydrofluorescein diacetate (DCFH-DA)

The ROS detection experiment *via* DCFH-DA assay was adapted from Hadrich et al.²⁸⁹. On day 8 of cell differentiation, the previous medium was eliminated and replaced with 100 μ L of fresh basal medium for vehicle control (untreated adipose cells), *N*-acetylcysteine (NAC) solution (5 and 10 mM) as the positive control, and the same volume of the culture medium (DMSO 0.1%) containing extracts of flowers, leaves, and bark of *A. saligna* in various concentration (25–200 μ g/mL) or isolated compounds (0.5 and 10 μ M) then incubated for 48 h. After discarding the supernatants, the cells were gently washed with PBS, added 10 μ M of DCFH-DA solution (100 μ L), covered with aluminium foil, and then incubated for 45 min at 37 °C. Afterwards, the supernatants were removed, and the cells are washed with HBBS, then added HBBS (100 μ L). The intensity of fluorescence corresponding to the intracellular ROS concentration was read at excitation and emission wavelength of 485 and 530 nm, respectively, with a plate fluorescence reader for 0-, 5-, 10-, and 15-min. The percentage of ROS level is calculated by:

$$\text{ROS level} = \frac{\text{Fluorescence of treated adipocytes}}{\text{Fluorescence of control}} \times 100\%$$

8.4.7. Experiment of cellular glucose uptake assay

A glucose uptake simulation has been carried out using a 2-NBDG fluorescent assay in 96-well polystyrene black microplates (Corning, USA) for all extracts and isolated compounds on 3T3-L1 adipocytes adapted from Nooron et al.⁴³⁵. On day-8 after the induction, the differentiated cells were serum-starved overnight in the humidified condition with low glucose DMEM and BSA 0.1%. After medium

removal, further incubation of the adipocytes for 1 h was carried out with the KRPH buffer solution. After another incubation for 30 min at 37 °C with the following treatment:

- 1) extracts (12.5 and 50 µg/mL) or isolated compounds (0.5 and 10 µM);
- 2) vehicle medium (vehicle control); and
- 3) insulin (100 nM) and metformin (10 µM) as the positive control 1 and 2, respectively;

all dissolved in the KRPH buffer (100 µL per well), another identical volume of KRPH buffer containing 2-NBDG (80 µM) was added into each well, followed by further incubation for 30 min.

After medium removal and washed by ice-cooled PBS, the fluorescence was measured using a microplate reader (PerkinElmer) at excitation (λ_{ex}) and emission wavelength (λ_{em}) of 485 and 535 nm, respectively. The glucose uptake values were expressed by:

$$\text{2-NBDG uptake} : \left(\frac{F_1}{F_0} \right) \times 100\%$$

where F_1 and F_0 were the fluorescence of a sample and the vehicle control, respectively.

8.5. Experiment of compound isolation and molecular structure elucidation

8.5.1. Materials for fractionation and isolation

Silica gel 60 Å/40–63 µm particle size for flash chromatography, silica gel (SiO_2) 60 F₂₅₄-coated Thin Layer Chromatography (TLC) aluminium sheets and methanol-d₄ were supplied by Sigma-Aldrich (St. Louis, MO, USA). The solvents used in the analytical grade were methanol, ethyl acetate, dichloromethane, and formic acid.

8.5.2. Thin Layer Chromatography (TLC) experiment

The tested extracts or fractions solution was spotted onto the baseline of the TLC plate and then placed in the closed TLC chamber for the separation development. Once the eluent reached the determined front line, the plate was removed from the chamber for solvent evaporation. The developed spots were inspected under a UV lamp at 254 nm wavelength.

8.5.2.1. Fractionation and TLC profile of FL-MeOH

The FL-MeOH extract (600 mg) was fractionated by column chromatography with silica gel 60 (Sigma-Aldrich, USA) packed in a column chromatography (socket joint 25/29, cone 19/26, Ø 18 mm, 200 mm effective length) by which DCM/MeOH (95:5, 90:10, 85:15, and 80:20) was the mobile phase according to the TLC

examination. The fractionation afforded three main fractions: FL-MeOH-A (109 mg), FL-MeOH-B (206 mg), and FL-MeOH-C (40 mg). Under a shortwave UV light, its TLC plate showed a single broad spot and two broad spots for FL-MeOH-A and -B, respectively, while a broad spot closer to the baseline was observed for FL-MeOH-C. According to its ¹H NMR profile, the fraction FL-MeOH-C was observed as impure -B. Therefore, a further column purification was carried out to the fractions A and B with details as follows:

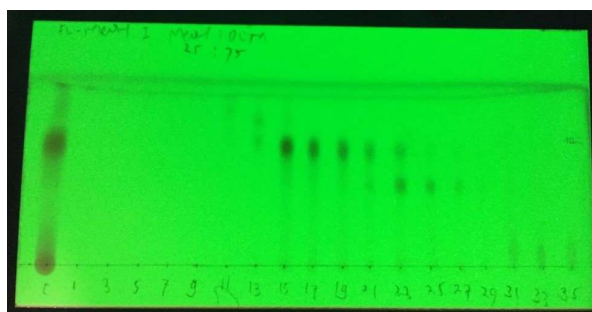
1. The normal phase silica column with the incremental gradient EtOAc/MeOH mobile phase (100:0 to 80:20) over FL-MeOH-A gave three sub-fractions, i.e., FL-MeOH-A1 (10.5 mg, R_f = 0.8, identified as naringenin **42**), -A2 (mixture), and -A3 (15.5 mg, R_f = 0.333 identified as naringenin-7O- α -L-arabinofuranose **76**).
2. The normal phase silica column with EtOAc/MeOH (100:0 to 80:20) over FL-MeOH-B gave six sub-fractions, i.e., FL-MeOH-B1a (0.2 mg, mixture of hydrocarbons), -B1b (9.13 mg, R_f = 0.528, identified as isosalipurposide **1**), -B2a (23.2 mg, impure B2b), -B2b (24.77 mg, R_f = 0.518, quercitrin **4**), -B3a (88.1 mg, impure B3b), and -B3b (15 mg, R_f = 0.168, identified as *D*-(+)-pinitol **79a**).

Table 22. Obtained fractions from the fractionation of FL-MeOH extract by the column chromatography

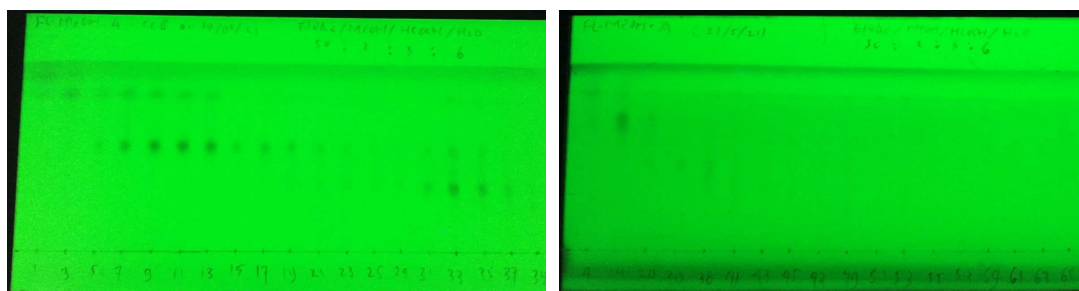
No	Mobile system (%v/v)		Collected fraction	Designed code	Weighed mass (mg) and percentage (w/w)
	DCM	MeOH			
1	100	0	1–13	FL-MeOH-A	109, 18.17%
	95	5			
2	90	10	14–23	FL-MeOH-B	206, 34.44%
4	85	15	24–29	FL-MeOH-C	40, 6.7%
5	0	100	-	Rest	245, 40.83%

Table 23. Obtained sub-fractions from the fractionation of FL-MeOH-A extract by the column chromatography

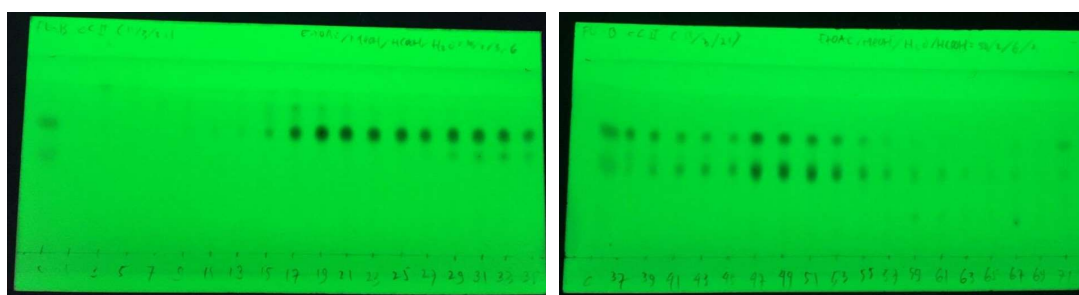
No	Mobile system (% v/v)		Collected fraction	Designed code	Weighed mass (mg) and percentage (w/w)	Identified compound
	EtOAc	MeOH				
1	100	0	1–4	FL-MeOH-A1	10.5, 9.63%	Naringenin 42
2	95	5	5–14	FL-MeOH-A2	12.2, 11.19%	-
3	90	10	15–20			
4	85	15	21 – 34	FL-MeOH-A3	15.5, 14.22%	Compound 76
			35 – 41			
5	0	100	-	Rest	70.8, 64.95%	-



(a)



(b)



(c)

Figure 119. Photographed images of TLC plates under a UV lamp at 254 nm for (a) FL-MeOH extract with a mobile phase of DCM/MeOH (75:25), (b) FL-MeOH-A fraction with EtOAc/MeOH/HCOOH/H₂O of 50:2:3:6, and (c) FL-MeOH-B fraction with EtOAc/MeOH/HCOOH/H₂O of 50:2:3:6.

Table 24. Obtained sub-fractions from the fractionation of FL-MeOH-B extract by the column chromatography

No	Mobile system (% v/v)		Collected fraction	Designed code	Weighed mass (mg) and percentage (w/w)	Identified compound
	EtOAc	MeOH				
1	100	0	1–13	FL-MeOH-B1a	0.2, 0.10%	-
			7–14	FL-MeOH-B1b	9.13, 4.43%	Isosalipurposide 1
2	95	5	14–20	FL-MeOH-B2a	23.3, 11.31%	-
			21–27	FL-MeOH-B2b	24.77, 12.02%	Quercitrin 4
3	90	10	28–46		88.1, 42.72%	-

No	Mobile system (% v/v)		Collected fraction	Designed code	Weighed mass (mg) and percentage (w/w)	Identified compound
	EtOAc	MeOH				
4	85	15	37–57	FL-MeOH-B3a	15, 7.28%	<i>D</i> -(+)-pinitol 79a
			58 – 68	FL-MeOH-B3b		
5	0	100	-	Rest	45.5, 22.09%	-

8.5.2.2. Fractionation and TLC profile of LF-MeOH

The LF-MeOH extract (1 g) was fractionated to give four major fractions: LF-MeOH-A (80 mg), -B (60 mg), -C (490 mg), and -D (50 mg). The proton NMR of LF-MeOH-D, assigned as 3-hydroxy-5-(2-aminoethyl) dihydrofuran-2(3*H*)-one **80** that the fraction was relatively pure, and no further purification was required. However, further purification using EtOAc/MeOH eluent system was conducted for the other three fractions resulting in some sub-fractions as follows:

1. Three sub-fractions, i.e., LF-MeOH-A1 (9 mg, assigned as (-)-epicatechin **77**), -A2 (mixture), and -A3 (10 mg, 2,4-di-*t*-butylphenol **78**) were obtained from the purification of fraction A.
2. Three sub-fractions were obtained from fraction B as LF-MeOH-B1 (2.3 mg, mixture of hydrocarbons), -B2 (27.5 mg, assigned as quercitrin **4**) and -B3 (12 mg, impure -B2).
3. Five sub-fractions: C1 (5 mg, mixture), C2a (26.8 mg, impure C2b), C2b (50 mg, assigned as myricitrin **11**), C2c (27.8 mg, mixture of C2b and C3), and C3 (80 mg, *D*-(-)-pinitol **79b**) were isolated from the fraction C of the methanolic extract of leaves.

Table 25. Obtained fractions from the fractionation of LF-MeOH extract by the column chromatography

No	Mobile system (% v/v)		Collected fraction	Designed code	Weighed mass (mg) and percentage (w/w)	Identified compound
	DCM	MeOH				
1	100	0	1–26	LF-MeOH-A	80, 8%	-
2	95	5	27–40			-
3	90	10	41–50	LF-MeOH-B	60, 6%	-
4	85	15	51–81	LF-MeOH-C	490, 49%	-
5	80	20	82–90	LF-MeOH-D	50, 6%	Compound 80
6	0	100	-	Rest	320, 32%	-

Table 26. Obtained sub-fractions from the fractionation of LF-MeOH-A extract by the column chromatography

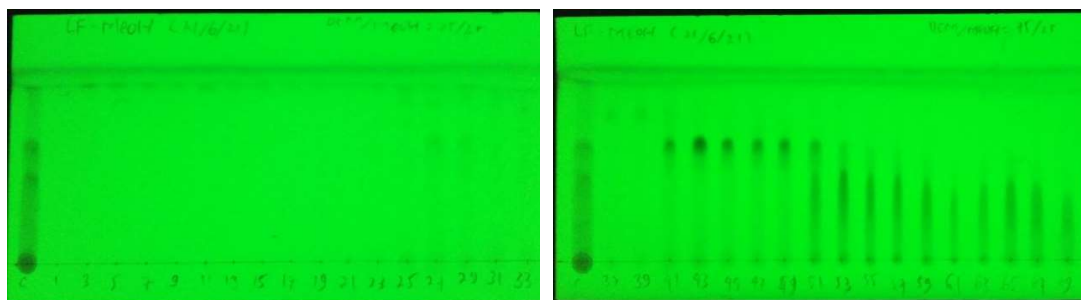
No	Mobile system (% v/v)		Collected fraction	Designed code	Weighed mass (mg) and percentage (w/w)	Identified compound
	EtOAc	MeOH				
1	100	0	1–4	LF-MeOH-A1	9, 11.25%	(–)-Epicatechin 77
2	95	5	5–9	LF-MeOH-A2	18.5, 23.13%	-
3	90	10	11–17	LF-MeOH-A3	10, 12.5%	Compound 78
4	0	100	-	Rest	42.5, 53.13%	-

Table 27. Obtained sub-fractions from the fractionation of LF-MeOH-B extract by the column chromatography

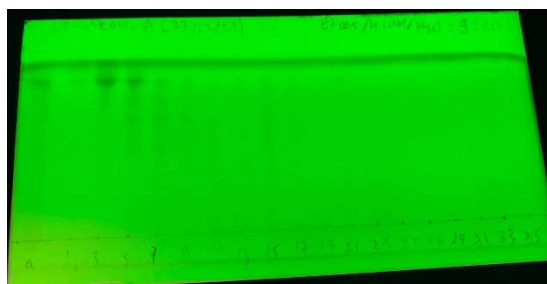
No	Mobile system (% v/v)		Collected fraction	Designed code	Weighed mass (mg) and percentage (w/w)	Identified compound
	EtOAc	MeOH				
1	100	0	1–5	LF-MeOH-B1	2.3, 3.83%	-
2	95	5	6–16	LF-MeOH-B2	28.6, 47.67%	Quercitrin 4
3	90	10	17-21	LF-MeOH-B3	12, 20%	-
4	0	100	-	Rest	17.1, 28.5%	-

Table 28. Obtained sub-fractions from the fractionation of LF-MeOH-C extract by the column chromatography

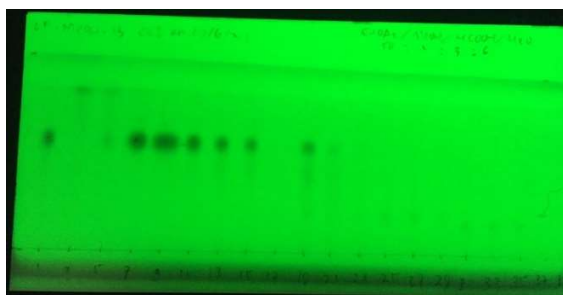
No	Mobile system (% v/v)		Collected fraction	Designed code	Weighed mass (mg) and percentage (w/w)	Identified compound
	EtOAc	MeOH				
1	100	0	1–13	LF-MeOH-C1	5, 1.02%	-
2	95	5	14–28	LF-MeOH-C2a	26.8, 5.47%	-
3	90	10	29–39	LF-MeOH-C2b	50, 10.20%	Myricitrin 11
			40–68	LF-MeOH-C2c	27.8, 5.67%	-
4	85	15	69–85	LF-MeOH-C3	80, 16.33%	(–)-Pinitol 79b
5	0	100	-	Rest	300.4, 61.31%	-



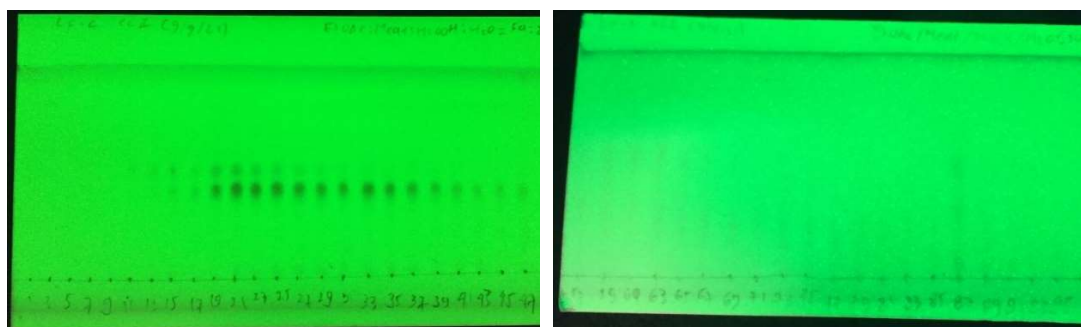
(a)



(b)



(c)



(d)

Figure 120. Photographed images of TLC plates under a UV lamp at 254 nm for (a) LF-MeOH extract with a mobile phase of DCM/MeOH (75:25), (b) LF-MeOH-A fraction with EtOAc/HCOOH/H₂O of 9:1:1, (c) LF-MeOH-B fraction with EtOAc/MeOH/HCOOH/H₂O of 50:2:3:6, and (d) LF-MeOH-C fraction with EtOAc/MeOH/HCOOH/H₂O of 50:2:3:6.

8.5.2.3. Fractionation and TLC profile of BK-MeOH

According to the proton NMR spectra of BK-MeOH extract, saccharide-derived compounds appeared as the major component in the methanolic extract, indicated by strong multiplet peaks between 3 and 4 ppm. Some minor peaks in the

aromatic region were also observed in the data representing possible phenolic derivation species. Given that the extracted components were most likely to be more polar, the mobile phase of the fractionation was EtOAc and MeOH with increasing polarity. Three main fractions, BK-MeOH-A, -B, and -C, were collected. Furthermore, each fraction can be grouped into two sub-fractions according to the TLC profile. The detailed assignment of the methanolic bark isolated compounds was as follows:

1. NMR peaks of sub-fraction BK-MeOH-A1 (7.6 mg) were identical with (–)-epicatechin **77**, while sub-fraction -A2 was impure (–)-epicatechin **77**.
2. The sub-fraction B2, assigned later as *D*-(+)-pinitol **79a** (53.5 mg), was estimated as the main isolated compound of the methanolic bark extract, whereas impure *D*-(+)-pinitol **79A** was in BK-MeOH-B1 (1.1 mg).
3. A common disaccharide, sucrose (25 mg), confirmed by its spectroscopic data, was found as the component of BK-MeOH-C2, along with its impure form in subfraction-C1 (33.5 mg).

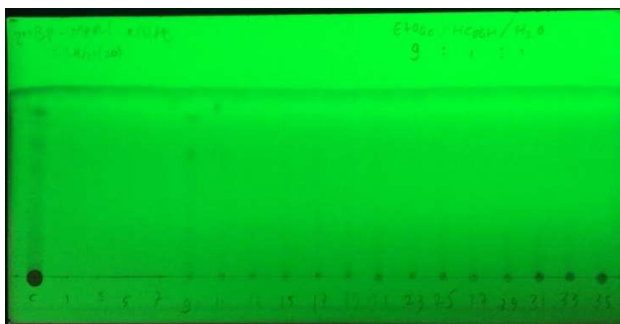


Figure 121. Photographed image of TLC plate under a UV lamp at 254 nm for BK-MeOH extract with a mobile phase of EtOAc/HCOOH/H₂O (9:1:1).

Table 29. Obtained fraction from the fractionation of BK-MeOH extract by the column chromatography

No	Mobile system (% v/v)		Collected fraction	Code of fraction	Weighed mass (mg) and percentage (w/w)	Identified compound
	EtOAc	MeOH				
1	100	0	1–8	BK-MeOH-A1	7.6, 2.53%	(–)-Epicatechin 77
2	95	5	9–11	BK-MeOH-A2 (mixture)	2.9, 1%	-
3	90	10		BK-MeOH-B1	1.1, 0.37%	-
4			12–20	BK-MeOH-B2	53.5, 17.83%	<i>D</i> -(+)-pinitol 79a
5	85	15		BK-MeOH-C1	33.5, 11.17%	-
6			21–30	BK-MeOH-C2	25, 8.33%	Sucrose
7	0	100	31–35	Rest	54.5, 18.17%	-

8.5.3. Structure identification of isolated compounds

Isolated pure compounds were structure characterised by specific optical rotation (Jasco P-2000 Polarimeter), melting point (Gallenkamp apparatus), GCMS (Agilent 6890GC coupled with Agilent 5973n MS (EI), FTIR (Nicolet-FTIR 6700), HRMS (Agilent 6510 QTOF Mass Spectrometer (ESI)), 1D and 2D NMR (Bruker 400 MHz and Agilent 500 MHz). Analysis of 1D NMR, including proton and carbon-13 & carbon-DEPT, was conducted to determine the main elemental components of the compounds. The 2D NMR analysis of the isolated phytochemicals, including COSY and HSQC, was carried out to build the molecule's connectivity.

8.5.3.1. Spectral data analysis of compounds from FL-MeOH

Naringenin **42**: FL-MeOH-A1 (10.5 mg, 1.75% w/w) is a yellow solid: IR (ν_{\max} , cm^{-1}) 3246.22 (-OH), 2919.77 (sp^3 CH), 1709.65 (C=O), 1597.51 (C=C aromatic), and 1013.25 cm^{-1} (C-O); HRMS (EI) m/z 273.0684 $[\text{M} + \text{H}]^+$, cald for $\text{C}_{15}\text{H}_{12}\text{O}_5$ 273.0685; m.p. 253–255 °C; $[\alpha]^{23} = -16.68^\circ$ (c 0.1, EtOH) [literature ⁴³⁶ $[\alpha]^{22} = -14.7^\circ$ (c 0.36, EtOH)].

Naringenin-7-*O*- α -L-arabinofuranoside **76**: FL-MeOH-A3 (15.5 mg, 2.58% w/w) is yellow powder: IR (ν_{\max} , cm^{-1}) 3300.70 (-OH stretching), 2920.64 (sp^3 CH stretching), 1710 C=O), 1605.11 (C=C), and 1021.40 cm^{-1} (C-O); HRMS (EI) m/z 405.1189 $[\text{M} + \text{H}]^+$, cald $\text{C}_{20}\text{H}_{20}\text{O}_9$ 405.1186; m.p. 229–230 °C; $[\alpha]^{23} = -44.54^\circ$ (c 0.1, MeOH).

Isolisalipurposide **1**: FL-MeOH-B1b is a yellow powder (9.13 mg, 1.52% w/w): IR (ν_{\max} , cm^{-1}) 3255.08 (-OH), 2930.83 (sp^3 CH), 1601.61 (C=O), 1550.28 (C=C), and 1070.60 cm^{-1} (C-O); HRMS (EI) m/z 435.1298 $[\text{M} + \text{H}]^+$, cald $\text{C}_{21}\text{H}_{22}\text{O}_{10}$ 435.1291; m.p. 174–175 °C; $[\alpha]^{23} = -119.02^\circ$ (c 0.1, MeOH).

Quercitrin **4**: FL-MeOH-B2b (24.77 mg, 4.13% w/w) is yellow powder: IR (ν_{\max} , cm^{-1}) 3248.57 (-OH), 2936.97 (sp^3 CH), 1652.71 (C=O), 1499.15 (C=C), 1198.56 and 1070.60 cm^{-1} (C-O); HRMS (EI) m/z 449.1072 $[\text{M} + \text{H}]^+$, cald $\text{C}_{21}\text{H}_{21}\text{O}_{11}$ 449.1084; m.p. 180–183 °C; $[\alpha]^{23} = -120.86^\circ$ (c 0.1, MeOH).

D-(+)-Pinitol **79a**: FL-MeOH-B3b (15 mg, 2.5% w/w) is white solid: IR (ν_{\max} , cm^{-1}) 3328.27 (-OH), 2918.85 (sp^3 CH), and 1034.21 cm^{-1} (C-O); HRMS (EI) m/z 195.0865 $[\text{M} + \text{H}]^+$, cald $\text{C}_7\text{H}_{14}\text{O}_6$ 195.0869; m.p. 171–172 °C; $[\alpha]^{23} = +44.80^\circ$ (c 0.1, H_2O) [lit. ³⁴⁵ $[\alpha]^{23} = +69.7^\circ$ (c 0.56, MeOH)].

8.5.3.2. Spectral data analysis of compounds from LF-MeOH

(-)-Epicatechin **77**: LF-MeOH A1 (9 mg, 0.9%) isolated as colourless solids: IR (ν_{\max} , cm^{-1}) 3270.79 (-OH); 2920.04 (sp^3 CH); 1598.57 (C=C); and 1013.97 cm^{-1}

(C–O); HRMS (EI) m/z 291.0871 $[M + H]^+$ calcd $C_{15}H_{14}O_6$ 291.0869; m.p. 240–243 °C; $[\alpha]^{23} = -69.06^\circ$ (c 0.1, MeOH) [lit. ⁴³⁷ $[\alpha]^{23} = -69.7^\circ$ (c 0.56, MeOH)].

2,4-di-*t*-butylphenol **78**: LF-MeOH-A3 (10 mg, 1% w/w) is a yellow solid: IR (ν_{\max} , cm^{-1}) 3330.29 (-OH), 2921.70 (sp^3 CH), 1592.96 (C=C, aromatic), and 1029.41 cm^{-1} (C–O); GC-MS analysis showed a single peak ($r_t = 13.919$ min) with m/z peak at 206.1, which represents $C_{14}H_{22}O$; m.p. 61–62 °C.

Quercitrin **4**: LF-MeOH-B2 (28.6 mg, 2.86% w/w) is yellow solid: IR (ν_{\max} , cm^{-1}) 3286.53 (-OH), 2927.28 (sp^3 CH), 1652.21 (C=O), 1599.51 and 1498.15 (C=C), 1197.61 and 1070.60 cm^{-1} (C–O); HRMS(EI) m/z 449.1081 $[M + H]^+$, calcd $C_{21}H_{21}O_{11}$ 449.1084; m.p. 180–183 °C; $[\alpha]^{23} = -212.80^\circ$ (c 0.1, MeOH).

Myricitrin **11**: LF-MeOH-C2b (50 mg, 5% w/w) is a yellow powder: IR (ν_{\max} , cm^{-1}) 3266.81 (-OH), 2930.51 (sp^3 CH), 1652.84 (C=O), 1499.04 (C=C aromatic), 1197.39 and 1070.60 cm^{-1} (C–O); HRMS (EI) m/z 465.1037 $[M + H]^+$, calcd $C_{21}H_{20}O_{12}$ 465.1033; m.p. 193–195 °C; $[\alpha]^{23} = -246.32^\circ$ (c 0.1, MeOH).

(-)-Pinitol **79b**: LF-MeOH-C3 (80 mg, 8%) a white solid: IR (ν_{\max} , cm^{-1}) 3389.09 (-OH), 3302.90 and 2907.93 (sp^3 CH), 1068.27 and 1070.60 cm^{-1} (C–O); HRMS (EI) m/z 195.0863 $[M + H]^+$, calcd $C_7H_{14}O_6$ 195.0869; m.p. 175–177 °C; $[\alpha]^{23} = -79.44^\circ$ (c 0.1, H₂O) [lit. ³⁴⁵ $[\alpha]^{20} = -61.5^\circ$ (c 0.19, H₂O)].

(3*S**,5*S**)-3-Hydroxy-5-(2-aminoethyl) dihydrofuran-2(3*H*)-one **80**: LF-MeOH-D (50 mg, 5% w/w) a colourless solid: IR (ν_{\max} , cm^{-1}) 3212.08 (OH), 2929.09 (sp^3 CH), 1707.74 (C=O) and 1053.09 (C–O), HRMS (EI) m/z 146.0818 $[M + H]^+$; calcd $C_6H_{11}NO_3$ 146.0817; m.p. 347–350 °C.

8.5.3.3. Spectral data analysis of compounds from BK-MeOH

(-)-Epicatechin **77**: BK-MeOH-A1 (7.6 mg, 2.53%) is colourless solid: IR (ν_{\max} , cm^{-1}) 3220.47 (-OH); 2919.54 (sp^3 CH); 1604.73 (C=C); and 1031.13 cm^{-1} (C–O); HRMS (EI) m/z 291.0859 $[M + H]^+$ calcd $C_{15}H_{14}O_6$ 291.0869; m.p. 240–243 °C; $[\alpha]^{23} = -28.72^\circ$ (c 0.1, MeOH) [lit. ⁴³⁷ $[\alpha]^{23} = -69.7^\circ$ (c 0.56, MeOH)].

D-(+)-Pinitol **79a**: BK-MeOH-B2 (53.5 mg, 17.83% w/w) is white solid: IR (ν_{\max} , cm^{-1}) 3290.16 (-OH), 2920.20 (sp^3 CH), 1066.12 and 1070.60 cm^{-1} (C–O); HRMS (EI) m/z 195.0865 $[M + H]^+$, calcd $C_7H_{14}O_6$ 195.0869; m.p. 171–172 °C; $[\alpha]^{23} = +90.82^\circ$ (c 0.1, H₂O) [lit. ³⁴⁵ $[\alpha]^{23} = +69.7^\circ$ (c 0.56, MeOH)].

8.6. Experiments of mt-ROS and MMP assays

8.6.1. Materials of mitochondrial assays

Unless otherwise mentioned, all chemicals were supplied by Sigma-Aldrich (St. Louis, MO, USA). The main chemicals for the assays were metformin, JC-1 (5,5,6,6'-tetrachloro-1,1',3,3' tetraethylbenzimidazolylcarbocyanine iodide), insulin, and bovine serum albumin (BSA). The MitoSOX (hydroethidine triphenylphosphonium cation) was purchased from Thermo-Fisher Scientific (USA).

8.6.2. Mt-ROS level measurement using mitoSOX staining reagent

A hydroethidine triphenylphosphonium cation (MitoSOX red) is a lipophilic hydroethidium member for staining mt-ROS. Due to the charge difference between the mitochondrial intermediate membrane and mitochondrial matrix, the triphenylphosphonium substituent (TPP^+) can stimulate the hydroethidium entry into the inner space of the mitochondrion. Then, the cation is attracted to the negatively charged environment of the mitochondrial matrix, where mt-ROS is most likely present. It can be oxidised by the mt-ROS to produce 2-hydroxyethidium that exhibits a red fluorescent emission at $\lambda_{\text{em}} 510$ ⁴³⁸. Hence, the more intense optical density indicates a higher level of the observed mt-ROS.

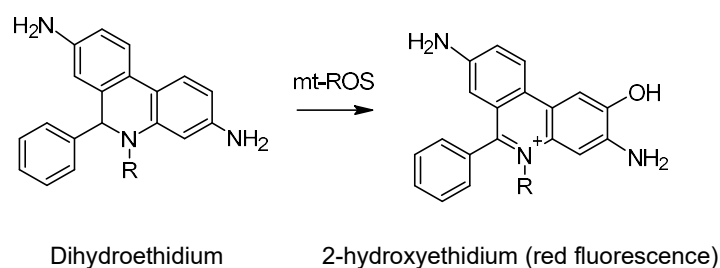


Figure 122. A simplified oxidation reaction of the dihydroethidium group to form the red dyeing indicator of mt-ROS ⁴³⁹.

The modified protocol from Kauffman et al. ⁴⁴⁰ was adapted for the experiment of the mt-ROS probe using the mitoSOX in the 96-well black plates. The mature 3T3-L1 adipocytes were incubated for 24 h with basal medium containing DMSO 0.1% and methanolic extracts (12.5 and 50 $\mu\text{g}/\text{mL}$) or isolated compounds (0.5, 5, and 10 μM). The basal medium (vehicle medium) was used as the blank control, while metformin (10 μM) was a positive control. Following the incubation and medium discarding, the treated mature adipose cells were then exposed to 5 μM of MitoSOX Red in 100 μL of PBS for tagging the mt-ROS, covered with aluminium foil, and incubated for 30 min. Afterwards, the cells were washed with PBS twice, and 100

μL of PBS was added. The fluorescence was read with the PerkinElmer microplate reader at λ_{ex} 510 and λ_{em} 580 nm. The obtained data were expressed in percentage of the observed parameter:

$$\text{Mt-ROS level (\%)} = \frac{\text{OD of treated adipocytes}}{\text{OD of blank control}} \times 100\%$$

where OD is the optical density of the fluorescence observation.

8.6.3. Mitochondrial membrane potential (MMP) measurement using JC-1 staining reagent

A fluorescent cationic dye, 5,5,6,6'-tetrachloro-1,1',3,3' tetraethylbenzimidazolcarbocyanine iodide (JC-1), is a lipophilic reagent that can be used to monitor the health status of mitochondria in cells⁴⁴¹. It can readily enter the inner side of the mitochondrial matrix, which is a more negatively charged region for a healthy mitochondrion due to proton transfer from the mitochondrial matrix to intermembrane space. Thus, it forms a complex product called J-aggregate. The difference in exhibiting fluorescence between unreacted JC-1 reagent (JC-1 monomer) and J-aggregate is green and red, respectively, which can predict the degree of MMP.

In a normal MMP and healthy mitochondrion, more accumulated J-aggregates are produced due to higher interaction between the cation and negatively charged matrix resulting in more intense red fluorescence in the assay. Unhealthy mitochondria with lower MMP will have a lower red fluorescence as the mitochondrial matrix has a less negative charge. Therefore, more JC-1 monomer is present, producing more intense green fluorescence. Hence, the ratio of red to the green shift of the probe expresses the status of MMP. The normal mitochondria have a higher MMP value, which can be indicated by a high ratio⁴⁰¹. The normal MMP status allows protons produced by the mitochondrial respiratory chains to transfer proportionally from the mitochondrial matrix to the intermembrane. It indicates the recovered mitochondrial respiration that can produce homeostasis energy. Moreover, inhibiting excessive mt-ROS reduction can protect endogenous antioxidant enzymes from oxidation and maintain mitochondrial redox balance.

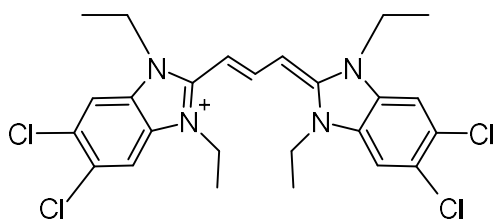


Figure 123. Molecular structure of JC-1 labelling agent.

The MMP measurement by JC-1 was carried out in the 96 multiwell black plates by following Harshkova et al. ⁴⁴² with a slight modification. Similar to those described for labelling mt-ROS, after the 24 h treatment with the methanolic extracts (12.5 and 50 µg/mL) or isolated compounds (0.5, 5, and 10 µM), blank control, and positive control of metformin (10 µM), the mitochondria of adipocytes were stained with 3 µM of JC-1 for 30 min in the humidified incubator. Following the PBS washing twice and PBS (100 µL) addition, the fluorescent optical density was read at λ_{ex} 488 nm and λ_{em} 530 nm (green JC-1 monomers) and λ_{ex} 443 nm and λ_{em} 590 nm (red JC-1 aggregates). The obtained data were converted to a ratio of J-aggregates to JC-1 monomers (R). The MMP was expressed as a percentage of the ratio of J-aggregates to JC-1 monomers for samples (Rs) normalised by the ratio for vehicle control (Rc).

$$\text{J-aggregates to JC-1 monomers ratio (\% of control)} = \frac{R_s}{R_c} \times 100\%$$

8.7. Experiment of immunoblot analysis

8.7.1. Materials for immunoblot study

The following materials were supplied by Merck (Germany): polyvinylidene fluoride (PDVF) membranes, skim milk powder, Immobilon ECL Ultra Western HRP substrate, RIPA lysis buffer, glycine, Bradford reagent, hydrochloric acid, sodium dodecyl sulfate (SDS). The other materials were Tween-20 (Vivantis Inc., USA), Tris (Vivantis Inc., USA), ammonium peroxide sulphate, sodium hydroxide, protein and ladder standard solution, acrylamide/bis-acrylamide solution 30% (HiMedia Laboratories, India), tetramethylethylenediamine or TEMED (PanReac AppliChem & ITW Reagents, Germany), and Laemmli sample buffer (BioRad Laboratories, USA). The following materials were purchased from Cell Signalling Technology (USA): protease inhibitor cocktail, primary antibodies (p-AMPK- α , AMPK- α , and α -tubulin), and goat anti-rabbit IgG horseradish peroxidase-conjugated (HRP-conjugated) secondary antibody.

8.7.2. Protocols for immunoblot study

The protocol of immunoblot analysis was adapted from Lee et al. ⁴⁴³ with a minor change. After being treated with the indicated agents, the cells were washed in ice-chilled PBS, harvested by 100 µL of lysis buffer, and then spun for 10 minutes at 12,000 RPM at 4°C. The Bradford-based protein content was carried out using BSA as the standard with a range of concentration (0.0375–6 mg/mL) in a 96-well plate. The lysates were then heated at 95 °C for 10 min and centrifugation at 5,000 RPM for 2 min.

Electrophoresis of supernatant containing 20 µg of proteins was performed using SDS-polyacrylamide (10%) gels followed by electrophoretic transfer of separated proteins to polyvinylidene fluoride (PDVF) membranes (Merck, Germany). Afterwards, the membranes were blocked with 5% non-fat milk (Merck, Germany) solution for 1 h and then incubated with the appropriate primary antibodies' solution of 1:1,000 (Cell signalling, USA) overnight at 4 °C. After washing with Tris-buffered saline and Tween 20 (0.1%), the membranes were incubated with goat anti-rabbit IgG horseradish peroxidase-conjugated (HRP-conjugated) secondary antibodies (1:10,000) for an hour at room temperature. Bands were then visualised with ECL western blotting reagents (Merck, Germany), and the chemiluminescent images were captured using Chemidoc (Amersham Image-quant 800). A stripping step was performed before reprobing with other antibodies (total AMPK and α-tubulin). The captured bands were analysed using Image J (National Institute of Health, USA) to quantify the protein expression.

8.8. Quantitative reverse transcription-polymerase chain reaction (RT-qPCR)

8.8.1. Materials for RT-qPCR

The following materials were supplied by Promega (Wisconsin, USA): nuclease-free water, dNTP mix (10 mM), reverse transcription kits of cDNA first-strand synthesis, and random primers. The following target primers (TaqMan™ GeneExpressionAssay (FAM)) were purchased from Thermo-Fisher Scientific (Massachusetts, USA):

Table 30. List of target primers used for the RT-qPCR experiments

No	Primers	Catalogue No
1	Adiponectin	4331182/ assay ID: Mm04933656_m1
2	PGC-1α	4331182/ assay ID: Mm01208835_m1
3	mtTFA	4331182/ assay ID: Mm00447485_m1
4	TNF-α	4331182/ assay ID: Mm00443258_m1
5	IL-6	4331182/ assay ID: Mm00446190_m1
6	β-Actin	4331182/ assay ID: Mm02619580_g1

The other materials were Trizol reagent for RNA isolation (Sigma-Aldrich, USA), 96-well PCR plate and adhesive seals (Bio-Rad, California, USA), solvents including isopropanol, chloroform and ethanol (Point of Care Diagnostics, Australia), and master mix for RT-PCR (Meridian Bioscience, Ohio, USA).

8.8.2. Protocol of the RT-qPCR experiment

The RNA of treated adipocytes was extracted using Trizol reagent, followed by precipitation with isopropyl alcohol, three times washing with 75% EtOH in

nuclease-free water, solvent evaporation, and dissolving in nuclease-free water. The concentration of RNA was quantified using a Nanodrop 2000 spectrometer (Thermo-Fisher Scientific, USA).

The first-strand cDNA was synthesised from 1 µg of the isolated RNA according to the protocol of the manufacturer. The reaction was conducted in a Bio-Rad T100 Thermal Cycler (California, USA). The concentration of cDNA product used as a template for amplification of RT-qPCR was estimated using the nanodrop apparatus.

The qPCR was carried out in a Bio-Rad CFX96 Real-Time System (California, USA) following the manufacturer of the kit. The reaction was conducted in the following stages: polymerase activation (95°C, 2 min), denaturation (95°C, 10 s), and annealing step (60°C, 30 s) for 50 cycles.

8.9. Statistical analysis

A descriptive analysis using GraphPad Prism 9 (San Diego, CA, USA) was conducted to determine the mean \pm standard error mean (SEM) from the three separate experiments ($n = 3$). The difference between the two means of each sample and the vehicle control optical densities were calculated using a one-way ANOVA followed by Tukey's or Dunnett's post hoc tests where $p < 0.05$ was considered significant.

REFERENCES

- (1) WHO. *Global report on diabetes*; WHO Press, 2016.
- (2) WHO. *Noncommunicable diseases country profiles 2018*; WHO Press, 2018.
- (3) WHO. *Classification of diabetes mellitus*; WHO, 2019.
- (4) IDF. *Diabetes atlas third edition*; The International Diabetes Federation (IDF), 2006.
- (5) Buren, J. Glucose and lipid metabolism in insulin resistance – an experimental study in fat cells. Umeå University, Umeå, 2002. <https://www.diva-portal.org/smash/get/diva2:142848/FULLTEXT01.pdf>.
- (6) Golay, A.; Ybarra, J. Link between obesity and type 2 diabetes. *Best practice & research Clinical endocrinology & metabolism* **2005**, *19* (4), 649-663.
- (7) Pi, J.; Collins, S. Reactive oxygen species and uncoupling protein 2 in pancreatic β -cell function. *Diabetes, Obesity and Metabolism* **2010**, *12*, 141-148.
- (8) Gupta, D.; B Krueger, C.; Lastra, G. Over-nutrition, obesity and insulin resistance in the development of β -cell dysfunction. *Current diabetes reviews* **2012**, *8* (2), 76-83.
- (9) Al-Goblan, A. S.; Al-Alfi, M. A.; Khan, M. Z. Mechanism linking diabetes mellitus and obesity. *Diabetes, metabolic syndrome and obesity: targets and therapy* **2014**, *7*, 587.
- (10) Ford, E. S.; Williamson, D. F.; Liu, S. Weight change and diabetes incidence: findings from a national cohort of US adults. *American journal of epidemiology* **1997**, *146* (3), 214-222.
- (11) Halpern, A.; Mancini, M. C. Diabetes. *Treatments in endocrinology* **2005**, *4* (2), 65-74.
- (12) Stumvoll, M.; Goldstein, B. J.; Van Haefen, T. W. Type 2 diabetes: principles of pathogenesis and therapy. *The Lancet* **2005**, *365* (9467), 1333-1346.
- (13) Gregor, M. F.; Hotamisligil, G. S. Inflammatory mechanisms in obesity. *Annual review of immunology* **2011**, *29*, 415-445.
- (14) Hotamisligil, G. S.; Shargill, N. S.; Spiegelman, B. M. Adipose expression of tumor necrosis factor- α : direct role in obesity-linked insulin resistance. *Science* **1993**, *259* (5091), 87-91.
- (15) Hotamisligil, G. S.; Peraldi, P.; Budavari, A.; Ellis, R.; White, M. F.; Spiegelman, B. M. IRS-1-mediated inhibition of insulin receptor tyrosine kinase activity in TNF- α -and obesity-induced insulin resistance. *Science* **1996**, *271* (5249), 665-670.
- (16) Hotamisligil, G. S.; Arner, P.; Caro, J. F.; Atkinson, R. L.; Spiegelman, B. M. Increased adipose tissue expression of tumor necrosis factor- α in human obesity and insulin resistance. *The Journal of clinical investigation* **1995**, *95* (5), 2409-2415.
- (17) Gutiérrez-Rodelo, C.; Roura-Guiberna, A.; Olivares-Reyes, J. A. Molecular mechanisms of insulin resistance: An update. *Gac Med Mex* **2017**, *153* (2), 214-228.
- (18) Donath, M. Y.; Shoelson, S. E. Type 2 diabetes as an inflammatory disease. *Nature Reviews Immunology* **2011**, *11* (2), 98-107.
- (19) Donath, M. Y. Targeting inflammation in the treatment of type 2 diabetes: time to start. *Nature reviews Drug discovery* **2014**, *13* (6), 465-476.
- (20) Butcher, M. J.; Hallinger, D.; Garcia, E.; Machida, Y.; Chakrabarti, S.; Nadler, J.; Galkina, E. V.; Imai, Y. Association of proinflammatory cytokines and islet resident leucocytes with islet dysfunction in type 2 diabetes. *Diabetologia* **2014**, *57* (3), 491-501.

- (21) Gerber, P. A.; Rutter, G. A. The role of oxidative stress and hypoxia in pancreatic beta-cell dysfunction in diabetes mellitus. *Antioxidants & redox signaling* **2017**, *26* (10), 501-518.
- (22) Lei, X. G.; Vatamaniuk, M. Z. Two tales of antioxidant enzymes on β cells and diabetes. *Antioxidants & redox signaling* **2011**, *14* (3), 489-503.
- (23) Rochette, L.; Zeller, M.; Cottin, Y.; Vergely, C. Diabetes, oxidative stress and therapeutic strategies. *Biochimica et Biophysica Acta (BBA)-General Subjects* **2014**, *1840* (9), 2709-2729.
- (24) Ying, W.; Fu, W.; Lee, Y. S.; Olefsky, J. M. The role of macrophages in obesity-associated islet inflammation and β -cell abnormalities. *Nature Reviews Endocrinology* **2019**, 1-10.
- (25) Pociot, F.; McDermott, M. Genetics of type 1 diabetes mellitus. *Genes & Immunity* **2002**, *3* (5), 235-249.
- (26) Paschou, S. A.; Petsiou, A.; Chatzigianni, K.; Tsatsoulis, A.; Papadopoulos, G. K. Type 1 diabetes as an autoimmune disease: the evidence. *Diabetologia* **2014**, *57* (7), 1500-1501.
- (27) Sheehan, J. P.; Ulchaker, M. M. *Obesity and type 2 diabetes mellitus*; Oxford University Press, 2010.
- (28) Højlund, K.; Mogensen, M.; Sahlin, K.; Beck-Nielsen, H. Mitochondrial dysfunction in type 2 diabetes and obesity. *Endocrinology and metabolism clinics of North America* **2008**, *37* (3), 713-731.
- (29) Olokoba, A. B.; Obateru, O. A.; Olokoba, L. B. Type 2 diabetes mellitus: a review of current trends. *Oman medical journal* **2012**, *27* (4), 269.
- (30) Nimse, S. B.; Pal, D. Free radicals, natural antioxidants, and their reaction mechanisms. *Rsc Advances* **2015**, *5* (35), 27986-28006.
- (31) Brownlee, M. Biochemistry and molecular cell biology of diabetic complications. *Nature* **2001**, *414* (6865), 813-820.
- (32) Furukawa, S.; Fujita, T.; Shimabukuro, M.; Iwaki, M.; Yamada, Y.; Nakajima, Y.; Nakayama, O.; Makishima, M.; Matsuda, M.; Shimomura, I. Increased oxidative stress in obesity and its impact on metabolic syndrome. *The Journal of clinical investigation* **2017**, *114* (12), 1752-1761.
- (33) Jiang, Z.-Y.; Woollard, A. C.; Wolff, S. P. Hydrogen peroxide production during experimental protein glycation. *FEBS letters* **1990**, *268* (1), 69-71.
- (34) Masella, R.; Vari, R.; D'Archivio, M.; Santangelo, C.; Scazzocchio, B.; Maggiorella, M. T.; Sernicola, L.; Titti, F.; Sanchez, M.; Di Mario, U. Oxidised LDL modulate adipogenesis in 3T3-L1 preadipocytes by affecting the balance between cell proliferation and differentiation. *FEBS letters* **2006**, *580* (10), 2421-2429.
- (35) Kuniyasu, A.; Tokunaga, M.; Yamamoto, T.; Inoue, S.; Obama, K.; Kawahara, K.; Nakayama, H. Oxidized LDL and lysophosphatidylcholine stimulate plasminogen activator inhibitor-1 expression through reactive oxygen species generation and ERK1/2 activation in 3T3-L1 adipocytes. *Biochimica et Biophysica Acta (BBA)-Molecular and Cell Biology of Lipids* **2011**, *1811* (3), 153-162.
- (36) Bordt, E. A.; Polster, B. M. NADPH oxidase-and mitochondria-derived reactive oxygen species in proinflammatory microglial activation: a bipartisan affair? *Free Radical Biology and Medicine* **2014**, *76*, 34-46.
- (37) Pelletier, M.; Lepow, T. S.; Billingham, L. K.; Murphy, M. P.; Siegel, R. M. New tricks from an old dog: mitochondrial redox signaling in cellular inflammation. In *Seminars in immunology*, 2012; Elsevier: Vol. 24, pp 384-392.
- (38) Rains, J. L.; Jain, S. K. Oxidative stress, insulin signaling, and diabetes. *Free Radical Biology and Medicine* **2011**, *50* (5), 567-575.

- (39) Roberts, C. K.; Barnard, R. J.; Sindhu, R. K.; Jurczak, M.; Ehdaie, A.; Vaziri, N. D. Oxidative stress and dysregulation of NAD (P) H oxidase and antioxidant enzymes in diet-induced metabolic syndrome. *Metabolism* **2006**, *55* (7), 928-934.
- (40) Arai, K.; Maguchi, S.; Fujii, S.; Ishibashi, H.; Oikawa, K.; Taniguchi, N. Glycation and inactivation of human Cu-Zn-superoxide dismutase. Identification of the in vitro glycosylated sites. *Journal of Biological Chemistry* **1987**, *262* (35), 16969-16972.
- (41) Wolff, S. P.; Dean, R. Glucose autoxidation and protein modification. The potential role of 'autoxidative glycosylation' in diabetes. *Biochemical journal* **1987**, *245* (1), 243-250.
- (42) Sottero, B.; Gargiulo, S.; Russo, I.; Barale, C.; Poli, G.; Cavalot, F. Postprandial dysmetabolism and oxidative stress in type 2 diabetes: pathogenetic mechanisms and therapeutic strategies. *Medicinal research reviews* **2015**, *35* (5), 968-1031.
- (43) Kawahito, S.; Kitahata, H.; Oshita, S. Problems associated with glucose toxicity: role of hyperglycemia-induced oxidative stress. *World journal of gastroenterology: WJG* **2009**, *15* (33), 4137.
- (44) Rebolledo, O.; Dato, S. A. Postprandial hyperglycemia and hyperlipidemia-generated glycoxidative stress: its contribution to the pathogenesis of diabetes complications. *European review for medical and pharmacological sciences* **2005**, *9* (4), 191.
- (45) Hatia, S.; Septembre-Malaterre, A.; Le Sage, F.; Badiou-Bénéteau, A.; Baret, P.; Payet, B.; Lefebvre d'Hellencourt, C.; Gonthier, M.-P. Evaluation of antioxidant properties of major dietary polyphenols and their protective effect on 3T3-L1 preadipocytes and red blood cells exposed to oxidative stress. *Free radical research* **2014**, *48* (4), 387-401.
- (46) Yan, J.; Zhao, Y.; Suo, S.; Liu, Y.; Zhao, B. Green tea catechins ameliorate adipose insulin resistance by improving oxidative stress. *Free Radical Biology and Medicine* **2012**, *52* (9), 1648-1657.
- (47) Deng, W.; Fang, X.; Wu, J. Flavonoids function as antioxidants: by scavenging reactive oxygen species or by chelating iron? *Radiation Physics and Chemistry* **1997**, *50* (3), 271-276.
- (48) Kicinska, A.; Jarmuszkiewicz, W. Flavonoids and mitochondria: activation of cytoprotective pathways? *Molecules* **2020**, *25* (13), 3060.
- (49) Xiong, J.; Grace, M. H.; Esposito, D.; Komarnytsky, S.; Fei, W.; Lila, M. A. Polyphenols isolated from *Acacia mearnsii* bark with anti-inflammatory and carbolytic enzyme inhibitory activities. *Chinese journal of natural medicines* **2017**, *15* (11), 816-824.
- (50) Delgadillo Puga, C.; Cuchillo Hilario, M.; Espinosa Mendoza, J. G.; Medina Campos, O.; Molina Jijón, E.; Díaz Martínez, M.; Álvarez Izazaga, M. A.; Ledesma Solano, J. Á.; Pedraza Chaverri, J. Antioxidant activity and protection against oxidative-induced damage of *Acacia shaffneri* and *Acacia farnesiana* pods extracts: in vitro and in vivo assays. *BMC Complementary and Alternative Medicine* **2015**, *15*, 1-8.
- (51) Berg, L. JM; Tymoczko, JL; Stryer, Biochemistry 5th ed., 5th editio. *New York* **2002**.
- (52) Baron, A. D. Postprandial hyperglycaemia and α -glucosidase inhibitors. *Diabetes Research and Clinical Practice* **1998**, *40*, S51-S55.
- (53) Mitrakou, A.; Kelley, D.; Veneman, T.; Jenssen, T.; Pangburn, T.; Reilly, J.; Gerich, J. Contribution of abnormal muscle and liver glucose metabolism to postprandial hyperglycemia in NIDDM. *Diabetes* **1990**, *39* (11), 1381-1390.

- (54) Leiter, L. A.; Ceriello, A.; Davidson, J. A.; Hanefeld, M.; Monnier, L.; Owens, D. R.; Tajima, N.; Tuomilehto, J.; Group, I. G. R. P. S. Postprandial glucose regulation: New data and new implications. *Clinical therapeutics* **2005**, *27*, S42-S56.
- (55) Pratley, R.; Weyer, C. The role of impaired early insulin secretion in the pathogenesis of type II diabetes mellitus. *Diabetologia* **2001**, *44* (8), 929-945.
- (56) Bock, G.; Dalla Man, C.; Campioni, M.; Chittilapilly, E.; Basu, R.; Toffolo, G.; Cobelli, C.; Rizza, R. Pathogenesis of pre-diabetes: mechanisms of fasting and postprandial hyperglycemia in people with impaired fasting glucose and/or impaired glucose tolerance. *Diabetes* **2006**, *55* (12), 3536-3549.
- (57) Ceriello, A.; Colagiuri, S.; Gerich, J.; Tuomilehto, J. Guideline for management of postmeal glucose. *Nutrition, Metabolism and Cardiovascular Diseases* **2008**, *18* (4), S17-S33.
- (58) Yki-Järvinen, H. Glucose toxicity. *Endocrine Reviews* **1992**, *13* (3), 415-431.
- (59) Robertson, R. P.; Gavareski, D. J.; Porte, D.; Bierman, E. L. Inhibition of in vivo insulin secretion by prostaglandin E 1. *The Journal of clinical investigation* **1974**, *54* (2), 310-315.
- (60) Metz, S. A.; Robertson, R. P.; Fujimoto, W. Y. Inhibition of prostaglandin E synthesis augments glucose-induced insulin secretion in cultured pancreas. *Diabetes* **1981**, *30* (7), 551-557.
- (61) Giugliano, D.; Di Pinto, P.; Torella, R.; Frascolla, N.; Saccomanno, F.; Passariello, N.; D'Onofrio, F. A role for endogenous prostaglandin E in biphasic pattern of insulin release in humans. *American Journal of Physiology-Endocrinology and Metabolism* **1983**, *245* (6), E591-E597.
- (62) Baron, A. D.; Laakso, M.; Brechtel, G.; Edelman, S. V. Mechanism of insulin resistance in insulin-dependent diabetes mellitus: a major role for reduced skeletal muscle blood flow. *The Journal of Clinical Endocrinology & Metabolism* **1991**, *73* (3), 637-643.
- (63) Dimitriadis, G.; Lambadiari, V.; Mitrou, P.; Maratou, E.; Boutati, E.; Panagiotakos, D. B.; Economopoulos, T.; Raptis, S. A. Impaired postprandial blood flow in adipose tissue may be an early marker of insulin resistance in type 2 diabetes. *Diabetes Care* **2007**, *30* (12), 3128-3130.
- (64) Bohlen, H.; Niggli, B. Arteriolar anatomical and functional abnormalities in juvenile mice with genetic or streptozotocin-induced diabetes mellitus. *Circulation research* **1979**, *45* (3), 390-396.
- (65) Baron, A.; Brechtel, G.; Wallace, P.; Edelman, S. Rates and tissue sites of non-insulin- and insulin-mediated glucose uptake in humans. *American Journal of Physiology-Endocrinology And Metabolism* **1988**, *255* (6), E769-E774.
- (66) Sies, H.; Stahl, W.; Sevanian, A. Nutritional, dietary and postprandial oxidative stress. *The Journal of nutrition* **2005**, *135* (5), 969-972.
- (67) Victor, V. M.; Rocha, M.; Sola, E.; Banuls, C.; Garcia-Malpartida, K.; Hernandez-Mijares, A. Oxidative stress, endothelial dysfunction and atherosclerosis. *Current pharmaceutical design* **2009**, *15* (26), 2988-3002.
- (68) Förstermann, U. Endothelial NO synthase as a source of NO and superoxide. *European Journal of Clinical Pharmacology* **2006**, *62* (1), 5-12.
- (69) Lebovitz, H. E. Effect of the postprandial state on nontraditional risk factors. *The American journal of cardiology* **2001**, *88* (6), 20-25.
- (70) Taslimi, P.; Aslan, H. E.; Demir, Y.; Oztaskin, N.; Maraş, A.; Gulçin, İ.; Beydemir, S.; Goksu, S. Diarylmethanon, bromophenol and diarylmethane compounds: Discovery of potent aldose reductase, α -amylase and α -glycosidase inhibitors as new therapeutic approach in diabetes and functional hyperglycemia. *International journal of biological macromolecules* **2018**, *119*, 857-863.

- (71) Dhameja, M.; Gupta, P. Synthetic heterocyclic candidates as promising α -glucosidase inhibitors: An overview. *European journal of medicinal chemistry* **2019**, *176*, 343-377.
- (72) Jang, J. H.; Park, J. E.; Han, J. S. Scopoletin increases glucose uptake through activation of PI3K and AMPK signaling pathway and improves insulin sensitivity in 3T3-L1 cells. *Nutrition Research* **2020**, *74*, 52-61.
- (73) Lee, J. H.; Park, J. E.; Han, J. S. Fucoidan Stimulates Glucose Uptake via the PI3K/AMPK Pathway and Increases Insulin Sensitivity in 3T3-L1 Adipocytes. *Journal of Life Science* **2021**, *31* (1), 1-9.
- (74) Schultze, S. M.; Hemmings, B. A.; Niessen, M.; Tschopp, O. PI3K/AKT, MAPK and AMPK signalling: protein kinases in glucose homeostasis. *Expert reviews in molecular medicine* **2012**, *14*.
- (75) Ogihara, T.; Asano, T.; Katagiri, H.; Sakoda, H.; Anai, M.; Shojima, N.; Ono, H.; Fujishiro, M.; Kushiyama, A.; Fukushima, Y. Oxidative stress induces insulin resistance by activating the nuclear factor- κ B pathway and disrupting normal subcellular distribution of phosphatidylinositol 3-kinase. *Diabetologia* **2004**, *47* (5), 794-805.
- (76) Gao, C. L., Zhu, C., Zhao, Y.P., Chen, X.H., Ji, C.B., Zhang, C.M., Zhu, J.G., Xia, Z.K., Tong, M.L., and Guo, X.R. Mitochondrial dysfunction is induced by high levels of glucose and free fatty acids in 3T3-L1 adipocytes. *Molecular and cellular endocrinology* **2010**, *320* (1-2), 25-33.
- (77) Fazakerley, D. J.; Minard, A. Y.; Krycer, J. R.; Thomas, K. C.; Stöckli, J.; Harney, D. J.; Burchfield, J. G.; Maghzal, G. J.; Caldwell, S. T.; Hartley, R. C. Mitochondrial oxidative stress causes insulin resistance without disrupting oxidative phosphorylation. *Journal of Biological Chemistry* **2018**, *293* (19), 7315-7328.
- (78) Pessler, D.; Rudich, A.; Bashan, N. Oxidative stress impairs nuclear proteins binding to the insulin responsive element in the GLUT4 promoter. *Diabetologia* **2001**, *44* (12), 2156-2164.
- (79) Nishikawa, T.; Kukidome, D.; Sonoda, K.; Fujisawa, K.; Matsuhisa, T.; Motoshima, H.; Matsumura, T.; Araki, E. Impact of mitochondrial ROS production in the pathogenesis of insulin resistance. *Diabetes research and clinical practice* **2007**, *77* (3), S161-S164.
- (80) Nishikawa, T.; Araki, E. Impact of mitochondrial ROS production in the pathogenesis of diabetes mellitus and its complications. *Antioxidants & redox signaling* **2007**, *9* (3), 343-353.
- (81) Choi, Y. M. K., H.K., Shim, W., Anwar, M.A., Kwon, J.W., Kwon, H.K., Kim, H.J., Jeong, H., Kim, H.M., and Hwang, D. Mechanism of cisplatin-induced cytotoxicity is correlated to impaired metabolism due to mitochondrial ROS generation. *PloS one* **2015**, *10* (8), e0135083.
- (82) Kukidome, D.; Nishikawa, T.; Sonoda, K.; Imoto, K.; Fujisawa, K.; Yano, M.; Motoshima, H.; Taguchi, T.; Matsumura, T.; Araki, E. Activation of AMP-activated protein kinase reduces hyperglycemia-induced mitochondrial reactive oxygen species production and promotes mitochondrial biogenesis in human umbilical vein endothelial cells. *Diabetes* **2006**, *55* (1), 120-127.
- (83) Fujisawa, K.; Nishikawa, T.; Kukidome, D.; Imoto, K.; Yamashiro, T.; Motoshima, H.; Matsumura, T.; Araki, E. TZDs reduce mitochondrial ROS production and enhance mitochondrial biogenesis. *Biochemical and biophysical research communications* **2009**, *379* (1), 43-48.
- (84) Vial, G.; Demaille, D.; Guigas, B. Role of mitochondria in the mechanism (s) of action of metformin. *Frontiers in endocrinology* **2019**, *10*, 294.
- (85) Carling, D. The AMP-activated protein kinase cascade—a unifying system for energy control. *Trends in biochemical sciences* **2004**, *29* (1), 18-24.

- (86) Rena, G.; Hardie, D. G.; Pearson, E. R. The mechanisms of action of metformin. *Diabetologia* **2017**, *60* (9), 1577-1585.
- (87) Van Leeuwen, N.; Nijpels, G.; Becker, M.; Deshmukh, H.; Zhou, K.; Stricker, B.; Uitterlinden, A.; Hofman, A.; van't Riet, E.; Palmer, C. A gene variant near ATM is significantly associated with metformin treatment response in type 2 diabetes: a replication and meta-analysis of five cohorts. *Diabetologia* **2012**, *55*, 1971-1977.
- (88) Nathan, D.; Buse, J.; Davidson, M.; Ferrannini, E.; Holman, R. R.; Sherwin, R.; Zinman, B. Medical management of hyperglycaemia in type 2 diabetes mellitus: a consensus algorithm for the initiation and adjustment of therapy: a consensus statement from the American Diabetes Association and the European Association for the Study of Diabetes. *Diabetologia* **2009**, *52*, 17-30.
- (89) Priyanka, A.; Nisha, V.; Anusree, S.; Raghu, K. Bilobalide attenuates hypoxia induced oxidative stress, inflammation, and mitochondrial dysfunctions in 3T3-L1 adipocytes via its antioxidant potential. *Free Radical Research* **2014**, *48* (10), 1206-1217.
- (90) Kim, T. Y.; Leem, E.; Lee, J. M.; Kim, S. R. Control of reactive oxygen species for the prevention of Parkinson's disease: the possible application of flavonoids. *Antioxidants* **2020**, *9* (7), 583.
- (91) Kim, Y.-R.; Kim, M.-A.; Cho, H.-J.; Oh, S.-K.; Lee, I.-K.; Kim, U.-K.; Lee, K.-Y. Galangin prevents aminoglycoside-induced ototoxicity by decreasing mitochondrial production of reactive oxygen species in mouse cochlear cultures. *Toxicology Letters* **2016**, *245*, 78-85.
- (92) Dragicevic, N.; Smith, A.; Lin, X.; Yuan, F.; Copes, N.; Delic, V.; Tan, J.; Cao, C.; Shytle, R. D.; Bradshaw, P. C. Green tea epigallocatechin-3-gallate (EGCG) and other flavonoids reduce Alzheimer's amyloid-induced mitochondrial dysfunction. *Journal of Alzheimer's Disease* **2011**, *26* (3), 507-521.
- (93) Naoi, M.; Maruyama, W.; Shamoto-Nagai, M. Disease-modifying treatment of Parkinson's disease by phytochemicals: Targeting multiple pathogenic factors. *Journal of Neural Transmission* **2022**, 1-17.
- (94) Rebollo-Hernanz, M.; Zhang, Q.; Aguilera, Y.; Martín-Cabrejas, M. A.; de Mejia, E. G. Phenolic compounds from coffee by-products modulate adipogenesis-related inflammation, mitochondrial dysfunction, and insulin resistance in adipocytes, via insulin/PI3K/AKT signaling pathways. *Food and Chemical Toxicology* **2019**, *132*, 110672.
- (95) Kim, J.; Yang, G.; Kim, Y.; Kim, J.; Ha, J. AMPK activators: mechanisms of action and physiological activities. *Experimental & molecular medicine* **2016**, *48* (4), e224-e224.
- (96) Frøsig, C.; Pehmøller, C.; Birk, J. B.; Richter, E. A.; Wojtaszewski, J. F. Exercise-induced TBC1D1 Ser237 phosphorylation and 14-3-3 protein binding capacity in human skeletal muscle. *The Journal of physiology* **2010**, *588* (22), 4539-4548.
- (97) Merrill, G. F.; Kurth, E. J.; Hardie, D.; Winder, W. AICA riboside increases AMP-activated protein kinase, fatty acid oxidation, and glucose uptake in rat muscle. *American Journal of Physiology-Endocrinology And Metabolism* **1997**, *273* (6), E1107-E1112.
- (98) Lin, H.-Y.; Weng, S.-W.; Chang, Y.-H.; Su, Y.-J.; Chang, C.-M.; Tsai, C.-J.; Shen, F.-C.; Chuang, J.-H.; Lin, T.-K.; Liou, C.-W. The causal role of mitochondrial dynamics in regulating insulin resistance in diabetes: link through mitochondrial reactive oxygen species. *Oxidative Medicine and Cellular Longevity* **2018**, 2018.
- (99) Yin, X.; Lanza, I. R.; Swain, J. M.; Sarr, M. G.; Nair, K. S.; Jensen, M. D. Adipocyte mitochondrial function is reduced in human obesity independent of

- fat cell size. *The Journal of Clinical Endocrinology & Metabolism* **2014**, *99* (2), E209-E216.
- (100) Hunter, C. A.; Kartal, F.; Koc, Z. C.; Murphy, T.; Kim, J. H.; Denvir, J.; Koc, E. C. Mitochondrial oxidative phosphorylation is impaired in TALLYHO mice, a new obesity and type 2 diabetes animal model. *The international journal of biochemistry & cell biology* **2019**, *116*, 105616.
- (101) Wu, Z.; Puigserver, P.; Andersson, U.; Zhang, C.; Adelmant, G.; Mootha, V.; Troy, A.; Cinti, S.; Lowell, B.; Scarpulla, R. C. Mechanisms controlling mitochondrial biogenesis and respiration through the thermogenic coactivator PGC-1. *Cell* **1999**, *98* (1), 115-124.
- (102) Skov, V.; Glintborg, D.; Knudsen, S.; Jensen, T.; Kruse, T. A.; Tan, Q.; Brusgaard, K.; Beck-Nielsen, H.; Højlund, K. Reduced expression of nuclear-encoded genes involved in mitochondrial oxidative metabolism in skeletal muscle of insulin-resistant women with polycystic ovary syndrome. *Diabetes* **2007**, *56* (9), 2349-2355.
- (103) Heinonen, S.; Buzkova, J.; Muniandy, M.; Kaksonen, R.; Ollikainen, M.; Ismail, K.; Hakkarainen, A.; Lundbom, J.; Lundbom, N.; Vuolteenaho, K. Impaired mitochondrial biogenesis in adipose tissue in acquired obesity. *Diabetes* **2015**, *64* (9), 3135-3145.
- (104) Scarpulla, R. C. Nuclear control of respiratory chain expression by nuclear respiratory factors and PGC-1-related coactivator. *Annals of the New York Academy of Sciences* **2008**, *1147* (1), 321-334.
- (105) Feige, J. N.; Auwerx, J. Transcriptional coregulators in the control of energy homeostasis. *Trends in cell biology* **2007**, *17* (6), 292-301.
- (106) Chen, X.-H.; Zhao, Y.-P.; Xue, M.; Ji, C.-B.; Gao, C.-L.; Zhu, J.-G.; Qin, D.-N.; Kou, C.-Z.; Qin, X.-H.; Tong, M.-L. TNF- α induces mitochondrial dysfunction in 3T3-L1 adipocytes. *Molecular and cellular endocrinology* **2010**, *328* (1-2), 63-69.
- (107) Houstis, N.; Rosen, E. D.; Lander, E. S. Reactive oxygen species have a causal role in multiple forms of insulin resistance. *Nature* **2006**, *440* (7086), 944-948.
- (108) Choo, H.-J.; Kim, J.-H.; Kwon, O.-B.; Lee, C.; Mun, J.; Han, S.; Yoon, Y.-S.; Yoon, G.; Choi, K.-M.; Ko, Y.-G. Mitochondria are impaired in the adipocytes of type 2 diabetic mice. *Diabetologia* **2006**, *49*, 784-791.
- (109) Bournat, J. C.; Brown, C. W. Mitochondrial dysfunction in obesity. *Current opinion in endocrinology, diabetes, and obesity* **2010**, *17* (5), 446.
- (110) Wang, C. H., Wang, C.C., Huang, H.C., and Wei, Y.H. Mitochondrial dysfunction leads to impairment of insulin sensitivity and adiponectin secretion in adipocytes. *The FEBS journal* **2013**, *280* (4), 1039-1050.
- (111) Jäger, S.; Handschin, C.; St.-Pierre, J.; Spiegelman, B. M. AMP-activated protein kinase (AMPK) action in skeletal muscle via direct phosphorylation of PGC-1 α . *Proceedings of the National Academy of Sciences* **2007**, *104* (29), 12017-12022.
- (112) Iwabu, M.; Yamauchi, T.; Okada-Iwabu, M.; Sato, K.; Nakagawa, T.; Funata, M.; Yamaguchi, M.; Namiki, S.; Nakayama, R.; Tabata, M. Adiponectin and AdipoR1 regulate PGC-1 α and mitochondria by Ca²⁺ and AMPK/SIRT1. *Nature* **2010**, *464* (7293), 1313-1319.
- (113) Yan, W.; Zhang, H.; Liu, P.; Wang, H.; Liu, J.; Gao, C.; Liu, Y.; Lian, K.; Yang, L.; Sun, L. Impaired mitochondrial biogenesis due to dysfunctional adiponectin-AMPK-PGC-1 α signaling contributing to increased vulnerability in diabetic heart. *Basic research in cardiology* **2013**, *108*, 1-15.
- (114) Kusminski, C. M.; Scherer, P. E. Mitochondrial dysfunction in white adipose tissue. *Trends in endocrinology & metabolism* **2012**, *23* (9), 435-443.

- (115) Hawley, S. A.; Ross, F. A.; Chevtzoff, C.; Green, K. A.; Evans, A.; Fogarty, S.; Towler, M. C.; Brown, L. J.; Ogunbayo, O. A.; Evans, A. M. Use of cells expressing γ subunit variants to identify diverse mechanisms of AMPK activation. *Cell metabolism* **2010**, *11* (6), 554-565.
- (116) Suchankova, G.; Nelson, L. E.; Gerhart-Hines, Z.; Kelly, M.; Gauthier, M.-S.; Saha, A. K.; Ido, Y.; Puigserver, P.; Ruderman, N. B. Concurrent regulation of AMP-activated protein kinase and SIRT1 in mammalian cells. *Biochemical and biophysical research communications* **2009**, *378* (4), 836-841.
- (117) Rezvan, N.; Moini, A.; Gorgani-Firuzjaee, S.; Hosseinzadeh-Attar, M. J. Oral quercetin supplementation enhances adiponectin receptor transcript expression in polycystic ovary syndrome patients: a randomized placebo-controlled double-blind clinical trial. *Cell Journal (Yakhteh)* **2018**, *19* (4), 627.
- (118) Zebisch, K.; Voigt, V.; Wabitsch, M.; Brandsch, M. Protocol for effective differentiation of 3T3-L1 cells to adipocytes. *Analytical biochemistry* **2012**, *425* (1), 88-90.
- (119) Ruiz-Ojeda, F. J.; Rupérez, A. I.; Gomez-Llorente, C.; Gil, A.; Aguilera, C. M. Cell models and their application for studying adipogenic differentiation in relation to obesity: a review. *International journal of molecular sciences* **2016**, *17* (7), 1040.
- (120) Gregoire, F. M.; Smas, C. M.; Sul, H. S. Understanding adipocyte differentiation. *Physiological reviews* **1998**, *78* (3), 783-809.
- (121) Green, H.; Kehinde, O. An established preadipose cell line and its differentiation in culture II. Factors affecting the adipose conversion. *Cell* **1975**, *5* (1), 19-27.
- (122) Rubin, C. S.; Hirsch, A.; Fung, C.; Rosen, O. M. Development of hormone receptors and hormonal responsiveness in vitro. Insulin receptors and insulin sensitivity in the preadipocyte and adipocyte forms of 3T3-L1 cells. *Journal of Biological Chemistry* **1978**, *253* (20), 7570-7578.
- (123) Russell, T. R.; Ho, R.-J. Conversion of 3T3 fibroblasts into adipose cells: triggering of differentiation by prostaglandin F₂alpha and 1-methyl-3-isobutyl xanthine. *Proceedings of the National Academy of Sciences* **1976**, *73* (12), 4516-4520.
- (124) Green, H.; Meuth, M. An established pre-adipose cell line and its differentiation in culture. *Cell* **1974**, *3* (2), 127-133.
- (125) Ramirez-Zacarias, J.; Castro-Munozledo, F.; Kuri-Harcuch, W. Quantitation of adipose conversion and triglycerides by staining intracytoplasmic lipids with Oil red O. *Histochemistry* **1992**, *97* (6), 493-497.
- (126) Eriksson, J. W. Metabolic stress in insulin's target cells leads to ROS accumulation—a hypothetical common pathway causing insulin resistance. *FEBS letters* **2007**, *581* (19), 3734-3742.
- (127) Boden, G.; Homko, C.; Barrero, C. A.; Stein, T. P.; Chen, X.; Cheung, P.; Fecchio, C.; Koller, S.; Merali, S. Excessive caloric intake acutely causes oxidative stress, GLUT4 carbonylation, and insulin resistance in healthy men. *Science translational medicine* **2015**, *7* (304), 304re307-304re307.
- (128) Ambrose, M.; Gatti, R. A. Pathogenesis of ataxia-telangiectasia: the next generation of ATM functions. *Blood, The Journal of the American Society of Hematology* **2013**, *121* (20), 4036-4045.
- (129) Kahn, S. E.; Haffner, S. M.; Heise, M. A.; Herman, W. H.; Holman, R. R.; Jones, N. P.; Kravitz, B. G.; Lachin, J. M.; O'Neill, M. C.; Zinman, B. Glycemic durability of rosiglitazone, metformin, or glyburide monotherapy. *New England Journal of Medicine* **2006**, *355* (23), 2427-2443.
- (130) Matthaei, S.; Bierwirth, R.; Fritsche, A.; Gallwitz, B.; Haering, H.-U.; Joost, H.-G.; Kellerer, M.; Kloos, C.; Kunt, T.; Nauck, M. Medical antihyperglycaemic

- treatment of type 2 diabetes mellitus. *Experimental and clinical endocrinology & diabetes* **2009**, *117* (09), 522-557.
- (131) Viollet, B.; Guigas, B.; Garcia, N. S.; Leclerc, J.; Foretz, M.; Andreelli, F. Cellular and molecular mechanisms of metformin: an overview. *Clinical science* **2012**, *122* (6), 253-270.
- (132) Petrie, J. R.; Guzik, T. J.; Touyz, R. M. Diabetes, hypertension, and cardiovascular disease: clinical insights and vascular mechanisms. *Canadian Journal of Cardiology* **2018**, *34* (5), 575-584.
- (133) Ahrén, B. Creative use of novel glucose-lowering drugs for type 2 diabetes: where will we head in the next 50 years? *Diabetologia* **2015**, *58* (8), 1740-1744.
- (134) Brown, E.; Rajeev, S. P.; Cuthbertson, D. J.; Wilding, J. P. A review of the mechanism of action, metabolic profile and haemodynamic effects of sodium-glucose co-transporter-2 inhibitors. *Diabetes, Obesity and Metabolism* **2019**, *21*, 9-18.
- (135) Rasalam, R.; Barlow, J.; Kennedy, M.; Phillips, P.; Wright, A. GLP-1 Receptor Agonists for Type 2 Diabetes and Their Role in Primary Care: An Australian Perspective. *Diabetes Therapy* **2019**, 1-13.
- (136) Bailey, C. The current drug treatment landscape for diabetes and perspectives for the future. *Clinical Pharmacology & Therapeutics* **2015**, *98* (2), 170-184.
- (137) Inzucchi, S. E.; Bergenstal, R. M.; Buse, J. B.; Diamant, M.; Ferrannini, E.; Nauck, M.; Peters, A. L.; Tsapas, A.; Wender, R.; Matthews, D. R. Management of hyperglycemia in type 2 diabetes, 2015: a patient-centered approach: update to a position statement of the American Diabetes Association and the European Association for the Study of Diabetes. *Diabetes care* **2015**, *38* (1), 140-149.
- (138) Tahrani, A. A.; Barnett, A. H.; Bailey, C. J. Pharmacology and therapeutic implications of current drugs for type 2 diabetes mellitus. *Nature Reviews Endocrinology* **2016**, *12* (10), 566.
- (139) Christensen, K. B.; Petersen, R. K.; Petersen, S.; Kristiansen, K.; Christensen, L. P. Activation of PPAR γ by metabolites from the flowers of purple coneflower (*Echinacea purpurea*). *Journal of natural products* **2009**, *72* (5), 933-937.
- (140) Puhl, A. C.; Bernardes, A.; Silveira, R. L.; Yuan, J.; Campos, J. L.; Saidenberg, D. M.; Palma, M. S.; Cvorovic, A.; Ayers, S. D.; Webb, P. Mode of peroxisome proliferator-activated receptor γ activation by luteolin. *Molecular pharmacology* **2012**, *81* (6), 788-799.
- (141) Sasikumar, P.; Prabha, B.; Reshmitha, T.; Veluthoor, S.; Pradeep, A.; Rohit, K.; Dhanya, B.; Sivan, V.; Jithin, M.; Kumar, N. A. Comparison of antidiabetic potential of (+) and (-)-hopeaphenol, a pair of enantiomers isolated from *Ampelocissus indica* (L.) and *Vateria indica* Linn., with respect to inhibition of digestive enzymes and induction of glucose uptake in L6 myotubes. *RSC advances* **2016**, *6* (80), 77075-77082.
- (142) Sohn, E. J.; Kim, C.-S.; Kim, Y. S.; Jung, D. H.; Jang, D. S.; Lee, Y. M.; Kim, J. S. Effects of magnolol (5, 5'-diallyl-2, 2'-dihydroxybiphenyl) on diabetic nephropathy in type 2 diabetic Goto-Kakizaki rats. *Life sciences* **2007**, *80* (5), 468-475.
- (143) Kawser Hossain, M.; Abdal Dayem, A.; Han, J.; Yin, Y.; Kim, K.; Kumar Saha, S.; Yang, G.-M.; Choi, H. Y.; Cho, S.-G. Molecular mechanisms of the anti-obesity and anti-diabetic properties of flavonoids. *International journal of molecular sciences* **2016**, *17* (4), 569.
- (144) Zhang, B.-w.; Li, X.; Sun, W.-l.; Xing, Y.; Xiu, Z.-l.; Zhuang, C.-l.; Dong, Y.-s. Dietary flavonoids and acarbose synergistically inhibit α -glucosidase and lower postprandial blood glucose. *Journal of agricultural and food chemistry* **2017**, *65* (38), 8319-8330.

- (145) Cazarolli, L. H.; Zanatta, L.; Alberton, E. H.; Figueiredo, R. B.; Santos, M.; Folador, P.; Damazio, R. G.; Pizzolatti, M. G.; Mena Barreto Silva, F. R. Flavonoids: cellular and molecular mechanism of action in glucose homeostasis. *Mini reviews in medicinal chemistry* **2008**, *8* (10), 1032-1038.
- (146) Jo, S.; Ka, E.; Lee, H. Comparison of antioxidant potential and rat intestinal α -glucosidases inhibitory activities of quercetin, rutin, and isoquercetin. **2009**.
- (147) Dhanya, R.; Arya, A.; Nisha, P.; Jayamurthy, P. Quercetin, a lead compound against type 2 diabetes ameliorates glucose uptake via AMPK pathway in skeletal muscle cell line. *Frontiers in Pharmacology* **2017**, *8*, 336.
- (148) Pinent, M.; Blay, M.; Blade, M.; Salvado, M.; Arola, L.; Ardevol, A. Grape seed-derived procyanidins have an antihyperglycemic effect in streptozotocin-induced diabetic rats and insulinomimetic activity in insulin-sensitive cell lines. *Endocrinology* **2004**, *145* (11), 4985-4990.
- (149) Arumugam, B.; Palanisamy, U. D.; Chua, K. H.; Kuppusamy, U. R. Potential antihyperglycaemic effect of myricetin derivatives from *Syzygium malaccense*. *Journal of functional foods* **2016**, *22*, 325-336.
- (150) Dua, T. K.; Joardar, S.; Chakraborty, P.; Bhowmick, S.; Saha, A.; De Feo, V.; Dewanjee, S. Myricitrin, a glycosyloxyflavone in *Myrica esculenta* bark ameliorates diabetic nephropathy via improving glycemic status, reducing oxidative stress, and suppressing inflammation. *Molecules* **2021**, *26* (2), 258.
- (151) Gao, J.; Chen, S.; Qiu, Z.; Fang, L.; Zhang, L.; Guo, C.; Chen, T.; Qiu, L. Myricitrin ameliorates ethanol-induced steatosis in mouse AML12 liver cells by activating AMPK, and reducing oxidative stress and expression of inflammatory cytokines. *Molecular medicine reports* **2018**, *17* (5), 7381-7387.
- (152) He, C.; Liu, X.; Jiang, Z.; Geng, S.; Ma, H.; Liu, B. Interaction Mechanism of Flavonoids and α -Glucosidase: Experimental and Molecular Modelling Studies. *Foods* **2019**, *8* (9), 355.
- (153) Zygumt, K.; Faubert, B.; MacNeil, J.; Tsiani, E. Naringenin, a citrus flavonoid, increases muscle cell glucose uptake via AMPK. *Biochemical and biophysical research communications* **2010**, *398* (2), 178-183.
- (154) Yang, J.-Y.; Della-Fera, M. A.; Rayalam, S.; Ambati, S.; Hartzell, D. L.; Park, H. J.; Baile, C. A. Enhanced inhibition of adipogenesis and induction of apoptosis in 3T3-L1 adipocytes with combinations of resveratrol and quercetin. *Life Sciences* **2008**, *82* (19-20), 1032-1039.
- (155) Peng, X.; Zhang, G.; Liao, Y.; Gong, D. Inhibitory kinetics and mechanism of kaempferol on α -glucosidase. *Food chemistry* **2016**, *190*, 207-215.
- (156) Zhang, Y.; Zhen, W.; Maechler, P.; Liu, D. Small molecule kaempferol modulates PDX-1 protein expression and subsequently promotes pancreatic β -cell survival and function via CREB. *The Journal of nutritional biochemistry* **2013**, *24* (4), 638-646.
- (157) Matsui, T.; Tanaka, T.; Tamura, S.; Toshima, A.; Tamaya, K.; Miyata, Y.; Tanaka, K.; Matsumoto, K. α -Glucosidase inhibitory profile of catechins and theaflavins. *Journal of Agricultural and Food Chemistry* **2007**, *55* (1), 99-105.
- (158) Daisy, P.; Balasubramanian, K.; Rajalakshmi, M.; Eliza, J.; Selvaraj, J. Insulin mimetic impact of Catechin isolated from *Cassia fistula* on the glucose oxidation and molecular mechanisms of glucose uptake on Streptozotocin-induced diabetic Wistar rats. *Phytomedicine* **2010**, *17* (1), 28-36.
- (159) He, J.-H.; Chen, L.-X.; Li, H. Progress in the discovery of naturally occurring anti-diabetic drugs and in the identification of their molecular targets. *Fitoterapia* **2019**.
- (160) Kandasamy, N.; Ashokkumar, N. Protective effect of bioflavonoid myricetin enhances carbohydrate metabolic enzymes and insulin signaling molecules in

- streptozotocin–cadmium induced diabetic nephrotoxic rats. *Toxicology and applied pharmacology* **2014**, 279 (2), 173-185.
- (161) Proença, C.; Freitas, M.; Ribeiro, D.; Oliveira, E. F.; Sousa, J. L.; Tomé, S. M.; Ramos, M. J.; Silva, A. M.; Fernandes, P. A.; Fernandes, E. α -Glucosidase inhibition by flavonoids: an in vitro and in silico structure–activity relationship study. *Journal of enzyme inhibition and medicinal chemistry* **2017**, 32 (1), 1216-1228.
- (162) Chai, W.; Ou-Yang, C.; Ma, Z.; Song, S.; Huang, Q.; Wei, Q.; Peng, Y. Anti- α -glucosidase and antityrosinase activity of condensed tannins from the bark of *Clausena lansium* (Lour.) Skeels with antiproliferative and apoptotic properties in B16 mouse melanoma cells. *Process Biochemistry* **2019**, 86, 205-214.
- (163) Ernawati, T.; Radji, M.; Hanafi, M.; Mun'im, A.; Yanuar, A. Cinnamic Acid Derivatives as α -Glucosidase Inhibitor Agents. *Indonesian Journal of Chemistry* **2017**, 17 (1), 151-160.
- (164) Prabhakar, P. K.; Doble, M. Interaction of cinnamic acid derivatives with commercial hypoglycemic drugs on 2-deoxyglucose uptake in 3T3-L1 adipocytes. *Journal of agricultural and food chemistry* **2011**, 59 (18), 9835-9844.
- (165) Zheng, Y.; Liu, K.; Jia, G.; Li, H.; Han, L.; Kimura, Y. Effect of hot-water extract of coffee seeds on postprandial blood glucose concentration in rats. **2007**.
- (166) Ong, K. W.; Hsu, A.; Tan, B. K. H. Chlorogenic acid stimulates glucose transport in skeletal muscle via AMPK activation: a contributor to the beneficial effects of coffee on diabetes. *PLoS one* **2012**, 7 (3).
- (167) Oboh, G.; Agunloye, O. M.; Adefegha, S. A.; Akinyemi, A. J.; Ademiluyi, A. O. Caffeic and chlorogenic acids inhibit key enzymes linked to type 2 diabetes (in vitro): a comparative study. *Journal of Basic and Clinical Physiology and Pharmacology* **2015**, 26 (2), 165-170.
- (168) Huang, D.-W.; Shen, S.-C.; Wu, J. S.-B. Effects of caffeic acid and cinnamic acid on glucose uptake in insulin-resistant mouse hepatocytes. *Journal of agricultural and food chemistry* **2009**, 57 (17), 7687-7692.
- (169) Megawati; Darmawan, A.; Fajriah, S.; Primahana, G.; Dewi, R. T.; Minarti; Meiliawati, L. Antioxidant and α -glucosidase activities of benzoic acid derivate from the bark of *Myristica fatua* Houtt. In *AIP Conference Proceedings*, 2017; AIP Publishing LLC: Vol. 1904, p 020027.
- (170) Vinayagam, R.; Xu, B. Antidiabetic properties of dietary flavonoids: a cellular mechanism review. *Nutrition & metabolism* **2015**, 12 (1), 60.
- (171) Khangholi, S.; Majid, F. A. A.; Berwary, N. J. A.; Ahmad, F.; Abd Aziz, R. B. The mechanisms of inhibition of advanced glycation end products formation through polyphenols in hyperglycemic condition. *Planta medica* **2016**, 82 (01/02), 32-45.
- (172) Gulati, V. Investigation of traditional Australian Aboriginal and Indian Ayurvedic medicinal plants for their role in management of type 2 diabetes. **2013**.
- (173) Subhan, N. Phytochemical and pharmacological investigations of Australian Acacia: An ethnomedicine-guided bioprospective approach. *Doctor of Philosophy Charles Sturt University* **2016**.
- (174) Bai, N.; He, K.; Roller, M.; Zheng, B.; Chen, X.; Shao, Z.; Peng, T.; Zheng, Q. Active compounds from *Lagerstroemia speciosa*, insulin-like glucose uptake-stimulatory/inhibitory and adipocyte differentiation-inhibitory activities in 3T3-L1 cells. *Journal of agricultural and food chemistry* **2008**, 56 (24), 11668-11674.
- (175) Bharti, S. K.; Krishnan, S.; Kumar, A.; Kumar, A. Antidiabetic phytoconstituents and their mode of action on metabolic pathways. *Therapeutic Advances in Endocrinology and metabolism* **2018**, 9 (3), 81-100.
- (176) Kar, A.; Choudhary, B.; Bandyopadhyay, N. Comparative evaluation of hypoglycaemic activity of some Indian medicinal plants in alloxan diabetic rats. *Journal of ethnopharmacology* **2003**, 84 (1), 105-108.

- (177) Patel, D.; Prasad, S. K.; Kumar, R.; Hemalatha, S. An overview on antidiabetic medicinal plants having insulin mimetic property. *Asian Pacific journal of tropical biomedicine* **2012**, *2* (4), 320-330.
- (178) Wickens, K.; Pennacchio, M. A search for novel biologically active compounds in the phyllodes of Acacia species. *Conservation Science Western Australia* **2002**, *4* (3), 139-144.
- (179) Cock, I. E. Medicinal and aromatic plants—Australia. *Ethnopharmacology section, Biological, Physiological and Health Sciences, Encyclopedia of Life Support Systems (EOLSS)* **2011**.
- (180) Williams, C. *Medicinal Plants in Australia Volume 2: Gums, Resins, Tannin and Essential Oils*; Rosenberg Publishing, 2011.
- (181) Saini, M. L.; Saini, R.; Roy, S.; Kumar, A. Comparative pharmacognostical and antimicrobial studies of Acacia species (Mimosaceae). *Journal of Medicinal Plants Research* **2008**, *2* (12), 378-386.
- (182) Gulati, V.; Harding, I. H.; Palombo, E. A. Enzyme inhibitory and antioxidant activities of traditional medicinal plants: potential application in the management of hyperglycemia. *Bmc complementary and alternative medicine* **2012**, *12* (1), 77.
- (183) Jæger, D.; Ndi, C. P.; Crocoll, C.; Simpson, B. S.; Khakimov, B.; Guzman-Genuino, R. M.; Hayball, J. D.; Xing, X.; Bulone, V.; Weinstein, P. Isolation and structural characterization of echinocystic acid triterpenoid saponins from the Australian medicinal and food plant *Acacia ligulata*. *Journal of natural products* **2017**, *80* (10), 2692-2698.
- (184) Gulati, V.; Gulati, P.; Harding, I. H.; Palombo, E. A. Exploring the anti-diabetic potential of Australian Aboriginal and Indian Ayurvedic plant extracts using cell-based assays. *BMC complementary and alternative medicine* **2015**, *15* (1), 8.
- (185) Ikarashi, N.; Toda, T.; Okaniwa, T.; Ito, K.; Ochiai, W.; Sugiyama, K. Anti-obesity and anti-diabetic effects of acacia polyphenol in obese diabetic KKAy mice fed high-fat diet. *Evidence-Based Complementary and Alternative Medicine* **2011**, 2011.
- (186) Imperato, F. A new chalcone glucoside and isosalipurposide from *Acacia cyanophylla*. *Phytochemistry (UK)* **1978**.
- (187) Al-Huqail, A. A.; Behiry, S. I.; Salem, M. Z.; Ali, H. M.; Siddiqui, M. H.; Salem, A. Z. Antifungal, antibacterial, and antioxidant activities of *Acacia saligna* (Labill.) HL Wendl. flower extract: HPLC analysis of phenolic and flavonoid compounds. *Molecules* **2019**, *24* (4), 700.
- (188) Ghribia, L.; Ghouilaa, H.; Omrib, A.; Besbesb, M.; Janneta, H. B. Antioxidant and anti-acetylcholinesterase activities of extracts and secondary metabolites from *Acacia cyanophylla*. *Asian Pacific journal of tropical biomedicine* **2014**, *4*, S417-S423.
- (189) El Sissi, H.; El Sherbeiny, A. The flavanoid components of the leaves of *Acacia saligna*. *Qualitas Plantarum et Materiae Vegetabiles* **1967**, *14* (3), 257-266.
- (190) El-Toumy, S. A.; Salib, J.; Mohamed, W.; Morsy, F. Phytochemical and antimicrobial studies on *Acacia saligna* leaves. *Egypt J Chem* **2010**, *53*, 705-717.
- (191) Gumgumjee, N.; Hajar, A. Antimicrobial efficacy of *Acacia saligna* (Labill.) HL Wendl. and *Cordia sinensis* Lam. leaves extracts against some pathogenic microorganisms. *Int. J. Microbiol. Immunol. Res* **2015**, *3*, 51-57.
- (192) El Ayeb-Zakhama, A.; Sakka-Rouis, L.; Bergaoui, A.; Flamini, G.; Ben Jannet, H.; Harzallah-Skhiri, F. Chemical composition and allelopathic potential of essential oils obtained from *Acacia cyanophylla* Lindl. cultivated in Tunisia. *Chemistry & biodiversity* **2015**, *12* (4), 615-626.

- (193) Sadiq, M. B.; Hanpithakpong, W.; Tarning, J.; Anal, A. K. Screening of phytochemicals and in vitro evaluation of antibacterial and antioxidant activities of leaves, pods and bark extracts of *Acacia nilotica* (L.) Del. *Industrial Crops and Products* **2015**, *77*, 873-882.
- (194) Tung, Y.-T.; Wu, J.-H.; Huang, C.-Y.; Kuo, Y.-H.; Chang, S.-T. Antioxidant activities and phytochemical characteristics of extracts from *Acacia confusa* bark. *Bioresource technology* **2009**, *100* (1), 509-514.
- (195) Wei, S.-D.; Zhou, H.-C.; Lin, Y.-M.; Liao, M.-M.; Chai, W.-M. MALDI-TOF MS analysis of condensed tannins with potent antioxidant activity from the leaf, stem bark and root bark of *Acacia confusa*. *Molecules* **2010**, *15* (6), 4369-4381.
- (196) Gedara, S. R.; Galala, A. A. New cytotoxic spirostane saponin and biflavonoid glycoside from the leaves of *Acacia saligna* (Labill.) HL Wendl. *Natural product research* **2014**, *28* (5), 324-329.
- (197) Buttner, D. H.; Reddy, S.; Koekemoer, T.; van de Venter, M. An in vitro assessment of the potential antidiabetic activity and cytotoxic effects of ethanolic and aqueous extracts from three invasive Australian acacias. *South African Journal of Botany* **2021**, *141*, 1-11.
- (198) Maslin, B. R. Studies in the genus *Acacia* 3: The taxonomy of *A. saligna* (Labill.) H. Wendl. *Nuytsia* **1974**, *1*, 332-340.
- (199) Orchard, A. E. *Flora of Australia*; Csiro, 2001.
- (200) Maslin, B. Understanding *Acacia saligna*. *Wattle We Eat for Dinner* **2011**, *16*, 18.
- (201) Millar, M. A. *Acacia saligna* as a sustainable agroforestry crop for southern Australia: a genetic assessment. 2008.
- (202) Muylt, A. *Bush Invaders of South-East Australia: A guide to the identification and control of environmental weeds found in south-east Australia*; RG and FJ Richardson, 2001.
- (203) Doran, J. C.; Turnbull, J. W. Australian trees and shrubs: species for land rehabilitation and farm planting. **1997**.
- (204) Muslin, B.; Mc Donald, M. *Evaluation of Acacia as a woody crop option for Southern Australia*; Report, 2004.
- (205) Millar, M.; Byrne, M.; O'Sullivan, W. Corrigendum to: Defining entities in the *Acacia saligna* (Fabaceae) species complex using a population genetics approach. *Australian Journal of Botany* **2011**, *59* (5), 507-507.
- (206) George, N.; Byrne, M.; Maslin, B.; Yan, G. Genetic differentiation among morphological variants of *Acacia saligna* (Mimosaceae). *Tree Genetics & Genomes* **2006**, *2*, 109-119.
- (207) Millar, M.; Mezgebe, K.; Hagazi, N.; Cunningham, P.; Byrne, M. Genetic assignment, diversity, and divergence of naturalised *Acacia saligna* (Fabaceae) in Tigray, Ethiopia. *Tree Genetics & Genomes* **2020**, *16*, 1-11.
- (208) Thompson, G. D.; Bellstedt, D. U.; Richardson, D. M.; Wilson, J. R.; Le Roux, J. J. A tree well travelled: global genetic structure of the invasive tree *Acacia saligna*. *Journal of Biogeography* **2015**, *42* (2), 305-314.
- (209) Thompson, G. D.; Bellstedt, D. U.; Byrne, M.; Millar, M. A.; Richardson, D. M.; Wilson, J. R.; Le Roux, J. J. Cultivation shapes genetic novelty in a globally important invader. *Molecular Ecology* **2012**, *21* (13), 3187-3199.
- (210) Fajraoui, A.; Nasr, J. B.; Lacoste, C.; Amar, M. B.; Dony, P.; Odof, S.; El Halouani, F. Coloration of the polylactic acid with the natural dye extracted from *acacia cyanophylla* flowers. *Polymer Testing* **2019**, *78*, 105988.
- (211) Ghouila, H.; Meksi, N.; Haddar, W.; Mhenni, M.; Jannet, H. B. Extraction, identification and dyeing studies of Isosalipurposide, a natural chalcone dye from *Acacia cyanophylla* flowers on wool. *Industrial Crops and Products* **2012**, *35* (1), 31-36.

- (212) Verma, N.; Shukla, S. Impact of various factors responsible for fluctuation in plant secondary metabolites. *Journal of Applied Research on Medicinal and Aromatic Plants* **2015**, *2* (4), 105-113.
- (213) Ahn, C.-H.; Hossain, M. A.; Lee, E.; Kanth, B. K.; Park, P. B. Increased salt and drought tolerance by D-pinitol production in transgenic *Arabidopsis thaliana*. *Biochemical and biophysical research communications* **2018**, *504* (1), 315-320.
- (214) Chapman, J. M.; Muhlemann, J. K.; Gayomba, S. R.; Muday, G. K. RBOH-dependent ROS synthesis and ROS scavenging by plant specialized metabolites to modulate plant development and stress responses. *Chemical research in toxicology* **2019**, *32* (3), 370-396.
- (215) El-Toumy, S. Flavonoids from *Acacia saligna* leaves and Evaluation of Antihyperglycaemic Effect of Aqueous Extract. *Planta Medica* **2006**, *72* (11), P_004.
- (216) Elansary, H. O., Szopa, A., Kubica, P. Ekiert, H., Al-Mana, F., and Al-Yafsi, M.A. Antioxidant and biological activities of *Acacia saligna* and *Lawsonia inermis* natural populations. *Plants* **2020**, *9* (7), 908.
- (217) Abdelhamid, A.; Lajili, S.; Elkaibi, M. A.; Ben Salem, Y.; Abdelhamid, A.; Muller, C. D.; Majdoub, H.; Kraiem, J.; Bouraoui, A. Optimized extraction, preliminary characterization and evaluation of the in vitro anticancer activity of phlorotannin-rich fraction from the brown seaweed, *Cystoseira sedoides*. *Journal of Aquatic Food Product Technology* **2019**, *28* (9), 892-909.
- (218) Guneidy, R. A.; Amer, M. A.; Hakim, A. E. E.; Abdel-Shafy, S.; Allam, S. A. Effect of polyphenols extracted from *Punica granatum* and *Acacia saligna* plants on glutathione S-transferase of the cattle tick *Rhipicephalus (Boophilus) annulatus* (Acari: Ixodidae). *Journal of Parasitic Diseases* **2021**, *45* (2), 524-538.
- (219) Gumgumjee, N.; Hajar, A. Antimicrobial efficacy of *Acacia saligna* (Labill.) HL Wendl. and *Cordia sinensis* Lam. leaves extracts against some pathogenic microorganisms. *Int. J. Microbiol. Immunol. Res* **2015**, *3* (4), 51-57.
- (220) Almazroui, M.; Nazrul Islam, M.; Athar, H.; Jones, P.; Rahman, M. A. Recent climate change in the Arabian Peninsula: annual rainfall and temperature analysis of Saudi Arabia for 1978–2009. *International Journal of Climatology* **2012**, *32* (6), 953-966.
- (221) Alghamdi, A. G.; Aly, A. A.; Majrashi, M. A.; Ibrahim, H. M. Impact of climate change on hydrochemical properties and quality of groundwater for domestic and irrigation purposes in arid environment: A case study of Al-Baha region, Saudi Arabia. *Environmental Earth Sciences* **2023**, *82* (1), 39.
- (222) Bahnasy, M.; Khamis, M. Distribution pattern of trees diversity in Orman Botanical Garden. *Middle East J. Agric. Res* **2019**, *8*, 1-11.
- (223) Okba, S. K.; Mazrou, Y.; Mikhael, G. B.; Farag, M. E.; Alam-Eldein, S. M. Magnetized Water and Proline to Boost the Growth, Productivity and Fruit Quality of 'Taifi' Pomegranate Subjected to Deficit Irrigation in Saline Clay Soils of Semi-Arid Egypt. *Horticulturae* **2022**, *8* (7), 564.
- (224) Świeca, M. Elicitation with abiotic stresses improves pro-health constituents, antioxidant potential and nutritional quality of lentil sprouts. *Saudi journal of biological sciences* **2015**, *22* (4), 409-416.
- (225) Kiani, R.; Arzani, A.; Mirmohammady Maibody, S. Polyphenols, flavonoids, and antioxidant activity involved in salt tolerance in wheat, *Aegilops cylindrica* and their amphidiploids. *Frontiers in plant science* **2021**, *12*, 646221.
- (226) Salem, M. Z.; Mohamed, A. A.; Ali, H. M.; Al Farraj, D. A. Characterization of Phytoconstituents from Alcoholic Extracts of Four Woody Species and Their Potential Uses for Management of Six *Fusarium oxysporum* Isolates Identified from Some Plant Hosts. *Plants* **2021**, *10* (7), 1325.

- (227) Subhan, N.; Burrows, G. E.; Kerr, P. G.; Obied, H. K. Phytochemistry, ethnomedicine, and pharmacology of *Acacia*. *Studies in Natural Products Chemistry* **2018**, *57*, 247-326.
- (228) Al-Huqail, A. A.; Behiry, S.I., Salem, M.Z., Ali, H.M.; Siddiqui, M.H.; Salem, A.Z. Antifungal, antibacterial, and antioxidant activities of *Acacia saligna* (Labill.) HL Wendl. flower extract: HPLC analysis of phenolic and flavonoid compounds. *Molecules* **2019**, *24*, 700-714.
- (229) Youzbachi, N.; Elfalleh, W.; Tlili, N.; Gregoire, S.; Berdeaux, O.; Salles, C.; Triki, S.; Khouja, M. L.; Khaldi, A.; Nasri, N. Unexploited *Acacia cyanophylla* seeds: potential food sources of ω 6 fatty acids and antioxidants? *Journal of the Science of Food and Agriculture* **2012**, *92* (7), 1526-1532.
- (230) El-Manawaty, M.; Gohar, L. In vitro alpha-glucosidase inhibitory activity of Egyptian plant extracts as an indication for their antidiabetic activity. *Vitro* **2018**, *11*, 360-367.
- (231) Abdallah, H. M.; Ammar, N. M.; Abdelhameed, M. F.; Gendy, A. E.-N. G. E.; Ragab, T. I.; Abd-ElGawad, A. M.; Farag, M. A.; Alwahibi, M. S.; Elshamy, A. I. Protective mechanism of *Acacia saligna* butanol extract and its nano-formulations against ulcerative colitis in rats as revealed via biochemical and metabolomic assays. *Biology* **2020**, *9* (8), 195.
- (232) Thompson, G. D.; Robertson, M. P.; Webber, B. L.; Richardson, D. M.; Le Roux, J. J.; Wilson, J. R. Predicting the subspecific identity of invasive species using distribution models: *Acacia saligna* as an example. *Diversity and Distributions* **2011**, *17* (5), 1001-1014.
- (233) Abd El Gawad, A.; El-Amier, Y. Allelopathy and potential impact of invasive *Acacia saligna* (Labill.) wendl. on plant diversity in the Nile delta coast of Egypt. *International Journal of Environmental Research* **2015**, *9* (3).
- (234) Menezes, J. C.; Orlikova, B.; Morceau, F.; Diederich, M. Natural and synthetic flavonoids: structure–activity relationship and chemotherapeutic potential for the treatment of leukemia. *Critical reviews in food science and nutrition* **2016**, *56* (sup1), S4-S28.
- (235) Chang, H.; Mi, M.; Ling, W.; Zhu, J.; Zhang, Q.; Wei, N.; Zhou, Y.; Tang, Y.; Yuan, J. Structurally related cytotoxic effects of flavonoids on human cancer cells in vitro. *Archives of pharmacal research* **2008**, *31*, 1137-1144.
- (236) Touil, Y. S.; Fellous, A.; Scherman, D.; Chabot, G. G. Flavonoid-induced morphological modifications of endothelial cells through microtubule stabilization. *Nutrition and cancer* **2009**, *61* (3), 310-321.
- (237) Al-ghulikah, H. A.; Mughal, E. U.; Elkaeed, E. B.; Naeem, N.; Nazir, Y.; Alzahrani, A. Y. A.; Sadiq, A.; Shah, S. W. A. Discovery of chalcone derivatives as potential α -glucosidase and cholinesterase inhibitors: Effect of hyperglycemia in paving a path to dementia. *Journal of Molecular Structure* **2023**, *1275*, 134658.
- (238) Khan, H.; Amin, S.; Kamal, M. A.; Patel, S. Flavonoids as acetylcholinesterase inhibitors: Current therapeutic standing and future prospects. *Biomedicine & Pharmacotherapy* **2018**, *101*, 860-870.
- (239) Hutton, P.; White, C.; Durmic, Z.; Vercoe, P. *Eremophila glabra* is an Australian plant that reduces lactic acid accumulation in an in vitro glucose challenge designed to simulate lactic acidosis in ruminants. *animal* **2009**, *3* (9), 1254-1263.
- (240) Akkari, H.; Darghouth, M.; Salem, H. B. Preliminary investigations of the anti-nematode activity of *Acacia cyanophylla* Lindl.: Excretion of gastrointestinal nematode eggs in lambs browsing *A. cyanophylla* with and without PEG or grazing native grass. *Small Ruminant Research* **2008**, *74* (1-3), 78-83.

- (241) Yousef, M. I. Reproductive performance, blood testosterone, lipid peroxidation and seminal plasma biochemistry of rabbits as affected by feeding *Acacia saligna* under subtropical conditions. *Food and chemical toxicology* **2005**, *43* (2), 333-339.
- (242) Howard, D. M. The value of *Acacia saligna* as a source of fodder for ruminants. Curtin University, 2002.
- (243) Degen, A.; Blanke, A.; Becker, K.; Kam, M.; Benjamin, R.; Makkar, H. The nutritive value of *Acacia saligna* and *Acacia salicina* for goats and sheep. *Animal Science* **1997**, *64* (2), 253-259.
- (244) Gebreslassie, G.; Yayneshet, T. Utilization of wheat bran and dried *Acacia saligna* (Labill) HL Wendl leaves by highland rams. *African Journal of Agricultural Research* **2017**, *12* (15), 1286-1292.
- (245) Shaer, E. Utilization of *Acacia saligna* as livestock fodder in arid and semi-arid areas in Egypt. *Cahiers Options Mediterraneennes* **2000**, (45), 213-217.
- (246) Salem, H. B.; Nefzaoui, A.; Salem, L. B.; Ferchichi, H.; Tisserand, J. Intake and digestion in sheep given fresh or air-dried *Acacia cyanophylla* Lindl foliage. In *Annales de zootechnie*, 1997; Vol. 46, pp 361-374.
- (247) Krebs, G.; Howard, D.; Dods, K. The effects of feeding *Acacia saligna* on feed intake, nitrogen balance and rumen metabolism in sheep. *Asian-Australasian Journal of Animal Sciences* **2007**, *20* (9), 1367-1373.
- (248) El-Waziry, A.; Basmakil, S.; Al-Owaimer, A.; Metwally, H.; Ali, M.; Al-Harbi, M. Effect of replacing alfalfa hay with acacia foliage on the growth performance, in vitro gas production and rumen fermentation in goats. *Adv. Anim. Vet. Sci* **2019**, *7* (9), 738-744.
- (249) Ee, K.; Yates, P. Nutritional and antinutritional evaluation of raw and processed Australian wattle (*Acacia saligna*) seeds. *Food chemistry* **2013**, *138* (2-3), 762-769.
- (250) Kebede, M.; Tadesse, A.; Hagazi, N. Section C: nutritional value of *Acacia saligna* seeds. *Acacia species for food security and environmental rehabilitation in the dryland areas of Northern Ethiopia* **2014**, *7*, 114.
- (251) Harwood, C. Australian acacia seeds for human food in developing countries: Looking back and looking forward. *Wattle We Eat for Dinner* **2011**, *16*, 18.
- (252) George, N. A. *Koojong (Acacia Saligna), a Species with Potential as a Perennial Forage for Dryland Salinity Management: Genetic Variation, Feed Quality and Reproductive Biology*; University of Western Australia, 2005.
- (253) Yates, P. Australian Acacias. *The potential to combat child malnutrition build agricultural resilience and support adaptation to climate change in semi-arid Africa*. Charles Darwin University, Western Australia **2010**.
- (254) Nasri, N.; Elfalleh, W.; Tlili, N.; Hannachi, H.; Triki, S.; Khaldi, A. Minor lipid components of some *Acacia* species: potential dietary health benefits of the unexploited seeds. *Lipids in Health and Disease* **2012**, *11* (1), 1-5.
- (255) Yates, P. A. Australian Acacias for food security in semi-arid Africa: A multidisciplinary assessment. *Doctorate in Tropical Environmental Management, Charles Darwin University* **2014**.
- (256) Boughton, B. A.; Reddy, P.; Boland, M. P.; Roessner, U.; Yates, P. Non-protein amino acids in Australian acacia seed: Implications for food security and recommended processing methods to reduce djenkolic acid. *Food chemistry* **2015**, *179*, 109-115.
- (257) Sultana, B.; Anwar, F.; Ashraf, M. Effect of extraction solvent/technique on the antioxidant activity of selected medicinal plant extracts. *Molecules* **2009**, *14* (6), 2167-2180.
- (258) Fraga, C. G. *Plant phenolics and human health: biochemistry, nutrition and pharmacology*; John Wiley & Sons, 2009.

- (259) Zhang, Q.-W.; Lin, L.-G.; Ye, W.-C. Techniques for extraction and isolation of natural products: A comprehensive review. *Chinese medicine* **2018**, *13* (1), 1-26.
- (260) Pavlíková, D.; Pavlík, M.; Vašíčková, S.; Száková, J.; Vokáč, K.; Balík, J.; Tlustoš, P. Development of a procedure for the sequential extraction of substances binding trace elements in plant biomass. *Analytical and bioanalytical chemistry* **2005**, *381* (4), 863-872.
- (261) Altemimi, A.; Lakhssassi, N.; Baharlouei, A.; Watson, D. G.; Lightfoot, D. A. Phytochemicals: Extraction, isolation, and identification of bioactive compounds from plant extracts. *Plants* **2017**, *6* (4), 42.
- (262) Mulinacci, N.; Prucher, D.; Peruzzi, M.; Romani, A.; Pinelli, P.; Giaccherini, C.; Vincieri, F. Commercial and laboratory extracts from artichoke leaves: estimation of caffeoyl esters and flavonoidic compounds content. *Journal of Pharmaceutical and Biomedical Analysis* **2004**, *34* (2), 349-357.
- (263) Santos-Sánchez, N. F.; Salas-Coronado, R.; Villanueva-Cañongo, C.; Hernández-Carlos, B. *Antioxidant compounds and their antioxidant mechanism*; IntechOpen London, UK, 2019.
- (264) Kim, D.-O.; Jeong, S. W.; Lee, C. Y. Antioxidant capacity of phenolic phytochemicals from various cultivars of plums. *Food chemistry* **2003**, *81* (3), 321-326.
- (265) Kim, D.-O.; Lee, C. Y. Comprehensive study on vitamin C equivalent antioxidant capacity (VCEAC) of various polyphenolics in scavenging a free radical and its structural relationship. *Critical reviews in food science and nutrition* **2004**, *44* (4), 253-273.
- (266) Chun, O. K.; Kim, D. O.; Smith, N.; Schroeder, D.; Han, J. T.; Lee, C. Y. Daily consumption of phenolics and total antioxidant capacity from fruit and vegetables in the American diet. *Journal of the Science of Food and Agriculture* **2005**, *85* (10), 1715-1724.
- (267) Chatatikun, M.; Chiabchalard, A. Thai plants with high antioxidant levels, free radical scavenging activity, anti-tyrosinase and anti-collagenase activity. *BMC complementary and alternative medicine* **2017**, *17* (1), 1-9.
- (268) Hayakawa, T., Noda, Kondo, Takaharu. and NOBUYOSHI OKUMURA. *Nagoya J. Med. Sci* **1984**, *47*, 35-41.
- (269) Lin, A. H.-M.; Ao, Z.; Quezada-Calvillo, R.; Nichols, B. L.; Lin, C.-T.; Hamaker, B. R. Branch pattern of starch internal structure influences the glucogenesis by mucosal Nt-maltase-glucoamylase. *Carbohydrate polymers* **2014**, *111*, 33-40.
- (270) Sim, L.; Quezada-Calvillo, R.; Sterchi, E. E.; Nichols, B. L.; Rose, D. R. Human intestinal maltase–glucoamylase: crystal structure of the N-terminal catalytic subunit and basis of inhibition and substrate specificity. *Journal of molecular biology* **2008**, *375* (3), 782-792.
- (271) Chiasson, J.-L.; Josse, R. G.; Gomis, R.; Hanefeld, M.; Karasik, A.; Laakso, M.; Group, S.-N. T. R. Acarbose treatment and the risk of cardiovascular disease and hypertension in patients with impaired glucose tolerance: the STOP-NIDDM trial. *Jama* **2003**, *290* (4), 486-494.
- (272) Şöhretoğlu, D.; Sari, S. Flavonoids as alpha-glucosidase inhibitors: Mechanistic approaches merged with enzyme kinetics and molecular modelling. *Phytochemistry Reviews* **2019**, 1-12.
- (273) Xiao, J.; Hogger, P. Dietary polyphenols and type 2 diabetes: current insights and future perspectives. *Current medicinal chemistry* **2015**, *22* (1), 23-38.
- (274) Missio, A. L.; Tischer, B.; dos Santos, P. S.; Codevilla, C.; de Menezes, C. R.; Barin, J. S.; Haselein, C. R.; Labidi, J.; Gatto, D. A.; Petutschnigg, A. Analytical characterization of purified mimosa (*Acacia mearnsii*) industrial tannin extract:

- Single and sequential fractionation. *Separation and Purification Technology* **2017**, *186*, 218-225.
- (275) Enev, V.; Sedláček, P.; Kubíková, L.; Sovová, Š.; Doskočil, L.; Klučáková, M.; Pekař, M. Polarity-based sequential extraction as a simple tool to reveal the structural complexity of humic acids. *Agronomy* **2021**, *11* (3), 587.
- (276) Bouazzi, S.; El Mokni, R.; Nakbi, H.; Dhaouadi, H.; Joshi, R. K.; Hammami, S. Chemical composition and antioxidant activity of essential oils and hexane extract of *Onopordum arenarium* from Tunisia. *Journal of Chromatographic Science* **2020**, *58* (4), 287-293.
- (277) Sutton, P. A.; Wilde, M. J.; Martin, S. J.; Cvačka, J.; Vrkoslav, V.; Rowland, S. J. Studies of long chain lipids in insects by high temperature gas chromatography and high temperature gas chromatography–mass spectrometry. *Journal of Chromatography A* **2013**, *1297*, 236-240.
- (278) Ghribia, L., et al. Antioxidant and anti-acetylcholinesterase activities of extracts and secondary metabolites from *Acacia cyanophylla*. *Asian Pacific journal of tropical biomedicine* **2014**, *4*, S417-S423.
- (279) Elansary, H. O., et al. Antioxidant and biological activities of *Acacia saligna* and *Lawsonia inermis* natural populations. *Plants* **2020**, *9*, 908-925.
- (280) Salem, M. Z. M., et al. Characterization of Phytoconstituents from Alcoholic Extracts of Four Woody Species and Their Potential Uses for Management of Six *Fusarium oxysporum* Isolates Identified from Some Plant Hosts. *Plants* **2021**, *10*, 1325-1342.
- (281) Zheng, J., et al. Regulation of phytochemicals in fruits and berries by environmental variation—Sugars and organic acids. *J. Food Biochem.* **2019**, *43*, e12642-12660.
- (282) Elmi, A.; Spina, R.; Risler, A.; Philippot, S.; Mérito, A.; Duval, R. E.; Abdoul-Latif, F. M.; Laurain-Mattar, D. Evaluation of antioxidant and antibacterial activities, cytotoxicity of *Acacia seyal* Del bark extracts and isolated compounds. *Molecules* **2020**, *25* (10), 2392.
- (283) Satoh, T.; Igarashi, M.; Yamada, S.; Takahashi, N.; Watanabe, K. Inhibitory effect of black tea and its combination with acarbose on small intestinal α -glucosidase activity. *Journal of Ethnopharmacology* **2015**, *161*, 147-155.
- (284) Pollini, L.; Riccio, A.; Juan, C.; Tringaniello, C.; Ianni, F.; Blasi, F.; Mañes, J.; Macchiarulo, A.; Cossignani, L. Phenolic acids from *Lycium barbarum* leaves: In vitro and in silico studies of the inhibitory activity against porcine pancreatic α -amylase. *Processes* **2020**, *8* (11), 1388.
- (285) Wu, H.; Xu, B. Inhibitory effects of onion against α -glucosidase activity and its correlation with phenolic antioxidants. *International Journal of Food Properties* **2014**, *17* (3), 599-609.
- (286) Adisakwattana, S.; Sookkongwaree, K.; Roengsumran, S.; Petsom, A.; Ngamrojanavanich, N.; Chavasiri, W.; Deesamer, S.; Yibchok-anun, S. Structure–activity relationships of trans-cinnamic acid derivatives on α -glucosidase inhibition. *Bioorganic & medicinal chemistry letters* **2004**, *14* (11), 2893-2896.
- (287) Ernawati, T.; Mun'im, A.; Hanafi, M.; Yanuar, A. Synthesis of cinnamide derivatives and their α -glucosidase inhibitory activities. *Sains Malaysiana* **2020**, *49* (2), 315-322.
- (288) Eruslanov, E.; Kusmartsev, S. Identification of ROS using oxidized DCFDA and flow-cytometry. *Advanced protocols in oxidative stress II* **2010**, 57-72.
- (289) Hadrich, F., Garcia, M., Maalej, A., Moldes, M., Isoda, H., Feve, B., and Sayadi, S. Oleuropein activated AMPK and induced insulin sensitivity in C2C12 muscle cells. *Life Sciences* **2016**, *151*, 167-173.

- (290) Yamada, K.; Nakata, M.; Horimoto, N.; Saito, M.; Matsuoka, H.; Inagaki, N. Measurement of glucose uptake and intracellular calcium concentration in single, living pancreatic β -cells. *Journal of Biological Chemistry* **2000**, *275* (29), 22278-22283.
- (291) Yoshioka, K.; Oh, K.; Saito, M.; Nemoto, Y.; Matsuoka, H. Evaluation of 2-[N-(7-nitrobenz-2-oxa-1, 3-diazol-4-yl) amino]-2-deoxy-D-glucose, a new fluorescent derivative of glucose, for viability assessment of yeast *Candida albicans*. *Applied microbiology and biotechnology* **1996**, *46* (4), 400-404.
- (292) Kao, T.-Y.; Wu, H.-W.; Lee, S.-S.; Liang, P.-H.; Guh, J.-H.; Hsu, L.-C. Characterization of a fluorescent glucose derivative 1-NBDG and its application in the identification of natural SGLT1/2 inhibitors. *Journal of Food & Drug Analysis* **2021**, *29* (3).
- (293) Yoshioka, K.; Saito, M.; Oh, K.-B.; Nemoto, Y.; Matsuoka, H.; Natsume, M.; Abe, H. Intracellular fate of 2-NBDG, a fluorescent probe for glucose uptake activity, in *Escherichia coli* cells. *Bioscience, biotechnology, and biochemistry* **1996**, *60* (11), 1899-1901.
- (294) Hsu, C. L.; Yen, G. C. Induction of cell apoptosis in 3T3-L1 pre-adipocytes by flavonoids is associated with their antioxidant activity. *Molecular nutrition & food research* **2006**, *50* (11), 1072-1079.
- (295) Brodie, A. E.; Manning, V. A.; Ferguson, K. R.; Jewell, D. E.; Hu, C. Y. Conjugated linoleic acid inhibits differentiation of pre- and post-confluent 3T3-L1 preadipocytes but inhibits cell proliferation only in pre-confluent cells. *The Journal of nutrition* **1999**, *129* (3), 602-606.
- (296) Lin, Y.; Sun, X.; Qiu, L.; Wei, J.; Huang, Q.; Fang, C.; Ye, T.; Kang, M.; Shen, H.; Dong, S. Exposure to bisphenol A induces dysfunction of insulin secretion and apoptosis through the damage of mitochondria in rat insulinoma (INS-1) cells. *Cell death & disease* **2013**, *4* (1), e460-e460.
- (297) Madsen, L.; Petersen, R. K.; Sørensen, M. B.; Jørgensen, C.; Hallenborg, P.; Pridal, L.; Fleckner, J.; Amri, E.-Z.; Krieg, P.; Furstenberger, G. Adipocyte differentiation of 3T3-L1 preadipocytes is dependent on lipoxygenase activity during the initial stages of the differentiation process. *Biochemical Journal* **2003**, *375* (3), 539-549.
- (298) Jang, Y. J.; Koo, H. J.; Sohn, E.-H.; Kang, S. C.; Rhee, D.-K.; Pyo, S. Theobromine inhibits differentiation of 3T3-L1 cells during the early stage of adipogenesis via AMPK and MAPK signaling pathways. *Food & function* **2015**, *6* (7), 2365-2374.
- (299) Tzeng, T.-F.; Liu, I.-M. 6-Gingerol prevents adipogenesis and the accumulation of cytoplasmic lipid droplets in 3T3-L1 cells. *Phytomedicine* **2013**, *20* (6), 481-487.
- (300) Student, A. K.; Hsu, R. Y.; Lane, M. D. Induction of fatty acid synthetase synthesis in differentiating 3T3-L1 preadipocytes. *Journal of Biological Chemistry* **1980**, *255* (10), 4745-4750.
- (301) Amri, E.; Bertrand, B.; Ailhaud, G.; Grimaldi, P. Regulation of adipose cell differentiation. I. Fatty acids are inducers of the aP2 gene expression. *Journal of Lipid Research* **1991**, *32* (9), 1449-1456.
- (302) Gomez, F. E.; Bauman, D. E.; Ntambi, J. M.; Fox, B. G. Effects of stercularic acid on stearoyl-CoA desaturase in differentiating 3T3-L1 adipocytes. *Biochemical and Biophysical Research Communications* **2003**, *300* (2), 316-326.
- (303) Ali, A. T.; Hochfeld, W. E.; Myburgh, R.; Pepper, M. S. Adipocyte and adipogenesis. *European journal of cell biology* **2013**, *92* (6-7), 229-236.
- (304) Cao, Z.; Umek, R. M.; McKnight, S. L. Regulated expression of three C/EBP isoforms during adipose conversion of 3T3-L1 cells. *Genes & development* **1991**, *5* (9), 1538-1552.

- (305) Farmer, S. R. Transcriptional control of adipocyte formation. *Cell metabolism* **2006**, 4 (4), 263-273.
- (306) Nam, W.; Nam, S. H.; Kim, S. P.; Levin, C.; Friedman, M. Anti-adipogenic and anti-obesity activities of purpurin in 3T3-L1 preadipocyte cells and in mice fed a high-fat diet. *BMC complementary and alternative medicine* **2019**, 19 (1), 1-12.
- (307) Asmara, A. P.; Prasansuklab, A.; Tencomnao, T.; Ung, A. T. Identification of Phytochemicals in Bioactive Extracts of *Acacia saligna* Growing in Australia. *Molecules* **2023**, 28 (3), 1028.
- (308) Marimoutou, M.; Le Sage, F.; Smadja, J.; Lefebvre d'Helencourt, C.; Gonthier, M.-P.; Robert-Da Silva, C. Antioxidant polyphenol-rich extracts from the medicinal plants *Antirhea borbonica*, *Doratoxylon apetalum* and *Gouania mauritiana* protect 3T3-L1 preadipocytes against H₂O₂, TNF α and LPS inflammatory mediators by regulating the expression of superoxide dismutase and NF- κ B genes. *Journal of Inflammation* **2015**, 12, 1-15.
- (309) Heim, K. E.; Tagliaferro, A. R.; Bobilya, D. J. Flavonoid antioxidants: chemistry, metabolism and structure-activity relationships. *The Journal of nutritional biochemistry* **2002**, 13 (10), 572-584.
- (310) Verri Jr, W. A., Vicentini, F.T.M.C., Baracat, M.M., Georgetti, S.R., Cardoso, R.D.R., Cunha, T.M., Ferreira, S.H., Cunha, F.Q., Fonseca, M.J.V., and Casagrande, R. Flavonoids as anti-inflammatory and analgesic drugs: mechanisms of action and perspectives in the development of pharmaceutical forms. *Studies in natural products chemistry* **2012**, 36, 297-330.
- (311) Luan, G.; Li, L.; Yue, H.; Li, Y.; Lv, H.; Wang, Y. Phenols from *Potentilla anserina* L. Improve Insulin Sensitivity and Inhibit Differentiation in 3T3-L1 Adipocytes in Vitro. *Chemistry & biodiversity* **2023**.
- (312) Lee, C.-L.; Lee, S.-L.; Chen, C.-J.; Chen, H.-C.; Kao, M.-C.; Liu, C.-H.; Chen, J.-Y.; Lai, Y.-T.; Wu, Y.-C. Characterization of secondary metabolites from purple *Ipomoea batatas* leaves and their effects on glucose uptake. *Molecules* **2016**, 21 (6), 745.
- (313) Gothai, S.; Ganesan, P.; Park, S.-Y.; Fakurazi, S.; Choi, D.-K.; Arulselvan, P. Natural phyto-bioactive compounds for the treatment of type 2 diabetes: inflammation as a target. *Nutrients* **2016**, 8 (8), 461.
- (314) Manaharan, T.; Ming, C. H.; Palanisamy, U. D. *Syzygium aqueum* leaf extract and its bioactive compounds enhances pre-adipocyte differentiation and 2-NBDG uptake in 3T3-L1 cells. *Food chemistry* **2013**, 136 (2), 354-363.
- (315) Shi, L.; Zhang, W.; Zhou, Y.-Y.; Zhang, Y.-N.; Li, J.-Y.; Hu, L.-H.; Li, J. Corosolic acid stimulates glucose uptake via enhancing insulin receptor phosphorylation. *European journal of pharmacology* **2008**, 584 (1), 21-29.
- (316) Gutiérrez, G.; Giraldo-Dávila, D.; Combariza, M. Y.; Holzgrabe, U.; Tabares-Guevara, J. H.; Ramírez-Pineda, J. R.; Acín, S.; Muñoz, D. L.; Montoya, G.; Balcazar, N. Serjanic acid improves immunometabolic markers in a diet-induced obesity mouse model. *Molecules* **2020**, 25 (7), 1486.
- (317) Du, Q.; Jerz, G.; Winterhalter, P. Preparation of three flavonoids from the bark of *Salix alba* by high-speed countercurrent chromatographic separation. *Journal of liquid chromatography & related technologies* **2004**, 27 (20), 3257-3264.
- (318) Andersen, O. M.; Markham, K. R. *Flavonoids: chemistry, biochemistry and applications*; CRC press, 2005.
- (319) Olsen, H. T.; Stafford, G. I.; Van Staden, J.; Christensen, S. B.; Jäger, A. K. Isolation of the MAO-inhibitor naringenin from *Mentha aquatica* L. *Journal of ethnopharmacology* **2008**, 117 (3), 500-502.
- (320) Zhang, Z.; ElSohly, H. N.; Li, X.-C.; Khan, S. I.; Broedel, S. E.; Raulli, R. E.; Cihlar, R. L.; Walker, L. A. Flavanone glycosides from *Miconia trillii*. *Journal of natural products* **2003**, 66 (1), 39-41.

- (321) Hendra, R.; Willis, A.; Keller, P. A. Phytochemical studies on the Australian native plant species *Acacia pycnantha* and *Jacaranda mimosifolia* D. Don. *Natural product research* **2019**, *33* (14), 1997-2003.
- (322) Sofa, F.; Akhmad, D.; Megawati, M.; Muhammad, H. Isolation and identification of quercetin derivatives and their alpha-glucosidase inhibitory activities from *Bryophyllum pinnatum*. *Res J Chem Environ* **2018**, *22*, 114-119.
- (323) Kim, Y.-K.; Kim, Y. S.; Choi, S. U.; Ryu, S. Y. Isolation of flavonol rhamnosides from *Loranthus tanakae* and cytotoxic effect of them on human tumor cell lines. *Archives of pharmacal research* **2004**, *27* (1), 44-47.
- (324) Seo, J.-H.; Kim, J.-E.; Shim, J.-H.; Yoon, G.; Bang, M.; Bae, C.-S.; Lee, K.-J.; Park, D.-H.; Cho, S.-S. HPLC analysis, optimization of extraction conditions and biological evaluation of *Corylopsis coreana* Uyeki Flos. *Molecules* **2016**, *21* (1), 94.
- (325) Iio, M.; Yoshioka, A.; Imayoshi, Y.; Koriyama, C.; Ayako, M. Effect of flavonoids on α -glucosidase and β -fructosidase from yeast. *Agricultural and biological chemistry* **1984**, *48* (6), 1559-1563.
- (326) Utari, F.; Itam, A.; Syafrizayanti, S.; Putri, W. H.; Ninomiya, M.; Koketsu, M.; Tanaka, K.; Efdi, M. Isolation of flavonol rhamnosides from *Pometia pinnata* leaves and investigation of α -glucosidase inhibitory activity of flavonol derivatives. *Journal of Applied Pharmaceutical Science* **2019**, *9* (08), 053-065.
- (327) Raya-Gonzalez, D.; Pamatz-Bolanos, T.; Rosa, E.; Martinez-Munoz, R. E.; Ron-Echeverria, O.; Martinez-Pacheco, M. M. D-(+)-pinitol, a component of the heartwood of *Enterolobium cyclocarpum* (Jacq.) Griseb. *Zeitschrift für Naturforschung C* **2008**, *63* (11-12), 922-924.
- (328) Anderson, A. B.; MacDonald, D.; Fischer, H. O. The structure of pinitol. *Journal of the American Chemical Society* **1952**, *74* (6), 1479-1480.
- (329) Chaubal, R.; Pawar, P. V.; Hebbalkar, G. D.; Tungikar, V. B.; Puranik, V. G.; Deshpande, V. H.; Deshpande, N. R. Larvicidal Activity of *Acacia nilotica* Extracts and Isolation of D-Pinitol—A Bioactive Carbohydrate. *Chemistry & biodiversity* **2005**, *2* (5), 684-688.
- (330) Bates, S. H.; Jones, R. B.; Bailey, C. J. Insulin-like effect of pinitol. *British journal of pharmacology* **2000**, *130* (8), 1944-1948.
- (331) Yap, A.; Nishiumi, S.; Yoshida, K.-i.; Ashida, H. Rat L6 myotubes as an in vitro model system to study GLUT4-dependent glucose uptake stimulated by inositol derivatives. *Cytotechnology* **2007**, *55* (2-3), 103-108.
- (332) Lee, E.; Lim, Y.; Kwon, S. W.; Kwon, O. Pinitol consumption improves liver health status by reducing oxidative stress and fatty acid accumulation in subjects with non-alcoholic fatty liver disease: A randomized, double-blind, placebo-controlled trial. *The Journal of nutritional biochemistry* **2019**, *68*, 33-41.
- (333) Bhat, K. A.; Lone, S. H.; Malik, F. A. Click chemistry inspired facile synthesis and bioevaluation of novel triazolyl analogs of D-(+)-pinitol. *Arabian Journal of Chemistry* **2019**, *12* (8), 3479-3489.
- (334) Belghit, S.; Driche, E. H.; Bijani, C.; Zitouni, A.; Sabaou, N.; Badji, B.; Mathieu, F. Activity of 2, 4-Di-tert-butylphenol produced by a strain of *Streptomyces mutabilis* isolated from a Saharan soil against *Candida albicans* and other pathogenic fungi. *Journal de mycologie medicale* **2016**, *26* (2), 160-169.
- (335) Dharni, S.; Maurya, A.; Samad, A.; Srivastava, S. K.; Sharma, A.; Patra, D. D. Purification, characterization, and in vitro activity of 2, 4-di-tert-butylphenol from *Pseudomonas monteilii* PsF84: conformational and molecular docking studies. *Journal of agricultural and food chemistry* **2014**, *62* (26), 6138-6146.
- (336) Zhao, F.; Wang, P.; Lucardi, R. D.; Su, Z.; Li, S. Natural sources and bioactivities of 2, 4-di-tert-butylphenol and its analogs. *Toxins* **2020**, *12* (1), 35.

- (337) Johnson, J.; Citarasu, T.; Manjusha, W. Antimicrobial screening and identification of bioactive compounds present in marine sponge *Zygomycala* sp. collected from Kanyakumari coast. *J. chem. biol. phys. sci* **2012**, *2* (1842), e1848.
- (338) Yoon, M.-A.; Jeong, T.-S.; Park, D.-S.; Xu, M.-Z.; Oh, H.-W.; Song, K.-B.; Lee, W. S.; Park, H.-Y. Antioxidant effects of quinoline alkaloids and 2, 4-di-tert-butylphenol isolated from *Scolopendra* subspinipes. *Biological and Pharmaceutical Bulletin* **2006**, *29* (4), 735-739.
- (339) Varsha, K. K.; Devendra, L.; Shilpa, G.; Priya, S.; Pandey, A.; Nampoothiri, K. M. 2, 4-Di-tert-butyl phenol as the antifungal, antioxidant bioactive purified from a newly isolated *Lactococcus* sp. *International journal of food microbiology* **2015**, *211*, 44-50.
- (340) Khiralla, A.; Spina, R.; Varbanov, M.; Philippot, S.; Lemiere, P.; Slezack-Deschaumes, S.; André, P.; Mohamed, I.; Yagi, S. M.; Laurain-Mattar, D. Evaluation of antiviral, antibacterial and antiproliferative activities of the endophytic fungus *Curvularia papendorffii*, and isolation of a new polyhydroxyacid. *Microorganisms* **2020**, *8* (9), 1353.
- (341) Chuah, T.; Norhafizah, M.; Ismail, B. Evaluation of the biochemical and physiological activity of the natural compound, 2, 4-ditert-butylphenol on weeds. *Crop and Pasture Science* **2015**, *66* (2), 214-223.
- (342) Huang, X.; Li, Y.; Jiang, P.; Zhang, X.; Zhang, X.; Tan, P.; Tian, W. Identification of chrysanthemum root exudates and allelopathic effects of the three plants. *Hubei Agric. Sci* **2017**, *56*, 1061-1071.
- (343) Kamel, M.; Hammad, S. A. The Allelopathic Effect of the Exotic Tree *Acacia saligna* on the Germination of Wheat and Canola. *Ecologia Balkanica* **2015**, *7* (1).
- (344) Hwang, I.-W.; Chung, S.-K. Isolation and identification of myricitrin, an antioxidant flavonoid, from daebong persimmon peel. *Preventive nutrition and food science* **2018**, *23* (4), 341.
- (345) Hudlicky, T.; Price, J. D.; Rulin, F.; Tsunoda, T. Efficient and enantiodivergent synthesis of (+)-and (-)-pinitol. *Journal of the American Chemical Society* **1990**, *112* (25), 9439-9440.
- (346) Obendorf, R. L.; Górecki, R. J. Soluble carbohydrates in legume seeds. *Seed Science Research* **2012**, *22* (4), 219.
- (347) Schweizer, T. F.; Horman, I.; Würsch, P. Low molecular weight carbohydrates from leguminous seeds; a new disaccharide: galactopinitol. *Journal of the Science of Food and Agriculture* **1978**, *29* (2), 148-154.
- (348) Ismayati, M.; Nakagawa-izumi, A.; Ohi, H. Structural elucidation of condensed tannin from the bark waste of *Acacia crassicarpa* plantation wood in Indonesia. *Journal of Wood Science* **2017**, *63* (4), 350-359.
- (349) Kamiya, K.; Watanabe, C.; Endang, H.; Umar, M.; Satake, T. Studies on the Constituents of Bark of *Parameria laevigata* MOLDENKE1. *Chemical and pharmaceutical bulletin* **2001**, *49* (5), 551-557.
- (350) Roux, D.; Maihs, E. Condensed tannins. 3. Isolation and estimation of (-)-7: 3': 4': 5'-tetrahydroxyflavan-3-ol, (+)-catechin and (+)-galocatechin from black-wattle-bark extract. *Biochemical Journal* **1960**, *74* (1), 44.
- (351) Drewes, S.; Roux, D.; Saayman, H.; Eggers, S.; Feeney, J. Some stereochemically identical biflavanols from the bark tannins of *Acacia mearnsii*. *Journal of the Chemical Society C: Organic* **1967**, 1302-1308.
- (352) Kayed, A. M.; Genady, E. A.; Kadry, H. A.; Elghaly, E.-S. M. New phytoconstituents, anti-microbial and cytotoxic activities of *Acacia etbaica* Schweinf. *Natural Product Research* **2020**, 1-10.

- (353) Obendorf, R. L.; Górecki, R. J. Soluble carbohydrates in legume seeds. *Seed Science Research* **2012**, *22* (4), 219-242.
- (354) Hernández-García, E.; García, A.; Avalos-Alanís, F. G.; Rivas-Galindo, V. M.; Delgadillo-Puga, C.; del Rayo Camacho-Corona, M. Nuclear magnetic resonance spectroscopy data of isolated compounds from *Acacia farnesiana* (L) Willd fruits and two esterified derivatives. *Data in brief* **2019**, *22*, 255-268.
- (355) Ahmad, S. Phytochemical and Bioactivity Studies of *Mangifera Pajang* Kosterm, *Aglaia Odoratissima* Blume and *Acacia Albida* Delile. Universiti Putra Malaysia, 2014.
- (356) Matsuo, Y.; Kusano, R.; Ogawa, S.; Yazaki, Y.; Tanaka, T. Characterization of the α -amylase inhibitory activity of oligomeric proanthocyanidins from *Acacia mearnsii* Bark Extract. *Natural Product Communications* **2016**, *11* (12), 1934578X1601101219.
- (357) Dunn, J. D.; Alvarez, L. A.; Zhang, X.; Soldati, T. Reactive oxygen species and mitochondria: A nexus of cellular homeostasis. *Redox biology* **2015**, *6*, 472-485.
- (358) Kim, J.-a.; Wei, Y.; Sowers, J. R. Role of mitochondrial dysfunction in insulin resistance. *Circulation research* **2008**, *102* (4), 401-414.
- (359) Fan, Y.; Yang, Q.; Yang, Y.; Gao, Z.; Ma, Y.; Zhang, L.; Liang, W.; Ding, G. Sirt6 suppresses high glucose-induced mitochondrial dysfunction and apoptosis in podocytes through AMPK activation. *International journal of biological sciences* **2019**, *15* (3), 701.
- (360) Chen, Q.; Chen, X.; Han, C.; Wang, Y.; Huang, T.; Du, Y.; Dong, Z. FGF-2 transcriptionally down-regulates the expression of BNIP3L via PI3K/Akt/FoxO3a signaling and inhibits necrosis and mitochondrial dysfunction induced by high concentrations of hydrogen peroxide in H9c2 cells. *Cellular Physiology and Biochemistry* **2016**, *40* (6), 1678-1691.
- (361) Campbell, I.; Campbell, H. Mechanisms of insulin resistance, mitochondrial dysfunction and the action of the ketogenic diet in bipolar disorder. Focus on the PI3K/AKT/HIF1- α pathway. *Medical Hypotheses* **2020**, *145*, 110299.
- (362) Peng, Y.; Liu, J.; Shi, L.; Tang, Y.; Gao, D.; Long, J.; Liu, J. Mitochondrial dysfunction precedes depression of AMPK/AKT signaling in insulin resistance induced by high glucose in primary cortical neurons. *Journal of neurochemistry* **2016**, *137* (5), 701-713.
- (363) Yano, M.; Watanabe, K.; Yamamoto, T.; Ikeda, K.; Senokuchi, T.; Lu, M.; Kadomatsu, T.; Tsukano, H.; Ikawa, M.; Okabe, M. Mitochondrial dysfunction and increased reactive oxygen species impair insulin secretion in sphingomyelin synthase 1-null mice. *Journal of Biological Chemistry* **2011**, *286* (5), 3992-4002.
- (364) Sharoyko, V. V.; Abels, M.; Sun, J.; Nicholas, L. M.; Mollet, I. G.; Stamenkovic, J. A.; Göhring, I.; Malmgren, S.; Storm, P.; Fadista, J. Loss of TFB1M results in mitochondrial dysfunction that leads to impaired insulin secretion and diabetes. *Human molecular genetics* **2014**, *23* (21), 5733-5749.
- (365) Lee, J. W.; Kim, W. H.; Yeo, J.; Jung, M. H. ER stress is implicated in mitochondrial dysfunction-induced apoptosis of pancreatic beta cells. *Molecules and cells* **2010**, *30* (6), 545-549.
- (366) Kirkman, D. L.; Muth, B. J.; Ramick, M. G.; Townsend, R. R.; Edwards, D. G. Role of mitochondria-derived reactive oxygen species in microvascular dysfunction in chronic kidney disease. *American Journal of Physiology-Renal Physiology* **2018**, *314* (3), F423-F429.
- (367) Miller, D. J.; Cascio, M. A.; Rosca, M. G. Diabetic retinopathy: the role of mitochondria in the neural retina and microvascular disease. *Antioxidants* **2020**, *9* (10), 905.

- (368) Grammas, P.; Martinez, J.; Miller, B. Cerebral microvascular endothelium and the pathogenesis of neurodegenerative diseases. *Expert reviews in molecular medicine* **2011**, *13*.
- (369) Wu, M.-Y.; Yiang, G.-T.; Lai, T.-T.; Li, C.-J. The oxidative stress and mitochondrial dysfunction during the pathogenesis of diabetic retinopathy. *Oxidative medicine and cellular longevity* **2018**, *2018*.
- (370) Chen, W.; Zhu, X.; Lu, Q.; Zhang, L.; Wang, X.; Liu, R. C-ring cleavage metabolites of catechin and epicatechin enhanced antioxidant activities through intestinal microbiota. *Food Research International* **2020**, *135*, 109271.
- (371) Ao, C.; Higa, T.; Ming, H.; Ding, Y.-t.; Tawata, S. Isolation and identification of antioxidant and hyaluronidase inhibitory compounds from *Ficus microcarpa* L. fil. bark. *Journal of Enzyme Inhibition and Medicinal Chemistry* **2010**, *25* (3), 406-413.
- (372) Panat, N. A.; Amrute, B. K.; Bhattu, S.; Haram, S. K.; Sharma, G. K.; Ghaskadbi, S. S. Antioxidant Profiling of C3 Quercetin Glycosides: Quercitrin, Quercetin 3- β -D-glucoside and Quercetin 3-O-(6"-O-malonyl)- β -Dglucoside in cell free environment. *Free Radicals and Antioxidants* **2015**, *5* (2), 90-100.
- (373) Li, X.; Mai, W.; Chen, D. Chemical Study on Protective Effect Against Hydroxyl-induced DNA Damage and Antioxidant Mechanism of Myricitrin. *Journal of the Chinese Chemical Society* **2014**, *61* (3), 383-390.
- (374) Chen, W.; Feng, L.; Shen, Y.; Su, H.; Li, Y.; Zhuang, J.; Zhang, L.; Zheng, X. Myricitrin inhibits acrylamide-mediated cytotoxicity in human Caco-2 cells by preventing oxidative stress. *BioMed research international* **2013**, *2013*.
- (375) Li, X.; Jiang, Q.; Wang, T.; Liu, J.; Chen, D. Comparison of the antioxidant effects of quercitrin and isoquercitrin: Understanding the role of the 6"-OH group. *Molecules* **2016**, *21* (9), 1246.
- (376) Wu, W.-M.; Lu, L.; Long, Y.; Wang, T.; Liu, L.; Chen, Q.; Wang, R. Free radical scavenging and antioxidative activities of caffeic acid phenethyl ester (CAPE) and its related compounds in solution and membranes: A structure–activity insight. *Food Chemistry* **2007**, *105* (1), 107-115.
- (377) Cai, R.; Li, X.; Chen, B.; Xie, Y.; Xie, H.; Chen, D. Antioxidant change in biosynthesis from naringenin chalcone to flavonoid apigenin. *ChemistrySelect* **2019**, *4* (17), 5155-5159.
- (378) Ouyang, X.; Li, X.; Lu, W.; Zhao, X.; Chen, D. A null B-ring improves the antioxidant levels of Flavonol: a comparative study between Galangin and 3, 5, 7-Trihydroxychromone. *Molecules* **2018**, *23* (12), 3083.
- (379) Priscilla, D., et al. Naringenin inhibits α -glucosidase activity: A promising strategy for the regulation of postprandial hyperglycemia in high fat diet fed streptozotocin induced diabetic rats. *Chemico-Biological Interactions* **2014**, *210*, 77–85.
- (380) Jung, H. A.; Paudel, P.; Seong, S. H.; Min, B.-S.; Choi, J. S. Structure-related protein tyrosine phosphatase 1B inhibition by naringenin derivatives. *Bioorganic & Medicinal Chemistry Letters* **2017**, *27* (11), 2274-2280.
- (381) Miao, J.; Li, X.; Zhao, C.; Gao, X.; Wang, Y.; Gao, W. Active compounds, antioxidant activity and α -glucosidase inhibitory activity of different varieties of *Chaenomeles* fruits. *Food chemistry* **2018**, *248*, 330-339.
- (382) Zhang, L.-L.; Han, L.; Yang, S.-Y.; Meng, X.-M.; Ma, W.-F.; Wang, M. The mechanism of interactions between flavan-3-ols against α -glucosidase and their in vivo antihyperglycemic effects. *Bioorganic Chemistry* **2019**, *85*, 364-372.
- (383) Gong, T.; Yang, X.; Bai, F.; Li, D.; Zhao, T.; Zhang, J.; Sun, L.; Guo, Y. Young apple polyphenols as natural α -glucosidase inhibitors: In vitro and in silico studies. *Bioorganic Chemistry* **2020**, *96*, 103625.

- (384) Tadera, K., et al. Inhibition of alpha-glucosidase and alpha-amylase by flavonoids. *J Nutr Sci Vitaminol* **2006**, *52*, 149–153.
- (385) Proença, C., et al. α -Glucosidase inhibition by flavonoids: an in vitro and in silico structure–activity relationship study. *Journal of enzyme inhibition and medicinal chemistry* **2017**, *32*, 1216-1228.
- (386) He, C., et al. Interaction Mechanism of Flavonoids and α -Glucosidase: Experimental and Molecular Modelling Studies. *Foods* **2019**, *8*, 355-361.
- (387) Şöhretoğlu, D., Sari, S. Flavonoids as alpha-glucosidase inhibitors: Mechanistic approaches merged with enzyme kinetics and molecular modelling. *Phytochemistry Reviews* **2020**, *19*, 1081–1092.
- (388) Sanchez-Hidalgo, M., et al. D-Pinitol: a cyclitol with versatile biological and pharmacological activities. *Phytochem Rev* **2021**, *20*, 211–224.
- (389) Kidruangphokin, M.; Suphrom, N.; Boonphong, S. α -Glucosidase Inhibitory and Antioxidant Activities of Ethanolic Extracts of Different Parts of *Lysiphyllum strychnifolium* and Their Constituents. *Journal of Herbs, Spices & Medicinal Plants* **2023**, *29* (3), 274-287.
- (390) Deepa, P. R.; Vandhana, S.; Jayanthi, U.; Krishnakumar, S. Therapeutic and toxicologic evaluation of anti-lipogenic agents in cancer cells compared with non-neoplastic cells. *Basic & clinical pharmacology & toxicology* **2012**, *110* (6), 494-503.
- (391) Nishina, A.; Sato, D.; Yamamoto, J.; Kobayashi-Hattori, K.; Hirai, Y.; Kimura, H. Antidiabetic-like effects of Naringenin-7-O-glucoside from Edible *Chrysanthemum* 'Kotobuki' and Naringenin by Activation of the PI3K/Akt Pathway and PPAR γ . *Chemistry & Biodiversity* **2019**, *16* (1), e1800434.
- (392) Ardevol, A.; Blade, C.; Salvado, M.; Arola, L. Changes in lipolysis and hormone-sensitive lipase expression caused by procyanidins in 3T3-L1 adipocytes. *International journal of obesity* **2000**, *24* (3), 319-324.
- (393) Choi, S. J.; Kim, J. K.; Kim, H. K.; Harris, K.; Kim, C.-J.; Park, G. G.; Park, C.-S.; Shin, D.-H. 2, 4-Di-tert-butylphenol from sweet potato protects against oxidative stress in PC12 cells and in mice. *Journal of medicinal food* **2013**, *16* (11), 977-983.
- (394) Luan, G.; Wang, Y.; Wang, Z.; Zhou, W.; Hu, N.; Li, G.; Wang, H. Flavonoid glycosides from fenugreek seeds regulate glycolipid metabolism by improving mitochondrial function in 3T3-L1 adipocytes in vitro. *Journal of agricultural and food chemistry* **2018**, *66* (12), 3169-3178.
- (395) Cao, G., Sofic, E., and Prior, R.L. Antioxidant and prooxidant behavior of flavonoids: structure-activity relationships. *Free radical biology and medicine* **1997**, *22* (5), 749-760.
- (396) Wali, A. F., Rashid, S., Rashid, S.Mu., Ansari, M.A., Khan, M.R., Haq, N., Alhareth, D.Y., Ahmad, A., and Rehman, M.U. Naringenin regulates doxorubicin-induced liver dysfunction: impact on oxidative stress and inflammation. *Plants* **2020**, *9* (4), 550.
- (397) Wang, K., Chen, Z., Huang, L., Meng, B., Zhou, X., Wen, X., and Ren, D. Naringenin reduces oxidative stress and improves mitochondrial dysfunction via activation of the Nrf2/ARE signaling pathway in neurons. *International Journal of Molecular Medicine* **2017**, *40* (5), 1582-1590.
- (398) Chaturvedi, D. Sesquiterpene lactones: structural diversity and their biological activities, In-Opportunity, Challenges and Scope of Natural Products in Medicinal Chemistry. ISBN: 978-81-308-0448-4, *Research Signpost, Trivandrum* **2011**, 313-334.
- (399) Limasset, B., Le Doucen, C., Dore, J.C., Ojasoo, T., Damon, M., and De Paulet, A.C. Effects of flavonoids on the release of reactive oxygen species by

- stimulated human neutrophils: Multivariate analysis of structure-activity relationships (SAR). *Biochemical pharmacology* **1993**, *46* (7), 1257-1271.
- (400) Lebedzinska, M., Karkucinska-Wieckowska, A., Giorgi, C., Karczmarewicz, E., Pronicka, E., Pinton, P., Duszynski, J., Pronicki, M., and Wieckowski, M.R. Oxidative stress-dependent p66Shc phosphorylation in skin fibroblasts of children with mitochondrial disorders. *Biochimica et Biophysica Acta (BBA)-Bioenergetics* **2010**, *1797* (6-7), 952-960.
- (401) Elefantova, K., Lakatos, B., Kubickova, J., Sulova, Z., and Breier, A. Detection of the mitochondrial membrane potential by the cationic dye JC-1 in L1210 cells with massive overexpression of the plasma membrane ABCB1 drug transporter. *International journal of molecular sciences* **2018**, *19* (7), 1985.
- (402) Muthaiah, V. P. K.; Venkatasamy, L.; Michael, F. M.; Chandrasekar, K.; Venkatachalam, S. Neuroprotective role of naringenin on carbaryl induced neurotoxicity in mouse neuroblastoma cells. *Journal of pharmacology & pharmacotherapeutics* **2013**, *4* (3), 192.
- (403) Rahaman, M. S., Akter, M., Rahman, M.M., Sikder, M.T., Hosokawa, T., Saito, T., and Kurasaki, M. Investigating the protective actions of D-pinitol against arsenic-induced toxicity in PC12 cells and the underlying mechanism. *Environmental Toxicology and Pharmacology* **2020**, *74*, 103302.
- (404) López-Domènech, S.; Bañuls, C.; de Marañón, A. M.; Abab-Jiménez, Z.; Morillas, C.; Gómez-Abril, S. Á.; Rovira-Llopis, S.; Víctor, V. M.; Hernández-Mijares, A.; Rocha, M. Pinitol alleviates systemic inflammatory cytokines in human obesity by a mechanism involving unfolded protein response and sirtuin 1. *Clinical nutrition* **2018**, *37* (6), 2036-2044.
- (405) Annadurai, T., Muralidharan, A.R., Joseph, T., Hsu, M.J., Thomas, P.A., and Geraldine, P. Antihyperglycemic and antioxidant effects of a flavanone, naringenin, in streptozotocin–nicotinamide-induced experimental diabetic rats. *Journal of physiology and biochemistry* **2012**, *68* (3), 307-318.
- (406) Sadler, D. G., Barlow, J., Draijer, R., Jones, H., Thijssen, D.H.J., and Stewart, C.E. (–)-Epicatechin alters reactive oxygen and nitrogen species production independent of mitochondrial respiration in human vascular endothelial cells. *Oxidative medicine and cellular longevity* **2022**, *2022*.
- (407) Li, H.; Liu, L.; Cao, Z.; Li, W.; Liu, R.; Chen, Y.; Li, C.; Song, Y.; Liu, G.; Hu, J. Naringenin ameliorates homocysteine induced endothelial damage via the AMPK α /Sirt1 pathway. *Journal of Advanced Research* **2021**, *34*, 137-147.
- (408) Mladenova, S. G.; Vasileva, L. V.; Savova, M. S.; Marchev, A. S.; Tews, D.; Wabitsch, M.; Ferrante, C.; Orlando, G.; Georgiev, M. I. Anti-Adipogenic Effect of *Alchemilla monticola* is Mediated Via PI3K/AKT Signaling Inhibition in Human Adipocytes. *Frontiers in Pharmacology* **2021**, *12*.
- (409) Zhao, C.; Zhao, C.; Zhao, H. Defective insulin receptor signaling in patients with gestational diabetes is related to dysregulated miR-140 which can be improved by naringenin. *The International Journal of Biochemistry & Cell Biology* **2020**, *128*, 105824.
- (410) Fan, C.; Liang, W.; Wei, M.; Gou, X.; Han, S.; Bai, J. Effects of D-Chiro-Inositol on Glucose Metabolism in db/db Mice and the Associated Underlying Mechanisms. *Frontiers in pharmacology* **2020**, *11*, 354.
- (411) Do, G.-M.; Choi, M.-S.; Kim, H.-J.; Woo, M.-N.; Lee, M.-K.; Jeon, S.-M. Soy pinitol acts partly as an insulin sensitizer or insulin mediator in 3T3-L1 preadipocytes. *Genes & nutrition* **2008**, *2* (4), 359-364.
- (412) Molonia, M. S.; Occhiuto, C.; Muscarà, C.; Speciale, A.; Ruberto, G.; Siracusa, L.; Cristani, M.; Saija, A.; Cimino, F. Effects of a pinitol-rich *Glycyrrhiza glabra* L. leaf extract on insulin and inflammatory signaling pathways in palmitate-induced hypertrophic adipocytes. *Natural Product Research* **2021**, 1-8.

- (413) Álvarez-Cilleros, D.; Martín, M. Á.; Ramos, S. Protective effects of (-)-epicatechin and the colonic metabolite 3, 4-dihydroxyphenylacetic acid against glucotoxicity-induced insulin signalling blockade and altered glucose uptake and production in renal tubular NRK-52E cells. *Food and chemical toxicology* **2018**, *120*, 119-128.
- (414) Álvarez-Cilleros, D.; Martín, M. Á.; Ramos, S. (-)-Epicatechin and the Colonic 2, 3-Dihydroxybenzoic Acid Metabolite Regulate Glucose Uptake, Glucose Production, and Improve Insulin Signaling in Renal NRK-52E Cells. *Molecular nutrition & food research* **2018**, *62* (4), 1700470.
- (415) Cordero-Herrera, I.; Martín, M. Á.; Goya, L.; Ramos, S. Cocoa flavonoids attenuate high glucose-induced insulin signalling blockade and modulate glucose uptake and production in human HepG2 cells. *Food and Chemical Toxicology* **2014**, *64*, 10-19.
- (416) Ueda, M.; Furuyashiki, T.; Yamada, K.; Aoki, Y.; Sakane, I.; Fukuda, I.; Yoshida, K.-i.; Ashida, H. Tea catechins modulate the glucose transport system in 3T3-L1 adipocytes. *Food & function* **2010**, *1* (2), 167-173.
- (417) Pessler, D.; Rudich, A.; Bashan, N. Oxidative stress impairs nuclear proteins binding to the insulin responsive element in the GLUT4 promoter. *Diabetologia* **2001**, *44*, 2156-2164.
- (418) Choi, Y. M.; Kim, H. K.; Shim, W.; Anwar, M. A.; Kwon, J. W.; Kwon, H. K.; Kim, H. J.; Jeong, H.; Kim, H. M.; Hwang, D. Mechanism of cisplatin-induced cytotoxicity is correlated to impaired metabolism due to mitochondrial ROS generation. *PloS one* **2015**, *10* (8), e0135083.
- (419) Wang, C. H.; Wang, C. C.; Huang, H. C.; Wei, Y. H. Mitochondrial dysfunction leads to impairment of insulin sensitivity and adiponectin secretion in adipocytes. *The FEBS journal* **2013**, *280* (4), 1039-1050.
- (420) Serra, D.; Mera, P.; Malandrino, M. I.; Mir, J. F.; Herrero, L. Mitochondrial fatty acid oxidation in obesity. *Antioxidants & redox signaling* **2013**, *19* (3), 269-284.
- (421) Jayarathne, S.; Stull, A. J.; Miranda, A.; Scoggin, S.; Claycombe-Larson, K.; Kim, J. H.; Moustaid-Moussa, N. Tart cherry reduces inflammation in adipose tissue of Zucker fatty rats and cultured 3T3-L1 adipocytes. *Nutrients* **2018**, *10* (11), 1576.
- (422) Pessler-Cohen, D.; Pekala, P. H.; Kovsan, J.; Bloch-Damti, A.; Rudich, A.; Bashan, N. GLUT4 repression in response to oxidative stress is associated with reciprocal alterations in C/EBP alpha and delta isoforms in 3T3-L1 adipocytes. *Archives of physiology and biochemistry* **2006**, *112* (1), 3-12.
- (423) Rebello, C. J.; Greenway, F. L.; Lau, F. H.; Lin, Y.; Stephens, J. M.; Johnson, W. D.; Coulter, A. A. Naringenin promotes thermogenic gene expression in human white adipose tissue. *Obesity* **2019**, *27* (1), 103-111.
- (424) L'Abbate, S.; Nicolini, G.; Forini, F.; Marchetti, S.; Di Lascio, N.; Faita, F.; Kusmic, C. Myo-inositol and D-Chiro-inositol oral supplementation ameliorate cardiac dysfunction and remodeling in a mouse model of diet-induced obesity. *Pharmacological Research* **2020**, *159*, 105047.
- (425) Sente, T.; Van Berendoncks, A. M.; Franssen, E.; Vrints, C. J.; Hoymans, V. Y. Tumor necrosis factor- α impairs adiponectin signalling, mitochondrial biogenesis, and myogenesis in primary human myotubes cultures. *American Journal of Physiology-Heart and Circulatory Physiology* **2016**, *310* (9), H1164-H1175.
- (426) Yi, Z.; Wu, Y.; Zhang, W.; Wang, T.; Gong, J.; Cheng, Y.; Miao, C. Activator-mediated pyruvate kinase M2 activation contributes to endotoxin tolerance by promoting mitochondrial biogenesis. *Frontiers in Immunology* **2021**, *11*, 595316.

- (427) Zhang, Q.; Zhang, J.; Shen, J.; Silva, A.; Dennis, D. A.; Barrow, C. J. A simple 96-well microplate method for estimation of total polyphenol content in seaweeds. *Journal of applied phycology* **2006**, *18* (3), 445-450.
- (428) Nurcholis, W.; Putri, D. N. S. b.; Husnawati, H.; Aisyah, S. I.; Priosoeryanto, B. P. Total flavonoid content and antioxidant activity of ethanol and ethyl acetate extracts from accessions of *Amomum compactum* fruits. *Annals of Agricultural Sciences* **2021**, *66* (1), 58-62.
- (429) Jiang, Y.; Li, D.; Ma, X.; Jiang, F.; He, Q.; Qiu, S.; Li, Y.; Wang, G. Ionic liquid–ultrasound-based extraction of biflavonoids from *Selaginella helvetica* and investigation of their antioxidant activity. *Molecules* **2018**, *23* (12), 3284.
- (430) Chen, Z. G.; Bishop, K. S.; Tanambell, H.; Buchanan, P.; Smith, C.; Quek, S. Y. Characterization of the bioactivities of an ethanol extract and some of its constituents from the New Zealand native mushroom *Hericium novae-zealandiae*. *Food & function* **2019**, *10* (10), 6633-6643.
- (431) Konan, K.; Le Tien, C.; Mateescu, M. Electrolysis-induced fast activation of the ABTS reagent for an antioxidant capacity assay. *Analytical Methods* **2016**, *8* (28), 5638-5644.
- (432) Re, R.; Pellegrini, N.; Proteggente, A.; Pannala, A.; Yang, M.; Rice-Evans, C. Antioxidant activity applying an improved ABTS radical cation decolorization assay. *Free radical biology and medicine* **1999**, *26* (9-10), 1231-1237.
- (433) Ning, Z.-w.; Zhai, L.-x.; Huang, T.; Peng, J.; Hu, D.; Xiao, H.-t.; Wen, B.; Lin, C.-y.; Zhao, L.; Bian, Z.-x. Identification of α -glucosidase inhibitors from *Cyclocarya paliurus* tea leaves using UF-UPLC-Q/TOF-MS/MS and molecular docking. *Food & function* **2019**, *10* (4), 1893-1902.
- (434) Kraus, N. A.; Ehebauer, F.; Zapp, B.; Rudolphi, B.; Kraus, B. J.; Kraus, D. Quantitative assessment of adipocyte differentiation in cell culture. *Adipocyte* **2016**, *5* (4), 351-358.
- (435) Nooron, N., Athipornchai, A., Suksamrarn, A., and Chiabchalard, A. Mahanine enhances the glucose-lowering mechanisms in skeletal muscle and adipocyte cells. *Biochemical and biophysical research communications* **2017**, *494* (1-2), 101-106.
- (436) Giorgio, E.; Parrinello, N.; Caccamese, S.; Rosini, C. Non-empirical assignment of the absolute configuration of (-)-naringenin, by coupling the exciton analysis of the circular dichroism spectrum and the ab initio calculation of the optical rotatory power. *Organic & biomolecular chemistry* **2004**, *2* (24), 3602-3607.
- (437) Kim, H. J.; Lee, J. Y.; Kim, S. M.; Park, D.-A.; Jin, C.; Hong, S. P.; Lee, Y. S. A new epicatechin gallate and calpain inhibitory activity from *Orostachys japonicus*. *Fitoterapia* **2009**, *80* (1), 73-76.
- (438) Zhao, H.; Kalivendi, S.; Zhang, H.; Joseph, J.; Nithipatikom, K.; Vásquez-Vivar, J.; Kalyanaraman, B. Superoxide reacts with hydroethidine but forms a fluorescent product that is distinctly different from ethidium: potential implications in intracellular fluorescence detection of superoxide. *Free Radical Biology and Medicine* **2003**, *34* (11), 1359-1368.
- (439) Mailloux, R. J. Teaching the fundamentals of electron transfer reactions in mitochondria and the production and detection of reactive oxygen species. *Redox biology* **2015**, *4*, 381-398.
- (440) Kauffman, M. E., Kauffman, M.K., Traore, K., Zhu, H., Trush, M.A., Jia, Z., and Li, Y.R. MitoSOX-based flow cytometry for detecting mitochondrial ROS. *Reactive oxygen species (Apex, NC)* **2016**, *2* (5), 361.
- (441) Sivandzade, F.; Bhalerao, A.; Cucullo, L. Analysis of the mitochondrial membrane potential using the cationic JC-1 dye as a sensitive fluorescent probe. *Bio-protocol* **2019**, *9* (1).

- (442) Harshkova, D.; Zielińska, E.; Aksmann, A. Optimization of a microplate reader method for the analysis of changes in mitochondrial membrane potential in *Chlamydomonas reinhardtii* cells using the fluorochrome JC-1. *Journal of Applied Phycology* **2019**, *31* (6), 3691-3697.
- (443) Lee, J. O., Lee, S.K., Kim, J.H., Kim, N., You, G.Y., Moon, J.W., Kim, S.J., Park, S.H., and Kim, H.S. Metformin regulates glucose transporter 4 (GLUT4) translocation through AMP-activated protein kinase (AMPK)-mediated Cbl/CAP signaling in 3T3-L1 preadipocyte cells. *Journal of Biological Chemistry* **2012**, *287* (53), 44121-44129.
- (444) Al-Soqeer, A. Nutritive value assessment of Acacia species using their chemical analyses and in vitro gas production technique. *Res. J. Agric. Biol. Sci* **2008**, *4* (6), 688-694.
- (445) Salem, H. B.; Nefzaoui, A.; Salem, L. B.; Tisserand, J. Effect of Acacia cyanophylla Lindl. foliage supply on intake and digestion by sheep fed lucerne hay-based diets. *Animal feed science and technology* **1997**, *68* (1-2), 101-113.
- (446) Hamiltons-Amachree, A.; Uzoekwe, S. A. GC-MS analysis of oil rich in polyenoic fatty acid methyl esters from leaves of *Justicia secunda* Vahl growing abundantly in the lowland rain forests of the Niger Delta region of Nigeria. *American Journal of Essential Oils and Natural Products* **2017**, *5* (4), 1-4.
- (447) Ravichandiran, V.; Shanmugam, K.; Anupama, K.; Thomas, S.; Princy, A. Structure-based virtual screening for plant-derived SdiA-selective ligands as potential antivirulent agents against uropathogenic *Escherichia coli*. *European journal of medicinal chemistry* **2012**, *48*, 200-205.
- (448) Jayaram, H.; Marigowda, V.; Thara Saraswathi, K. J. Secondary Metabolite Production and Terpenoid Biosynthesis in Endophytic Fungi *Cladosporium cladosporioides* Isolated from Wild *Cymbopogon martinii* (Roxb.) Wats. *Microbiology Research* **2021**, *12* (4), 812-827.
- (449) Bohman, B.; Weinstein, A. M.; Mozuraitis, R.; Flematti, G. R.; Borg-Karlson, A.-K. Identification of (Z)-8-heptadecene and n-pentadecane as electrophysiologically active compounds in *Ophrys insectifera* and its *Argogorytes* pollinator. *International journal of molecular sciences* **2020**, *21* (2), 620.
- (450) Mileva, M.; Krumova, E.; Miteva-Staleva, J.; Kostadinova, N.; Dobрева, A.; Galabov, A. S. Chemical compounds, in vitro antioxidant and antifungal activities of some plant essential oils belonging to Rosaceae family. *Compt. Rend. Acad. Bulg. Sci* **2014**, *67* (10), 1363-1368.
- (451) Hashem, F.; Saleh, M. Antimicrobial components of some cruciferae plants (*Diplotaxis harra* Forsk. and *Erucaria microcarpa* Boiss.). *Phytotherapy Research: An International Journal Devoted to Pharmacological and Toxicological Evaluation of Natural Product Derivatives* **1999**, *13* (4), 329-332.
- (452) Safaei-Ghomi, J.; Akhoondi, S.; Batooli, H.; Dackhili, M. Chemical variability of essential oil components of two *Rosa x damascena* genotypes growing in Iran. *Chemistry of natural compounds* **2009**, *45* (2), 262-264.
- (453) Selli, S.; Prost, C.; Serot, T. Odour-active and off-odour components in rainbow trout (*Oncorhynchus mykiss*) extracts obtained by microwave assisted distillation–solvent extraction. *Food Chemistry* **2009**, *114* (1), 317-322.
- (454) Hu, Z.; Wang, C.; Shen, H.; Zhang, K.; Leng, P. Antioxidant effect of aromatic volatiles emitted by *Lavandula dentata*, *Mentha spicata*, and *M. piperita* on mouse subjected to low oxygen condition. *Bioscience, Biotechnology, and Biochemistry* **2017**, *81* (12), 2386-2395.
- (455) Cheng-ke, B. Analysis of Chemical Constituents of Volatile Oil from Different Parts of *Melia azedarach* L. by GC-MS. *Natural Product Research & Development* **2008**, *20* (4).

- (456) Abouelenein, D.; Angeloni, S.; Caprioli, G.; Genovese, J.; Mustafa, A. M.; Nzekoue, F. K.; Petrelli, R.; Rocculi, P.; Sagratini, G.; Tappi, S. Effect of Plasma Activated Water on Selected Chemical Compounds of Rocket-Salad (*Eruca sativa* Mill.) Leaves. *Molecules* **2021**, *26* (24), 7691.
- (457) Zhou, Y.; Tang, N.; Huang, L.; Zhao, Y.; Tang, X.; Wang, K. Effects of Salt Stress on Plant Growth, Antioxidant Capacity, Glandular Trichome Density, and Volatile Exudates of *Schizonepeta tenuifolia* Briq. *International journal of molecular sciences* **2018**, *19* (1), 252.
- (458) Ogunwande, I.; Flamini, G.; Adefuye, A.; Lawal, N.; Moradeyo, S.; Avoseh, N. Chemical compositions of *Casuarina equisetifolia* L., *Eucalyptus toreliana* L. and *Ficus elastica* Roxb. ex Hornem cultivated in Nigeria. *South African Journal of Botany* **2011**, *77* (3), 645-649.
- (459) Kang, W.; Ji, Z.; Wang, J. Composition of the essential oil of *Adiantum flabellulatum*. *Chemistry of natural compounds* **2009**, *45* (4), 575-577.
- (460) Salem, A.-F. Z.; Salem, M. Z.; Gonzalez-Ronquillo, M.; Camacho, L.; Cipriano, M. Major chemical constituents of *Leucaena leucocephala* and *Salix babylonica* leaf extracts. *Journal of Tropical Agriculture* **2011**, *49*, 95-98.
- (461) Javidnia, K.; Miri, R.; Soltani, M.; Khosravi, A. Essential oil composition of *biebersteinia multifida* DC.(Biebersteiniaceae) from Iran. *Journal of Essential Oil Research* **2010**, *22* (6), 611-612.
- (462) Lazari, D. M.; Skaltsa, H. D.; Constantinidis, T. Composition of the essential oil of *Herniaria incana* Lam. from Greece. *Journal of Essential Oil Research* **2000**, *12* (4), 435-437.
- (463) Ogunwande, I. A.; Sonibare, M. A.; Thang, T. D.; Dung, N. X.; Soladoye, M. O.; Morohunfolu, O. O. Comparative analysis of the oils of three *Ficus* species from Nigeria. *Journal of Essential Oil Research* **2008**, *20* (5), 386-389.
- (464) Sonibare, M. A.; Sonibare, O. O.; Akharam, O. E.; Soladoye, M. O. Chemical Composition of Essential Oils of *Ficus elasticoidies* De Wild., *Ficus ovata* Vahl and *Ficus natalensis* subsp. *leprieurii* (Miq.) CC Berg from Nigeria. *Journal of Essential Oil Bearing Plants* **2009**, *12* (3), 282-286.
- (465) Chibani, S.; Gherboudj, W.; Kabouche, A.; Touzani, R.; Aburjai, T.; Kabouche, Z. GC-MS analysis of *Senecio giganteus* Desf. from Algeria. *Journal of Essential Oil Bearing Plants* **2013**, *16* (1), 123-125.
- (466) Choi, H.-S. Chemical composition of *Cirsium japonicum* var. *ussuriense* Kitamura and the quantitative changes of major compounds by the harvesting season. *The Korean Journal of Food And Nutrition* **2016**, *29* (3), 327-334.
- (467) Choi, H.-S. Analysis of Essential Oils Extracted from Fresh and Shade-dried Leaves of *Synurus deltoides* (Arr.) Nakai. *The Korean Journal of Food And Nutrition* **2021**, *34* (2), 224-232.
- (468) Sun, Y.; Yang, A. W. H.; Lenon, G. B. Phytochemistry, ethnopharmacology, pharmacokinetics and toxicology of *Cnidium monnieri* (L.) Cusson. *International Journal of Molecular Sciences* **2020**, *21* (3), 1006.
- (469) Yuvaraj, R.; Rao, M. R. K.; Prabhu, K.; Sundram, R. L.; Shil, S.; Kumar, M. S.; Vijayalakshmi, N. The gas chromatography–mass spectrometry study of one medicinal plant, *Stachytarpheta indica*. *Drug Invention Today* **2019**, *12* (8).
- (470) Ahmed, O. H.; Abbas, A. H.; Yaseen, Y. S.; Ezghayer, M. A. GC-MS Analysis of Hexane Fraction of *Indigofera Suffruticosa* Plant Naturally Growing in Iraq. *NeuroQuantology* **2022**, *20* (4), 393-396.
- (471) Wood, W. F.; Palmer, T. M.; Stanton, M. L. A comparison of volatiles in mandibular glands from three *Crematogaster* ant symbionts of the whistling thorn acacia. *Biochemical Systematics and Ecology* **2002**, *30* (3), 217-222.

- (472) Debi, C.; Parkash, V. Influence of microbial bioinoculants on the accumulation of new phytochemicals in *Oroxylum indicum* (L.) Benth. ex Kurz. *GSC Biological and Pharmaceutical Sciences* **2020**, *13* (3), 228-243.
- (473) Murugan, K.; Iyer, V. V. Antioxidant activity and gas chromatographic-mass spectrometric analysis of extracts of the marine algae, *Caulerpa peltata* and *Padina gymnospora*. *Indian journal of pharmaceutical sciences* **2014**, *76* (6), 548.
- (474) Lesuffleur, F.; Paynel, F.; Bataillé, M.-P.; Le Deunff, E.; Cliquet, J.-B. Root amino acid exudation: measurement of high efflux rates of glycine and serine from six different plant species. *Plant and soil* **2007**, *294* (1), 235-246.
- (475) Bhuiyan, M. N. I.; Begum, J.; Bhuiyan, M. N. H. Analysis of essential oil of eaglewood tree (*Aquilaria agallocha* Roxb.) by gas chromatography mass spectrometry. *Bangladesh Journal of Pharmacology* **2009**, *4* (1), 24-28.
- (476) Adsul, V.; Khatiwora, E.; Kulkarni, M.; Tambe, A.; Pawar, P.; Deshpande, N. GC-MS study of fatty acids, esters, alcohols from the leaves of *Ipomoea carnea*. *Int J Pharm Tech Res* **2009**, *1*, 1224-1226.
- (477) Mastelić, J.; Jerković, I.; Mesić, M. Volatile constituents from flowers, leaves, bark and wood of *Prunus mahaleb* L. *Flavour and fragrance journal* **2006**, *21* (2), 306-313.
- (478) Misra, L.; Mishra, P.; Pandey, A.; Sangwan, R. S.; Sangwan, N. S. 1, 4-Dioxane and ergosterol derivatives from *Withania somnifera* roots. *Journal of Asian natural products research* **2012**, *14* (1), 39-45.
- (479) Mitra, S.; Sarkar, N.; Barik, A. Long-chain alkanes and fatty acids from *Ludwigia octovalvis* weed leaf surface waxes as short-range attractant and ovipositional stimulant to *Altica cyanea* (Weber)(Coleoptera: Chrysomelidae). *Bulletin of entomological research* **2017**, *107* (3), 391-400.
- (480) Dandekar, R.; Fegade, B.; Bhaskar, V. GC-MS analysis of phytoconstituents in alcohol extract of *Epiphyllum oxypetalum* leaves. *Journal of pharmacognosy and phytochemistry* **2015**, *4* (1).
- (481) Khatua, S.; Pandey, A.; Biswas, S. J. Phytochemical evaluation and antimicrobial properties of *Trichosanthes dioica* root extract. *Journal of Pharmacognosy and Phytochemistry* **2016**, *5* (5), 410.
- (482) Al Bratty, M.; Makeen, H. A.; Alhazmi, H. A.; Syame, S. M.; Abdalla, A. N.; Homeida, H. E.; Sultana, S.; Ahsan, W.; Khalid, A. Phytochemical, cytotoxic, and antimicrobial evaluation of the fruits of miswak plant, *Salvadora persica* L. *Journal of Chemistry* **2020**, 2020.
- (483) Ahmad, M.; Baba, W. N.; Gani, A.; Wani, T. A.; Gani, A.; Masoodi, F. Effect of extraction time on antioxidants and bioactive volatile components of green tea (*Camellia sinensis*), using GC/MS. *Cogent Food & Agriculture* **2015**, *1* (1), 1106387.
- (484) Angelini, P.; Tirillini, B.; Properzi, A.; Rol, C.; Venanzoni, R. Identification and bioactivity of the growth inhibitors in *Tuber* spp. methanolic extracts. *Plant Biosystems-An International Journal Dealing with all Aspects of Plant Biology* **2015**, *149* (6), 1000-1009.
- (485) Rosselli, S.; Tundis, R.; Bruno, M.; Leporini, M.; Falco, T.; Gagliano Candela, R.; Badalamenti, N.; Loizzo, M. R. *Ceiba speciosa* (A. St.-Hil.) seeds oil: Fatty acids profiling by GC-MS and NMR and bioactivity. *Molecules* **2020**, *25* (5), 1037.
- (486) So, H. M.; Lee, S.; Baek, K.-H.; Roh, H.-S.; Kim, S.; Jo, M. S.; Baek, S. C.; Seok, S.; Ryoo, R.; Kim, K. H. Bioactivity-based analysis and chemical characterization of cytotoxic compounds from a poisonous mushroom, *Amanita spissacea*, in human lung cancer cells in vitro. *Natural Product Research* **2021**, *35* (4), 649-654.

- (487) Omoruyi, B. E.; Afolayan, A. J.; Bradley, G. Chemical composition profiling and antifungal activity of the essential oil and plant extracts of *Mesembryanthemum edule* (L.) bolus leaves. *African Journal of Traditional, Complementary and Alternative Medicines* **2014**, *11* (4), 19-30.
- (488) Mozirandi, W.; Tagwireyi, D.; Mukanganyama, S. Evaluation of antimicrobial activity of chondrillasterol isolated from *Vernonia adoensis* (Asteraceae). *BMC complementary and alternative medicine* **2019**, *19* (1), 1-11.
- (489) Ezzat, S. M.; Salama, M. M. A new α -glucosidase inhibitor from *Achillea fragrantissima* (Forssk.) Sch. Bip. growing in Egypt. *Natural Product Research* **2014**, *28* (11), 812-818.
- (490) Shen, Y.; Han, C.; Liu, J.; Liu, A.; Ji, X.; Liu, C. Analysis of volatile components of *Pseudostellaria heterophylla* (Miq.) Pax by microwave-assisted solvent extraction and GC-MS. *Chromatographia* **2008**, *68* (7), 679-682.
- (491) Chen, J.-J.; Duh, C.-Y.; Chen, I.-S. Cytotoxic chromenes from *Myriactis humilis*. *Planta medica* **2005**, *71* (04), 370-372.
- (492) Piyatida, P.; Kimura, F.; Sato, M.; Kato-Noguchi, H. Isolation of [Beta]-sitosterol from *Hibiscus sabdariffa* L. *Allelopathy Journal* **2013**, *32* (2), 289.
- (493) Alqahtani, S. S.; Makeen, H. A.; Menachery, S. J.; Moni, S. S. Documentation of bioactive principles of the flower from *Caralluma retrospiciens* (Ehrenb) and in vitro antibacterial activity-Part B. *Arabian Journal of Chemistry* **2020**, *13* (10), 7370-7377.
- (494) Villaseñor, I. M.; Canlas, A. P.; Faustino, K. M.; Plana, K. G. Evaluation of the bioactivity of triterpene mixture isolated from *Carmona retusa* (Vahl.) Masam leaves. *Journal of ethnopharmacology* **2004**, *92* (1), 53-56.
- (495) Henneh, I. T.; Huang, B.; Musayev, F. N.; Al Hashimi, R.; Safo, M. K.; Armah, F. A.; Ameyaw, E. O.; Adokoh, C. K.; Ekor, M.; Zhang, Y. Structural elucidation and in vivo anti-arthritic activity of β -amyrin and polpunonic acid isolated from the root bark of *Ziziphus abyssinica* HochstEx. A Rich (Rhamnaceae). *Bioorganic chemistry* **2020**, *98*, 103744.
- (496) Ramos-Hernández, J.; Calderón-Santoyo, M.; Navarro-Ocaña, A.; Barros-Castillo, J.; Ragazzo-Sánchez, J. Use of emerging technologies in the extraction of lupeol, α -amyrin and β -amyrin from sea grape (*Coccoloba uvifera* L.). *Journal of food science and technology* **2018**, *55* (7), 2377-2383.
- (497) Csapi, B.; Hajdú, Z.; Zupkó, I.; Berényi, Á.; Forgo, P.; Szabó, P.; Hohmann, J. Bioactivity-guided isolation of antiproliferative compounds from *Centaurea arenaria*. *Phytotherapy research* **2010**, *24* (11), 1664-1669.
- (498) Klein, E. J.; Nathia-Neves, G.; Vardanega, R.; Meireles, M. A. A.; da Silva, E. A.; Vieira, M. G. A. Supercritical CO₂ extraction of α -/ β -amyrin from uvaia (*Eugenia pyriformis* Cambess.): effects of pressure and co-solvent addition. *The Journal of Supercritical Fluids* **2019**, *153*, 104595.
- (499) Karen Cardoso, B.; Line Marko de Oliveira, H.; Zonta Melo, U.; Mariano Fernandez, C. M.; Franco de Araújo Almeida Campo, C.; Gonçalves, J. E.; Laverde Jr, A.; Barion Romagnolo, M.; Andrea Linde, G.; Cristiani Gazim, Z. Antioxidant activity of α and β -amyrin isolated from *Myrcianthes pungens* leaves. *Natural Product Research* **2020**, *34* (12), 1777-1781.
- (500) Abdel-Raouf, N.; Al-Enazi, N. M.; Al-Homaidan, A. A.; Ibraheem, I. B. M.; Al-Othman, M. R.; Hatamleh, A. A. Antibacterial β -amyrin isolated from *Laurencia microcladia*. *Arabian Journal of Chemistry* **2015**, *8* (1), 32-37.
- (501) Keawsa-Ard, S.; Natakankitkul, S.; Liawruangrath, S.; Teerawutgulrag, A.; Trisuwan, K.; Charoenying, P.; Pyne, S. G.; Liawruangrath, B. Anticancer and antibacterial activities of the isolated compounds from *Solanum spirale* Roxb. leaves. *Chiang Mai J. Sci* **2012**, *39* (3), 445-454.

- (502) Gilani, S.; Najafpour, G. Evaluation of the extraction process parameters on bioactive compounds of cinnamon bark: A comparative study. *Process Biochemistry* **2022**, *114*, 93-101.
- (503) Pham, T. V.; Hoang, H. N. T.; Nguyen, H. T.; Nguyen, H. M.; Huynh, C. T.; Vu, T. Y.; Do, A. T.; Nguyen, N. H.; Do, B. H. Anti-Inflammatory and Antimicrobial Activities of Compounds Isolated from *Distichochlamys benenica*. *BioMed research international* **2021**, *2021*.
- (504) Majouli, K.; Hamdi, A.; Msaada, K.; Kenani, A. A bioactivity guided study on the antibacterial activity of *Hertia cheirifolia* L. extracts. *Microbial pathogenesis* **2017**, *106*, 113-118.
- (505) de Carvalho Rodrigues, V.; da Silva, M. V.; dos Santos, A. R.; Zielinski, A. A.; Haminiuk, C. W. Evaluation of hot and cold extraction of bioactive compounds in teas. *International Journal of Food Science & Technology* **2015**, *50* (9), 2038-2045.
- (506) Bock, C. H.; Shapiro-Ilan, D. I.; Wedge, D. E.; Cantrell, C. L. Identification of the antifungal compound, trans-cinnamic acid, produced by *Photobacterium luminescens*, a potential biopesticide against pecan scab. *Journal of Pest Science* **2014**, *87* (1), 155-162.
- (507) de Sousa, C. B. d. C.; dos Anjos, G. L.; Nobrega, R. S.; Magaton, A. d. S.; de Miranda, F. M.; Dias, F. d. S. Greener ultrasound-assisted extraction of bioactive phenolic compounds in *Croton heliotropiifolius* Kunth leaves. *Microchemical Journal* **2020**, *159*, 105525.
- (508) Moreira, G. C.; de Souza Dias, F. Mixture design and Doehlert matrix for optimization of the ultrasonic assisted extraction of caffeic acid, rutin, catechin and trans-cinnamic acid in *Physalis angulata* L. and determination by HPLC DAD. *Microchemical Journal* **2018**, *141*, 247-252.
- (509) Vedak, S.; Raut, S. V. Study on antibacterial compounds from methanolic extract of bark of *Prosopis juliflora* (Vilayati babhul). *Int J Pharmaceu Sci Bus Manag* **2014**, *2* (6), 1-14.
- (510) Tangavelou, A.; Viswanathan, M.; Balakrishna, K.; Patra, A. Phytochemical Analysis in the Leaves of *Chamaecrista nigricans* (Leguminosae). *Pharm. Anal. Acta* **2018**, *9*.
- (511) Larbie, C. *Tetrapleura tetraptera* of Ghanaian origin: phytochemistry, antioxidant and antimicrobial activity of extracts of plant parts. *Antioxidant and Antimicrobial Activity of Extracts of Plant Parts (December 17, 2020)* **2020**.
- (512) Kang, M.-C.; Ding, Y.; Kim, E.-A.; Choi, Y. K.; De Araujo, T.; Heo, S.-J.; Lee, S.-H. Indole derivatives isolated from brown alga *Sargassum thunbergii* inhibit adipogenesis through AMPK activation in 3T3-L1 preadipocytes. *Marine drugs* **2017**, *15* (4), 119.
- (513) Cha, S.-H.; Hwang, Y.; Heo, S.-J.; Jun, H.-S. Indole-4-carboxaldehyde isolated from seaweed, *Sargassum thunbergii*, attenuates methylglyoxal-induced hepatic inflammation. *Marine drugs* **2019**, *17* (9), 486.
- (514) Luan, C.; Zhang, M.; Devahastin, S.; Liu, Y. Effect of two-step fermentation with lactic acid bacteria and *Saccharomyces cerevisiae* on key chemical properties, molecular structure and flavor characteristics of horseradish sauce. *LWT* **2021**, *147*, 111637.
- (515) Srinivasan, S.; Priya, V. Phytochemical screening and GC-MS analysis of *Cyperus dubius*, Rottb.(Cyperaceae). *Journal of Medicinal Plants* **2019**, *7* (2), 89-98.
- (516) Dinesh, S.; Sudharsana, S.; Mohanapriya, A.; Itami, T.; Sudhakaran, R. Molecular docking and simulation studies of *Phyllanthus amarus* phytochemicals against structural and nucleocapsid proteins of white spot syndrome virus. *3 Biotech* **2017**, *7* (5), 1-12.

- (517) Rameshkumar, R.; Satish, L.; Pandian, S.; Rathinapriya, P.; Rency, A. S.; Shanmugaraj, G.; Pandian, S. K.; Leung, D. W.; Ramesh, M. Production of squalene with promising antioxidant properties in callus cultures of *Nilgirianthus ciliatus*. *Industrial Crops and Products* **2018**, *126*, 357-367.
- (518) Rama, V.; Bharathi Muruganatham, K. D.; Muthusami, S. Molecular docking analysis of estrogen receptor binding phytocomponents identified from the ethyl acetate extract of *Salicornia herbacea* (L). *Bioinformation* **2022**, *18* (3), 273-283.
- (519) Anusiya, G.; Bharathi, S.; Mukesh Praveen, K.; Sainandhini, G. Extraction and molecular characterization of biological compounds from water hyacinth. *Journal of Medicinal Plants* **2020**, *8* (5), 14-19.
- (520) Ricciardelli, A.; Casillo, A.; Papa, R.; Monti, D. M.; Imbimbo, P.; Vrenna, G.; Artini, M.; Selan, L.; Corsaro, M. M.; Tutino, M. L. Pentadecanal inspired molecules as new anti-biofilm agents against *Staphylococcus epidermidis*. *Biofouling* **2018**, *34* (10), 1110-1120.
- (521) Cho, S.-Y.; Min, N.-R.; Kim, Y. O.; Kim, D. Anti-Viral Hemorrhagic Septicemia Virus (VHSV) Activity of 3-Methyl Catechol. *Korean Journal of Fisheries and Aquatic Sciences* **2021**, *54* (5), 644-651.
- (522) Wu, Y.; Chen, H.-P.; Wei, J.-Y.; Yang, K.; Tian, Z.-F.; Li, X.-L.; Wang, P.-J.; Wang, C.-F.; Du, S.-S.; Cai, Q. Repellent constituents of essential oil from *Citrus wilsonii* stem barks against *Tribolium castaneum*. *Natural Product Communications* **2014**, *9* (10), 1934578X1400901028.
- (523) Lawal, O.; Hutchings, A.; Oyedeji, O. Chemical Composition of the Leaf Oil of *Plectranthus neochilus* Schltr. *Journal of Essential Oil Research* **2010**, *22* (6), 546-547.
- (524) Doshi, G. M.; Nalawade, V. V.; Mukadam, A. S.; Chaskar, P. K.; Zine, S. P.; Somani, R. R.; Une, H. D. Structural elucidation of chemical constituents from *Benincasa hispida* seeds and *Carissa congesta* roots by gas chromatography: Mass spectroscopy. *Pharmacognosy research* **2015**, *7* (3), 282.
- (525) Vahedi, H.; Lari, J.; Halimi, M.; Nasrabadi, M.; Vahedi, A. Chemical composition of the n-hexane extract of *Verbascum speciosum* growing wild in Iran. *Journal of Essential Oil Bearing Plants* **2012**, *15* (6), 895-899.
- (526) Indrayan, A.; Sharma, S.; Durgapal, D.; Kumar, N.; Kumar, M. Determination of nutritive value and analysis of mineral elements for some medicinally valued plants from Uttaranchal. *Current science* **2005**, 1252-1255.
- (527) Chen, S.; Yong, T.; Xiao, C.; Su, J.; Zhang, Y.; Jiao, C.; Xie, Y. Pyrrole alkaloids and ergosterols from *Grifola frondosa* exert anti- α -glucosidase and anti-proliferative activities. *Journal of functional foods* **2018**, *43*, 196-205.
- (528) Tan, D. C.; Kassim, N. K.; Ismail, I. S.; Hamid, M.; Ahmad Bustamam, M. S. Identification of antidiabetic metabolites from *Paederia foetida* l. twigs by gas chromatography-mass spectrometry-based metabolomics and molecular docking study. *BioMed research international* **2019**, 2019.
- (529) Yao, L.; Gerde, J. A.; Lee, S.-L.; Wang, T.; Harrata, K. A. Microalgae lipid characterization. *Journal of agricultural and food chemistry* **2015**, *63* (6), 1773-1787.
- (530) Belanger, P.; Zintel, J.; Heuvel, W. V.; Smith, J. Identification by combined gas-liquid chromatography-mass spectrometry of sterols isolated from *Scenedesmus obliquus* grown in light and heavy water. *Canadian Journal of Chemistry* **1973**, *51* (19), 3294-3298.
- (531) Anandan, A.; Eswaran, R.; Doss, A.; Sangeetha, G.; Anand, S. Chemical compounds investigation of *Cassia auriculata* leaves—a potential folklore medicinal plant. *Bulletin of Environment, Pharmacology & Life Sciences* **2011**, *1* (1), 20-23.

- (532) Prabhadevi, V.; Sahaya, S. S.; Johnson, M.; Venkatramani, B.; Janakiraman, N. Phytochemical studies on *Allamanda cathartica* L. using GC–MS. *Asian Pacific Journal of Tropical Biomedicine* **2012**, *2* (2), S550-S554.
- (533) Fang, Y.; Li, Y.; Yi, W.; Liu, S.; Bai, X. Fractionation of pyroligneous acid: the first step for the recovery of levoglucosan. *BioResources* **2017**, *12* (1), 981-991.
- (534) Yip, J.; Chen, M.; Szeto, Y.; Yan, S. Comparative study of liquefaction process and liquefied products from bamboo using different organic solvents. *Bioresource Technology* **2009**, *100* (24), 6674-6678.
- (535) Wang, X.; Bei, H.; Du, R.; Chen, Q.; Wu, F.; Chen, J.; Bo, H. Metabolomic analysis of serum reveals the potential effective ingredients and pathways of Danggui Buxue Tang in promoting erythropoiesis. *Complementary Therapies in Medicine* **2020**, *48*, 102247.
- (536) Robinson, T. D-amino acids in higher plants. *Life sciences* **1976**, *19* (8), 1097-1102.
- (537) Indrasari, S. D.; Arofah, D.; Handoko, D. D. Volatile compounds profile of some Indonesian shallot varieties. In *IOP Conference Series: Earth and Environmental Science*, 2021; IOP Publishing: Vol. 746, p 012009.
- (538) Ding, Y.; Zhou, X.; Zhong, Y.; Wang, D.; Dai, B.; Deng, Y. Metabolite, volatile and antioxidant profiles of black garlic stored in different packaging materials. *Food Control* **2021**, *127*, 108131.

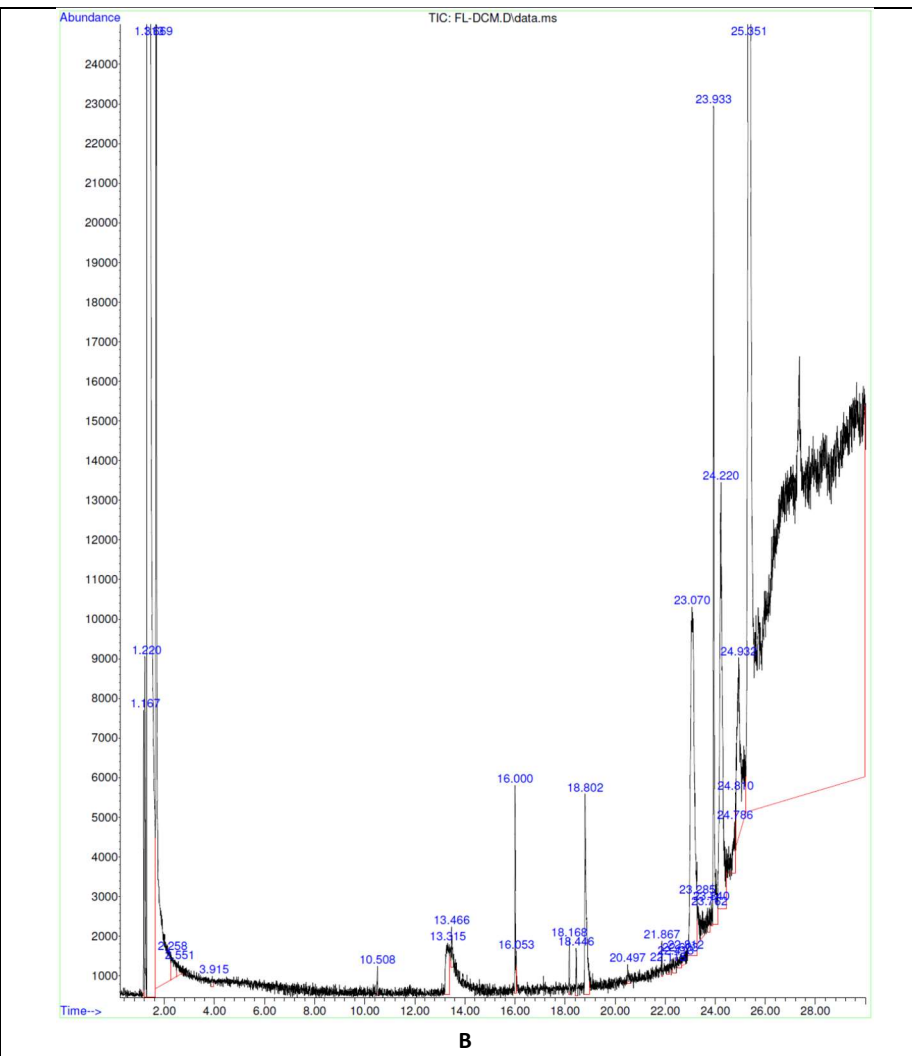
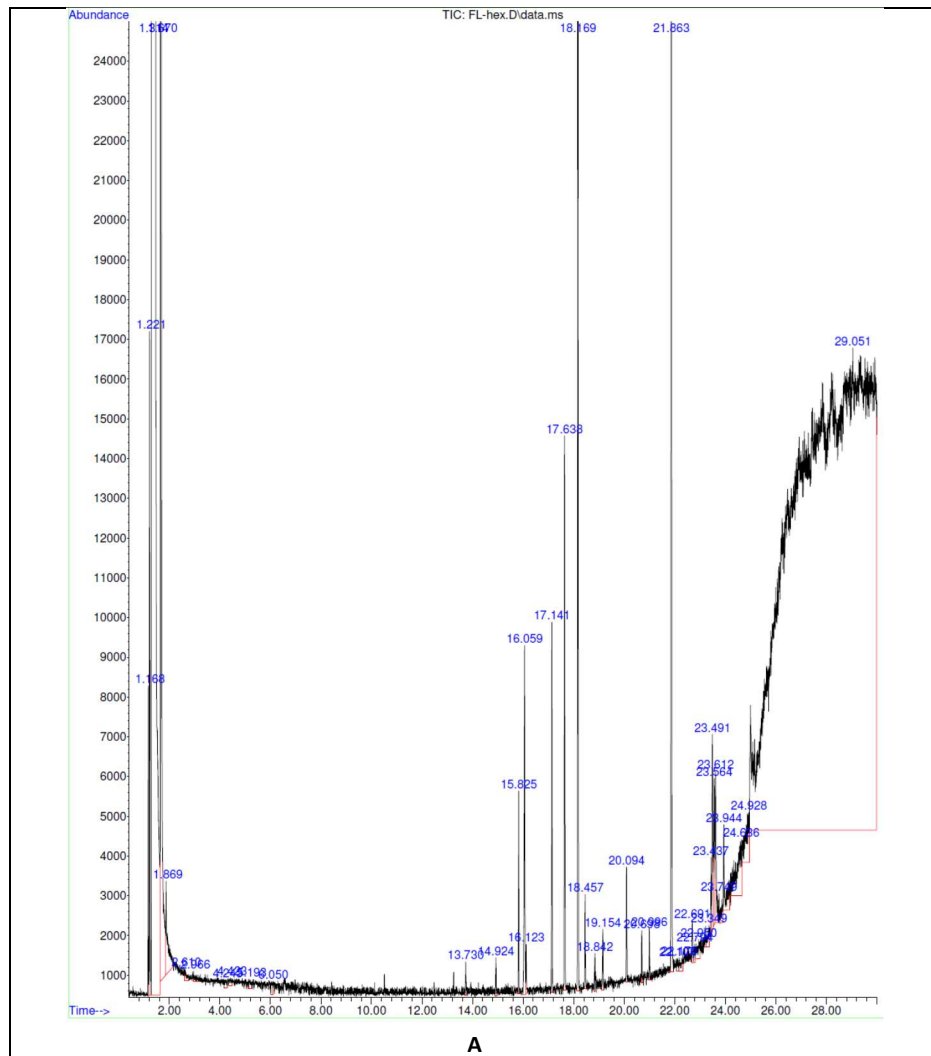
Appendix A

Table S1. Summary of reported bioactivities of various parts of *A. saligna* along with the possibly responsible phytochemicals

No	Bioactivities	Plant parts	Harvesting location	Compound identification methods	Corresponding compounds	Reference
1	Antioxidant	Flowers	Tunisia	NMR and mass spectrometry	Isosalipurposide 1 , quercetin 3 , and naringenin 42	197
			Egypt	HPLC	Quercetin 3 , kaempferol 22 , benzoic acid 24 , syringic acid 28 , <i>p</i> -hydroxy benzoic acid 31 , salicylic acid 32 , caffeic acid 35 , <i>o</i> -coumaric acid 36 , <i>p</i> -coumaric acid 37 , ferulic acid 38 , naringenin 42 , ellagic acid 44 , catechol 45 , and caffeine 46	196
		Leaves	Egypt	NMR and mass spectrometry	Quercitrin 4 , myricitrin 11 , myricetin-3- <i>O</i> -rhamnoside (<i>C</i> ⁷ - <i>O</i> - <i>C</i> ⁷) myricetin-3- <i>O</i> -rhamnoside 33 , erythrodiol 73 , 3β- <i>O</i> - <i>trans-p</i> -coumaryl erythrodiol 74 , and 25 <i>S</i> -5β-spirostan-3β-yl-3- <i>O</i> -β- <i>D</i> -xylopyranosyl (1→3)- <i>O</i> -β- <i>D</i> -xylopyranosyl (1→4)-β- <i>D</i> -galactopyranoside 75	54
			Saudi Arabia	HPLC	Quercetin 3 , rutin 6 , miquelianin 7 , isoquercetin 8 , hyperoside 9 , apigetrin 17 , gallic acid 25 , salipurpin 18 , and <i>p</i> -coumaric acid 37	220
		Seeds	Tunisia		Polyphenols, flavonoids, and fatty acids	231
		Barks	Egypt	HPLC	Quercetin 3 , rutin 6 , kaempferol 22 , benzoic acid 24 , gallic acid 25 , vanillin 29 , caffeic acid 35 , <i>o</i> -coumaric acid 37 , <i>p</i> -coumaric acid 36 , ferulic acid 38 , rosmarinic acid 39 , chlorogenic acid 40 , and caffeine 46	230
2	Antibacterial	Flowers	Egypt	HPLC	Quercetin 3 , kaempferol 22 , benzoic acid 24 , syringic acid 28 , <i>p</i> -hydroxy benzoic acid 31 , salicylic acid 32 , caffeic acid 35 , <i>o</i> -coumaric acid 36 , <i>p</i> -coumaric acid 37 , ferulic acid 38 , naringenin 42 , ellagic acid 44 , catechol 45 , and caffeine 46	196
		Leaves	Saudi Arabia	HPLC	Quercetin 3 , quercitrin 4 , rutin 6 , miquelianin 7 , isoquercetin 8 , hyperoside 9 , apigetrin 17 , salipurpin 18 , gallic acid 25 , and <i>p</i> -coumaric acid 37	220
			Egypt	NMR and mass spectrometry	Quercetin 3 , quercitrin 4 , quercetin-3- <i>O</i> -arabinoside 5 , myricetin 10 , myricitrin 11 , myricetin-3- <i>O</i> -arabinoside 12 , myricetin-3- <i>O</i> -glucoside 13 , catechin 14 , 7- <i>O</i> -Galloyl-cathecin 15 , apigenin 16 , apigetrin 17 , luteolin 19 , luteolin-7- <i>O</i> -glucoside 20 , gallic acid 25 , and methyl gallate 26	199
3	Antifungal	Flowers	Egypt	HPLC	Quercetin 3 , kaempferol 22 , benzoic acid 24 , syringic acid 28 , <i>p</i> -hydroxy benzoic acid 31 , salicylic acid 32 , caffeic acid 35 , <i>o</i> -coumaric acid 36 , <i>p</i> -	196

No	Bioactivities	Plant parts	Harvesting location	Compound identification methods	Corresponding compounds	Reference
					coumaric acid 37 , ferulic acid 38 , naringenin 42 , ellagic acid 44 , catechol 45 , and caffeine 46	
		Leaves	Saudi Arabia	HPLC	Quercetin 3 , rutin 6 , miquelianin 7 , isoquercetin 8 , gallic acid 25 , hyperoside 9 , apigetrin 17 , salipurpin 18 , and <i>p</i> -coumaric acid 37	220
		Barks	Egypt	HPLC	Quercetin 3 , rutin 6 , kaempferol 22 , benzoic acid 24 , gallic acid 25 , vanillin 29 , caffeic acid 35 , <i>o</i> -coumaric acid 36 , <i>p</i> -coumaric acid 37 , ferulic acid 38 , rosmarinic acid 39 , chlorogenic acid 40 , and caffeine 46	230
4	Anticancer	Leaves	Egypt	NMR and mass spectrometry	Quercitrin 4 , myricitrin 11 , myricetin-3- <i>O</i> -rhamnoside (<i>C</i> ⁷ - <i>O</i> - <i>C</i> ⁷) myricetin-3- <i>O</i> -rhamnoside 33 , erythrodiol 73 , 3 β - <i>O</i> - <i>trans</i> - <i>p</i> -coumaryl erythrodiol 74 , 25 <i>S</i> -5 β -spirostan-3 β -yl-3- <i>O</i> - β - <i>D</i> -xylopyranosyl (1 \rightarrow 3)- <i>O</i> - β - <i>D</i> -xylopyranosyl (1 \rightarrow 4)- β - <i>D</i> -galactopyranoside 75	54
			Saudi Arabia	HPLC	Quercetin 3 , rutin 6 , miquelianin 7 , isoquercetin 8 , hyperoside 9 , apigetrin 17 , salipurpin 18 , gallic acid 25 , and <i>p</i> -coumaric acid 37	220
5	Anti-acetylcholine-esterase	Flowers	Tunisia	NMR and mass spectrometry	Isosalipurposide 1	197
6	Allelopathic	Flowers, leaves, stems, roots	Tunisia	GC-FID and GC/MS	<p><i>Roots</i>: benzyl benzoate 69, benzyl benzoate 69, hexahydrofarnesyl acetone 71, phenylethyl salicylate, 2-phenylethyl benzoate</p> <p><i>Stems</i>: dodecanoic acid (syn. Lauric acid), tetradecanoic acid, pentadecane 62, dodecanoic acid 64, tetradecanoic acid 70, hexahydrofarnesyl acetone 71, heptyl valerate, heptadecane, pentadecane, and benzyl butyrate</p> <p><i>Leaves</i>: linalool 47, nonanal 48, α-terpineol 49, decanal 50, geraniol 52, thymol 54, 2-methyl butyl heptanoate 56, eugenol 57, decanoic acid 58, (<i>E</i>)-geranyl acetone 59, (<i>E</i>)-β-ionone 60, pentadecane 62, tridecanal 63, dodecanoic acid 64, tetradecanal 65, benzophenone 66, pentadecan-2-one 67, pentadecanal 68, benzyl benzoate 69, hexahydrofarnesyl acetone 71, pentadecanal, benzyl benzoate, and heptadecane-2-one 72</p> <p><i>Flowers</i>: linalool 47, α-terpineol 49, β-cyclocitral 51, geraniol 52, (<i>E</i>)-dec-2-enal 53, 1,2-dihydro-1,1,6-trimethylnaphthalene 55, decanoic acid 58, (<i>E</i>)-geranyl acetone 59, (<i>E</i>)-β-ionone 60, tridecan-2-one 61, dodecanoic acid</p>	201

No	Bioactivities	Plant parts	Harvesting location	Compound identification methods	Corresponding compounds	Reference
					64 , pentadecan-2-one 67 , pentadecanal 68 , tetradecanoic acid 70 , hexahydrofarnesyl acetone 71 , heptadecane-2-one <i>Pods</i> : 2-methyl butyl heptanoate 56 , (<i>E</i>)-geranyl acetone 59 , (<i>E</i>)- β -ionone 60 , tridecan-2-one 61 , dodecanoic acid 64 , hexahydrofarnesyl acetone 71 , , heptadecane, and methyl hexadecanoate	
7	Fermentation inhibition	Leaves & twigs	Saudi Arabia		Tannins	232
		Stems	Australia		Tannins	233
8	Anti-parasite	Leaves	Egypt	HPLC	Quercetin 3 , rutin 6 , catechin 14 , gallic acid 25 , methyl gallate 26 , propyl gallate 27 , syringic acid 28 , vanillin 29 , cinnamic acid 34 , caffeic acid 35 , <i>p</i> -coumaric acid 37 , ferulic acid 38 , chlorogenic acid 40 , taxifolin 41 , naringin 43 , and ellagic acid 44	222
			Tunisia		Tannins	234 235
9	α -glucosidase inhibition	Barks & leaves	South Africa		Phenolics	205
10	Antihyperglycemic	Leaves	Egypt	HPLC	Quercetin 3 , quercitrin 4 , quercetin 3- <i>O</i> -arabinoside 5 , miquelianin 7 , myricetin 10 , myricitrin 11 , myricetin 3- <i>O</i> -arabinoside 12 , myricetin 3- <i>O</i> -glucoside 13 , luteolin 19 , luteolin 7- <i>O</i> -glucoside 20 , and luteolin 7- <i>O</i> - β -arabinoside 21	219
11	Antiinflammation	Shoots	Egypt	HPLC	Quercetin 3 , rutin 6 , catechin 14 , taxifolin 41 , kaempferol 22 , gallic acid 25 , methyl gallate 26 , syringic acid 28 , cinnamic acid, caffeic acid 35 , coumaric acid 36 , ferulic acid 38 , chlorogenic acid 40 , naringenin 42 , and ellagic acid 44	236



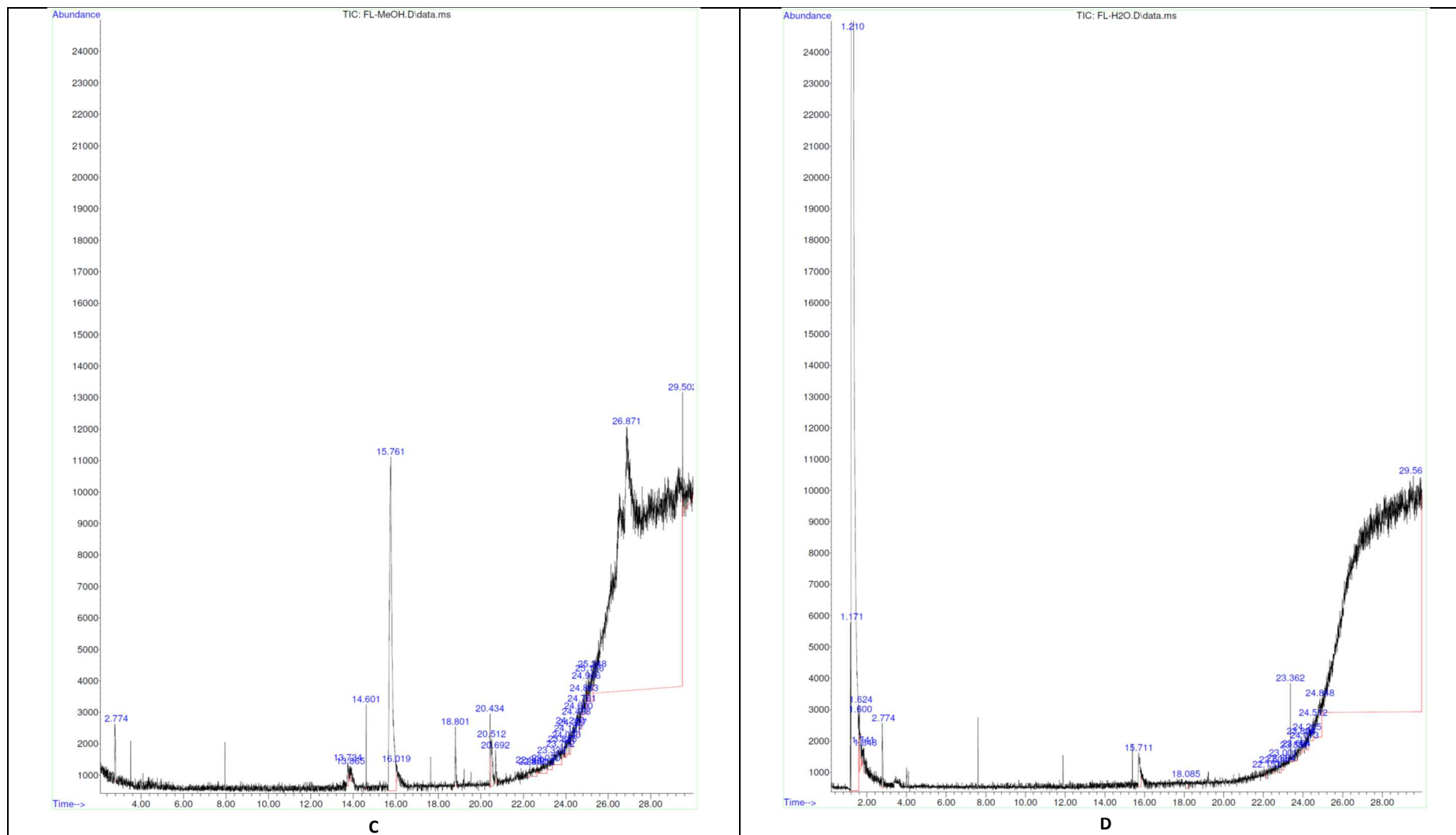
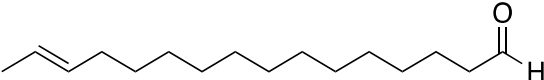
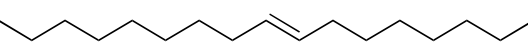
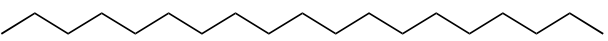
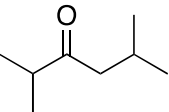
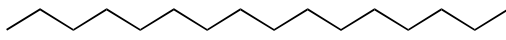
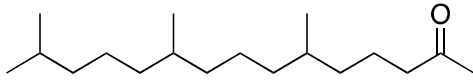
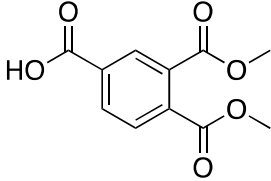
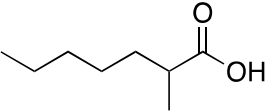
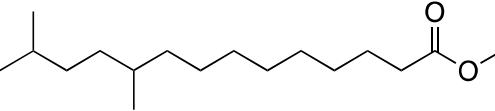
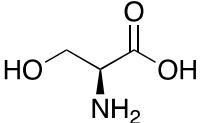
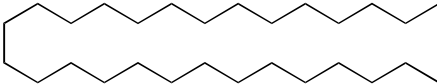
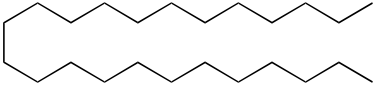
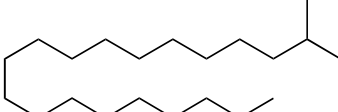
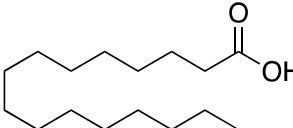
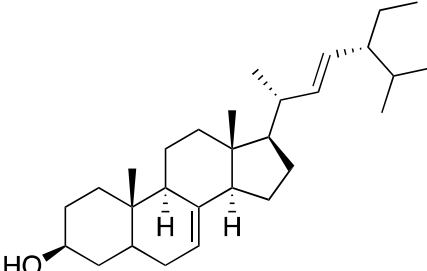


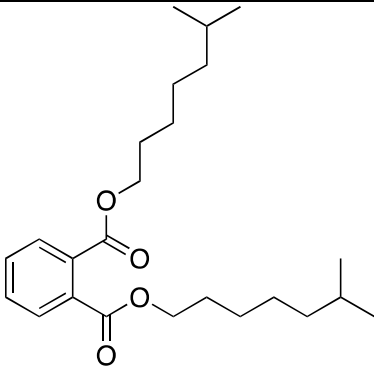
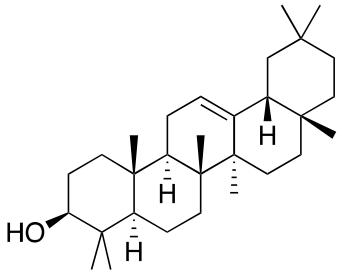
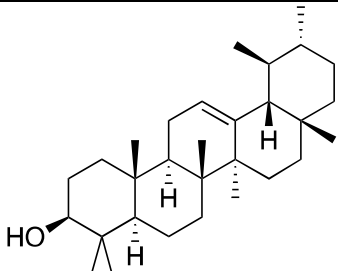
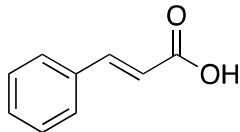
Figure S1. Spectral images of GCMS analysis of (A) FL-hex, (B) FL-DCM, (C) FL-MeOH, and (D) FL-H₂O extracts

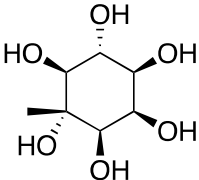
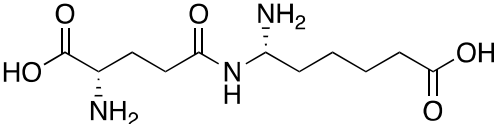
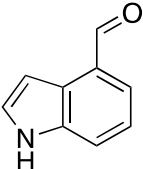
Table S2. The list of identified compounds in hexane flower extract of *Acacia saligna* by GCMS

No	Extract	Compound name/ group/ molecular formula	Retention time (min)	Area (%)	Structure	Reported sources	Bioactivities
1	FL-hex	(<i>E</i>)-14-Hexadecanal (alkenal, C ₁₆ H ₃₀ O)	14.93	0.01		Leaves of <i>Justicia secunda</i> Vahl [279]; <i>Melia dubia</i> barks [280]; leaves of <i>Cymbopogon martini</i> [281]	ND
2	FL-hex	8-Heptadecene (alkene, C ₁₇ H ₃₄)	15.83	0.06		Leaves of <i>Cymbopogon martini</i> [281]; <i>Ophrys insectifera</i> flowers [282]	ND
3	FL-hex	Nonadecane (alkane, C ₁₉ H ₄₀)	16.05	0.15		<i>Rosaceae</i> plant family [286]; <i>Diploaxis harra</i> and <i>Erucaria macrocarpa</i> [287]; <i>Rosa damascena</i> Mill [288]	Antioxidant, antifungal [286]; antimicrobial [287]
4	FL-hex	2,5-Dimethyl-3-hexanone (ketone, C ₈ H ₁₆ O)	16.12	0.02		<i>Oncorhynchus mykiss</i> [290]; <i>Mentha piperita</i> [291]; <i>Melia azedarach</i> [292]; <i>Eruca sativa</i> Mill. Leaves [293]; <i>Schizonepeta tenuifolia</i> Briq [294]	Antioxidant [291]
5	FL-hex	Hexadecane (alkane, C ₁₆ H ₃₄)	17.14	0.11		<i>Rosa damascena</i> Mill [288]	ND
6	FL-hex	6,10,14-Trimethyl-2-pentadecanone (ketone, C ₁₈ H ₃₆ O)	17.63	0.18		Leaves of <i>Ficus elastica</i> Roxb. ex Hornem [296]; roots and leaves of <i>Adiantum flabellulatum</i> [297]; leaves of <i>Leucaena leucocephala</i> (Lamk.) de Wit [298]; <i>Biebersteinia multifida</i> DC. (Biebersteiniaceae) [299]; <i>Herniaria incana</i> Lam. [300]; <i>Ficus lutea</i> Vahl., <i>Ficus polita</i> Vahl., and <i>Ficus thonningii</i> Blume [301]; leaves of <i>Ficus Linn.</i> (Moraceae), <i>Ficus elasticoides</i> De Wild., <i>Ficus ovata</i> Vahl and <i>Ficus natalensis</i> subsp. <i>leprieurii</i> (Miq.) C. C. Berg [302]; aerial parts of <i>Senecio giganteus</i> Desf. [303]; <i>Cirsium japonicum</i> var. <i>ussuriense</i>	ND

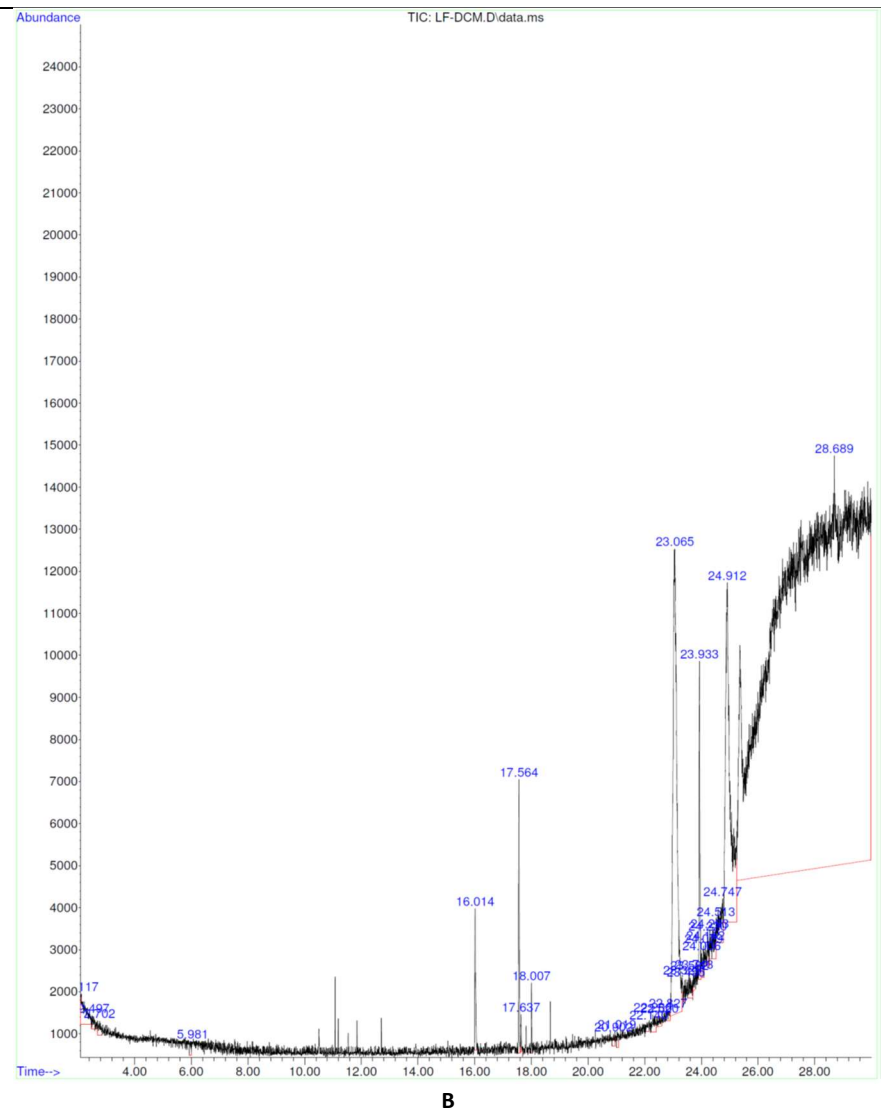
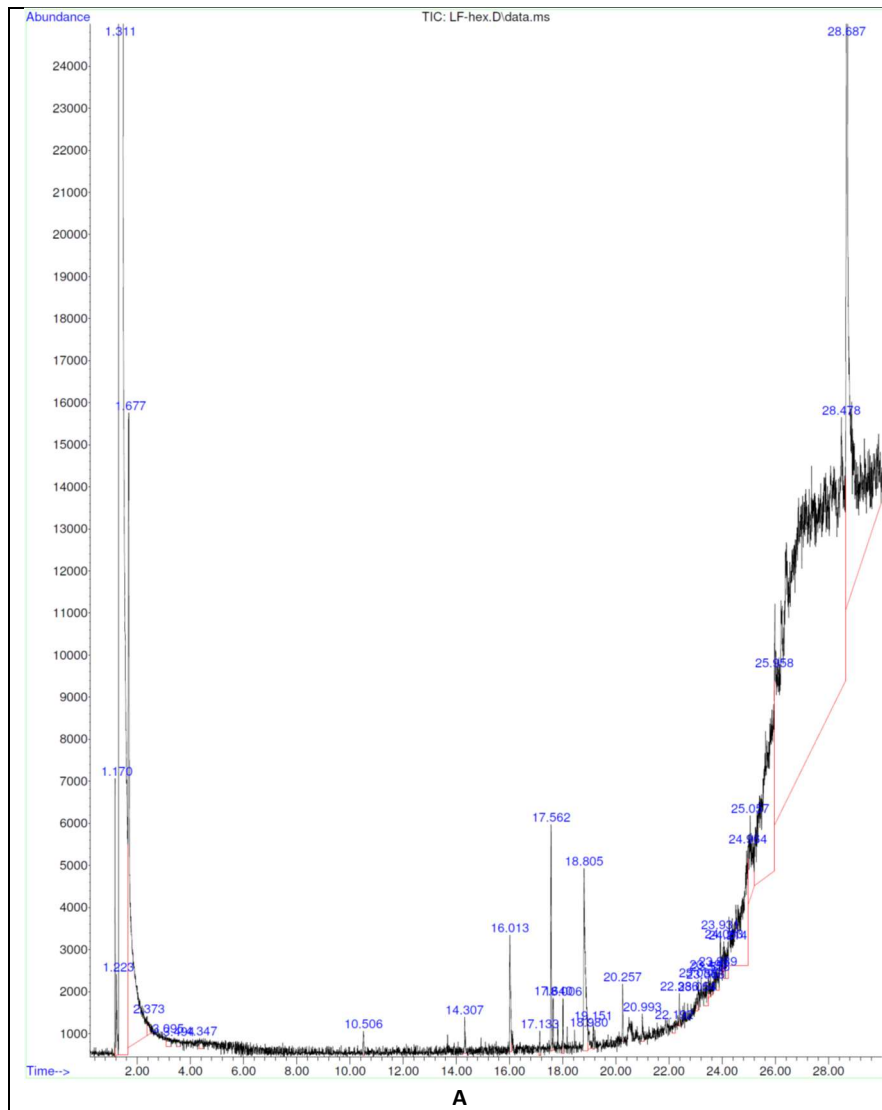
No	Extract	Compound name/ group/ molecular formula	Retention time (min)	Area (%)	Structure	Reported sources	Bioactivities
						Kitamura [304]; leaves of <i>Synurus deltoides</i> (Arr.) Nakai [305]	
7	FL-hex	1,2,4- Benzenetricarbo- xylic acid, 1,2- dimethyl ester (carboxylic acid, C ₁₁ H ₁₀ O ₆)	18.19	0.41		<i>Cnidium monnieri</i> (L.) Cusson [317]	ND
8	FL-hex	2-Methylhepta-noic acid (carboxylic acid, C ₈ H ₁₆ O ₂)	18.47	0.03		Leaves of <i>Stachytarpheta indica</i> [318]; leaves of <i>Indigofera suffruticosa</i> [319]; <i>Creumatogaster</i> species: <i>C. mimosae</i> , <i>C. nigriceps</i> , and <i>C. sjostedti</i> [320]	ND
9	FL-hex	Tetradecanoic acid, 10,13-dimethyl-, methyl ester (carboxylic acid, C ₁₇ H ₃₄ O ₂)	18.45	0.01		Roots of <i>Oroxylum indicum</i> (L.) Benth. ex Kurz [321]; <i>Caulerpa peltate</i> [322]	Antioxidant [322]
10	FL-hex	L-Serine (amino acid, C ₃ H ₇ NO ₃)	19.15	0.02		<i>Trifolium repens</i> L., <i>Lolium perenne</i> L., <i>Zea mays</i> L., <i>Brassica napus</i> L., <i>Lycopersicon esculentum</i> Mill. and <i>Medicago sativa</i> L. [323]	ND
11	FL-hex	Octacosane (alkane, C ₂₈ H ₅₈)	20.69	0.02		<i>Aquilaria agallocha</i> Roxb [329]; leaves of <i>Ipomoea carnea</i> [330]; flowers of <i>Prunus mahaleb</i> L. [309]; <i>Withania somnifera</i> roots [331]; leaves of <i>Ludwigia octovalvis</i> (Jacq.) Raven [332]	ND
12	FL-hex	Tetracosane (alkane, C ₂₄ H ₅₀)	21.86	0.02		<i>Rosa damascena</i> Mill [288]	ND

No	Extract	Compound name/ group/ molecular formula	Retention time (min)	Area (%)	Structure	Reported sources	Bioactivities
13	FL-hex	2-Methyleicosane (alkane, C ₂₁ H ₄₄)	21.88	0.46		<i>Epiphyllum oxypetalum</i> leaves [333]; <i>Trichosanthes dioica</i> root [334]; fruits of <i>Salvadora persica</i> L. [335]	Antimicrobial [334, 335]
14	FL-DCM	<i>n</i> -Hexadecanoic acid or palmitic acid (fatty acid, C ₁₆ H ₃₂ O ₂)	18.80	0.20		Leaves of green tea (<i>Camellia sinensis</i>) [336]; fruits of <i>Tuber melanosporum</i> , <i>T. aestivum</i> , <i>T. magnatum</i> and <i>T. borchii</i> [337]; fruits of <i>Ceiba speciosa</i> (A. St.-Hil.) [338]; and fruiting bodies of <i>Amanita spissacea</i> [339]; <i>Cirsium japonicum</i> var. <i>ussuriense</i> Kitamura [304]; <i>Mesembryanthemum edule</i> (L.) Bolus leaves [340]	Allelopathic [337]; antioxidant and α-glucosidase inhibitor [338]; and anticancer [339]; antifungal [340]
15	FL-DCM	Chondrillasterol (steroid, C ₂₉ H ₄₈ O)	23.08	0.83		Leaves of <i>Vernonia adoensis</i> [341]; aerial parts of <i>Achillea fragrantissima</i> (Forssk.) Sch. Bip. [342]; root of <i>Pseudostellaria heterophylla</i> (Miq.) Pax [343]; and <i>Myriactis humilis</i> Merr. [344]	Antibacterial [341]; α-glucosidase inhibitor [342]; anticancer [344]; allelopathic activity [345]

No	Extract	Compound name/ group/ molecular formula	Retention time (min)	Area (%)	Structure	Reported sources	Bioactivities
16	FL-DCM	1,2-Benzenedicarboxylic acid, diisooctyl ester or diisooctyl phthalate (diester, C ₂₄ H ₃₈ O ₄)	23.93	0.40		Flower of <i>Caralluma retropiciens</i> [346]	Antibacterial [346]
17	FL-DCM	β-Amyrin (triterpenoid, C ₃₀ H ₅₀ O)	24.22	0.68		<i>Carmona retusa</i> leaves [347]; root bark of <i>Ziziphus abyssinica HochstEx. A Rich</i> (Rhamnaceae) [348]; leaves, stem, and fruits of <i>Coccoloba uvifera</i> L. [349]; <i>Centaurea arenaria</i> M.B. ex Willd [350]; <i>Eugenia pyriformis</i> leaves [351]; <i>Myrcianthes pungens</i> leaves [352]; and <i>Laurencia microcladia</i> Kutzing [353]	Antidiarrheal activity [347]; anti-arthritic activity [348]; anticancer [350]; antioxidant activity [351, 352]; antimicrobial [353]
18	FL-DCM	α-Amyrin (triterpenoid, C ₃₀ H ₅₀ O)	2.93	0.43		<i>Carmona retusa</i> leaves [347]; fruits of <i>Coccoloba uvifera</i> L. [349]; <i>Eugenia pyriformis</i> leaves [351]; <i>Myrcianthes pungens</i> leaves [352]	Antidiarrheal activity [347]; antioxidant activity [351, 352]
19	FL-MeOH	<i>trans</i> -Cinnamic acid (unsaturated carboxylic acid, C ₉ H ₈ O ₂)	13.72	0.16		<i>Solanum spirale</i> Roxb. Leaves [354]; cinnamon barks [355]; rhizomes of <i>Distichochlamys benenica</i> [356]; flowers of <i>Hertia cheirifolia</i> L. [357]; tea leaves [358]; nematode symbiont	Inhibitor of α-glucosidase enzyme [362]; anticancer, cytotoxic and antibacterial activities [354];

No	Extract	Compound name/ group/ molecular formula	Retention time (min)	Area (%)	Structure	Reported sources	Bioactivities
						<i>Photorhabdus luminescens</i> [359]; <i>Croton heliotropiifolius</i> Kunth leaves [360]; roots and aerial parts of <i>Physalis angulata</i> L. [361]	anti-inflammatory and antibacterial [356]; antibacterial [357]; antioxidant [358]; antifungal [359]
20	FL-MeOH	4-C-Methyl- <i>myo</i> -inositol or laminitol (polyol, C ₇ H ₁₄ O ₆)	15.68	6.42		Barks of <i>Prosopis juliflora</i> (Sw.) DC [367]; Leaves of <i>Chamaecrista nigricans</i> [368]; fruits of <i>Tetrapleura tetraptera</i> [369]	Antioxidant and antimicrobial [369]
21	FL-MeOH	γ -Glutamyl- ϵ -lysine (dipeptides, C ₁₁ H ₂₁ N ₃ O ₅)	20.44	0.36		ND	ND
22	FL-MeOH	Indole-4-carboxaldehyde (heteroarene carbaldehyde, C ₉ H ₇ NO)	20.76	0.17		Brown alga <i>Sargassum thunbergii</i> [370, 371]	Anti-obesity [370]; anti-inflammatory effect [371]

ND = no documentation



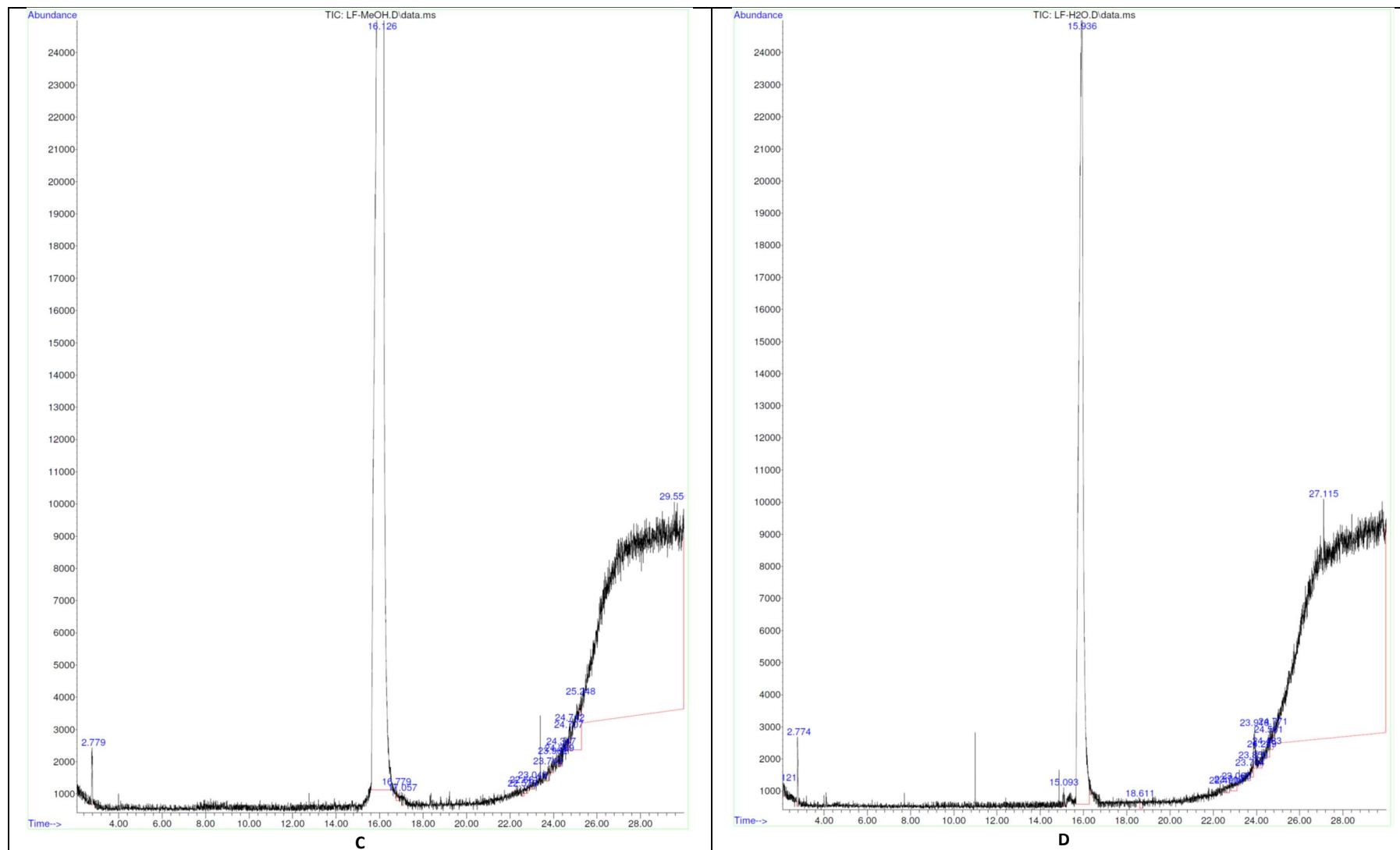
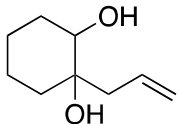
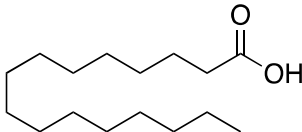
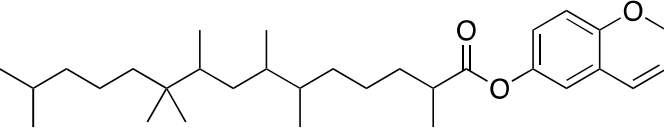
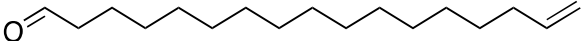
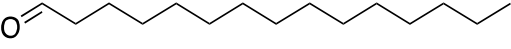
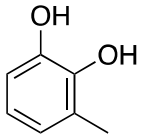
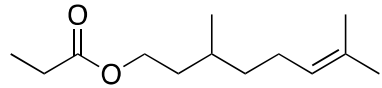
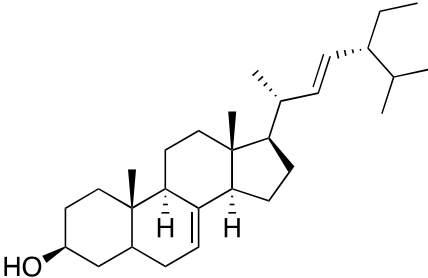
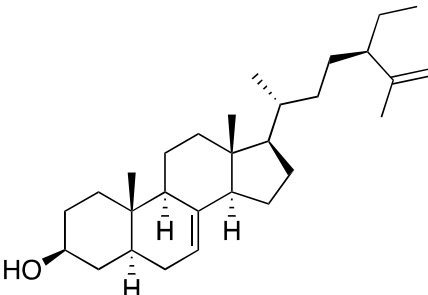
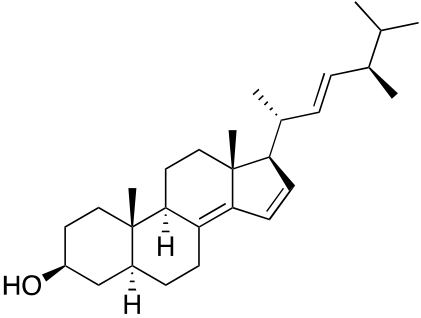
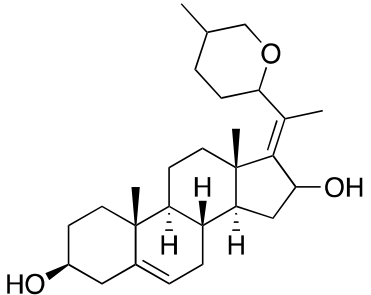
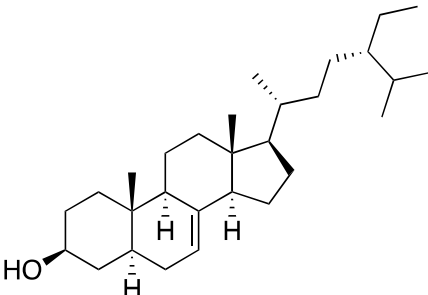
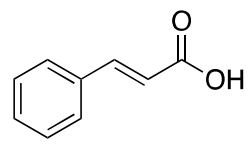


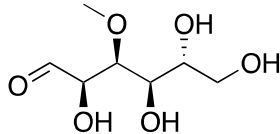
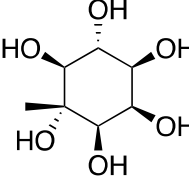
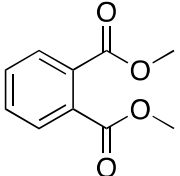
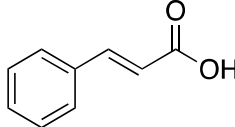
Figure S2. Spectral images of GCMS analysis of (A) LF-hex, (B) LF-DCM, (C) LF-MeOH, and (D) LF-H₂O extracts

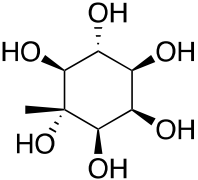
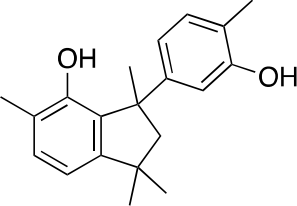
Table S3. The list of identified compounds in *Acacia saligna* leaves extracts by GCMS

No	Extract	Compound name/ group/ molecular formula	Retention time (min)	Area (%)	Structure	Reported sources	Bioactivities
1	LF-hex	1-Allylcyclo-hexane- 1,2-diol (alcohol, C ₉ H ₁₆ O ₂)	16.02	0.07		Horseradish sauce produced by lactic acid bacteria and <i>Saccharomyces cerevisiae</i> [372]	Antioxidant [372]
2	LF-hex	Palmitic acid (fatty acid, C ₁₆ H ₃₂ O ₂)	18.81	0.19		Leaves of green tea (<i>Camellia sinensis</i>) [336]; fruits of <i>Tuber melanosporum</i> , <i>T. aestivum</i> , <i>T. magnatum</i> and <i>T. borchii</i> [337]; fruits of <i>Ceiba speciosa</i> (A. St.-Hil.) [338]; and fruiting bodies of <i>Amanita spissacea</i> [339]; <i>Cirsium japonicum</i> var. ussuriense Kitamura [304]; <i>Mesembryanthemum edule</i> (L.) Bolus leaves [340]	Allelopathic [337]; antioxidant and α- glucosidase inhibitor [338]; and anticancer [339]; antifungal [340]
3	LF-hex	2 <i>H</i> -1-Benzopyran-6- ol, 3,4-Dihydro- 2,5,7,8-tetramethyl- 2-(4,8,12- trimethyltridecyl)- acetate (tocotrienol, C ₃₁ H ₅₀ O ₃)	26.69	1.03		<i>Cyperus dubius</i> Rottb. [373]	Antiviral [374]
4	LF-DCM	16-Heptadecenal (alkenal, C ₁₇ H ₃₂ O)	17.57	0.49		Leaves & nodes of <i>Nilgiranthus ciliates</i> [375]; <i>Salicornia herbacea</i> (L) [376]; the shoots of <i>Eichhornia crassipes</i> [377]	ND

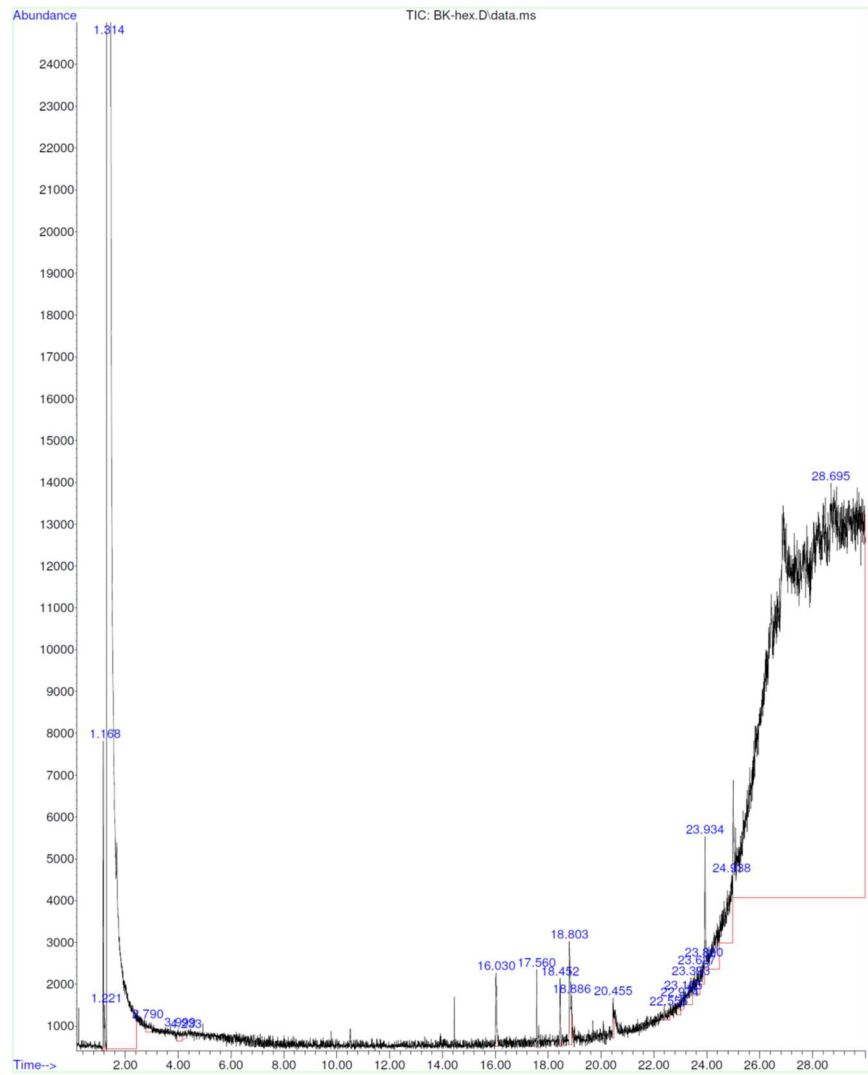
No	Extract	Compound name/ group/ molecular formula	Retention time (min)	Area (%)	Structure	Reported sources	Bioactivities
5	LF-DCM	Pentadecanal (alkenal, C ₁₅ H ₃₀ O)	16.01	0.33		Bacterium <i>Pseudoalteromonas haloplanktis</i> [378]	Antibacteria [378]
6	LF-DCM	3-Methyl-catechol (phenolic, C ₇ H ₈ O ₂)	18.01	0.08		Green tea leaves [379]	Antioxidant and antiviral [379]
7	LF-DCM	3,7-Dimethyl propanoate-6-octen- 1-ol or citronellyl propionate (alkenyl ester, C ₁₃ H ₂₄ O ₂)	17.82	0.06		<i>Citrus wilsonii</i> Tanaka stems and barks [380]; leaves of <i>Plectranthus neochilus</i> [381]	Natural repellent [380]
8	LF-DCM	Chondrillasterol (stigmastane, C ₂₉ H ₄₈ O)	23.05	4.96		Leaves of <i>Vernonia adoensis</i> [341]; aerial parts of <i>Achillea fragrantissima</i> (Forssk.) Sch. Bip. [342]; root of <i>Pseudostellaria heterophylla</i> (Miq.) Pax [343]; and <i>Myriactis humilis</i> Merr .[344]	Antibacterial [341]; α- glucosidase inhibitor [342]; anticancer [344]; allelopathic activity [345]
9	LF-DCM	(3β,5α)-Stigmasta- 7,25-dien-3-ol (steroid, C ₂₉ H ₄₈ O)	23.93	0.71		<i>Carissa congesta</i> root [384]; Leaves of <i>Verbascum speciosum</i> were [385]; the leaves of <i>Nelumbo nucifera</i> (Gaertn.) [386]	ND

No	Extract	Compound name/ group/ molecular formula	Retention time (min)	Area (%)	Structure	Reported sources	Bioactivities
10	LF-DCM	(3 β ,5 α ,22 <i>E</i>)- Ergosta- 8(14),15,22-trien-3- ol (steroid, C ₂₈ H ₄₄ O)	24.89	4.16		Fruiting body of <i>Grifola frondose</i> [387]	Inhibitor of α - glucosidase [387]
11	LF-DCM	Cholesta-5,17(20)- diene-3 β ,16-diol, 22,26-epoxy- (steroid, C ₂₇ H ₄₂ O ₃)	24.92	0.21		ND	ND
12	LF-DCM	(3 β ,5 α ,24 <i>S</i>)- Stigmast-7-en-3-ol (steroid, C ₂₉ H ₅₀ O)	25.36	0.38		Twigs of <i>Paederia foetida</i> L. (Rubiaceae) [388]; microalga <i>Nannochloropsis</i> sp. [389]; <i>Scenedesmus obliquus</i> algae [390]	Inhibitor of α - glucosidase [388]
13	LF-MeOH	<i>trans</i> -Cinnamic acid (unsaturated carboxylic acid, C ₉ H ₈ O ₂)	4.09	0.15		<i>Solanum spirale</i> Roxb. Leaves [354]; cinnamon barks [355]; rhizomes of <i>Distichoclamys benenica</i> [356]; flowers of <i>Hertia cheirifolia</i> L. [357]; tea	Inhibitor of α - glucosidase enzyme [362]; anticancer, cytotoxic and antibacterial activities [354]; anti-inflammatory

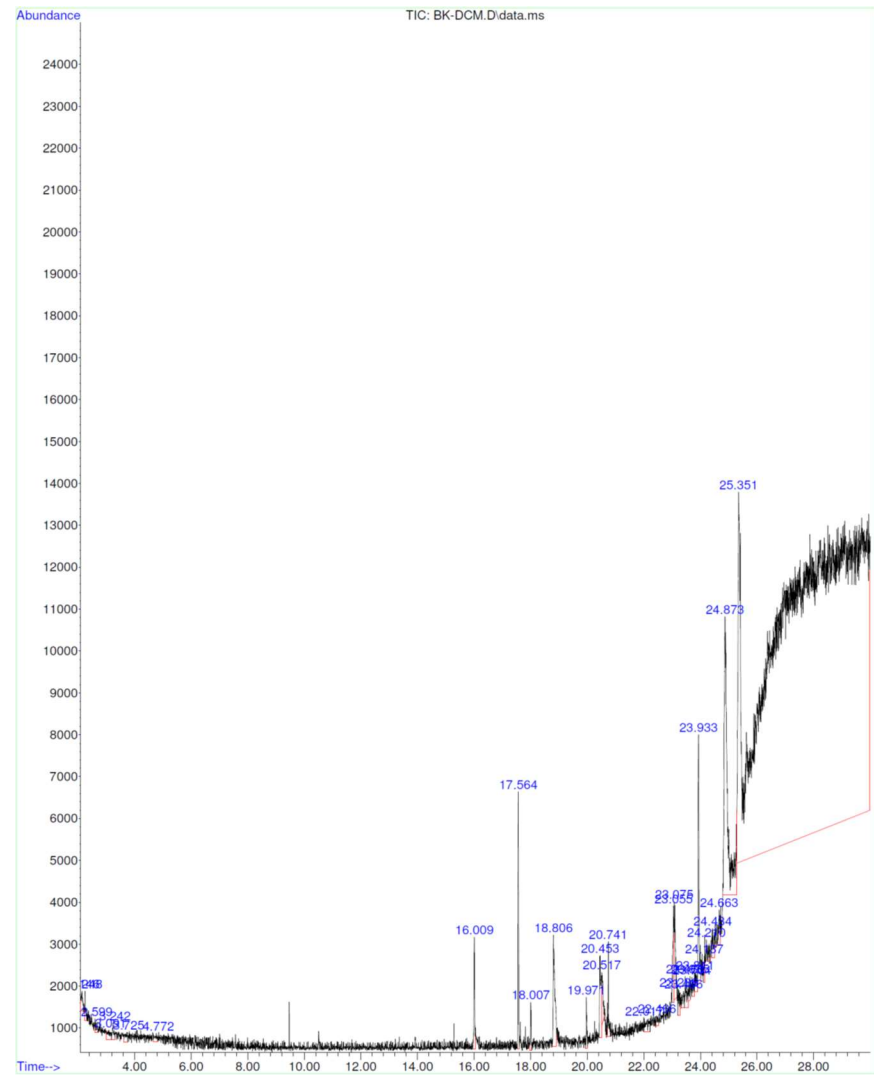
No	Extract	Compound name/ group/ molecular formula	Retention time (min)	Area (%)	Structure	Reported sources	Bioactivities
						leaves [358]; nematode symbiont <i>Photorhabdus luminescens</i> [359]; <i>Croton heliotropiifolius</i> Kunth leaves [360]; roots and aerial parts of <i>Physalis angulata</i> L. [361]	and antibacterial [356]; antibacterial [357]; antioxidant [358]; antifungal [359]
14	LF-MeOH	3-O-Methyl-D- glucose (carbohydrate, C ₇ H ₁₄ O ₆)	16.14	0.06		<i>Cassia auriculata</i> leaves [365]; leaves and stems of <i>Allamanda cathartica</i> L. [366]	ND
15	LF-MeOH	4-C-Methyl- <i>myo</i> - inositol or lamitol (polyols, C ₇ H ₁₄ O ₆)	15.68	42.74		Barks of <i>Prosopis juliflora</i> (Sw.) DC [367]; Leaves of <i>Chamaecrista nigricans</i> [368]; fruits of <i>Tetrapleura tetraptera</i> [369]	Antioxidant and antimicrobial [369]
16	LF-MeOH	1,2-Benzenedicar- boxylic acid-1,2- dimethyl ester, or dimethyl phthalate (diester, C ₁₀ H ₁₀ O ₄)	23.40	0.06		ND	ND
17	LF-H ₂ O	<i>trans</i> -Cinnamic acid (unsaturated carboxylic acid, C ₉ H ₈ O ₂)	4.10	0.21		<i>Solanum spirale</i> Roxb. Leaves [354]; cinnamon barks [355]; rhizomes of <i>Distichoclamys benenica</i> [356]; flowers of <i>Hertia cheirifolia</i> L. [357]; tea leaves [358]; nematode symbiont <i>Photorhabdus luminescens</i> [359];	Inhibitor of α- glucosidase enzyme [362]; anticancer, cytotoxic and antibacterial activities [354]; anti-inflammatory and antibacterial [356]; antibacterial [357]; antioxidant

No	Extract	Compound name/ group/ molecular formula	Retention time (min)	Area (%)	Structure	Reported sources	Bioactivities
						<i>Croton heliotropiifolius</i> Kunth leaves [360]; roots and aerial parts of <i>Physalis angulata</i> L. [361]	[358]; antifungal [359]
18	LF-H ₂ O	4-C-Methyl- <i>myo</i> -inositol or lamitol (polyols, C ₇ H ₁₄ O ₆)	15.99	18.77		Barks of <i>Prosopis juliflora</i> (Sw.) DC [367]; Leaves of <i>Chamaecrista nigricans</i> [368]; fruits of <i>Tetrapleura tetraptera</i> [369]	Antioxidant and antimicrobial [369]
19	LF-H ₂ O	3-(3-Hydroxy-4-methylphenyl)-1,1,3,5-tetramethylindan-4-ol (aryl alcohol, C ₂₀ H ₂₄ O ₂)	23.89	0.20		Lignocellulosic biomass [393, 394]	ND

ND = no documentation



A



B

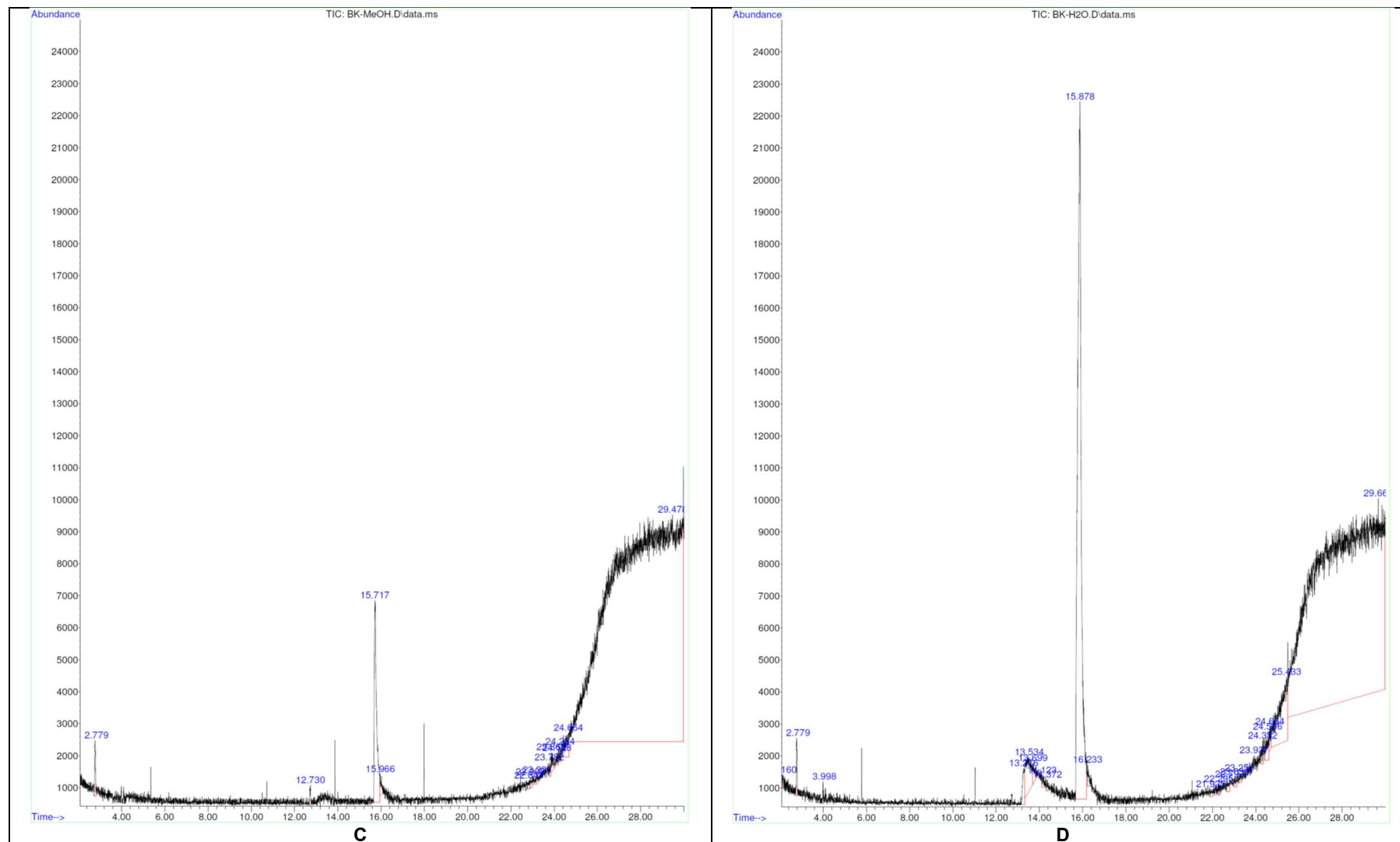
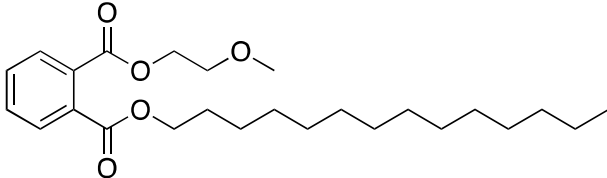
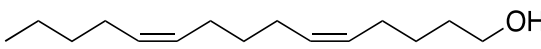
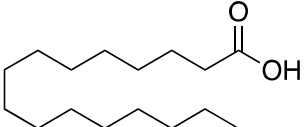
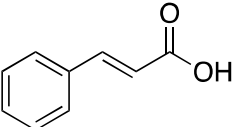


Figure S3. Spectral images of GCMS analysis of (A) BK-hex, (B) BK-DCM, (C) BK-MeOH, and (D) BK-H₂O extracts

Table S4. The list of identified compounds in *Acacia saligna* bark extracts by GCMS

No	Extract	Compound name/ group/ molecular formula	Retention time (min)	Area (%)	Structure	Reported sources	Bioactivities
1	BK-hex	Phthalic acid, 2-methoxyethyltetradecyl ester (ester dicarboxylic, C ₂₅ H ₄₀ O ₅)	23.934	0.21		ND	ND
2	BK-DCM	(Z,Z)-5,10-Pentadecadien-1-ol (alkenol, C ₁₅ H ₂₈ O)	17.56	0.56		Roots of <i>Astragalii Radix</i> and <i>Angelica Sinensis Radix</i> [395]	Erythropoiesis activity [395]
3	BK-DCM	<i>n</i> -Hexadecanoic acid or palmitic acid (fatty acid, C ₁₆ H ₃₂ O ₂)	18.83	0.70		Leaves of green tea (<i>Camellia sinensis</i>) [336]; fruits of <i>Tuber melanosporum</i> , <i>T. aestivum</i> , <i>T. magnatum</i> and <i>T. borchii</i> [337]; fruits of <i>Ceiba speciosa</i> (A. St.-Hil.) [338]; and fruiting bodies of <i>Amanita spissacea</i> [339]; <i>Cirsium japonicum</i> var. <i>ussuriense</i> Kitamura [304]; <i>Mesembryanthemum edule</i> (L.) Bolus leaves [340]	Allelopathic [337]; antioxidant and α-glucosidase inhibitor [338]; and anticancer [339]; antifungal [340]
4	BK-MeOH	<i>trans</i> -Cinnamic acid (unsaturated carboxylic acid, C ₉ H ₈ O ₂)	4.09	0.27		<i>Solanum spirale</i> Roxb. Leaves [354]; cinnamon barks [355]; rhizomes of <i>Distichochlamys benenica</i> [356]; flowers of <i>Hertia cheirifolia</i> L. [357]; tea leaves [358]; nematode symbiont <i>Photorhabdus luminescens</i> [359]; <i>Croton heliotropifolius</i> Kunth leaves [360]; roots and aerial parts of	Inhibitor of α-glucosidase enzyme [362]; anticancer, cytotoxic and antibacterial activities [354]; anti-inflammatory and antibacterial [356]; antibacterial [357]; antioxidant

No	Extract	Compound name/ group/ molecular formula	Retention time (min)	Area (%)	Structure	Reported sources	Bioactivities
						<i>Physalis angulata</i> L. [361]	[358]; antifungal [359]
5	BK-MeOH	4-C-Methyl- <i>myo</i> - inositol (polyols, C ₇ H ₁₄ O ₆)	15.73	2.94		Barks of <i>Prosopis juliflora</i> (Sw.) DC [367]; Leaves of <i>Chamaecrista nigricans</i> [368]; fruits of <i>Tetrapleura tetraptera</i> [369]	Antioxidant and antimicrobial [369]
6	BK-MeOH	<i>D</i> -Asparagine (amino acid, C ₄ H ₈ N ₂ O ₃)	15.67	0.16		Plants [392]	ND
7	BK-MeOH	Thymidine-5'- monophosphate (nucleoside, C ₁₀ H ₁₅ N ₂ O ₈ P)	22.44	0.06		ND	ND
8	BK-H ₂ O	1-(1-Propenylthio) propane (alkenyl sulfide, C ₆ H ₁₂ S)	5.871	0.06		Shallot [396]; black garlic [397]	ND
9	BK-H ₂ O	3-O-Methyl- <i>D</i> - glucose (carbohydrate, C ₇ H ₁₄ O ₆)	15.83	16.23		<i>Cassia auriculata</i> leaves [365]; leaves and stems of <i>Allamanda cathartica</i> L. [366]	ND

ND = no documentation

Table S5. DPPH scavenging activity of the extracts of *A. saligna*

No	Extract	DPPH scavenging percentage (%) at the indicated concentration (µg/mL)										IC ₅₀ (µg/mL)
		7.8125	15.625	31.25	62.5	125	250	500	1,000	2,000	4,000	
1	FL-hex	-	-	6.306 ± 3.09	7.537 ± 2.97	12.19 ± 4.03	10.47 ± 4.30	11.07 ± 4.56	11.5 ± 6.78	13.64 ± 6.44	19.1 ± 6.40	>4000 ^a
2	FL-DCM	-	-	0.645 ± 6.16	3.976 ± 6.61	2.068 ± 7.92	3.639 ± 9.03	8.673 ± 6.85	15.91 ± 5.14	14.36 ± 5.94	22.87 ± 3.57	>4000 ^a
3	FL-MeOH	8.67 ± 5.44	8.05 ± 4.06	9.32 ± 1.461	16.48 ± 0.91	27.8 ± 0.03	41.57 ± 1.3	61.07 ± 1.30	74.34 ± 0.87	-	-	331.5 ± 17.21 ^{****}
4	FL-H ₂ O	-	-	1.07 ± 2.96	2.54 ± 2.95	4.32 ± 3.34	5.45 ± 4.09	10.51 ± 2.65	18.09 ± 3.42	20.92 ± 2.11	34.78 ± 5.75	>4000 ^a

No	Extract	DPPH scavenging percentage (%) at the indicated concentration (µg/mL)										IC ₅₀ (µg/mL)
		7.8125	15.625	31.25	62.5	125	250	500	1,000	2,000	4,000	
5	LF-hex	-	-	10.04 ± 10.46	12.43 ± 8.05	18.1 ± 5.99	18.82 ± 3.36	18.96 ± 8.98	22.26 ± 7.29	34.45 ± 9.91	60.47 ± 11.55	3,283 ± 774.3****
6	LF-DCM	-	-	1.391 ± 10.24	4.17 ± 15.54	3.49 ± 9.81	5.7 ± 8.78	14.81 ± 7.81	27.72 ± 7.85	24.3 ± 7.28	37.41 ± 7.09	>4000 ^a
7	LF-MeOH	10.75 ± 6.58	13.33 ± 7.44	21.33 ± 7.21	25.89 ± 7.56	38.66 ± 8.94	58.2 ± 9.95	82.6 ± 6.20	89.33 ± 0.61	-	-	190.1 ± 59.15****
8	LF-H ₂ O	-	-	3.61 ± 2.90	5.06 ± 3.31	7.55 ± 4.40	8.12 ± 6.56	14.03 ± 7.4	26.06 ± 5.18	31.14 ± 5.65	47.9 ± 5.08	>4000 ^a
9	BK-hex	-	-	2.27 ± 7.00	5.57 ± 6.03	12.39 ± 2.51	10.06 ± 3.23	9.764 ± 4.26	11.4 ± 4.02	15.11 ± 5.61	26.8 ± 5.72	>4000 ^a
10	BK-DCM	-	-	1.793 ± 5.00	1.497 ± 5.40	2.304 ± 5.96	6.771 ± 6.70	14.09 ± 5.68	26.35 ± 6.87	30.49 ± 5.64	49.32 ± 8.42	>4000 ^a
11	BK-MeOH	10.29 ± 5.22	16.13 ± 3.92	26.42 ± 2.99	37.79 ± 4.60	56.85 ± 7.27	81.14 ± 6.06	88.55 ± 0.81	89.97 ± 0.53	-	-	94.24 ± 19.89
12	BK-H ₂ O	-	-	3.256 ± 4.36	5.436 ± 4.93	7.886 ± 6.37	11.27 ± 5.48	19.53 ± 5.53	32.34 ± 6.68	42.35 ± 7.06	71.69 ± 8.54	2,446 ± 527.4****

^aNo activity higher than 50% was observed at the highest tested concentration (4000 µg/mL). Data expressed as mean ± SEM, *****p* < 0.0001 of samples against vitamin C (*n* = 3, ANOVA).

Table S6. Scavenging activity (%) and IC₅₀ values of vitamin C from DPPH scavenging assay

No	Sample	DPPH scavenging percentage (%) at c the indicated concentration (µg/mL)							IC ₅₀ (µg/mL)
		1.56	3.125	6.25	12.5	25	50	100	
1	Vitamin C	1.10 ± 3.90	3.616 ± 2.89	5.15 ± 3.26	11.91 ± 4.52	24.59 ± 4.79	51.57 ± 9.65	86.88 ± 5.38	49.97 ± 10.76****

Data in mean ± SEM; *****p* < 0.0001, *p* value was from comparing FL-MeOH and vitamin C (*n* = 3, one-way ANOVA, Tukey's post hoc tests).

Table S7. ABTS** scavenging activity of the extracts of *A. saligna*

No	Sample	ABTS** scavenging percentage (%) at the indicated concentration (µg/mL)										IC ₅₀ (µg/mL)
		7.8125	15.625	31.25	62.5	125	250	500	1000	2000	4000	
1	FL-hex	-	-	3.576 ± 7.18	4.182 ± 6.08	4.969 ± 6.37	5.11 ± 8.65	8.021 ± 7.32	11.48 ± 3.99	18.64 ± 7.78	30.49 ± 4.99	>4000 ^a
2	FL-DCM	-	-	2.534 ± 6.72	5.685 ± 6.17	10.12 ± 8.06	21.08 ± 6.79	29.53 ± 6.95	41.58 ± 6.71	54.65 ± 1.00	69.16 ± 0.85	1,579 ± 240.8****
3	FL-MeOH	7.884 ± 3.18	9.104 ± 2.21	12.09 ± 2.4	17.22 ± 1.37	27.71 ± 0.79	45.09 ± 0.60	62.72 ± 0.33	89.97 ± 2.28	-	-	316.6 ± 11.45****
4	FL-H ₂ O	-	-	2.719 ± 4.60	4.937 ± 5.69	6.898 ± 3.36	11.08 ± 3.37	18.01 ± 4.12	28.77 ± 3.38	43.6 ± 0.22	70.28 ± 5.39	2,433 ± 103.5****

No	Sample	ABTS ^{•+} scavenging percentage (%) at the indicated concentration (µg/mL)										IC ₅₀ (µg/mL)
		7.8125	15.625	31.25	62.5	125	250	500	1000	2000	4000	
5	LF-hex	-	-	-1.047 ± 1.45	2.395 ± 0.20	8.864 ± 0.42	7.013 ± 1.67	13.06 ± 1.39	23.57 ± 0.98	35.42 ± 1.41	65.73 ± 0.32	2,951 ± 75.9 ^{****}
6	LF-DCM	-	-	3.193 ± 0.97	7.741 ± 3.71	12.18 ± 0.69	14.69 ± 0.60	23.84 ± 1.63	37.31 ± 0.13	56.49 ± 0.78	84.04 ± 0.18	1,633 ± 41.55 ^{****}
7	LF-MeOH	9.964 ± 1.74	14.58 ± 0.85	20.71 ± 0.83	27.21 ± 0.03	43.98 ± 0.02	72.22 ± 0.55	99.63 ± 0.05	99.89 ± 0.05	-	-	146.7 ± 0.99
8	LF-H ₂ O	-	-	5.21 ± 0.17	6.959 ± 2.68	8.885 ± 1.94	18.07 ± 4.66	22.23 ± 6.35	31.56 ± 6.61	44.34 ± 0.39	71 ± 1.16	2,422 ± 148.8 ^{****}
9	BK-hex	-	-	0.611 ± 1.77	1.13 ± 0.08	0.039 ± 0.64	3.449 ± 0.55	3.463 ± 2.23	9.726 ± 0.99	14.92 ± 3.10	30.56 ± 0.50	>4000 ^a
10	BK-DCM	-	-	-3.323 ± 0.28	-2.756 ± 3.54	4.297 ± 1.63	13.23 ± 1.25	22.49 ± 0.33	30.96 ± 2.62	42.35 ± 1.82	62.81 ± 3.04	2,764 ± 165.3 ^{****}
11	BK-MeOH	10.23 ± 6.29	16.81 ± 6.19	31.91 ± 5.20	52.46 ± 1.65	80.41 ± 7.44	96.87 ± 0.45	92.53 ± 3.37	99.87 ± 0.01	-	-	55.44 ± 6.84
12	BK-H ₂ O	-	-	-1.072 ± 6.05	3.195 ± 8.07	5.123 ± 3.34	11.29 ± 5.27	22.59 ± 4.59	40.95 ± 4.10	69.81 ± 1.83	93.68 ± 2.52	1,241 ± 97.93 ^{****}

^aNo activity higher than 31% was observed at the highest tested concentration (4000 µg/mL); Data in mean ± SEM; ^{****}*p* < 0.0001, *p* value was from comparing the indicated samples and vitamin C (*n* = 3, one-way ANOVA, Tukey's post hoc tests).

Table S8. ABTS^{•+} scavenging activity (%) and IC₅₀ values of vitamin C

No	Sample	ABTS scavenging percentage (%) at the indicated concentration (µg/mL)							IC ₅₀ (µg/mL)
		1.56	3.125	6.25	12.5	25	50	100	
1	Vitamin C	2.387 ± 5.29	1.026 ± 4.74	3.058 ± 5.04	6.223 ± 6.18	17.29 ± 3.44	31.21 ± 4.53	73.56 ± 2.64	72.25 ± 4.42 ^{****}

Data in mean ± SEM; ^{****}*p* < 0.0001, *p* value was from comparing FL-MeOH and vitamin C (*n* = 3, one-way ANOVA, Tukey's post hoc tests).

Table S9. Percentage of α -glucosidase inhibition (%) of flower extracts

No	Extract	Percentage of inhibition (%) at the indicated concentration ($\mu\text{g/mL}$)						IC ₅₀ ($\mu\text{g/mL}$)
		3.125	6.25	12.5	25	50	100	
1	FL-hex	-2.523 \pm 4.02	-3.158 \pm 4.96	1.291 \pm 0.72	2.861 \pm 2.15	4.050 \pm 1.79	4.652 \pm 2.35	>100 ^a
2	FL-DCM	-1.785 \pm 2.53	-1.682 \pm 2.22	0.339 \pm 2.86	0.845 \pm 3.09	0.277 \pm 1.89	1.875 \pm 5.5	>100 ^a
3	FL-H ₂ O	-1.323 \pm 2.81	-2.124 \pm 3.21	-3.898 \pm 4.64	-2.675 \pm 5.69	-4.222 \pm 6.54	-4.312 \pm 6.65	>100 ^a

^aNo activity higher than 5% was observed at the highest tested concentration (100 $\mu\text{g/mL}$). Data in mean \pm SEM.

Table S10. Percentage of α -glucosidase inhibition (%) of methanolic flower extract

No	Extract	Percentage of inhibition (%) at the indicated concentration ($\mu\text{g/mL}$)						IC ₅₀ ($\mu\text{g/mL}$)
		25	30	40	50	60	80	
1	FL-MeOH	20.04 \pm 2.45	36.39 \pm 3.26	62.55 \pm 10.26	83.47 \pm 0.86	85.59 \pm 0.48	87.93 \pm 0.43	34.93 \pm 2.67 ^{***}

Data in mean \pm SEM; ^{***} $p = 0.0004$, p value was from comparing the inhibition of the extract and acarbose ($n = 3$, ANOVA).

Table S11. Percentage of α -glucosidase inhibition (%) of leaf extracts

No	Extract	Percentage of inhibition (%) at the indicated concentration ($\mu\text{g/mL}$)						IC ₅₀ ($\mu\text{g/mL}$)
		31.25	62.5	125	250	500	1000	
1	LF-hex	-0.727 \pm 3.28	-0.581 \pm 3.69	17.89 \pm 7.03	31.74 \pm 16.58	50.91 \pm 15.02	67.31 \pm 11.81	285.5 \pm 100.9
2	LF-DCM	-2.421 \pm 6.73	0.188 \pm 5.83	-2.172 \pm 5.67	-342.1 \pm 335	-340.6 \pm 335.1	-8.070 \pm 4.38	>1000 ^a
3	LF-H ₂ O	-8.004 \pm 8.82	-6.791 \pm 8.11	-5.323 \pm 7.40	-0.630 \pm 4.68	22.97 \pm 2.10	58.34 \pm 3.61	882.6 \pm 48.01

^aNo activity higher than 1% was observed at the highest tested concentration (1000 $\mu\text{g/mL}$). Data in \pm SEM, ($n = 3$, ANOVA)

Table S12. Percentage of α -glucosidase inhibition (%) of the methanolic leaf extract

No	Extract	Percentage of inhibition (%) at the indicated concentration ($\mu\text{g/mL}$)						IC ₅₀ ($\mu\text{g/mL}$)
		25	30	40	50	60	80	
1	LF-MeOH	15.23 \pm 2.68	28.86 \pm 1.33	50.30 \pm 2.33	80.31 \pm 0.89	84.85 \pm 0.95	86.79 \pm 0.77	38.69 \pm 1.01 ^{***}

Data in mean \pm SEM; ^{***} $p = 0.0004$, p value was from comparing the inhibition of the extract and acarbose ($n = 3$, one-way ANOVA, Tukey's hoc tests).

Table S13. Percentage of α -glucosidase inhibition (%) of bark extracts

No	Extract	Percentage of inhibition (%) at the indicated concentration ($\mu\text{g/mL}$)						IC ₅₀ ($\mu\text{g/mL}$)
		31.25	62.5	125	250	500	1000	
1	BK-hex	1.114 \pm 1.43	14.27 \pm 6.99	17.77 \pm 4.19	42.19 \pm 5.31	77.07 \pm 1.55	85.22 \pm 2.05	289.9 \pm 29.17
2	BK-DCM	-1.116 \pm 2.49	-3.464 \pm 1.02	4.055 \pm 3.39	30.78 \pm 13.83	53.23 \pm 13.84	44.14 \pm 16.84	>1000 ^a
3	BK-H ₂ O	-4.953 \pm 3.53	9.056 \pm 3.14	22.09 \pm 6.16	56.44 \pm 7.51	79.68 \pm 3.94	86.34 \pm 0.09	23.27 \pm 3.88 ^{****}

^a No activity higher than 45% was observed at the highest tested concentration (1000 $\mu\text{g/mL}$); Data in mean \pm SEM, ^{****} $p < 0.0001$, p value was from comparing the IC₅₀ of BK-H₂O and acarbose ($n = 3$, one-way ANOVA, Tukey's post hoc tests).

Table S14. Percentage of α -glucosidase inhibition (%) of methanolic bark extract

No	Extract	Percentage of inhibition (%) at the indicated concentration ($\mu\text{g/mL}$)						IC ₅₀ ($\mu\text{g/mL}$)
		3	4	5	6	8	10	
1	BK-MeOH	29.20 \pm 4.85	40.10 \pm 2.72	57.28 \pm 7.44	75.46 \pm 2.15	84.45 \pm 0.17	85.35 \pm 0.25	4.37 \pm 0.24****

Data in mean \pm SEM, **** $p < 0.0001$, p value was from comparing the IC₅₀ of BK-MeOH and acarbose ($n = 3$, one-way ANOVA, Tukey's post hoc tests).

Table S15. Percentage of α -glucosidase inhibition (%) of acarbose

No	Sample	Percentage of inhibition (%) at the indicated concentration ($\mu\text{g/mL}$)						IC ₅₀ ($\mu\text{g/mL}$)
		31.25	62.5	125	250	500	1000	
1	Acarbose	16.62 \pm 3.95	23.06 \pm 3.99	35.20 \pm 2.41	47.16 \pm 2.18	59.39 \pm 1.37	70.64 \pm 1.38	254 \pm 22.18

Table S16. Viable 3T3-L1 preadipocytes treated with flower extracts for 24, 48, and 72 h

No	Extract	Incubation (h)	Viable cells (%) at concentrations of ($\mu\text{g/mL}$)			
			25	50	100	200
1	FL-hex	24	119 \pm 11.85	120.5 \pm 10.27	121.2 \pm 21.74	139.6 \pm 13.95**
		48	96.31 \pm 4.26	99.79 \pm 3.02	104.5 \pm 5.24	103.9 \pm 5.85
		72	90.48 \pm 1.98	101.3 \pm 0.85	97.93 \pm 0.45	95.92 \pm 1.16
2	FL-DCM	24	111.4 \pm 10.43	111.7 \pm 6.85	123.3 \pm 14.47*	120.5 \pm 7.91*
		48	88.95 \pm 4.42	98.48 \pm 1.82	95.34 \pm 5.27	104.5 \pm 4.48
		72	87.31 \pm 1.35	98.44 \pm 1.09	93.95 \pm 1.94	95.2 \pm 0.52
3	FL-MeOH	24	112.5 \pm 8.15	116.8 \pm 3.31*	129.6 \pm 8.14***	139.9 \pm 3.66****
		48	100.8 \pm 7.37	108.9 \pm 3.94	117.3 \pm 3.20*	118.7 \pm 4.28*
		72	86.43 \pm 4.11	102.5 \pm 3.01	106.4 \pm 0.73	105.3 \pm 1.77
4	FL-H ₂ O	24	107.9 \pm 8.86	124.6 \pm 6.44*	126.5 \pm 9.38*	129.1 \pm 16.22**
		48	87.47 \pm 2.57	104.3 \pm 2.77	104.4 \pm 0.85	105.9 \pm 4.36
		72	81.02 \pm 5.12	101.8 \pm 2.34	100.1 \pm 3.68	98.43 \pm 1.03

Data in mean \pm SEM; * $p = 0.04$; ** $p = 0.004$; *** $p = 0.0001$; **** $p < 0.0001$, p values were from comparing the indicated samples and vehicle control ($n = 3$, one-way ANOVA, Dunnett's post hoc tests).

Table S17. Viable 3T3-L1 preadipocytes treated with leaf extracts for 24, 48, and 72 h

No	Extract	Incubation (h)	Viable cells (%) at concentrations of ($\mu\text{g/mL}$)			
			25	50	100	200
1	LF-hex	24	109.3 \pm 6.75	124.3 \pm 12.45*	123.6 \pm 15.51*	120.8 \pm 10.44
		48	91.22 \pm 4.61	98.83 \pm 2.60	100.6 \pm 2.77	97.28 \pm 4.11
		72	90.81 \pm 2.60	91.6 \pm 3.20	99 \pm 3.24	90.95 \pm 2.12
2	LF-DCM	24	107.4 \pm 6.06	116.1 \pm 9.92	117.8 \pm 11.97	127.4 \pm 13.1**
		48	95.28 \pm 1.89	93.51 \pm 5.09	99.52 \pm 2.05	99.88 \pm 3.88
		72	90.9 \pm 2.17	91.3 \pm 1.95	98.97 \pm 1.96	92.44 \pm 1.80
3	LF-MeOH	24	115.3 \pm 7.67	111.2 \pm 3.49	72.55 \pm 5.19***	41.6 \pm 0.59****
		48	98.35 \pm 2.78	87.91 \pm 2.02	64.41 \pm 0.52****	38.76 \pm 8.63****
		72	84.36 \pm 5.46	79 \pm 3.25**	70.16 \pm 3.96****	54.27 \pm 7.80****
4	LF-H ₂ O	24	113.6 \pm 10.33	118.7 \pm 11.9	125.8 \pm 14.27*	118.6 \pm 12.68
		48	93.69 \pm 4.01	93.27 \pm 2.34	105.6 \pm 3.41	95.17 \pm 4.12

No	Extract	Incubation (h)	Viable cells (%) at concentrations of ($\mu\text{g/mL}$)			
			25	50	100	200
		72	91.17 \pm 2.26	90.8 \pm 1.63	99.24 \pm 4.32	90.71 \pm 7.05

Data in mean \pm SEM; * p = 0.03; ** p = 0.006; *** p = 0.0004; **** p < 0.0001, p values were from comparing the indicated samples and vehicle control (n = 3, one-way ANOVA, Dunnett's post hoc tests).

Table S18. Viable 3T3-L1 preadipocytes treated with bark extracts for 24, 48, and 72 h

No	Extract	Incubation (h)	Viable cells (%) at concentrations of ($\mu\text{g/mL}$)			
			25	50	100	200
1	BK-hex	24	108.5 \pm 3.71	107.5 \pm 6.00	112.7 \pm 3.91	118.6 \pm 7.67**
		48	104 \pm 2.46	91.88 \pm 6.14	95.75 \pm 4.18	101.2 \pm 4.97
		72	97.15 \pm 3.88	91.33 \pm 0.96	90.73 \pm 2.13	99.57 \pm 4.38
2	BK-DCM	24	106.6 \pm 2.00	97.54 \pm 8.23	106.5 \pm 4.17	111.5 \pm 1.76
		48	106.3 \pm 3.59	92.63 \pm 3.72	92.3 \pm 2.42	93.19 \pm 6.29
		72	97.01 \pm 1.30	89.15 \pm 1.69	88.55 \pm 2.03	98.29 \pm 1.45
3	BK-MeOH	24	83.08 \pm 11.03	61.86 \pm 3.23****	32.64 \pm 4.22****	45.74 \pm 6.31****
		48	78.44 \pm 3.95*	45.67 \pm 3.02****	16.19 \pm 2.22****	22.33 \pm 7.69****
		72	81.56 \pm 1.01	67.46 \pm 4.70***	34.28 \pm 11.35****	18.16 \pm 6.18****
4	BK-H ₂ O	24	94.74 \pm 7.36	109.6 \pm 6.75	91.27 \pm 10.38	59.01 \pm 9.38***
		48	101.3 \pm 2.70	104.2 \pm 3.45	78.19 \pm 4.85	41.15 \pm 10.07****
		72	91.69 \pm 3.81	90.61 \pm 6.10	74.79 \pm 8.71*	65.71 \pm 14.56**

Data in mean \pm SEM; * p = 0.03; ** p = 0.008; *** p = 0.0007; **** p < 0.0001, p values were from comparing the indicated samples and vehicle medium (n = 3, one-way ANOVA, Dunnett's post hoc tests).

Table S19. Viable 3T3-L1 adipocytes treated with flowers extracts for 24, 48, and 72 h

No	Extract	Incubation (h)	Viable cells (%) at concentrations of ($\mu\text{g/mL}$)			
			25	50	100	200
1	FL-hex	24	92.35 \pm 2.70	104 \pm 2.90	100.8 \pm 4.64	95.33 \pm 6.44
		48	90.9 \pm 3.39	100.6 \pm 4.44	99.38 \pm 5.64	97.99 \pm 5.32
		72	95.55 \pm 7.78	104.9 \pm 8.35	106 \pm 9.66	105.1 \pm 11.99
2	FL-DCM	24	96.93 \pm 2.07	114 \pm 2.37	110.6 \pm 3.08	110.8 \pm 3.31
		48	97.32 \pm 1.85	115.1 \pm 1.21	109.9 \pm 3.70	112.5 \pm 5.00
		72	102.4 \pm 6.31	117.7 \pm 4.96*	116.1 \pm 6.95*	118.2 \pm 8.72*
3	FL-MeOH	24	93.7 \pm 1.47	105 \pm 3.15	104.7 \pm 3.41	100.7 \pm 0.42
		48	95.13 \pm 1.73	104.2 \pm 1.78	105.8 \pm 3.45	105.2 \pm 2.89
		72	99.67 \pm 5.59	109.4 \pm 3.97	107.3 \pm 0.51	115.3 \pm 1.70**
4	FL-H ₂ O	24	97.96 \pm 2.85	110.2 \pm 2.82	110.7 \pm 2.4	106.9 \pm 2.86
		48	100.6 \pm 3.41	112.3 \pm 4.83	116.3 \pm 2.77	110.3 \pm 3.58
		72	104.5 \pm 6.90	116.4 \pm 6.39	122.8 \pm 7.63**	116.3 \pm 7.82

Data in mean \pm SEM, * p = 0.02; ** p = 0.002, p values were from comparing the indicated samples and vehicle control (n = 3, one-way ANOVA, Dunnett's post hoc tests).

Table S20. Viable 3T3-L1 adipocytes treated with leaves extracts for 24, 48, and 72 h

No	Extract	Incubation (h)	Viable cells (%) at concentrations of ($\mu\text{g/mL}$)			
			25	50	100	200
1	LF-hex	24	100.4 \pm 2.00	101.4 \pm 3.40	115.8 \pm 3.51	101.5 \pm 2.21
		48	101 \pm 2.72	100.9 \pm 4.52	116.1 \pm 2.43*	104.1 \pm 4.66
		72	105.1 \pm 5.98	105.3 \pm 5.79	120.9 \pm 6.44**	109.5 \pm 8.07
2	LF-DCM	24	100.3 \pm 2.51	105.2 \pm 3.13	120.3 \pm 3.5**	102.6 \pm 2.50
		48	103.4 \pm 3.01	105.8 \pm 3.06	120.2 \pm 2.18**	104 \pm 3.49
		72	106.7 \pm 5.60	110.2 \pm 6.15	124.4 \pm 5.90***	103.3 \pm 1.47
3	LF-MeOH	24	95.08 \pm 1.68	94.53 \pm 3.66	100.4 \pm 4.14	102.8 \pm 5.21
		48	95.93 \pm 1.00	93.33 \pm 0.56	96.24 \pm 2.46	98.23 \pm 3.38
		72	97.18 \pm 3.65	98.95 \pm 2.10	103.7 \pm 1.72	103.7 \pm 3.26
4	LF-H ₂ O	24	101.4 \pm 1.45	98.92 \pm 3.51	105.2 \pm 1.37	105.7 \pm 3.36
		48	102.6 \pm 1.61	94.81 \pm 1.26	105.9 \pm 0.51	109 \pm 2.48
		72	105.8 \pm 1.36	101.7 \pm 3.92	106.8 \pm 3.93	110.8 \pm 2.59*

Data in mean \pm SEM; * p = 0.02; ** p = 0.001; *** p = 0.0001, p values were from comparing the indicated samples and vehicle medium (n = 3, one-way ANOVA, Dunnett's post hoc tests).

Table S21. Viable 3T3-L1 adipocytes treated with barks extracts for 24, 48, and 72 h

No	Extract	Incubation (h)	Viable cells (%) at concentrations of ($\mu\text{g/mL}$)			
			25	50	100	200
1	BK-hex	24	109.9 \pm 1.83	100.9 \pm 2.85	97.77 \pm 3.68	117 \pm 2.61**
		48	116.5 \pm 1.11**	100.1 \pm 2.97	99.56 \pm 2.49	115.6 \pm 1.88**
		72	117.2 \pm 4.79**	103.3 \pm 3.16	103.4 \pm 5.66	114.1 \pm 2.74*
2	BK-DCM	24	106.9 \pm 1.87	94.18 \pm 2.46	99.16 \pm 3.11	112.7 \pm 2.61*
		48	112.4 \pm 1.09*	96.04 \pm 1.46	99.32 \pm 1.78	113.5 \pm 0.44*
		72	115.6 \pm 5.76**	99.87 \pm 2.53	107.2 \pm 6.68	111.3 \pm 3.32
3	BK-MeOH	24	103.1 \pm 1.59	94.65 \pm 1.94	93.74 \pm 3.42	102.5 \pm 5.23
		48	104.7 \pm 3.10	100.3 \pm 2.37	94.17 \pm 0.96	99.57 \pm 3.07
		72	102.1 \pm 3.04	100.2 \pm 2.16	98.34 \pm 1.39	97.81 \pm 3.33
4	BK-H ₂ O	24	111.2 \pm 2.40*	107.6 \pm 1.83	99.51 \pm 4.04	104.3 \pm 3.66
		48	110.3 \pm 1.55*	113.5 \pm 0.22**	96.63 \pm 1.91	106.6 \pm 3.42
		72	111.1 \pm 3.64*	112.7 \pm 2.52**	101.7 \pm 1.99	109.1 \pm 1.45

Data in mean \pm SEM; * p = 0.02; ** p = 0.003, p values were from comparing the indicated samples and vehicle control (n = 3, one-way ANOVA, Dunnett's post hoc tests).

Table S22. Estimated lipid content from adipogenesis assay with ORO staining agent on the 3T3-L1 adipocytes treated with extracts

No	Sample	Fold change of adipogenesis (%)	
		12.5 $\mu\text{g/mL}$	50 $\mu\text{g/mL}$
1	Vehicle control	100 \pm 8.13	
2	FL-hex	105.1 \pm 10.08	90.04 \pm 12.87
3	FL-DCM	131.3 \pm 8.38	112.2 \pm 6.66
4	FL-MeOH	92.45 \pm 11.17	95.36 \pm 10.84
5	FL- H ₂ O	83.19 \pm 10.67	91.46 \pm 16.75
6	LF-hex	104.8 \pm 1.46	89.82 \pm 2.54

No	Sample	Fold change of adipogenesis (%)	
		12.5 µg/mL	50 µg/mL
7	LF-DCM	123 ± 10.97	140.9 ± 5.32*
8	LF-MeOH	84.65 ± 4.08	71.32 ± 3.77**
9	LF- H ₂ O	110 ± 9.52	108.5 ± 7.98
10	BK-hex	122.1 ± 7.01	108.3 ± 1.12
11	BK-DCM	145.9 ± 8.56**	129.7 ± 8.21
12	BK-MeOH	130.4 ± 4.94**	88.1 ± 4.73
13	BK-H ₂ O	99.56 ± 4.16	95.95 ± 6.30
14	NAC 5 mM	77.86 ± 5.77	
15	NAC 10 mM	70.45 ± 5.45*	

Data in mean ± SEM; * $p = 0.02$; ** $p = 0.009$, p values were from comparing the indicated samples and vehicle control ($n = 3$, one-way ANOVA, Tukey's post hoc tests).

Table S23. The estimated ROS level in adipocytes exposed to extracts for 48 h

No	Extracts	Cellular ROS level (%) at the corresponding concentration (µg/mL)			
		25	50	100	200
1	FL-hex	97.61 ± 6.84	105.6 ± 15.43	105.7 ± 16.51	105.5 ± 19.43
2	FL-DCM	118.1 ± 12.33	136.5 ± 19.54	128.9 ± 21.59	103.4 ± 15.07
3	FL-MeOH	136 ± 13.18	100.5 ± 6.83	93.52 ± 3.77	86.13 ± 9.93
4	FL-H ₂ O	97.55 ± 7.29	92.61 ± 8.36	95.5 ± 11.9	112.9 ± 14.45
5	LF-hex	118.5 ± 6.84	125.4 ± 9.09	131.2 ± 12.9	120.8 ± 9.58
6	LF-DCM	120.6 ± 7.17	121.7 ± 9.909	107.4 ± 3.75	109 ± 10.3
7	LF-MeOH	93.44 ± 4.41	85.56 ± 3.82	85.13 ± 2.18	78.06 ± 4.92
8	LF- H ₂ O	105 ± 1.90	105.6 ± 5.13	100.3 ± 6.44	92.53 ± 9.20
9	BK-hex	103.3 ± 8.72	99.09 ± 4.96	103.7 ± 1.49	101 ± 0.55
10	BK-DCM	98.9 ± 3.29	104 ± 2.973	105.2 ± 1.35	97.66 ± 4.47
11	BK-MeOH	89.11 ± 3.67	78.87 ± 2.90	70.66 ± 4.98 [†]	62.57 ± 0.96**
12	BK-H ₂ O	93.39 ± 4.39	87.78 ± 7.3	85.32 ± 3.89	85.62 ± 2.27

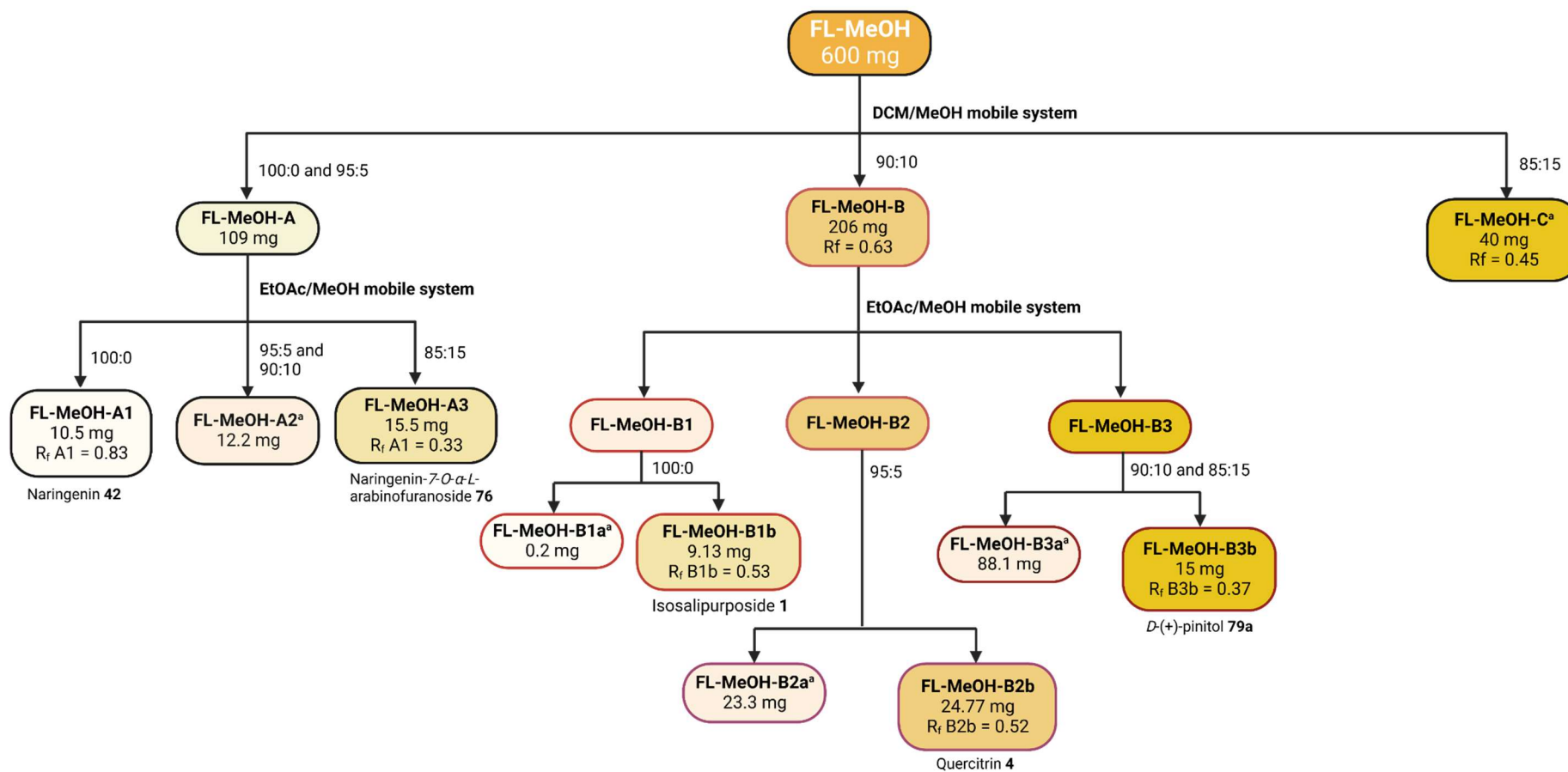
Data in mean ± SEM; [†] $p = 0.03$, ** $p = 0.003$, p values were from the inhibition of the extract vs vehicle control ($n = 3$, one-way ANOVA, Tukey's post hoc tests).

Table S24. Observed data of glucose uptake simulation with the fluoroprobe 2-NBDG assay for all extracts on the 3T3-L1 adipocytes.

Sample	2-NBDG uptake percentage (%)	
	12.5 µg/mL	50 µg/mL
Vehicle	100 ± 6.54	
FL-hex	74.97 ± 1.54	89.15 ± 6.80
FL-DCM	91.74 ± 6.51	95.89 ± 23.05
FL-MeOH	141.5 ± 27.94	185.3 ± 41.52**
FL-H ₂ O	87.01 ± 6.63	96.55 ± 8.45
LF-hex	89.48 ± 8.04	101.6 ± 4.84
LF-DCM	119.8 ± 18.74	120.9 ± 19.54
LF-MeOH	113.5 ± 6.1	198 ± 42.61**
LF-H ₂ O	97.69 ± 4.01	101.4 ± 5.51
BK-hex	109.4 ± 7.73	139.9 ± 18.76
BK-DCM	86.49 ± 9.82	103 ± 14.90
BK-MeOH	118.3 ± 9.517	161.6 ± 10.76
BK-H ₂ O	121.8 ± 14.63	132.2 ± 22.81
Insulin 100 nM	140.6 ± 18.36	
Metformin 10 µM	138 ± 28.26	

Data in mean ± SEM; ** $p = 0.007$ for FL-MeOH and ** $p = 0.006$, p values were from comparing the indicated samples and vehicle control ($n = 3$, one-way ANOVA, Dunnett's post hoc tests).

Appendix B

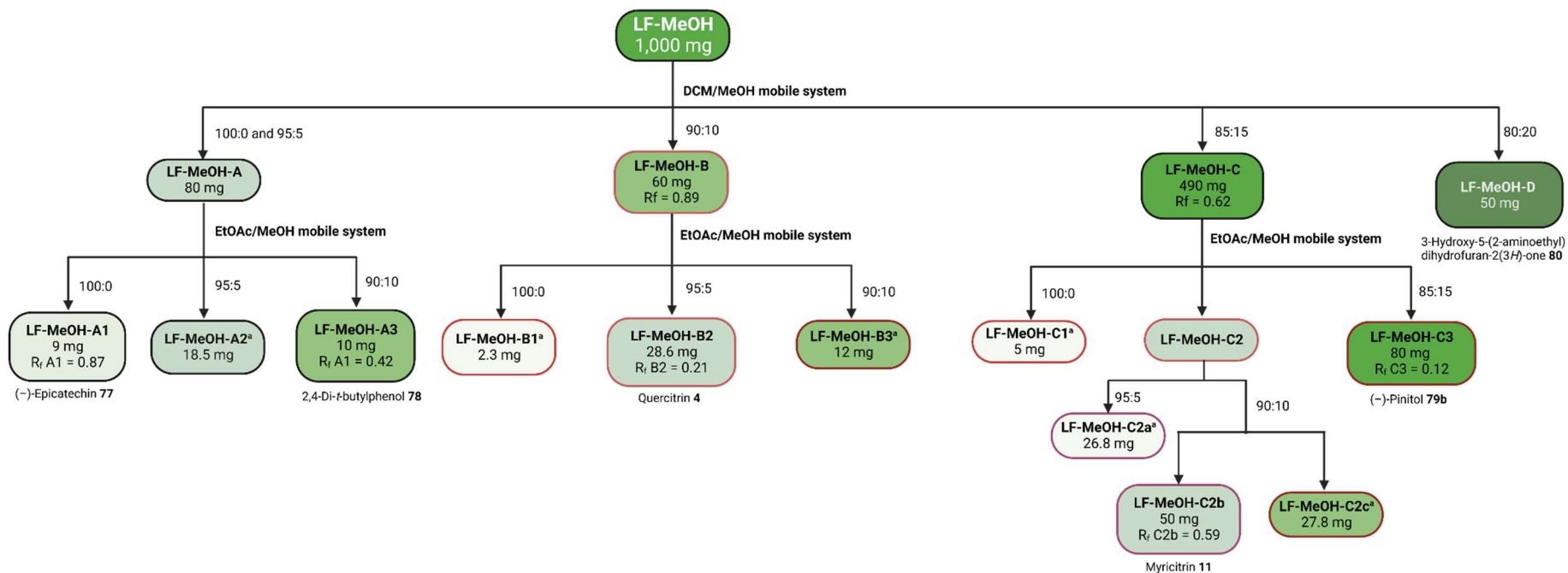


^aNote:

According to the proton NMR spectra, the following fractions were:

- 1) FL-MeOH-A2 = mixture of subfraction A1 and A3
- 2) FL-MeOH-B1a = mixture of hydrocarbons (δ ^1H = 0–1.8 ppm)
- 3) FL-MeOH-B2a = impure subfraction B2b
- 4) FL-MeOH-B3a = impure subfraction B3b
- 5) FL-MeOH-C = impure fraction B

Figure S4. Schematic representation of the outcomes of fractionation of FL-MeOH extract of *A. saligna*

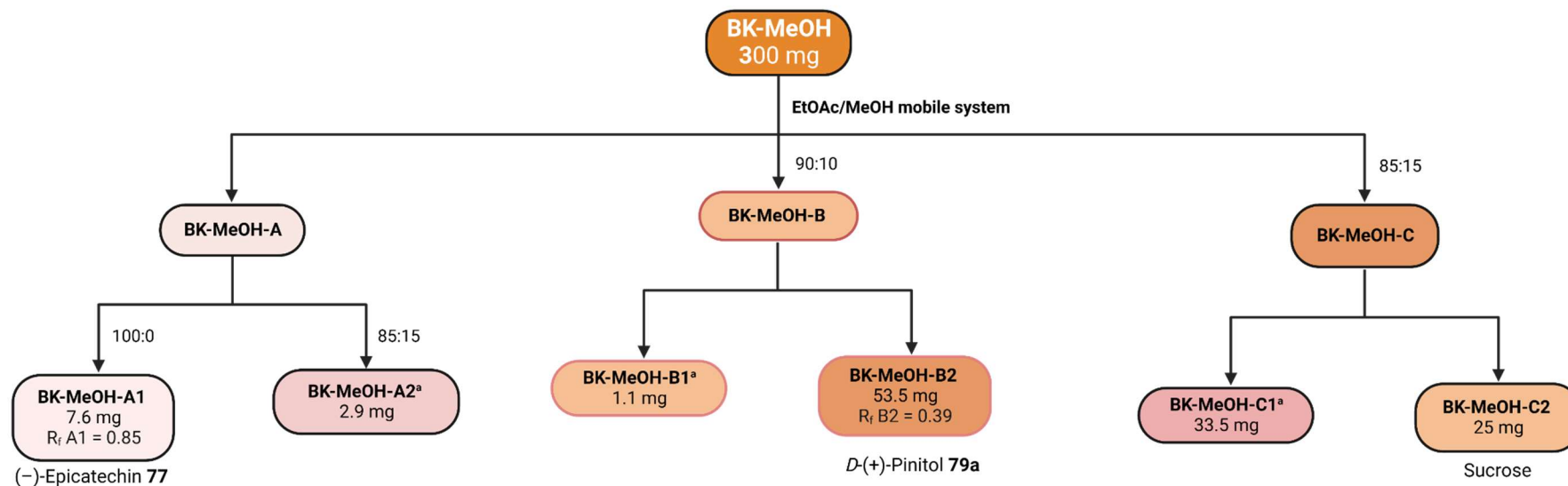


^aNote:

According to the proton NMR spectra, the following fractions were:

- 1) LF-MeOH-A2 = mixture of subfraction A1 and A3
- 2) LF-MeOH-B1 = mixture of hydrocarbons (δ ¹H = 0–1.8 ppm)
- 3) LF-MeOH-B3 = impure subfraction B2
- 4) LF-MeOH-C1 = mixture of hydrocarbons (δ ¹H = 0–1.8 ppm)
- 5) LF-MeOH-C2a = impure subfraction C2b
- 6) LF-MeOH-C2c = mixture of subfraction C2b and C3

Figure S5. Schematic representation of the outcomes of fractionation of LF-MeOH extract of *A. saligna*



^a Note:

According to the proton NMR spectra, the following fractions were:

- 1) BK-MeOH-A2 = impure sub-fraction A1
- 2) LF-MeOH-B1 = impure sub-fraction B1
- 3) LF-MeOH-C1 = mixture of B2 and C2

Figure S6. Schematic representation of the outcomes of fractionation of BK-MeOH extract of *A. saligna*

Appendix C

Table S25. The DPPH scavenging properties of the isolated compounds

No	Sample	Scavenging percentage (%) at the indicated concentration (μM)								IC ₅₀ (μM)
		62.5	125	250	500	1,000	2,000	5,000	10,000	
1	Isosalipurposide 1	-	15.14 \pm 1.24	18.65 \pm 1.74	25.34 \pm 0.46	37.83 \pm 2.00	56.78 \pm 2.75	61.44 \pm 2.74	-	1,559 \pm 28.16 ^{***}
2	Naringenin 42	-	-	10.06 \pm 1.61	12.34 \pm 1.02	14.91 \pm 0.56	21.46 \pm 0.74	26.55 \pm 3.29	34.51 \pm 0.39	>10,000 ^a
3	Quercitrin 4	9.75 \pm 0.72	18.71 \pm 1.82	38.91 \pm 2.00	68.99 \pm 1.13	86.6 \pm 0.39	90.5 \pm 0.17	-	-	322.6 \pm 14.05 ^{****}
4	Myricitrin 11	14.44 \pm 1.88	28.65 \pm 0.70	57.71 \pm 1.33	93.77 \pm 0.50	95.01 \pm 0.14	95.38 \pm 0.17	-	-	199.9 \pm 4.83 ^{****}
5	Naringenin-7- <i>O</i> - α -L-arabinofuranose 76	-	-	1.62 \pm 0.37	2.62 \pm 1.68	3.98 \pm 0.47	7.35 \pm 2.14	16.08 \pm 5.11	19.62 \pm 0.53	>10,000 ^a
6	<i>D</i> -(+)-pinitol 79a	-	-	8.23 \pm 2.52	15.77 \pm 2.41	29.25 \pm 3.11	58.31 \pm 1.55	88.25 \pm 1.58	87.38 \pm 0.56	1,675 \pm 65.72 ^{****}
7	(-)-pinitol 79b	-	-	12.39 \pm 3.61	14.62 \pm 1.37	20.22 \pm 0.16	28.10 \pm 0.57	42.58 \pm 1.00	59.93 \pm 2.21	6,865 \pm 69.08 ^{****}
8	(-)-Epicatechin 77	14.04 \pm 3.44	23.44 \pm 2.00	43.22 \pm 1.91	65.65 \pm 9.73	87.84 \pm 6.31	95.28 \pm 0.28	-	-	278 \pm 8.62 ^{****}
9	2,4-Di- <i>t</i> -butylphenol 78	-	-	8.00 \pm 3.65	10.16 \pm 3.02	12.05 \pm 3.42	21.75 \pm 4.18	24.47 \pm 3.73	36.9 \pm 4.20	>10,000 ^a
10	3-Hydroxy-5-(2-aminoethyl) dihydroxyfuran-2(3H)-one 80	-	-	-6.10	-3.31	0.02 \pm 5.07	5.78 \pm 5.61	8.92 \pm 4.58	14.37 \pm 5.29	>10,000 ^a
11	Vitamin C	1.86 \pm 1.45	5.71 \pm 2.28	6.738 \pm 1.43	20.65 \pm 1.62	46.58 \pm 2.18	87.17 \pm 2.15	-	-	1,072 \pm 47.64

^aNo activity higher than 37% was observed at the highest tested concentration (10 mM); Data in mean \pm SEM, *** p = 0.0002; **** p < 0.0001, p values were from comparing the indicated compounds and vitamin C (n = 3, one-way ANOVA, Tukey's post hoc tests).

Table S26. The ABTS^{•+} scavenging properties of the isolated compounds

No	Sample	Scavenging percentage (%) at the indicated concentration (μM)								IC ₅₀ (μM)
		62.5	125	250	500	1,000	2,000	5,000	10,000	
1	Isosalipurposide 1	-	-	13.98 \pm 0.26	23.37 \pm 1.96	36.21 \pm 2.37	56.01 \pm 2.29	80.17 \pm 1.90	93.27 \pm 0.45	1,686 \pm 95.26 ^{****}
2	Naringenin 42	-	19.55 \pm 1.05	26.91 \pm 0.12	35.88 \pm 0.80	43.71 \pm 0.72	55.46 \pm 4.06	79.89 \pm 0.76	-	1,525 \pm 316.5 ^{****}

No	Sample	Scavenging percentage (%) at the indicated concentration (μM)								IC ₅₀ (μM)
		62.5	125	250	500	1,000	2,000	5,000	10,000	
3	Quercitrin 4	14.01 \pm 2.14	24.82 \pm 0.34	37.36 \pm 0.73	63.06 \pm 1.37	85.56 \pm 1.67	99.03 \pm 0.06	-	-	355.3 \pm 12.08
4	Myricitrin 11	14.29 \pm 4.22	29.41 \pm 2.13	44.56 \pm 1.02	67.66 \pm 1.4	82.1 \pm 1.07	91.98 \pm 0.95	-	-	285.9 \pm 7.21
5	Naringenin-7 <i>O</i> - α -L-arabinofuranoside 76	-	15.36 \pm 2.00	24.98 \pm 1.42	29.92 \pm 1.69	34.82 \pm 1.07	38.65 \pm 3.00	56.29 \pm 1.34	-	4,146 \pm 99.15****
6	<i>D</i> -(+)-pinitol 79a	6.55 \pm 5.32	15.61 \pm 5.01	27.6 \pm 4.14	50.66 \pm 2.31	92.43 \pm 0.19	99.96 \pm 0.34	-	-	475 \pm 24.20
7	(-)-pinitol 79b	-	5.87 \pm 0.16	2.98 \pm 0.83	18.5 \pm 2.05	28.61 \pm 1.83	48.48 \pm 1.37	82.87 \pm 3.41	-	2,096 \pm 70.40****
8	(-)-Epicatechin 77	35.88 \pm 3.58	63.17 \pm 4.09	90.85 \pm 2.43	99.56 \pm 0.04	99.67 \pm 0.09	99.85 \pm 0.13	-	-	92.58 \pm 13.03
9	2,4-Di- <i>t</i> -butylphenol 78	-	10.89 \pm 1.68	11.94 \pm 2.44	19.29 \pm 0.04	27.88 \pm 1.19	41.91 \pm 0.25	70.9 \pm 3.48	-	2,715 \pm 64.02****
10	3-Hydroxy-5-(2-aminoethyl) dihydrofuran-2(3 <i>H</i>)-one 80	-	4.35 \pm 4.02	8.67 \pm 6.85	1.68 \pm 2.58	5.84 \pm 1.27	10.46 \pm 3.85	22.49 \pm 5.44	-	>10,000 ^a
11	Vitamin C	9.40 \pm 1.74	13.86 \pm 3.70	30.4 \pm 6.61	53.52 \pm 4.17	80.4 \pm 1.65	96.39 \pm 1.71	-	-	460.2 \pm 56.29

^aNo activity higher than 23% was observed at the highest tested concentration (5 mM). Data in mean \pm SEM, **** p < 0.0001, p value was from comparing the indicated compounds and vitamin C (n = 3, one-way ANOVA, Tukey's post hoc tests).

Table S27. The quantified inhibitory activity of the isolated compounds against the α -glucosidase enzyme

No	Sample	Inhibitory percentage (%) at the corresponding concentrations (μM)						IC ₅₀ (μM)
		31.25	62.5	125	250	500	1,000	
1	Isosalipurposide 1	32.27 \pm 5.61	37.36 \pm 7.32	52.19 \pm 3.49	63.69 \pm 2.47	73.88 \pm 1.29	82.3 \pm 1.00	116.5 \pm 26.40
2	Naringenin 42	28.81 \pm 3.89	40.78 \pm 2.19	65.64 \pm 5.77	77.64 \pm 4.81	93.37 \pm 0.75	98.59 \pm 0.61	89.71 \pm 10.22*
3	Quercitrin 4	18.01 \pm 2.18	28.32 \pm 2.61	41.66 \pm 3.69	58.19 \pm 0.84	76.97 \pm 0.99	87.03 \pm 4.46	177.3 \pm 11.34
4	Myricitrin 11	13.01 \pm 6.59	16.52 \pm 4.71	21.58 \pm 6.71	43.06 \pm 4.48	59.48 \pm 1.73	88.06 \pm 1.19	351.6 \pm 24.88
5	Naringenin-7 <i>O</i> - α -L-arabinofuranoside 76	8.11 \pm 2.03	14.07 \pm 4.44	17.2 \pm 1.41	20.81 \pm 1.80	34.41 \pm 2.66	76.34 \pm 21.72	769.1 \pm 95.82****
6	<i>D</i> -(+)-pinitol 79a	16 \pm 3.03	39 \pm 1.59	89.22 \pm 2.40	99.74 \pm 0.57	100.6 \pm 0.54	100.5 \pm 0.64	74.69 \pm 0.23*
7	(-)-pinitol 79b	0.29 \pm 6.45	1.18 \pm 0.97	31.64 \pm 1.35	78.43 \pm 4.73	93.46 \pm 1.77	96.17 \pm 1.85	164.2 \pm 8.36
8	(-)-Epicatechin 77	33.01 \pm 6.84	48.53 \pm 4.50	78.04 \pm 4.6	92.36 \pm 2.23	97.14 \pm 0.82	99.15 \pm 0.38	63.58 \pm 11.83*
9	2,4-Di- <i>t</i> -butylphenol 78	18.57 \pm 4.45	18.73 \pm 5.06	27.11 \pm 5.58	55.17 \pm 10.98	79.26 \pm 10.49	89.86 \pm 7.42	259 \pm 58.34
10	3-Hydroxy-5-(2-aminoethyl) dihydrofuran-2(3 <i>H</i>)-one 80	5.99 \pm 7.41	12.28 \pm 5.13	13.5 \pm 3.35	12.55 \pm 4.46	14.01 \pm 1.03	10.47 \pm 1.06	>1000 ^a

No	Sample	Inhibitory percentage (%) at the corresponding concentrations (μM)						IC ₅₀ (μM)
		31.25	62.5	125	250	500	1,000	
11	Acarbose	17.88 \pm 1.97	28.34 \pm 1.44	35.48 \pm 3.47	50.6 \pm 2.46	64.13 \pm 1.65	74.34 \pm 1.09	239.9 \pm 31.74

^aNo activity higher than 11% was observed at the highest tested concentration (1 mM); Data in mean \pm SEM, * p = 0.03; **** p < 0.0001, p values were from comparison between the indicated the compounds and acarbose (n = 3, one-way ANOVA, Tukey's post hoc tests).

Table S28. Viable 3T3-L1 preadipocytes and adipocytes treated with naringenin **42** for 24, 48, and 72 h

No	Incubation (h)	Viable pre-adipocytes (%) at concentrations of (μM)				Viable adipocytes (%) at concentrations of (μM)			
		15.63	31.25	62.5	125	15.63	31.25	62.5	125
1	24	85.76 \pm 2.59 [*]	85.03 \pm 0.62 ^{**}	89.93 \pm 3.16	96.9 \pm 2.45	98.67 \pm 3.21	99.29 \pm 3.58	97.92 \pm 3.91	93.54 \pm 1.92
2	48	94.8 \pm 5.29	94.4 \pm 4.23	91.9 \pm 7.01	93.84 \pm 5.66	91.82 \pm 8.36	98.59 \pm 4.79	98.18 \pm 4.63	94.33 \pm 3.55
3	72	91.34 \pm 0.94	89.89 \pm 1.32	84.01 \pm 1.30 ^{**}	83.67 \pm 2.78 ^{**}	92.65 \pm 5.58	84.54 \pm 6.28	87.11 \pm 7.49	78.31 \pm 2.28 ^{**}

Data in mean \pm SEM, ^{*} $p = 0.013$; ^{**} $p = 0.003$, p values were from comparison between the indicated samples and vehicle control ($n = 3$, one-way ANOVA, Dunnett's post hoc tests).

Table S29. Viable 3T3-L1 preadipocytes and adipocytes treated with naringenin-7O- α -L-arabinofuranoside **76** for 24, 48, and 72 h

No	Incubation (h)	Viable pre-adipocytes (%) at concentrations of (μM)				Viable adipocytes (%) at concentrations of (μM)			
		15.63	31.25	62.5	125	15.63	31.25	62.5	125
1	24	85 \pm 2.43 ^{**}	94.59 \pm 1.57	82.08 \pm 7.24 ^{***}	82.91 \pm 1.85 ^{**}	100.6 \pm 1.39	97.51 \pm 1.27	97.53 \pm 2.69	96.47 \pm 3.10
2	48	92.54 \pm 5.02	96.35 \pm 2.94	96.1 \pm 2.82	93.79 \pm 4.48	96.53 \pm 8.24	94.4 \pm 6.88	91.69 \pm 6.60	90.01 \pm 10.17
3	72	89.67 \pm 2.5	86.07 \pm 2.11 ^{**}	83.11 \pm 1.57 ^{**}	85.88 \pm 1.96 ^{**}	78.09 \pm 4.08 [*]	78.99 \pm 5.77 [*]	89.79 \pm 5.81	90.06 \pm 4.65

Data in mean \pm SEM, ^{*} $p = 0.01$; ^{**} $p = 0.004$; ^{***} $p = 0.0008$, p values were from comparison between the indicated samples and vehicle control ($n = 3$, one-way ANOVA, Dunnett's post hoc tests).

Table S30. Viable 3T3-L1 preadipocytes and adipocytes treated with isosalipurposide **1** for 24, 48, and 72 h

No	Incubation (h)	Viable pre-adipocytes (%) at concentrations of (μM)				Viable adipocytes (%) at concentrations of (μM)			
		15.63	31.25	62.5	125	15.63	31.25	62.5	125
1	24	89.99 \pm 5.82	94.12 \pm 4.96	89.9 \pm 4.81	86.14 \pm 5.831	93.75 \pm 0.57 [*]	96.26 \pm 1.82	96.65 \pm 2.25	96.92 \pm 1.87
2	48	86.43 \pm 3.16	84.12 \pm 5.36	86.08 \pm 4.88	67.71 \pm 10.32 ^{***}	93.21 \pm 0.10	93.78 \pm 2.31	95.64 \pm 3.49	95.71 \pm 1.44
3	72	98.9 \pm 1.94	93.48 \pm 3.26	93.14 \pm 0.78	83.81 \pm 11.98	100.2 \pm 4.14	101 \pm 3.92	101 \pm 4.02	101.3 \pm 3.07

Data in mean \pm SEM, ^{*} $p = 0.04$; ^{***} $p = 0.0008$, p values were from comparison between the indicated samples and vehicle control ($n = 3$, one-way ANOVA, Dunnett's post hoc tests).

Table S31. Viable 3T3-L1 preadipocytes and adipocytes treated with quercitrin **4** for 24, 48, and 72 h

No	Incubation (h)	Viable pre-adipocytes (%) at concentrations of (μM)				Viable adipocytes (%) at concentrations of (μM)			
		15.63	31.25	62.5	125	15.63	31.25	62.5	125
1	24	91.81 \pm 4.69	95.37 \pm 2.14	100.2 \pm 4.62	97.9 \pm 5.92	97.81 \pm 1.83	99.16 \pm 1.23	99.1 \pm 0.98	98.46 \pm 1.56
2	48	90.86 \pm 1.12	96.71 \pm 2.11	98.23 \pm 2.52	92.13 \pm 4.16	95.74 \pm 1.42	96.33 \pm 0.94	98.02 \pm 1.59	96.99 \pm 2.34
3	72	95.78 \pm 0.04	93.21 \pm 2.52	90.57 \pm 2.81	90.03 \pm 2.69	98.54 \pm 1.3	98.76 \pm 1.56	99.32 \pm 1.59	99.92 \pm 2.12

Data in mean \pm SEM ($n = 3$).

Table S32. Viable 3T3-L1 preadipocytes and adipocytes treated with *D*-(+)-pinitol **79a** for 24, 48, and 72 h

No	Incubation (h)	Viable pre-adipocytes (%) at concentrations of (μM)				Viable adipocytes (%) at concentrations of (μM)			
		15.63	31.25	62.5	125	15.63	31.25	62.5	125
1	24	87.44 \pm 6.55	91.1 \pm 4.07	87.94 \pm 7.09	83.78 \pm 10.65*	93.58 \pm 3.19	92.6 \pm 2.69	93.65 \pm 3.39	95.3 \pm 3.63
2	48	96.42 \pm 2.98	95.46 \pm 1.99	94.25 \pm 2.89	86.69 \pm 2.50	94.42 \pm 4.16	97.64 \pm 3.42	95.06 \pm 3.84	95.32 \pm 4.72
3	72	99.3 \pm 1.67	96.96 \pm 0.15	96.3 \pm 0.73	88.58 \pm 1.05	97.92 \pm 4.66	98.62 \pm 4.07	98.19 \pm 3.04	97.54 \pm 3.11

Data in mean \pm SEM, * p = 0.02, p value was from comparison between the indicated samples and vehicle control (n = 3, one-way ANOVA, Dunnett's post hoc tests).

Table S33. Viable 3T3-L1 preadipocytes and adipocytes treated with (-)-pinitol **79b** for 24, 48, and 72 h

No	Incubation (h)	Viable pre-adipocytes (%) at concentrations of (μM)				Viable adipocytes (%) at concentrations of (μM)			
		15.63	31.25	62.5	125	15.63	31.25	62.5	125
1	24	97.69 \pm 7.54	95.84 \pm 6.01	96.87 \pm 9.44	87.89 \pm 3.58	91.36 \pm 2.37	91.89 \pm 2.19	91.36 \pm 1.73	93.41 \pm 2.65
2	48	94.34 \pm 4.67	96.21 \pm 4.1	94.96 \pm 4.13	86.38 \pm 1.72	92.01 \pm 3.03	93.7 \pm 3.96	93.45 \pm 3.92	93.35 \pm 3.85
3	72	101.1 \pm 2.25	99.96 \pm 1.24	98.48 \pm 2.39	93.05 \pm 2.50	94.38 \pm 2.90	93.97 \pm 4.30	93.58 \pm 3.58	95.94 \pm 3.92

Data in mean \pm SEM (n = 3).

Table S34. Viable 3T3-L1 preadipocytes and adipocytes treated with (-)-epicatechin **77** for 24, 48, and 72 h

No	Incubation (h)	Viable pre-adipocytes (%) at concentrations of (μM)				Viable adipocytes (%) at concentrations of (μM)			
		15.63	31.25	62.5	125	15.63	31.25	62.5	125
1	24	83.76 \pm 4.13**	86.55 \pm 5.15**	88.55 \pm 4.27*	96.15 \pm 4.63	98.17 \pm 1.55	100.1 \pm 0.94	100 \pm 0.41	99.31 \pm 0.77
2	48	93.15 \pm 3.31	91.24 \pm 3.39	96.33 \pm 3.56	100.7 \pm 1.64	97.94 \pm 3.33	97.78 \pm 4.22	98.39 \pm 4.32	97.73 \pm 1.01
3	72	91.39 \pm 1.138	88.25 \pm 1.407*	84.78 \pm 2.49**	88.57 \pm 2.10*	88.74 \pm 7.24	94.62 \pm 2.01	92.28 \pm 1.38	86.87 \pm 6.90*

Data in mean \pm SEM, * p = 0.03; ** p = 0.001, p values were from comparison of the indicated samples and vehicle control (n = 3, one-way ANOVA, Dunnett's post hoc tests).

Table S35. Viable 3T3-L1 preadipocytes and adipocytes treated with 2,4-di-*t*-butylphenol **78** for 24, 48, and 72 h

No	Incubation (h)	Viable pre-adipocytes (%) at concentrations of (μM)				Viable adipocytes (%) at concentrations of (μM)			
		15.63	31.25	62.5	125	15.63	31.25	62.5	125
1	24	89.31 \pm 2.59*	97.67 \pm 4.13	75.34 \pm 7.34****	83.19 \pm 1.54***	100.7 \pm 1.05	98.31 \pm 2.16	101.2 \pm 1.52	101.5 \pm 1.60
2	48	89.89 \pm 4.05*	85.75 \pm 4.46**	86.91 \pm 1.01**	76.29 \pm 0.36****	97.8 \pm 4.18	90.83 \pm 1.07	101.4 \pm 3.42	101.5 \pm 4.69
3	72	87.16 \pm 0.71*	81.78 \pm 1.77***	80.36 \pm 0.816***	73.66 \pm 2.19****	98.8 \pm 1.35	82 \pm 5.34*	88.6 \pm 10.96	90.2 \pm 7.58

Data in mean \pm SEM, * p = 0.01; ** p = 0.001; **** p < 0.0001, p values were from comparison between the indicated samples and vehicle control (n = 3, one-way ANOVA, Dunnett's post hoc tests).

Table S36. Viable 3T3-L1 preadipocytes and adipocytes treated with myricitrin **11** for 24, 48, and 72 h

No	Incubation (h)	Viable pre-adipocytes (%) at concentrations of (μM)				Viable adipocytes (%) at concentrations of (μM)			
		15.63	31.25	62.5	125	15.63	31.25	62.5	125
1	24	99.07 \pm 6.02	91.45 \pm 5.79	67.47 \pm 6.12**	35.62 \pm 8.23****	98.77 \pm 0.29	97.99 \pm 3.07	100 \pm 0.70	100.4 \pm 1.57
2	48	93.24 \pm 1.16	81.22 \pm 3.39	58.5 \pm 7.67****	18.41 \pm 9.38****	95.91 \pm 2.47	94.4 \pm 3.99 [†]	95.05 \pm 3.17	95.6 \pm 1.52
3	72	99.31 \pm 1.50	91.81 \pm 3.18	70.22 \pm 7.59**	27.3 \pm 13.61****	104.6 \pm 5.07	105.4 \pm 5.27	102.7 \pm 2.84	104 \pm 3.47

Data in mean \pm SEM, [†] $p = 0.05$; ** $p = 0.001$; **** $p < 0.0001$, p values were from comparison of the indicated samples and vehicle control ($n = 3$, one-way ANOVA, Dunnett's post hoc tests).

Table S37. Viable 3T3-L1 preadipocytes and adipocytes treated with 3-hydroxy-5-(2-aminoethyl) dihydrofuran-2(3H)-one **80** for 24, 48, and 72 h

No	Incubation (h)	Viable pre-adipocytes (%) at concentrations of (μM)				Viable adipocytes (%) at concentrations of (μM)			
		15.63	31.25	62.5	125	15.63	31.25	62.5	125
1	24	85.26 \pm 2.22**	83.29 \pm 3.94***	79.62 \pm 2.90****	80.56 \pm 2.16****	100.2 \pm 1.41	100.9 \pm 1.80	97.23 \pm 4.11	98.67 \pm 1.84
2	48	82.4 \pm 1.62***	74.3 \pm 1.32****	68.46 \pm 0.71****	64.26 \pm 1.50****	96.19 \pm 5.80	96.76 \pm 5.56	95.56 \pm 6.77	96.84 \pm 3.16
3	72	71.71 \pm 5.92****	70.59 \pm 5.20****	57.63 \pm 3.09****	47.93 \pm 1.76****	82.7 \pm 3.24 [†]	95.72 \pm 3.18	89.75 \pm 6.28	85.22 \pm 4.60 [†]

Data in mean \pm SEM, [†] $p = 0.02$; ** $p = 0.002$; *** $p = 0.0002$; **** $p < 0.0001$, p values were from comparison between the indicated samples and vehicle control ($n = 3$, one-way ANOVA, Dunnett's post hoc tests).

Table S38. Estimated lipid content from adipogenesis assay with ORO staining agent on the 3T3-L1 adipocytes treated with isolated compounds within the differentiation process (day-0 to day-8)

No	Sample	Fold change of adipogenesis (%)	
		0.5 μM	10 μM
1	Vehicle control	100 \pm 0.81	
2	Naringenin 42	90.69 \pm 2.41	85.59 \pm 1.77
3	Naringenin-7O- α -L-arabinofuranoside 76	92.41 \pm 4.34	92.16 \pm 5.98
4	Isosalipurposide 1	97.18 \pm 8.43	100.5 \pm 13.98
5	Quercitrin 4	94.1 \pm 4.59	88.12 \pm 5.32
6	D-(+)-pinitol 79a	92.38 \pm 8.41	89.12 \pm 5.64
7	(-)-Pinitol 79b	94.99 \pm 5.72	83.08 \pm 1.58
8	(-)-Epicatechin 77	87.85 \pm 8.40	78.85 \pm 5.68
9	2,4-Di- <i>t</i> -butylphenol 78	96.27 \pm 3.76	90.14 \pm 3.85
10	Myricitrin 11	96.55 \pm 2.78	74.72 \pm 3.67*
11	3-Hydroxy-5-(2-aminoethyl) dihydrofuran-2(3H)-one 80	84.12 \pm 7.54	80.87 \pm 5.62
12	NAC 5 mM	57.69 \pm 1.16****	
13	NAC 10 mM	48.87 \pm 2.86****	
14	Undifferentiated	57.70 \pm 0.25****	

Data in mean \pm SEM; * $p = 0.03$, **** $p = 0.00008$, p values were from comparison between the indicated samples and vehicle control ($n = 3$, one-way ANOVA, Tukey's post hoc tests)

Table S39. The estimated ROS level of adipocytes exposed to isolated compounds for 48 h

No	Isolated compounds	Cellular ROS level (%) at the corresponding concentrations (μM)	
		0.5	10
1	Naringenin 42	98.7 \pm 2.89	75.82 \pm 6.20 [†]

No	Isolated compounds	Cellular ROS level (%) at the corresponding concentrations (μM)	
		0.5	10
2	Naringenin-7O- α -L-arabinofuranoside 76	99.06 \pm 10.95	76.64 \pm 5.16
3	Isosalipurposide 1	98.33 \pm 2.27	80.13 \pm 7.52
4	Quercitrin 4	102.9 \pm 0.36	87.65 \pm 0.72
5	D-(+)-pinitol 79a	89.84 \pm 0.88	69.24 \pm 3.90**
6	(-)-Pinitol 79b	88.76 \pm 2.96	79.57 \pm 6.40
7	(-)-Epicatechin 77	105.5 \pm 3.99	71.45 \pm 4.82**
8	2,4-Di- <i>t</i> -butylphenol 78	99.95 \pm 0.93	87.94 \pm 5.29
9	Myricitrin 11	100.5 \pm 7.66	78.64 \pm 6.14
10	3-Hydroxy-5-(2-aminoethyl) dihydrofuran-2(3 <i>H</i>)-one 80	99.6 \pm 6.24	92.67 \pm 3.20

Data in mean \pm SEM, * p = 0.05, ** p = 0.002, p values were from the inhibition of the isolated compound vs blank control (n = 3, one-way ANOVA, Tukey's post hoc tests)

Table S40. Estimated mt-ROS level (%) and J aggregates/JC-1 monomers percentage in 3T3-L1 adipocytes treated by methanolic extracts

Sample	Mt-ROS level (%)		J aggregates (red)/JC-1 monomers (green) percentage (%)	
	12.5 $\mu\text{g/mL}$	50 $\mu\text{g/mL}$	12.5 $\mu\text{g/mL}$	50 $\mu\text{g/mL}$
Vehicle control	100 \pm 8.78		100 \pm 9.81	
FL-MeOH	103 \pm 28.33	68.44 \pm 27.5	138.1 \pm 23.81	303.5 \pm 7.60***
LF-MeOH	98.36 \pm 9.05	47.43 \pm 19.67	97.18 \pm 2.06	178.8 \pm 18.9
BK-MeOH	103.3 \pm 24.13	42.35 \pm 3.74	123.7 \pm 32.67	246.8 \pm 28.65*
Metformin 10 μM	65.74 \pm 2.16		206.8 \pm 41.87	
Undifferentiated cells	70.45 \pm 7.89		191.1 \pm 11.10	

Data in mean \pm SEM, * p = 0.03, *** p = 0.0002, p values were from comparison between the indicated samples and vehicle control (n = 3, one-way ANOVA, Tukey's post hoc tests).

Table S41. Estimated mt-ROS content and J aggregates/JC-1 monomers ratio in 3T3-L1 adipocytes treated by isolated compounds.

Sample	Mt-ROS level (%)			J aggregates/JC-1 monomers percentage (%)		
	0.5 μM	5 μM	10 μM	0.5 μM	5 μM	10 μM
Vehicle control	100 \pm 8.78			100 \pm 9.81		
Naringenin 42	65.1 \pm 6.03	64.53 \pm 7.70	49.12 \pm 10.76**	94.6 \pm 2.72	173 \pm 13.06	267.3 \pm 31.14****
Compound 76	72.21 \pm 2.60	69.02 \pm 3.03	57.19 \pm 5.56*	107.4 \pm 10.22	124.3 \pm 16.7	206.4 \pm 10.5*
Isosalipurposide 1	78.4 \pm 2.21	63.67 \pm 5.00	57.01 \pm 7.08*	89.28 \pm 7.21	127 \pm 8.40	163.7 \pm 6.25
Quercitrin 4	90.66 \pm 2.30	71.63 \pm 8.97	57.13 \pm 3.75*	74.23 \pm 11.96	104.6 \pm 20.54	128.1 \pm 6.69
D-(+)-pinitol 79a	71.3 \pm 7.07	71.53 \pm 2.65	56.44 \pm 7.68*	120.8 \pm 20.13	141.9 \pm 15.46	301 \pm 42.09****
(-)-Pinitol 79b	103.5 \pm 4.31	63.83 \pm 5.35	54.61 \pm 2.56*	196.2 \pm 27.88	224.2 \pm 29.28*	238.2 \pm 20.74**
(-)-Epicatechin 77	67.21 \pm 7.36	55.8 \pm 9.62*	45.94 \pm 3.54**	118.5 \pm 12.86	120.2 \pm 17.45	224.7 \pm 31.68**
2,4-Di- <i>t</i> -butylphenol 78	73.23 \pm 1.37	68.17 \pm 7.09	45.82 \pm 8.21**	91.93 \pm 5.01	147.9 \pm 23.75	164.9 \pm 8.61
Myricitrin 11	83.97 \pm 15.37	70.42 \pm 17.29	67.73 \pm 5.36	126.8 \pm 13.49	132.2 \pm 21.66	193.5 \pm 14.24
Compound 80	95.02 \pm 18.26	89.12 \pm 6.65	77.78 \pm 7.92	147.9 \pm 24.71	134.6 \pm 15.02	186.7 \pm 23.12
Metformin 10 μM	65.74 \pm 2.16			206.8 \pm 41.87		
Undifferentiated cells	70.45 \pm 7.89			191.1 \pm 11.10		

Data in mean \pm SEM; * p = 0.03, ** p = 0.001, *** p = 0.0002, **** p = 0.000001, p values were from comparison between the indicated samples and vehicle control (n = 3, one-way ANOVA, Tukey's post hoc tests).

Table S42. Observed data of glucose uptake simulation with 2-NBDG fluorescence assay for isolated compounds on the 3T3-L1 adipocytes.

No	Sample	2-NBDG uptake percentage (%)	
		0.5 μ M	10 μ M
1	Vehicle	100 \pm 6.54	
2	Naringenin 42	89.3 \pm 9.47	127.3 \pm 15
3	Naringenin-7 <i>O</i> - α -L-arabinofuranoside 76	107.6 \pm 7.89	156.4 \pm 22.26
4	Isosalipurposide 1	110.7 \pm 13.26	161 \pm 39.47
5	Quercitrin 4	101.6 \pm 14.07	151 \pm 10.03
6	<i>D</i> -(+)-pinitol 79a	108.5 \pm 11.36	143.9 \pm 12.56
7	(-)-Pinitol 79b	96.99 \pm 3.25	125.6 \pm 13.27
8	(-)-Epicatechin 77	108.3 \pm 1.12	187.9 \pm 41.95*
9	2,4-Di- <i>t</i> -butylphenol 78	86.39 \pm 10.81	131.2 \pm 21.57
10	Myricitrin 11	122.7 \pm 10.74	152.3 \pm 24.02
11	3-Hydroxy-5-(2-aminoethyl) dihydrofuran-2(3 <i>H</i>)-one 80	89.56 \pm 7.20	96.64 \pm 10.97
12	Insulin 100 nM	140.6 \pm 18.36	
13	Metformin 10 μ M	138 \pm 28.26	

Data in mean \pm SEM; * p = 0.01, p value was from the indicated sample against the vehicle control (n = 3, One-way ANOVA, Dunnett's post hoc).

Table S43. Quantitative data of ratio of expressed p-AMPK- α to AMPK- α (%) by adipocytes exposed to the tested MeOH extracts

No	Treatment	Ratio of p-AMPK- α to AMPK- α (%)	
		12.5 μ g/mL	50 μ g/mL
1	Vehicle control	100 \pm 17.16	
2	Metformin 10 μ M	166.4 \pm 14.08	
3	FL-MeOH	128.1 \pm 10.56	177 \pm 16.98*
4	LF-MeOH	128.9 \pm 12.97	158.5 \pm 13.76
5	BK-MeOH	129.7 \pm 22.79	149.1 \pm 25.85

* p = 0.02, p value was of the sample against the vehicle control (n = 3, one-way ANOVA, Tukey)

Table S44. Quantitative data of ratio of expressed p-AMPK- α to AMPK- α (%) by adipocytes exposed to the tested isolated compounds

No	Treatment	Ratio of p-AMPK- α to AMPK- α (%)	
		0.5 μ M	10 μ M
1	Vehicle	100 \pm 13.36	
2	Metformin 10 μ M	191.8 \pm 21.86**	
3	Naringenin 42	123.8 \pm 2.34	148.4 \pm 13.56
3	Naringenin-7 <i>O</i> - α -L-arabinofuranoside 76	139.1 \pm 13.04	211.8 \pm 30.27***
4	Isosalipurposide 1	129.8 \pm 14.7	196.6 \pm 20.33**
5	Quercitrin 4	110.7 \pm 11.33	148.6 \pm 12.2
6	Myricitrin 11	109.4 \pm 10.11	156 \pm 8.11
7	(-)-Pinitol 79b	94.05 \pm 7.39	102.7 \pm 22.67
8	(-)-Epicatechin 77	99.62 \pm 3.88	143.2 \pm 17.25
9	<i>D</i> -(+)-Pinitol 79a	91.72 \pm 6.07	98.61 \pm 8.55

Data in mean \pm SEM; * p = 0.003, *** p = 0.0002, p values were from comparison between the indicated samples and vehicle control (n = 3, one-way ANOVA, Tukey's post hoc tests)

Table S45. Quantitative data of the expression of the target mRNA normalised by β -actin from the RT-qPCR of adipocytes treated with MeOH extracts

Treatment	Concentration	mRNAs related to mitochondrial biogenesis			Inflammatory markers' mRNAs	
		Adiponectin	PGC-1 α	mtTFA	TNF- α	IL-6
Vehicle control	-	95.98 \pm 2.08	125.4 \pm 2.50	125.7 \pm 0.08	175.5 \pm 2.81	152.6 \pm 1.65
Metformin	10 μ M	98.15 \pm 1.67	127.1 \pm 1.9	129.4 \pm 1.63	172.2 \pm 0.23	148.2 \pm 0.83
FL-MeOH	12.5 μ g/mL	102.6 \pm 1.00	129.7 \pm 2.76	127.4 \pm 3.58	179.3 \pm 4.87	151.5 \pm 3.25
	50 μ g/mL	124.9 \pm 11.87*	136.8 \pm 2.91*	137.2 \pm 0.81**	159.6 \pm 9.72	142.1 \pm 3.19*
LF-MeOH	12.5 μ g/mL	99.94 \pm 1.68	134.1 \pm 1.85	128.4 \pm 4.16	174.7 \pm 4.39	151.9 \pm 5.10
	50 μ g/mL	106.1 \pm 2.72	138.8 \pm 0.36**	134.4 \pm 1.53	163.9 \pm 7.75	142.2 \pm 10.89
BK-MeOH	12.5 μ g/mL	102.8 \pm 4.94	135.3 \pm 0.69*	136.4 \pm 1.69*	180.3 \pm 3.35	156.9 \pm 0.45
	50 μ g/mL	113.8 \pm 12.33	136.1 \pm 2.71*	138.3 \pm 1.47**	163.5 \pm 1.56	153.4 \pm 1.22

Data in mean \pm SEM; * p = 0.02, ** p = 0.002, p values were comparison between the indicated samples and vehicle control (n = 3, one-way ANOVA, Tukey's post hoc tests)

Table S46. Quantitative data of the expression of the target mRNA normalised by β -actin from the RT-qPCR of adipocytes treated with MeOH isolated compounds

Treatment	Concentration (μ M)	mRNAs related to mitochondrial biogenesis			Inflammatory markers' mRNAs	
		Adiponectin	PGC-1 α	mtTFA	TNF- α	IL-6
Vehicle control	-	95.98 \pm 2.08	125.4 \pm 2.5	125.7 \pm 0.08	175.5 \pm 2.81	152.6 \pm 1.65
Metformin	10	98.15 \pm 1.67	127.1 \pm 1.9	129.4 \pm 1.63	172.2 \pm 0.23	148.2 \pm 0.83
Naringenin 42	0.5	97.07 \pm 1.97	125.8 \pm 1.52	126.9 \pm 1.72	170.6 \pm 6.91	151.6 \pm 3.16
	10	110.4 \pm 12.19*	131.6 \pm 2.33	132.1 \pm 0.73	164.5 \pm 7.90	148.7 \pm 3.03
Naringenin-7O- α -L-arabinofuranoside 76	0.5	96.93 \pm 2.52	127 \pm 1.71	129.1 \pm 3.44	176.6 \pm 1.14	152 \pm 2.56
	10	103.2 \pm 2.56	132.4 \pm 2.86	133.3 \pm 2.96	161.3 \pm 5.45*	151.1 \pm 2.52
Isosalipurposide 1	0.5	95.85 \pm 0.55	127.3 \pm 2.46	130 \pm 1.69	168.4 \pm 2.88	152.3 \pm 3.95
	10	97.8 \pm 1.14	128.4 \pm 2.54	131.4 \pm 1.61	165.9 \pm 3.54	151.7 \pm 3.22
Quercitrin 4	0.5	95.38 \pm 1.30	127.1 \pm 3.45	128 \pm 0.85	169.2 \pm 4.88	152.9 \pm 4.52
	10	97.38 \pm 0.54	130.4 \pm 2.52	131.4 \pm 2.55	162.8 \pm 6.23	146.1 \pm 1.68
D-(+)-Pinitol 79a	0.5	95.4 \pm 2.59	130.4 \pm 1.51	128.8 \pm 1.04	166.7 \pm 2.32	151.4 \pm 2.98
	10	97.49 \pm 1.83	137.5 \pm 2.89*	130.2 \pm 1.73	155.9 \pm 6.45*	147.9 \pm 3.29
(-)-Pinitol 79b	0.5	94.24 \pm 3.10	126.6 \pm 0.71	128 \pm 3.84	169 \pm 10.08	148.5 \pm 5.62
	10	95.41 \pm 3.66	127.4 \pm 1.24	130.3 \pm 5.79	163 \pm 10.05	146.5 \pm 4.17
(-)-Epicatechin 77	0.5	95.42 \pm 0.52	126.9 \pm 2.46	126.8 \pm 0.93	172.3 \pm 6.54	150.1 \pm 3.41
	10	95.92 \pm 1.03	128.5 \pm 2.25	129 \pm 2.10	168.4 \pm 5.74	148.1 \pm 1.79
Myricitrin 11	0.5	96.18 \pm 0.69	126.2 \pm 1.59	130.2 \pm 2.25	170.9 \pm 6.85	155.4 \pm 3.44
	10	98.52 \pm 0.70	134.1 \pm 1.02	131.8 \pm 0.72	165.6 \pm 5.68	145.6 \pm 9.24

Data in mean \pm SEM; * p = 0.02, p value was from comparison between the indicated samples and vehicle control (n = 3, one-way ANOVA, Tukey's post hoc tests).